

CHARACTERISATION OF THE  
HERPES SIMPLEX VIRUS TYPE 1 (HSV-1)  
TRIPLEX PROTEINS

BY

CHRISTOPHER JOHN BOUTELL

A THESIS FOR THE DEGREE OF DOCTOR OF PHILOSOPHY  
IN THE FACULTY OF SCIENCE AT GLASGOW UNIVERSITY

MRC VIROLOGY UNIT  
INSTITUTE OF VIROLOGY  
CHURCH STREET  
GLASGOW  
G11 5JR

SEPTEMBER, 2000

ProQuest Number: 13818557

All rights reserved

INFORMATION TO ALL USERS

The quality of this reproduction is dependent upon the quality of the copy submitted.

In the unlikely event that the author did not send a complete manuscript and there are missing pages, these will be noted. Also, if material had to be removed, a note will indicate the deletion.



ProQuest 13818557

Published by ProQuest LLC (2018). Copyright of the Dissertation is held by the Author.

All rights reserved.

This work is protected against unauthorized copying under Title 17, United States Code  
Microform Edition © ProQuest LLC.

ProQuest LLC.  
789 East Eisenhower Parkway  
P.O. Box 1346  
Ann Arbor, MI 48106 – 1346

GLASGOW  
UNIVERSITY  
LIBRARY

12036-Copy 1

# Contents

## ACKNOWLEDGEMENTS

## ABSTRACT

## ABBREVIATIONS

<b>1.0 INTRODUCTION .....</b>	<b>1</b>
1.1 CLASSIFICATION OF THE HERPESVIRUSES .....	1
1.1.1 <i>Subfamily classification of herpesviruses</i> .....	2
1.1.2 <i>Classification of herpesviruses based upon sequence analysis</i> .....	3
1.1.3 <i>Divergence of the Herpesviridae family</i> .....	4
1.2 HERPESVIRUSES WHICH INFECT HUMANS .....	4
1.3 VIRION ARCHITECTURE .....	5
1.3.1 <i>The HSV-1 genome</i> .....	5
1.3.2 <i>The "α" sequence</i> .....	5
1.3.3 <i>DNA structure within the nucleocapsid</i> .....	6
1.4 VIRION MORPHOLOGY .....	7
1.4.1 <i>The tegument</i> .....	7
1.4.1.1 <i>Tegument assembly</i> .....	8
1.4.1.2 <i>Tegument structure</i> .....	8
1.4.3 <i>The capsid</i> .....	9
1.4.3.1 <i>Structural composition of the capsid</i> .....	10
1.4.3.2 <i>Protein composition of the HSV-1 capsid</i> .....	11
1.4.3.3 <i>Minor capsid proteins</i> .....	16
1.5 THE HSV-1 LYTIC LIFE CYCLE .....	17
1.5.1 <i>Attachment and entry of HSV-1 into the cell</i> .....	17
1.5.2 <i>Nucleocapsid transport</i> .....	18
1.5.3 <i>Disruption of host cell protein synthesis</i> .....	18
1.5.4 <i>HSV-1 gene expression</i> .....	19
1.5.5 <i>DNA replication</i> .....	20
1.5.6 <i>Packaging of progeny DNA</i> .....	20
1.5.7 <i>Tegument acquisition and virion egress</i> .....	21
1.6 OVERVIEW OF HSV-1 LATENCY .....	23
1.6.1 <i>Definition of latency</i> .....	23
1.6.2 <i>Establishment of latency</i> .....	23
1.6.3 <i>Maintenance of latency</i> .....	24
1.6.4 <i>Reactivation from latency</i> .....	25
1.7 CAPSID STRUCTURE .....	25
1.7.1 <i>Capsid architecture and the requirement for redundancy</i> .....	26
1.7.2 <i>Quasi-equivalence</i> .....	26
1.7.3 <i>Departure from quasi-equivalence</i> .....	27
1.7.4 <i>Flexibility of proteins within capsid structures</i> .....	28
1.7.5 <i>Flexibility of proteins within quasi-equivalent capsid structures</i> .....	29
1.7.6 <i>Symmetry mismatches in capsids</i> .....	29
1.8 HSV-1 CAPSID STRUCTURE .....	31
1.8.1 <i>Asymmetric unit</i> .....	31
1.8.2 <i>Protein composition of the capsomeres</i> .....	32
1.8.2.1 <i>Pentons and hexons are composed of VP5</i> .....	32
1.8.2.2 <i>Triplexes are heterotrimers of VP19c and VP23</i> .....	33
1.8.2.3 <i>VP26 is located on the tips of the hexons</i> .....	34
1.8.3 <i>Internal scaffold composition</i> .....	34
1.8.4 <i>Quasi-equivalence within the HSV-1 capsid</i> .....	36
1.8.5 <i>The non-equivalence of triplexes</i> .....	37

---

1.8.6 Quasi-equivalence within the procapsids.....	37
1.9 CAPSID ASSEMBLY .....	38
1.9.1 Nuclear assembly of HSV-1 capsids.....	38
1.9.2 HSV-1 capsid assembly analysis within insect cells.....	39
1.9.3 In vitro HSV-1 capsid assembly and procapsid formation.....	40
1.9.4 The structure of the procapsid.....	42
1.9.5 Identification of procapsids during HSV-1 infection.....	42
1.9.6 Other capsid assembly models .....	43
1.9.7 P22 capsid assembly .....	44
1.9.8 The molten globule-like characteristics of the P22 scaffold protein (gp8) .....	45
<b>2.1 MATERIALS .....</b>	<b>47</b>
<b>2.2 METHODS.....</b>	<b>55</b>
2.2.1 RECOMBINANT DNA MANIPULATION .....	55
2.2.1.1 Preparation of electrocompetent bacteria.....	55
2.2.1.2 Transformation of electrocompetent bacteria.....	55
2.2.1.3 Glycerol stock preparation.....	56
2.2.1.4 Small scale plasmid DNA isolation.....	56
2.2.1.5 Phenol/chloroform extraction and ethanol precipitation of DNA.....	56
2.2.1.6 Large scale plasmid DNA isolation.....	57
2.2.1.7 Restriction endonuclease digestion of DNA .....	57
2.2.1.8 Analytical DNA agarose gel electrophoresis .....	58
2.2.1.9 Purification of DNA from agarose .....	58
2.2.1.10 DNA ligation .....	58
2.2.1.11 Linker ligation.....	59
2.2.1.12 Oligonucleotide purification .....	59
2.2.1.13 PAGE of synthetic oligonucleotides .....	59
2.2.2 M13 PHAGE SITE DIRECTED MUTAGENESIS OF UL18.....	60
2.2.2.1 Preparation of uracil enriched pETUL18 ssDNA.....	60
2.2.2.2 Oligonucleotide mutagenesis .....	61
2.2.3 GENERATION OF MONOCLONAL ANTIBODIES.....	62
2.2.4 IMMUNOFLUORESCENCE ANALYSIS.....	64
2.2.4.1 Transfection of plasmid DNA .....	64
2.2.4.2 Immuno staining and microscopy analysis .....	64
2.2.5 YEAST MANIPULATION.....	65
2.2.5.1 Glycerol stock preparation.....	65
2.2.5.2 Transformation of plasmid DNA into yeast.....	66
2.2.5.2.1 Preparation of yeast cells.....	66
2.2.5.2.2 Transformation of competent yeast cells.....	66
2.2.5.3 Yeast colony selection .....	67
2.2.5.3 Replica plating and picking of yeast colonies .....	67
2.2.5.4 $\beta$ -galactosidase filter assay.....	68
2.2.5.5 Isolation of plasmid DNA from yeast .....	68
2.2.5.6 TCA extraction of proteins from yeast cells .....	69
2.2.5.6.1 Yeast cell culture and preparation for protein extraction.....	69
2.2.5.6.2 TCA protein extraction.....	69
2.2.5.7 Random PCR mutagenesis .....	70
2.2.6 TISSUE CULTURE AND VIRUS MANIPULATION .....	71
2.2.6.1 Baculovirus manipulation .....	71
2.2.6.1.1 SF cell culture .....	71
2.2.6.1.2 Freezing and storage of SF cells.....	71
2.2.6.1.3 Recovery of SF21 cells .....	71
2.2.6.1.4 Construction of recombinant baculoviruses.....	72
2.2.6.1.5 Isolation of recombinant viruses .....	72
2.2.6.1.6 Production of low titre baculovirus stocks.....	73
2.2.6.1.7 Production of high titre baculovirus stocks.....	73
2.2.6.1.8 Baculovirus titration .....	74
2.2.6.2 BHK-21 C13 cell culture.....	74

---

---

2.2.6.3 Vero cell culture .....	75
2.2.6.4 Complementation of UL18 null mutant virus (K23Z).....	75
2.2.6.5 Titration of complemented HSV-1 UL18 null mutant virus (K23Z) .....	76
2.2.7 EXPRESSION OF RECOMBINANT PROTEINS .....	76
2.2.7.1 Protein expression in BL21 DE3 bacteria .....	76
2.2.7.2 Protein expression using the baculovirus expression system.....	77
2.2.8 PURIFICATION OF 6XHis EPI TOPE TAGGED PROTEINS .....	77
2.2.8.1 Ni-NTA agarose column chromatography .....	77
2.2.8.2 Preparation of bacterial extracts for Ni-NTA purification .....	78
2.2.8.3 Preparation of SF21 cell extracts for Ni-NTA purification.....	78
2.2.8.4 Ni-NTA agarose purification.....	78
2.2.8.5 Ni-NTA agarose pull downs .....	79
2.2.8.6 Quantification of protein concentration.....	80
2.2.9 ANALYSIS OF PURIFIED PROTEINS.....	80
2.2.9.1 SDS-polyacrylamide gel electrophoresis (SDS-PAGE) .....	80
2.2.9.2 Semi-dry Western blot analysis .....	81
2.2.9.2.1 Protein transfer .....	81
2.2.9.2.2 Detection of proteins .....	81
2.2.9.4 Stripping and re-probing nitro-cellulose membranes .....	82
2.2.9.3 TCA precipitation.....	82
2.2.9.4 Sucrose gradient sedimentation .....	82
2.2.9.5 Capsid assembly analysis.....	83
2.2.9.5.1 In vitro capsid assembly.....	83
2.2.9.5.2 In vivo capsid assembly.....	83
2.2.10 BIOPHYSICAL CHARACTERISATION TECHNIQUES .....	84
2.2.10.1 Fluorescence and ANS binding. ....	84
2.2.10.2 Circular-dichroism (CD).....	85
2.2.10.3 Digital scanning calorimetry (DSC). ....	85
2.2.10.4 Size exclusion chromatography.....	85
<b>3.1 REVERSE YEAST TWO HYBRID SYSTEM .....</b>	<b>87</b>
3.1.1 YEAST TWO HYBRID SYSTEM.....	87
3.1.1.1 Yeast two hybrid analysis of HSV-1 capsid protein interactions .....	87
3.1.1.2 Deletion mapping of protein-protein interactions within the yeast two hybrid system.....	88
3.1.2 REVERSE YEAST TWO HYBRID SYSTEM.....	89
3.1.3 REVERSE YEAST TWO HYBRID ANALYSIS OF VP19C AND VP23 .....	89
3.1.3.1 Generation of mutant alleles .....	89
3.1.3.2 Negative selection of mutant alleles.....	90
3.1.3.3 Regulation of URA3 and lacZ reporter genes within MaV103 cells .....	90
3.1.3.4 Other reporter genes within MaV103 cells .....	91
3.1.3.5 GAL4 fusion vectors used in the reverse yeast two hybrid system .....	91
3.1.3.6 Cloning of UL18 into pPc86 .....	91
3.1.3.7 Cloning of VP19c into pPc97.....	92
3.1.3.8 Fusion protein C-terminal truncations.....	92
3.1.3.9 Cloning strategy for UL38 pp65 epitope tagged into pPc97 .....	92
3.1.6 CONCLUSIONS.....	93
3.1.6.1 Yeast two hybrid analysis.....	93
3.1.6.2 Expression of UL38 and UL38Epi in the yeast two hybrid system .....	94
3.1.6.3 Reverse yeast two hybrid analysis.....	95
3.1.6.4 FOA selection.....	95
3.1.6.5 Analysis of negatively selected mutant alleles.....	96
3.1.6.6 Future work.....	98
<b>3.2 CHARACTERISATION OF MONOCLONAL ANTIBODIES .....</b>	<b>100</b>
3.2.1 IMMUNISATION PROTOCOL.....	100
3.2.2 ANTIBODY SCREENING BY WESTERN BLOT ANALYSIS.....	101
3.2.2.1 Monoclonal antibodies generated from BALB/c mouse #4.....	101
3.2.2.2 Monoclonal antibodies generated from BALB/c mice #1-3 .....	102
3.2.3 CONCLUSIONS AND FUTURE WORK.....	103

---

<b>3.3 CHARACTERISATION OF THE TRIPLEX PROTEIN VP23.....</b>	<b>104</b>
3.3.1 CONSTRUCTION AND EXPRESSION OF PETUL18 .....	104
3.3.1.1 Cloning of the UL18 ORF into pET28MOD .....	104
3.3.1.2 Bacterial expression of VP23His in BL21 DE3 cells.....	104
3.3.2 PURIFICATION OF VP23His.....	105
3.3.2.1 Nickle-nitrilotriacetic acid (Ni-NTA) agarose affinity chromatography.....	105
3.3.2.2 Ni-NTA agarose purification of VP23His .....	105
3.3.3 SIZE EXCLUSION CHROMATOGRAPHY AND SUCROSE GRADIENT SEDIMENTATION.....	106
3.3.3.1 Size exclusion chromatography of purified VP23His in G-150 buffer.....	106
3.3.3.2 VP23His purification and characterisation in buffer O.....	108
3.3.5 SUCROSE GRADIENT SEDIMENTATION ANALYSIS OF PURIFIED VP23His IN BUFFER O.....	109
3.3.6 CHARACTERISATION OF PURIFIED VP23His DIMERS .....	110
3.3.6.1 Thermolability of VP23 dimers .....	110
3.3.7 DISULPHIDE LINKAGE ANALYSIS OF VP23 .....	111
3.3.7.1 VP23 dimer formation in the absence of reducing agents .....	111
3.3.7.2 VP23 sequence analysis .....	112
3.3.8 VP23 CYSTEINE MUTAGENESIS .....	113
3.3.8.1 Expression of VP23His cysteine mutants .....	113
3.3.8.2 Ni-NTA purification of VP23 cysteine mutants .....	114
3.3.9 IMMUNFLUORESCENCE ANALYSIS OF VP23 AND VP23CYS MUTANTS.....	115
3.3.9.1 Cloning of UL18 and UL18CYS mutant ORFs into pCMV <sub>10</sub> .....	115
3.3.9.1 Intracellular localisation of VP23His and VP19c.....	116
3.3.10 VIRAL GROWTH ANALYSIS OF UL18CYS MUTANTS .....	117
3.3.11 CONCLUSIONS.....	118
3.3.11.1 VP23 dimerisation.....	118
3.3.11.2 VP23 cysteine analysis .....	120
3.3.11.3 Future Work .....	121
<b>3.4 CHARACTERISATION OF THE TRIPLEX PROTEIN VP19C.....</b>	<b>123</b>
3.4.1 CONSTRUCTION AND EXPRESSION OF PETUL38. ....	123
3.4.1.1 Cloning of the UL38 ORF into pET28MOD .....	123
3.4.1.2 Bacterial expression of VP19cHis.....	123
3.4.2 VP19CHIS ISOLATION FROM RECOMBINANTLY EXPRESSED TRIPLEXES .....	124
3.4.3 PURIFICATION OF RECOMBINANTLY EXPRESSED VP19CHIS FROM SF21 CELLS INFECTED WITH AC381 .....	126
3.4.3.1 Cloning of the UL38 ORF into pAcCL29-1.....	126
3.4.3.2 Expression and purification of VP19cHis .....	126
3.4.4 NI-NTA PULL DOWN ASSAYS.....	128
3.4.4.1 Characterisation of in vitro triplex formation.....	129
3.4.5 SIZE EXCLUSION CHROMATOGRAPHY OF VP19CHIS .....	130
3.4.6 SUCROSE GRADIENT SEDIMENTATION .....	131
3.4.6.1 in vitro formation of triplexes from purified proteins.....	131
3.4.7 CONCLUSIONS.....	133
3.4.7.1 Future work.....	136
<b>3.5 CHARACTERISATION OF THE HSV-1 TRIPLEX.....</b>	<b>137</b>
3.5.1 CONSTRUCTION AND EXPRESSION OF PETUL1838. ....	137
3.5.1.1 Cloning of the 6xHis tagged UL18 ORF into pETUL38.....	137
3.5.1.2 Expression of triplex proteins VP23His and VP19cHis in BL21 DE3 bacteria.....	137
3.5.1.3 Ni-NTA agarose purification of VP23His and VP19cHis from induced BL21 DE3 bacteria expressing pETUL1838.....	138
3.5.2 CO-EXPRESSION OF VP23 AND VP19C TRIPLEX PROTEINS WITHIN SF21 CELLS.....	139
3.5.2.1 Cloning of the UL18 ORF into the baculovirus transfer vector pAcAB3 containing the UL38 ORF (pAcAB3.10) .....	139
3.5.2.2 Expression of Ac18638 within SF21 cells.....	140
3.5.3 CLONING AND EXPRESSION OF AC18386.....	140
3.5.3.1 Cloning of the 6x His epitoped tagged UL38 ORF and UL18 ORF into the baculovirus transfer vector pAcAB3.....	141

3.5.3.2 <i>Expression of Ac18386 in SF21 cells</i> .....	141
3.5.4 NI-NTA AGAROSE PURIFICATION OF TRIPLEX PROTEINS EXPRESSED WITHIN SF21 CELLS INFECTED EITHER WITH AC18638 OR AC18386 .....	142
3.5.4.1 <i>Purification of triplexes</i> .....	142
3.5.4.2 <i>Solubility of triplexes at 4°C</i> .....	142
3.5.5 DISULPHIDE BOND ANALYSIS OF PURIFIED TRIPLEX PROTEINS.....	144
3.5.6 SIZE EXCLUSION CHROMATOGRAPHY ANALYSIS OF PURIFIED TRIPLEX PROTEINS.....	145
3.5.7 SUCROSE GRADIENT SEDIMENTATION ANALYSIS OF NI-NTA AGAROSE PURIFIED TRIPLEXES .....	147
3.5.8 CONCLUSIONS.....	148
3.5.9.1 <i>Future work</i> .....	150
<b>3.6 FUNCTIONAL AND BIOPHYSICAL CHARACTERISATION OF PURIFIED TRIPLEXES AND TRIPLEX PROTEINS.....</b>	<b>151</b>
3.6.1 IN VIVO AND IN VITRO CAPSID ASSEMBLY ANALYSIS.....	151
3.6.2 BIOPHYSICAL CHARACTERISATION OF THE HSV-1 TRIPLEXES AND TRIPLEX PROTEIN CONSTITUENTS .....	153
3.6.2.1 <i>Homogeneity of Ni-NTA agarose purified triplexes and triplex proteins used for biophysical experimental analysis</i> .....	153
3.6.2.2 <i>Ni-NTA purified triplexes and triplex proteins are folded protein molecules</i> .....	154
3.6.2.3 <i>GndHCl induced unfolding of triplexes and triplex proteins</i> .....	155
3.6.2.4 <i>Far-UV CD analysis of the secondary structure within triplexes and triplex proteins</i> .....	156
3.6.2.5 <i>Near-UV CD analysis of the tertiary structure within triplexes and triplex proteins</i> .....	159
3.6.2.6 <i>DSC analysis of the tertiary structure within triplexes and triplex proteins</i> .....	160
3.6.2.7 <i>Partial folding within purified triplexes and triplex proteins</i> .....	165
3.6.3 CONCLUSIONS.....	166
3.6.3.1 <i>Ni-NTA agarose purified triplexes and triplex proteins are functionally active</i> .....	166
3.6.3.2 <i>Molten globularity of purified VP23His and VP19cHis</i> .....	167
3.6.3.3 <i>Mutual protein co-folding within the triplex</i> .....	169
3.6.3.4 <i>Partial folding within the triplex</i> .....	169
3.6.3.5 <i>Future work</i> .....	171
<b>4.0 DISCUSSION.....</b>	<b>173</b>
4.1 QUASI-EQUIVALENCE AND CONFORMATIONAL FLEXIBILITY WITHIN THE HSV-1 CAPSID.....	173
4.2 NON-EQUIVALENT INTERACTIONS OF TRIPLEXES WITHIN THE HSV-1 CAPSID.....	174
4.3 HOW DO THE TRIPLEXES OCCUPY A 3-FOLD ROTATIONAL AXIS? .....	175
4.4 CONFORMATIONAL FLEXIBILITY WITHIN THE TRIPLEX .....	176
4.5 MOLTEN GLOBULE CHARACTERISTICS OF THE TRIPLEX.....	177
4.6 GROSS CONFORMATIONAL REARRANGEMENTS AND THE CAPSID FLOOR.....	178
4.7 HETEROTRIMER OPPOSED TO HOMOTRIMER, THE REQUIREMENT FOR VP23 WITHIN THE TRIPLEX.....	180
4.7.1 <i>The function of VP23 within the triplex</i> .....	181
4.8 VP5 CAPSOMER FLEXIBILITY .....	182
<b>5.0 SUMMARY .....</b>	<b>185</b>
5.1 PARTIAL FOLDING AND CAPSID ASSEMBLY.....	185
5.2 PARTIAL FOLDING AND HSV-1 CAPSID ASSEMBLY .....	186

## REFERENCES

## List of figures:

### Introduction:

<u>Fig. number:</u>	<u>Title:</u>	<u>Following page number:</u>
Fig. 1.1	Electron micrograph of a frozen hydrated HSV-1 virion.	..... 1
Fig. 1.2	Schematic illustration of the divergence over time for some of the herpesviruses within the herpesviridae family.	..... 3
Fig. 1.3	Schematic illustration of the structure of the HSV-1 genome.	..... 5
Fig. 1.4	Cross-section through a cryo-EM reconstruction of the HSV-1 virion resolved to 20Å.	..... 6
Fig. 1.5	Visualisation of the icosahedrally ordered tegument proteins.	..... 7
Fig. 1.6	Schematic illustration of the structural organisation of the HSV-1 genes UL26 and UL26.5.	..... 15
Fig. 1.7	Schematic overview of the lytic reproductive cycle of HSV-1.	..... 17
Fig. 1.8	Schematic diagram depicting triangulation symmetry.	..... 26
Fig. 1.9	3D Surface reconstruction of the HSV-1 B-capsid at 8.5Å.	..... 31
Fig. 1.10	Asymmetric unit of the HSV-1 capsid.	..... 31
Fig. 1.11	3D reconstruction of the HSV-1 triplex to 13Å.	..... 33
Fig. 1.12	Schematically illustration of the protein-protein interactions within the HSV-1 capsid determined through immunofluorescence.	..... 39
Fig. 1.13	EM analysis of negative stained <i>in vitro</i> formed procapsids and mature B-capsids.	..... 40
Fig. 1.14	Schematic representation of the intermediate stages in HSV-1 capsid assembly.	..... 41
Fig. 1.15	Structural changes that accompany HSV-1 procapsid maturation.	..... 42
Fig. 1.16	Schematic illustration of the capsid assembly pathway of the bacteriophage P22.	..... 44
Fig. 1.17	Diagrammatic representation of a molten-globule state.	..... 45

### Results (section 3.1):

Fig. 3.1.1	Schematic representation of the yeast two hybrid system.	..... 87
Fig. 3.1.2	Schematic representation of the reverse yeast two-hybrid system.	..... 89
Fig. 3.1.3	Schematic representation of pPc86 and pPc97 GAL4 fusion vectors.	..... 91
Fig. 3.1.4	Cloning strategy of UL18 ORF into pPc86.	..... 92
Fig. 3.1.5	Cloning strategy of UL38 ORF into pPc97.	..... 92
Fig. 3.1.6	Cloning strategy of pPc97UL38Epi.	..... 92
Fig. 3.1.7	Phenotypic characterisation of the MaV103 yeast cells.	..... 93
Fig. 3.1.8	Yeast two hybrid analysis and $\beta$ -galactosidase filter assay.	..... 93
Fig. 3.1.9	Analysis of pPc97UL38Epi (VP19cDB.Epi).	..... 94
Fig. 3.1.10	Recombination and gap repair of mutant UL18 PCR alleles into linearised pPc86 vector.	..... 95
Fig. 3.1.11	FOA negatives selection of mutants UL18 alleles.	..... 96
Fig. 3.1.12	Second round FOA selection of mutant UL18 alleles.	..... 96
Fig. 3.1.13	SDS-PAGE and Western blot analysis of yeast cell protein extracts.	..... 97
Fig. 3.1.14	1% TBE gel of plasmid DNA purified from yeast.	..... 97

**Results (section 3.2):**

Fig. 3.2.1	Characterisation of monoclonal antibodies produced from BALB/c mouse #4.	..... 101
Fig. 3.2.2	Characterisation of monoclonal antibodies produced from BALB/c mice #1-3.	..... 102

**Results (section 3.3):**

Fig. 3.3.1	Construction of the pET28MOD expression vector.	..... 104
Fig. 3.3.2	Schematic representation of the bacterial expression vector pETUL18.	..... 104
Fig. 3.3.3	SDS-PAGE and Western blot analysis of VP23His expression in BL21 DE3 bacteria.	..... 104
Fig. 3.3.4	Schematic representation of Ni-NTA and Ni-NTA binding to two His residues from the 6xHis epitope tag.	..... 105
Fig. 3.3.5	SDS-PAGE analysis of Ni-NTA agarose purified VP23His in sonication buffer.	..... 105
Fig. 3.3.6	Size exclusion chromatography and SDS-PAGE analysis of Ni-NTA agarose purified VP23His in G150 buffer.	..... 106
Fig. 3.3.7	Size exclusion chromatography of protein standards and generation of a standard curve.	..... 107
Fig. 3.3.8	Size exclusion chromatography of purified VP23His analysed at 0.25, 0.5, and 1.5 mg/ml in G150 buffer.	..... 107
Fig. 3.3.9	SDS-PAGE and Western blot analysis of Ni-NTA agarose purified VP23His in buffer O.	..... 108
Fig. 3.3.10	Size exclusion chromatography and SDS-PAGE analysis of Ni-NTA agarose purified VP23His in buffer O.	..... 108
Fig. 3.3.11	Sucrose gradient sedimentation and SDS-PAGE analysis of Ni-NTA purified VP23His in buffer O.	..... 109
Fig. 3.3.12	Size exclusion chromatography of Ni-NTA agarose purified VP23His in buffer O before and after incubation at 4°C.	..... 110
Fig. 3.3.13	SDS-PAGE analysis of Ni-NTA agarose purified VP23His in the presence and absence of 20mM $\beta$ -mercaptoethanol.	..... 111
Fig. 3.3.14	Size exclusion chromatography of Ni-NTA agarose purified VP23His in buffer O before and after incubation in the presence of 10mM DTT.	..... 112
Fig. 3.3.15	Amino acid sequence alignment of VP23 homologues.	..... 112
Fig. 3.3.16	Cysteine mutagenesis of UL18.	..... 113
Fig. 3.3.17	Western blot and SDS-PAGE analysis of VP23His and VP23His cysteine mutants.	..... 114
Fig. 3.3.18	SDS-PAGE analysis of purified VP23His Cysteine mutants -1, -3, and -4 in buffer O.	..... 114
Fig. 3.3.19	Schematic representation of the cloning strategy for UL18 ORF and mutant UL18CYS ORFs into pCMV <sub>10</sub> .	..... 115
Fig. 3.3.20	Immunofluorescence analysis showing the intracellular localisation of VP23 and VP19c.	..... 116
Fig. 3.3.21	Immunofluorescence analysis showing intracellular localisation of VP23 and VP19c co-expressed within BHK-21 C13 cells.	..... 116
Fig. 3.3.22	Immunofluorescence analysis showing the intracellular distribution of VP23His and VP23HisCYS mutants 1, 3, and 4 with VP19c.	..... 116
Fig. 3.3.23	Titration of complemented UL18 null mutant virus K23Z in Vero cells or G5-11 cells.	..... 117

**Results (section 3.4):**

Fig.3.4.1	Schematic representation of the bacterial expression vector pETUL38.	..... 123
Fig.3.4.2	SDS-PAGE and Western blot analysis of VP19cHis expression in BL21 DE3 bacteria.	..... 124
Fig.3.4.3	SDS-PAGE analysis of VP19cHis isolated from Ni-NTA agarose purified triplexes denatured in 3M urea.	..... 125
Fig.3.4.4	SDS-PAGE and fluorescence spectroscopy analysis of Ni-NTA agarose purified VP19cHis isolated from denatured triplexes in 3M urea.	..... 125
Fig.3.4.5	Schematic representation of pAcCL29381.	..... 126
Fig.3.4.6	SDS-PAGE analysis of SF21 cells infected with Ac381.	..... 126
Fig.3.4.7	SDS-PAGE analysis of VP19cHis purified in buffer O.	..... 127
Fig.3.4.8	SDS-PAGE and Western blot analysis of Ni-NTA agarose purified VP19cHis.	..... 127
Fig.3.4.9	SDS-PAGE and Western blot analysis of Ni-NTA agarose VP19cHis pull down of VP23.	..... 128
Fig.3.4.10	SDS-PAGE analysis of VP19cHis/VP23 interaction in the presence or absence of 1M NaCl.	..... 129
Fig.3.4.11	SDS-PAGE analysis of VP19cHis/VP23 interaction at 0°C.	..... 129
Fig.3.4.12	Size exclusion chromatography and SDS-PAGE analysis of Ni-NTA agarose purified VP19cHis in buffer O.	..... 130
Fig.3.4.13	SDS-PAGE analysis Ni-NTA agarose purified VP19cHis in the presence or absence of 20mM $\beta$ -mercaptoethanol.	..... 130
Fig.3.4.14	Sucrose gradient sedimentation and SDS-PAGE analysis of Ni-NTA purified VP19cHis in buffer O.	..... 131
Fig.3.4.15	Sucrose gradient sedimentation and SDS-PAGE/Western blot analysis of Ni-NTA purified VP19cHis and VP23His in buffer O.	..... 132

**Results (section 3.5):**

Fig. 3.5.1	Schematic representation of the cloning strategy for UL18 ORF into pETUL38 to generate pETUL1838.	..... 137
Fig. 3.5.2	SDS-PAGE analysis of pETUL1838 expression in BL21 DE3 bacteria.	..... 137
Fig. 3.5.3	Western blot analysis of pETUL18 and pETUL1838 expression in BL21 DE3 bacteria.	..... 137
Fig. 3.5.4	SDS-PAGE analysis of Ni-NTA agarose purified bacterially expressed triplex proteins (VP23His+VP19cHis).	..... 138
Fig. 3.5.5	Schematic representation of the cloning strategy for the insertion of the UL18 ORF into the baculovirus transfer vector pAcAB3.10 to generate pAcABUL18638 (Ac18638).	..... 139
Fig. 3.5.6	SDS-PAGE analysis of [ <sup>35</sup> S]methionine-labelled SF21 cell infected with the recombinant baculovirus Ac18638 co-expressing VP23His and VP19c.	..... 139
Fig. 3.5.7	SDS-PAGE analysis of Ni-NTA agarose purified triplex proteins VP23His and VP19c from SF21 cells infected with Ac18638.	..... 140
Fig. 3.5.8	Schematic representation of the baculovirus transfer vector pAcAB3. The red sites indicate the unique restriction sites used in the construction of pAcABUL18386.	..... 141
Fig. 3.5.9	Schematic representation for the orientation of the UL18 and UL38 ORFs within the baculovirus transfer vector pAcAB3 to generate pAcABUL18386 (Ac18386).	..... 141
Fig. 3.5.10	SDS-PAGE analysis of SF21 cells infected with Ac18386 co-expressing the triplex proteins VP19cHis and VP23.	..... 141
Fig. 3.5.11	SDS-PAGE analysis of Ni-NTA agarose purified triplex proteins upon incubation at 4°C.	..... 142
Fig. 3.5.12	SDS-PAGE analysis of Ni-NTA agarose purified triplex proteins in buffer OG before and after o/n storage at 4°C.	..... 143

---

Fig. 3.5.13	Ni-NTA agarose purification of triplex proteins in the presence of 8M urea.	..... 144
Fig. 3.5.14	SDS-PAGE analysis of Ni-NTA agarose purified triplex proteins in the presence (+) or absence (-) of 20mM $\beta$ -mercaptoethanol.	..... 144
Fig. 3.5.15	Ni-NTA agarose purification of triplex proteins and size exclusion chromatography.	..... 145
Fig. 3.5.16	SDS-PAGE and ratio analysis of triplex proteins.	..... 146
Fig. 3.5.17	Sucrose gradient sedimentation analysis of Ni-NTA purified triplex proteins.	..... 147

### Results (section 3.6):

Fig. 3.6.1	Functional analysis of recombinantly expressed 6xHis tagged proteins.	..... 151
Fig. 3.6.2	Intrinsic fluorescence spectra of Ni-NTA agarose purified VP23His, VP19cHis and triplexes.	..... 154
Fig. 3.6.3	Structural stability analysis of Ni-NTA agarose purified VP23His, VP19cHis and triplexes by GdnHCl induced unfolding.	..... 155
Fig. 3.6.4	Far-UV CD analysis and CONTIN estimation of secondary structure of purified VP23His, VP19cHis, and triplex.	..... 156
Fig. 3.6.5	Near-UV CD analysis of monomeric, and dimeric VP23His and triplexes.	..... 159
Fig. 3.6.6	Differential scanning calorimetry (DSC) of Ni-NTA agarose purified VP23His.	..... 160
Fig. 3.6.7	Differential scanning calorimetry (DSC) of Ni-NTA agarose purified VP19cHis.	..... 161
Fig. 3.6.8	Differential scanning calorimetry (DSC) of Ni-NTA agarose purified triplexes.	..... 163
Fig. 3.6.9	Differential scanning calorimetry (DSC) of Ni-NTA agarose purified triplexes.	..... 165

### Discussion:

Fig. 4.1	Surface reconstruction of the HSV-1 capsid at 8.5Å resolution.	..... 174
Fig. 4.2	Heterotrimeric arrangement of VP23 and VP19c interactions within the triplex.	..... 175
Fig. 4.3	Predicted $\alpha$ -helices within the two VP23 molecules of an averaged triplex.	..... 176
Fig. 4.4	Visualisation of the heterotrimeric interactions within the triplex.	..... 176
Fig. 4.5	Model for the folding events and cellular localisation of the triplex proteins during capsid assembly.	..... 184

---

## List of tables:

<u>Table number:</u>	<u>Title:</u>	<u>Following page number:</u>
Table 1.1	Summary of human herpesviruses including primary and associated illnesses.	..... 4
Table 1.2	Summary of the HSV-1 tegument proteins and their known properties.	..... 8
Table 1.3	Summary of HSV-1 glycoproteins and their known properties.	..... 9
Table 1.4	Summary of the major capsid proteins within HSV-1 A-, B-, and C-capsids.	..... 10
Table 1.5	Summary of the essential HSV-1 DNA replication proteins.	..... 20
Table 1.6	Summary of the HSV-1 DNA packaging proteins.	..... 21
Table 2.2.1	Summary of the immunisation regime of BALB/c mice for the production of VP19c and VP23 monoclonal antibodies.	..... 63*
Table 2.2.2	Summary of antibody dilutions used in immunofluorescence analysis.	..... 65*
Table 3.2.1	Summary of the monoclonal antibodies generated from BALB/c mouse #4.	..... 101
Table 3.2.2	Summary of the monoclonal antibodies generated from BALB/c mice #1-#3.	..... 102
Table 3.5.1	Summary table of buffers used in the solubilisation of Ni-NTA agarose purified triplex proteins.	..... 143
Table 3.6.1	Functional analysis of triplexes and triplex protein samples to support <i>in vitro</i> and <i>in vivo</i> capsid formation.	..... 152

\* Table on page number shown.

## Acknowledgements

I would like to thank all the members of lab 209 who have provided me with constant support, encouragement, and technical expertise. I would like to particularly thank Dr Frazer Rixon for his advice throughout the course of my project and for proof reading my thesis so thoroughly (if nothing else Frazer at least my spelling is getting better). I would also like to thank Joyce Mitchell and David McNab for being so patient over the years and providing their valuable and technical experience so willingly.

With regards to the biophysical characterisation experiments presented within this thesis I would especially like to thank Dr David McClelland, for his advice and help throughout the course of my PhD, Dr Marina Kirkitadze, for providing her technical expertise during the DSC analysis, Sharon Kelly and Professor Nick Price for all their help, advice, and great patience during the near and far-UV CD analysis.

I would also like to acknowledge Professor Wah Chiu, Dr Hong Zhou, and their respective groups (Baylor College of Medicine, Texas, USA), for providing all the cryo-EM image reconstructions, and generous hospitality during my visit.

All the results presented within this thesis were obtained by the author's own efforts, unless stated otherwise.

I would personally like to thank my family for all their support, the Siege Boy'z and Girl'z for their great friendships, laughter, and humorous outings to Dumby. I would also like to thank Angus Cameron for his love, friendship, and encouragement over the last four years in the good and the not so good times.

Last, but by no means least, I would like to thank Alison Kerr for giving her love unconditionally and for putting up with me over the past six months. This thesis is dedicated to you and our future together.

---

## Abstract

Within the herpes simplex type-1 (HSV-1) capsid the heterotrimeric protein complex, the triplex, plays an essential structural role in both the capsid assembly pathway and subsequent conformational changes involved in the maturation of the procapsid into the WT polyhedral T=16 icosahedral capsid. Cryo-EM has shown that the HSV-1 capsid contains 6 different types of triplexes ( $T_a$ - $T_f$ ) which contribute to a single asymmetric unit and occupy the local and, with respect to triplex ' $T_f$ ', global 3-fold rotational axes. These triplexes in themselves represent unique asymmetrical structures within the HSV-1 capsid that violate the rules of quasi-equivalence. The triplexes have been shown not only to be involved in the interconnection of hexon and penton capsomers but also to interact with, and probably influence the development of, the capsid floor. This thesis analyses the structural relationship between the single copy of VP19c and the two copies of VP23 which make up the triplex and the means by which these unique asymmetric structures form their unusual interactions within the HSV-1 capsid.

The interactions between the triplex proteins were analysed by using a genetic approach based on the yeast two-hybrid system, termed the reverse yeast two-hybrid system (described in section 3.1). Using this system, VP23 and VP19c were shown to interact within yeast.

Since little is known about the structure of the individual HSV-1 capsid proteins, it was decided to analyse their biophysical properties through the use of size exclusion chromatography, near and far-UV circular dichroism (CD), differential scanning calorimetry (DSC), fluorescence spectroscopy, and 8-anilino-1-naphthalene sulfonate (ANS) binding studies. In order to carry out these experiments both bacterial and baculovirus recombinant expression systems were employed to express the individual triplex proteins VP23 and VP19c, as well as, co-expressing these proteins to form triplexes *in vivo*. Proteins were engineered to contain a 6xHis epitope tag at their N-termini. Using this tag, purification strategies were developed to maximise the recovery and solubility of the recombinantly expressed proteins. Monoclonal antibodies raised against these proteins were used in their characterisation.

---

VP23 was shown to exist either as a monomer or a dimer, depending on the purification buffer used during the analysis, and both were shown to be functionally active in capsid assembly. Dimers were shown not to be linked by inter-molecular disulphide bonds. Conserved cysteine residues within VP23 were also shown not to be essential for either triplex formation or capsid assembly.

Biophysical experiments were performed on both triplexes and triplex proteins purified to homogeneity through the use of Ni-NTA agarose affinity chromatography and shown to be functionally active via *in vitro* capsid assembly experiments. Fluorescence and far-UV CD analysis demonstrated that these purified proteins and complexes were folded and contained high levels of secondary structure. DSC and near-UV CD analysis demonstrated that VP23, either as a monomer or dimer, contained little or no stable tertiary structure. This was also demonstrated for purified VP19c. ANS binding studies demonstrated that these proteins were able to bind ANS and that the organic moiety could become fluorescent following excitation. This indicates that ANS had access to the hydrophobic core of these proteins suggesting that they were able to undergo further conformational rearrangements. Triplexes, in comparison, were shown to contain well-defined tertiary structure while still retaining the ability to bind ANS that could become fluorescent following excitation.

Taken together, the results show that the individual triplex proteins exist in a "molten globule" like intermediate state of folding. Molten globule-like proteins typically demonstrate a compact state with a high degree of secondary structure but with little or no rigid tertiary structure. Triplexes were shown to contain well-defined tertiary structure but still retained some of the characteristics of a molten globule. These results suggest that partial folding of the triplex proteins plays an important role in the formation of the triplex and its extensive interactions with other capsid proteins required for procapsid assembly and subsequent maturation. These results are discussed in relation to the known functions of the triplex and their overall importance to capsid structure.

---

---

## Abbreviations

### • A

Ac	<i>Autographa californica</i>
AD	Activation domain
Amp	Ampicillin
ANS	8-anilino-1-naphthalene sulfonate
ATP	Adenosine triphosphate

### • B

BHK	Baby hamster kidney
bp	base pair
BM	Boiling mix
BSA	Bovine serum albumin
BTV	Blue tongue virus

### • C

C-	Carboxy
°C	degrees centigrade
CCV	Channel catfish virus
CD	Circular dichroism
Ci	Curie
CIP	Calf intestinal phosphatase
CO <sub>2</sub>	Carbon dioxide
CPE	Cytopathic effect
Cryo-EM	electron cyro-microscopy

### • D

3D	Three-dimensional
Da	Dalton
DB	DNA binding domain
dH <sub>2</sub> O	deionised water
DMSO	dimethyl sulphoxide
DNA	deoxyribonucleic acid
DR	Direct repeat
ds	Double stranded
DSC	Differential scanning calorimetry
DTT	dithiothreitol

### • E

E.coli	<i>Escherichia coli</i>
EBV	Epstein-Barr virus
EDR	envelopment, deenvelopment, reenvelopment pathway
EDTA	ethylenediaminetetra-acetic acid
EHV	Equine herpesvirus
ELISA	Enzyme linked immunoabsorbent assay
EM	Electron microscope/microscopy
EtBr	Ethidium bromide

---

• **F**

FCS	Foetal calf serum
FITC	fluorescein thiocyanate
FOA	5-fluoroorotic acid

• **G**

GAGS	Glycosaminoglycans
GFP	Green fluorescent protein
GHV	Gallid herpesvirus
GMEM	Glasgow modified medium
GdnHCl	Guanidine hydrochloride

• **H**

HCl	Hydrochloric acid
HCMV	Human cytomegalovirus
HHV	Human herpesvirus
6xHis	6 histidines
HSV	Herpes simplex virus
Hve	Herpesvirus mediator

• **I**

ICP	Infected cell protein
IE	Immediate early
Ig	Immunoglobulin
IRL	internal repeat long
ISL	internal repeat short
IPTG	isopropylthio- $\beta$ -D-galactoside

• **K**

k	kilo ( $10^3$ )
kan	kanamycin
kbp	kilobase pair
KS	kaposi's sarcoma

• **L**

l	Litre
LAT	Latency associated transcript

• **M**

m	milli ( $10^{-3}$ )
M	Molar
mA	milliamps
mAb	Monoclonal antibody
MCP	Major capsid protein
min	Minute
mg	milligrams
ml	millilitres
mM	millimolar
m.o.i.	Multiplicity of infection
MW	Molecular weight
mRNA	Messenger ribonucleic acid

• **N**

n	nano ( $10^{-9}$ )
N-	amino
NaCl	Sodium chloride
NCS	Newborn calf serum
Ni <sup>2+</sup>	Nickle ion
NP40	nonidet P40
NPT	non-permissive temperature
NTA	Nitrilo-tri-acetic acid

• **O**

OBP	Origin binding protein
OD	Optical density
o/n	Overnight
ORF	Open reading frame
ori	Origin of replication

• **P**

PAGE	Polyacrylamide gel electrophoresis
PBS	Phosphate buffered saline
PCR	Polymerase chain reaction
p.f.u.	Plaque forming units
pH	Plate harvest
pi	Post-infection
PRV	pseudorabies virus
PS	Penicillin/streptomycin
PT	Permissive temperature

• **R**

RGB	Resolving gel buffer
RNA	ribonucleic acid
RnaseA	Ribonuclease A
r.p.m.	Revolutions per minute
RT	Room temperature

• **S**

<sup>35</sup> [S]	Sulphur-35-radioisotope
SCMV	Simian cytomegalovirus
SDS	Sodium dodecyl sulphate
SF	<i>Spodoptera frugiperda</i>
SGB	Stacking gel buffer
ss	Single stranded
SV40	Simian virus 40

• **T**

TCA	Trichloroacetic acid
TEMED	N,N,N',N'-tetramethylethylene diamine
TNF	Tumour necrosis factor
Tris	tris (hydroxymethyl) aminoethane
ts	temperature sensitive

- **U**

μ	Micro (10 <sup>-6</sup> )
μg	Microgram
μl	Microlitre
UL	Unique long
US	Unique short
UV	Ultra violet

- **V**

V	Volts
VHS	Virion host shut-off protein
v/v	Volume to volume ratio
v/w	Volume to weight ratio
VZV	Varicella-zoster virus

- **W**

WT	Wild type
----	-----------

- **X**

X-gal	5-bromo-4-chloro-3-indolyl-β-D-galactosidase
-------	--

- **Amino acid abbreviations**

<u>Amino acid</u>	<u>Three letter code</u>	<u>One letter code</u>
Alanine	Ala	A
Arginine	Arg	R
Asparagine	Asn	N
Aspartic acid	Asp	D
Cysteine	Cys	C
Glutamine	Gln	Q
Glutamic acid	Glu	E
Glycine	Gly	G
Histidine	His	H
Isoleucine	Ile	I
Leucine	Leu	L
Lysine	Lys	K
Methionine	Met	M
Phenylalanine	Phe	F
Proline	Pro	P
Serine	Ser	S
Threonine	Thr	T
Tryptophan	Trp	W
Tyrosine	Tyr	Y
Valine	Val	V

- **DNA/RNA letter abbreviations**

<u>Base</u>	<u>One letter code</u>
Adenine	A
Cytosine	C
Guanine	G
Thymidine	T
Uracil	U

# Chapter 1

## Introduction

# 1.0 Introduction

## 1.1 Classification of the Herpesviruses

Herpesviruses belong to the family of *Herpesviridae*, a large family of viruses containing over 112 known species that infect a wide variety of warm and cold blooded animals (reviewed by Roizman and Sears, 1996). The virions of all species that belong to the *Herpesviridae* consist of 4 morphological compartments:

- I. The nucleic acid - a linear double stranded (ds) DNA molecule, typically 120-250kb in length, with variable G+C content (31-75%).
- II. The capsid - an icosahedral protein shell which surrounds the nucleic acid.
- III. The tegument - an amorphous protein shell that surrounds the capsid.
- IV. The envelope - the outermost layer of the virion composed of a lipid bilayer containing glycoprotein spikes protruding from its surface.

The architecture of a typical HSV-1 virion is shown in fig: 1.1.

All members of the *Herpesviridae* also share 4 common biological properties (reviewed by Roizman, 1992):

- I. Their respective nucleic acid encodes all the enzymes and co-factors that are required for nucleic acid synthesis and metabolism.
- II. The synthesis of viral DNA, capsid assembly, and packaging of viral DNA occurs within the nucleus. Envelopment of the capsid occurs by the budding of the capsid through the inner nuclear envelope. Viral membrane proteins within the envelope may become modified upon transit through the Golgi apparatus.
- III. Production of infectious progeny virus invariably leads to the destruction of the infected cell.

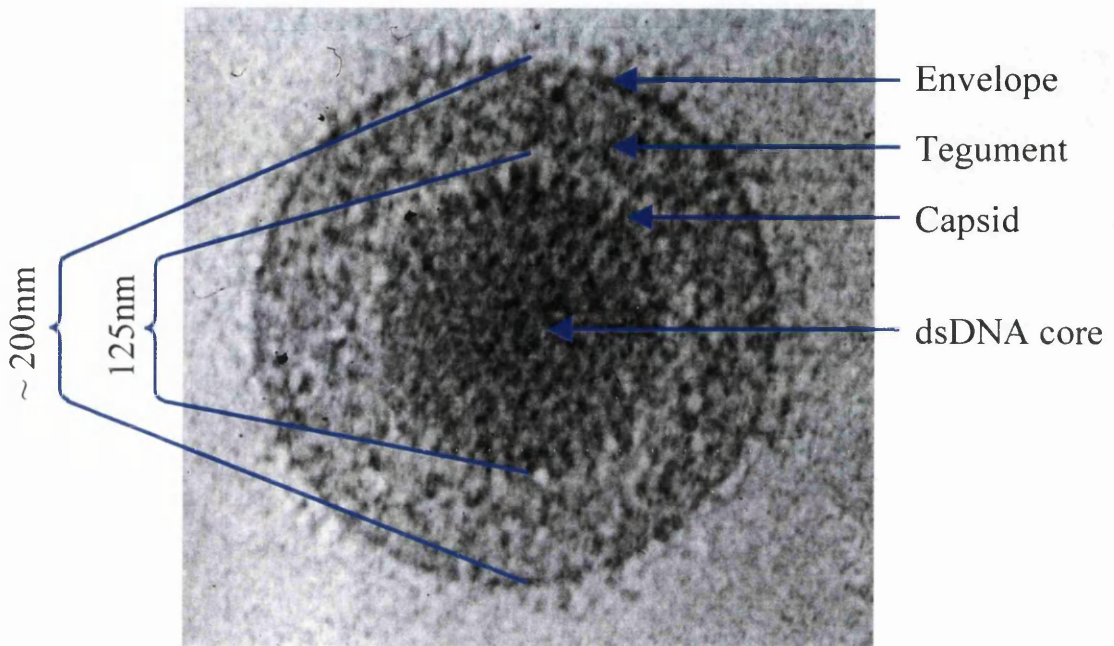


Fig. 1.1: Electron micrograph of a frozen hydrated HSV-1 virion.

The major structural features of the virion, including envelope, tegument, capsid, and DNA core are indicated by the appropriate arrows. The diameter of capsid and the approximate diameter of the virion are also indicated.

This figure was reproduced with permission from W. Chiu, Baylor College of Medicine, USA.

- IV. All herpesviruses examined to date are capable of establishing and maintaining a latent state of infection within their natural hosts where genome expression is restricted to a small subset of viral genes.

#### *1.1.1 Subfamily classification of herpesviruses*

Herpesviruses are widely distributed throughout nature with most vertebrate animals so far examined being a natural reservoir to at least one herpesvirus. Historically herpesviruses have been classified into three subfamilies based upon their biological properties. The three subfamilies are the *Alpha-*, *Beta-*, and *Gamma-herpesvirinae*. The basis for such subfamily classification has historically included such characteristics as host range, duration of reproductive cycle, cytopathology, and characteristics of latent infection. However, more recently genome sequencing has provided a more detailed understanding of the evolutionary relatedness of herpesviruses within the *Herpesviridae* (Roizman, 1992; McGeoch et al., 1995). The three distinct subfamilies of herpesviruses are briefly summarised below:

- *Alphaherpesvirinae*

Herpesviruses within this subfamily demonstrate a variable host range *in vitro*, relative short reproductive cycle (<24 hours), rapid spread within tissue culture that results in the efficient destruction of infected cells, and a capacity to establish a latent state of infection predominantly within the sensory ganglia. The subfamily of *Alphaherpesvirinae* has been further divided into two genera; *Simplexviruses*, which include herpes simplex virus type-1 and type-2 (HSV-1 and HSV-2), and *Varicelloviruses*, which includes varicella-zoster virus (VZV).

- *Betaherpesvirinae*

Herpesviruses within this subfamily demonstrate a restricted host range *in vitro*, a long reproductive cycle, and slow spread in tissue culture. Infected cells commonly demonstrate an enlarged appearance (cytomegalia). Viruses within this family predominantly maintain a latent state of infection within lymphoreticular cells. The

subfamily of *betaherpesvirinae* has been further divided into three genera; *Cytomegalovirus*, which includes the human cytomegalovirus (HCMV-1), *Muromegalovirus*, which includes murine cytomegalovirus, and *Roseolovirus*, which includes the human herpes virus type-6 and type-7 (HHV-6 and HHV-7).

- *Gammaherpesvirinae*

Herpesviruses within this subfamily typically demonstrate an *in vitro* host range restricted to the family or order to which the natural host belongs. *In vitro* all members of this subfamily replicate in lymphoblastoid cells and some also cause lytic infection within epithelial and fibroblastic cells. Within the natural host, viruses tend to be specific for either T or B-lymphocytes. Viruses within this subfamily frequently maintain a latent state of infection within lymphoid tissue. The subfamily of *Gammaherpesvirinae* has been further divided into two genera; *Lymphocryptovirus*, which includes the Epstein-Barr virus (EBV), and *Rhadinovirus*, which includes human herpes virus type-8 (HHV-8).

### 1.1.2 Classification of herpesviruses based upon sequence analysis

Mirroring the remarkable developments in DNA sequencing and sequence analysis over the past two decades the classification of herpesviruses within the three subfamilies has been reanalysed based upon DNA sequence homology and genome organisation. Factors taken into consideration include the arrangement of terminal sequences required for DNA packaging, conservation and positioning of genes and gene clusters, and the presence of nucleotides subject to methylation (reviewed by Roizman, 1992; McGeoch et al, 1995). Fortunately the historical classification based upon the biological properties of the viruses has proved remarkably accurate. However, there are a few notable exceptions. The most prominent is that of gallid herpesvirus type-1 (GHV-1, also known as Marek's disease virus) which was originally classified as a member of the *Gammaherpesvirinae*. The assignment of GHV-1 to the *Gammaherpesvirinae* subfamily was based upon the virus's ability to cause tumour like growths within lymphoid tissue of chickens. However, sequence analysis demonstrated that the GHV-1 genome arrangement resembled that of *Alphaherpesvirinae* rather than *Gammaherpesvirinae* and it was subsequently reassigned (Buckmaster et al., 1988). Similarly, both HHV-6 and HHV-7 were originally classified

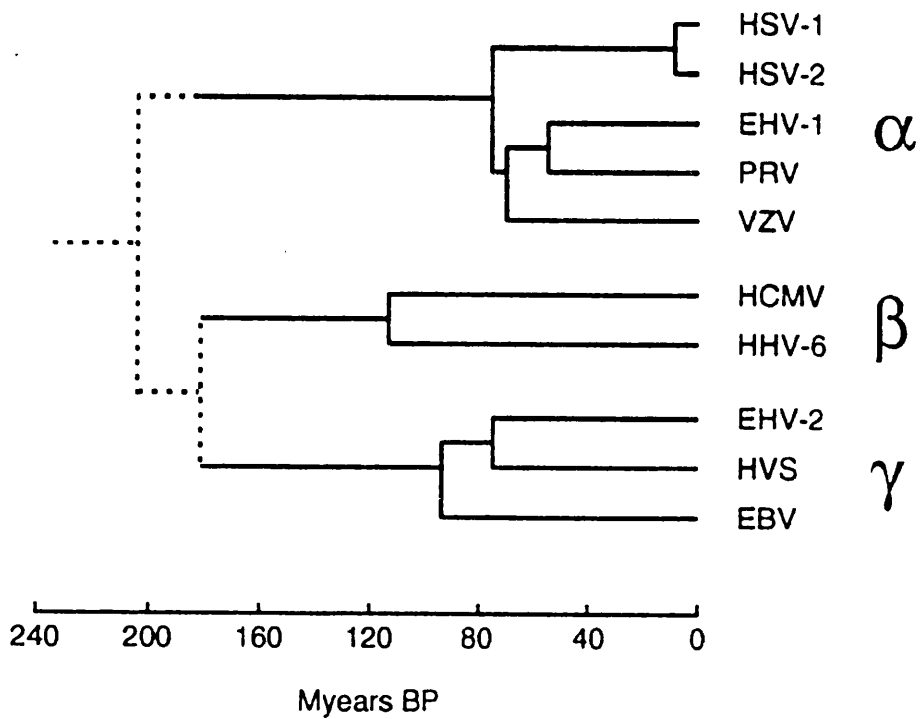


Fig. 1.2: This figure is reproduced from McGeoch et al., (1995) and illustrates the divergence over time for some of the herpesviruses within the herpesviridae family from a common ancestor. Horizontal lines of branches are proportional to their respective time of divergence. Subfamily groups are indicated by the presence of their appropriate Greek letter. The oldest parts of the tree are indicated by broken lines to represent the low confidence in the exact time scale of divergence.

as *Gammaherpesvirinae* as they exhibited lymphotropism, but were subsequently reassigned to the *Betaherpesvirinae* following sequence analysis.

### *1.1.3 Divergence of the Herpesviridae family*

Detailed sequence examination and phylogenetic analysis of those herpesviruses that have been sequenced has clearly demonstrated a common ancestry among the *Alpha-*, *Beta-*, and *Gamma-herpesvirinae* (McGeoch et al, 1995). It has been estimated that the divergence of the three subfamilies arose approximately 180-200 million years ago with divergence within individual subfamilies occurring approximately 80 million years ago. Fig: 1.2 schematically illustrates the sequence relatedness between some of the herpesviruses within the three subfamilies and demonstrates their evolutionary divergence over time.

## **1.2 Herpesviruses which infect humans**

There are currently eight herpesviruses that have been isolated from humans (summarised in table 1.1). Most of these viruses are widespread and are distributed both in the developed and underdeveloped world. As with all herpesviruses, infection can result in the establishment of a latent infection. The viral DNA remains associated with the host for its entire life as a circular episome within the nuclei of cells. Sporadic reactivation from latency into a full lytic infection is poorly understood but usually requires external or internal stimulus. Such stimuli include; mental and physical stress, hormonal changes, immunocompromisation, and exposure to UV radiation (reviewed by Roizman and Sears, 1996). HSV-1 latency is discussed in further detail within section 1.6.

Human herpesvirus	Subfamily (genus) <sup>1</sup>	Site of latency <sup>1</sup>	G + C content <sup>1,2</sup>	Genome size (kb) <sup>2,3</sup>	Primary associate illness <sup>3,4,5,6</sup>	Other associated illnesses <sup>3,4,5,6</sup>
HSV-1	Alpha- ( <i>Simplexvirus</i> )	Sensory nerve ganglia	68.3	152	Cold sores	Genital lesions, conjunctivitis, herpetic whitlow, keratitis, encephalitis
HSV-2	Alpha- ( <i>Simplexvirus</i> )	Sensory nerve ganglia	70.4	152	Genital lesions	Oral lesions, conjunctivitis, herpetic whitlow, keratitis, encephalitis
VZV	Alpha- ( <i>Varicellovirus</i> )	Sensory nerve ganglia	46	125	Chicken pox/fever	Reactivation can lead to shingles
HCMV-1	Beta- ( <i>Cytomegalovirus</i> )	Leukocytes, epithelial cells	57	229	Congenital abnormalities, mononucleosis, hepatitis	Immuno-compromised individuals suffer from gastro-enteritis and retinitis
HHV-6	Beta- ( <i>Roseolovirus</i> )	T-lymphocytes	42	160	Infant rash exanthem subitum	Associated with certain malignancies- lymphoma, leukaemia, co-factor in cervical and oral carcinoma
HHV-7	Beta- ( <i>Roseolovirus</i> )	T-lymphocytes	45	145	Febrile illness	-
HHV-8	Gamma- ( <i>Rhadinovirus</i> )	Lymphocytes	54	170	Associated with Kaposi's sarcoma	-
EBV	Gamma- ( <i>Lymphocryptovirus</i> )	B-lymphocytes	60	172	Glandular fever, mononucleosis	Burkitt lymphoma, nasopharyngeal carcinoma

Table 1.1: Summary of human herpesviruses including primary and associated illnesses

(1) Roizman, (1992); (2) Subak-Sharpe and Dargan, (1998); (3) Levy, (1997); (4) Gold and Nankervis, (1991); (5) Evans and Niederman, (1991); (6) Nahmias et al., (1991).

## 1.3 Virion architecture

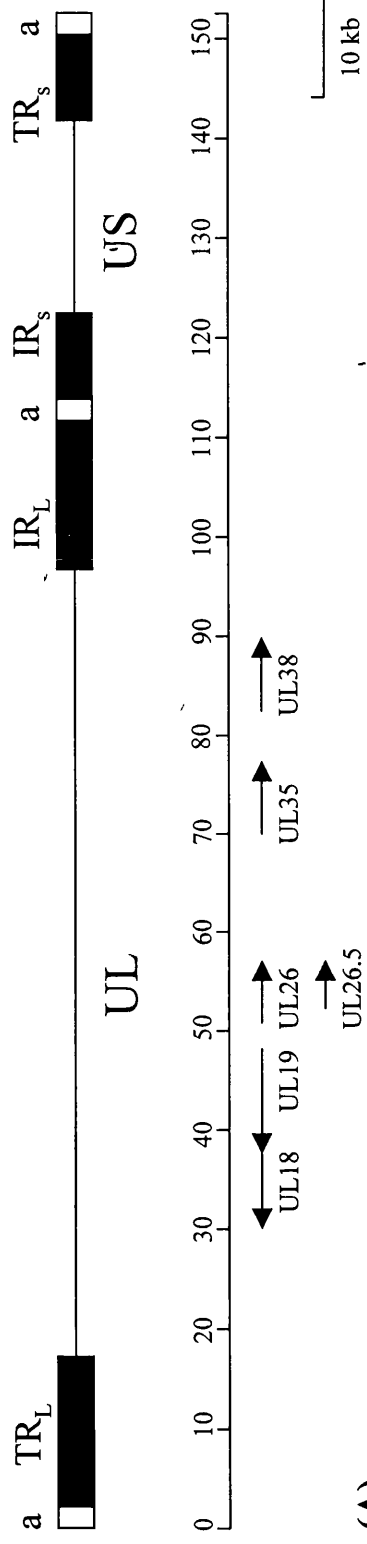
The architecture of the virion is conserved throughout the herpesviridae and comprises four distinct components; DNA core, nucleocapsid, tegument, and envelope (fig. 1.1) (Wildy et al., 1960). Attention will be paid to the architecture of the HSV-1 virion, especially the structure and composition of the capsid, as this forms the basis to the work presented within this thesis.

### 1.3.1 *The HSV-1 genome*

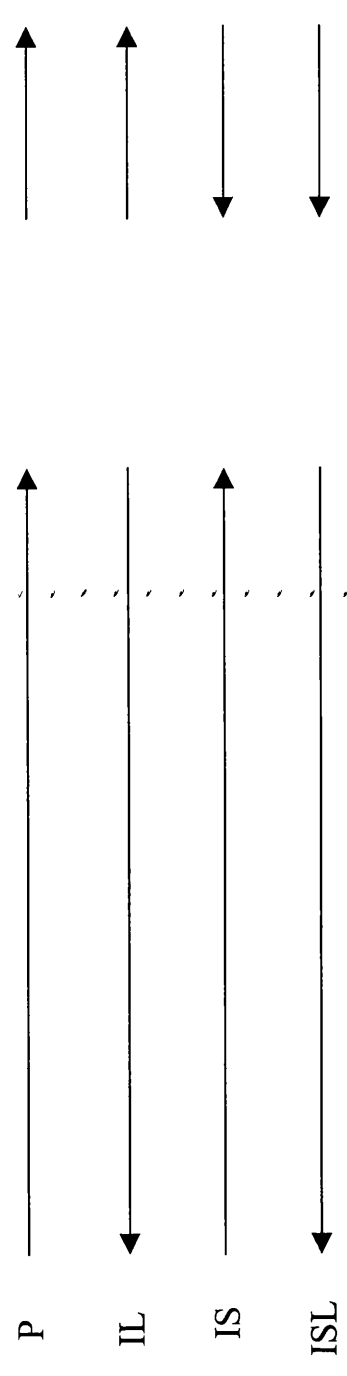
The entire genome of HSV-1 (strain 17) has been sequenced and consists of 152,260bp of dsDNA encoding a minimum of 73 open reading frames (ORFs) with an overall G+C content of 68.3% (McGeoch et al., 1988). The genome of HSV-1 consists of two regions, unique long (UL) and unique short (US). Genes within these unique sequences are prefixed with either UL or US and are numbered according to their relative position within the genome. These sequences are flanked by internal and terminal repeat sequences designated TR<sub>L</sub>/IR<sub>L</sub> and IR<sub>S</sub>/TR<sub>S</sub> (fig. 1.3, panel A). A sequence of variable length, termed the “a” sequence, is present as a direct repeat at each terminus of the DNA molecule and as an inverted repeat at the L-S junction. During infection the UL and US sequences can invert relative to each other with progeny viral DNA typically being present in equimolar amounts of the four isomers. These isomers are termed; P (prototype), IL (inversion of L), IS (inversion of S), and ISL (inversion of both S and L) (summarised in fig. 1.3, panel B).

### 1.3.2 *The “a” sequence.*

The “a” sequence mediates a number of important functions during the life cycle of herpesviruses and is composed of a number of repeat elements (reviewed in Roizman and Sears, 1996). It is directly involved in the inversion of L and S segments, the circularisation of DNA following infection, site specific recombination, and plays an integral role in the cleavage of replicated DNA during packaging. The HSV-1 “a” sequence can be divided into both unique (U) and directly repeated (DR) elements. The structure of the “a” sequence in HSV-1 (strain F) is represented as:



(A)



(B)

Fig. 1.3: (A) Schematic illustration of the structure of the HSV-1 genome containing unique long (UL) and unique short (US) sequences. The positions of the “ $\alpha$ ” sequences, the terminal repeats ( $TR_L$  and  $TR_S$ ) and internal repeats ( $IR_L$  and  $IR_S$ ) are shown. The position of the six capsid protein genes encoded in the UL sequence are shown on the line below (not to scale, diagram modified from Homa and Brown, 1997). (B) Schematic illustration of the four possible isomers of the UL and US sequences: P (prototype), IL (inversion of L), IS (inversion of S), and ISL (inversion of both S and L).

---

DR1-U<sub>b</sub>-DR2<sub>n</sub>-DR4<sub>m</sub>-U<sub>c</sub>-DR1

Where U<sub>b</sub> and U<sub>c</sub> consist of unique sequences of 65 and 68bp in length and DR1, DR2, and DR4 are direct repeats containing 20, 12, and 37bp respectively. DR2 is present in 19 to 23 copies, and DR4 is present in 2 to 3 copies per “a” sequence. The size of the “a” sequence varies depending on the strain and generally reflects the number of repeats of DR2 and DR4. Linear virion DNA contains asymmetric ends with the terminal “a” sequences of the L component ending in 18bp of DR1 and that of the S component ending in 1bp of DR1. A single 3’ residue overhang occurs at both termini and allows the linear DNA molecule to circularise. The number of “a” sequences at the L-S junction and at the L terminus can vary, although only a single “a” sequence is present at the S terminus. The relevance of the “a” sequence is discussed further in section 1.5.5.

### *1.3.3 DNA structure within the nucleocapsid*

The DNA within the nucleocapsid of HSV-1 virions was originally proposed to exist as a toroid by Furlong et al., (1972). Analysis of thin sections of HSV-1 virions and gradient purified capsids by EM showed that the DNA within the nucleocapsids of these samples appeared as an electron-opaque toroid partially surrounding a less dense cylindrical mass. This led the authors to speculate that the DNA was wound around a central protein plug. The plug was proposed to be composed of VP21 by Gibson and Roizman (1972). However, Puvion-Dutilleul et al., (1987) argued that the toroid structure of DNA observed within the core was a direct result of dehydrating agents used in the specimen preparation. Cryo-EM and computer reconstruction analysis of HSV-1 capsids has not provided any supporting evidence for a toroid arrangement of viral DNA coiled around a central protein plug. Booy et al., (1991) proposed that the DNA within the nucleocapsid was packaged in a liquid crystalline state, similar to that observed for bacteriophage  $\lambda$  and T4, where the DNA is packaged in parallel bundles. The packaging of DNA in this manner into the core of icosahedral capsids circumvents the requirement for a central protein plug to wind the DNA around (Lepault et al., 1987). Recent cryo-EM analysis upon purified HSV-1 virions has provided additional support for the packaging of viral DNA into HSV-1 capsids in the absence of a central protein plug. Zhou et al., (1999) showed the DNA within HSV-1

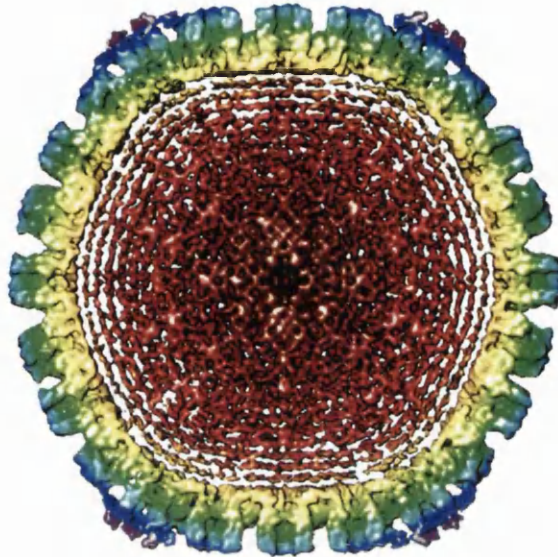


Fig. 1.4: Cross-section through a cryo-EM reconstruction of the HSV-1 virion resolved to 20Å.

The cross-section is viewed along a 2-fold axis and illustrates the concentric layers of DNA packaged within the capsid (coloured in brown). The spacing between the concentric layers of DNA is approximately 26Å. The capsid is radially coloured from light (yellow/interior) to dark (purple/exterior). Inner and outer capsid shells are coloured yellow and green respectively. The icosahedrally ordered tegument is coloured blue and purple.

This figure was reproduced with permission from W. Chiu, Baylor College of Medicine, USA.

virions was packaged as regularly spaced concentric layers approximately 26Å apart. Up to 10 concentric layers of DNA could be successfully resolved at the resolution of analysis with the DNA occupying 90% of the total internal volume of the capsid. The structure of the DNA within the HSV-1 capsid is consistent with a spooling model of DNA packaging, as seen within the T7 bacteriophage (Harrison, 1983; Cerritelli et al., 1997). However, unlike that of T7 bacteriophage, no central protein plug was observed around which the genome could be spooled. Instead, Zhou et al., (1999) speculated that the linear DNA molecule wrapped itself around the inner surface of the capsid shell accumulating one layer at a time with the DNA becoming less densely packaged further away from the inner surface of the capsid (fig. 1.4). Although the DNA is closely associated with the inner surface of the capsid shell no icosahedral symmetry could be detected and therefore it seems unlikely that the viral DNA makes any specific DNA/protein interactions (Zhou et al., 1999).

## **1.4 Virion morphology**

The HSV-1 genome encodes over 73 major ORFs of which approximately 40 are reported to encode proteins that can be found within the mature virion. Therefore, over 50% of the HSV-1 genome encodes proteins that are utilised in the production of infectious progeny virions. However, it should be noted that not all of the proteins found within mature virion are required for infectivity. Indeed, transfection of naked HSV-1 DNA into cells is sufficient for initiating infection. The majority of the virion proteins are responsible for effectively delivering the viral DNA into the cell nucleus and directing the process of infection (Rixon, 1993).

### *1.4.1 The tegument*

The tegument is an amorphous protein layer situated between the capsid and the envelope (see fig. 1.1) (Wildy et al., 1960). In comparison to the rest of the virion, little is known about the structural organisation of the tegument (reviewed by Rixon, 1993). However, the tegument accounts for approximately 50% of the total volume of the virion and consists of at least 18 viral proteins (Haarr and Skulstad, 1994). Although some of these proteins have yet to be assigned functional roles, proteins within the tegument are

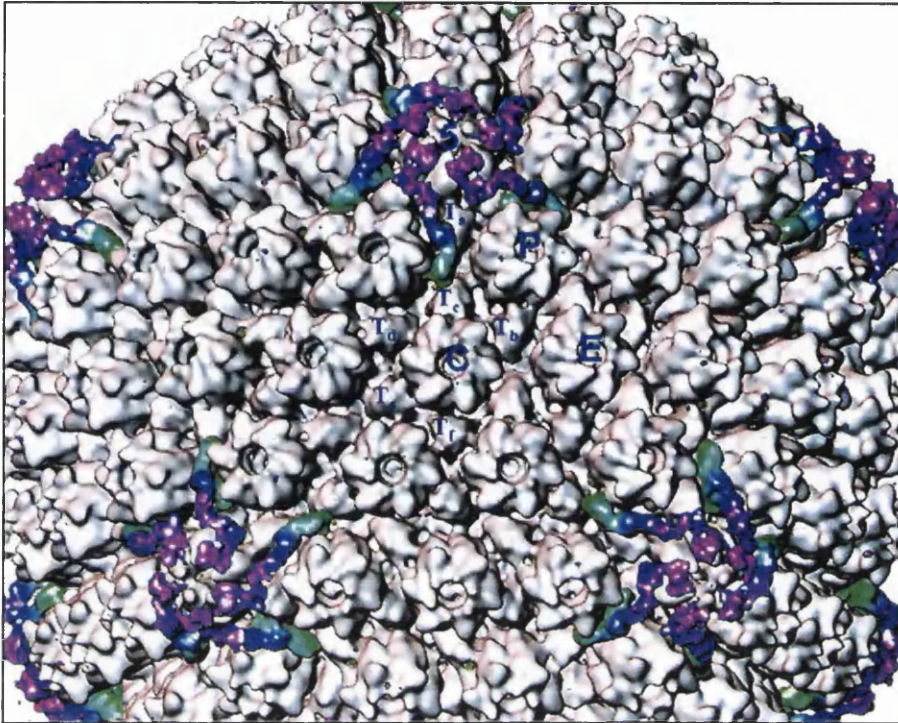


Fig. 1.5: Visualisation of the icosahedrally ordered tegument proteins.

The tegument proteins are coloured from light (green/low) to dark (purple/high) representing their radial distance from the center of the capsid. Protein densities attributed to the B-capsid are coloured in gray. Structural components which make up one asymmetric unit, 1 penton (P), hexons (E, and C), and triplexes ( $T_a$ - $T_p$ ) are labeled in blue.

This figure was reproduced with permission from W. Chiu, Baylor College of Medicine, USA.

generally considered to be involved in virion morphogenesis, uncoating, and regulation of gene expression. The functions of the known tegument proteins are summarised in table 1.2.

#### *1.4.1.1 Tegument assembly*

Although little is known about tegument assembly and virion tegument acquisition it should be noted that the tegument does contain a degree of structural organisation. Szilagi and Cunningham (1991) demonstrated that tegument proteins could assemble into stable particles (L-particles) that sediment more slowly than normal HSV-1 virions during gradient purification. These particles were shown to consist solely of tegument and envelope proteins (Rixon et al., 1992). L-particles are unable to initiate infection, due to the lack of a viral genome, but are capable of penetrating cells and increasing the efficiency of HSV-1 lytic replication (McLauchlan et al., 1992; Dargan and Subak-Sharpe, 1997). The tegument proteins found within L-particles also appeared similar to those proteins found within mature virions indicating that the capsid is not required for tegument formation (McLauchlan and Rixon, 1992).

#### *1.4.1.2 Tegument structure*

Recent cryo-EM analysis performed by Zhou et al., (1999) upon gradient purified virions demonstrated that some of the tegument proteins associated with the capsid are icosahedrally ordered (see fig. 1.5). Although these proteins have yet to be identified their extensive interactions around the penton lead the authors to speculate that they may be involved in the regulation of DNA transport through the penton channel.

It is of interest to note that similar cryo-EM analysis performed upon purified HCMV virions reveals significant differences in the structural organisation of the icosahedrally ordered tegument proteins surrounding the capsid (Chen et al., 1999). The principle difference in HCMV can be seen in the extensive association of tegument protein complexes with both pentons and hexons. The tegument densities surrounding the HCMV capsid also appear conformationally distinct from those surrounding the penton in the HSV-1 virion. As with HSV-1 these icosahedrally ordered tegument proteins have yet to

Gene	Protein	Approx. Mr (kDa)	Properties	Reference(s)
UL11		~ 17-22	Myristylated, role in envelopment and virion transport	MacLean et al., (1989)
UL13	VP18.5	57	Protein kinase, phosphorylates VP22 (UL49)	Baines and Roizman, (1992) Prod'hon et al., (1996)
UL21	-	-	Function unknown, dispensable in tissue culture	Baines et al., (1994)
UL25	-	63	Required for packaging but not cleavage of replicated viral DNA	McNab et al., (1998)
UL36	VP1/2	270	Possible DNA binding protein	McNabb and Courtney, (1992)
UL37	-	121	Phosphoprotein, function unknown	Schmitz et al., (1995)
UL41	vhs	55	Virion host shut (vhs) off protein	Everly and Read, (1999)
UL46	VP11/12	79	Modulates Vmw65 ( $\alpha$ TIF/VP16) and TK transactivation	Zhang et al., (1991) Zhang and McKnight, (1993)
UL47	VP13/14	74	Modulates Vmw65 ( $\alpha$ TIF/VP16) and TK transactivation	Zhang et al., (1991) Zhang and McKnight, (1993)
UL48	Vmw65 (VP16)	55	Transactivates IE genes	Berk et al., (1998)
UL49	VP22	32	Stabilises microtubule assembly	Elliott and O'Hare, (1998)
UL54	Vmw63	55	IE2 transcription/post-transcriptional regulator	Sinclair et al., (1994)
UL56	-	-	Function unknown,	Kehm et al., (1998)
RL2	Vmw110 (ICP0)	110	IE1 transcriptional activator, blocks mitosis, disrupts ND10 domains	Lomonte and Everett, (1999)
RS1	Vmw175 (ICP4)	133	Transcription activator	Muller and Dejean, (1999) Allen and Everett, (1997)
US3	-	53	Protein kinase, partial inhibitor of apoptosis	Jerome et al., (1999)
US9	-	10	Ubiquitinated phosphoprotein, function unknown	Brandimarti and Roizman, (1997)
US10	-	34	Phosphoprotein, function unknown	Yamada et al., (1997)
US11	-	18	RNA binding regulatory protein associated with 60S ribosome	Roller et al., (1996)

Table 1.2: Summary of the HSV-1 tegument proteins and their known properties.

be identified. However, the substantial differences in their structural organisation are probably indicative of their divergent roles during infection.

#### *1.4.2 The envelope*

The outer layer of the HSV-1 virion is composed of a trilaminar envelope that contains a large number of prominent protein spikes protruding from its surface (fig. 1.1) (Wildy et al., 1960). Utilising immuno-gold labelling Stannard et al., (1987) demonstrated that these protruding spikes corresponded to HSV-1 glycoproteins which varied in length (80-240Å) and shape. There are currently 11 glycoproteins which have been identified. Although no glycoprotein has been shown to be essential for virion assembly, four glycoproteins are necessary for infectivity (reviewed by Spears, 1993; Haarr and Skulstad, 1994). The properties of the 11 glycoproteins are summarised in table 1.3. The nomenclature of glycoproteins is alphabetical, with the prefix “g” denoting the protein as being fully processed. Originally the list contained glycoprotein A (gA). However, this glycoprotein was later shown to be indistinguishable from glycoprotein B (gB) (Eberle and Courtney, 1980). Similarly, Glycoprotein F (gF) originally discovered in HSV-2 was subsequently shown to be the homologue of glycoprotein C (gC) in HSV-1 (Zezulak and Spear, 1984). Consequently both gA and gF are absent from the summary table.

#### *1.4.3 The capsid*

The HSV-1 capsid is an icosahedral protein shell (~125nm in diameter, see fig. 1.13) that directly surrounds the viral DNA (Wildy et al., 1960). Gibson and Roizman (1972) originally demonstrated that three distinct types of capsid could be isolated from HSV-1 infected Hep-2 cells. Three types of capsids could be observed by EM within the nuclei of infected cells which appeared uniform in size and conformation. Two types of capsid could be separated based upon differences in their respective mass by gradient sedimentation. The upper band was termed A-capsids and the lower band B-capsids. Characterisation of the proteins found within these capsids lead Gibson and Roizman (1972) to propose that A-capsids, which lacked VP22a and VP21, differed from B-capsids in their internal core protein composition. B-capsids also appeared to contain approximately 10x more DNA than A-capsids. The third type of capsid, termed the C-

Protein	Gene	Approx. Mr (kDa)	Properties
gB	<u>UL27</u>	120	Forms homooligomers, required for viral penetration and cell fusion
gC	UL44	120	Mediates cell attachment, may be required for entry on some polarised cell types
gD	<u>US6</u>	60	Required for viral penetration and cell fusion
gE	US8	80	Forms oligomers with gI, involved in cell-to-cell spread
gG	US4	60	Non-essential for viral replication in cultured cells
gH	<u>UL22</u>	115	Forms heterooligomers with gL, required for viral penetration and cell fusion
gI	US7	70	Forms oligomers with gE, involved in cell-to-cell spread
gJ	US5	10	Non-essential for viral replication in cultured cells
gK	UL53	40	Involved in cell fusion
gL	<u>UL1</u>	40	Forms heterooligomers with gH, required for viral penetration and cell fusion
gM	UL10	60	Phosphorylated by US3 protein kinase, non-essential for viral replication in cultured cells

Table 1.3: Summary of HSV-1 glycoproteins and their known properties.

Those genes underlined are essential for viral infectivity.

(Subak-Sharpe and Dargan, 1998; Steven and Spear, 1997; Haarr and Skulstad, 1994).

capsid, was isolated from infectious virions present within the cytoplasm of infected cells. Treatment of virions with the non-ionic detergent NP-40 and urea removed the surrounding envelope and tegument layers. C-capsids, as with B-capsids, were found to contain DNA and lack the internal protein VP22a. When C-capsids were sedimented on sucrose gradients in conjunction with A and B capsids they appeared as a faint band beneath B-capsids. Subsequent to this work, all three types of capsid have been purified from the nuclei of infected cells (reviewed by Rixon, 1993).

The three types of capsid are now defined as:

- I. A capsids - empty capsids with no internal structure.
- II. B capsids - intermediate capsids that lack viral DNA but contain a core in the form of a proteinaceous layer.
- III. C capsids - capsids that contain the viral DNA and lack the internal proteinaceous core.

A fourth type of capsid, termed the procapsid, has recently been identified from *in vitro* capsid assembly experiments (Newcomb et al., 1996; Trus et al., 1996). This type of capsid was proposed to be a precursor to mature capsids. Procapsids have subsequently been characterised in and isolated from HSV-1 infected cells and therefore represent a true assembly intermediate during virion assembly (Rixon and McNab, 1999; Newcomb et al., 2000). The procapsid is discussed in further detail within section 1.9.

#### *1.4.3.1 Structural composition of the capsid*

Gibson and Roizman (1972 and 1974) originally characterised the protein composition of B capsids and identified six virion proteins (VP); VP5, VP19, VP21, VP22a, VP23, and VP24. Heilman et al., (1979) and Cohen et al., (1980) further identified the presence of a small (12kDa) capsid protein which they termed p12 and NC-7 respectively. Newcomb and Brown (1991) standardised the nomenclature of the capsid proteins and renamed the p12/NC-7 capsid protein as VP26. The virion protein VP19 was also renamed to VP19c in order to differentiate it from a glycosylated virion protein that co-migrated during SDS-

Gene	Protein	Mr (Da)	Location in capsid	No. of copies per capsid	Presence in A-, B-, and C-capsids
UL18	VP23	34,268	Triplexes	640	A, B, C
UL19	VP5	149,075	Hexons & Pentons	960	A, B, C
UL26-N	VP24	26,618	Internal scaffold	~ 147	A, B, C
UL26-C	VP21	39,875	Internal scaffold	~ 87	B
UL26.5	VP22a	33,765	Internal scaffold	~ 1153	B
UL35	VP26	12,095	Tips of Hexons	900	A, B, C
UL38	VP19c	50,260	Triplexes	320	A, B, C

Table 1.4: Summary of the major capsid proteins within HSV-1 A-, B-, and C-capsids (table modified from Homa and Brown, 1997).

PAGE analysis (Heine et al., 1974; Newcomb and Brown, 1991). The individual capsid proteins are discussed in detail below and summarised in table 1.4.

#### 1.4.3.2 Protein composition of the HSV-1 capsid

- VP5 (UL19)

The 155kDa capsid protein VP5 was first shown to be a constituent of the virion by Spear and Roizman (1972) and subsequently identified as a component of the capsid by Gibson and Roizman (1972).

VP5 is encoded by the UL19 ORF, initiating at 40528 and terminating at 36406, see fig. 1.3 (Costa et al., 1984; McGeoch et al., 1988). The UL19 ORF encodes a protein with a predict MW of approximately 150kDa which corresponds well to the observed MWs of 150-155kDa indicating that the protein does not undergo any significant post-translational modification (Gibson and Roizman, 1972; Cohen et al., 1980; Rixon et al., 1990). VP5 has been shown to make up 60-70% of the protein mass of HSV capsids and commonly is referred to as the major capsid protein (MCP). Indeed, VP5 has been shown to make up the entire mass of the pentons and the majority of the mass of hexons (Gibson and Roizman 1972; Newcomb et al., 1993; Zhou et al., 1994).

As VP5 is the MCP it is not surprising therefore that it is essential for capsid formation. Weller et al., (1987) demonstrated that *ts* mutations within the UL19 ORF were sufficient to prevent the formation of capsids at non-permissive temperatures. Similarly, experiments performed by Desai et al., (1993) demonstrated that insertion of the *lacZ* gene into the beginning of the UL19 ORF to generate a VP5 null mutant virus (K5ΔZ) abolished the formation of capsid particles in non-permissive Vero cells. Furthermore, infection of non-permissive cells with the K5ΔZ mutant produced similar levels of concatameric viral DNA as was seen within permissive cells. However, mutant viruses were defective in the processing of concatameric DNA into genome length molecules suggesting that capsid formation is a prerequisite for DNA cleavage to occur. HSV-1 capsid assembly analysis utilising the baculovirus expression system has also demonstrated that VP5 is essential for the formation of capsids both *in vivo* and *in vitro* (Newcomb et al., 1994; Tatman et al.,

1994; Thomsen et al., 1994; Newcomb et al., 1999). The fact the VP5 is essential for capsid formation is consistent with the observation that VP5 is the MCP and present within all capsid types. The structural organisation of VP5 within the capsid is discussed in further detail within section 1.8. It is interesting to note that VP5 has been shown by non-reducing SDS-PAGE to be covalently linked to VP19c within purified HSV-2 capsids (Zweig et al., 1979). The high degree of conservation between HSV-1 and HSV-2 would suggest that such an interaction should also exist in HSV-1 although attempts to identify it within HSV-1 capsids have failed so far (personal communication; Rixon, 1996).

VP5 has been directly implicated in binding to the C-terminal 25 amino acid of the internal scaffold proteins encoded by UL26 and UL26.5 (Thomsen et al., 1994; Kennard et al., 1995; Desai and Person, 1996; Hong et al., 1996). The residues within VP5 that participate in this interaction have yet to be identified, although recent experiments utilising second site mutations within VP5 to rescue scaffold protein mutants that are unable to undergo maturational cleavage, have indicated that residues within the N-terminus of VP5 may be involved (Desai and Person, 1999).

- VP19c (UL38)

The 53kDa capsid protein VP19c was first shown to be a constituent of the virion by Spear and Roizman (1972) and subsequently identified as a component of the capsid by Gibson and Roizman (1972).

VP19c is encoded by the UL38 ORF, initiating at 84531 and terminating at 85926, see fig. 1.3 (McGeoch et al., 1988; Rixon et al., 1990). The UL38 ORF encodes a protein with a predicted MW of approximately 50kDa which corresponds well to the observed MWs of 50-54kDa indicating that the protein does not undergo any significant post-translational modifications (Gibson and Roizman, 1972; Cohen et al., 1980; McGeoch et al., 1988; Rixon et al., 1990).

VP19c forms part of the heterotrimeric complex termed the triplex, discussed in further detail within section 1.8.2 (Newcomb et al., 1993). The VP19c homologue within HSV-2

capsids has been reported to be covalently linked to VP5, although this has yet to be identified with HSV-1 capsids (Zweig et al., 1979).

VP19c has been shown to be essential for capsid formation and is present within A, B, and C-capsids. Pertuiset et al., (1989) demonstrated that a *ts* mutant (A44*ts*2) that located to the UL38 ORF could not form capsids at the non-permissive temperature. Like the VP5 mutants described above, A44*ts*2 mutant virus, although not defective in DNA replication, was defective in the processing of concatameric DNA into genome length molecules. Similarly, a VP19c null mutant virus was shown to be inhibited in the formation of virions on non-permissive cells (Person and Desai, 1998). Furthermore, capsid assembly analysis utilising the baculovirus expression system has also demonstrated that VP19c is essential for the formation of capsids both *in vivo* and *in vitro* (Newcomb et al., 1994; Tatman et al., 1994; Thomsen et al., 1994; Newcomb et al., 1999).

- VP23 (UL18)

The 33kDa capsid protein VP23 was first shown to be a constituent of the virion by Spear and Roizman (1972) and subsequently identified as a component of the capsid by Gibson and Roizman (1972).

VP23 is encoded by the UL18 ORF (Rixon et al., 1990), initiating at 36051 and terminating at 35097, see fig. 1.3 (McGeoch et al., 1988). The UL18 ORF encodes a protein with a predicted MW of approximately 34kDa which corresponds well to the observed MWs of 30-34kDa indicating that the protein does not undergo any significant post-translational modifications (Gibson and Roizman, 1972; Cohen et al., 1980; McGeoch et al., 1988; Rixon et al., 1990).

Two copies of VP23 interact with a single copy of VP19c to form a heterotrimeric complex termed the triplex, discussed in further detail within section 1.8.2 (Newcomb et al., 1993).

VP23 has also been shown to be essential for the formation of WT polyhedral capsids in the baculovirus expression system (Newcomb et al., 1994; Tatman et al., 1994; Thomsen et

al., 1994; Newcomb et al., 1999). A null mutant virus (K23Z) generated by the insertion of the *lacZ* gene into coding region of VP23 failed to produce capsids on non-permissive cells (Desai et al., 1993). K23Z mutant virus synthesised WT levels of DNA but was defective in the processing of concatameric DNA into genome length molecules. Furthermore, baculovirus analysis has shown that in the absence of VP23 VP5/VP19c particles form that are smaller and more densely stained than WT capsids (Tatman et al., 1994; Thomsen et al., 1994; Rixon et al., 1996; Saad et al., 1999).

- VP26 (UL35)

VP26 is the smallest structural protein associated with the capsid and was originally identified by Heilman et al., (1979).

VP26 is encoded by the UL35 ORF, initiating at 70566 and terminating at 70902, see fig. 1.3 (McGeoch et al., 1988; Davison et al., 1992). The UL35 ORF encodes a protein of a predicted MW of approximately 12kDa which corresponds exactly to the observed MW of 12kDa indicating that the protein does not undergo any post-translational modifications (Heilman et al., 1979; Cohen et al., 1980; McGeoch et al., 1988; Rixon et al., 1990).

VP26 is located on the tips of the hexons and is present within A, B, and C-capsids, discussed in further detail within section 1.8.2 (Trus et al., 1992; Booy et al., 1994; Zhou et al., 1994; Zhou et al., 1995; Wingfield et al., 1997; Desai and Person, 1998).

Capsid assembly analysis utilising the baculovirus expression system has shown VP26 to be non-essential for the formation of capsids both *in vivo* and *in vitro* (Tatman et al., 1994; Thomsen et al., 1994). VP26 has also been shown to be absent from purified HSV-1 procapsids (Newcomb et al., 2000). The function of VP26 therefore remains ambiguous. However, Desai et al., (1998) demonstrated that a VP26 null mutant virus (K $\Delta$ 26Z), which replicated at WT levels in tissue culture, had a 30- to 100-fold decrease in virus yield from the trigeminal ganglia compared to that of WT virus. Furthermore, latent K $\Delta$ 26Z genomes also had a reduced ability in reactivate from latency compared to latent WT virus. VP26 therefore appears to be important for infectious virus production within neuronal cells.

- VP21, VP24, and VP22a (UL26/UL26.5)

VP21, VP24, and VP22a are the three major capsid scaffold proteins and are encoded by overlapping in-frame genes UL26 (VP21 and VP24) and UL26.5 (VP22a) (illustrated schematically in fig. 1.6; Liu and Roizman, 1991a and 1991b; reviewed by Rixon, 1993 and Steven and Spear, 1997). Both genes are essential for the efficient maturation of capsids that are capable of packaging viral DNA (Gao et al., 1994; Sheaffer et al., 2000).

UL26 encodes an N-terminal protease (VP24) and a C-terminal oligomerisation and VP5 binding protein domain (VP21) (Preston et al., 1992; Pelletier et al., 1997). The UL26 ORF initiates at 50809 and terminates at 52714, see fig. 1.3 (Davison et al., 1992; McGeoch et al., 1988). Following translation the proteolytic activity of the N-terminal VP24 domain results in self-cleavage between alanine 247 and serine 248 to generate two cleavage products, namely VP24 and preVP21 (DiIanni et al., 1993; Weinheimer et al., 1993). Further proteolytic cleavage of preVP21 by VP24 between alanine 610 and serine 611 results in the removal of the C-terminal 25 amino acids and the production of mature VP21. VP24 and VP21 have observed MWs of 24-26kDa and 40-44kDa respectively (Gibson and Roizman, 1972, Cohen et al., 1980, and Rixon et al., 1990).

VP22a is encoded by the UL26.5 gene (Liu and Roizman (1991b); Davison et al., 1992). The UL26.5 ORF initiates at 51727 (within the UL26 ORF) and terminates at 52714 (McGeoch et al., 1988). The full-length UL26.5 gene product is termed preVP22a and can be proteolytically processed by VP24 between alanine 610 and serine 611 resulting in the cleavage of the C-terminal 25 amino acids to produce mature VP22a, see fig.1.6.

Differential regulation of the UL26 and UL26.5 promoters results in the increased expression of VP22a over that of VP21 and VP24. As a consequence VP22a is present in much higher quantities within B-capsids, approximately 1000-1500 copies per capsid, than either VP24 or VP21, approximately 100 copies per capsid (Liu and Roizman, 1991a, and 1991b; Newcomb et al., 1993).

Mature forms of VP22a and VP21 are expelled from the capsid upon packaging of viral DNA (Gibson and Roizman, 1974; Addison et al., 1990). Consequently, VP21 and VP22a

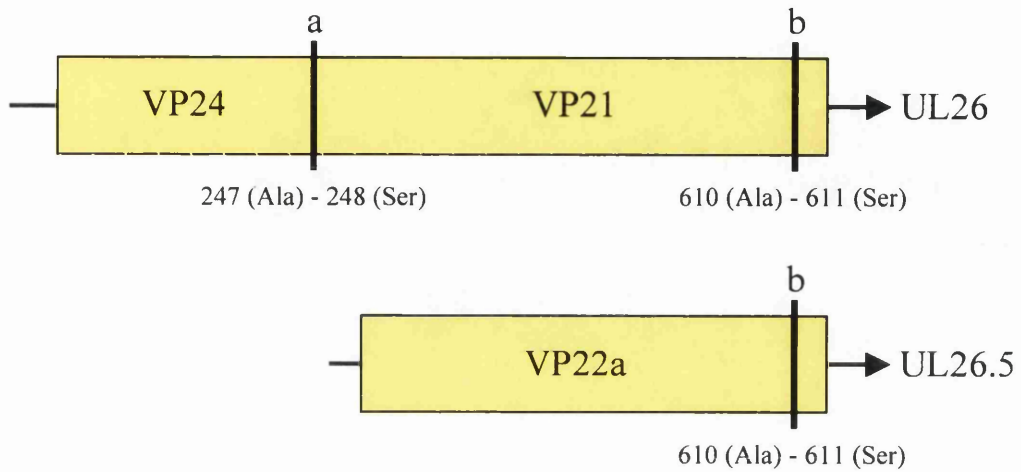


Fig. 1.6: Schematic illustration of the structural organisation of the HSV-1 genes UL26 and UL26.5. The two 3' co-terminal mRNAs are represented by the arrows and their respective ORFs by the yellow boxes. The vertical lines indicate sites of proteolytic cleavage between Alanine (Ala) and Serine (Ser) residues. Cleavage at site (a) results in the release of capsid proteins VP21 and VP24. Cleavage at site (b) results in the removal of the C-terminal 25 amino acids from either preVP21 or preVP22a.

can only be detected within B-capsids. The relevance of the C-terminal 25 amino acids of preVP21 and preVP22a for HSV-1 capsid assembly is discussed in further detail within section 1.8.3. VP24 can be detected within all three types of capsids as well as within mature HSV-1 virions (Gibson and Roizman 1974, Sheaffer et al., 2000).

#### *1.4.3.3 Minor capsid proteins*

Six proteins encoded by UL6, UL12.5, UL15, UL17, UL25, and UL28 have recently been identified as minor constituent proteins of the capsid. However, both *in vivo* and *in vitro* capsid assembly analysis has shown that these proteins are not required for efficient capsid assembly to occur (Tatman et al., 1994; Thomsen et al., 1994; Newcomb et al., 1996; Newcomb et al., 1999). Although these proteins may not be required for the assembly of capsids they have a strong association with the capsid. For example, gene products of the UL6, UL12.5, and UL15 have been shown to be resistant to extraction from capsids treated with 2M GdnHCl (Patel and MacLean, 1995; Bronstein et al., 1997; Salmon and Baines, 1998). Similar treatment of purified B-capsids by Newcomb et al., (1993) demonstrated that 2M GdnHCl could induce the disassociation of VP26 from the tips of the hexons, pentons from the 5-fold vertices and strip triplexes T<sub>a</sub> and T<sub>c</sub>. These minor capsid proteins are associated with the cleavage and packaging of viral DNA into the capsid (discussed in further detail in section 1.5.5 and summarised in table 1.5). Therefore, although these proteins are not required for the assembly of viral capsids their strong association to the capsid highlights the direct correlation between capsid assembly and the efficient cleavage and packaging of viral DNA.

## 1.5 The HSV-1 lytic life cycle

The processes involved in the lytic reproduction of HSV-1, from initial infection through to the release of progeny virions resulting in cell death, are briefly discussed below and summarised schematically in fig. 1.7.

### *1.5.1 Attachment and entry of HSV-1 into the cell*

Attachment of HSV-1 virions to the cell surface and subsequent fusion requires a chain of events involving several of the 11 glycoproteins within the envelope of the HSV-1 virion (reviewed by Spear, 1993; Steven and Spear, 1997). Initial attachment of the virion to the cell is thought to involve the glycoproteins gC and/or gB binding to cell surface glycosaminoglycans (GAGS), preferentially heparan sulfate (Shieh and Spear, 1994). However, the initial attachment to GAGS is not sufficient for virus penetration (Lee and Fuller, 1993). Recently a group of receptors termed the herpesvirus entry mediators (HveA-D) have been implicated in the entry of herpesviruses into a number of cell types. However, the specificity of these receptors varies and they can be cell specific. For example, HveA is a member of the tumour necrosis factor receptor family and has been shown to be the principle receptor for HSV-1 within human lymphoid cells but will not support the entry of other  $\alpha$ -herpesviruses such as PRV (Montgomery et al., 1996). HveB-D are related to the poliovirus receptor proteins which belong to the immunoglobulin superfamily. Both HveB and HveD have been shown to be specific entry mediators for a number of  $\alpha$ -herpesvirus but do not support the entry of various strains of WT HSV-1. Conversely, HveC has been shown to be an entry mediator of HSV-1 and binds strongly to gD. It has also been shown to be an active entry mediator for a number of other  $\alpha$ -herpesviruses, including HSV-2, PRV and BHV-1 (Geraghty et al., 1998; Krummenacher et al., 1998).

Following attachment fusion of the viral envelope with the host cell membrane occurs in a pH-independent manner and requires the presence of number of glycoproteins including gD, gB, and the gH-gL complex (Wittels and Spear, 1991; Spear, 1993).



Fig. 1.7: Schematic overview of the lytic reproductive cycle of HSV-1

(1-3) Virions bind to the cell surface, initially through cell surface glycosaminoglycans, and Hve receptor-mediated fusion occurs (discussed in section 1.5.1). (4) Following internalisation, tegument proteins are released into the cytoplasm (discussed in section 1.5.3) and the capsid is transported along microtubules to the nucleus (discussed in section 1.5.2). (5a-5c) Tegument proteins become localised, either to the nucleus where they stimulate viral transcription or remain within the cytoplasm where they restrict host protein synthesis (discussed in section 1.5.3 and 1.5.4). (6+7) Transported capsids dock at the nuclear pore where the viral DNA is released into the nucleus and circularises to form an episome. (8+9) The gene cascade begins with immediate early (IE) transcription. Transcripts move into the cytoplasm and become translated. IE gene products are transported into the nucleus where they activate early gene transcription and regulate IE gene transcription. (10-12b) Early gene transcription results in the production of proteins primarily involved in viral DNA replication (gene expression cascade is discussed in section 1.5.4). (13) DNA replication results in the production of long concatamers (discussed in section 1.5.5). (14+15) Late gene expression predominantly results in the production of structural proteins (late gene expression discussed in section 1.5.4). (16a-16d) Membrane associated structural proteins, predominantly glycoproteins, become incorporated into the rough endoplasmic reticulum. Membrane proteins may then become modified by glycosylation and localise to both inner and outer nuclear membranes and the endoplasmic reticulum. Further modification occurs within the Golgi apparatus. Mature glycoproteins become transported to the plasma membrane. (17) Some late proteins, including capsid proteins, are transported to the nucleus. (18) Capsid assembly initiates (discussed in section 1.9 and 4.0) and DNA packaging occurs (discussed in section 1.4.3.3 and 1.5.6). (19) DNA containing capsids, in association with tegument proteins, acquire an envelope by budding through the inner nuclear membrane and pass into the lumen of the endoplasmic reticulum. The exact processes concerning virion egress remain unresolved and much debated. However, two popular theories exist regarding virion transport to the cell surface. Both the de-envelopment and luminal pathways are discussed in further detail in section 1.5.7. (19a-19c) Depicts the de-envelopment pathway. The enveloped virus fuses to the endoplasmic reticulum membrane and naked capsids and associated tegument proteins become released into the cytoplasm. Further accumulation of tegument proteins occurs within the cytoplasm before fusing with late Golgi compartments containing mature viral membrane associated proteins. (20a-20e) Depicts the luminal pathway. Enveloped virus is engulfed by a transport vesicle and delivered to the Golgi compartments. The precursor viral envelope proteins are processed *in situ* as part of the virion. In both cases the mature virion is then transported to the plasma membrane and released via exocytosis. (23) Progeny virions in the extracellular space can infect surrounding epithelial cells or neuronal cells where they may become transported to the sensory ganglia and establish a latent state of infection (discussed in section 1.6). Diagram reproduced from Flint et al., (2000).

### *1.5.2 Nucleocapsid transport.*

The events following fusion of the viral envelope with the cell membrane are not particularly well defined but must involve the release of the nucleocapsid from the envelope and subsequent release of tegument proteins into the cytoplasm of the host cell. Once inside the cell the capsid is rapidly transported to the vicinity of the nucleus. Due to the high viscosity and the presence of steric obstacles within the cytoplasm, capsids cannot diffuse efficiently to the nucleus from the cell membrane. Within neurones transport occurs by retrograde transport along the axon from the presynaptic membrane to the nucleus (Lycke et al., 1988; Penfold et al., 1994). However, the transport mechanism within other cell types, particularly epithelial cells, is less well understood. Cytoskeletal assisted transport has recently been implicated in the transport of capsids from the periphery of cells to the nucleus (Sodeik et al., 1997). Capsids are thought to bind to cytoplasmic dynein, a microtubule-dependent motor protein. This binding is thought in part to be mediated by a virion protein encoded by UL34 (Ye et al., 2000). Capsids are then propelled along microtubules towards the nucleus by an unknown mechanism and in an ATP dependent manner. Once at the nucleus the capsid attaches to the nuclear pore and the DNA is released into the nucleus where it circularises into an episome (Tognon et al., 1981; Batterson et al., 1983; Ojala et al., 2000).

### *1.5.3 Disruption of host cell protein synthesis*

Uncoating of the virion following fusion of the viral envelope with the cell membrane results in the release of the tegument proteins into the cytoplasm of the host cell. Some of these proteins serve to stall host protein synthesis and accelerate the activation of viral gene transcription (reviewed by Roizman and Sears, 1996). The primary mechanism that initiates the shut-off of host protein synthesis during the initial stages of infection is regulated by the virion associated host shut-off (VHS) protein. The 53kDa VHS protein, encoded by the UL41 ORF, has been shown to degrade both cellular and viral mRNAs in a non-specific manner. Although viral mRNA is also degraded, its rate of synthesis is greater than that of VHS-induced degradation (Schek and Bachenheimer, 1985; Kwong and Frenkel, 1987; Kwong et al., 1988; Elgadi et al., 1999). However, it should be noted that VHS is not solely responsible for regulating host protein synthesis. The IE protein

ICP27 and the UL13 protein kinase have also been shown to play roles in the regulation of host cell protein synthesis (Overton et al., 1994; Sandri-Goldin, 1998; Laurent et al., 1998).

#### *1.5.4 HSV-1 gene expression*

Transcription of the viral DNA within the nucleus of host cells is carried out by DNA dependent RNA polymerase II and occurs in a regulated cascade (reviewed by Roizman and Sears, 1996). There are three main groups of genes that have been classified according to their time of expression during the viral replication cycle. These are: immediate early (IE or  $\alpha$ ), early (E or  $\beta$ ), and late (L or  $\gamma$ ) genes (Hones and Roizman, 1974).

Following initial infection, the tegument protein VP16 ( $\alpha$ TIF) together with the cellular transcription factor oct-1 (octamer DNA-binding protein) induce the expression of IE ( $\alpha$ ) proteins by binding to the upstream consensus  $\alpha$ -promoter element 'TATGARAT'. There are five gene products that are expressed within the IE cascade: ICP0 (Vmw110), ICP4 (Vmw175), ICP22 (Vmw68), ICP27 (Vmw63), and ICP47 (Vmw12). IE protein expression serves to transactivate early ( $\beta$ ) gene expression, with IE protein synthesis peaking at 2-4 hours post-infection. The early genes primarily encode proteins that are generally required for DNA replication such as: DNA polymerase, single stranded DNA-binding protein (SSB or ICP8), DNA helicase-primase, and the origin binding protein. Early genes also include enzymes that are required for nucleotide metabolism and DNA repair. The synthesis of early genes can be detected as early as 3 hours post-infection and reaches a peak at 5-7 hours post-infection. Viral DNA synthesis commences shortly after the onset of early gene expression and continues up to 15 hours post-infection, with a peak between 7-10 hours post-infection. The regulated cascade of gene expression ends with the expression of late genes that generally encode structural proteins of the virion, such as the capsid proteins. Late genes can be subdivided into leaky late, such as VP5 encoded by UL19, and true late, such as VP19c encoded by UL38. Leaky late genes are expressed in the absence of DNA although their expression is enhanced during DNA replication whereas true late genes are only expressed after the onset of DNA replication. Late gene expression peaks at 8-10 hours post-infection and persists for the remainder of the lytic cycle (Harris-Hamilton and Bachenheimer, 1985).

### 1.5.5 DNA replication

As early as 30 minutes post-infection the input viral DNA reaches the nucleus where it forms a circular episome. Following early gene expression the replication of the viral DNA occurs at specific sites within the nucleus (Quinlan et al., 1984; de Bruyn Kops and Knipe, 1994; de Bruyn Kops et al., 1998). DNA replication is thought to be initiated by a *theta* mode of replication. However, at some point, by an unknown mechanism, *theta* replication switches to the rolling circle mode of DNA replication (reviewed by Lehman and Boehmer, 1999; Boehmer and Lehman, 1997). Seven HSV-1 genes are required for ori (origin of replication) dependent DNA replication. These genes are UL5, UL8, UL9, UL29, UL30, UL42, and UL52. Their properties are summarised in table 1.5.

Initiation of replication occurs at one of the three *cis*-acting elements within the HSV-1 genome that function as origins of replication (ori). The origin binding protein (UL9) forms a homodimer and binds to specific sequences within the ori in association with the single stranded DNA binding protein ICP8 (UL29). Helicase activity associated with UL9, stimulated by the presence of ICP8, separates the two DNA strands permitting entry of the DNA polymerase complex (a heterodimer of UL30/UL40). DNA replication commences by a *Theta* mode of replication before switching to a rolling circle mode of replication and the addition of the DNA helicase-primase (primosome) complex comprising of a 1:1:1 ratio of UL5/UL8/UL52 gene products respectively. DNA synthesis is continuous along one strand and discontinuous along the other strand. The progeny viral DNA accumulates as large concatemeric molecules at specific sites within the nucleus (de Bruyn Kops et al., 1998). Other HSV-1 viral proteins important in DNA replication include those involved in nucleic acid metabolism, such as thymidine kinase (UL23), ribonucleotide reductase (UL39 and UL40) and dUTPase (UL50), and proteins which have been implicated in DNA repair, such as uracil DNA glycosylase (UL2) and alkaline exonuclease (UL12).

### 1.5.6 Packaging of progeny DNA

Cleavage and packaging of DNA into capsids are tightly linked processes and require 6 essential gene products (UL6, UL15, UL25, UL28, UL32, and UL33). Although the exact role of these individual gene products has yet to be identified, their correlation to DNA

Gene	Approx. Mr (kDa)	Properties
UL5	98	Subunit of the primosome holoenzyme required for DNA helicase-primase activity
UL8	79	Stimulates primer synthesis. Subunit of the primosome holoenzyme required for DNA helicase-primase activity. Required for optimal DNA-helicase and DNA-dependent ATPase activity
UL9	94	Homodimeric origin binding protein, complexes with UL29
UL29	128	Commonly referred to as ICP8. Binds single stranded DNA, increases helicase and DNA-dependent ATPase activity of UL9
UL30	136	DNA polymerase with exonuclease (3'→5') and RNaseH activity, forms a heterodimer with UL42
UL42	51	phosphoprotein with dsDNA binding activity, forms a heterodimer with UL30; increases processivity of UL30
UL52	114	Subunit of the primosome holoenzyme required for DNA helicase-primase activity, proposed divalent metal binding motif

Table 1.5: Summary of the essential HSV-1 DNA replication proteins. (Boehmer and Lehman, 1997; Lehman and Boehmer, 1999).

cleavage and/or packaging has typically been characterised through the use of *ts* mutants (the properties of these gene products are summarised in table 1.6 and reviewed by Homa and Brown, 1997).

DNA replication results in the production of large, branched, head-to-tail concatamers of viral DNA (Zhang et al., 1994). The UL12 and UL12.5 genes encode alkaline nucleases, which although not essential for cleavage or packaging of viral DNA, aid the processing of branched DNA molecules prior to cleavage. Mutants that fail to produce an alkaline nuclease have been shown to reduce viral yield by 100- to 1000-fold (Martinez et al., 1996; Bronstein et al., 1997).

Replicated DNA is packaged into the capsid and cleaved into unit length monomers at the novel a-a junction. This results in a single copy of the genome being packaged per capsids, with an “a” sequence being present at each terminus of the DNA molecule (Mocarski and Roizman, 1982). The “a” sequence therefore appears to act as a marker in order to determine when a full genome length has been package and should be cleaved. The cleavage of DNA is also dependent upon capsid formation as mutants that fail to express either the UL19 (VP5) or UL18 (VP23) capsid proteins appear to be unable to cleave concatemeric DNA (Desai et al., 1993). Indeed, several of the DNA packaging proteins have been shown to be strongly associated to capsids (summarised in table 1.6). The exact mechanism by which DNA enters the capsid has yet to be identified. However, the structure of the DNA within virions (discussed in section 1.3.3) would suggest that the DNA is packaged by a spooling mechanism forming coiled layers (Zhou et al., 1999). During infection the DNA is thought to be released from the capsid in a reverse process, whereby the DNA uncoils from the centre outwards (Zhou et al., 1999).

#### *1.5.7 Tegument acquisition and virion egress*

Following DNA packaging the capsid leaves the nucleus and acquires tegument and envelope layers before mature virions leave the cell via the exocytic pathway (reviewed by Rixon, 1993 and Steven and Spear, 1996). Although the exact mode of tegument and envelope acquisition is not known there are currently two popular models to describe this stage in the HSV-1 lytic reproductive cycle (schematically illustrated in fig. 1.6). One

Gene	Approx Mr (kDa)	Capsid association	Function	Reference(s)
<u>UL6</u>	74	YES	Associated with DNA cleavage and packaging	Patel et al., (1996)
UL12	67.5	NO	Alkaline nuclease thought to be involved in DNA processing prior to encapsidation	Shao et al., (1993); Goldstein and Weller (1998)
UL12.5	67.5	YES	Capsid associated alkaline nuclease thought to be involved in DNA processing during packaging	Bronstein et al., (1997)
<u>UL15</u>	81	YES	Associated with DNA cleavage and packaging. Homologous to bacteriophage T4 terminase. Transports UL28 to the nucleus	Yu and Weller (1998); Koslowski et al., (1999)
UL17	77	YES	Associated with DNA cleavage and packaging	Goshima et al., (2000); Salmon et al., (1998)
<u>UL25</u>	62.5	YES	Associated with DNA packaging	McNab et al., (1998)
<u>UL28</u>	85.5	YES	Associated with DNA cleavage and packaging	Cavalcoli et al., (1993)
<u>UL32</u>	64	Unknown	Associated with DNA cleavage and packaging	Lamberti and Weller (1998)
<u>UL33</u>	19	NO	Associated with DNA cleavage and packaging	Reynolds et al., (2000); Patel et al., (1996)

Table 1.6: Summary of the HSV-1 DNA packaging proteins. Genes that are underlined are essential for DNA cleavage and/or DNA packaging

model, the luminal pathway, proposes that the capsids acquire an envelope at the inner nuclear membrane, with subsequent modifications to the tegument and envelope glycoproteins occurring as the virion exits the cell through the Golgi apparatus by the exocytic pathway (schematically illustrated in fig.1.6, 20a-20e). The second model, the envelopment, deenvelopment, and reenvelopment (EDR) pathway, proposes that capsids exiting the nucleus acquire an envelope by budding through the inner nuclear membrane into the perinuclear space. These membrane bound capsids are then deenveloped at the outer nuclear membrane and naked capsids are released into the cytoplasm. Capsids acquire a tegument on route to the Golgi apparatus where they are reenveloped and acquire membrane-associated proteins before exiting the cell via an exocytic pathway (schematically illustrated in fig.1.6, 19a-19c). EM analysis of infected cells supports both models with enveloped capsids within cytoplasmic vesicles and naked capsids having been observed (Campadelli-Fiume et al., 1991; Steven and Spear, 1997).

However, recently there is a growing body of data to support the EDR pathway of virion egress. Van Genderen et al., (1994) demonstrated that the phospholipid composition of extracellular virions resembles that of membranes derived from the Golgi apparatus and plasma membranes as opposed to that of membranes derived from the nuclei of infected cells. However, the authors could not rule out that the lipids present within extracellular virions were not typical of those associated with the inner nuclear membrane, nor could they rule out that the phospholipid composition was modified during virion egress.

The most conclusive evidence for the EDR pathway comes from the use of recombinant HSV-1 viruses. HSV-1 mutants expressing modified forms of the glycoproteins gD and gH that carry an ER retention signal to localise these proteins to the inner nuclear membrane have been shown to produce non-infectious progeny virions. This therefore supports the theory of deenvelopment at the outer nuclear membrane, with the loss of glycoproteins gD and gH, and the reenvelopment at the Golgi apparatus. The envelopment of virus particles in the absence of gD and gH therefore results in the production of non-infectious progeny virions (Browne et al., 1996; Whiteley et al., 1999). Furthermore, it has been recently shown through time lapse confocal microscopy that the tegument protein VP22 does not enter the nucleus of cells during the course of HSV-1 lytic infection (Elliot and O'Hare, 1999). This led the authors to conclude that at least some of the tegument

proteins are acquired within the cytoplasm during egress and providing further evidence to substantiate the EDR pathway.

## **1.6 Overview of HSV-1 latency**

One of the unusual characteristics of all herpesviruses is their ability to establish a life-long dormant or latent state of infection within the natural host. Sporadic reactivation of latent viral genomes can lead to recurrent lesions at the initial site of peripheral infection. The viral mechanisms involved in establishing and maintaining a latent state of infection have been, and still are, extensively studied and as such a detailed account is outside the remit of this general introduction into the HSV-1 life cycle. However, as latency is such an integral part of the viral life cycle a brief summary is given below (for detailed reviews see Preston, 2000; Wagner and Bloom, 1997; Steiner and Kennedy, 1995).

### *1.6.1 Definition of latency*

HSV-1 latency can be defined as the maintenance of viral genomes within the nuclei of infected cells without the production of virus particles. The genome is genetically equivalent to that present within the mature virus particle but the highly regulated cascade of gene expression (described above) does not occur. However, the virus genome retains the ability to reactivate and resume replication that can lead to the recurrence of disease.

### *1.6.2 Establishment of latency*

Following lytic replication at the site of peripheral infection HSV-1 enters the nerve termini and becomes transported intra-axonally to the sensory ganglia, frequently the trigeminal ganglia, by retrograde transport. Infected neurones can support viral replication. However, in most instances latency is soon established and the viral genome becomes sequestered in its non-replicative state within the nuclei of infected cells as a non-integrated circular episome. There are estimated to be 10-100 copies of the viral genome per latently infected neurone. Although the exact mode in which viral genomes become suppressed is not known, the lack of certain viral factors, such as Vmw65 (ICP27), and the

presence of cellular regulatory factors, such as the transcription factor Oct-2, have been implicated in the down regulation of viral gene expression (Lillycrop et al., 1993; Steiner and Kennedy, 1995).

### *1.6.3 Maintenance of latency*

During latent infection no viral gene expression associated with the lytic replication cycle can be detected. The only detectable gene expression is that of a major class of transcripts termed the latency associated transcripts (LATs), the major accumulative products of which are 2.0 and 1.5-1.4kb RNAs that are transcribed anti-sense to, and partially overlapping the coding sequences of Vmw110 (ICP0). These are thought to represent stable non-polyadenylated introns cleaved from a longer 8.3kb precursor RNA which is in part complementary to the entire coding sequence of Vmw110 (Wagner and Bloom, 1997). The number of LATs varies, ranging between 40,000-100,000 copies per neurone, and their stability is thought to be attributed to their non-linear structure making them resistant to degradation (Rodahl and Haarr, 1997). The exact biological role of LATs remains unclear and much debated, as they appear to have a minimal effect upon the establishment and reactivation of viral genomes. However, a number of popular theories exist. For example, Perng et al., (2000) recently demonstrated through the use of a LAT<sup>-</sup> mutant HSV-1 virus (dLAT2903), that infected neurones were more susceptible to apoptosis than neurones infected with LAT<sup>+</sup> HSV-1. Thus, Perng and co-workers postulated that LATs promote neuronal survival following HSV-1 infection. LATs contain a number of ORFs suggesting that they could possibly encode an as yet, unidentified viral protein. Thomas et al., (1999) demonstrated that the deregulated expression of the 2 kb LAT, both in neuronal and non-neuronal cells, promoted the growth of HSV-1 in a protein rather than an RNA specific manner. Therefore, the LAT may encode a tightly regulated viral protein, the expression of which although non-essential, could enhance the reactivation of latent HSV-1 genomes. Alternatively, as LATs are partially complementary to the Vmw110 ORF they may act as antisense inhibitors repressing genome expression and therefore maintaining latency, as Vmw110 has been shown to specifically enhance IE gene expression and consequently viral replication (reviewed by Preston, 2000; Everett, 2000).

### *1.6.4 Reactivation from latency*

HSV-1 reactivation, as with other elements of HSV-1 latency, is not fully understood. Reactivation of latent HSV-1 genomes within humans can be induced by local stimuli, for example tissue damage to surrounding neurones harbouring latent genomes, and by systemic conditions, such as UV radiation, stress, and immunosuppression. With such a wide variety of stimuli inducing reactivation it appears likely that both viral and cellular factors are involved in triggering the onset of reactivation. Reactivation results in the production of infectious progeny virions without significant destruction of the host neurones (Gominak et al., 1990). Furthermore, repeated recurrences of reactivation of HSV-1 appear to have no deleterious effects upon the function or physiology of the trigeminal ganglia (Wagner and Bloom, 1997).

## **1.7 Capsid Structure**

Capsid assembly plays an essential role in the life cycle of most viruses characterised to date. Successful formation of the capsid is fundamental in order to provide a robust structure that can enclose and thus protect the viral nucleic acid. Therefore, viruses have evolved specific assembly pathways to produce regular macromolecular structures that are capable of packaging their viral genomes. Furthermore, these intricate and comparatively large structures are produced in the context of a limited coding capacity. For example, herpesvirus capsids are composed of approximately 4000 proteins that become associated to form a structure of  $\sim 1250\text{\AA}$  in diameter. The construction of this complex piece of protein architecture only requires the expression of 7 virally encoded genes (Tatman et al., 1994; Thomsen et al., 19994; Steven and Spear, 1997). As the processes involved in the assembly of viral capsids become better understood, principally through developments in image processing and a better understanding of protein folding pathways, the analysis of capsid assembly is beginning to provide general insights into the assembly of large cellular macromolecular multiprotein complexes.

### *1.7.1 Capsid architecture and the requirement for redundancy*

Crick and Watson (1956) realised that small viruses lacked sufficient coding capacity within their nucleic acid genomes to encode a single asymmetric coat protein molecule large enough to surround and protect the viral genome. From this observation they deduced that virus capsids, both helical and icosahedral, were comprised of one or a small number of protein molecules organised in symmetrical arrays where an individual subunit would have specific bonding properties that were repeated exactly throughout the particle. The repetition of a single subunit within a capsid structure was termed redundancy. Their hypothesis holds true for helical viruses such as tobacco mosaic virus (TMV). The inter-subunit connections within this capsid are essentially identical within the mature virion, with the exception of those subunits at the ends of the helical array which have unsatisfied bonding capacities. (Namba et al., 1989; Casjens, 1997). In relation to icosahedral viruses, Crick and Watson (1956) specifically proposed that these particles were composed of 60 subunits, where each subunit was identically bound to its neighbouring subunit. Although this theory holds true for small icosahedral capsids, such as satellite tobacco necrosis virus (STNV) which is composed of a single repeated polypeptide subunit, their theory could not account for icosahedral viruses which were observed to contain considerably more than 60 identical subunits.

### *1.7.2 Quasi-equivalence*

Caspar and Klug (1962) subsequently suggested a hypothesis that circumvented this paradox. They postulated that if inter-subunit bonds could be “deformed” this would allow certain multiples of 60 subunits, termed the triangulation (T) number, to be incorporated into an icosahedral protein shell. T represents the total number of bonding differences a protein subunit would encounter within a single icosahedral face. The simplest icosahedron would therefore be created from 60 subunits (T=1) with 12 vertices, 20 triangular facets, and 30 edges (see fig. 1.8). Caspar and Klug (1962) envisaged that within an icosahedral capsid where more than 60 identical subunits were used, subunits would be symmetrically inserted between the rings of five subunits (pentamers) at the 12 vertices, as rings of six subunits (hexamers). Incorporation of pentamers at the 12-icosahedral vertices would therefore provide the curvature required, within a hexamer

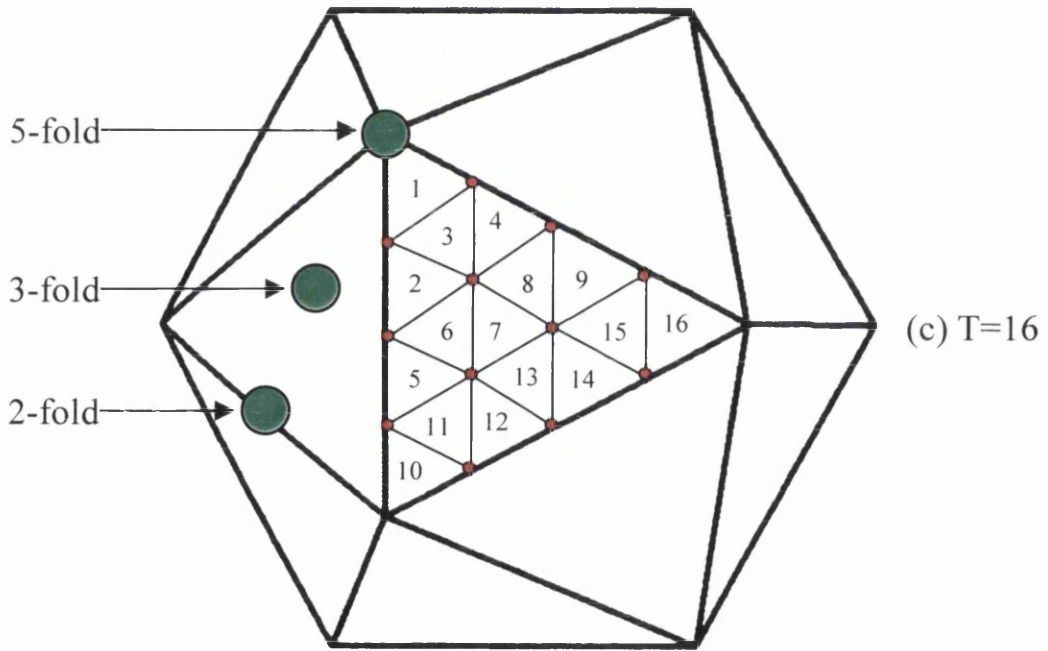
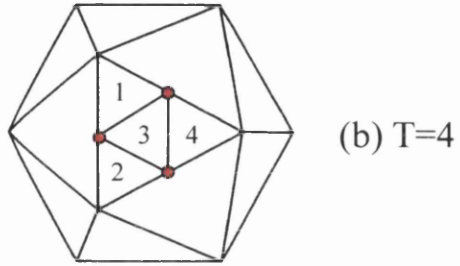
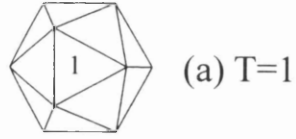


Fig. 1.8: Schematic diagram depicting triangulation symmetry

Following the theory of quasi-equivalence (Caspar and Klug, 1962) icosahedral capsids could be composed from multiples of 60 subunits by the insertion of hexons (represented by the red dots in b and c) between the pentons located at the 5-fold vertices. Where  $T$  would represent the total number of bonding differences a protein subunit would have to encounter within an icosahedral face. The simplest icosahedron ( $T=1$ ) is composed of 60 subunits (a). (b)  $T=4$  icosahedron would contain 240 ( $4 \times 60$ ) subunits via the insertion of 3 hexons per icosahedral face. (c)  $T=16$  icosahedron would contain 960 subunits via the insertion of 12 hexons per icosahedral face. The global 5-, 3-, and 2-fold icosahedral axes of symmetry are highlighted in (c) by green circles.

lattice, in order to form a closed spherical particle (see fig. 1.10, panel B). Thus, a  $T=4$  capsid would be composed of 240 ( $4 \times 60$ ) subunits where each subunit would have to take on 4 slightly different conformations within an icosahedral face. If the subunits assembled totally from hexamers then the surface lattice formed would be a flat sheet and would be unable to form a closed particle which could encapsidate nucleic acid. Caspar and Klug (1962) postulated that the individual protein molecules within a given subunit structure would have to display subtle differences in their bonding relationships, in order to form both hexons and pentons. The subtle non-equivalence in bonding capacity between individual protein molecules was subsequently labelled “quasi-equivalent” and defined as ‘any small non-random variation in regular bonding pattern that leads to a more stable structure than does strictly equivalent bonding’ (Caspar and Klug, 1962; Johnson, 1996; Casjens, 1997; Johnson and Speir, 1997).

The general principles of quasi-equivalence have been applied to a number of virus structures that display icosahedral symmetry. A good example of quasi-equivalence is the core particle of blue tongue virus (BTV). The icosahedral BTV contains two layers, an outer layer, which is primarily involved in cell attachment and penetration, and a core layer that contains the segmented dsRNA genome (Mertens, et al., 1987). The 700Å diameter core of BTV has recently been resolved to 3.5Å by X-ray crystallography and has been shown to be segregated into a further two layers (Grimes et al., 1998). The outer core layer is composed of 780 copies of a single polypeptide (VP7) arranged in a lattice of 260 essentially identical trimers. A single asymmetric unit comprises 13 VP7 molecules ( $T=13$  icosahedral symmetry) arranged into 5 quasi-equivalent trimers (P, Q, R, S, and T). The bonding interactions between these trimers follows the quasi-equivalent hypothesis put forward by Caspar and Klug (1962) and allows the outer core layer to form a robust structure. The size of the outer core layer is determined by the inner core (discussed below in section 1.7.1.5).

### *1.7.3 Departure from quasi-equivalence*

The principle of quasi-equivalence put forward by Caspar and Klug (1962) showing how icosahedral viruses could be composed of more than 60 identical subunits, provides a convenient means by which capsid architecture can be described. However, increased

structural data accumulated through X-ray crystallography and high-resolution electron microscopy analysis has challenged the universality of quasi-equivalence (Rossmann, 1984; Casjens, 1997). Indeed, many capsid proteins demonstrate a remarkable ability to break the rules of geometrical symmetry, such that chemically identical subunits that occupy distinct lattice sites have significantly different conformational structures and bonding relationships.

#### *1.7.4 Flexibility of proteins within capsid structures*

The breakdown in the principles of quasi-equivalence is dramatically highlighted within the icosahedral structure of polyoma virus. Low resolution X-ray crystallography of the polyoma virus capsid to 22.5Å revealed that all the hexon positions were occupied by pentons thereby contradicting the rules of quasi-equivalence (Rayment et al, 1982). High-resolution structures of SV40 to 3.8Å demonstrated that these pentamers, composed of 5 copies of VP1, were inter-linked by their  $\alpha$ -helical C-terminal arms which inserted into their adjacent pentamer subunits. The flexibility of these  $\alpha$ -helical arms ensured the correct specificity of interaction with adjacent pentamers without requiring rigid capsomer geometry and strong symmetry restrictions (Liddington et al., 1991; Steven et al., 1997). The structure of papillomavirus, another member of the genus papovaviruses, has recently been solved to 9Å and also demonstrates similar pentamer lattice arrangements and inter-pentameric connections (Trus et al., 1997). Although pentamers occupy both pentamer and hexamer positions within the icosahedral lattice, there are distinct conformational differences between the capsomers. In the centre of the hexavalent capsomers there is a 25Å hole that is occluded in the pentavalent capsomers. Both pentavalent and hexavalent capsomers are predominantly composed of L1 protein but the occlusion of the hole in the pentavalent capsomers may be attributed to an additional protein mass from the minor capsid protein L2 (Trus et al., 1997). This would therefore suggest the L1 protein exhibits conformational flexibility in order to accommodate the incorporation of the L2 protein into the pentavalent capsomer.

### *1.7.5 Flexibility of proteins within quasi-equivalent capsid structures*

Even in those virus structures that display quasi-equivalence, flexibility between protein structures plays an essential role in virion assembly. This is particularly highlighted by the inner sub-core of BTV and the interactions it forms with the outer core. As previously discussed, the outer core of BTV forms a strictly quasi-equivalent T=13 icosahedral lattice (section 1.7.1.2). However, the inner core of BTV has been shown by X-ray crystallography to form a T=2 lattice (Grimes et al., 1998). This triangulation number should not occur under the rules of quasi-equivalence. However, the BTV inner subcore circumvents the rules of quasi-equivalence by forming a flexible, triangular shaped, elongated dimer, composed of two molecules of the same protein, designated VP3A and VP3B. Five of these dimers are arranged around the 5-fold rotational axis which bind together through different protein interfaces to form an intermediate decamer, with a total of 12 decamers forming the inner subcore. The conformational flexibility required for this arrangement is centred on an  $\alpha$ -helix within the VP3 dimerisation domain. The modest pivoting provided by the  $\alpha$ -helix and conformational differences within the loop regions of VP3A and VP3B allow the subunits to form close fitting interlocking decamers while still retaining a local two-fold symmetry axis (Grimes et al., 1998). Flexibility within the BTV virion is further highlighted by the interactions between the outer core composed of VP7 trimers, and inner VP3 subcore. Due to the symmetry mismatch there are 13 different sets of contacts between the outer (T=13) and inner (T=2) cores. The polymerisation of trimers around the inner core is predominantly achieved through subtle alterations in the hydrophobic interactions between inner and outer cores. The flexibility in this protein-protein interface provides the outer core with a scaffold for assembly of the strict quasi-equivalent T=13 shell.

### *1.7.6 Symmetry mismatches in capsids.*

Although such large deviations from quasi-equivalence have only been highlighted comparatively recently due to the advances in high-resolution imaging. Breakdowns in symmetry and consequent divergences from quasi-equivalence have been observed for some time. The basic capsid shell often requires the addition of specific proteins to the outer capsid layer, which contribute important functional attributes that are essential in the

production of infectious virions. However, addition of further structural proteins into the geometrical capsid lattice can introduce symmetry mismatch at the point of introduction, commonly the 5-fold symmetry axis, and therefore requires capsomer flexibility in order to be accommodated (Steven et al., 1997). Viruses that have been well documented to have such symmetry mismatches include bacteriophages, such as P22,  $\lambda$ , and T4, and adenovirus (Valpuesta, 1994; Hendrix, 1978; Steven et al., 1997). Bacteriophages have a tail spike that protrudes from one of the 12 pentonal vertices and is responsible for the attachment to and delivery of the viral nucleic acid into the new bacterial host. The adenovirus capsid has 12 fibres, approximately 120 to 330Å in length, that project out from the 12 pentons at each 5-fold axis. These are responsible for receptor binding and internalisation within the host cell (Philipson et al., 1968). Both adenovirus and bacteriophage capsids have been shown to assemble in the absence of their fibres and tail spikes respectively. Although virion infectivity in both cases is greatly impaired the attachment of these structural proteins is non-essential for the assembly of their respective capsid structures (Falgout and Ketner, 1988; Bazinet and King, 1988). Since they are not themselves pentamers, incorporation of fibres and tail spikes into their capsid structures must cause alterations in the symmetry of the bonding relationships between their surrounding capsomers. Tail and fibre attachment must therefore require capsomer flexibility at the site of attachment for efficient incorporation without subsequent disruption of the surrounding capsomer bonding interfaces. Indeed, this has been demonstrated to occur within the penton base and fibre attachment of adenovirus capsids. Recombinant expression within the baculovirus system of the penton base from adenovirus type 3 (Ad3) in the absence of other capsid proteins leads to the production of dodecahedral particles. Cryo-EM and computer reconstruction analysis of these particles in the presence and absence of fibres demonstrates a remarkable difference in the conformation of the penton base structure in the presence of the fibre (Schoehn et al., 1996). The conformational rearrangements observed are thought to be due to the movement of densities attributed to flexible loops within the penton base. The degree of individual capsomer flexibility involved in these examples, far exceeds the limited deformable interactions implied by the theory of quasi-equivalence.

## 1.8 HSV-1 capsid structure

The HSV-1 capsid is one of the largest and most complex of virus icosahedral particles and as such there has been considerable interest in analysing its three dimensional structure. Through the use of EM the HSV-1 capsid has long been known to consist of 150 hexons and 12 pentons, arranged in T=16 icosahedral symmetry (Wildy et al., 1960; Furlong et al., 1978). The overall structure of the HSV-1 capsid appears to be well conserved throughout the herpesvirus family. Similar structures have been identified from a wide variety of herpesviruses whose natural hosts span those from mammals, such as HSV-1 (Schrag et al., 1989), SCMV (Trus et al., 1999), and HCMV (Butcher et al., 1998), to fish, such as the channel catfish virus (Booy et al., 1996), and invertebrates, such as oyster herpes virus (personal communication, Andrew Davison 2000). Cryo-EM analysis in conjunction with three-dimensional computer image processing has provided the clearest detail of the native structure of the HSV-1 capsid (to date) to a resolution of 8.5Å, see fig. 1.9 (Zhou et al., 2000). The capsid shell, comprising outer, middle, and inner (or floor) areas, is 125nm in diameter and approximately 15nm thick. The outer shell is composed of protruding capsomers, 150 hexons and 12 pentons, that are interconnected in the middle area by 320 triplexes. These capsomeric subunits associate to form a densely packed network, which makes up the 4nm thick inner or capsid floor area (Wildy et al., 1960; Schrag et al., 1989; Booy et al., 1991; Zhou et al., 1994; Zhou et al., 1998).

### 1.8.1 Asymmetric unit

The asymmetric unit is a single building block that contains all the structural information required to build a capsid. With respect to the HSV-1 capsid, each of the 20 icosahedral faces is composed of three asymmetric subunits consisting of one fifth of a penton, one P-hexon, one C-hexon, one-half of an E-hexon, one of each of the five triplexes  $T_a$ - $T_e$  triplexes, and one third of the triplex  $T_f$  (Zhou et al., 1994; Zhou et al., 1998). A single asymmetric unit is illustrated schematically in relation to a single icosahedral face in fig. 1.10 (panel B).

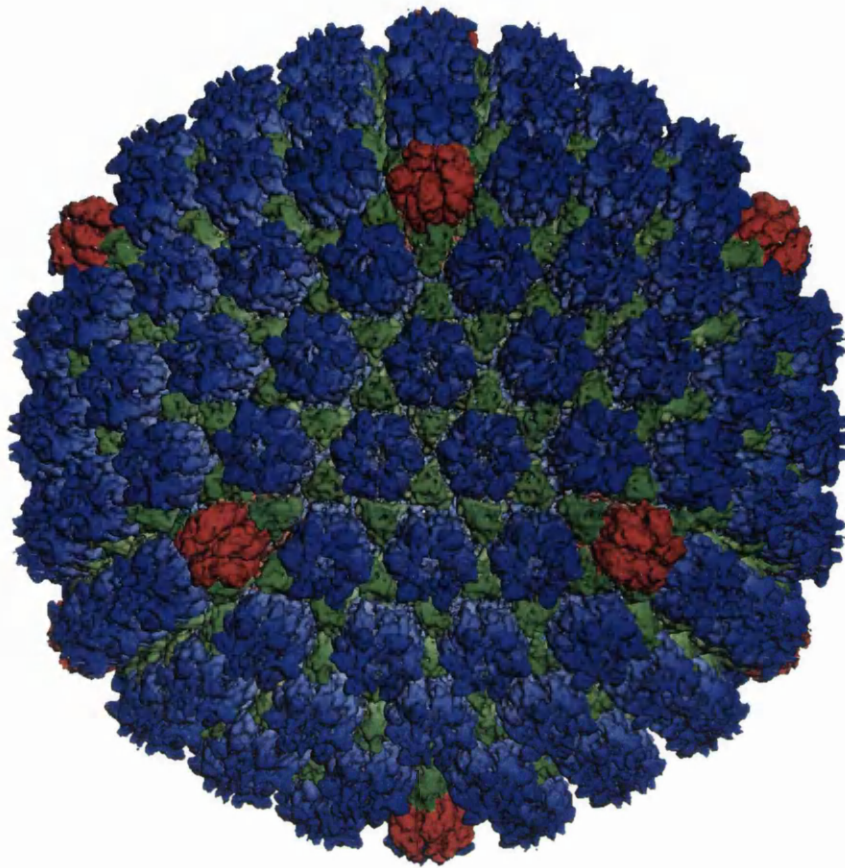


Fig. 1.9: 3D Surface reconstruction of the HSV-1 B-capsid at 8.5Å, generated by cryo-EM and image processing.

The outer shell of the HSV-1 capsid consists of 162 capsomers arranged around T=16 icosahedral symmetry. Out of the 162 capsomers; 150 are hexons (coloured blue) and 12 are pentons (coloured red). The capsomers are interconnected by 320 triplexes (coloured green).

This figure was reproduced with permission from W. Chiu, Baylor College of Medicine, USA.

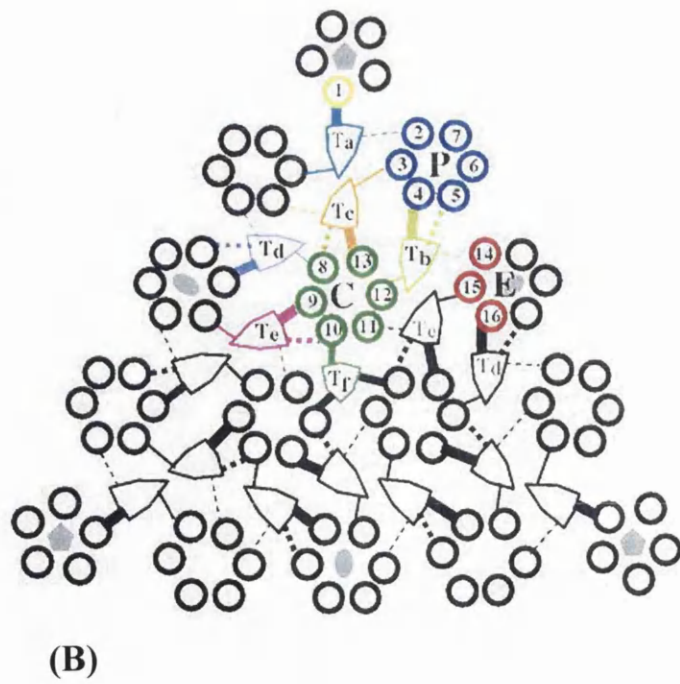
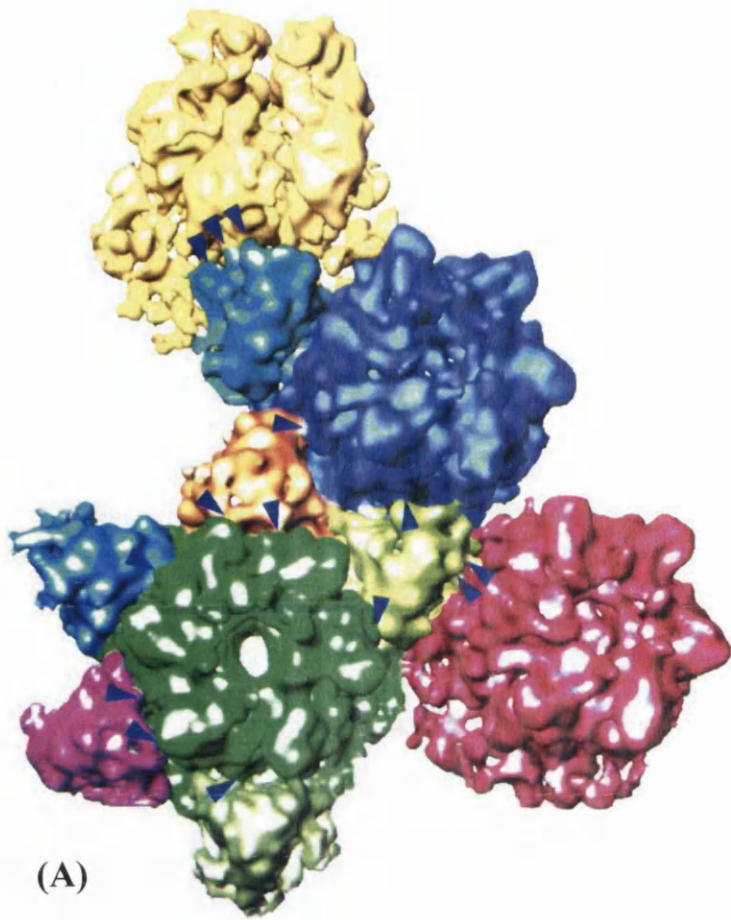


Fig. 1.10: Asymmetric unit of the HSV-1 capsid

3D reconstruction to 13Å resolution of the contiguous morphological components making up a single asymmetric unit from the HSV-1 B-capsid. Shown in (A) are one penton (coloured in yellow), one P-hexon (coloured in blue), one C-hexon (coloured in green), one E-hexon (coloured in pink), and the six different types of triplexes ( $T_a$ ,  $T_b$ ,  $T_c$ ,  $T_d$ ,  $T_e$ , and  $T_f$ ) (highlighted in various colours). The arrows indicate the positions of external attachment above the capsid floor between triplexes and their adjacent hexons and/or penton. (B) Schematic diagram of one triangular face of the HSV-1 capsid illustrating the interactions between the VP5 subunits from the penton and hexons (1-16) with their respective triplexes  $T_a$ - $T_f$ . Subunits comprising a single asymmetric unit are highlighted in the same colours as for (A). The four types of interaction between the triplex and VP5 are represent by the thickness of line; strong triplex head connection (thick solid line), weak triplex head connection (thick dashed line), triplex tail connection (thin solid line), and triplex arm connection (thin dashed line).

This figure was reproduced with permission from W. Chiu, Baylor College of Medicine, USA.

### *1.8.2 Protein composition of the capsomers*

Although the icosahedral structure of the HSV-1 capsid has been established for some time (Wildy et al., 1960; Schrag et al., 1989) the protein composition of capsomers has only been resolved comparatively recently. Two approaches, namely antibody labelling (Trus et al., 1992) and systematic depletion of structural components from purified capsids (Newcomb and Brown, 1989; Newcomb and Brown, 1991; Newcomb et al., 1993) have been employed. Newcomb and Brown (1989) originally demonstrated through the use of argon ( $\text{Ar}^+$ ) etching that VP5, VP19c, and VP23 were more readily disassociated from the capsid than VP21, VP24, and VP22a when purified B-capsids were exposed to low doses of ion plasma. From this they concluded that VP5, VP19c, and VP23 were present on the outer surface of the capsid whereas VP21, VP24, and VP22a were more likely to be internal components of the capsid as they required longer periods of exposure to become disassociated. Similar depletion analysis utilising denaturants, such as urea and GdnHCl, in conjunction with cryo-EM and SDS-PAGE analysis have determined which proteins make up the various structures.

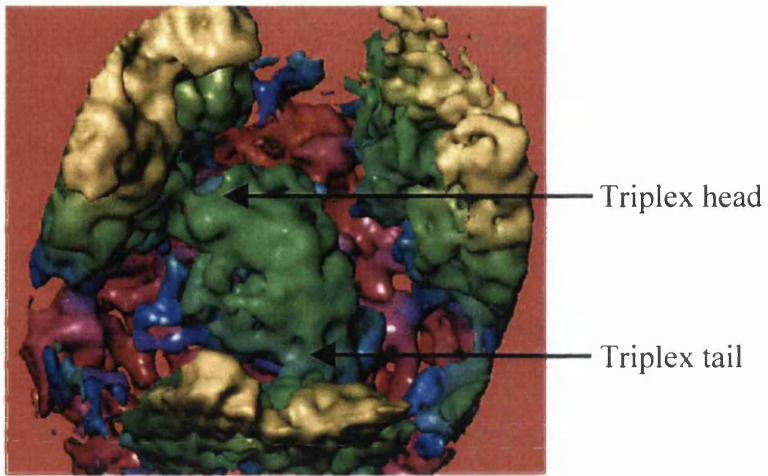
#### *1.8.2.1 Pentons and hexons are composed of VP5*

Trus et al., (1992) demonstrated through cryo-EM analysis of immune precipitated capsids, utilising monoclonal antibodies against VP5, that both the pentons and hexons within the HSV-1 capsid were composed of VP5. The fact that the pentons as well as the hexons were composed of VP5 was consistent with the observation that VP5 was the MCP (Gibson and Roizman, 1972). Newcomb and Brown (1991) went on to demonstrate that the pentons could be disassociated when purified capsids were treated with 2M GdnHCl. Subsequent SDS-PAGE analysis confirmed the findings of Trus et al., (1992) that indeed the pentons were composed of VP5. Quantitative analysis showed that pentons were composed of five copies of VP5 (Newcomb et al., 1993). However, high-resolution cryo-EM analysis has provided the best insight into the structural arrangement of VP5 within capsomers. Each penton can be readily observed to be composed of five copies of VP5 that form a cylindrical tower 145Å in diameter and 140Å in height. A channel runs through the centre of the penton tower with a diameter of 50Å. Each VP5 subunit within the penton is well separated from its neighbouring subunits (Zhou et al., 1994; Zhou et al.,

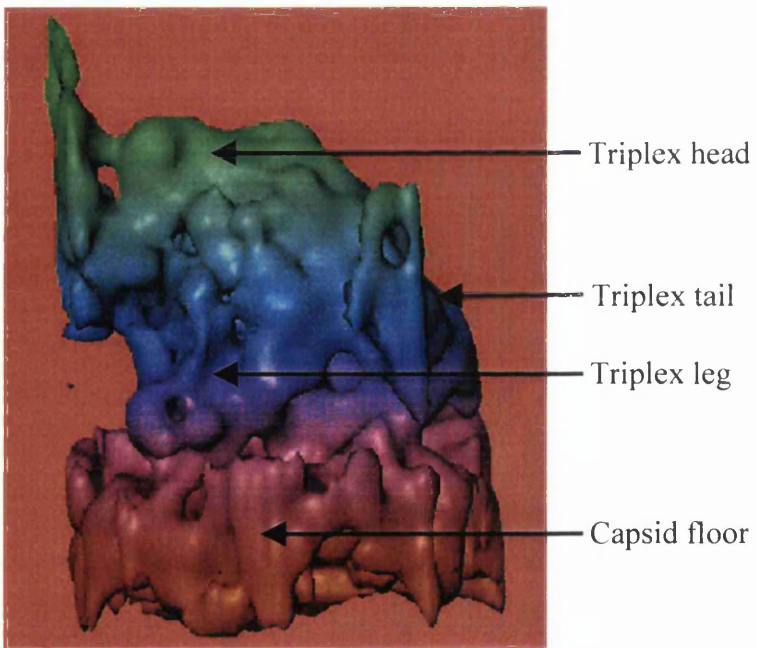
1998). In comparison, each hexon is composed of six copies of VP5 that are not as well separated as those within the penton. The incorporation of an additional VP5 subunit into the hexon also highlights the conformationally flexible nature of VP5 (discussed in further detail within section 1.8.4 and 4.0). The quasi-equivalent P (peripentonal), E (edge) and C (central) hexons, are similar but not identical in their overall conformation, reflecting their slightly different quasi-equivalent environments within the icosahedral face. Each hexon is cylindrical in shape with a diameter of 170Å and a height of 140Å. Located on top of each hexon is a horn shape density attributed VP26 (Trus et al., 1995, Zhou et al., 1995). The hexons, as with the pentons, have a channel running throughout their centre. However, unlike the channel within the penton, the hexon channel is constricted by a bundle of short  $\alpha$ -helices (Zhou et al., 1994; Zhou et al., 2000; personal communication Frazer Rixon 2000). As VP5 is the MCP and contributes the entire mass of pentons and the majority of the mass of hexons it is not surprising that VP5 also comprises the majority of the mass within the capsid floor area. Here it is thought that the termini of the VP5 molecules from individual capsomers form an intricate network of connections (Baker et al., 1990; Zhou et al., 2000).

#### *1.8.2.2 Triplexes are heterotrimers of VP19c and VP23*

Early negative stain EM analysis of capsids originally identified triplexes, initial termed fibrils, as a component of the capsid lattice, interconnecting adjacent capsomers (Vernon et al., 1974). Mirroring the early developments in cryo-EM analysis, low-resolution images of the capsid identified the triplexes as Y-shaped masses located at the 3-fold axes of symmetry interconnecting adjacent capsomers (Schrag et al., 1989; Baker et al., 1990; Booy et al., 1991). However, it has only been comparatively recently that the composition and the structural nature of the triplex has been identified. Newcomb et al., (1993) demonstrated that 2M GdnHCl treatment of purified capsids could disassociate triplexes surrounding the penton, namely triplexes T<sub>a</sub> and T<sub>c</sub>. Quantitative analysis of the proteins associated with the removal of these triplexes suggested that the triplexes were probably a heterotrimer comprising of one copy of VP19c and two copies of VP23. Furthermore, high-resolution cryo-EM analysis of the capsid has subsequently demonstrated that most of the triplexes are asymmetrical, and not Y-shaped (Zhou et al., 1994; Zhou et al., 1998). There are a total of six different types of triplex (termed T<sub>a</sub>-T<sub>f</sub>) that contribute to a single



(A)



(B)

Fig. 1.11: 3D reconstruction of the HSV-1 triplex to 13Å.

Aerial view of an averaged triplex connecting two out of three surrounding hexons (A). Side view of a triplex connecting to an adjacent capsomer through protein densities in the head domain of the triplex attributed to VP19c (B). Triplex leg and tail domains anchor the triplex to the capsid floor. Both (A) and (B) are coloured from light (yellow/high) to dark (red/low) representing their radial distance from the center of the capsid.

This figure was reproduced with permission from W. Chiu, Baylor College of Medicine, USA.

asymmetric unit with a total of 16 triplexes within a single icosahedral face (see fig. 1.10). The extent of interaction between the triplexes and their surrounding capsomers varies and depends upon their position within the icosahedral lattice. For example, the head connection made by triplex  $T_a$  to the penton is significantly different to that of the head connections made by triplexes  $T_b$ - $T_e$  to their respective hexon capsomers (personal communication, Zhou, 1999). The exact nature of the interactions between triplex  $T_f$  and its surrounding hexons remains unresolved. Triplex  $T_f$  is located at the global 3-fold axis of symmetry (see fig. 1.10, panel B) and as a consequence image processing in conjunction with computer reconstructions makes it appear symmetrical. However, from triplexes  $T_a$ - $T_e$  four types of exterior triplex connections to surrounding VP5 capsomers have been shown to occur. These consist of strong and weak head connections, and tail and arm connections (Saad et al., 1999; Zhou et al., 1994; Zhou et al., 1998). The triplex is discussed in further detail within section 1.8.5 and section 4.0 in association with the findings presented within this thesis and other current published data.

#### *1.8.2.3 VP26 is located on the tips of the hexons*

The location of VP26 within the capsid was initially suggested by comparison of penton and hexon subunits and through depletion analysis of purified capsids, in conjunction with cryo-EM (Zhou et al., 1994). Newcomb and Brown (1991) demonstrated that VP26 could be readily detached from purified capsids treated with either urea or GdnHCl. Subsequently, Booy et al., (1994) demonstrated by cryo-EM analysis of VP26 depleted and VP26 re-associated capsids that VP26 was specifically located to the tips of the hexons. Six copies of VP26 are thought to bind to each hexon and form a star-shaped ring at each hexon tip (Zhou et al., 1995; Wingfield, 1997).

#### *1.8.3 Internal scaffold composition*

Although the external characteristics of the HSV-1 capsid have been known for some time the internal core composition has only comparatively recently been resolved. As previously stated, Newcomb and Brown (1989) originally demonstrated through  $Ar^+$  etching of purified B-capsids that VP22a, VP21 and VP24 were relatively well protected from erosion by low intensity plasma. This led the authors to conclude that these proteins

formed internal components of the capsid. Subsequent to this, cryo-EM comparison of A-, and B-capsids highlighted additional protein masses within the interior of B-capsids that correlated to the presence of internal core proteins (Baker et al., 1990). It is now known that the major internal scaffold component of B-capsids is VP22a, with over 1000 copies per capsid compared to VP21 and VP24, which are present in approximately 100 copies per capsid (Newcomb et al., 1993). The scaffold has been shown to exist in two forms within the interior of capsids. Large cored capsids, where the C-terminal 25 amino acids of either preVP22a and/or preVP21 have not been cleaved by the VP24 protease, or small cored capsids, where the C-terminal cleavage has taken place. Large cored capsids can be made using the baculovirus system by omitting the UL26 gene, encoding VP21 and the scaffold protease VP24 (Tatman et al., 1994; Thomsen et al., 1994). Temperature sensitive (*ts*) mutants within the UL26 gene, such as *ts1201*, that are defective in the processing of the UL26 into VP21 and VP24 at the non-permissive temperature also produce large cored capsids. Downshifting *ts1201* infected cells to their permissive temperature results in the correct processing of UL26, and the production of small cored capsids (Preston et al., 1983).

The interaction between preVP22a and VP5 has specifically been shown to occur through the C-terminal 25 amino acids and as such these residues are essential for capsid formation (Kennard et al., 1995; Matusick-Kumar et al., 1995; Hong et al., 1996). Cryo-EM has recently shown that the majority of the scaffold mass, either within large or small cored capsids, exhibits no icosahedral symmetry. However, some localised regions of the scaffold do appear to be icosahedrally arranged and form rod-like densities, approximately 40Å in length, protruding into the interior of the capsid. These densities appear to be located beneath the triplexes T<sub>b</sub>, T<sub>c</sub>, T<sub>d</sub> and T<sub>e</sub> and are thought to represent the positions at which the C-terminus of the scaffold interacts with capsid shell (Zhou et al., 1998).

Through baculovirus studies, the minor constituent scaffold protein, preVP21, has been shown to be able to substitute for preVP22a in the formation of capsids. However, the efficiency with which capsids were assembled was greatly impaired. Furthermore, larger numbers of aberrant shells were formed when compared to UL26.5 mediated assembly (Newcomb et al., 1993; Thomsen et al., 1994; Tatman et al., 1994). Sheaffer et al., (2000) went on to demonstrate that UL26 mediated capsid assembly, in the absence of UL26.5

expression occurred without the increased incorporation of VP21 and VP24 into the capsid. This led the authors to conclude that although preVP21 to preVP22a shared C-terminal sequence identity, capsid assembly could occur, although substantially less efficiently, on a minimal scaffold composed of VP21.

#### *1.8.4 Quasi-equivalence within the HSV-1 capsid*

As previously stated, VP5 comprises the entire mass of pentons (5 copies of VP5) and the majority of the mass of hexons (6 copies of VP5). Computational separation of VP5 molecules from pentons and hexons demonstrates that the individual VP5 molecules have similar conformational arrangements that display overlapping mass densities (Zhou et al., 1994). Although the exact bonding relationship between VP5 molecules within individual hexon and penton subunits remains unresolved at the current resolution, VP5 molecules clearly display similar interactions and therefore fit the criteria required by the theory of quasi-equivalence (Zhou et al., 1994; Zhou et al., 1998; Zhou et al., 2000; personal communication; Jing He, 2000; personal communication, Frazer Rixon). However, it should be noted that three distinct conformational differences have been identified between individual VP5 molecules from pentons and hexons. The most obvious is the presence of an additional horn shape density at the distal tip of VP5 from hexons attributed to VP26 (Zhou et al., 1995). Hexons also contain an extra mass density in the middle domain of VP5, attributed to a bundle of seven short  $\alpha$ -helices, which constricts the hexon channel (Zhou et al., 2000). Further differences in mass density can also be seen within the lower domains of VP5 molecules, in particular the predicted long N-terminal  $\alpha$ -helix. Differences in the angle of this  $\alpha$ -helix can be seen not only between VP5 molecules from pentons and hexons but also between VP5 molecules from the P, E and C hexons. Indeed, these quasi-equivalent hexons appear skewed in relation to each other, reflecting their slightly different locations within the icosahedral lattice (Zhou et al., 1994; Zhou et al., 2000). Although subtle differences in the density masses do exist between the various quasi-equivalent hexons they typically display good 6-fold local symmetry throughout their structures, particularly in the tower regions which are highly conserved (personal communication, Jing He, 2000).

### 1.8.5 *The non-equivalence of triplexes*

Triplexes occupy positions of local, and with respect to the triplex  $T_f$  global, 3-fold symmetry. However, due to the apparent asymmetry of the triplex molecule, as determined by cryo-EM and computer reconstruction, and the heterotrimeric arrangement of this complex (2 copies of VP23:1 copy of VP19c) it has been difficult to elucidate how this complex occupies a 3-fold symmetrical positions since rotation of a triplex around its axis would not result in equivalent interactions (Zhou et al., 1994; Zhou et al., 1998; Zhou et al., 2000). Furthermore, cryo-EM and computer reconstruction analysis of the HSV-1 capsid has long since demonstrated that the triplexes  $T_a$ - $T_f$  have slightly different degrees of interaction with their adjacent capsomers. The most significant different is that of triplex  $T_a$  compared to that of triplexes  $T_b$ - $T_c$ , (Zhou et al., 1994; Zhou et al., 1998). The variation in the degree of association between triplexes with pentons and hexons can also be detected biochemically possibly reflecting differences in their respective bonding interfaces. Newcomb et al., (1993) demonstrated that the peripentonal triplexes ( $T_a$  and  $T_c$ ) were more readily disassociated from capsids treated with 2M GdnHCl than those triplexes surrounding adjacent hexons. Conway et al., (1993) demonstrated similar findings between perihexonal and peripentonal triplexes when capsids were treated with high doses of radiation.

Although the differences in bonding between triplexes with their surrounding capsomers, and their clear asymmetry, violate the rules of quasi-equivalence, analysis of the triplex connections to the capsid floor at 8.5Å resolution has recently revealed how triplexes occupy a 3-fold rotational axis (Zhou et al., 2000). This is discussed in detail in section 4.0 in relation to the results presented within this thesis.

### 1.8.6 *Quasi-equivalence within the procapsids*

During the assembly of HSV-1 capsids the initial assembly product is a transient intermediate termed the procapsid (discussed within section 1.9.3 and 1.9.4; Newcomb et al., 1996; Rixon and McNab, 1999; Newcomb et al., 1999; Newcomb et al., 2000). The procapsid is markedly rounder than the mature capsid and lacks the flat facets, angular edges, and vertices associated with the mature icosahedron (see fig. 1.13; Newcomb et al.,

1996). The pentons and hexons within the procapsid are less compact than those of the mature capsid with individual VP5 subunits making little connection to each other or adjacent capsomers (Trus et al., 1996). Thus, although the capsomers are arranged on a T=16 icosahedral lattice, the general spherical and porous nature of the procapsid, in conjunction with the loose packing of individual capsomers, reflects a high degree of non-equivalence within the procapsid. The non-equivalent nature of VP5 subunits within hexon capsomers of the procapsid, opposed to that of mature capsid, also makes procapsid hexons unable to bind VP26 (Newcomb et al., 1999). Thus, the high degree of non-equivalence within the procapsid prevents the procapsid from fitting the criteria required by the theory of quasi-equivalence proposed by Caspar and Klug (1962).

## 1.9 Capsid assembly

Although the structure of the HSV-1 capsid has been extensively studied over a number of decades the mechanisms involved in the actual assembly of the capsid have only comparatively recently been examined. Developments in recombinant protein expression techniques, such as the baculovirus expression system, have provided a means by which the mechanisms involved in HSV-1 capsid assembly can be investigated. Utilising this approach the minimal protein components required for the assembly of HSV-1 capsids have been identified (discussed in section 1.9.2) and their structural locations within the capsid have been revealed (Tatman et al., 1994; Thomsen et al., 1994; Zhou et al., 1995). Furthermore, the assembly of HSV-1 capsids has been reconstituted *in vitro* using infected cell extracts and more recently from individual purified capsid protein components (Newcomb et al., 1994; Newcomb et al., 1996; Newcomb et al., 1999). Such recent developments have led to a better understanding of the protein-protein interactions associated with HSV-1 capsid assembly and of the protein folding pathways that are required to form such a large and architecturally complex structure.

### 1.9.1 Nuclear assembly of HSV-1 capsids

One of the defining characteristics of all herpesviruses is that DNA replication, capsid assembly and subsequent DNA packaging occur within the nucleus. This therefore,

necessitates that HSV-1 capsid proteins translated within the cytoplasm must be transported to the nucleus. Immunofluorescent analysis performed by Nicholson et al, (1994) and Rixon et al., (1996) demonstrated how the major structural components of the capsid were localised to the nucleus. VP19c and preVP22a were shown to be capable of localising to the nucleus independently, whereas VP5, VP23, and VP26 were unable to localise selectively to the nucleus. PreVP22a was shown to associate with VP5, whereas VP19c could associate with either VP5 or VP23, and in turn localise these proteins to the nucleus. However, it was observed that VP26 did not localise to the nucleus when expressed with either preVP22a or VP19c. Co-expression of VP26 with VP5, and either VP19c or preVP22a, did result in the nuclear localisation of VP26. This led the authors to conclude that VP26 binds directly to VP5 and subsequent interactions between VP5 and either VP19c and/or preVP22a resulted in the efficient nuclear localisation of VP26. Furthermore, detailed analysis of capsid protein nuclear localisation utilising confocal microscopy has demonstrated that capsid assembly occurs at defined foci within the nucleus. This has led to suggestion that capsid assembly occurs at specific sites within the nucleus in close proximity to DNA replication compartments (Ward et al., 1996; de Bruyn Kops et al., 1998). The capsid protein interactions identified through their nuclear localisation capability are summarised in fig. 1.12.

### *1.9.2 HSV-1 capsid assembly analysis within insect cells*

Comparatively recent advances in recombinant expression techniques have allowed the study of HSV-1 capsid protein interactions to be accomplished in greater detail than by electrophoretic and electron microscopy analysis alone. One approach that has been integral in the study of HSV-1 capsid assembly is that of the baculovirus expression system. Baculoviruses naturally infect arthropods and can be recombinantly manipulated to express single or multiple genes of interest within cultured insect cells. One of the most commonly utilised insect cell lines is that of *Spodoptera frugiperda* (SF). Infection of these cells with recombinant baculoviruses expressing gene(s) of interest under the strong late polyhedrin promoter results in high levels of protein expression. Tatman et al., (1994) and Thomsen et al., (1994) utilised the baculovirus expression system to analyse the requirement for HSV-1 gene products in the assembly of HSV-1 capsids. Capsid particles, resembling those of WT B-capsids, of normal composition and structure were

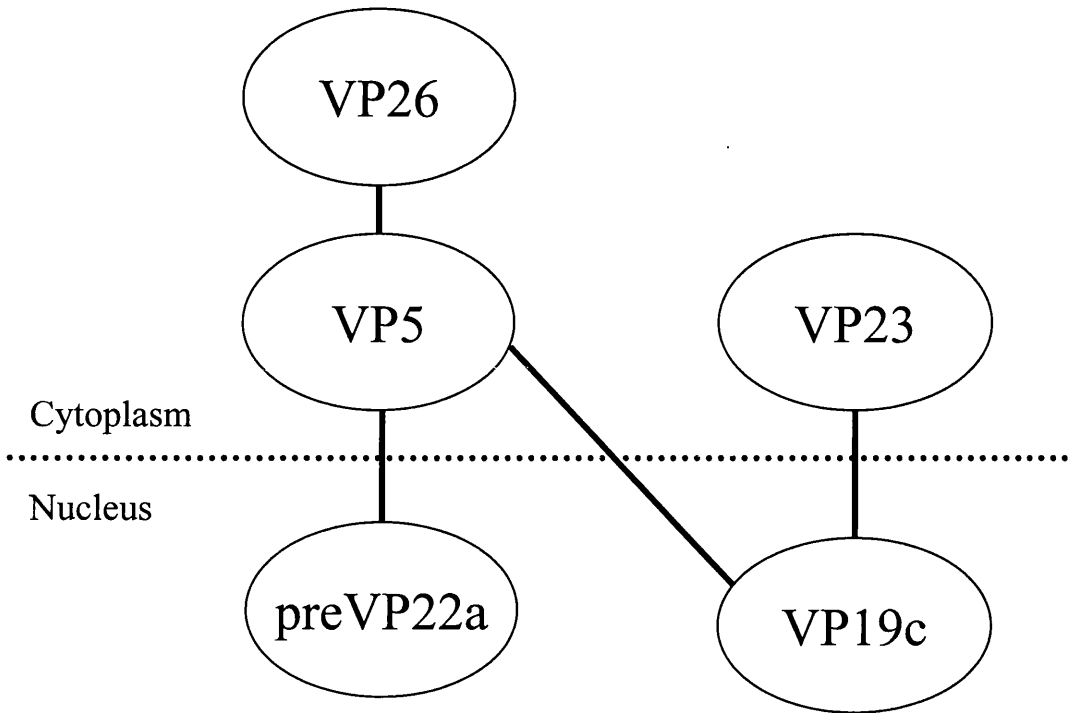


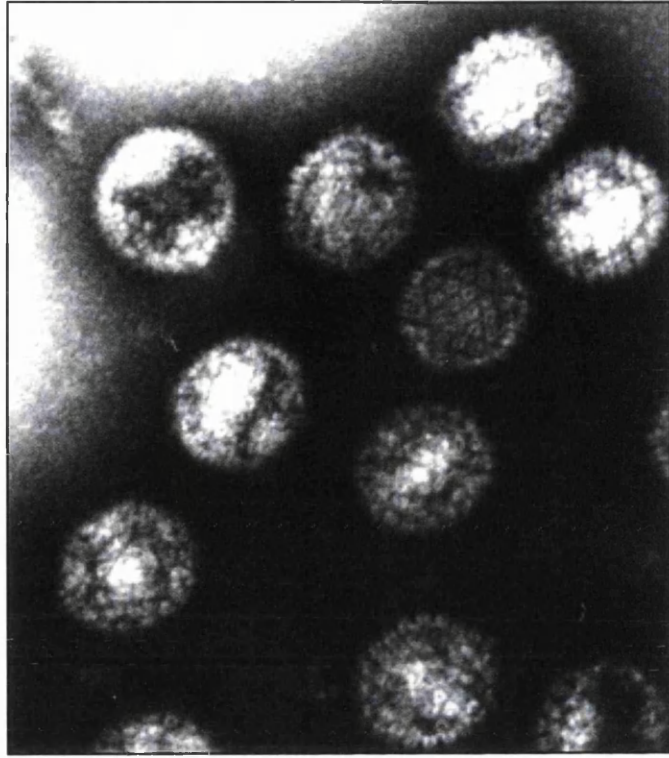
Fig.1.12: Diagram schematically illustrating the protein-protein interactions within the HSV-1 capsid determined through the re-localisation of HSV-1 capsid proteins from the cytoplasm to the nucleus (Nicholson et al., 1994; Rixon et al., 1996).

produced by infecting insect cells with a panel of baculoviruses (designated Ac) expressing six capsid protein genes: AcUL19 (VP5), AcUL18 (VP23), AcUL38 (VP19c), AcUL35 (VP26), AcUL26 (VP21/VP24), and AcUL26.5 (preVP22a). Omission of AcUL35 (VP26) had little effect on the production of capsids indicating that it is not required for the efficient formation of capsids. However, omission of either AcUL19 (VP5), AcUL18 (VP23), or AcUL38 (VP19c) prevented the formation of capsids.

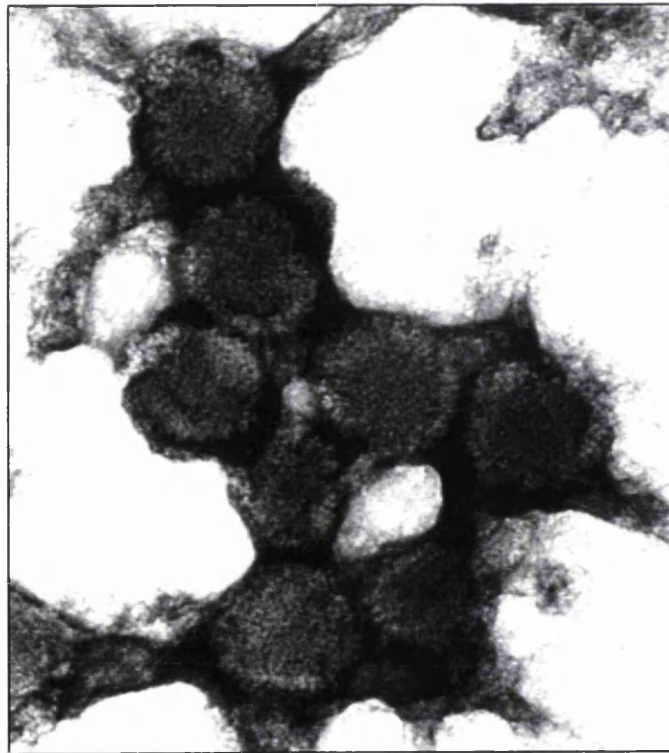
These studies also demonstrated that capsid assembly was not prevented by the omission of either one of the scaffold protein genes, AcUL26 (VP21/VP24) or AcUL26.5 (preVP22a). Therefore, the expression of preVP21 or preVP22a was sufficient to serve as a scaffold for the formation of capsids. However, omission of both scaffold protein genes prevented the formation of capsids leading instead to the formation of aberrant particles and curved capsid shells. Although co-infection with AcUL26 could support the assembly of capsids, in the absence UL26.5, the number of capsid produced was significantly lower than that of AcUL26.5 mediated assembly. This could possibly reflect the higher copy number incorporation of preVP22a, over 1000 copies per B-capsid, compared to that of preVP21, approximately 100 copies per B-capsid (Newcomb et al., 1993). Indeed, subsequent analysis into the specific incorporation of preVP21 into capsids during assembly was shown to be lower than that of preVP22a even in the presence of excess preVP21 protein. Thus, capsid formation can occur on a minimal scaffold but at reduced efficiency (Sheaffer et al., 2000). Expression of AcUL26.5 alone results in the production of large numbers of core-like structures indicating that preVP22a can self assemble in the absence of other capsid proteins (Newcomb and Brown, 1991; Preston et al., 1994). Gradient purified scaffold particles have been shown to be sufficient to act as scaffold material for the formation of capsid particles *in vitro* (personal communication, McClelland, 1999; Newcomb et al., 1999).

### *1.9.3 In vitro HSV-1 capsid assembly and procapsid formation*

Recombinant expression of capsid proteins utilising the baculovirus system has led to the development of an *in vitro* based capsid assembly model. Newcomb et al., (1994) originally demonstrated through the mixing of lysed SF cell extracts, which had been individually infected with baculoviruses expressing VP5, VP19c, VP23, and preVP22a,



(A)



(B)

100nm

Fig. 1.13: EM analysis of negative stained *in vitro* formed procapsids and mature B-capsids

Purified capsid proteins VP5, triplexes (VP19cHis + VP23), and preVP22a were mixed and incubated at 28°C for either 1 hour (B) or o/n (A) before being immunoprecipitated with a VP5 monoclonal antibody (DM165). Pelleted capsids and related structures were subsequently analysed under negative staining by EM. Panel (A) demonstrates a typical field of view of *in vitro* assembled mature B-capsids. Capsomers can be readily identified in their icosahedral lattices. Panel (B) demonstrates a typical field of view of *in vitro* assembled procapsids. Capsids appear more spherical in nature with individual capsomers appearing less defined. Scale bar represents 100nm.

This fig. was reproduced with permission from F. Rixon, MRC Virology Unit, Institute of Virology, Glasgow.

that capsid formation could occur *in vitro*. EM analysis of extracts incubated o/n at 28°C demonstrated the presence of capsids that resembled WT capsids in their size, morphology (T=16), and presentation of specific surface epitopes to monoclonal antibodies. The *in vitro* formation of capsids was also shown to be cold sensitive with particle formation being inhibited when extracts were incubated at 4°C. Subsequently, Newcomb et al., (1996) went on to identify a series of intermediate capsid structures by immune precipitation of complexes from *in vitro* assembly-competent reaction mixtures in conjunction with EM analysis. Partial capsids, closed spherical particles (procapsids), and mature polyhedral capsids could be identified 1 min, 90 min, and 8 hours respectively after combined extract incubation. EM analysis revealed partial capsids as arc-shaped wedges with angles ranging from 30° to greater than 270°. These partial capsids were suggested to be precursors to procapsids as they were rarely identified in reactions incubated over 90 min. Partial capsids consisted of an outer shell, composed of VP5, VP19c, and VP23, surrounding a region of scaffold. Procapsids were the predominant assembly product following 90 minutes of incubation. EM analysis of procapsids revealed that they were highly uniform in morphology consisting of a round closed outer shell with identifiable capsomer protrusions (composed of VP5, VP19c and VP23) surrounding a scaffold core (see fig. 1.13, panel B). Continued incubation of purified procapsids resulted in the production of mature, angularised, icosahedral particles (see fig. 1.13, panel A). This led the authors to conclude that procapsids were indeed a true HSV-1 capsid assembly intermediate which does not require the association of further viral proteins to induce capsid maturation. Intriguingly, both partial capsids and procapsids disintegrated upon incubation at 2°C, whereas angularised particles resembling those of mature B-capsids appeared stable at 2°C. The cold sensitivity of these particles was consistent with other well documented dsDNA viruses which assembled through procapsid intermediates, such as T4 phage, and with earlier *in vitro* cell-free capsid assembly data (Steven et al., 1976; Newcomb et al., 1994). Newcomb and co-workers went on to propose a model for the assembly of HSV-1 capsids based upon their *in vitro* observations. Capsid assembly begins with the nuclear localisation of capsid proteins and the initial formation of partial arc-shaped capsids. These arcs grow in size by the addition of further capsomer subunits and triplexes until they form a closed spherical particle (procapsid). The procapsid then undergoes maturation to form a mature angularised polyhedral capsid. The stages in capsid assembly and morphogenesis are schematically depicted in fig. 1.14.

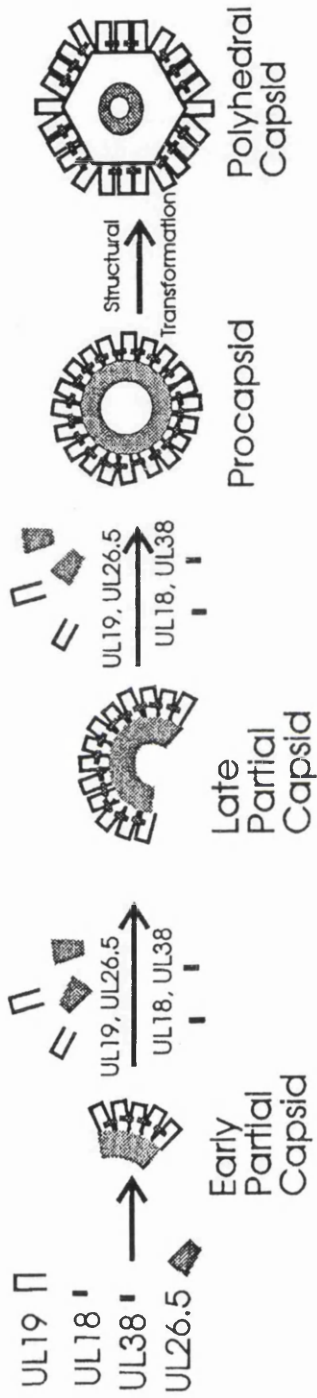


Fig. 1.14: Schematic representation of the intermediate stages in HSV-1 capsid assembly

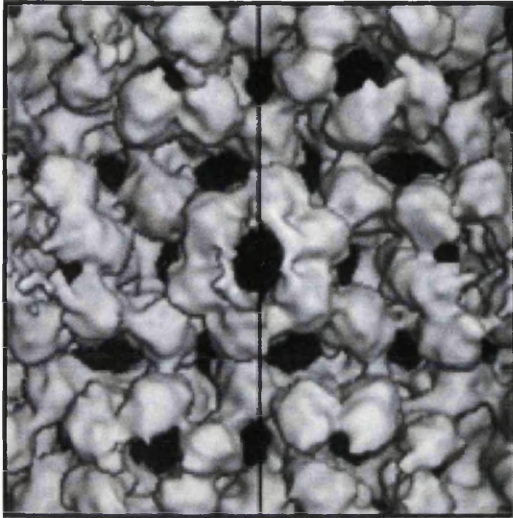
Following the localisation of capsid proteins to the nucleus capsid assembly begins with the formation of early, arc shaped, partial capsids. These early arcs enlarge to form late partial capsids which finally close to create a closed spherical particle or procapsid. The procapsid then undergoes maturation and angularises to form a mature polyhedral capsid. Only those gene products required for assembly are illustrated within the assembly pathway, namely VP5 (UL19), VP19c (UL38), VP23 (UL18), preVP22a (UL26.5). Diagram modified from Newcomb et al., (1996).

#### 1.9.4 The structure of the procapsid

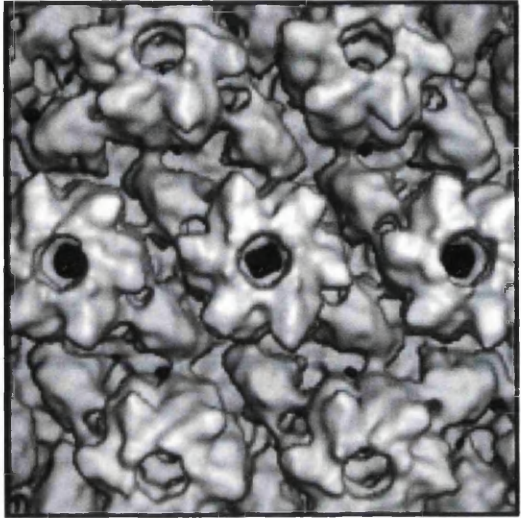
Cryo-EM analysis of procapsids to 27Å performed by Trus et al., (1996) revealed that procapsids were indeed spherical, and not polyhedral as with mature HSV-1 capsids, consisting of 162 capsomers lying on a T=16 icosahedral lattice. A large number of differences could be visualised between procapsids and mature polyhedral capsids. The most evident is that procapsid were more open and porous than mature capsids, with relatively little contact between the VP5 subunits within either the pentons or hexons except at their bases. The axial channels are fully open in both pentons and hexons with individual capsomers having no direct contact with surrounding capsomers. The capsomers are held together principally through the triplexes located at the local 3-fold axis of symmetry which appear more trimeric than the triplexes within mature polyhedral capsids. Large gaps are also evident within the procapsid floor which are absent from mature polyhedral capsids, indicating that capsid floor development occurs during capsid maturation and not initial assembly (see fig. 1.15). The hexons varied slightly in size within the procapsid and were not 6-fold symmetrical, but formed distorted oval (E-, and P-hexons) and triangular shaped (C-hexons) capsomers. The structure of the procapsid and procapsid maturation is discussed further in section 4.0.

#### 1.9.5 Identification of procapsids during HSV-1 infection

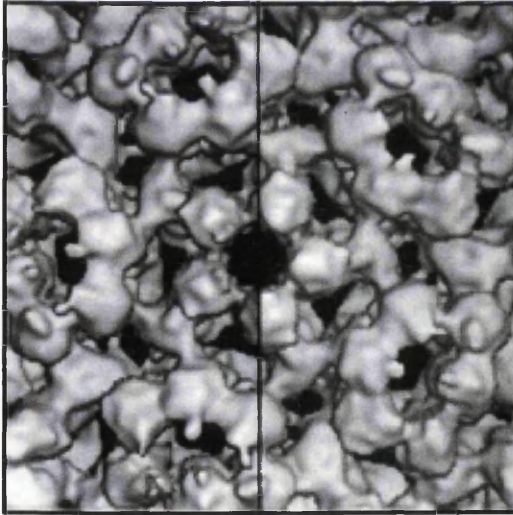
Initial *in vitro* observations that HSV-1 capsids assembled through a procapsid intermediate stage prompted analysis of HSV-1 infected cells to identify such an intermediate during the lytic reproductive cycle. Rixon and McNab (1999) demonstrated through the use of the HSV-1 *ts* mutant (*ts1201*) that capsids at the non-permissive temperature were cold sensitive and disassembled upon incubation at 0°C in the same manner as *in vitro* formed procapsids (Newcomb et al., 1996). *Ts1201* contains a *ts* lesion within the UL26 protease responsible for maturational cleavage of scaffold proteins (Addison et al., 1984). Infection of cells with *ts1201* at the non-permissive temperature results in the production of large cored B-capsids (B<sub>LC</sub>-capsids) containing uncleaved scaffold core. Downshifting *ts1201* B<sub>LC</sub>-capsids to their permissive temperature results in the reactivation of the protease and subsequent cleavage of the scaffolding proteins. These particles can then go on to mature into A-, B-, and C-capsids, and finally mature virions if



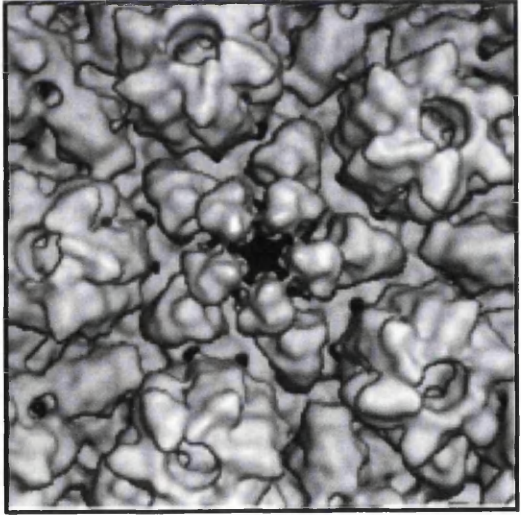
(A)



(B)



(C)



(D)

Fig. 1.15: Structural changes that accompany HSV-1 procapsid maturation

Cryo-EM reconstruction to 18Å of procapsids before (panels A and C) and after (panels B and D) maturation. Procapsids were isolated from *m100* infected cells (see section 1.9.5 for details). The outer shell surface is shown in each instance. Panels A and B represent protein masses surround the E-hexon. Panels C and D represent protein masses surrounding the penton. In the left hand side of panels A and C the less ordered density represents the protein mass associated with the monoclonal antibody utilised in procapsid precipitation (computationally removed in the right hand side of panels A and C). Procapsids demonstrate a more open and porous nature compared to that of the mature capsid with little intercapsomer connections other than through the triplexes located at the 3-fold axis of symmetry. The floor of the capsid remains undefined within the procapsid compared to that of the mature capsid. Triplexes also appear more Y-shaped than in the mature capsid where they form their unique asymmetric connections between their respective hexon and penton capsomers (picture modified from Newcomb et al., 2000).

the infection is left to proceed (Preston et al., 1983; Addison et al., 1990). Downshifting B<sub>LC</sub>-capsids to their permissive temperature resulted in the loss of their cold sensitive phenotype in the same manner as those *in vitro* purified procapsids that were allowed to angularise. Through the use of HSV-1 *ts1201* mutant Rixon and McNab (1999) concluded that the procapsid had a biologically relevant role within the virus life cycle. They also speculated that the cleavage of the scaffold may be directly responsible for procapsid maturation and that, as B<sub>LC</sub>-capsids capsids can mature into DNA containing C-capsids, DNA packaging may occur during the procapsid state. Newcomb et al., (1999) went on to isolate procapsids from cells infected with a HSV-1 mutant *m100*, which was deficient in the protease, and a second HSV-1 mutant *tsProt.A*, which (as with *ts1201*) contained a reversible temperature sensitive lesion within the protease. Isolated procapsids were shown by cryo-EM to be indistinguishable from those procapsids assembled *in vitro*. Furthermore, isolated procapsids from *tsProt.A* infected cells that were down shifted to their permissive temperature matured into polyhedral capsids identical to those isolated from WT HSV-1 infected cells.

#### 1.9.6 Other capsid assembly models

Although the general principles in HSV-1 capsid assembly are now becoming better understood, the precise mechanisms involved in the folding of proteins during the assembly of HSV-1 capsids remains largely unknown. As the HSV-1 capsid structure is determined to higher resolutions the greater the number of discrepancies away from the predicted quasi-equivalence structure become identified. Indeed, if individual protein subunits within capsomers can interact with their neighbouring subunits in a number of different bonding configurations, as depicted by quasi-equivalence or non-equivalent bonding, then in principle a myriad of “incorrect” capsid related structures as well as the “correct” capsid structure should be formed. However, capsid assembly appears to be universally economical in the production of effective structures that can package viral nucleic acid during the course of a normal infection. It is becoming increasingly evident that capsid subunits undergo a series of folding transitions as they assemble and polymerise into their respective native structures. Indeed, procapsid formation in some instances represents a late stage along the capsid protein folding-assembly pathway. For example, during P22 procapsid maturation little change in the secondary structure of

individual capsid protein subunits occurs but extensive changes in the packing of their respective side chains takes place upon maturation (Prevelige et al., 1993a; Tuma et al., 1998). Therefore, individual protein subunits of P22 represent partially folded proteins that only achieve their “true” native conformation within the mature capsid particle. Some of the principles involved in protein folding are discussed below in relation to P22 capsid assembly, one of the most comprehensively studied dsDNA viruses, in order to introduce terminology discussed elsewhere within this thesis and to provide a more general understanding of other capsid assembly pathways.

### *1.9.7 P22 capsid assembly*

The bacteriophage P22 is a dsDNA virus of *Salmonella typhimurium* (reviewed by Hendrix and Garcea, 1994; King and Chiu, 1997). The capsid assembly pathway of P22 has been extensively studied and is generally regarded as the prototype for capsid assembly in dsDNA bacteriophages (summarised schematically in fig. 1.16). Furthermore, the mechanisms involved in the protein folding pathways of individual capsid proteins have also been extensively studied.

The mature capsid of P22 is composed of 60 hexamers and 12 pentamers and conforms to T=7 icosahedral symmetry. The capsomers are linked by connecting arms which form 7 distinct intercapsomeric connections reflecting each of the T=7 quasi-equivalent environments (Prasad et al., 1993). The capsid has been shown to pass through a procapsid intermediate stage during which the scaffold core is removed and the viral dsDNA becomes packaged (Prevelige and King, 1993). The P22 procapsid is composed of 420 47kDa coat protein subunits (gp5) surrounding a scaffold core of 300 34kDa subunits (gp8). Assembly initiates around the portal complex, composed of 12 copies of the 90kDa portal protein (gp1), located on an eventual 5-fold axis of symmetry. Following procapsid assembly additional minor capsid proteins attach to the capsid, including gp16, gp20, and gp7, which are required for the injection of the viral DNA into the new host following attachment. However, these proteins, and the portal complex, are dispensable for capsid assembly *in vitro* (Fuller and King, 1982; Prevelige et al., 1988; Prevelige et al., 1993a). The P22 procapsid, like the HSV-1 procapsid (described above), is spherical and contains holes at the 6-fold axes that are absent within the mature P22 capsid (Prasad et al., 1993;

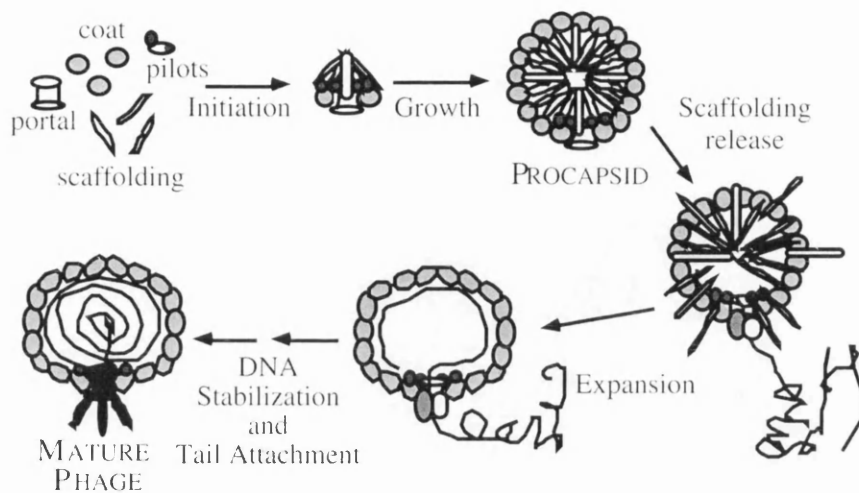


Fig. 1.16: Schematic illustration of the capsid assembly pathway of the bacteriophage P22

Assembly initiates by multiple copies of the coat protein (gp5) and scaffold protein (gp8) locating around the portal complex (composed of 12 copies of gp1). Further polymerisation of the capsid shell continues by subsequent addition of coat proteins surrounding a scaffold core until a closed spherical particle, the procapsid, is formed with T=7 icosahedral symmetry. Addition pilot proteins (gp16, gp20, and gp7) are subsequently added and the scaffold protein is released through holes in the procapsid structure. Scaffold proteins can be utilised for future rounds of assembly. The dsDNA is packaged into the procapsid and the portal closed by the addition of gp4, gp10, and gp26. The procapsid subsequently undergoes maturation and expansion increasing in diameter by ~10% and becoming more polyhedral. Tail attachment represents the final stage in assembly. Diagram reproduced from Zhang et al., (2000).

Zhang et al., 2000). The capsomers appear skewed in comparison to their larger and more regular mature form. The holes are thought to be the sites at which the internal scaffold protein exits the procapsid prior to or during maturation (Greene and King, 1994). Maturation is thought to be initiated by the packaging of the DNA genome through the portal complex and results in a 10% expansion in the total volume of the capsid in an ATP dependent manner (Earnshaw and Casjens, 1980; Galisteo and King, 1993). However, scaffold release can be triggered *in vitro* by treating procapsids with low concentrations of denaturants or by mild heating (Fuller and King, 1981; Prevelige et al., 1988; Galisteo and King, 1993). During maturation the most extensive conformational transformations to occur are around the trimer clusters, termed the trimer tips, located at the strict 3-fold axes on the procapsid inner surface. The trimer tips have been shown to be the positions at which the scaffold binds on the inner surface of the procapsid. As a consequence this implicates the scaffold protein not only in the assembly of the P22 capsids but also directly in the maturation of the capsid during DNA packaging (Zhang et al., 2000).

Interestingly, unlike HSV-1, the scaffold of P22 does not undergo any proteolytic cleavage and can therefore go on to aid the assembly of other P22 procapsids following its release (King and Casjens, 1974). The efficient release of scaffold proteins from the interior of the procapsid is thought to be due to its flexible nature (Tuma and Thomas, 1997).

#### *1.9.8 The molten globule-like characteristics of the P22 scaffold protein (gp8)*

Recent characterisation of gp8 by Tuma and Thomas (1997) demonstrated that the scaffold protein contains a high degree of  $\alpha$ -helical secondary structure but contains little measurable tertiary structure. Such characteristics are indicative of molten globule proteins, proteins that are in an intermediate stage of protein folding. The concept of molten globular proteins was originally introduced to describe equilibrium intermediates in protein folding pathways (reviewed by Ptitsyn, 1995a; Privalov, 1996). Molten globular proteins usually have a relatively compact and near native conformation, with much of their secondary structural features, in particular  $\alpha$ -helices, having been formed. However, molten globules typically contain little defined tertiary structure due to an absence in the packing of amino acid side chains and terminal loops. Such folding characteristics give

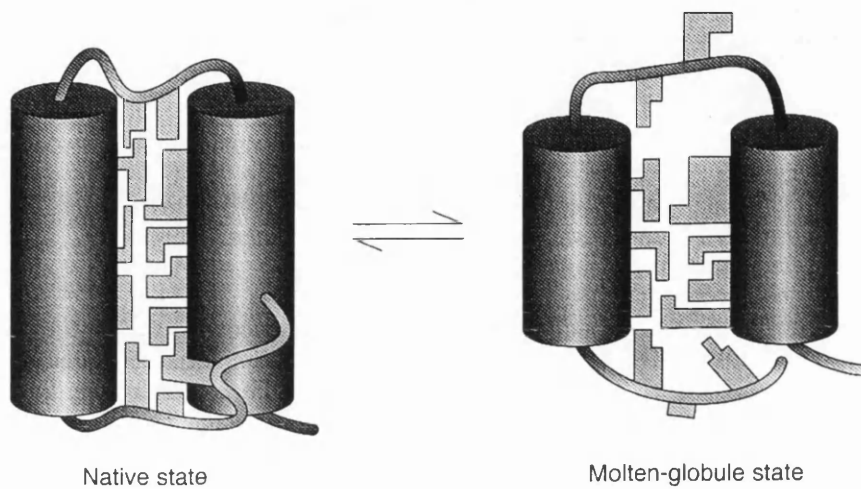


Fig. 1.17: Diagrammatic representation of a molten-globule state.

The molten globule contains the overall structural features of its native state, in particular secondary structural elements such as  $\alpha$ -helices (represented by shaded cylinders), but lacks tertiary structural features through the looser packing of amino acid side chains (represented by shaded blocks) and greater mobility of loops and ends of protein chains (represented by shaded lines). Diagram reproduced from Ptitsyn (1995).

these proteins a large amount of domain flexibility (the molten globule-like state is schematically illustrated in fig. 1.17).

The native molten globule-like character of gp8 is likely therefore to play a fundamental role in the scaffold exit from procapsids, since an elongated and flexible gp8 molecule could exit through the 25Å holes present at the 6-fold axes of symmetry. The lack of a rigid tertiary core would therefore make exiting these holes relatively easy. The interaction between the highly  $\alpha$ -helical structure of gp8 is thought to be stabilised by the highly  $\beta$ -stranded nature of the gp5 coat protein. Their interaction stabilises the  $\alpha$ -helical nature of gp8, and provides sufficient structure to form the procapsid shell (Tuma and Thomas, 1997). The onset of DNA packaging is thought to disrupt this balance causing the scaffold protein to exit the procapsid shell resulting in the initiation of maturation.

The molten globule-like nature of other proteins are discussed in relation to the findings within this thesis in sections 3.0 and 4.0.

# Chapter 2

## Materials & Methods

## 2.1 Materials

### 2.1.1 Chemicals

Chemicals and reagents used for EM analysis were purchased from either Agar Aids or TAAB laboratories. All other chemicals and reagents were purchased from either Sigma Chemical Company or BDH chemicals UK unless otherwise stated below or in subsequent sections:

<u>Chemical</u>	<u>Supplier</u>
Acetic acid	Rhone-poulenc Ltd
Ammonium hydroxide	Fisons
Ampicillin	Beecham Research Laboratories Ltd
APS (ammonium persulphate)	Aldrich
Butanol	Prolabo
Chloroform	May and Baker Ltd
Citifluor	Citifluor Ltd
Complete Protease Inhibitors	Boehringer Mannheim
Coomassie Brilliant Blue	Aldrich
DMSO (dimethyl sulphoxide)	Koch-Light Laboratories Ltd
dNTPs	Pharmacia
ECL	Amersham Pharmacia Biotech UK Ltd
Ethanol (ultra pure)	Joseph Mills Ltd
Formaldehyde and formamide	Fluka
Glacial acetic acid	Prolabo
Gluteraldehyde	Agar Scientific Ltd
Glycerol	Prolabo
Hydrochloric acid	Rhone-poulenc Ltd
IPTG	Gibco-BRL
Isopropanol	Prolabo
Methanol	Joseph Mills Ltd
Nitro-cellulose membrane	Hybond
Octyl- $\beta$ -glucoside	Pierce
Rainbow Markers™	Amersham Pharmacia Biotech UK Ltd
S.O.C.	Gibco-BRL
TEMED (N,N,N',N'-tetramethylethylene)	Aldrich

- Radiochemicals

ChemicalSupplier[<sup>35</sup>S]-L-methionine (10 $\mu$ Ci/ $\mu$ l)

Amersham

## 2.1.2 Enzymes

All enzymes and their appropriate buffers were purchased either from Boehringer Mannheim, Gibco-BRL, or New England Biolabs (NEB).

## 2.1.3 Oligonucleotides

All oligonucleotides were synthesised in house (MRC Institute of Virology, Glasgow) by D. McNab or A. Orr on a Biosearch 8600 DNA synthesiser.

## 2.1.4 Tissue culture

- *Spodoptera frugiperda* 21 (SF21) insect cells were derived from Ovarian tissue (Vaughn et al., 1977). SF21 cells were cultured in TC100/5 medium which consists of TC100 medium (Gibco/BRL) supplemented with 5% foetal calf serum (FCS) (Gibco/BRL) and 1% P/S (1000 units/ml penicillin, 10mg/ml streptomycin) (Gibco/BRL).
- Baby hamster kidney-21 C13 (BHK-21 C13) fibroblast cells were derived from baby hamster's kidney (MacPherson and Stoker, 1962). BHK-21 C13 cells were cultured in ETC/10 medium which consists of Glasgow-modified Eagles medium (GMEM) (Gibco-BRL) supplemented with 10% (v/v) tryptose phosphate broth, 10% newborn calf serum (NCS) (Gibco-BRL) and 1% P/S.

Variation: EMC/10 – Eagles medium containing 1% carboxymethyl cellulose and 10%NCS

- Vero cells were derived from African green monkey's kidney. Vero cells were grown in MEM/10 medium which consists of Dulbecco's modified Eagle's medium (DMEM)

(Gibco-BRL) supplemented with 10% FCS and 1% P/S. G5-11 cells (UL18 complementing Vero cell line) was a kind gift from P. Desai (Desai et al., 1993). G5-11 cells were grown in MEM/10.

### 2.1.5 Viruses

- Baculoviruses: *Autographica californica* nuclear polyhedrosis virus (AcNPV) and a polyhedrin negative derivative which has a *lacZ* gene under the control of the polyhedrin promoter (AcPAK6) were both gifts to the MRC Institute of Virology (Glasgow) from R. Possee.
- HSV-1 UL18 null mutant virus (K23Z) was a kind gift from P. Desai (Desai et al, 1993).

### 2.1.6 Bacterial culture medium

All bacteria were cultured using Lauria-Bertani medium (LB) described below:

<u>Medium</u>	<u>Composition</u>
L-Broth (pH7.5):	10g/l NaCl, 10g/l bactopectone, 5g/l yeast extract
L-Broth agar	L-Broth + 1.5% agar
Supplemented antibiotics:	Ampicillin (50µg/ml), Kanamycin (25µg/ml)

### 2.1.7 Bacteria

- *E.coli* BL21 (DE3) pLysS: Commercially available bacterial cells (Promega) used for protein expression vectors under the control of the T7 promoter, for example pET28a.
- *E.coli* DH5α: Used for the maintenance and propagation of plasmid DNA.

- *E.coli* CJ236 *dut<sup>-</sup> ung<sup>-</sup>*: Commercially available bacteria (New England Biolabs) used in site directed mutagenesis to produce uracil enriched ssDNA plasmid DNA (Kunkel et al., 1985).
- *E.coli* GM48 *dam<sup>-</sup> dcm<sup>-</sup>*: Commercially available bacterial cells (New England Biolabs) used in the preparation of unmethylated DNA.

### 2.1.8 Yeast culture medium

Yeast were cultured using either YPD medium or synthetic dropout (SD) medium (Clontech) supplemented with the appropriate 10X dropout (DO) amino acid powder mix (Clontech) described below:

<u>Medium</u>	<u>Composition</u>
YPD (pH5.8)	20g/L Bacto peptone (Difco) + 10g/L Yeast extract (Difco), 20g/L Dextrose
YPD agar	YPD + 20g/L agar
SD	26.7 g/L Minimal SD base + DO (Clontech)
SD agar	46.7g/L Minimal SD agar base + DO (Clontech)
10X DO supplement:	- <i>Leu</i> (0.69g/L), - <i>Trp</i> (0.74g/L), - <i>Leu</i> - <i>Trp</i> (0.64g/L), - <i>Leu</i> - <i>Trp</i> - <i>Ura</i> (0.62g/L) (Clontech)

### 2.1.9 Yeast

- MaV103: Yeast strain used in all experiments, characterised in section 3.1. Gift from M. Vidal (Vidal et al., 1996a).
- MaV103pPc97UL38: MaV103 cells transformed and propagated with the pPc97 GAL4 DB fusion vector containing UL38. Used in the selection of FOA resistant colonies.

### 2.1.10 Plasmids

- pAcAB3: Commercially available (Pharming) baculovirus transfer vector
- pCMV<sub>10</sub>: Transient expression plasmid containing the immediate early promoter of HCMV and the RNA processing signals of SV40 (Stow et al., 1993).
- pET28a(+): Commercially available expression plasmid (Novagen) containing T7 RNA polymerase promoter.
- pPc86: Yeast expression plasmid containing a GAL4 activation domain (AD) downstream of the multicloning site. Gift from M. Vidal (Chevray and Nathans, 1992).
- pPc97: Yeast expression vector containing a GAL4 DNA binding (DB) domain downstream of the multicloning site. Gift from M. Vidal (Vidal et al., 1996a).

### 2.1.11 Antibodies

- Penta His antibody: Commercially available (Qiagen) mouse monoclonal antibody used against 6xHis epitope tagged proteins.
- 187: Rabbit polyclonal antibody used against VP23 protein in HSV-1, gene product of UL18. Gift from David McClelland.
- TrpE/VP19c: Rabbit polyclonal antibody used against VP19c protein in HSV-1, gene product of UL38. Antibody produced against TrpE- VP19c fusion peptides. Gift from W. Wold (Yei et al., 1990).
- GAM-HRP: Commercially available (Sigma) goat anti-mouse conjugated to horse radish peroxidase used in Western blots.

- FITC-GAM: Commercially available (Sigma) goat anti-mouse antibody conjugated to fluorescein isothiocyanate used in immunofluorescence studies.
- Cy3-GAR: Commercially available (Amersham Pharmacia Biotech) goat anti-rabbit antibody conjugated to Cy3 used in immunofluorescence studies.

### 2.1.11 Buffer and solutions

Some of the commonly used buffers and solutions are detailed below:

- Commonly used buffers:

<u>Buffer/Solution</u>	<u>Composition</u>
PBSa	170mM NaCl, 3.4mM KCl, 10mM Na <sub>2</sub> HPO <sub>4</sub> , 1.8mM KH <sub>2</sub> PO <sub>4</sub> (pH7.2)
PBScomplete	PBSa + 6.8 mM CaCl <sub>2</sub> , 4.9mM MgCl <sub>2</sub>
PBSa/T	PBSa, 0.05% Tween-20
PBSa/TN	PBSa/T, 5% NCS (Gibco-BRL)

- DNA manipulation:

<u>Buffer/Solution</u>	<u>Composition</u>
Phenol/chloroform (1:1)	Mixed phenol/chloroform (1:1) saturated with 10mM Tris (pH8.0)
Solution 1	25mM Tris (pH8.0), 10mM EDTA, 50mM glucose
Solution 2	0.2M NaOH, 1% SDS
Solution 3	150mM NaCl, 15mM trisodium citrate (pH7.5),
Loading buffer	40% sucrose, 0.25% bromophenol blue, 0.25% xylene cyanol
TBE	89mM Tris (pH8.0), 89mM boric acid, 2mM EDTA
TAE	20mM Tris (pH7.5), 0.5M NaCl, 1mM EDTA
TM buffer	200mM Tris (pH8.0), 50mM MgCl <sub>2</sub>

- Yeast solutions:

<u>Buffer/Solution</u>	<u>Composition</u>
10X TE	100mM Tris-HCl, 10mM EDTA (pH7.5)
10X LiAc	1M lithium acetate
50% PEG 4000	50g PEG 4000 per 100ml of dH <sub>2</sub> O
1X TE/LiAc	1:10 dilution of 10X TE + 10X LiAc
PEG/LiAc/TE solution	8:1:1 mix of 50% PEG 4000:10X LiAc:10X TE
Z-buffer	8.52g/L Na <sub>2</sub> HPO <sub>4</sub> , 5.5g/L NaH <sub>2</sub> PO <sub>4</sub> , 0.75g/l KCl, 0.246g/L MgSO <sub>4</sub> (pH7.0).
X-gal (20mg/ml) stock	100mg of X-gal made up in 5ml DMSO
Z buffer/X-gal Solution	100ml Z-buffer, 0.27% β-mercaptoethanol, 1.67ml X-gal stock solution
Yeast plasmid lysis solution	2% Triton X-100, 1% SDS, 100mM NaCl, 10mM Tris-HCl (pH8.0), 1mM EDTA
TCA buffer	20mM Tris-HCl (pH8.0), 50mM Ammonium acetate, 2mM EDTA

- Tissue culture:

<u>Buffer/Solution</u>	<u>Composition</u>
TBS	20mM Tris-HCl (pH7.5), 500mM NaCl
Trypsin	TBS, 0.25% (w/v) trypsin, 0.0002% phenol red
Versene	PBSa, 600mM EDTA, 0.0002% phenol red

- SDS-PAGE:

<u>Buffer/Solution</u>	<u>Composition</u>
BM	40% SGB, 10% glycerol, 4.75% β-mercaptoethanol, 2% SDS, 0.01% bromophenol blue
RGB	0.74M Tris-HCl (pH8.0), 1% SDS
SGB	0.122M Tris-HCl (pH6.7), 0.1% SDS
Tank buffer	52mM Tris, 53mM glycine, 0.1% SDS
Coomassie Brilliant Blue	Methanol:H <sub>2</sub> O:acetic acid (50:880:70), 0.2% Coomassie Brilliant Blue R250
Destain	Methanol:H <sub>2</sub> O:acetic acid (50:880:70)

- Western blotting:

<u>Buffer/Solution</u>	<u>Composition</u>
Transfer buffer	40mM Tris, 48mM glycine, 20% methanol, 0.4% SDS
Stripping buffer	100mM $\beta$ -mercaptoethanol, 2% SDS, 62.5 mM Tris pH6.7
PBS/T	PBSa, 0.05% Tween-20
Blocking buffer	PBS/T, 5% Marvel milk powder

- Common purification buffers:

<u>Buffer/Solution</u>	<u>Composition</u>
Sonication buffer	20mM Tris, 10% glycerol, 0.1% NP40
G-150 buffer	20mM Tris (pH8.0), 150mM NaCl, 0.1% Tween-20
Buffer O	150mM $\text{Na}_2\text{HPO}_4$ (pH7.5), 0.1% glycerol, 0.1% Octyl- $\beta$ -glucoside
Buffer OL	Buffer O, 0.1% NP40, 150mM NaCl
Buffer OG	Buffer O, 5% glycerol
Buffer P	20mM $\text{Na}_2\text{HPO}_4$ (pH7.5), 0.004% NP40

## 2.2 Methods

### 2.2.1 Recombinant DNA manipulation

#### 2.2.1.1 Preparation of electrocompetent bacteria

50ml of pre-warmed L-broth was inoculated with approximately 10 $\mu$ l of a glycerol stock of DH5 $\alpha$  or BL21 DE3 bacteria and incubated o/n in an orbital shaker at 37°C. This 50ml starter culture was used to inoculate 1 litre of pre-warmed L-broth media in a 2 litre flask and incubated at 37°C in an orbital shaker until the OD<sub>630nm</sub> reached 0.5-0.6. The culture was transferred to the appropriate number of pre-chilled 250ml Falcon tubes and allowed to chill on ice for 5 minutes. Bacteria were pelleted by centrifugation at 3500 r.p.m. for 15 minutes at 4°C in a Sorvall RT7 centrifuge. The supernatant was removed and the individual bacterial pellets were resuspended in ice-cold dH<sub>2</sub>O to a final volume of 160ml before being pelleted by centrifugation (as described above). The supernatant was removed and the individual bacterial pellets were combined by progressive resuspension in ice-cold dH<sub>2</sub>O to a final volume of 500ml. Bacteria were pelleted (as described above), the supernatant removed, and the pellet resuspended in 40ml of ice-cold dH<sub>2</sub>O containing 10% sterile glycerol. The culture was transferred to a pre-chilled 50ml (SS-34) tube and the bacteria pelleted at 6,000 r.p.m. for 15 minutes at 4°C in a Sorvall SS-34 rotor. The supernatant was removed and the pellet resuspended in 2ml of ice-cold dH<sub>2</sub>O containing 10% sterile glycerol, aliquoted (80 $\mu$ l) into pre-chilled 1.5ml reaction vials and frozen on dry ice before being stored at -70°C.

#### 2.2.1.2 Transformation of electrocompetent bacteria

Typically 1-3 $\mu$ l of DNA was mixed with approximately 80 $\mu$ l of electrocompetent bacteria and electroporated using a Hybond cell shock electroporator (following the manufacturers guidelines) in a 0.1cm gene pulser<sup>®</sup> cuvette (Bio-Rad). Following electroporation the bacteria were resuspended in 1ml of ultrapure S.O.C. medium (Gibco-BRL), and incubated a 37°C for 45 minutes in an orbital shaker. 50-200 $\mu$ l of this culture was plated out onto an

L-Broth agar plate containing the appropriate antibiotic and incubated o/n at 37°C. Single colonies were used to generate starter cultures.

#### *2.2.1.3 Glycerol stock preparation*

For long term storage of bacteria containing recombinant plasmids, 1.5ml of a bacterial starter culture was centrifuged at 6,500 r.p.m. for 1 min at RT in a microfuge. The culture supernatant was removed and the cell pellet was resuspended in 1ml of a sterile mixture consisting of 80% glycerol and 20% bactopectone. Glycerol stock cultures were subsequently frozen on dry ice and stored at -70°C.

#### *2.2.1.4 Small scale plasmid DNA isolation*

Small scale DNA preparations were performed using the alkaline lysis method (described by Maniatis et al., 1982). Briefly, 1.5ml of bacterial starter culture, grown from a single bacterial colony, was centrifuged at 6,500 r.p.m. for 1 minute at RT in a microfuge. The culture supernatant was removed and the cell pellet was resuspended in 100µl of ice-cold solution 1 (see Materials for solution details) and incubated for 5 minutes at RT. 200µl of freshly prepared solution 2 was added to the mixture and briefly vortexed before 150µl of ice-cold solution 3 was added. The mixture was briefly vortexed and incubated on ice for 5 minutes. The resulting white precipitate, consisting of cell debris, was pelleted by centrifugation at 14,000 r.p.m. for 5 minutes at RT in a microfuge. The supernatant was removed and the DNA recovered by phenol/chloroform extraction and ethanol precipitation (described below). DNA pellets were typically resuspended in 30µl of dH<sub>2</sub>O containing 10µg/ml of RNaseA.

#### *2.2.1.5 Phenol/chloroform extraction and ethanol precipitation of DNA*

If the volume of the original DNA solution was <200µl then the volume was brought up to 200µl by the addition of dH<sub>2</sub>O. An equal volume of phenol/chloroform (1:1) was added to the DNA solution and briefly vortexed before being centrifuged at 13,000 r.p.m. for 5 minutes at RT in a microfuge and the upper aqueous phase removed. If the aqueous phase appeared cloudy then the phenol/chloroform extraction was repeated until the aqueous

phase appeared clear. The DNA was precipitate by the addition of a 1/10<sup>th</sup> volume of 3M sodium acetate and 2 volumes of 100% ethanol. The mixture was vortexed and incubated for 20 minutes on dry ice. Precipitated DNA was pelleted by centrifugation at 13,000 r.p.m. for 5 minutes at RT in a microfuge. DNA pellets were washed in approximately 200-500µl of 70% ethanol to remove excess salts and the DNA pelleted by centrifugation at 13,000 r.p.m. for 5 minutes at RT DNA pellets were allowed to air dry before being resuspended in the appropriate volume of dH<sub>2</sub>O containing 10µg/ml RNaseA and stored at -20°C until required.

#### *2.2.1.6 Large scale plasmid DNA isolation*

Either a single colony from an L-broth agar plate or approximately 10µl of glycerol stock was used to inoculate 10ml of pre-warmed L-broth containing the appropriate antibiotic. This was incubated for 4-8 hours in an orbital shaker at 37°C and used to inoculate 100ml of pre-warmed L-broth (containing the appropriate antibiotic) in a 500ml flask. This bacterial culture was incubated o/n in an orbital shaker at 37°C. Cultures were transferred to 50ml (SS-34) tubes and the bacteria pelleted by centrifugation at 6,000 r.p.m. for 10 minutes at 4°C in a Sorvall SS-34 rotor. The supernatant was discarded and the DNA was extracted using a Qiagen midi prep kit following the manufacturer's guidelines (Qiagen).

#### *2.2.1.7 Restriction endonuclease digestion of DNA*

Restriction digests were carried out in the buffer and at the temperature specified by the manufacturer. The number of units of enzyme used was dependent upon the concentration of DNA, typically 10 units/1 µg of DNA. If the DNA was to be dephosphorylated then 1 unit of calf intestinal phosphatase (CIP) was added to the reaction mixture following digestion and incubated for an additional hour at 37°C. In situations where double restriction digestions were required and the buffer specifications were incompatible, the DNA was phenol/chloroform extracted and ethanol precipitated (as described in section 2.2.1.5) following the first digestion and resuspended in dH<sub>2</sub>O before the second digestion was carried out in the appropriate buffer.

### *2.2.1.8 Analytical DNA agarose gel electrophoresis*

DNA that was to be analysed was mixed with a 1/5<sup>th</sup> volume of loading buffer and loaded onto a horizontal (10cm by 11cm) 1% agarose gel made in 1x TBE containing EtBr (0.5 µg/ml). 1kb or 100bp size markers (Gibco-BRL) of known concentrations were run alongside the sample DNA in order to estimate fragment sizes. Electrophoresis was carried out with the gel submerged in 1x TBE at 75V for approximately 30-45 minutes. DNA was visualised using a short wave UV transilluminator and photographed using a digital camera.

### *2.2.1.9 Purification of DNA from agarose*

DNA fragments that were required for cloning procedures were purified from 1% agarose gels made in 1x TAE containing EtBr (0.5µg/ml). Electrophoresis was carried out (as described in section 2.2.1.8) with the gel submerged under 1x TAE buffer. The DNA was visualised using a long wave UV transilluminator in order to prevent UV nicking. The appropriate DNA band(s) was excised from the gel using a sterile disposable scalpel and placed into the appropriate number of 1.5ml reaction vials. DNA was extracted from the agarose by a Qiaquick gel extraction kit (Qiagen) following the manufacturer's guidelines. Extracted DNA was checked for its integrity by analysing it on a 1% agarose gel run in 1x TBE buffer (as described in section 2.2.1.8).

### *2.2.1.10 DNA ligation*

Vector and insert were digested with the relevant restriction endonucleases and purified. To prevent the vector from self-annealing it was typically treated with 1 unit of CIP per µg of DNA following the endonuclease digestion. DNA fragments were mixed at a vector to insert ration of 1:3 in the presence of 1x ligation buffer (Gibco-BRL) and 1 unit of T4 DNA ligase (Gibco-BRL) in a total volume of 20µl. The ligation mixture was incubated either at RT for 5 hours or o/n at 15°C. The DNA was subsequently electroporated into the appropriate electrocompetent bacteria or frozen at -20°C until required.

### 2.2.1.11 Linker ligation

If the cloning strategy required the addition of non-phosphorylated oligonucleotide linkers to a blunt ended recombinant DNA molecule then essentially the same procedure was carried out as described in section 2.2.1.10. Oligonucleotide linkers were used in a 50-fold molar excess over that of the blunt ended recombinant DNA molecule. DNA were blunt ended by the addition of dNTPs (50 $\mu$ M/dNTP) and 2 units of DNA polymerase I Klenow to digestion mixtures and incubated for an additional 20-30 minutes at 37°C.

### 2.2.1.12 Oligonucleotide purification

Synthetic oligonucleotides were prepared using a Biosearch 8600 DNA synthesiser courtesy of D. McNab and A. Orr.

The oligonucleotides were eluted from the preparation column over a period of approximately 60 minutes in 1.5ml of concentrated ammonium solution (Fisons). The ammonia/oligonucleotide solution was then transferred to a 1.5ml screw cap reaction vial and incubated for 5 hours at 55°C before being placed on ice for approximately 2 minutes. The solution was then aliquoted into 4 equal volumes in 1.5ml reaction vials and the ammonia solution removed by o/n evaporation in a rotary evaporator. The dried oligonucleotides were stored at -20°C until required.

### 2.2.1.13 PAGE of synthetic oligonucleotides.

Oligonucleotide pellets were resuspended in 100 $\mu$ l of a 1:1 mix of dH<sub>2</sub>O/formamide. Typically 25 $\mu$ l of the resuspended pellet was loaded on to a 10% Sequagel (National diagnostics) in 0.5% TBE. 10 $\mu$ l of loading dye (containing 0.5% (x/v) xylene cyanol and 0.5% (w/v) Bromophenol blue) was loaded into a neighbouring well to act as migration markers. The gel was electrophoresed in 0.5x TBE buffer at 50mA until the Bromophenol dye front had migrated to the bottom of the gel.

Following electrophoresis the gel was transferred on to cling film and the DNA visualised by short wave UV radiation. The oligonucleotides would appear as a dark band against an

imager enhancer screen. The area of which was marked in the gel using a sterile scalpel. The band was excised from the acrylamide gel in the absence of UV radiation and transferred to a universal bottle containing 3ml of dH<sub>2</sub>O. The oligonucleotides were allowed to diffuse from the gel slice by incubating the gel in the dH<sub>2</sub>O o/n at 37°C in an orbital shaker. The oligonucleotide solution was transferred to a 10ml snap cap tube and the DNA recovered by phenol/chloroform extraction and ethanol precipitation. Oligonucleotide pellets were typically resuspended in 100µl of dH<sub>2</sub>O and stored at -20°C until required. The concentration of the oligonucleotide was measured by absorbance at OD<sub>260</sub> (1 OD<sub>260</sub> unit = 20µg of ssDNA).

### 2.2.2 M13 phage site directed mutagenesis of UL18.

A modified version of the Kunkel method (Kunkel et al., 1985) was used to generate a panel of cysteine UL18 mutants. The specific oligonucleotides used during the mutagenesis are described in section 3.3. The stages involved in the mutagenesis are described below.

#### 2.2.2.1 Preparation of uracil enriched pETUL18 ssDNA

Electrocompetent CJ236 *dut<sup>-</sup> ung<sup>-</sup>* bacteria (NEB) were electroporated in the presence of 1µg of pETUL18 vector DNA and plated out on L-broth agar plates containing kanamycin (50µg/ml), as described in section 2.2.1.2. A single recombinant colony was used to inoculate 10ml of pre-warmed L-broth (containing 50µg/ml of kanamycin and 100µg/ml of uridine) and incubated o/n at 37°C in an orbital shaker. This starter culture was used to inoculate 200ml of pre-warmed L-broth (containing 50µg/ml of kanamycin and 100µg/ml of uridine) in a 2 litre flask and incubated at 37°C for an additional 30 minutes in an orbital shaker. This culture was infected with 10<sup>11</sup> p.f.u./flask of M13 R408 bacteriophage (Promega) which was incubate for a further 9 hours at 37°C. The bacteria were pelleted by centrifugation at 9,000 r.p.m. for 10 minutes at 4°C in a SS-34 rotor. The supernatant was transferred to a sterile 500ml GSA bottle and 0.25 volumes of a mixture containing 20% PEG 6000 in 2.5M NaCl was added, mixed by inversion, and incubated on ice for 30 minutes. The bacteriophage were pelleted by centrifugation at 12,000 r.p.m. for 15

minutes at 4°C in a SLA-3000 rotor. The supernatant was carefully removed and the phage pellet resuspended in 5 ml of the supernatant media. The resuspended phage were transferred to a 50 ml (SS-34) tube and pelleted by centrifugation at 7,000 r.p.m. for 15 minutes at 4°C in a SS-34 rotor. The supernatant was removed and the pellet resuspended in 2ml of 1x TE. This mixture was then transferred to a 10ml snap cap tube and an equal volume of phenol/chloroform was added and mixed for 1 hour on an end over end mixer with intermittent periods of vigorous vortexing. The mixture was then centrifuged at 4°C for 5 minutes at 3,000 rpm in a Sorvall RT7 centrifuge. The aqueous phase was removed to a fresh tube. The phenol/chloroform was re-extracted using 1ml of 1x TE. The aqueous phases were pooled and re-extracted with phenol/chloroform until the aqueous phase appeared clear. The DNA was precipitated by adding 80µl/ml of 4M NaCl, 50mM EDTA, and 2.5 volumes of 100% ethanol and incubating at -20°C for a minimum of 2 hours. The precipitated DNA was pelleted by centrifugation at 7,000 r.p.m. for 20 minutes at 4°C in a SM-24 rotor. The supernatant was removed and the phage DNA resuspended in 100µl of dH<sub>2</sub>O and stored at -20°C until required.

#### 2.2.2.2 Oligonucleotide mutagenesis

A series of oligonucleotides (sequences detailed in section 3.3) were phosphorylated in 1x kinase buffer (Gibco-BRL) containing 20mM ATP + 2 units T4 kinase (Gibco-BRL) and were incubated for 40 minutes at 37°C. The reaction mixture was heat inactivated at 70°C for 10 minutes and stored at -20°C until required.

Approximately 1.0µg of phosphorylated oligonucleotides were annealed separately to 0.5µg of the uracil enriched ssDNA by heating the mixture in a hot block to 70°C and allowing the block to cool naturally to RT. 30µl of a solution containing 1x ligation buffer (Gibco-BRL), 0.5 units of T4 ligase (Gibco-BRL), and 0.5 units of T7 polymerase (Gibco-BRL), was added to the annealed DNA. Samples were incubated for 1 hour at RT followed by an additional 1 hour at 37°C. The DNA was then phenol/chloroform extracted and ethanol precipitated (as described in section 2.2.1.5), resuspended in 20µl of dH<sub>2</sub>O and stored at -20°C until required.

The DNA was electroporated into electrocompetent DH5 $\alpha$  bacteria (as described in section 2.2.1.2) and individual colonies analysed for oligonucleotide incorporation by restriction mapping (as described in section 3.3). Those colonies that tested positive were subsequently sequenced in house on an ABI PRISM<sup>TM</sup> 377 DNA sequencer. 200ng of recombinant DNA was used per sequence analysis using commercially available T7 primers (Novagen). Correctly mutated plasmids were subsequently electroporated into electrocompetent BL21 DE3 bacteria and analysed for recombinant protein expression (as described in section 3.3).

### **2.2.3 Generation of monoclonal antibodies**

The production of monoclonal antibodies against the triplex proteins VP19c and VP23 was carried out in house by Susan Graham. BALB/c mice were immunised with recombinantly expressed and Ni-NTA agarose purified triplex proteins (described in section 3.2) following the protocol outline in table 2.2.1. Test bleeds were performed and analysed for the presence of anti-sera against the triplex proteins by quantitative ELISA analysis. Mice that had positive anti-sera against the triplex proteins were subsequently used in the production of hybridoma cell lines. Quantitative ELISA analysis and the production of hybridoma cell lines were carried out by Susan Graham. The supernatants from these cell lines were tested for their specific reactivity towards VP19c and VP23 by Western blot and immunofluorescence analysis (discussed in section 3.2).

Days post-immunisation	Immunisation/analysis details
1	Primary immunisation in FCA (20µg/triplex) SC
29	Boost in FIA (20µg/triplex) SC
43	Boost in FIA (20µg/triplex) SC
57	Boost in FIA (20µg/triplex) SC
64	Test bleed animals #1-4 – low ELISA titre (<1:50)
71	Boost in FIA (20µg/triplex) SC
86	Boost in FIA (20µg/triplex) SC
102	Final Boost in PBSa (200µg/triplex) IP
120	Test bleed animals #1-4. Fusion with spleen cells from animal #4
184	Boost in FIA (20µg/VP19cHis) SC
197	Boost in FIA (20µg/VP19cHis) SC
204	Test bleed animals #1-3
220	Final Boost in PBSa (200µg/VP19cHis) IP for animals #1 and #3
225	Fusion with spleen cells from animals #1 and #3
241	Final Boost in PBSa (200µg/VP19cHis) IP for animal #2
246	Fusion with spleen cells from animal #2

Table 2.2.1: Summary of the immunisation regime of BALB/c mice for the production of VP19c and VP23 monoclonal antibodies. Mice were initially immunised with purified triplexes (Ac18638) in FCA (Freund's complete adjuvant) and boosted in FIA (Freund's incomplete adjuvant). Following poor test bleed analysis by ELISA for VP19c, mice #1, #2, and #3 were subsequently immunised and boosted 184 days post-immunisation with VP19c denatured in urea (described in section 3.2.1). SC and IP denote subcutaneous and intraperitoneal injections respectively.

## 2.2.4 Immunofluorescence analysis

### 2.2.4.1 *Transfection of plasmid DNA*

13mm sterile coverslips were placed into limbro wells, seeded with BHK-21 C13 cells in ETC10 medium at  $1 \times 10^4$  cells/well and left to grow o/n at 37°C. In separate 15ml Falcon tubes, 1µg of plasmid DNA and 15µl of liposomes (Gibco-BRL) was mixed with 500µl of OPTIMEM (Gibco-BRL) and allowed to incubate for 15 minute at RT. The diluted liposomes were added to the DNA/OPTIMEM mixture, gently mixed by agitation, and allowed to incubate for a further 10 minutes at RT. Growth media was removed from the BHK-21 C13 cells and the cell monolayer (approximately 50% confluent) was washed in 1ml of serum-free OPTIMEM and drained thoroughly. 500µl of the liposome/DNA mix was added to each coverslip and incubated for 4 hours at 37°C before 500µl of ETC10 medium containing 10% FCS was added to each well and incubated for a further 16-24 hours at 37°C. The transfection mixture was then removed and the coverslips washed in PBSa before being fixed in pre-chilled methanol (-20°C). Coverslips were stored at -20°C in methanol until they were required for analysis.

### 2.2.4.2 *Immuno staining and microscopy analysis*

All incubations were carried out in a humidified chamber and all dilutions were made in PBSa/TN (PBSa, 0.05% Tween-20, 5% NCS (Gibco-BRL)). Using microscope forceps, coverslips were removed from the methanol and rehydrated in PBSa/TN for 10 minutes at RT. The coverslips were blotted dry and 50µl of the appropriately diluted primary antibody (see table 2.2.1) was added to each coverslip and incubated for 45 minutes at RT. Coverslips were then washed 3x by immersion in a beaker containing PBSa/TN and blotted dry between each wash. After the final wash the coverslips were blotted dry and 50µl of appropriately diluted secondary antibody was added and incubated for 45 minutes at RT. The coverslips were washed (as above) with a further 2 washes in dH<sub>2</sub>O. The coverslips were blotted dry and mounted cell side down onto a glass slide in Citifluor (approximately 10µl) and stored a 4°C in the dark until required. For long-term storage clear nail varnish was applied to the outer edge of the coverslip. Immunofluorescence

analysis was carried out on a Zeiss Axioplan fluorescence microscope. Photographs were taken using a mounted digital camera and edited using PhotoShop 3.1 software.

Antibody	Dilution
CB040 (MAb. VP23)	Neat
CB2017 (MAb. VP19c)	Neat
CB2032 (MAb. VP19c)	Neat
CB2034 (MAb. VP19c)	Neat
CB2040 (MAb. VP19c)	Neat
CB2064 (MAb. VP19c)	Neat
CB2068 (MAb. VP19c)	Neat
CB2184 (MAb. VP19c)	Neat
CB2231 (MAb. VP19c)	Neat
187 (PolyAb. VP23)	1:200
FITC	1:100
Cy3	1:100

Table 2.2.2: Summary of antibody dilutions used in immunofluorescence analysis.

## 2.2.5 Yeast manipulation

### 2.2.5.1 Glycerol stock preparation

In order to preserve the viability of yeast containing plasmid DNA constructs and for long term storage of yeast strains and isolates, 1.5ml of an o/n culture grown in the appropriate drop out medium (Clontech) was centrifuged at 6,500 r.p.m. for 1 minute at 4°C in a microfuge. The culture supernatant was removed and the cell pellet was gently resuspended in 1ml of 100% sterile glycerol, frozen on dry ice and stored at -70°C until required.

### *2.2.5.2 Transformation of plasmid DNA into yeast*

Yeast transformation was carried out following the method described in Clontech Matchmaker™ Two-Hybrid System product protocol manual which is briefly described below.

#### *2.2.5.2.1 Preparation of yeast cells*

A single colony, approximately 2-3mm in diameter, was used to inoculate 20ml of pre-warmed YPD medium and incubated o/n at 30°C in an orbital shaker. This starter culture was used to inoculate 300ml of pre-warmed YPD medium in a 1 litre flask to an OD<sub>600</sub> of 0.2. This culture was then incubated at 30°C in an orbital shaker for a further 3 hours before the yeast cells were transferred to a 250ml Falcon tube. The yeast cells were sedimented by centrifugation at 2,200 r.p.m. for 5 minutes at RT in a Sorvall RT7 centrifuge. The supernatant was removed and the cell pellet resuspended in 50ml of dH<sub>2</sub>O. The yeast cells were then pelleted (as described above), the supernatant removed, and the cell pellet resuspended in 1.5 ml of 1x TE/LiAc buffer (see Materials).

#### *2.2.5.2.2 Transformation of competent yeast cells*

0.1µg of the appropriate plasmid DNA and 100µg of salmon sperm carrier DNA (Sigma) were mixed in a 1.5ml sterile reaction vial. 100µl of competent yeast cells were added to each reaction vial, mixed thoroughly by pipetting, and 0.6ml of PEG/LiAc buffer (see Materials) was added. The reaction vials were placed into a 50ml Falcon tube and incubated for 30 minutes at 30°C in an orbital shaker. Following the incubation, 70µl of sterile DMSO was added to each reaction vial and gently mixed. The yeast cells were then heat shocked at 42°C for 15 minutes in a dry block before being transferred onto ice for 1 minute. The yeast cells were pelleted by centrifugation at 14,000 r.p.m. for 5 seconds at RT in a microfuge. The supernatant was removed and the cell pellets resuspended in 0.5 ml of 1x TE buffer.

### 2.2.5.2.3 *Yeast colony selection*

Yeast cells containing the appropriate plasmid construct(s) could be selected by their growth on the appropriate SD agar medium. For a 90mm Petri dish, 100µl of transformed yeast cells were plated out onto the appropriate synthetic selection medium and spread evenly across the surface using a flamed glass rod. The plates were then inverted and transferred to a 30°C incubator. Incubation times for single colony development varied depending on the stringency of selection. For selection of *leu* or *trp* plasmids, colonies could typically be observed after 2-3 days. Selection of colonies containing plasmids expressing hybrid proteins which have interacting Gal4 domains to induce uracil biosynthesis typically required 6-10 days incubation.

### 2.2.5.3 *Replica plating and picking of yeast colonies*

Replica plating was carried out using 220 x 220mm pieces of 100% cotton velvet. The velvets were placed over a 85mm wooden replica-plating block (made in house) and fixed into position using a metal ring. Master plates were inverted and gently lowered on to the velvet with even pressure to ensure a good lift of all yeast colonies across the entire plate. The master plate was then gently lifted off the velvet and a new selective plate containing the appropriate synthetic medium was lowered onto the velvet with even pressure. This plate was then replica cleaned to dilute the number of yeast cells on the plate by repeating the process with a sterile velvet. Replica plates were incubated at 30°C and colony formation would typically occur within 2-3 days. The velvets were cleaned by soaking them o/n in 1% Virkon, and washing thoroughly in warm water before being dried o/n at 37°C. Sets of 10 velvets were then wrapped in tin foil and sterilised by autoclaving.

In some instances, a minimal number of yeast cells were transferred from a single yeast colony using sterile cocktail sticks. These cells were then transferred directly either to a new selection plate, nitro-cellulose filter, or the appropriate liquid culture medium, before being incubated at 30°C.

#### 2.2.5.4 *β-galactosidase filter assay*

Colonies that were to be analysed for the presence of  $\beta$ -galactosidase were transferred by picking (as described above) onto their appropriate SD selective agar plate. These colonies were then incubated for 2 days at 30°C. A reinforced nitro-cellulose filter (Hybond) was cut to the appropriate size and pre-soaked in Z buffer/X-gal solution (see Materials). The filter was then transferred to the selective plate containing the transformed colonies and orientated to the plate by puncturing 3 holes at asymmetric points. The filter was gently lifted from the plate and submerged colony side up into a liquid nitrogen bath for 10 seconds then allowed to thaw at RT (approximately 10 seconds). The filter was then placed in the lid of a Petri dish onto 2 pieces of Whatman filter paper (Whatman #541) pre-soaked in Z buffer/X-gal solution. The Petri dish was then covered and incubated o/n at 37°C.

#### 2.2.5.5 *Isolation of plasmid DNA from yeast*

Plasmid isolation was carried out following the method described in Clontech Matchmaker™ Two-Hybrid System product protocol manual. Briefly, a single transformed yeast colony grown on the appropriate SD agar selection media was used to inoculate 2ml of YPD liquid medium and incubated o/n in an orbital shaker at 30°C. 1.5ml of this yeast suspension was transferred to a 1.5ml reaction vial and the yeast cells pelleted at 6,000 r.p.m. for 5 seconds at RT in a microfuge. The media was removed and the yeast cells resuspended in 200 $\mu$ l of yeast lysis solution (see Materials). To this mixture, 200 $\mu$ l of Phenol/Chloroform and 0.3g of acid washed glass beads (Sigma) were added. The mixture was vortexed continuously for a minimum of 2 minutes. The cellular debris was pelleted at 14,000 r.p.m. for 5 minutes at RT in a microfuge. The supernatant was transferred to a clean 1.5ml reaction vial and the DNA recovered by phenol/chloroform extraction and ethanol precipitation. The DNA pellets were typically resuspended in 20 $\mu$ l of dH<sub>2</sub>O and stored at -20°C.

### 2.2.5.6 TCA extraction of proteins from yeast cells

Yeast cells were prepared and proteins extracted using the TCA protein extraction protocol described in Clontech Laboratories Inc. yeast protocols handbook and is briefly described below.

#### 2.2.5.6.1 Yeast cell culture and preparation for protein extraction

A single colony was used to inoculate 5ml of the appropriate SD media and incubated o/n at 30°C in an orbital shaker. This starter culture was vortexed to break up any cell clumps and used to inoculate 50ml of pre-warmed YPD medium in a 500ml conical flask. This yeast culture was incubated for a further 4-8 hours until the OD<sub>600</sub> reached 0.4-0.6. For each culture the total number of OD<sub>600</sub> units was calculated using the equation below:

$$\text{OD}_{600} (1\text{ml sample}) \times \text{Total volume of culture} = \text{Total OD}_{600} \text{ units}$$

The yeast culture was transferred to a pre-chilled 250ml Falcon tube containing 100ml of ice and the yeast cells were pelleted by centrifugation at 1000 r.p.m. for 5 minutes at 4°C in a Sorvall RT7 centrifuge. The supernatant and any unmelted ice was poured off and the yeast cell pellet resuspended in 50ml of ice-cold dH<sub>2</sub>O. The yeast cells were pelleted (as described above) and the supernatant removed before the cell pellet was frozen on dry ice and stored at -70°C until required.

#### 2.2.5.6.2 TCA protein extraction

Unless otherwise stated all sample preparations were kept on ice. Frozen yeast cell pellets were thawed on ice and resuspended in 100µl/7.5 OD<sub>600</sub> units of ice cold TCA buffer. The mixture was transferred to a 1.5ml reaction vial containing 100µl of acid washed glass beads (Sigma) and 100µl of ice cold 20% (w/v) TCA per 7.5 OD<sub>600</sub> units. If the volume was greater than 1.5ml the sample was split between two 1.5ml reaction vials. The tubes were vortexed for 4x 1 minute intervals and were placed on ice between each period of vortexing for a minimum of 30 seconds. The glass beads were allowed to settle before the supernatant was transferred to a fresh pre-chilled 1.5ml reaction vial. 500µl of a 1:1 mix

of 20% TCA and TCA buffer was added to the glass beads and vortexed for a further 2x 1 minute intervals (as described above). The glass beads were allowed to settle and the supernatant was pooled with the first extract. The combined cell extracts were incubated on ice for an additional 1 minute to allow any glass beads carried over to settle. This supernatant was transferred to a fresh pre-chilled 1.5ml reaction vial and the proteins pelleted by centrifugation at 14,000 r.p.m. for 10 minutes at 4°C in a microfuge. The supernatant was removed and the pellet resuspended in 10µl/OD<sub>600</sub> unit of BM. The sample was heated in a dry block for 10 minutes at 100°C and stored at -70°C prior to SDS-PAGE analysis.

#### 2.2.5.7 Random PCR mutagenesis

Random PCR mutagenesis was carried out using universal primers that encoded sequences flanking the multicloning site of pPc86 plasmid (primers detailed in section 3.1). The 5' primer corresponds to sequences located within the activation domain (AD), approximately 100bp upstream of the multicloning site of pPc86. The 3' primer corresponds to sequences located within the yeast transcriptional terminator (Term) approximately 100bp downstream of the multicloning site. Thus, a DNA fragment amplified using these two primers can be re-incorporated back into a linearised (KpnI digested and CIP treated) pPC86 vector via gap repair by transforming yeast cells with the appropriate linearised vector and PCR products.

Random PCR mutagenesis was carried out using; 100ng of linear pPc86UL18 DNA (as a DNA template), 1µM of each of the AD and Term primers, 50µM of each dNTP, 50mM KCl, 10mM Tris (pH 9.0), 1.5mM MgCl<sub>2</sub>, and 5 units of *Taq* DNA polymerase. The PCR reaction was carried out in a final volume of 50µl initially for 10 elongation cycles (described below) before MnCl<sub>2</sub> was added to a final concentration of 100µM. The reaction was continued for a further 30 cycles (1 min at 94°C, 1 min at 45°C, 2 min at 72°C). Each PCR reaction was analysed by electrophoresis on a 1% agarose TBE gel.

## 2.2.6 Tissue culture and virus manipulation

### 2.2.6.1 *Baculovirus manipulation*

#### 2.2.6.1.1 *SF cell culture*

SF21 cells were passage every 3-4 days in large (600ml) tissue culture flasks containing 50-75ml of TC100/5 medium. The cells were removed from the base of the flask by the addition of 10ml of TC100/5 medium and gentle tapping of the flask against the hand. Cell clumps were broken up by pipetting the medium up and down. Confluent flasks were typically passaged using a 1:4 split. Where appropriate cell densities were calculated using a Neubauer counting chamber. Cells were counted using a inverted light microscope (Olympus).

#### 2.2.6.1.2 *Freezing and storage of SF cells*

SF21 cells were grown in large flasks (600ml) at 28°C until confluent. They were then harvested in 10ml of TC100/5 medium and the cell suspension transferred to a 15ml Falcon tube. Cells were pelleted by centrifugation at 1,500 r.p.m. for 5 minutes in a Sorvall RT7 centrifuge. The supernatant was removed and the cells resuspended in 2ml TC100/10 and a equal volume of ice cold freezing mix (80% (v/v) TC100/10, 20% (v/v) DMSO). The cell suspension was aliquoted into cryogenic vials (1ml/vial) before being frozen o/n at -70°C. Frozen cells were then transferred to liquid nitrogen for long term storage.

#### 2.2.6.1.3 *Recovery of SF21 cells*

Aliquots of SF21 cells removed from liquid nitrogen were thawed quickly in a water bath at 37°C before being resuspended in a small volume of TC100/5 (approximately 5ml). The cell suspension was then transferred to a 15ml Falcon tube, and cells pelleted by centrifugation at 1,000 r.p.m. for 5 minutes in a Sorvall RT7 centrifuge. The supernatant was discarded and the cell pellet resuspended in 5ml of TC100/5, which was used to seed

to a medium flask (200ml). The flask was incubated at 28°C until the cells had firmly attached to the solid substrate before the medium was replaced with fresh TC100/5. Once the monolayer had reached confluency the cells were passaged into a large (600ml) flask and cultured as normal.

#### 2.2.6.1.4 Construction of recombinant baculoviruses

Transfection of DNA into SF21 cells followed the method described by Rose et al (1991) utilising a synthetic lipid reagent. Transfections were performed in 35mm dishes at a cell density of 60-70%. 0.5µg of AcPAK6 DNA, which had been digested with Bsu361 and subsequently phosphatased using CIP, was mixed in a 15ml Falcon tube with 5µg of transfer vector DNA in 500µl of TC100 medium. To this mixture 15µl of liposomes was added, gently vortexed, and incubated at RT for 15 minutes. The medium from the SF21 cell monolayer was removed and the cells were washed with 2ml of TC100 medium containing no foetal calf serum. The wash medium was removed and the transfection mixture added to the cell monolayer with an additional 500µl of TC100 medium. The cells were incubated at 28°C for 4 hours before an additional 1ml of TC100/10 media was added. The cells were then incubated for a further 65 hours at 28°C when the supernatant was removed and transferred to a sterile 1.5ml reaction vial. Any cells that were carried over were pelleted by centrifugation at 14,000 r.p.m. for 2 minutes in a microfuge. The supernatant was transferred to a fresh 1.5ml screw cap reaction vial, frozen on dry ice and stored at -70°C until required.

#### 2.2.6.1.5 Isolation of recombinant viruses

Recombinant viruses were selected on their *lacZ*-minus phenotype. 100µl of the harvested transfection supernatant was assayed for plaque formation and *lacZ* phenotype at dilutions from neat to 10<sup>-3</sup> (described in section 2.2.6.1.8). Plaques that did not stain blue were picked under a plate microscope (WILD M7A, Heerbrugg) using a sterile Pasteur pipette and transferred to 1ml of TC100/5 medium in a sterile 1.5ml screw cap tube. Virus was released from the agar by freeze/thawing the samples on dry ice 3x before being stored at -70°C. Baculoviruses were subsequently grown by infecting 50% confluent monolayers of SF21 cells (1x10<sup>6</sup> cells/plate) in 35mm dishes. The media was removed from the cells and

500µl of released virus suspension was added and allowed to absorb for 1 hour at 28°C before an additional 1ml of TC100/5 media was added. After a further 4-5 day incubation the supernatant, termed plate harvest one (PH1), was harvested (as described above) and used for a second round of plaque purification. PH2 was used for a final round of plaque purification and the PH3 virus supernatant was subsequently used for generating low titre virus stocks. Cells from each round of plate harvests were analysed by SDS-PAGE and stained with Coomassie Brilliant Blue to assay for the continued expression of the recombinant protein of interest.

#### *2.2.6.1.6 Production of low titre baculovirus stocks.*

Small tissue culture flasks (200ml) were seeded with SF21 cells in TC100/5 media and allowed to grow at 28°C until the monolayer reached a confluency of 50%. The media was removed and 500µl of PH3 supernatant was inoculated onto the cells and allowed to absorb for 1 hour at 28°C. Following the incubation, 10ml of fresh TC100/5 media was added to the cells and incubated for a further 4-5 days at 28°C. The media was transferred into a 15ml Falcon tube and the cells pelleted by centrifugation at 2,000 r.p.m. for 5 minutes in a Sorvall RT7 centrifuge. The supernatant was transferred to a fresh 15ml Falcon tube and stored at -70°C until required. 5ml of this supernatant was used to infect a 50% confluent monolayer of SF21 cells in a large (600ml) flask (as described above). After absorption, 50ml of TC100/5 media was added to the cells, which were subsequently incubated for 4-5 days at 28°C, after which the supernatant was harvested (flask harvest, FH), as described above, and stored at -70°C. The FH was subsequently titered as described in section 2.2.6.1.8.

#### *2.2.6.1.7 Production of high titre baculovirus stocks*

High titre stocks of parental (AcPAK6) and recombinant baculoviruses were routinely grown in roller bottles containing SF21 cells at a cell density of  $5 \times 10^5$  cells/ml (typically 300ml/bottle). Cells were infected at a m.o.i. of 0.1 p.f.u./ml and cultured for 5 days at 28°C. Cultures were transferred to 250ml Falcon tubes and the cells pelleted by centrifugation at 3,000 r.p.m. for 5 minutes in a Sorvall RT7 centrifuge. The supernatant was removed and baculovirus pelleted by centrifugation at 12,000 r.p.m. for 5 hours at 4°C

---

in a Sorvall SLA-3000 rotor. Virus pellets were resuspended in TC100/5 media (typically 4ml/300ml supernatant), transferred to sterile 1.5ml screw cap tubes and stored at 4°C until required.

#### 2.2.6.1.8 *Baculovirus titration*

Stocks of baculovirus were titrated by the method first described by Brown and Faulkner (1977). 35mm dishes were seeded with  $1 \times 10^6$  SF21 cells in 1.5ml of TC100/5 medium and allowed to grow o/n at 28°C to generate a 70-80% confluent monolayer. Serial 10 fold dilutions of the virus were performed in TC100/5 medium from neat to  $10^{-6}$  for low titre stocks and from  $10^{-5}$  to  $10^{-10}$  for high titre stocks. The medium was removed from the cells and 100µl of the diluted virus was added to each 35mm dish and allowed to absorb for 1 hour at 28°C with occasional rocking to prevent the cell monolayer from drying out. Following absorption, 1ml of overlay medium was added (50% TC100/5 and 50% 3% LTG agarose (SeaPlaque)), which had been previously melted and incubated at 45°C to prevent the agar from setting. Once the overlay medium had set (approximately 10 minutes), 1.5ml of TC100/5 was added and the plates were incubated for a further 4-5 days at 28°C. The medium was removed and 1.5ml of neutral red stain (0.4% neutral chloride mixed 1:50 with TC100/5) was added on top of the agar and the plates incubated for a further 5 hours at 28°C. The stain was removed and the plates inverted onto tissue paper and allowed to air dry o/n at RT. Plaques were counted and the titre calculated as p.f.u./ml. If the titration was required to identify recombinant viruses then 250µg of X-gal/ml (made up as a 3mg/ml stock solution in DMSO) was added to the initial stain. Recombinant virus plaques (clear plaques) were selected for their absence of  $\beta$ -galactosidase activity due to the disruption of the *lacZ* gene within the parental baculovirus (AcPAK6).

#### 2.2.6.2 *BHK-21 C13 cell culture.*

BHK cells were typically passaged every 3-4 days in 850cm<sup>2</sup> roller bottles. The cell monolayer was washed with 40ml of versene and the cells removed from the substrate by trypsinisation, 2x washes of a 20ml trypsin/versene (1:4) solution. The cells were left until the monolayer dispersed before 10ml of ETC/10 was added. A confluent monolayer

typically yielded approximately  $1 \times 10^8$  cells. Sterile roller bottles were seeded with  $2 \times 10^7$  cells in 100ml of ETC/10, gassed with 5% CO<sub>2</sub> and incubated at 37°C with gentle rotation.

#### 2.2.6.3 Vero cell culture.

Vero cells were typically passaged every 3-4 days in large (600ml) tissue culture flasks containing 50-75ml of MEM/10. The monolayer was washed in 20ml of versene and the cells removed from the substrate by trypsinisation, 2x washes of a 20ml trypsin/versene (1:4) solution. The cells were left until the monolayer dispersed before 10ml of MEM/10 medium was added. Cell clumps were dispersed by pipetting the medium up and down. Confluent flasks were typically passaged 1:4. into sterile flasks containing fresh medium and gassed with 5% CO<sub>2</sub>. Flasks were incubated at 37°C.

#### 2.2.6.4 Complementation of UL18 null mutant virus (K23Z)

35mm dishes were seeded with  $4 \times 10^5$  BHK-21 C13 cells in ETC10 medium and allowed to grow o/n at 37°C in 5% CO<sub>2</sub>. 1µg of the appropriate plasmid DNA was transfected into cells using the transfection procedure described in section 2.2.4.1. 18-24 hours post transfection the medium was removed and the cell monolayer infected with the UL18 null mutant virus (K23Z) at a m.o.i. of 3 p.f.u./cell in 100µl of ETC10 medium. The construction of K23Z is described in Desai et al., (1993). The cells were incubated for 1 hour at 37°C in 5% CO<sub>2</sub> with occasional rocking to prevent the cell monolayer from drying out. Following the incubation the virus inoculum was removed and the cells washed with 1ml of sterile PBScomplete. Unpenetrated virus particles were removed from the surface of cells by acid washing in 500µl of pH3 buffer (see Materials) for 1 minute at RT. The cell monolayer was then washed in 1ml of ETC10 medium before 1ml of ETC10 medium was added to the cells and incubated for 24 hours at 37°C in 5% CO<sub>2</sub>. Following the incubation, the cells were removed from the plate by scraping into the culture medium, using a sterile 1ml syringe plunger. The medium was then transferred to a Bijoux bottle and briefly bath sonicated in a soni-bath (Kerry) to release virus particles.

### 2.2.6.5 Titration of complemented HSV-1 UL18 null mutant virus (K23Z)

HSV-1 UL18 null mutant virus progeny (generated as described in section 2.2.6.4) were titred on 80% confluent monolayers of Vero cells or G5-11 Vero cells (a UL18 complementing cell line, described in Desai et al., 1993) in 35mm dishes. The virus was diluted through 10-fold serial dilutions, the medium removed, and the cells inoculated with 100µl of serial 10-fold dilutions from neat to  $10^{-4}$  in MEM/10 medium. The plates were incubated at 37°C for 1 hour with occasional rocking to prevent the cell monolayer from drying out. Following the incubation 2ml of EMC/10 (see Materials) was gently added to each plate and they were incubated for a further 3-4 days at 37°C. To visualise plaques, the cells were fixed in 2ml of Giemsa stain for 4 hours at RT. Excess stain was removed by gentle washing in cold water before the plates were inverted and allow to air dry o/n on tissue paper. The plaques were then counted using a plate microscope (WILD M7A, Heerbrugg).

## 2.2.7 Expression of recombinant proteins

### 2.2.7.1 Protein expression in BL21 DE3 bacteria

A single colony or approximately 10µl of a glycerol stock was used to seed 5ml of pre-warmed L-Broth (containing the appropriate antibiotic) and incubated in an orbital shaker for 4-5 hours at 37°C. This starter culture was then used to inoculate 100ml of pre-warmed L-Broth (containing the appropriate antibiotic) in a 500ml flask and allowed to grow o/n at 37°C in an orbital shaker. 50ml of the o/n culture was transferred to a 2 litre flask containing 1 litre of pre-warmed L-Broth (containing the appropriate antibiotic) and cultured until the  $OD_{630nm}$  reached 0.5-0.6. Expression of the gene(s) of interest was induced by adding 0.1mM IPTG and incubating for a further 16 hours at 18°C (unless otherwise stated). 600ml of the induced bacterial suspension was then transferred to a GS3 centrifuge bottle and the bacteria pelleted by centrifugation at 6,000 r.p.m. for 15 minutes at 4°C in a Sorvall SLA-3000 rotor. The culture supernatant was removed and the bacterial pellets were frozen at -20°C until required.

### 2.2.7.2 Protein expression using the baculovirus expression system

Recombinant protein expression was carried out using 35mm or 60mm dishes that were seeded with  $1 \times 10^6$  or  $4 \times 10^6$  SF21 cells respectively, or roller bottles containing 300ml of SF21 cells at a cell density of  $1 \times 10^6$  cells/ml. In all instances, SF21 cells were infected with recombinant baculoviruses expressing the gene(s) of interest at 5 p.f.u./cell and incubated at 28°C for 48 hours. SF21 cells cultured on plates were allowed to reach a confluency of 80% (typically o/n post-seeding), after which the growth medium was removed. 100 $\mu$ l (for a 35mm dish) or 200 $\mu$ l (for a 60mm dish), of the appropriately diluted baculovirus in TC100/5, was added to the cell monolayer and incubated for 1 hour at 28°C with occasional rocking. Following absorption, 1.5ml (for a 35mm dish) or 3ml (for a 60mm dish) of TC100/5 was added to the cell monolayer and incubated for 48 hours at 28°C. The plates were harvested in 1 ml of PBSa by gentle pipetting before being transferred to a 1.5ml reaction vial, and pelleted by centrifugation at 6,500 r.p.m. for 1 minute at RT in a microfuge. The supernatant was removed and the cell pellet was frozen on dry ice and stored at -20°C until required. For SF21 cells cultured in roller bottles, baculovirus was added directly to the cell suspension. 48 hours post infection the cell suspension was transferred to a 250ml Falcon tube and the cells pelleted by centrifugation at 3,000 r.p.m. for 5 minutes at RT in a Sorvall RT7 centrifuge. The supernatant was removed and the cell pellets frozen on dry ice and store at -20°C until required.

## 2.2.8 Purification of 6xHis epitope tagged proteins

### 2.2.8.1 Ni-NTA agarose column chromatography

The majority of protein purification's shown in this thesis utilised the expression of recombinant proteins that had a 6xHis amino acid tag located at their N-termini. This allowed the purification of both bacterial and baculovirus expressed proteins through the use of Ni-NTA affinity chromatography. The principles of which are discussed in detail in section 3.3. The protocols outlined below describe the general methods involved in extracting and purifying recombinantly expressed proteins from bacteria and SF21 cell

extracts. The specific composition of buffers used in individual cases are detailed within the appropriate text sections and figure legend texts.

#### *2.2.8.2 Preparation of bacterial extracts for Ni-NTA purification*

Frozen 600ml bacterial pellets (grown and induced as described in section 2.2.7.1) were typically resuspended in 20ml of the appropriate purification buffer (see fig. legends for details) and lysed using a Branson sonifier 450 soni-probe over approximately 5x 20 second bursts set at the 50% duty cycle and an output of 5. The lysed bacterial suspension was then transferred to the appropriate number of 1.5ml reaction vials and clarified at 14,000 r.p.m. for 5 min at RT in a microfuge. The supernatant fraction was transferred to a 15ml falcon tube for Ni-NTA agarose purification (described in section 2.2.8.4).

#### *2.2.8.3 Preparation of SF21 cell extracts for Ni-NTA purification*

Frozen SF21 cell pellets from 300ml cultures (cultured and infected as described in section 2.2.7.2) were typically resuspended in 5ml of the appropriate purification buffer (see fig. legends for details) containing Complete<sup>TM</sup> (EDTA-free) protease inhibitors (Boehringer Mannheim) prepared following the manufacturer's instructions. The cell suspension was lysed by sonication in a soni-bath (Kerry) for approximately 5 minutes at RT. The cell suspension was then transferred to the appropriate number of 1.5ml reaction vials and clarified at 14,000 r.p.m. for 5 minutes at RT in a microfuge (unless otherwise stated). The supernatant fraction was then transferred to a 15ml Falcon tube for Ni-NTA agarose purification (described in section 2.2.8.4).

#### *2.2.8.4 Ni-NTA agarose purification*

350-700 $\mu$ l of Ni-NTA coupled to Sepharose<sup>®</sup> CL-6B (Qiagen), was typically equilibrated in a 1.5ml reaction vial over 4x 1.5ml washes in the appropriate purification buffer. After each wash stage the agarose was pelleted by centrifugation at 14,000 r.p.m. for 5 seconds at RT in a microfuge, the buffer phase removed, and the agarose gently resuspended in 1.5ml of fresh purification buffer. Following the final wash stage the agarose was resuspended in 1.5ml of the appropriate purification buffer and added to the soluble protein

fraction. The 6xHIS epitoped tagged recombinant proteins were allowed to bind by mixing end over end for 1 hour at RT (unless otherwise stated). The agarose and bound protein complexes were then pelleted by centrifugation at the appropriate temperature at 1,000 r.p.m. for 5 minutes in a Sorvall RT7 centrifuge. The supernatant was removed and the agarose gently resuspended in 10ml of the purification buffer. The agarose was pelleted and washed a further 2x (as described above) before being transfer to a disposable column (BIO-Rad) in 5ml of the appropriate buffer. The agarose was washed with a further 5ml of the appropriate purification buffer. When required the Ni-NTA agarose was washed with 10 ml of purification buffer containing low concentrations imidazole (typically <25mM) to remove cellular proteins that had non-specifically bound to the agarose. The 6xHIS epitoped tagged recombinant proteins were eluted from the Ni-NTA agarose using a suitable concentration of imidazole (typically between 100-250mM) in the desired volume of purification buffer and collected in 1.5ml reaction vials. Specific details for each protein purified using Ni-NTA agarose are described in their respective results sections.

#### 2.2.8.5 Ni-NTA agarose pull downs

Frozen 35mm or 60mm plate harvests of SF21 cells infected with recombinant baculoviruses (as described in section 2.2.7.2) were resuspended in 150 $\mu$ l of the appropriate purification buffer (see fig. legends for details). The cell extracts were allowed to lyse on ice for 15 minutes with intermittent vortexing before being clarified by ultracentrifugation at 30,000 r.p.m. for 5 minutes at 4°C in a Beckman TLA 100.2 rotor. The supernatant was transferred to a fresh 1.5ml reaction vial and mixed with a second lysed and clarified extract or with 200 $\mu$ l of buffer. The extracts were incubated for 1 hour at an appropriate temperature before being mixed with 20 $\mu$ l of equilibrated Ni-NTA agarose (Qiagen). The extracts were incubated for a further 15 minutes with intermittent vortexing. The Ni-NTA agarose was pelleted at 14,000 r.p.m. for 5 seconds in a microfuge and washed in 3x 1ml and 2x 200 $\mu$ l of the appropriate buffer + 500mM NaCl. If the experiment was carried out at 4°C then all buffers were pre-chilled on ice before use. Following the final wash, the Ni-NTA agarose was resuspended in 30 $\mu$ l of BM + 250mM imidazole and heated in a dry block for 5 minutes at 100°C. The extracts were stored at -20°C until required.

### 2.2.8.6 Quantification of protein concentration

Purified protein concentrations were calculated by measuring the OD<sub>280</sub> and calculating the amount of protein in mg/ml using the following equation:

$$\frac{\text{Extinction Co-efficient}}{\text{MW}} = \frac{\text{OD}_{280}}{\text{X (mg/ml)}}$$

## 2.2.9 Analysis of purified proteins

### 2.2.9.1 SDS-polyacrylamide gel electrophoresis (SDS-PAGE)

Protein samples in all cases were resolved using a 10% polyacrylamide gel (37.5:1 acrylamide:bisacrylamide, Bio-Rad) prepared in 1x resolving gel buffer (see materials) within a vertical mini gel plate system (Bio-Rad), on top of which a 5% polyacrylamide stacking gel prepared in 1x stacking gel buffer (see Materials) was poured. Both resolving and stacking gels were polymerised by adding 200µl of 10% ammonium persulphate and 10µl of TEMED. Unless otherwise stated, protein samples were prepared in boiling mix (BM) buffer (see Materials) and heated at 100°C for 2 minutes prior to loading. Gels were typically electrophoresed at 150-200 volts until the dye front had reached the bottom of the resolving gel. If protein standards were required then 3µl of Rainbow™ markers (Amersham Pharmacia Ltd) or 3µl of purified capsids (prepared in house by J. Mitchell) were analysed next to the protein samples for comparison. Gels that were not going to be used for Western blotting were fixed and stained using Coomassie Brilliant Blue stain (see Materials) solution for 10-20 minutes before being transferred into a destain solution to remove excess back ground staining. Gels were photographed using a digital camera and images processed using PhotoShop 3.1 software (Adobe).

### *2.2.9.2 Semi-dry Western blot analysis*

#### *2.2.9.2.1 Protein transfer*

The transfer of proteins to a nitro-cellulose membrane was carried out by semi-dry transfer. SDS-PAGE was carried out (as described in section 2.2.9.1) and the stacking gel was separated from the resolving gel. 6 pieces of 3mm Whatman paper and the nitro-cellulose membrane (Hybond) were cut to the appropriate size and pre-soaked for 5-10 minutes in transfer buffer. The nitro-cellulose membrane was placed on to a stack of 3 pieces of 3mm Whatman paper and the resolving gel was placed on to the nitro-cellulose before an additional stack of 3 pieces of 3mm Whatman paper were placed on top of the resolving gel. The transfer of proteins on to the nitro-cellulose membrane was carried out using a 2117 Multiphor II Electrophoresis Unit (Pharmacia) typically at 40mA for 3-4 hours.

#### *2.2.9.2.2 Detection of proteins*

When the transfer was complete, non-specific binding sites on the nitro-cellulose membrane were blocked by immersing the membrane in 100ml of 3% Marvel milk powder made up in PBSa/T and incubating at RT on a orbital shaker for a minimum of 1 hour. The blocked membrane was then washed 3x 15 minutes in approximately 50ml of PBSa/T. The membrane was subsequently probed at RT in approximately 10ml of PBSa/T, containing the appropriately diluted primary antibody, for a minimum of 1 hour on an orbital shaker. The membrane was then washed (as described above) before the addition of a secondary antibody, typically GAM-HRP or Protein A peroxidase (both used at 1:1000 dilution), which was incubated for a minimum of 1 hour at RT on an orbital shaker. The membrane was then thoroughly washed, 3x 15 minutes and 4x 5 minutes in approximately 50ml of PBSa/T. Immuno-detection was carried out using ECL (Amersham Pharmacia Ltd) following the manufacturers instructions. Kodak XS-1 film was used for visualisation of immuno-complexes and was exposed for variable amounts of time.

#### 2.2.9.4 Stripping and re-probing nitro-cellulose membranes

Nitro-cellulose membranes were stripped by incubating the blot in 50ml of stripping buffer (see Materials) for 30-40 minutes at 55°C. Blots were then washed a minimum of 3x in 30ml of PBSa/T before being blocked and re-probed (as described above).

#### 2.2.9.3 TCA precipitation

50% (w/v) TCA was added to the protein solution in a 1.5ml reaction vial to give a final concentration of 5%. The mixture was incubated on ice for 10 minutes and the precipitated proteins were pelleted by centrifugation at 14,000 r.p.m. for 5 minutes at RT in a microfuge. The pellet was washed in 100% ethanol and pelleted (as above) and resuspended in the appropriate volume of BM buffer. Samples were either analysed directly by SDS-PAGE or frozen at -20°C until required.

#### 2.2.9.4 Sucrose gradient sedimentation

5-20% sucrose gradients in buffer O were prepared in 13x51mm Ultra Clear tubes (Beckman) using a BIOC0MP gradient maker (Gradient Master#106), following the manufacturers guidelines. The gradients were allowed to cool at 4°C for a minimum of 5 hours before application of sample and ultracentrifugation. Typically 300µl of sample was mixed with 50µl of BSA (5mg/ml) and gently layered onto the top of the gradient. The gradient was then centrifuged at 40,000 r.p.m. for 16 hours at 4°C in a AH650 rotor. Following ultracentrifugation, the gradients were carefully removed from the rotor and placed into a clamp. A 1.5mm gauge needle (Microlance3) was used to pierce the centrifuge tube approximately 5mm from the base and successive 150µl fractions were collected into 1.5ml reaction vials (typically 35 fractions/gradient). Gradient protein profiles were analysed by SDS-PAGE, in conjunction with Coomassie Brilliant Blue staining or Western blot analysis, of every third fraction. Once the relative fractions containing the appropriate protein samples were identified, further SDS-PAGE analysis was carried out in conjunction with Coomassie Brilliant Blue staining or Western blot analysis. The relative intensity profile for each sample across the gradient was calculated by taking a digital picture of the appropriate SDS-PAGE gel or autoradiograph. This

profile was analysed using Quantity ONE software (BIO-Rad, following the manufactures guidelines) to provide an intensity profile of the protein samples across the gradient. These profiles were then plotted as a percentage change in relative intensity for each sample against their appropriate fraction number using Origin 3.1 software.

#### 2.2.9.5 Capsid assembly analysis

##### 2.2.9.5.1 *In vitro* capsid assembly

To test the functionality of purified proteins, *in vitro* capsid assembly was carried out as described by Newcomb et al (1994). Briefly, frozen cell pellets (typical 30ml) of SF21 cells infected singly at 5 p.f.u./cell with recombinant baculoviruses expressing one of the four essential capsid proteins; AcUL19 (VP5), AcUL26.5 (preVP22a), AcUL38 (VP19c), AcUL18 (VP23), were resuspended in 50 $\mu$ l of the appropriate buffer and freeze/thawed a minimum of 4x on dry ice. The lysates were clarified at 14,000 r.p.m. for 5 minutes at RT in a microfuge. The appropriate soluble lysate fractions were then mixed, typically 10 $\mu$ l of each clarified extract, and incubated o/n at 28°C to allow capsid formation to take place. Capsids were sedimented at 30,000 r.p.m. for 45 minutes at 4°C in a Beckman TLS-55 rotor. Following sedimentation the supernatant was removed and the pellet resuspended in 10-20 $\mu$ l of PBSa. Typically 5.0 $\mu$ l of the resuspended pellet was transferred to a parlodion coated copper grid and allowed to absorb for 2-3 minutes. Grids were then stained with 1% phosphotungstic acid, analysed for the presence of capsids using a JEOL 100S electron microscope and photographed using Kodak 4489 film.

##### 2.2.9.5.2 *In vivo* capsid assembly

35mm dishes of SF21 cells at 80% confluency were infected at 5 p.f.u./cell each with a panel of recombinant baculoviruses expressing individually one of the four essential capsid proteins; AcUL19 (VP5), AcUL26.5 (preVP22a), AcUL38 (VP19c), AcUL18 (VP23). Or in the case of the dual expression baculoviruses Ac18638 and 18386 which co-express VP19c/VP23His or VP19cHis/VP23 respectively, baculoviruses expressing AcUL18 (VP23) and AcUL38 (VP19c) were omitted. Infected cells were harvested at 48 hours post-infection in 1ml of PBScomplete and transferred to a BEEM capsule (TAAB

Laboratories). The cells were pelleted by centrifugation at 1,000 r.p.m. for 5 minutes at RT in a vertical centrifuge (Beckman microfuge-12). The supernatant was carefully removed and the cell pellets fixed o/n at 4°C in 500µl of 2.5% glutaraldehyde (1:10 dilution of 25% glutaraldehyde in PBScomplete). The pellets were subsequently washed 3x in PBS complete before being overlaid for 1 hour at RT with 100µl of osmium tetroxide. The fixed pellets were then wash 2x in PBScomplete before being dehydrated in consecutive 500µl washes of 30%, 50%, 70%, 90%, and 2x 100% ethanol. Each dehydration step was carried out for a minimum of 2 hours and care was taken not to dislodge the fixed cell pellet. After the final dehydration step the ethanol was removed and the fixed pellets were infiltrated with Epon100 resin and left o/n at RT. The resin was then removed by inverting the tube on to tissue paper and leaving it to drain for 30-60 minutes at RT. Fresh resin was overlaid and incubated o/n at RT and subsequently baked at 60°C for 2 days. The resin blocks were then cut into thin sections using a diamond knife on a ultra-microtome (Ultracut-E, Reichart-Jung) before being mounted on parlodion coated copper grids and stained for 1 hour with saturated uranyl acetate in 50% (v/v) ethanol. The grids were washed in dH<sub>2</sub>O and counter-stained with lead citrate for 1 minute before being gently rinsed in dH<sub>2</sub>O to remove excess stain. The sections were examined using a JEOL 100S electron microscope and photographed on Kodak 4489 film.

## 2.2.10 Biophysical characterisation techniques

### 2.2.10.1 Fluorescence and ANS binding.

Proteins analysed by fluorescence were purified to homogeneity using Ni-NTA affinity chromatography (as described in section 2.2.8.4). Protein fluorescence was monitored at RT using a Perkin-Elmer LS-50B spectrofluorimeter in a 1ml semimicrocuvette with a path length of 1 cm. The excitation wavelength was 295nm and the emission spectra were recorded between 310-380nm. For ANS binding experiments, ANS was added to the protein samples to a final concentration of 20µM. The samples were then excited at 370nm and the emission spectra were recorded between 440-540nm (unless otherwise stated). For both fluorescence and ANS spectra the appropriate buffer profiles were subtracted from the recorded emission spectra.

### 2.2.10.2 Circular-dichroism (CD)

CD spectra were obtained on a Jasco-600 spectropolarimeter (Japan Spectroscopic Co., Tokyo, Japan). Near-UV CD spectra (320-260nm) were recorded using a cylindrical quartz cell with a path length of 0.5 cm. Far-UV CD spectra (260-190nm) were recorded using a cylindrical quartz cell with a path length of 0.5 cm. The content of secondary structure was estimated by using the CONTIN procedure. All experiments were carried out at 25°C with appropriate buffer only control spectra being subtracted from the recorded emission spectra.

### 2.2.10.3 Digital scanning calorimetry (DSC).

Calorimetric measurements were carried out using a MC-2 precision differential scanning micro-calorimeter (Microcalc). The rate of heating was 1°C/min, and the excess pressure was kept at  $8 \times 10^6$  Pa. Protein was analysed at a concentration of 0.5mg/ml in the appropriate buffer. The molar heat capacity of the protein was calculated by comparison with duplicate samples containing the identical buffer from which the protein had been omitted.

### 2.2.10.4 Size exclusion chromatography.

Chromatography was carried out using a 25ml (1 by 30 cm) superose-12 gel filtration column (Pharmacia) in the appropriate buffer that had been filter through a 0.2µm filter. All protein samples were clarified before analysis, either by filtration through a 0.2µm filter or by ultracentrifugation at 35,000 r.p.m. for 10 minutes at RT in a Beckman TLA 100.2 rotor. In all experiments the column was run at 0.5 ml/min. Protein size standards used to generate a standard curve were; β-amylase (MW, 200,000), alcohol dehydrogenase (MW, 150,000), bovine serum albumin (MW, 66,000), ovalbumin (MW, 45,000), and carbonic anhydrase (MW, 29,000) (SIGMA). Protein standards were analysed in the same buffer at the same concentration as the protein sample for comparative analysis. Standard curves were generated by plotting peak elution volumes against their given  $\text{Log}_{10}$  MW (Sigma) using Origin 3.1 software. Linear regression analysis was performed upon the

data utilising the spreadsheet software to generate a best-fit line, from which the native MW of purified sample proteins could be calculated.

# Chapter 3

## Results

## 3.1 Reverse Yeast Two Hybrid System

Due to time constraints during my PhD the experimental work within this section was unable to be finished and is currently ongoing within the laboratory. However, as a record of work undertaken during the course of my PhD and for future reference the preliminary results are presented below and discussed in relation to published experimental findings.

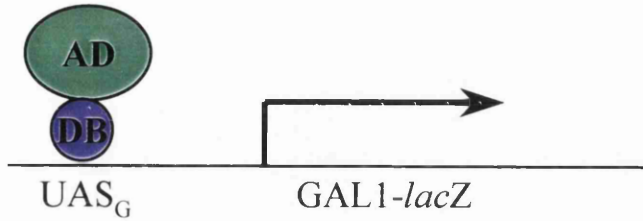
### 3.1.1 Yeast two hybrid system

Fields and Song (1989) were the first group to describe the use of the yeast two hybrid system to analyse protein-protein interactions within yeast *Saccharomyces cerevisiae*. They took advantage of the yeast transcriptional activator GAL4 that is required for the efficient expression of enzymes involved in the galactose utilisation pathway (Johnston et al., 1987). The GAL4 activator can be separated into two functional domains: an N-terminal DNA binding (DB) domain, which specifically binds to UAS<sub>G</sub> sequences; and a C-terminal activator domain (AD) containing acidic residues, which is required for efficient transcriptional activation (Ma and Ptashne, 1987). If these domains are expressed separately the activation domain cannot localise efficiently to the chromosome and activate gene expression. Fields and Song (1989) went onto describe the construction of plasmids expressing SNF1, a serine threonine protein kinase, fused to the DB domain of GAL4 and SNF4, a protein physically associated with SNF1, fused to the AD of GAL4. The interaction of these two proteins when expressed in *Saccharomyces cerevisiae* was sufficient to bring the AD and DB domains into close enough proximity to reconstitute GAL4 activity and induce the efficient expression of a *lacZ* reporter gene that was fused down stream of GAL1. Fig. 3.1.1 summarises the theory of the yeast two hybrid system described by Field and Song (1989).

#### 3.1.1.1 Yeast two hybrid analysis of HSV-1 capsid protein interactions

Desai and Person (1996) utilised the yeast two-hybrid system in conjunction with deletion mutagenesis to investigate the protein-protein interactions amongst the HSV-1 capsid

(a) Native GAL4



(b) Hybrid/GAL4 DNA binding domain  
Hybrid/GAL4 activation domain



(c) Interaction between hybrid proteins reconstitutes  
GAL4 activity

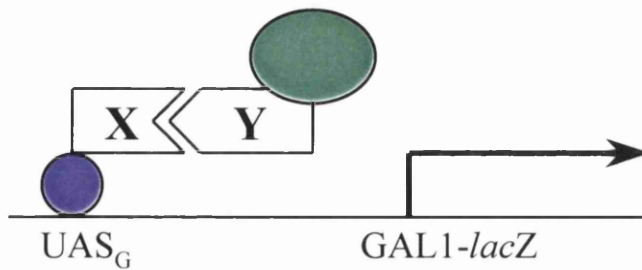


Fig. 3.1.1: Schematic representation of the yeast two hybrid system.  
X and Y represent recombinant proteins under analysis.  
(Modified from Fields & Song 1989)

proteins. Interestingly, the experiments by Desai and Person did not detect all the HSV-1 capsid protein interactions, specifically the interaction between VP19c and VP5. The inability to detect such an interaction could be explained in a number of ways. It is now becoming clear that virus capsid assembly is a dynamic process involving a number of folding stages (Trus et al., 1996; Newcomb et al., 1996; Johnson, 1996). Therefore, in order to detect certain protein-protein interactions utilising the yeast two hybrid system there may be a requirement for additional capsid proteins, over that of the two recombinantly expressed hybrid capsid proteins. In other words, the ability to present specific residues required for a detectable interaction may require the presence of a third partner in order to ensure the correct conformation required for further protein interactions to develop. However, in this specific instance, the interaction between VP5/VP19c, the requirement for a third capsid protein partner would seem unlikely. Immunofluorescence experiments performed by Rixon et al., (1996) demonstrated that VP19c can localise VP5 in the nucleus of transfected cells. This would imply therefore that these two proteins alone can form a stable protein-protein interaction in the absence of other capsid proteins. The lack of a detectable interaction between VP5/VP19c may be a direct result of the fusion of AD and DB domains to the termini of these proteins. The fusion of such domains may interfere with their folding or prevent specific amino acids or epitopes from being presented in the correct conformational arrangement required for a detectable protein-protein interaction.

#### *3.1.1.2 Deletion mapping of protein-protein interactions within the yeast two hybrid system*

It is worth noting that deletion mutagenesis, which is often applied in mapping protein-protein interactions, may affect protein stability. The deletion of an N- or C-terminal domain for example may present hydrophobic residues to the solute which would otherwise be buried within the interior of the protein or disrupt the protein backbone sufficiently to generate a mis-folded protein. Moreover, the sites of protein-protein interaction under analysis may be in broad non-overlapping domains and not condensed into a single specific domain. This would therefore not be detected using deletion mutagenesis and could lead to ambiguous and/or misleading results regarding sites of possible protein-protein interaction (Vidal and Legrain 1999; Desai and Person, 1996).

### 3.1.2 Reverse yeast two hybrid system

Vidal et al., (1996a and 1996b) were the first group to describe a reverse genetic selection, yeast two-hybrid system, termed the reverse yeast two-hybrid system. This yeast two-hybrid system could select, through the use of a counter-selectable marker, discrete single amino acid mutations that disrupted a defined protein-protein interaction. Vidal et al., (1996b) analysed the interaction between the transcription factor E2F1 and its partner DP1. They utilised random PCR mutagenesis to generate libraries of mutant E2F1 alleles and reverse genetic selection within yeast cells to identify those alleles with mutated amino acids, which abolished the interaction between E2F1 and DP1. Using this system they could identify, not only site specific mutations which affected the interaction but also second site compensatory mutations within DP1 which could restore the interaction. This ability to genetically select and map single mutations and compensatory mutations circumvented the typical problems associated with the yeast two hybrid system. For this reason, the reverse two-hybrid system was chosen to analyse the interaction between VP19c and VP23 and is summarised schematically in fig. 3.1.2 and discussed below.

### 3.1.3 Reverse yeast two hybrid analysis of VP19c and VP23

#### 3.1.3.1 Generation of mutant alleles

Libraries of mutant UL18 alleles were made by random PCR mutagenesis (as described in Methods) using generic forward and reverse primers (shown in fig. 3.1.10, panel B) located within the GAL4 AD and T<sub>ADC1</sub> (see fig. 3.1.3) sequences respectively (described by Vidal et al., 1996b). MaV103 cells that had already been transformed with pPc97UL38 (MaV103pPc97UL38) were subsequently transformed with the mutant UL18 alleles and a linearised EcoRI/NotI digested and CIP treated pPc86 backbone vector. Due to the overlapping AD and T<sub>ADC1</sub> sequences within the UL18 PCR products and the vector, recombination and gap repair can occur within yeast cells to regenerate a functional pPc86UL18Mut. plasmid. UL18 alleles that produced a mutated VP23AD fusion protein that abolished the interaction with VP19cDB were then selected for their resistance to the counter selectable marker.

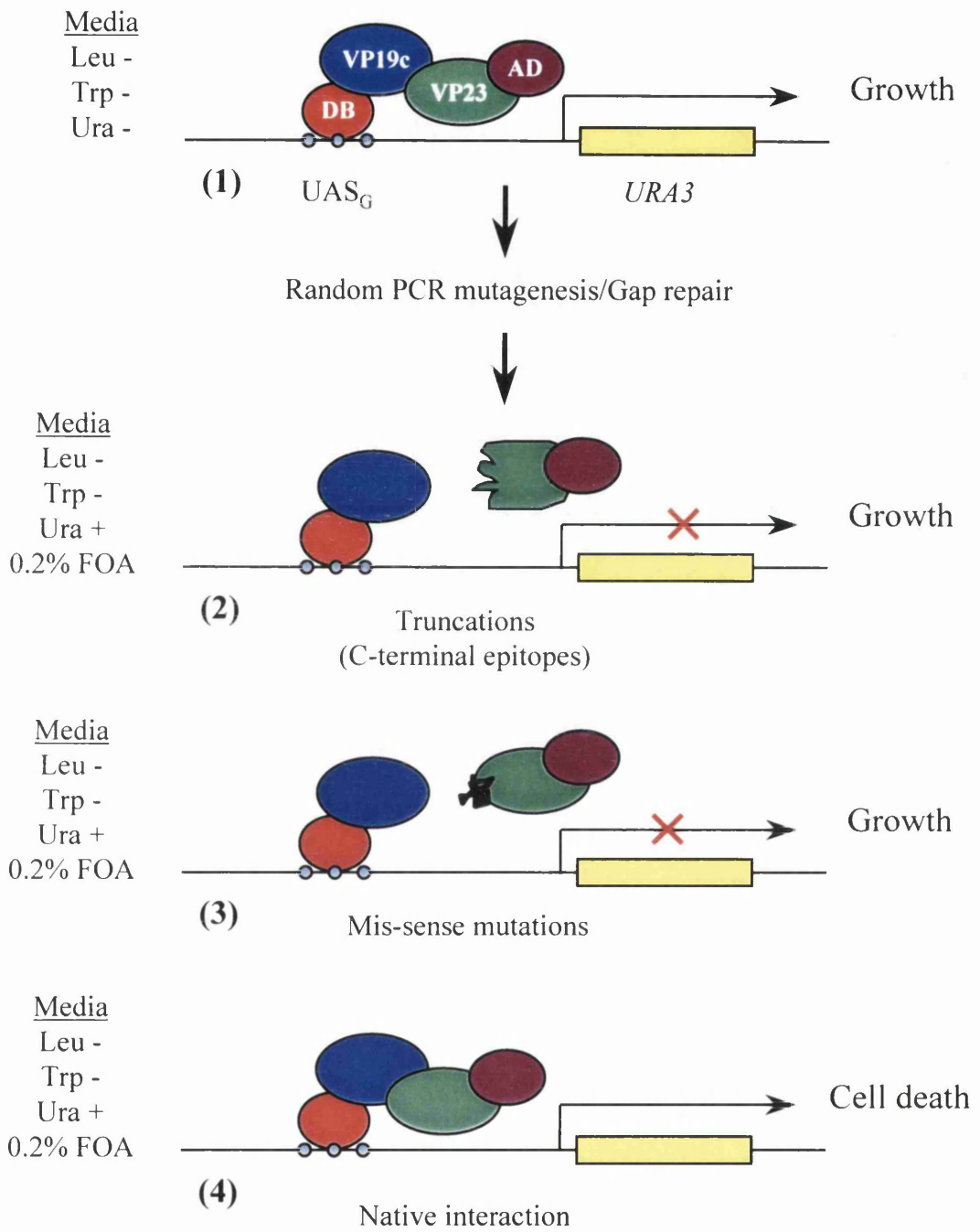


Fig. 3.1.2: Schematic representation of the reverse yeast two hybrid system

### 3.1.3.2 Negative selection of mutant alleles

The reporter gene *URA3* can act as both a negative and positive growth selection marker on medium containing 5-fluoroorotic acid (FOA) or on medium lacking uracil respectively. *URA3* encodes orotidine-5'-phosphate decarboxylase, an enzyme required for the biosynthesis of uracil. Orotidine-5'-phosphate decarboxylase can also convert the non-toxic FOA into a toxic uridine analogue 5-fluorouracil. Therefore, any transcriptional activation of *URA3* due to the interaction of hybrid AD and DB fusion proteins will result in the cell developing a FOA sensitive (FOA<sup>S</sup>) phenotype which will prevent growth. Thus, a large population of FOA<sup>S</sup> cells containing a few FOA resistant (FOA<sup>R</sup>) cells can be screened and those that are FOA<sup>R</sup> selected for further analysis.

### 3.1.3.3 Regulation of *URA3* and *lacZ* reporter genes within MaV103 cells

Basal levels of most GAL4 inducible promoters in *S. cerevisiae* are high enough to confer an FOA<sup>S</sup> phenotype. To counter this in MaV103 cells a *URA3* reporter gene promoter was manufactured to contain a strong cis-acting upstream repression sequence (URS). The URS containing element within the *URA3* reporter gene promoter is the yeast sporulation gene, *SPO13*, promoter. *SPO13* is tightly repressed within yeast cells during mitotic growth and only activated under sporulation conditions. Therefore the fusion of the *SPO13* promoter to the wild type *URA3* ORF confers a very tight *Ura*<sup>-</sup>, FOA<sup>R</sup> phenotype under normal growth conditions. To allow induction by GAL4 the *SPO13* promoter was modified to contain 10 GAL4-DNA binding sites (SPAL10::*URA3*) to allow efficient GAL4 dependent activation. To ensure stability and reproducibility of results within MaV103 cells the SPAL10::*URA3* promoter construct was integrated into the yeast genome replacing the endogenous, disrupted Ty element at the *ura3-52* locus on chromosome IV.

### 3.1.3.4 Other reporter genes within MaV103 cells

The *lacZ* reported gene is fused to the full length GAL1 promoter to generate *GAL1::lacZ* at an unknown locus within the yeast chromosome. MaV103 cells also contain an integrated single copy of the *His3* reporter gene linked to its own promoter containing an integrated 125bp GAL<sub>UAS</sub> sequence to generate *GAL1::HIS3*. HIS3 encodes imidazole glycerol phosphate dehydratase, an enzyme required in histidine biosynthesis. This enzyme can be inhibited in a dose dependent manner by 3-aminotriazole (3-AT). Therefore, the strength of GAL4 transcriptional activation can be titrated in a dose dependent manner by 3-AT, using the induction of transcriptional activation of *GAL1::HIS3* as a positive selection for interacting fusion proteins. Reporter gene construction and regulation is discussed in detail in Vidal et al., (1996a); Kishore and Shah (1988); Fields and Song (1989); Durfee et al. (1993).

### 3.1.3.5 GAL4 fusion vectors used in the reverse yeast two hybrid system

pPc86 and pPc97 expression vectors were obtained from Marc Vidal and are illustrated schematically in fig. 3.1.3 (panels A and B respectively). pPc86 encodes the GAL4(AD) sequence and pPc97 encodes the GAL4(DB) sequence, which are expressed from the yeast constitutive promoter P<sub>ADC1</sub>. The polylinker region is flanked by a terminator (T<sub>ADC1</sub>) sequence from the yeast *ADC1* gene. The pPc86 plasmid carries a *Trp1* selection marker and has a NLS sequence fused to the GAL4(AD) codons for efficient translocation of AD hybrid proteins to the nucleus. The pPc97 plasmid carries a *Leu2* selection marker. Both pPc86 and pPc97 encode a bacterial origin of replication (*ColE1 ori*), a yeast centromere (*CEN6*), a yeast origin of replication (*ARSH4*) and an ampicillin resistance gene (*Amp*). Unique restriction sites are marked in red. The construction of pPc86 and pPc97 is described in Chevray and Nathans (1992), and Vidal et al (1996b).

### 3.1.3.6 Cloning of UL18 into pPc86

The UL18 ORF was subcloned from pETUL18 (described in section 3.3) as a EcoRI/NotI fragment. This removed the ATG start codon and the 6xHis tag from the ORF. The pPc86 vector was digested with EcoRI/NotI and the overhanging ends dephosphorylated using

---

CIP (as described in Methods). The UL18 fragment was ligated into the linear vector and electroporated into DH5 $\alpha$  bacteria. Recombinant colonies were isolated and plasmid DNA obtained. Plasmids were analysed for the presence of the UL18 ORF by EcoRI/NotI digestion. The UL18 ORF cloning strategy is schematically represented in fig. 3.1.4.

#### *3.1.3.7 Cloning of VP19c into pPc97*

The UL38 ORF was sub cloned from pETUL38 as an EcoRI/NotI fragment, this removed the ATG and 6xHis tag from the ORF. This fragment was subcloned into the pPc86 vector to generate pPc86UL38 (as described above for the UL18 ORF cloning strategy). The UL38 ORF was then sub cloned out of pPc86UL38 as a Sall/NotI fragment and cloned in to Sall/NotI digested and CIP treated pPc97 vector. Recombinant plasmids were analysed for the presence of the UL38 ORF by a Sall/NotI digest. The UL38 ORF cloning strategy is schematically represented in fig. 3.1.5.

#### *3.1.3.8 Fusion protein C-terminal truncations*

One of the possible outcomes of random PCR mutagenesis is the generation of transcripts that encode a premature stop codon within the ORF and thus generate a truncated fusion protein. In order to screen out these truncated fusion proteins, and due to the lack of monoclonal antibodies against VP19c, it was decided to clone a small epitope tag onto the C-terminus of VP19c that could be screened for by Western blotting. The epitope chosen was pp65 from HCMV.

#### *3.1.3.9 Cloning strategy for UL38 pp65 epitope tagged into pPc97*

The UL38 ORF was sub cloned from the pETUL38 vector as a EcoRI/SphI fragment, removing the ATG and the 6xHis tag from the ORF. The SphI digest also removed the stop codon and the last 4bp of the UL38 ORF. The C-terminus was reconstructed by the ligation of an oligonucleotide (fig. 3.1.6, panel B) that encoded the pp65 epitope tag and contains an engineered NotI site down stream from the stop codon. The sense and anti-sense oligonucleotides were purified as described in Methods and heated in a dry block at 100°C for 2 minutes in the presence of 1x ligation buffer (Gibco-BRL). The

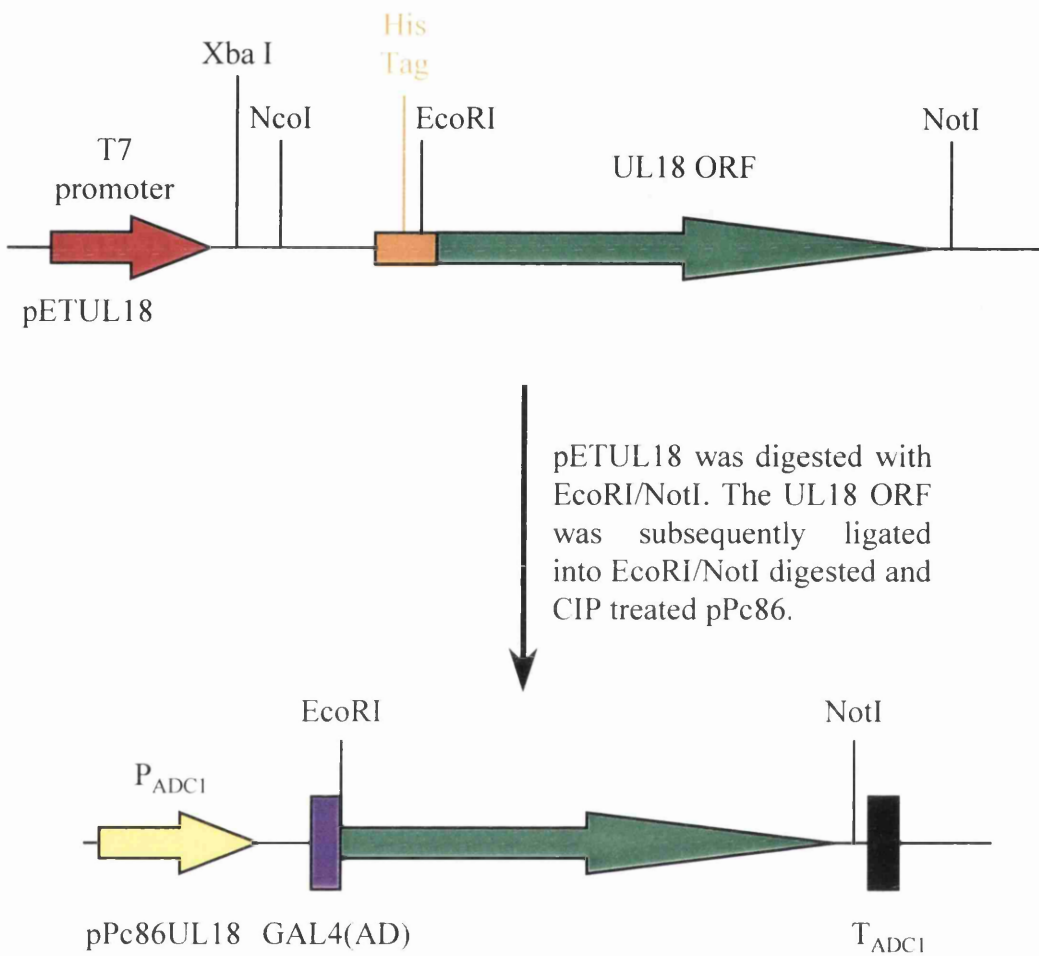


Fig. 3.1.4: Cloning strategy of UL18 ORF into pPc86

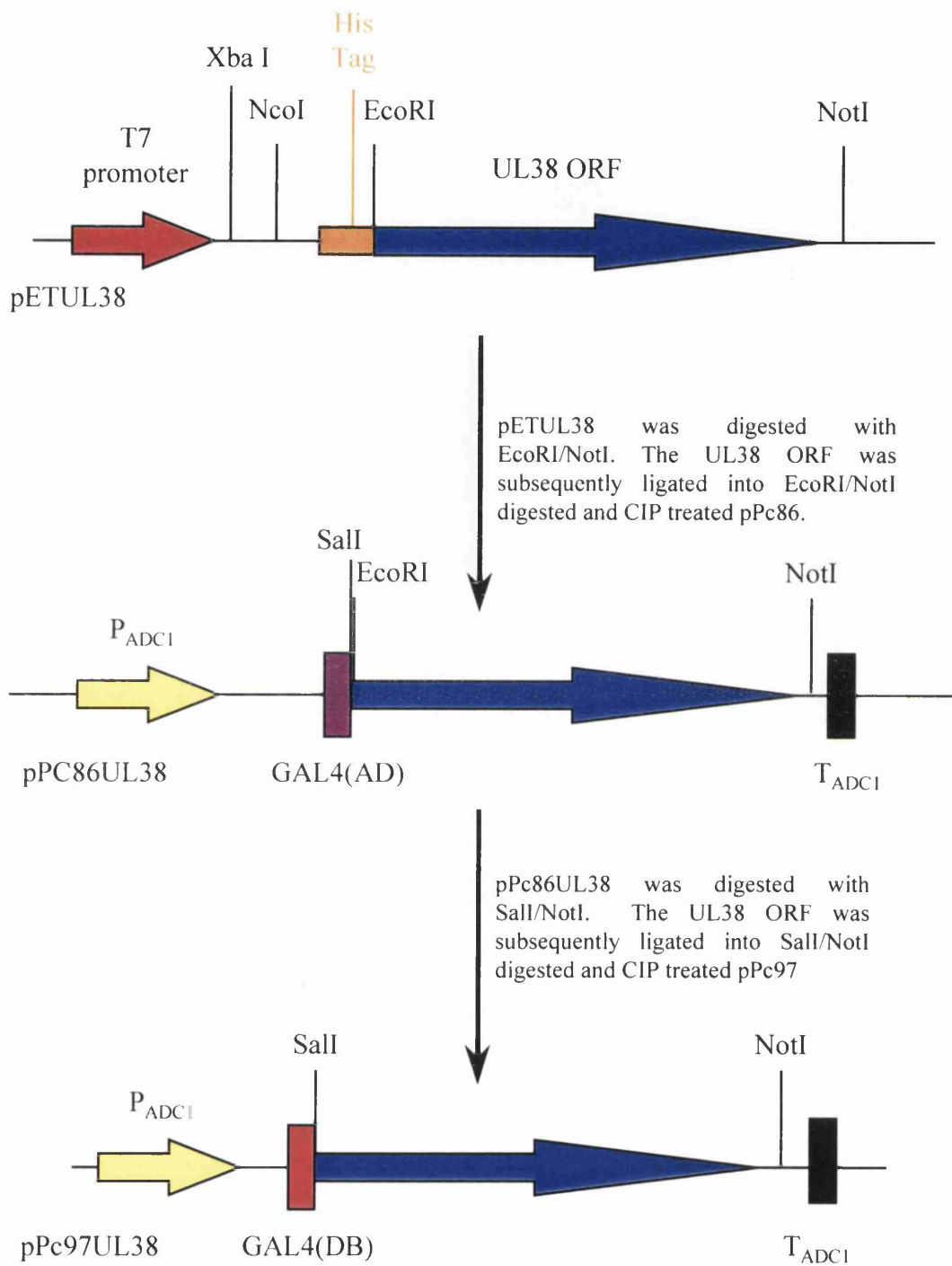
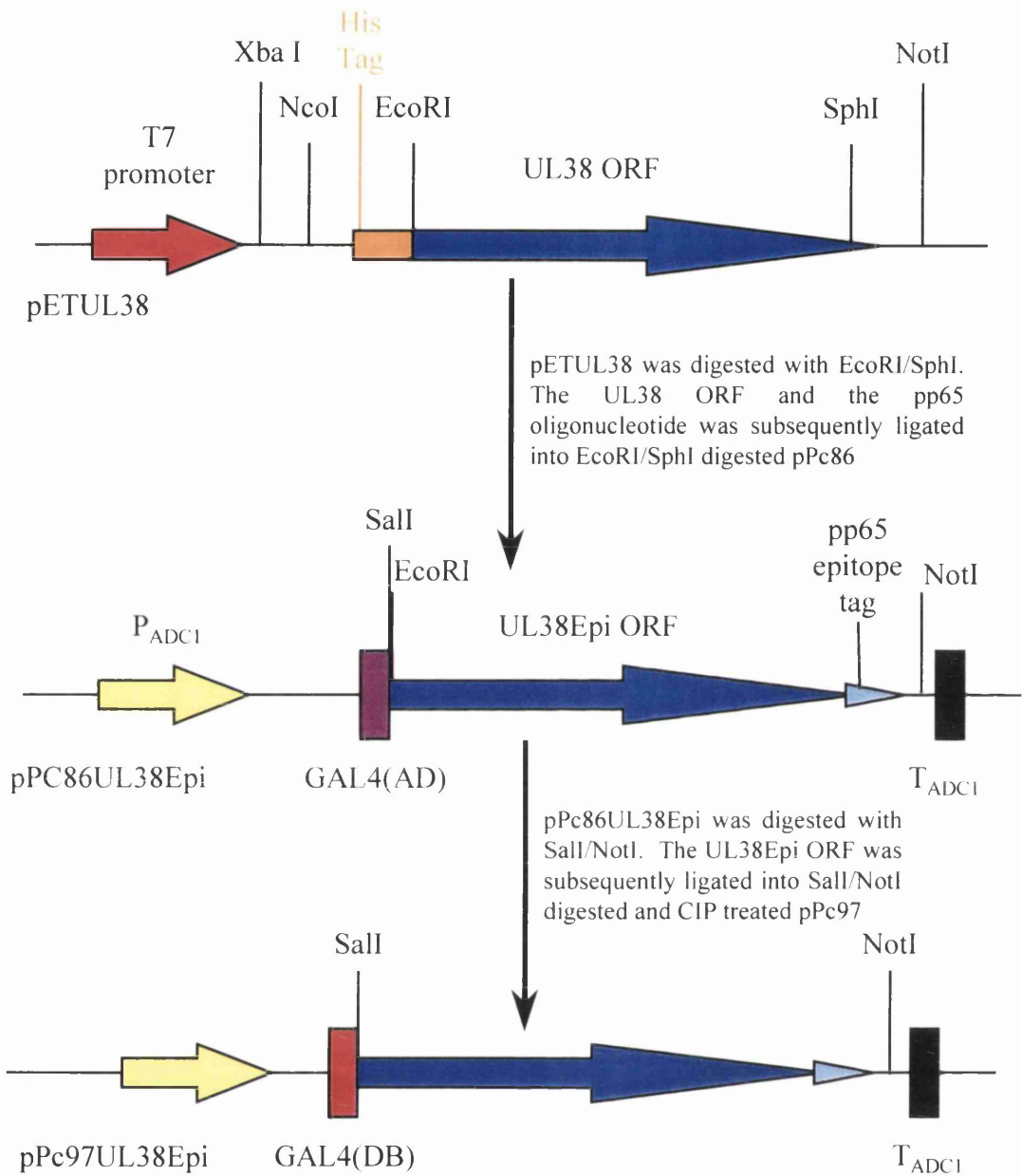
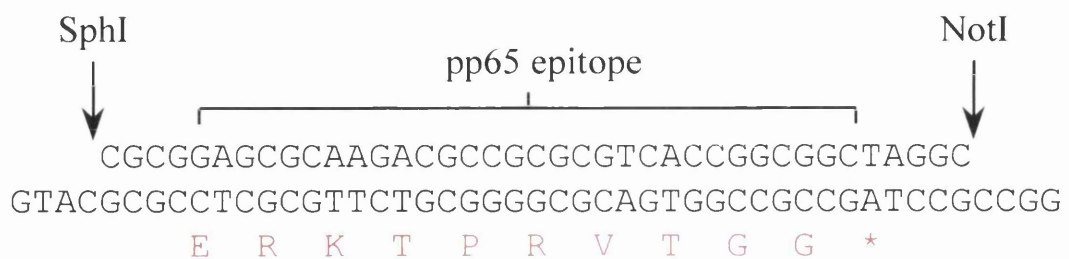


Fig. 3.1.5: Cloning strategy of UL38 ORF into pPc97



(A)



(B)

Fig. 3.1.6: Cloning strategy of pPc97UL38Epi (A) and nucleotide sequence for the sense and anti-sense pp65 epitope tag (B). Amino acid sequence encoded by the pp65 tag is highlight in red.

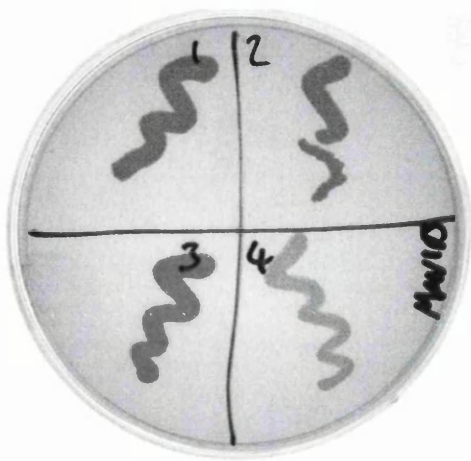
oligonucleotides were annealed by allowing the dry block to cool naturally to RT. The EcoRI/SphI UL38 ORF was ligated into EcoRI/NotI digested and CIP treated pPc86 vector in the presence of the annealed oligonucleotides. The ligation mix was electroporated into DH5 $\alpha$  bacteria and single recombinant colonies were grown. The plasmid DNA was screened for the presence of the reconstituted UL38 ORF by EcoRI/NotI digestion. Plasmids containing the correct insert (pPc86UL38Epi) released a DNA fragment of ~1500bp. The tagged UL38 ORF was sub cloned from pPc86UL38Epi as a Sall/NotI digest and ligated into Sall/NotI digested and CIP treated pPc97 vector. Recombinant plasmids were isolated and analysed for the presence of the UL38 ORF by a Sall/NotI digest. The cloning strategy is schematically represented in fig. 3.1.6, panel A.

### 3.1.6 Conclusions

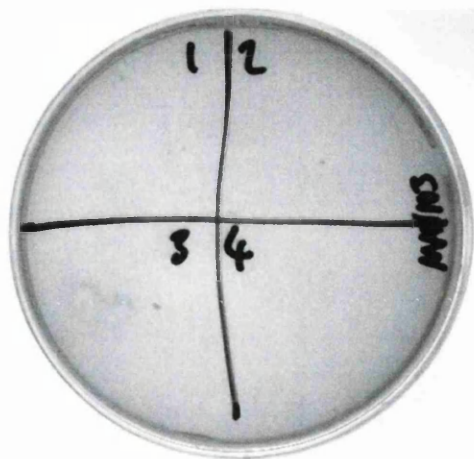
#### 3.1.6.1 Yeast two hybrid analysis

MaV103 cells were unable to grow on synthetic agar medium lacking either *Leu* or *Trp* (fig. 3.1.7). Growth of colonies was dependent on the successful transformation of either pPc86 or pPc97 yeast hybrid vectors when plated out on to synthetic medium lacking *Trp* or *Leu* respectively. Colony development of MaV103 cells only proceeded on synthetic agar medium lacking *Leu/Trp/Ura* when the MaV103 cells were co-transformed with plasmids expressing both the GAL4 AD and DB domains fused to VP23 and VP19c respectively (figs. 3.1.8, panel A). MaV103 cells expressing plasmids encoding only VP19c or VP23 but co-transformed with the appropriate complementing empty GAL4 fusion plasmid did not induce the transcriptional activation of *URA3* or  $\beta$ -galactosidase. This requirement for both capsid fusion proteins to be expressed indicates that the protein-protein interaction between VP19c and VP23 within yeast cells is sufficient to co-localise AD and DB domains and restore GAL4 transcriptional activity. This result also demonstrates that the fusion of the AD and DB domains on to VP23 and VP19c respectively does not appear to disrupt their interaction.

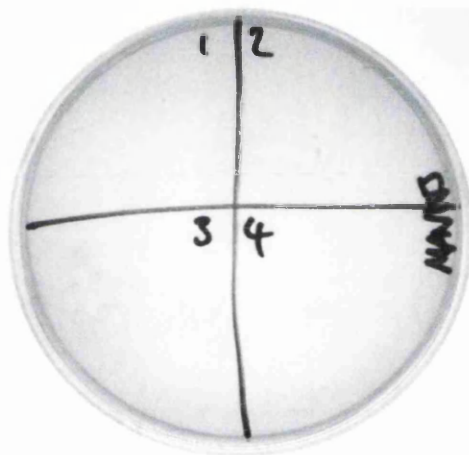
The interaction between VP19c and VP23 was further validated colourmetrically by the  $\beta$ -galactosidase filter assay (fig. 3.1.8, panel B). Only those cells co-transformed with



YPD



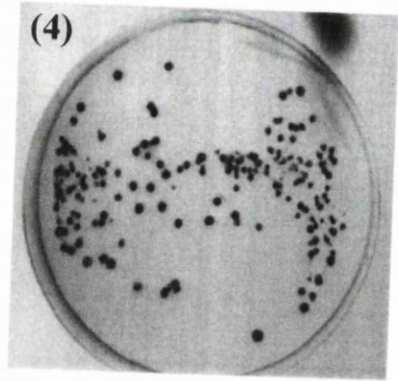
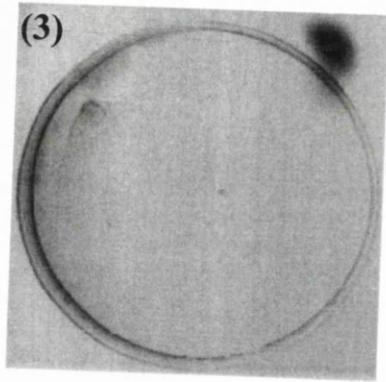
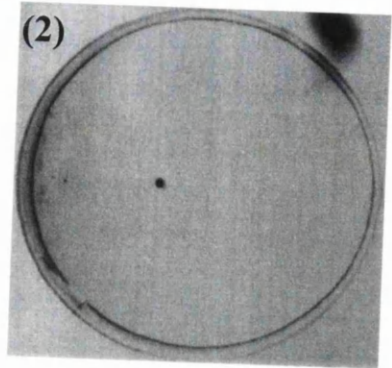
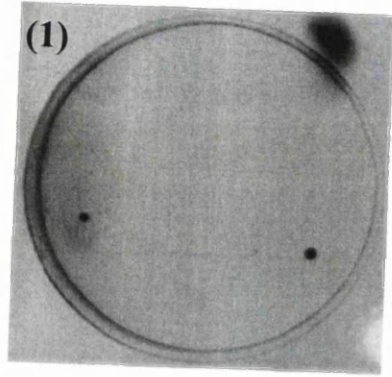
-*Trp*



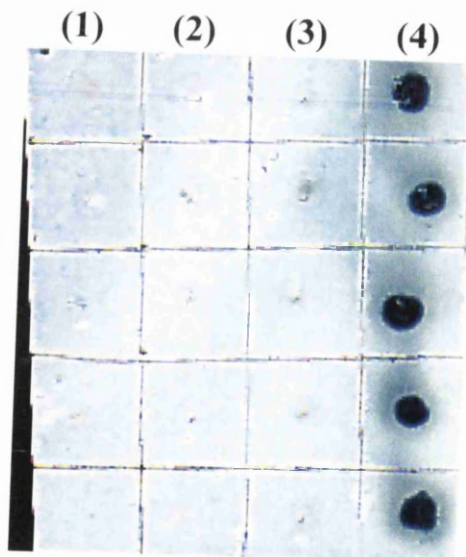
-*Leu*

Fig. 3.1.7: Phenotypic characterisation of the MaV103 yeast cells

Single MaV103 colonies were isolated from a master YPD-agar plate and resuspended in 200 $\mu$ l of sterile dH<sub>2</sub>O. A flamed loop was used to streak the individual resuspended colonies onto YPD agar or onto synthetic agar medium lacking *Trp* or *Leu* (as indicated). Plates were incubated for 2 days at 30°C before being photographed.



(A)



(B)

Fig. 3.1.8: Yeast two hybrid analysis and  $\beta$ -galactosidase filter assay.

MaV103 cells were co-transformed with the appropriate plasmids and plated out onto SD-agar plates deficient in *Leu/Trp/Ura*. Yeast colonies were allowed to grow for 10 days at 30°C before being photographed. MaV103 cells co-transformed with; (A) Panel 1: pPc86 and pPc97. Panel 2: pPc86 and pPc97UL38 (VP19cDB). Panel 3: pPc86UL18 (VP23AD) and pPC97. Panel 4: MaV103 pPc86UL18 (VP23AD) and pPc97UL38 (VP19cDB). (B)  $\beta$ -galactosidase filter assay. Colonies containing the appropriate plasmids (2-3 days old) were transferred to a reinforced nitrocellulose membrane and cultured as described in Methods. The cells were permeabilised in liquid nitrogen and assayed for the presence of  $\beta$ -galactosidase as described in Methods. MaV103 cells were co-transformed with; Lane 1: pPc86 and pPc97. Lane 2: pPc86 and pPc97UL38 (VP19cDB). Lane 3: pPc86UL18 (VP23AD) and pPC97. Lane 4: pPc86UL18 (VP23AD) and pPc97UL38 (VP19cDB).

plasmids expressing both VP23AD (pPc86UL18) and VP19cDB (pPc97UL38) were able to induce the transcriptional activation of  $\beta$ -galactosidase. As with *URA3*, the transcriptional activation of  $\beta$ -galactosidase requires the GAL4 AD and DB domains to be fused to VP23 and VP19c respectively. Cells expressing plasmids where one of the hybrid fusion proteins was absent were unable to reconstitute GAL4 binding and consequently failed to induce the transcriptional activation of *lacZ*. These results confirm the published findings of Desai and Person (1996) and demonstrate that VP23 and VP19c capsid proteins interact efficiently within yeast cells. The N-terminal GAL4 fusion domains do not appear to affect the ability of VP23 and VP19c to interact and bring the GAL4 domains together to reconstitute GAL4 transcriptional activity.

### 3.1.6.2 Expression of *UL38* and *UL38Epi* in the yeast two hybrid system

It is interesting to note that the *UL38* ORF cloned from the bacterial plasmid pETUL38 was able to restore GAL4 activity (fig. 3.1.9, panel 4), since pETUL38 expression of VP19c within bacteria is very poor and only detectable by Western blot analysis. The fact that the *UL38* ORF restored GAL4 activity within yeast cells with the appropriate hybrid partner suggests that the poor production of VP19c in bacteria is not due to mutations within the *UL38* ORF. However, the construction of a VP19cDB hybrid fusion protein containing a C-terminal pp65 epitope tag abolished the ability of VP19c to interact with VP23AD. This is shown by the inability of MaV103 cells expressing pPc86UL18 and pPc97UL38Epi to grow on synthetic agar medium lacking *Leu/Trp/Ura* (fig. 3.1.9), in contrast to the positive, pPc86UL18/pPc97UL38 control. This suggests that the C-terminal domain of VP19c is essential for the interaction with VP23 and that the insertion of the pp65 epitope tag blocked or changed the conformational arrangement of the C-terminal residues required for the interaction. Indeed, there is some evidence for this from the literature. Desai and Person (1996) could not detect any interaction between VP19c and VP23 utilising the yeast two-hybrid system when the C-terminal third of either protein was deleted. Spencer et al., (1998) also demonstrated by immune precipitation that deletion of just 15 amino acids from the C-terminus of VP19c could abolish the interaction with VP23. The C-terminal deletion mutant of VP19c was also unable to support *in vitro* capsid assembly from infected cell lysates demonstrating the essential requirement for these residues.

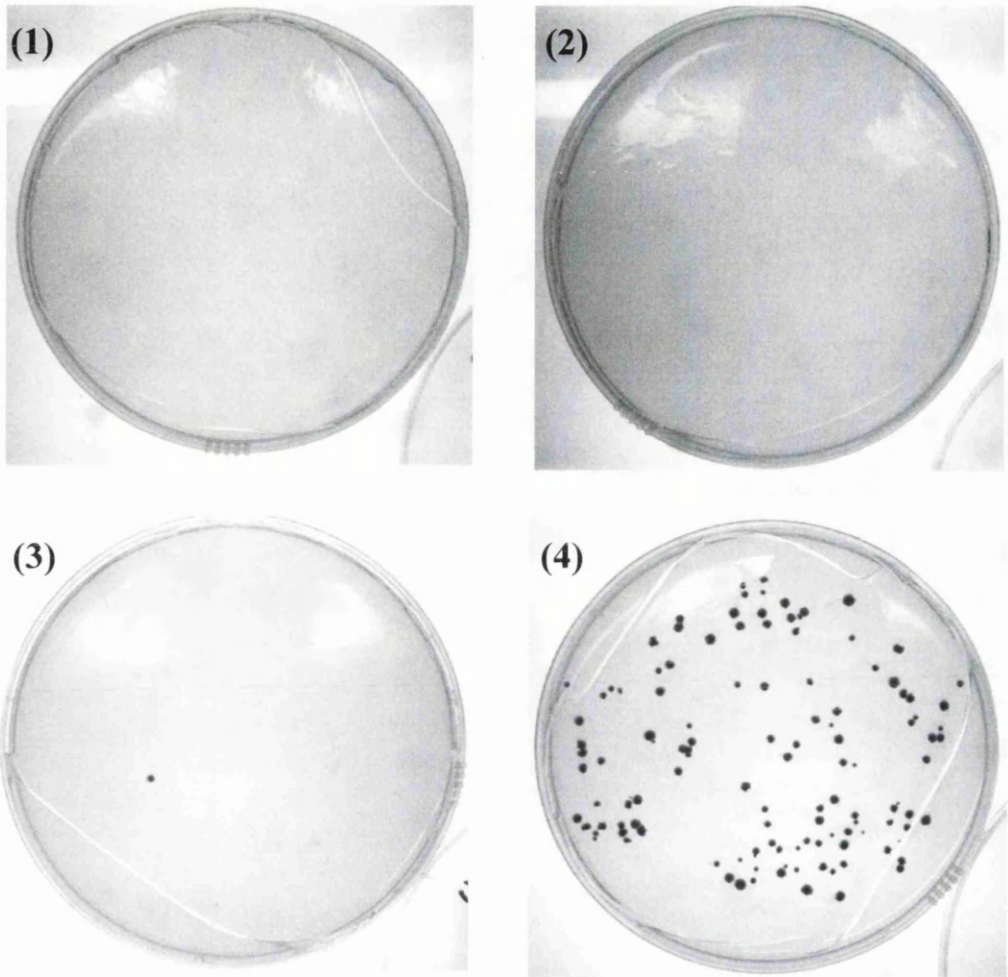


Fig. 3.1.9: Analysis of pPc97UL38Epi (VP19cDB.Epi).

MaV103 cells were co-transformed with the appropriate plasmids and plated out onto SD-agar plates deficient in *Leu/Trp/Ura*. Yeast colonies were allowed to grow for 10 days at 30°C before being photographed. MaV103 cells co-transformed with; Panel 1: pPc86 and pPc97. Panel 2: pPc86 and pPc97UL38 (VP19cDB). Panel 3: pPc86UL18 (VP23DB) and pPc97UL38Epi (VP19cDB.Epi). Panel 4: pPc86UL18 (VP23AD) and pPc97UL38 (VP19cDB).

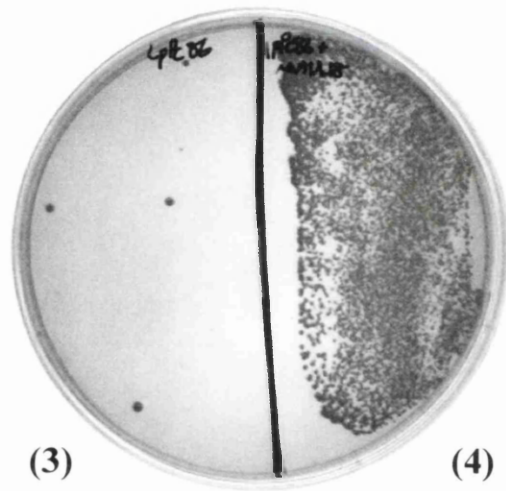
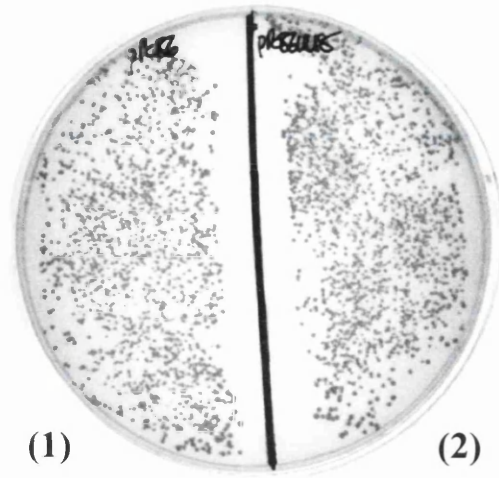
### 3.1.6.3 Reverse yeast two hybrid analysis

Co-transformation of the UL18 PCR products into MaV103 cells together with linear pPc86 vector DNA allowed homologous recombination and gap repair that regenerated replicating vectors that conferred a positive *Trp* selection phenotype (fig. 3.1.10, panel A). However, the only requirement for growth in this experiment is the regeneration of a replicating pPc86 plasmid with or without an insert. If the linearised vector was not dephosphorylated using CIP then the number of false positives increased (data not shown). Gap repair of linearised pPc86 was only detected when co-transformed with a UL18 PCR product (fig. 3.1.10, panel A). No gap repair was detected between the linearised pPc86 plasmid and endogenous pPc97UL38 within the MaV103pPc97UL38 cells (MaV103 cells transformed with pPc97UL38), fig. 3.1.11 (panel 1). This is important since pPc86 and pPc97 are closely related plasmids with much sequence homology.

### 3.1.6.4 FOA selection

As previously described in section 3.1.3.2, FOA can act as counter selectable marker for transcriptional activation of *URA3*. To illustrate this fig. 3.1.11 shows the growth phenotypes on medium lacking *Leu* & *Trp* and containing 0.2% FOA of MaV103 cells transformed with appropriate plasmids. In the presence of FOA the growth of MaV103 cells is dependent upon the disruption of the interaction between the GAL4 fusion proteins. This FOA<sup>R</sup> was demonstrated when the growth of MaV103pPc97UL38 cells transformed with pPc86 vector (fig. 3.1.11, panel 2) was compared to that of MaV103pPc97UL38 cells transformed with pPc86UL18 (fig. 3.1.11, panel 3). These experimental controls demonstrate that 0.2% FOA in the selection medium is sufficient to prevent the growth of colonies displaying an FOA<sup>S</sup> phenotype.

FOA<sup>R</sup> colonies could be selected when mutated UL18 alleles produced by random PCR mutagenesis were co-transformed together with linearised pPc86 into MaV103pPc97UL38 cells. MaV103 cells require both GAL4 hybrid vectors to be present in a circularised form in order to confer growth on media lacking *Leu* and *Trp* (fig. 3.1.11, panel 1 and 2). If one of the GAL4 hybrid vectors is present in a linear form then the cells cannot sustain growth due to the inability of the linear plasmid to replicate and confer selective growth (fig.



(A)

GAL4 AD: 5' CGCGTTTCCAATCACTACAGGG 3'

Term: 5' GGAGACTTGACCAAACCTCTGGCG 3'

(B)

Fig. 3.1.10: Recombination and gap repair of mutant UL18 PCR alleles into linearised pPc86 vector

MaV103 cells were co-transformed with the appropriate plasmids and PCR products and plated out onto SD-agar deficient *in Trp*. Yeast colonies were allowed to grow for 2 days at 30°C before being photographed (A). MaV103 cells transformed with; Panel 1: pPc86. Panel 2: pPc86UL18 (VP23AD). Panel 3: linear (EcoRI/NotI digested/CIP treated) pPc86. Panel 4: linear (EcoRI/NotI digested/CIP treated) pPc86 and Mut.UL18PCR product. (B) Generic forward (AD) and reverse (Term) PCR primers used in the generation of mutant UL18 alleles by random PCR mutagenesis (as described in Methods).

3.1.11, panel 1). Colony growth is therefore dependent on the reconstitution of circular GAL4 hybrid vectors by homologous recombination and gap repair. FOA selection ensures that only those colonies with a reconstituted pPc86 vector expressing a VP23AD fusion protein that cannot interact with VP19cDB, display a FOA<sup>R</sup> phenotype. This non-interaction has a selective advantage on synthetic media containing FOA due to the lack of transcriptional activation of *URA3* which prevents the formation of the toxic metabolite of FOA, 5-fluorouracil. The presence of uracil in the selective medium, ensures that colonies which contain the non-interacting proteins that confer the FOA<sup>R</sup> phenotype, are able to grow and form colonies. These colonies can subsequently be picked for further analysis.

It is worth noting that the number of colonies varied on plates where the pPc86 vector has been rescued by gap repair with different pools of mutated UL18 alleles (figs. 3.1.11, panels 4 and 5). This is unlikely to be due to variation in the final DNA concentration since the PCR reactions were analysed by agarose gel electrophoresis (data not shown) and the concentrations adjusted to keep an approximately uniform concentration of UL18 alleles. The variation in the number of colonies observed is likely to reflect the frequency of reading errors induced by MnCl<sub>2</sub> during PCR mutagenesis. Similarly, more than one *Taq* MnCl<sub>2</sub> induced error per UL18 ORF would also result in the amplification of multi-mutant alleles that had a greater chance of affecting protein-protein interactions between hybrid domain partners.

#### 3.1.6.5 Analysis of negatively selected mutant alleles.

To ensure that colony development was due to non-interacting GAL4 fusion hybrid proteins and not due to a failure in FOA to select FOA<sup>R</sup> colonies. Colonies were replica picked with the appropriate controls onto fresh synthetic agar medium lacking *Leu/Trp* and containing 0.2% FOA (fig. 3.1.12). The positive control for FOA<sup>R</sup>, MaV103 cells containing pPc86 + pPc97UL38 (fig.3.1.12, panel 3) grew successfully in these conditions. Conversely, the negative controls for FOA<sup>R</sup>, MaV103 cells containing pPc86UL18+pPc97UL38 (fig. 3.1.12, panel 2) did not display any growth. It is clear from fig. 3.1.12 (panel 1) that most of the colonies containing putative mutant UL18 alleles had retained their FOA<sup>R</sup> phenotype in the second round of selection. 4 colonies that readily grew on the second round selection plate were chosen randomly and analysed further. The

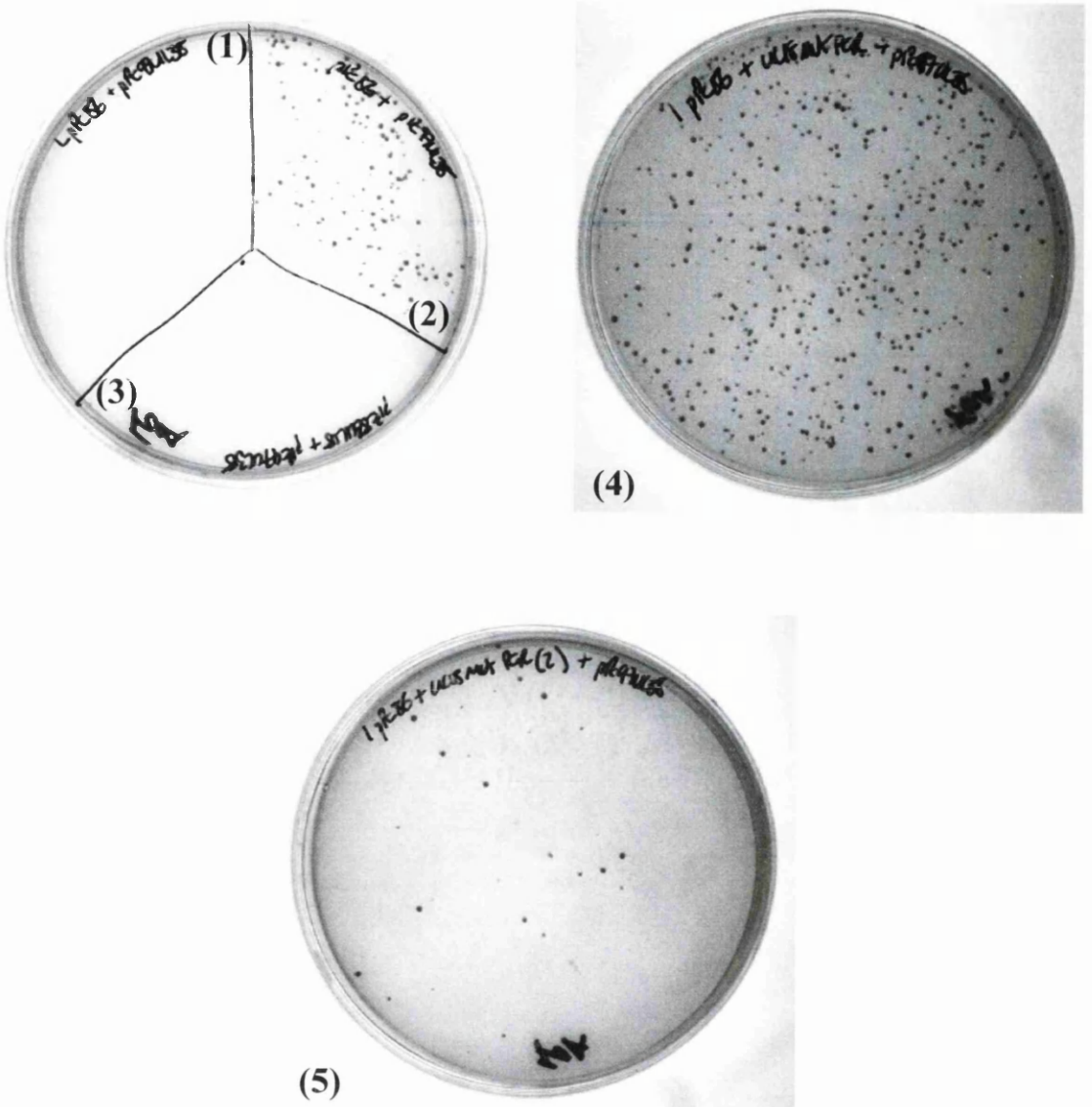


Fig. 3.1.11: FOA negatives selection of mutants UL18 alleles

MaV103pPc97UL38 cells were transformed with the appropriate plasmids and mutated UL18 PCR alleles (as describe in Methods) and plated out onto SD-agar medium lacking *Leu/Trp* containing 0.2% FOA. Yeast colonies were allowed to grow for 4 days at 30°C before being photographed. MaV103pPc97UL38 cells were transformed with; Panel 1: linear (EcoRI/NotI digested/CIP treated) pPc86. Panel 2: pPc86. Panel 3: pPc86UL18 (VP23AD). Panel 4: linear pPc86 and mutated UL18 alleles (PCR1). Panel 5: linear pPc86 and mutated UL18 alleles (PCR2).

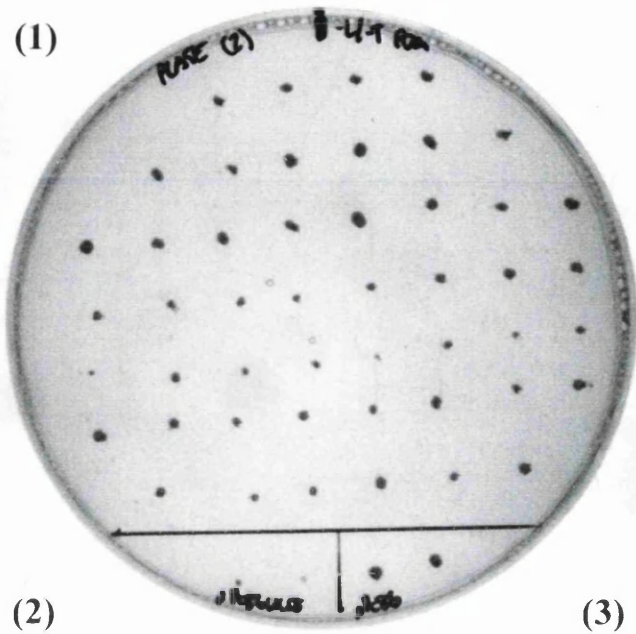
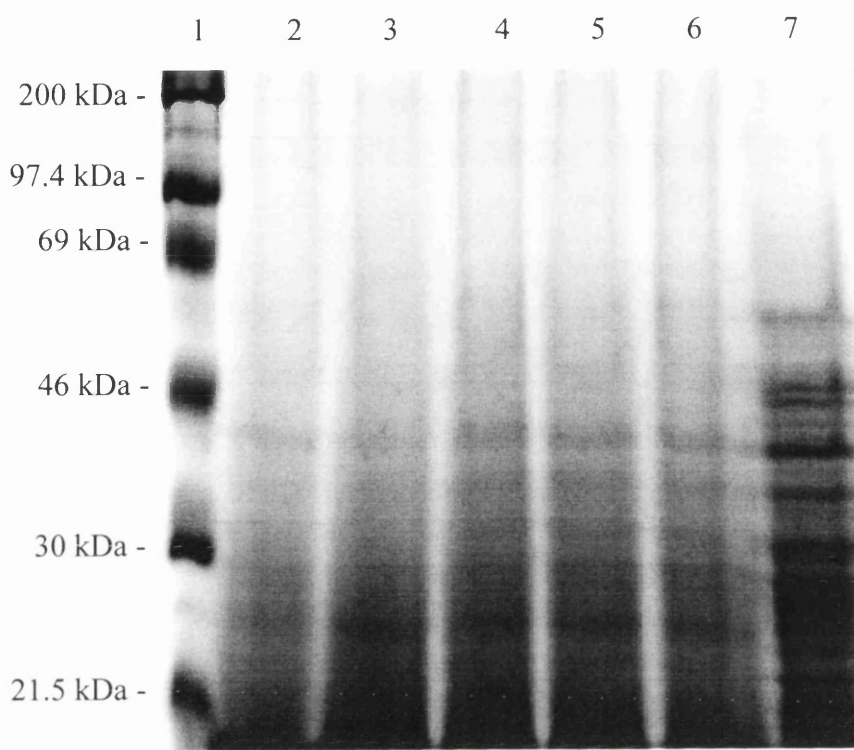


Fig. 3.1.12: Second round FOA selection of mutant UL18 alleles.

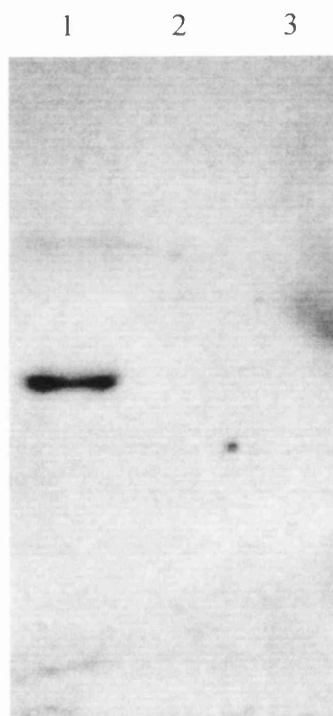
A mixture of colonies from the first round of negative selection were replica picked (as described in methods) with the appropriate controls onto a fresh SD-agar plate lacking *Leu/Trp* containing 0.2% FOA. Plates were incubated for 2 days at 30°C before being photographed. (1) Second round negative selection of picked colonies. (2) Negative control for non-interaction. Two individual replica picked colonies of MaV103pPc97UL38 cells transformed with pPc86UL18. (3) Positive control for non-interaction. Two individual replica picked colonies of MaV103pPc97UL38 cells transformed with pPc86.

possible outcomes of random PCR mutagenesis upon UL18 alleles and the resulting FOA phenotypes are summarised schematically in fig. 3.1.2. The three types of mutant allele that could be generated are: (I) Alleles that are mutated in regions that do not affect protein conformation or affect the sites of interaction with VP19c. These alleles will exhibit the same FOA<sup>S</sup> phenotype as the WT fusion protein and will not grow in the presence of FOA. (II) Alleles which contain mutations that generate stop codons within the ORF, leading to the production of truncated fusion proteins. If the truncation is severe enough to disrupt the interaction, these mutations will prevent GAL4 transcriptional activation of *URA3* and therefore confer a FOA<sup>R</sup> phenotype. (III) Alleles that have random mis-sense mutations within the ORF and generate full length proteins that cannot interact with their hybrid fusion partner. The disruption of interaction could be due, either to direct effects on specific sites involved in protein-protein interaction or to mutations elsewhere in the protein altering its conformation and disrupting the sites required for interaction. These mutations, like those generated in (II), would prevent GAL4 transcriptional activation of *URA3* and therefore colonies containing such alleles would have a FOA<sup>R</sup> phenotype and consequently grow in the presence of FOA.

In order to characterise which type of mutation (II or III) was responsible for the FOA<sup>R</sup> phenotype of the selected colonies, it was decided to screen for any truncated mutant proteins by Western blotting, probing the nitro-cellulose membrane with a monoclonal antibody that specifically recognised VP23. Protein cell extracts were generated from cultures grown from a single colony arising from the second round of FOA selection. Extracts were then analysed by SDS-PAGE and Western blotting. Repeated attempts were made to generate good yeast cell extracts using a variety of methods; these included Y-PER (Pierce) extraction buffer, urea/SDS extraction and TCA protein extraction protocols. The most successful of which was the TCA protein extraction method (described in Methods). The typical recovery of proteins extracted from yeast cells is shown Fig. 3.1.13 (panel A). The poor recovery of proteins from yeast cells is probably due to the thickness of the yeast cell wall and the inefficient cell lysis due to milling with acid washed glass beads. Repeated attempts were made to identify the VP23AD fusion protein by Western blotting, all of which failed (fig. 3.1.13, panel B). Therefore, in order to determine whether or not gap repair had worked plasmid DNA was purified from yeast cultures grown from single colonies derived from the second round FOA selection and digested



(A)



(B)

Fig. 3.1.13: SDS-PAGE and Western blot analysis of yeast cell protein extracts.

Proteins were extracted from yeast cells expressing the appropriate plasmids using the TCA extraction protocol as described in Methods. (A) 20 $\mu$ l of the appropriate extract and 3 $\mu$ l of Rainbow markers (lane 1) were analysed by SDS-PAGE and stained with Coomassie Brilliant Blue. MaV103pPc97UL38 cells transformed with; Lane 2: pPc86. Lane 3: pPc86UL18. Lane 4:  $\Delta$ 01 FOA resistant colony. Lane 5:  $\Delta$ 02 FOA resistant colony. Lane 6:  $\Delta$ 03 FOA resistant colony. Lane 7:  $\Delta$ 04 FOA resistant colony. (B) 20 $\mu$ l of the appropriate extract and 3 $\mu$ l of B capsids (lane 1) were analysed by SDS-PAGE and transferred to a nitro-cellulose membrane as described in Methods. The nitro-cellulose membrane was probed with a monoclonal antibody (CB003), which specifically recognises VP23. Lane 2: MaV103 pPc86UL18 cell extract. Lane 3: MaV103 cell extract.

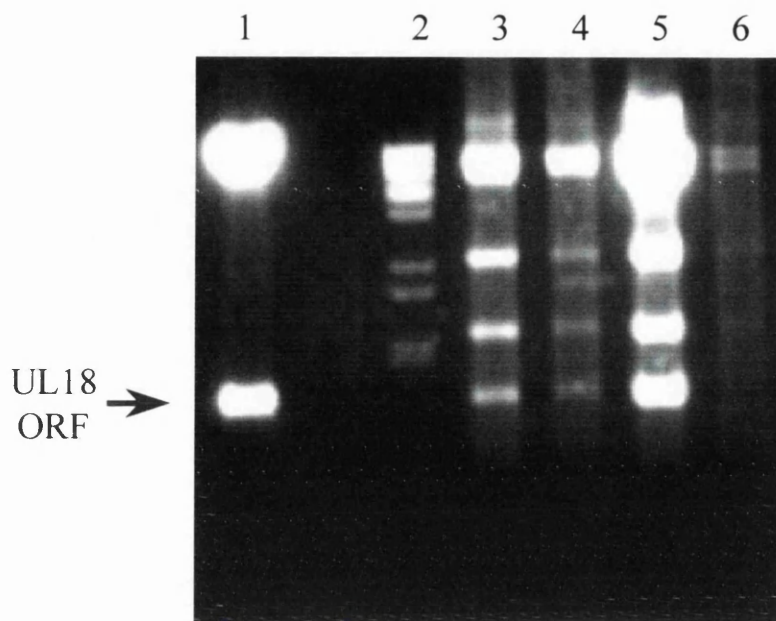


Fig. 3.1.14: 1% TBE gel of plasmid DNA purified from yeast.

Single yeast colonies from the second round of FOA selection were used to seed 5ml of YPD medium and cultured o/n at 30°C in an orbital shaker. Plasmid DNA was isolated from each culture, as described in Methods and analysed for the presence of a ~1000 bp UL18 fragment by an EcoRI/NotI restriction digest. 5µl of each analytical digest was electrophoresed on a 1% agarose gel in 1xTBE. Lane 1: EcoRI/NotI digested pPc86UL18 stock DNA. Lane 2: 1 kb  $\lambda$  BstEII marker. Lanes 3-6: EcoRI/NotI digested plasmid DNA from  $\Delta$ 01 -  $\Delta$ 04 FOA resistant colonies respectively.

with EcoRI/NotI to release the UL18 ORF from the pPc86 expression vector. The results of this digest are shown in fig. 3.1.14. A control digestion was set up (fig. 3.1.14, lane 1) using plasmid stock DNA of pPc86UL18 to identify the appropriate UL18 ORF DNA fragment (indicated by an arrow in fig. 3.1.14). 3 out of the 4 FOA resistant colonies gave DNA fragments of the appropriate size, approximately 1kb in length ( $\Delta 1-3$  FOA<sup>R</sup> colonies). This indicates that the gap repair and homologous recombination into the linear pPc86 vector was successful and that the FOA resistance was probably due to the VP23AD hybrid fusion protein containing mutation(s) which prevented interaction with VP19cDB. Unfortunately due to time constraints at the end of my PhD experiments to identify possible mutants could not be performed.

### 3.1.6.6 Future work

Due to the difficulty in obtaining good protein extracts from yeast cells, and due to the relative low level of expression of the VP23AD fusion protein, the characterisation of possible mutants for truncations and/or mis-sense mutations could not be carried out directly on yeast extracts. Other methods for generating yeast cell protein extracts could be tested in order to characterise possible VP23AD mutants by Western blotting. For example, enzymatic digestion of the yeast cell walls utilising lyticase. An alternative route of analysis would be to subclone possible mutant UL18 ORFs back into the bacterial expression vector pET28MOD. Plasmid DNA isolated from yeast cells could be analysed for the presence of the UL18 ORF by Southern blot analysis. This would provide direct evidence to establish the success of gap repair within yeast cells and provide a further means of testing FOA<sup>R</sup> colonies for the incorporation of UL18 alleles before subcloning.

Following cloning into pET28MOD, the mutated UL18 inserts could be analysed for expression of full length VP23, either by Western blotting, or by direct visualisation of the protein by SDS-PAGE and Coomassie Brilliant Blue staining. Any mutant UL18 alleles identified, which were shown to produce full length VP23AD, would need to be reanalysed for their ability to disrupt the VP19cDB interaction by re-introducing the isolated plasmid DNA back into the reverse yeast two hybrid system. The degree of disruption between the interacting hybrid partners could then be quantified using a  $\beta$ -galactosidase liquid culture assay and comparing the level of  $\beta$ -galactosidase activity to that of the WT hybrid

VP23DB and VP19cAD level. Mutants that demonstrate a significant decrease in the levels of  $\beta$ -galactosidase transcriptional activation could then be sequenced in order to identify the specific amino acid residues that are mutated. This assay could have been used on those colonies selected in the second round of FOA negative selection had time permitted. Mutations identified within the UL18 ORF that disrupt the interaction between VP23 and VP19c should be characterised further, either *in vivo* or *in vitro*, where the capsid proteins are expressed without the GAL4 AD and DB fusion domains, for example in *in vitro* capsid assembly experiments. Such experiments would demonstrate whether or not those mutations detected within the reverse two hybrid system directly affect protein-protein interactions between VP19c and VP23 or whether they their effects are specific to the reverse two hybrid system and abolish GAL4 transcriptional activation by some other mechanism.

---

## 3.2 Characterisation of monoclonal antibodies

One of the consistent problems throughout the course of my PhD was the lack of monoclonal antibodies that could be used to detect the triplex proteins VP19c and VP23. Although the majority of analyses performed upon these proteins involved the recombinant expression of proteins with N-terminal 6x His epitope tags, to which monoclonal antibodies are commercially available (Qiagen), in some cases, such as immunofluorescence, antibodies that could detect untagged proteins were required.

Following the successful purification of 6xHis tagged triplexes in buffer O (see section 3.5.4 for details) from Ac18638 infected SF cells, it was decided to generate a panel of monoclonal antibodies that could specifically recognise amino acid sequences within VP23 and/or VP19c.

### 3.2.1 Immunisation protocol

All immunisation, test bleeds, and fusion procedures were carried out by Susan Graham. BALB/c mice were immunised following the protocol described in Methods (section 2.2.3) and summarised in table 2.2.1. Immunisation was initially carried out using purified triplexes from Ac18638 (VP23His/VP19c) infected SF cells (following the purification strategy described in section 3.5.4). However, following poor detection of anti VP19c activity in test bleeds, it was decided to boost the remaining BALB/c mice with purified VP19cHis. Due to the difficulty associated at the time with purifying recombinantly expressed VP19cHis from SF cells infected with Ac381 (discussed in section 3.4.3), it was decided to purify VP19cHis by denaturing purified triplexes from Ac18386 (VP19cHis/VP23) infected SF cells. As the N-terminal 6xHis epitope tag was located on VP19c the majority of the VP23 was removed by denaturation in 3M urea. The urea was removed by washing the Ni-NTA agarose in buffer O. The bound protein, predominantly denatured VP19cHis, was eluted from the agarose by stripping the Ni<sup>2+</sup> from the NTA agarose resin in EDTA (see section 3.4.2 and fig. 3.4.3 for further details). The mice were boosted with denatured VP19cHis until test bleeds showed positive detection of VP19cHis

(approximately 60 days post VP19cHis immunisation) as determined by quantitative ELSIA analysis. Spleen cells from selected mice were used to generate hybridoma cell lines and the supernatant medium from each cell line was tested for the presence of antibodies against VP19c and VP23.

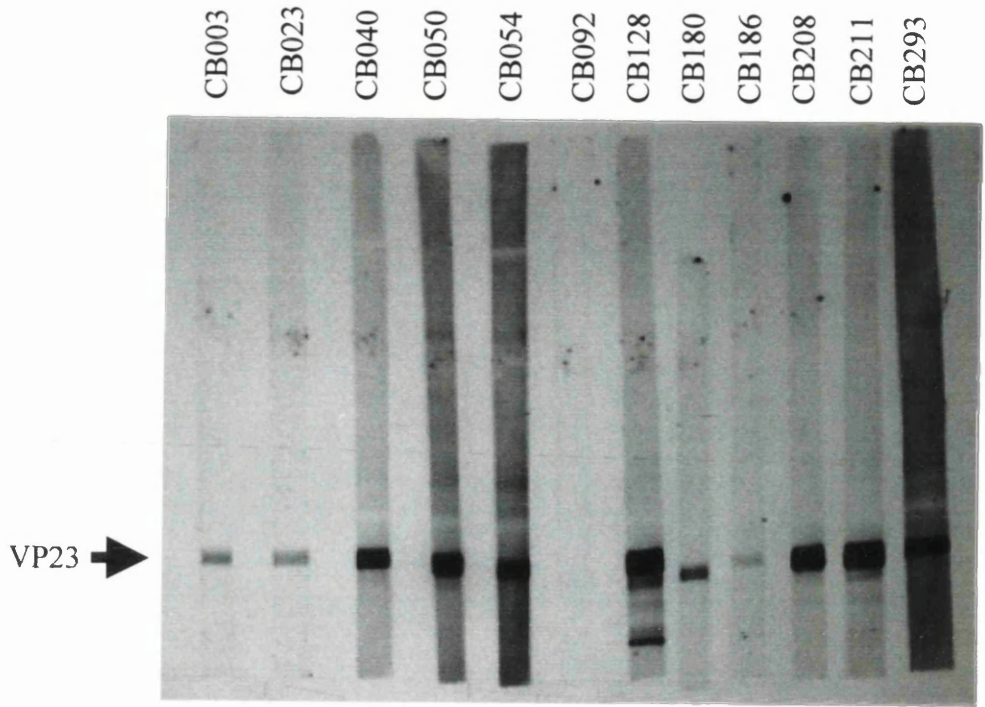
### 3.2.2 Antibody screening by Western blot analysis

#### 3.2.2.1 Monoclonal antibodies generated from BALB/c mouse #4.

Supernatants harvested from hybridoma cell lines generated from spleen cells of a BALB/c mouse (#4), immunised with purified triplexes only, were tested by Western blotting (as described in Methods) for the presence of monoclonal antibodies which recognised purified triplex proteins. Table 3.2.1 summarises the information generated from testing supernatants from 27 hybridoma cell lines. None of these supernatants gave a strong signal against VP19c, which confirms the findings of ELISA analysis showing poor anti-sera response against VP19c. 14 supernatants gave a strong signal against VP23His and these were tested by Western blotting against purified B-capsids in order to determine whether their specificity was directed towards the 6xHis epitope tag located on the N-terminus of VP23His. Fig. 3.2.1 (panel A) shows the results of the Western blot analysis against purified B-capsids. 7 out of the 12 supernatants tested gave a strong signal, 4 gave a good or detectable signal, and 1 (#CB092) failed to detect VP23 suggesting that it might be directed towards the N-terminal 6xHis epitope tag of VP23His. None of the antibodies tested against purified B-capsids recognised VP19c. Fig. 3.2.1 (panel B) shows the immunofluorescence analysis using CB040 to detect the cellular distribution of VP23His in BHK-21 C13 cells transfected with pE18H (a pCMV<sub>10</sub> based plasmid expressing VP23His, see section 3.3.9 for further details). In those cells expressing pE18H, VP23His could readily be detected throughout the cell as previously described by Nicholson et al., 1994 and Rixon et al., 1996.

MAb.	Western blot (18638)		Western blot (B-capsids)		IF
	VP23	VP19c	VP23	VP19c	
CB003	+++	-	++	-	n/t
CB023	+++	-	++	-	n/t
CB040	+++	+	+++	-	+++
CB050	+++	-	+++	-	n/t
CB054	+++	+	+++	-	n/t
CB076	+	-	n/t	n/t	n/t
CB078	-	-	n/t	n/t	n/t
CB084	-	-	n/t	n/t	n/t
CB092	+++	-	-	-	n/t
CB093	-	-	n/t	n/t	n/t
CB095	-	-	n/t	n/t	n/t
CB122	+	-	n/t	n/t	n/t
CB128	+++	-	+++	-	n/t
CB136	-	-	n/t	n/t	n/t
CB144	+	-	n/t	n/t	n/t
CB180	+++	-	++	-	n/t
CB186	++	-	+	-	n/t
CB187	-	-	n/t	n/t	n/t
CB188	+	-	n/t	n/t	n/t
CB197	-	-	n/t	n/t	n/t
CB208	+++	-	+++	-	n/t
CB211	+++	-	+++	-	n/t
CB293	+++	-	+++	-	n/t
CB318	-	-	n/t	n/t	n/t
CB341	+++	-	n/t	n/t	n/t
CB351	+++	+	n/t	n/t	n/t
CB495	+	+	n/t	n/t	n/t

Table 3.2.1: Summary of the monoclonal antibodies generated from BALB/c mouse #4 (120 days post-immunisation). The antibodies were rated for strength of signal by Western blotting against purified triplexes from SF cells infected with Ac18638 (VP23His/VP19c) or purified B-capsids, and by immunofluorescence against cells transfected with pE18H (IF, as described in fig. 3.2.1); +++ (very good), ++ (good), + (weak), - (not detectable), and n/t (not tested).



(A)



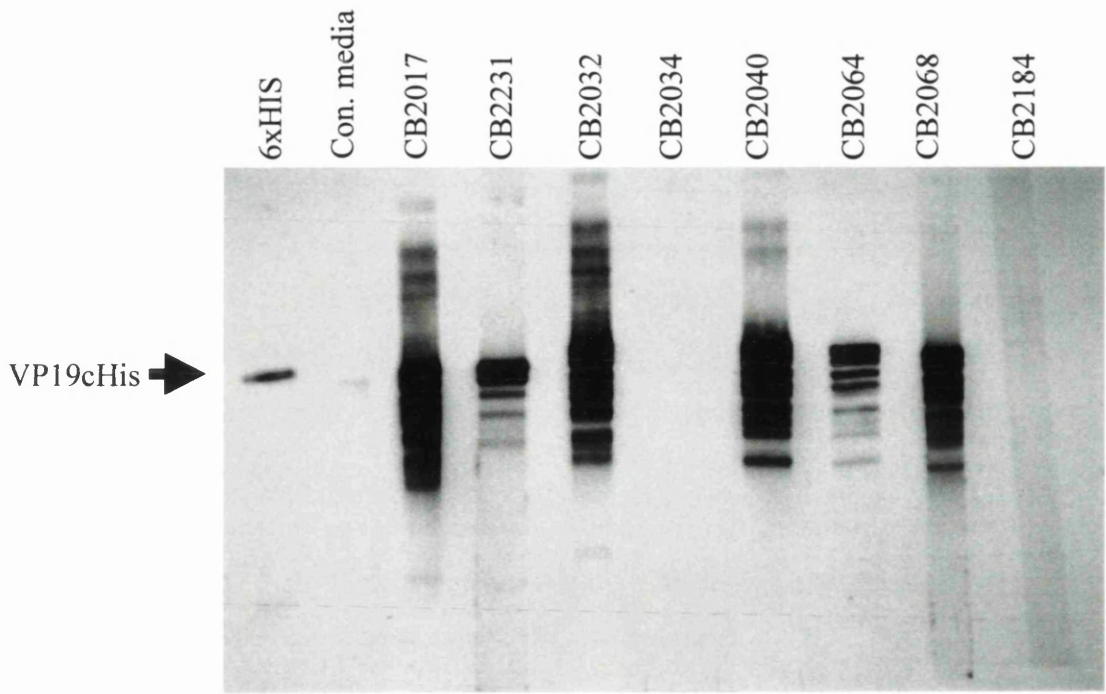
(B)

Fig. 3.2.1: Characterisation of monoclonal antibodies produced from BALB/c mouse #4

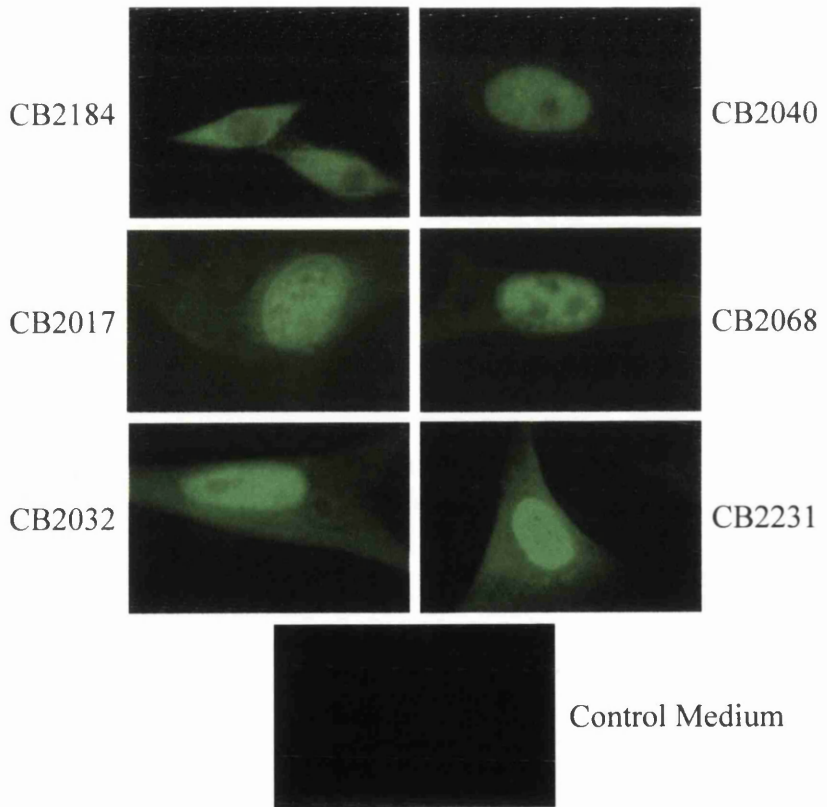
Western blot analysis was performed (as described in Methods) against purified B-capsids. Following protein transfer and membrane blocking, the nitro-cellulose membrane was cut into strips using a sterile scalpel. The strips were individually probed with hybridoma cell supernatants in order to test for the presence of monoclonal antibodies that specifically recognised VP23 (A). The arrow indicates the predicted position of VP23 as judged from transferred Rainbow markers. (B) BHK-21 C13 cells were transfected with pE18H (VP23His), as described in Methods. The cellular distribution of VP23His was analysed by immunofluorescence using the hybridoma cell supernatant CB040 and a secondary goat anti-mouse IgG antibody conjugated to FITC (Sigma).

### 3.2.2.2 Monoclonal antibodies generated from BALB/c mice #1-3

Supernatants harvested from hybridoma cell lines generated from spleen cells of the remaining three BALB/c mice (#1-3), boosted with denatured VP19cHis (designated by CB2), were analysed by Western blotting (as described in Methods). Fig. 3.2.2 (panel A) shows Western blot analysis of hybridoma supernatants tested for the presence of monoclonal antibodies that recognised purified VP19cHis from Ac381 infected SF cells. 6 out of the 8 supernatants tested gave a strong signal and 2 (#CB2034 and #CB2184) failed to detect the presence of purified VP19cHis. In order to determine whether or not their antibody specificity was directed towards the 6xHis epitope tag located on the N-terminus of VP19cHis, immunofluorescence was performed on BHK-21 C13 cells transfected with pE38 (a pCMV<sub>10</sub> based plasmid expressing VP19c, see section 3.3.9 for further details). Fig. 3.2.2 (panel B) shows the cellular distribution of VP19c as detected by CB2017, CB2032, CB2040, CB2068, and CB2231, compared to that of a control medium (sterile hybridoma growth medium) and CB2184 (negative controls). In those cells expressing pE38, VP19c gave a characteristic nuclear staining pattern as previously described by Nicholson et al., 1994 and Rixon et al., 1996, which could readily be detected within the nucleus using CB2017, CB2032, CB2040, CB2068, and CB2231. Control media failed to detect the presence of VP19c in pE38 transfected cells. As VP19c does not contain a His tag this suggests that these antibodies specifically recognise epitopes within VP19c and are not directed towards the N-terminal 6xHis tag of VP19cHis which was used during the immunisation process. CB2184, which failed to detect VP19cHis in Western blot analysis, gave an unusual staining pattern in BHK cells, demonstrating a predominantly cytoplasmic, rather than the typical nuclear, fluorescence. These results taken together would suggest that CB2184 has no specific activity towards VP19c. The characteristics of the monoclonal antibodies generated from BALB/c mice #1-3 are summarised in table 3.2.2.



(A)



(B)

Fig. 3.2.2: Characterisation of monoclonal antibodies produced from BALB/c mice #1-3

Western blot analysis was performed (as described in Methods) against VP19cHis purified from SF cells infected with Ac381 (as described in section 3.4.3). Following protein transfer and membrane blocking, the nitro-cellulose membrane was cut into strips using a sterile scalpel. The strips were individually probed with Hybridoma cell supernatants in order to test for the presence of monoclonal antibodies that specifically recognised VP19His (A). Control media (sterile hybridoma growth medium) and a commercially available monoclonal 6xHis antibody (Qiagen) were also analysed for comparative purposes. The arrow indicates the position of VP19cHis as detected by the 6xHis monoclonal antibody. (B) BHK-21 C13 cells were transfected with pE38 (VP19c), as described in Methods. The cellular distribution of VP19c was analysed by immunofluorescence using the hybridoma cell supernatants of CB2017, CB2032, CB2040, CB2068, and CB2231 and a secondary goat anti-mouse IgG antibody conjugated to FITC (Sigma). Control media and the hybridoma cell supernatant of CB184 were used as negative controls. CB2064 hybridoma cell line was not established prior to IF analysis and therefore remains untested.

MAb.	Western blot (381)	IF (pE38)
CB2017	+++	+++
CB2032	+++	+++
CB2034	-	n/t
CB2040	+++	+++
CB2064	+++	n/t
CB2068	+++	+++
CB2184	-	-
CB2231	+++	+++

Table 3.2.2: Summary of the monoclonal antibodies generated from BALB/c mice #1-#3 (225 days post-immunisation) and mouse #2 (246 days post-immunisation). The antibodies were rated for their respective strengths of signal by Western blotting and immunofluorescence; +++ (very good), ++ (good), + (weak), - (not detectable), and n/t (not tested).

### 3.2.3 Conclusions and future work

Following the solubilisation of triplex proteins a number of monoclonal antibodies were raised which specifically recognised amino acid sequence epitopes within either VP19c or VP23. Some of these antibodies have been used in further immunofluorescence analyses described within this thesis (sections 3.3.9 and 3.3.10). However, all the characterisation analyses described above and elsewhere in this thesis were performed using neat hybridoma supernatants. Work is currently on going within our laboratory to concentrate and purify these antibodies from large-scale cultures of their hybridoma cell lines through the use of affinity chromatography. Once purified these antibodies could be used to further characterise the interactions between VP23 and VP19c. This could be accomplished by antibody blocking studies, for example either using Ni-NTA agarose pull down analysis (described in section 3.4.4) or through ELISA blocking studies, and epitope mapping those antibodies which specifically prevent triplex formation.

## 3.3 Characterisation of the triplex protein VP23

### 3.3.1 Construction and expression of pETUL18

#### 3.3.1.1 Cloning of the UL18 ORF into pET28MOD

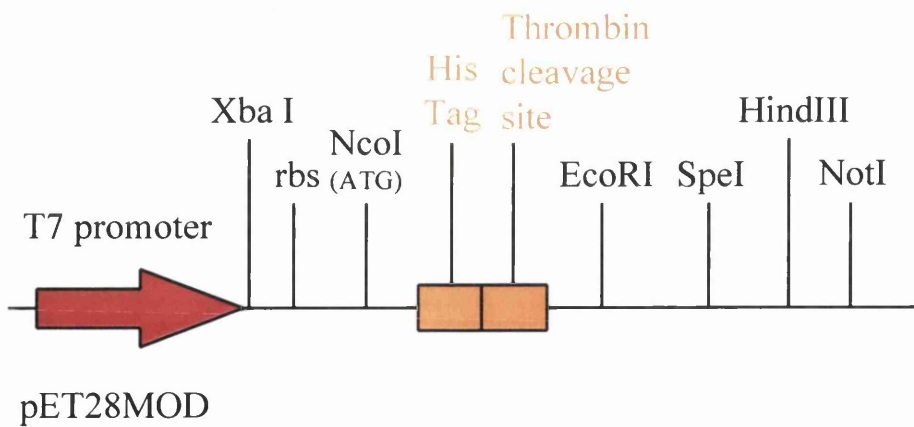
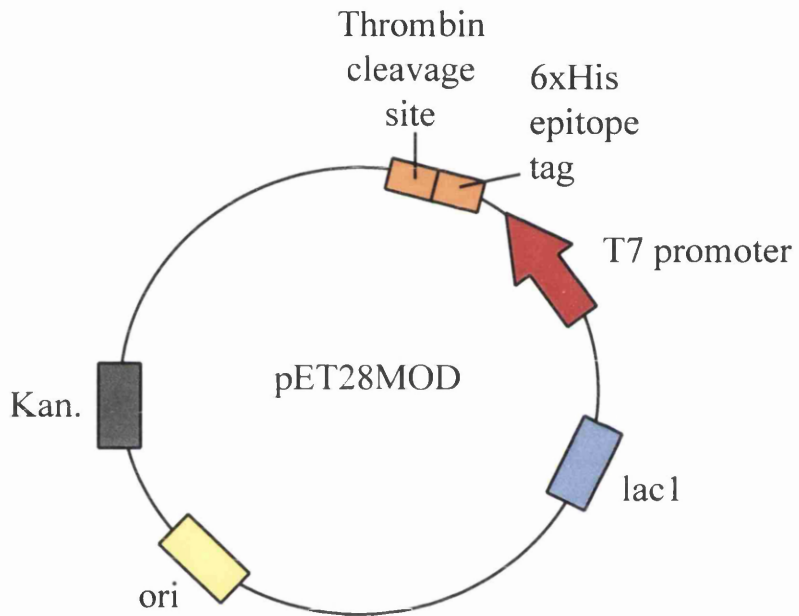
The cloning of the UL18 ORF into a modified version of the bacterial expression vector pET28a (Novagen Ltd.) was carried out by David McNab and is described in Kirkstadze et al. (1998). The cloning of the UL18 ORF into pET28MOD fuses 6 histidines (6x His) and a thrombin cleavage site onto the 5' end of the UL18 ORF (the pET28MOD expression vector is schematically illustrated in fig. 3.3.1). The T7 promoter controls gene regulation of the UL18 ORF. Expression of the pETUL18 vector within bacteria therefore results in the production of VP23 with an N-terminal 6xHis epitope tag (VP23His). The pETUL18 expression vector is schematically illustrated in fig. 3.3.2.

#### 3.3.1.2 Bacterial expression of VP23His in BL21 DE3 cells.

BL21 DE3 bacteria were electroporated in the presence of approximately 1 µg of pETUL18 or pET28MOD vector DNA and kanamycin resistant colonies were isolated. Single recombinant colonies were grown and induced (as described in Methods) and analysed for the expression of VP23His by SDS-PAGE analysis and Western blotting. Fig. 3.3.3 (panel A) shows the presence of a novel band in the induced pETUL18 sample when compared to that of the pET28MOD expression vector control. This novel band migrates with a slightly higher MW than that of VP23 from purified B-capsids, reflecting the additional amino acid sequences located at its N-terminus of VP23. This band was confirmed to be VP23 by Western blot analysis using the polyclonal VP23 antibody 187 (fig. 3.3.3, panel B).

5' TATGGGAATTCGGATCCACTAGTAC 3'  
 3' ACCCTTAAGGCCTAGGTGATCATGTTAA 5'

(A)



(B)

Fig. 3.3.1: Construction of the pET28MOD expression vector.

An oligonucleotide (A) was inserted into the NdeI and EcoRI sites of the bacterial expression vector pET28a (Novagen Ltd.) to generate pET28MOD. The insertion of this oligonucleotide resulted in the destruction of the existing EcoRI site and the incorporation of novel EcoRI and SpeI restriction sites (highlighted in red). (B) Schematic representation of the bacterial expression vector pET28MOD showing the 6xHis epitope tag, thrombin cleavage site, and some of the unique restriction sites.

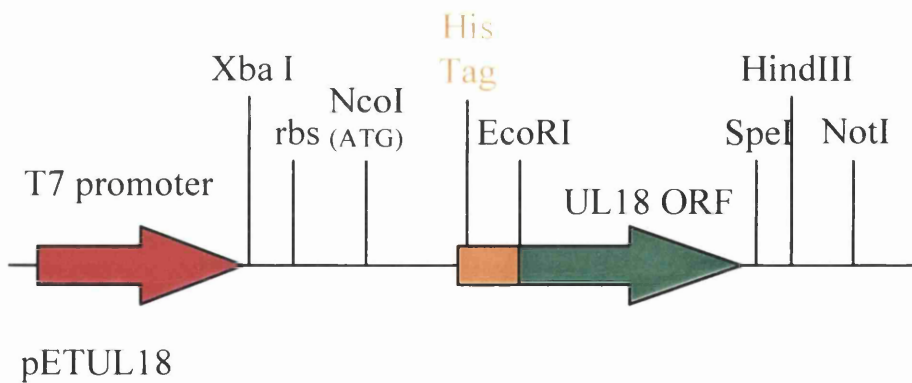
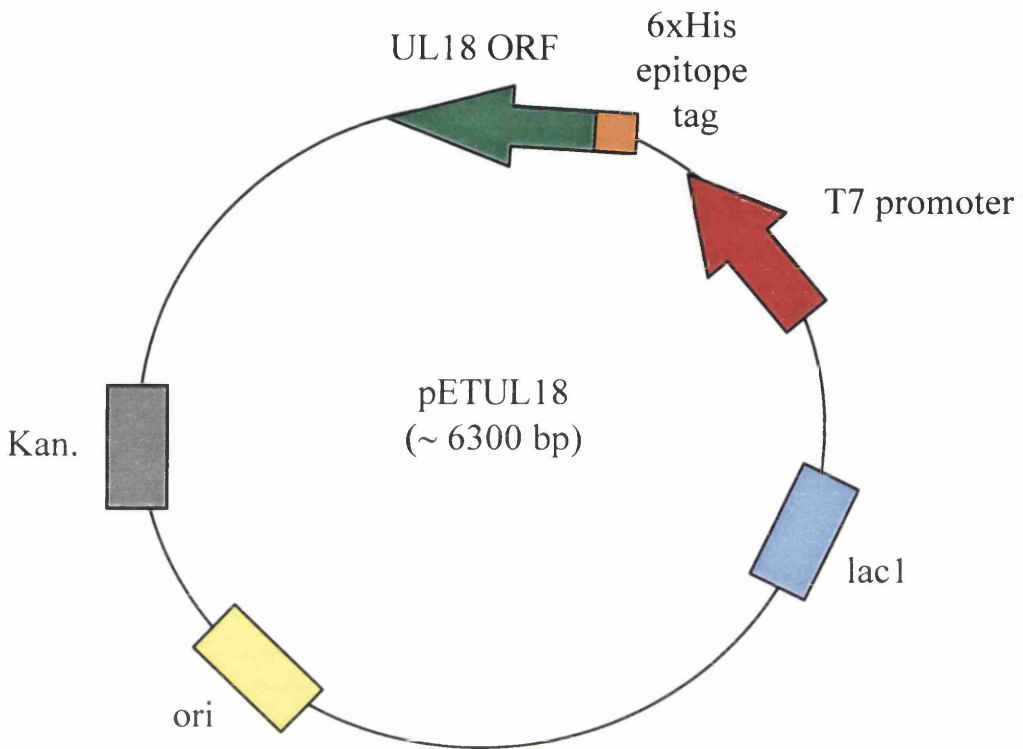
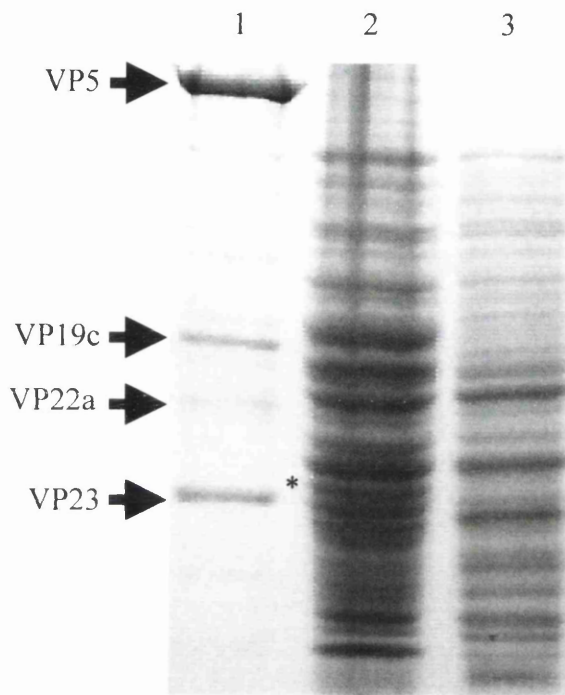
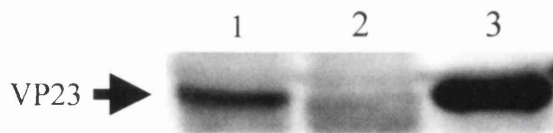


Fig. 3.3.2: Schematic representation of the bacterial expression vector pETUL18



(A)



(B)

Fig. 3.3.3: SDS-PAGE and Western blot analysis of VP23His expression in BL21 DE3 bacteria.

(A) BL21 DE3 bacterial cultures containing either pET28MOD vector (lane 3) or pETUL18 (lane 2) were grown and induced (as described in Methods). 1.5 ml of each culture was centrifuged at 14,000 r.p.m. for 30 seconds. The supernatant was removed and the bacterial pellet was resuspended in 200µl of BM and heated for 2 minutes at 100°C in a dry block. 15µl of each sample was analysed by SDS-PAGE and stained with Coomassie Brilliant Blue. Purified B-capsids were run for comparison (lane 1). Arrows indicate the relative positions of the capsid proteins as determined by the B-capsid profile. \* indicates the induced bacterial expression of VP23His. (B) Western blot analysis was performed on extracts from BL21 DE3 bacteria containing pETUL18 (lane 1), pET28MOD (lane 2), or on B-capsids (lane 3). The nitro-cellulose membrane was probed with a 1:1000 dilution of a polyclonal VP23 antibody (187). The arrow indicates the position of VP23.

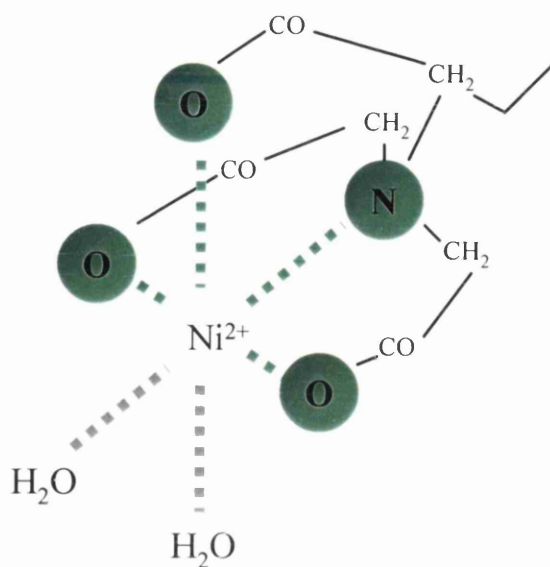
### 3.3.2 Purification of VP23His

#### 3.3.2.1 Nickel-nitrilotriacetic acid (Ni-NTA) agarose affinity chromatography.

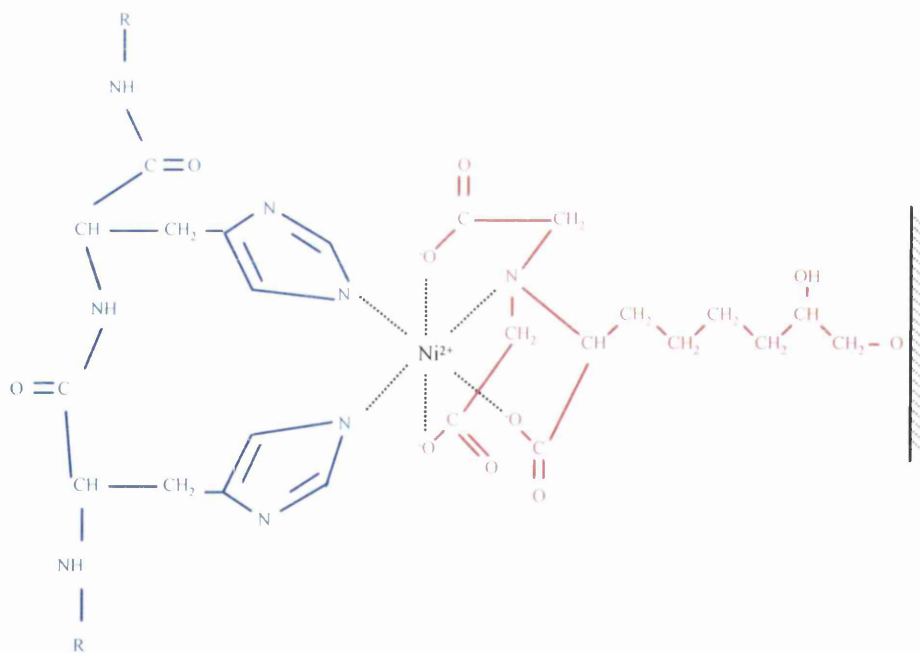
NTA is a tetradentate metal chelating adsorbent and occupies four out of the six ligand binding sites in a co-ordinated sphere around the  $\text{Ni}^{2+}$  ion, see fig 3.3.4 (panel A). This leaves two free  $\text{Ni}^{2+}$  sites to interact with the histidine residues from the 6x His epitope tag located on the terminus of a recombinantly expressed protein molecule (fig. 3.3.4, panel B). The Ni-NTA is coupled to Sepharose<sup>®</sup> CL-6B, which confers a high binding capacity with low non-specific binding and allows easy manipulation and purification of recombinantly expressed 6xHis tagged proteins by affinity chromatography. Ni-NTA agarose used in the purification of recombinantly expressed triplexes and triplex proteins was purchased from Qiagen.

#### 3.3.2.2 Ni-NTA agarose purification of VP23His

VP23His was readily purified using Ni-NTA agarose affinity chromatography from large-scale cultures of induced pETUL18 transformed BL21 DE3 bacteria (as described in Methods and fig. 3.3.5 legend). Fig. 3.3.5 shows a typical SDS-PAGE profile of purified VP23His. A single prominent band of approximately 34kDa was detected by Coomassie Brilliant Blue staining. The protein concentration for purified VP23His was typically in the range of 1.5-3.0 mg/ml for elution fractions 1 and 2 (as determined by  $\text{OD}_{280}$ ). Two other proteins were also purified (fig. 3.3.5, lane 2). A 70kDa protein, which was subsequently shown to be dimeric VP23His, and a 29kDa protein that was shown to be a breakdown/truncated VP23His product (discussed in section 3.3.3.2 and figs. 3.3.9). The MW of 34kDa for VP23His, as determined by SDS-PAGE analysis and comparison to Rainbow markers was in good agreement with the MW of 34268Da predict from the amino acid sequence (McGeoch et al., 1988).



(A)



(B)

Fig. 3.3.4: Schematic representation of Ni-NTA (A) and Ni-NTA binding to two His residues from the 6xHis epitope tag (B).

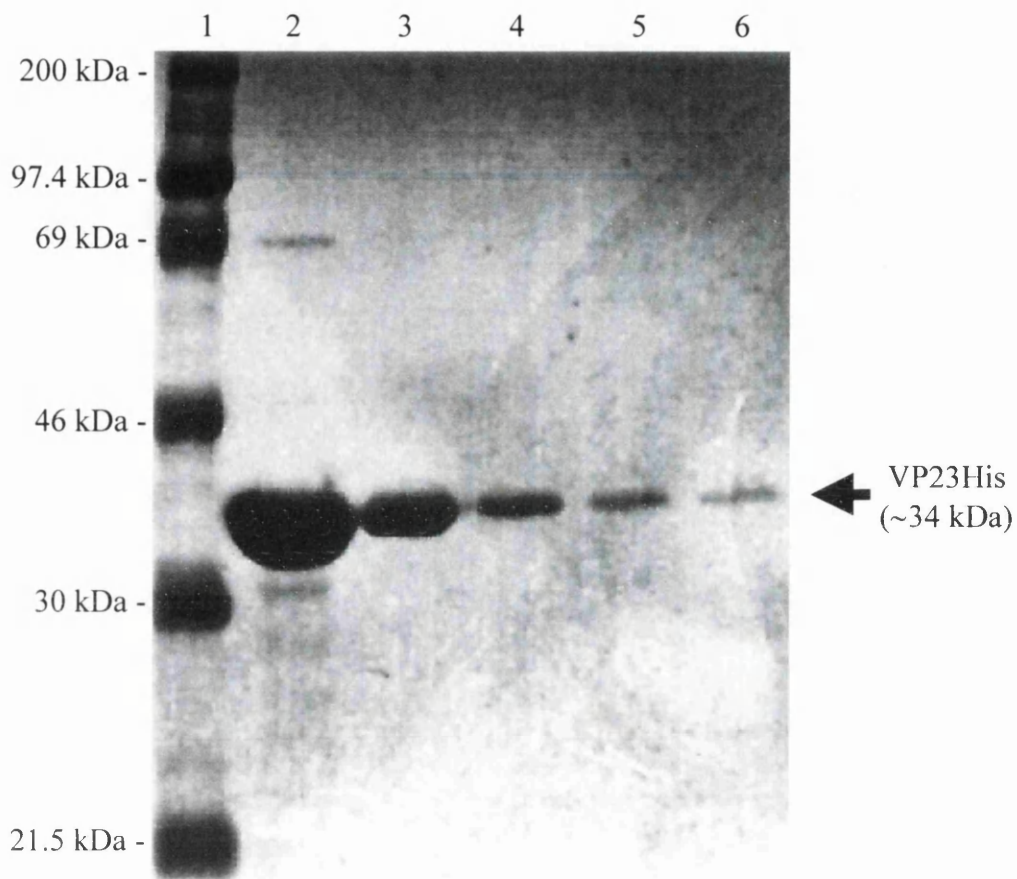


Fig. 3.3.5: SDS-PAGE analysis of Ni-NTA agarose purified VP23His in sonication buffer.

VP23His was purified using 700 $\mu$ l of Ni-NTA agarose equilibrated in sonication buffer (as described in Methods). Post-binding the Ni-NTA agarose was washed in 10ml of 20mM imidazole in sonication buffer to remove proteins that had non-specifically bound to the Ni-NTA agarose. VP23His was eluted from the agarose in 5x 1ml fractions of 250mM imidazole in sonication buffer (lanes 2-6 respectively). 20 $\mu$ l of each fraction and Rainbow markers (lane 1) were then analysed by SDS-PAGE and stained with Coomassie Brilliant Blue. The position of VP23His is indicated by an arrow.

### 3.3.3 Size exclusion chromatography and sucrose gradient sedimentation

#### 3.3.3.1 Size exclusion chromatography of purified VP23His in G-150 buffer

GdnHCl stripping of purified B-capsids in conjunction with quantitative SDS-PAGE analysis (performed by Newcomb et al., 1993) demonstrated that two copies of VP23 were present within each triplex. In order to determine the oligomeric status of VP23His, size exclusion chromatography was performed utilising a 25ml (1 by 30 cm) Superose 12 gel filtration column (Pharmacia). This column could resolve proteins from 20-200kDa in size. Preliminary attempts to size VP23His in sonication buffer failed due to column pressure limits exceeding those recommended by the column manufacturer (>3.0 Mpa). The high pressure within the column was due to the buffer, as the column pressure also exceeded 3.0MPa during column buffer calibration. The severe increase in column pressure may be attributable to micelle formation between the NP-40 detergent and the glycerol components of the buffer. Filtration of buffers and protein samples through a 0.2 $\mu$ M filter is standard procedure for column chromatography analysis (as described in Methods). However, filtration of sonication buffer did not prevent the column pressure from exceeding 3.0MPa.

As a consequence of this, VP23His was subsequently purified from bacteria using G-150 buffer (described in Materials) which lacks NP-40. Fig. 3.3.6 (panel B, lanes 2-4) shows the elution profile of VP23His purified in G-150 buffer. The Ni-NTA agarose elution profile was the same as that for VP23His purified in sonication buffer (fig. 3.3.4) with a prominent band observed at approximately 34kDa. 1ml of purified VP23His from fraction 1 (at a concentration of 0.5mg/ml) was analysed by size exclusion chromatography (fig. 3.3.6, Panel A). A single prominent peak was detected which eluted from the column at 14.03ml. 1.5ml fractions were collected from the column and the corresponding peak fraction was analysed by SDS-PAGE and shown to contain VP23His (fig. 3.3.6, panel B, lane 6). In order to determine an accurate native MW for VP23His, commercially available protein standards were purchased from Sigma and analysed under the same conditions. Fig. 3.3.7 (panel A) shows a compilation trace of the chromatography profiles of the protein standards analysed on the Superose 12 gel filtration column. The

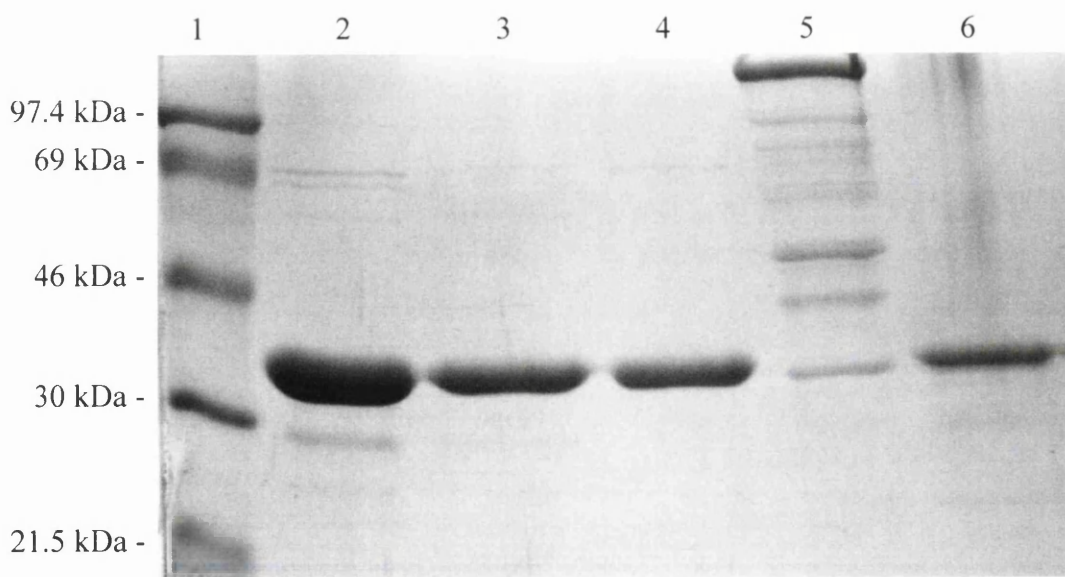
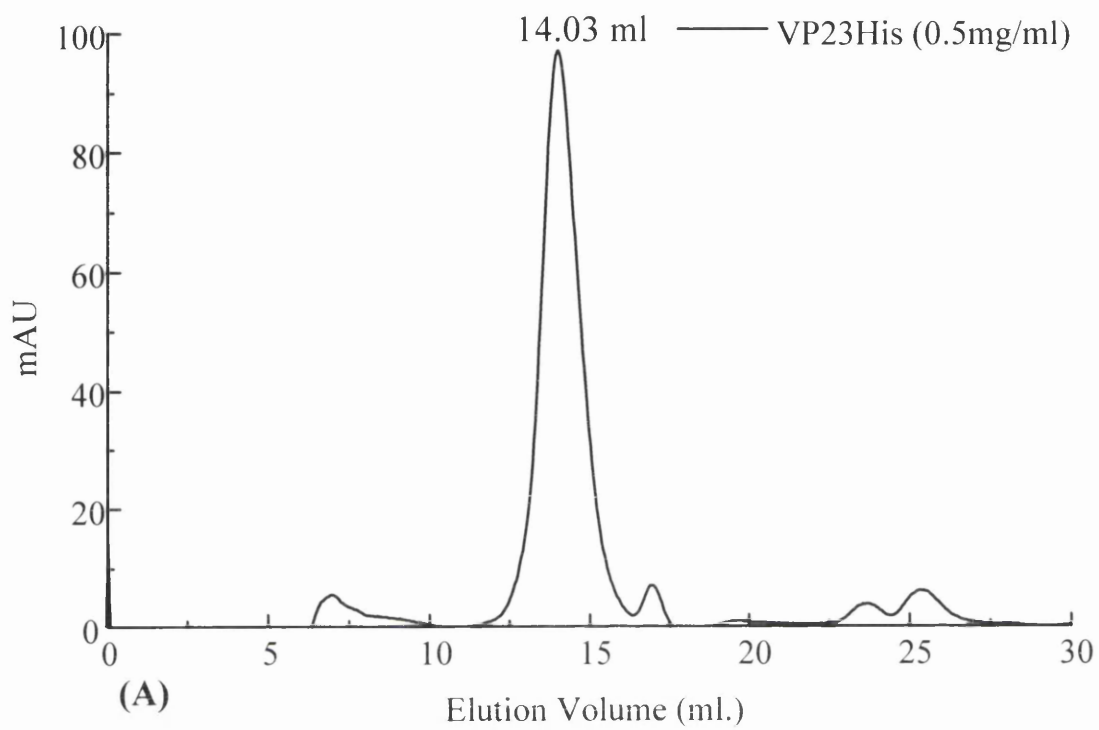


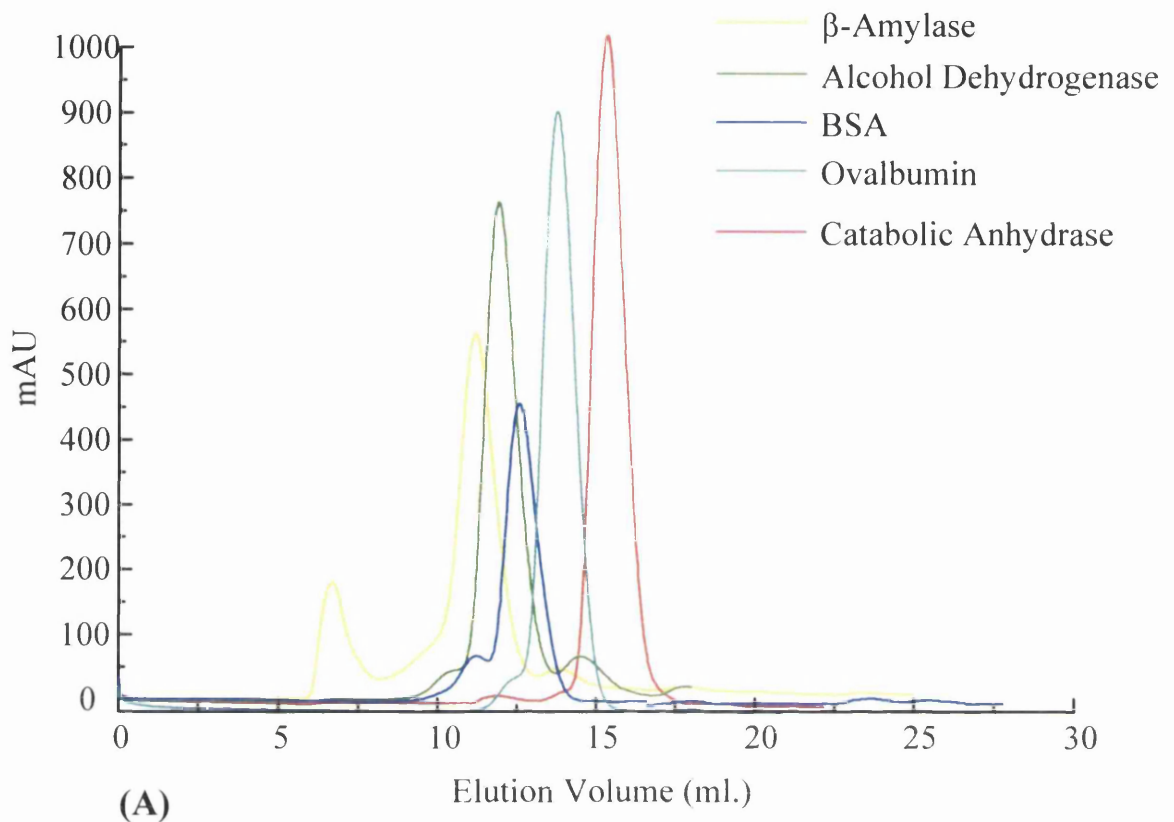
Fig. 3.3.6: Size exclusion chromatography and SDS-PAGE analysis of Ni-NTA agarose purified VP23His in G150 buffer.

VP23His was purified in G150 buffer (as described in Methods and in fig. 3.3.5). VP23His was eluted from the Ni-NTA agarose in 3x 1ml of G-150 buffer containing 250mM EDTA. Elution fraction 1 (0.5mg/ml) was analysed on a 25ml (1 by 30 cm) Superose 12 gel filtration column (Pharmacia) using a 1 ml injection superloop (as described in Methods) and 1.5ml fractions were collected. (A) Size exclusion chromatography profile for VP23His purified and analysed in G150 buffer + 250mM EDTA. (B) 20 $\mu$ l of purified VP23His from Ni-NTA agarose elution fractions 1-3 (lanes 2-4 respectively) and 20 $\mu$ l of the size exclusion chromatography peak fraction (lane 6) were analysed against Rainbow markers (lane 1) and purified B capsids (lane 5) by SDS-PAGE and stained with Coomassie Brilliant Blue.

information collected from the elution profile plots and the MW of each protein standard is summarised fig. 3.3.7 (panel B). These data were used to generate a standard curve using Origin 3.5 software, plotting  $\text{Log}_{10}$  MW against the elution volume for each protein standard. A best fit line was generated using linear regression analysis within the Origin 3.5 software package (fig. 3.3.7, panel C). Using the best fit line an accurate  $\text{Log}_{10}$  MW reading from the VP23His elution volume was recorded and the native MW calculated to be 36kDa.

The native MW of 36kDa for VP23His purified in G-150 buffer is in good agreement with the MW predicted from the amino acid sequence and suggests that purified VP23His exists as a monomer. Hydrodynamic studies performed by Marina Kirkitadze (described in Kirkitadze et al. 1998) on purified VP23His obtained from our laboratory demonstrated that its oligomeric status was dependent on protein concentration. Sedimentation analysis revealed that it was predominantly monomeric at concentrations of up to 0.8 mg/ml. This, therefore, supports the size exclusion chromatography data for VP23His analysed at a concentration of 0.5 mg/ml. However, at higher concentrations (1mg/ml) VP23His formed dimers with a MW of 70kDa, while at concentrations above 1.0 mg/ml it formed oligomers with a MWs of over 100kDa. As the purified VP23His used in these experiments was diluted from a concentrated stock, the oligomeric status of VP23His was thought to be reversible (Kirkitadze et al., 1998).

In order to detect such increases in the oligomeric status of VP23His, purified VP23His was analysed at different protein concentrations using size exclusion chromatography. Fig. 3.3.8 shows a compilation plot of VP23His size exclusion chromatography profiles of VP23His analysed at 0.25, 0.5, and 1.5 mg/ml in G-150 buffer. From these profiles no observable shift in the peak elution volume could be detected for the three concentrations tested. This would suggest that VP23His exists as a monomer under the buffer conditions used in the analysis.



Marker Protein	MW (kDa)	Log <sub>10</sub> MW (kDa)	Elution Volume (ml.)
β-Amylase	200	5.301	11.19
Alcohol Dehydrogenase	150	5.176	11.92
BSA	66	4.820	12.56
Ovalbumin	45	4.653	13.74
Carbonic Anhydrase	29	4.462	15.30

(B)

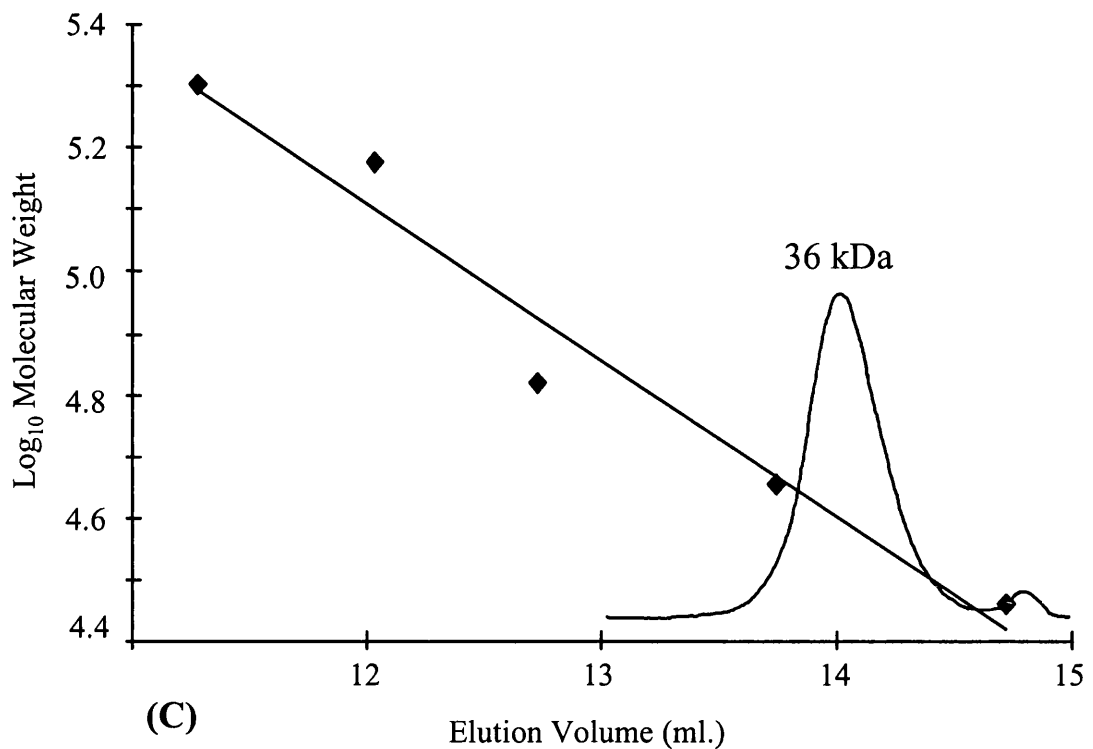


Fig. 3.3.7: Size exclusion chromatography of protein standards and generation of a standard curve.

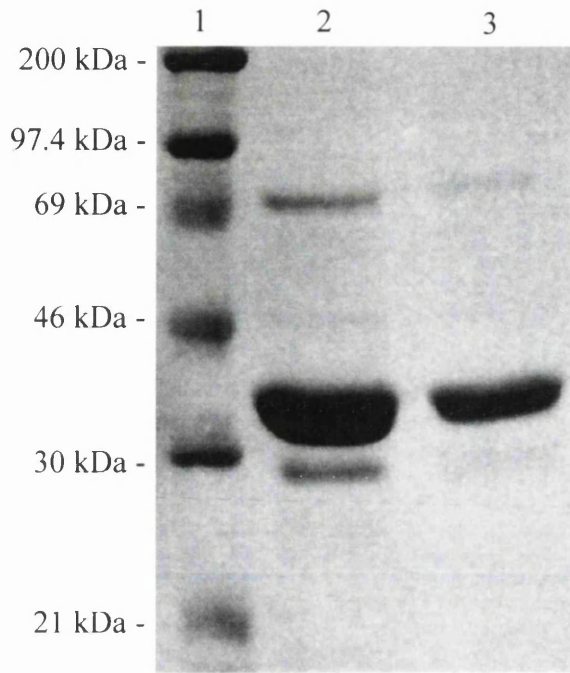
Size exclusion chromatography was carried out on commercially available protein standards (Sigma);  $\beta$ -amylase (200,000 Da), alcohol dehydrogenase (150,000 Da), bovine serum albumin (66,000 Da), ovalbumin (45,000 Da), and catabolic anhydrase (29,000 Da). 0.5 mg of each protein standard was resuspended in 1ml of G150 buffer + 250mM EDTA and analysed individually on a 25 ml (1 by 30 cm) Superose 12 gel filtration column (Pharmacia) using a 1 ml injection superloop (as described in Methods). (A) Compilation plot of the size exclusion chromatography profiles of the 5 protein standards described above. (B) Summary table of size exclusion data obtained from the protein standards. (C) Standard curve generated from the peak elution volumes for size standards with an overlay of the VP23His elution profile plot. The native MW (36,000 Da) for purified VP23His was calculated using linear regression analysis software within the Origin 3.5 software package.

### 3.3.3.2 VP23His purification and characterisation in buffer O

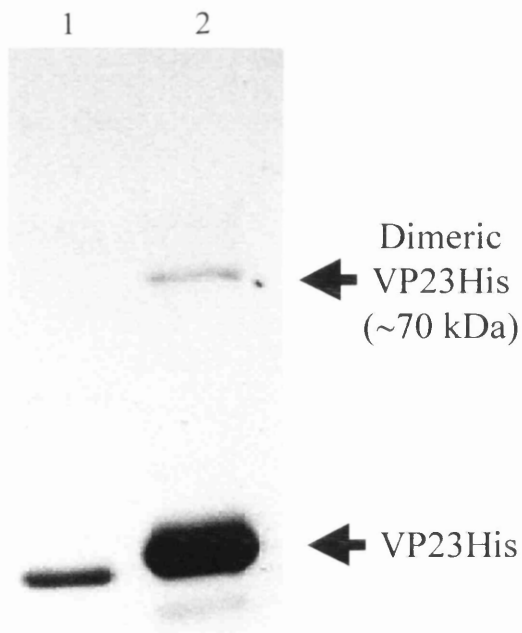
Solubilisation of recombinantly expressed triplexes (described in section 3.5) required them to be purified in a phosphate buffer, buffer O (described in Materials). It was consequently decided to re-examine VP23His in buffer O to allow legitimate biophysical comparison.

Fig. 3.3.9 (panel A) shows the Ni-NTA agarose purification profile of VP23His in buffer O. The same elution pattern was observed as that of VP23His in sonication buffer (fig. 3.3.5) and G-150 buffer (fig. 3.3.6, panel B). Western blot analysis demonstrated that both the 70 and 29kDa bands contained VP23 sequences (fig. 3.3.9, panel B) and were assumed to represent SDS resistant dimers and truncated or proteolytically cleaved versions of VP23His respectively.

In order to determine the oligomeric status of VP23His purified in buffer O, size exclusion chromatography analysis was repeated. Fig. 3.3.10 (panel A) shows the peak elution volume for VP23His and the standard curve generated from protein standards analysed in buffer O. VP23His was detected as a single prominent peak with a native MW of approximately 63kDa. This peak was confirmed to be VP23His by SDS-PAGE analysis (fig. 3.3.10, panel B). The detection of a single dimeric peak corresponding to VP23His at a concentration of 0.5 mg/ml implies that the reversibility in oligomeric status detected by hydrodynamic studies may have been a buffer related effect. Numerous size exclusion chromatography runs were performed on purified VP23His in buffer O and in all cases a single peak corresponding to dimeric VP23His was detected.



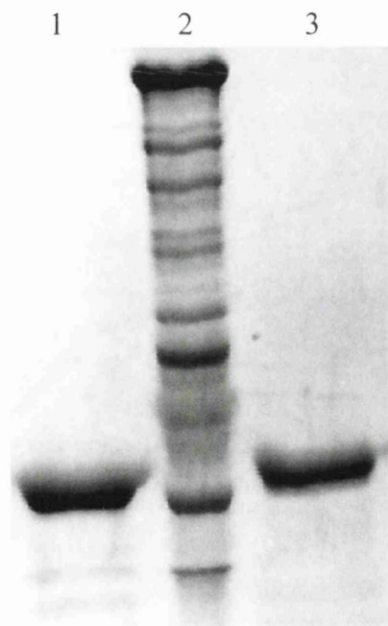
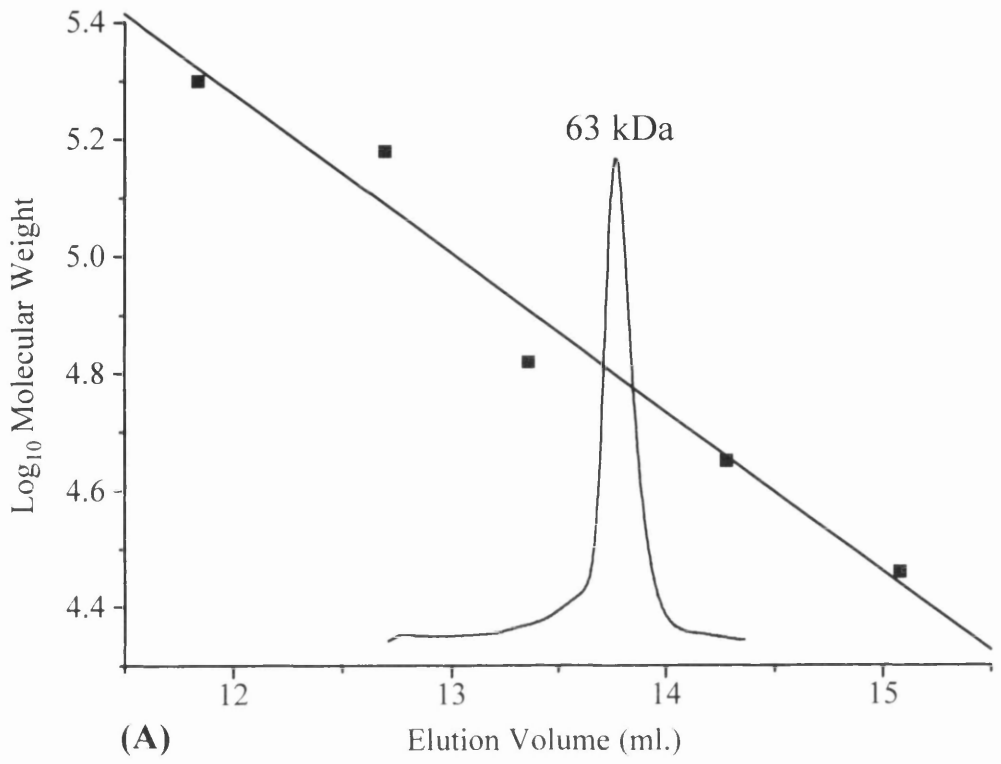
(A)



(B)

Fig. 3.3.9: SDS-PAGE and Western blot analysis of Ni-NTA agarose purified VP23His in buffer O.

VP23His was purified in buffer O (150mM Na<sub>2</sub>HPO<sub>4</sub> (pH7.5), 0.1% octyl-β-glucoside, 0.1% glycerol) as described in Methods and fig. 3.3.5. VP23His was eluted from the Ni-NTA agarose in 5x 1ml fractions of 250mM imidazole in buffer O. 20μl of VP23His elution fractions 1 and 2 (lanes 2 and 3) were analysed by SDS-PAGE against Rainbow markers (lane 1) and stained with Coomassie Brilliant Blue (A). (B) Western blot analysis of purified VP23His in buffer O (lane 2) and purified B-capsids (lane 1). The nitro-cellulose membrane was probed with a 1:1000 dilution of a polyclonal VP23 antibody (187). Monomeric and dimeric VP23His are indicated by the appropriate arrows.



(B)

Fig. 3.3.10: Size exclusion chromatography and SDS-PAGE analysis of Ni-NTA agarose purified VP23His in buffer O.

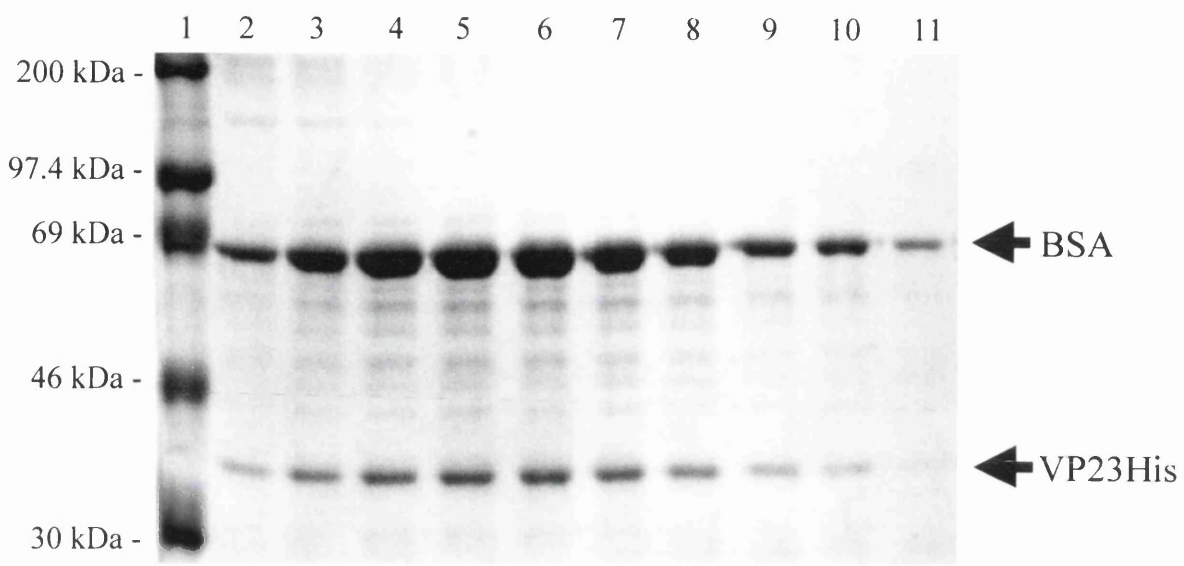
VP23His was purified in buffer O (as described in Methods and fig. 3.3.5). Purified VP23His (0.5mg/ml) was analysed on a 25ml (1 by 30 cm) Superose 12 gel filtration column (Pharmacia) using a 1ml injection superloop (as described in Methods) and 1.5ml fractions were collected. (A) Size exclusion chromatography elution volume profile for VP23His purified and analysed in buffer O. A Standard curve was generated (as described in fig. 3.3.7). All protein standards were resuspended and analysed in buffer O at a concentration of 0.5 mg/ml. The native MW for VP23His purified in buffer O (63 kDa) was calculated using linear regression analysis software within the Origin 3.5 software package. (B) 20 $\mu$ l of purified VP23His prior to analysis (lane 1) and 20 $\mu$ l of the size exclusion chromatography peak fraction (lane 3) was analysed by SDS-PAGE against purified B-capsids (lane 2) and stained with Coomassie Brilliant Blue.

### 3.3.5 Sucrose gradient sedimentation analysis of purified VP23His in buffer O.

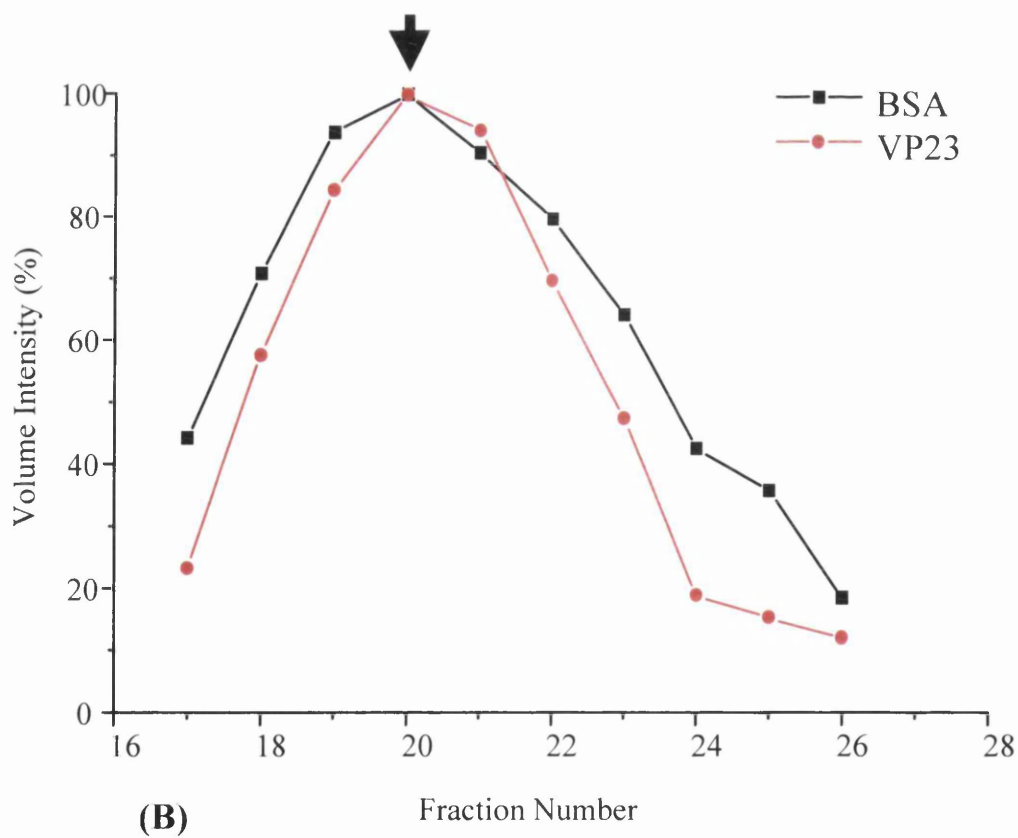
To confirm the dimeric status of VP23His purified in buffer O, it was co-sedimented with the protein standard BSA (66kDa) through a 5ml 5-25% sucrose gradient in buffer O.

Approximately 35x 150 $\mu$ l fractions were collected (as described in Methods) and every third fraction was analysed by SDS-PAGE in order to identify where VP23His localised within the gradient (data not shown). VP23His could be detected over a number of 150 $\mu$ l fractions as determined by Coomassie Brilliant Blue staining. Fig. 3.3.10 (panel A) shows the SDS-PAGE analysis of fractions 17 to 26. The relative intensities were calculated for each fraction, for both VP23His and BSA, and plotted as a percentage (%) change in volume intensity against their appropriate fraction number (fig. 3.3.11, panel B). The VP23His peak intensity sediments to the same position on the gradient as that of the internal 66kDa BSA protein standard (indicated by an arrow in fig. 3.3.11, panel B). The sedimentation analysis data clearly indicates that purified VP23His in buffer O can form stable dimers and therefore supports the observations made by size exclusion chromatography that purified VP23His exists as a stable dimer in buffer O.

The ability to purify VP23His on Ni-NTA agarose implies that the N-terminal 6x His tag on VP23 must be exposed to the solvent and not buried within the interior of the VP23 protein. The fact that VP23His exists as a purifiable dimer in buffer O would also imply that at least one of the N-termini is not directly involved in the dimerisation of VP23. While the work described in this thesis was in progress, Spencer et al. (1998) published that VP23 expressed in SF9 cells infected with a recombinant baculovirus could form stable dimers. This evidence supports the findings reported here, and demonstrates that these dimers are not attributed to the presence of the 6xHis tag utilised in the purification process. Monomeric VP23His which was detected by size exclusion chromatography and hydrodynamic studies is probably a result of the disassociation of VP23 dimers due to the non-physiological nature of the purification buffers used in the isolation of VP23His. The presence of NP-40 and/or NaCl in these buffers may be sufficient to interfere or compete



(A)



(B)

Fig. 3.3.11: Sucrose gradient sedimentation and SDS-PAGE analysis of Ni-NTA purified VP23His in buffer O.

VP23His was purified in buffer O (as described in Methods and fig. 3.3.5). 300 $\mu$ l of purified VP23His and 50 $\mu$ l BSA (5mg/ml resuspended in buffer O) were mixed and layer onto a 5ml 5-25% sucrose gradient and sedimented together at 4°C for 16 hours at 40,000 r.p.m. in a AH650 rotor and fractions collected (as described in Methods). (A) 20 $\mu$ l of fractions 17-26 (lanes 2-11 respectively) and Rainbow markers (lane 1) were analysed by SDS-PAGE and stained with Coomassie Brilliant Blue. The position of BSA and VP23His are indicated by the appropriate arrows. The relative intensity of the Coomassie stained protein profiles was calculated individually for both VP23His and BSA protein profiles using Quantity ONE software (BIO-Rad) as described in Methods. The data was plotted as percentage (%) change in volume intensity for each individual protein profile against their eluted fraction number (B). An arrow indicates the gradient peak elution of VP23His.

with any hydrophobic or electrostatic interactions between VP23 molecules and therefore result in the monomerisation of VP23.

### 3.3.6 Characterisation of purified VP23His dimers

#### 3.3.6.1 Thermolability of VP23 dimers

Newcomb et al., (1996) were the first group to identify a procapsid transition during the assembly of the HSV-1 capsids. Rixon and McNab (1999) subsequently showed that HSV-1 procapsids could be detected *in vivo* using a mutant of HSV-1 (*ts1201*) which had a temperature sensitive lesion in the UL26 protease. One of the defining characteristics of procapsids is their thermolability and they were shown to disassemble at 0°C (Newcomb et al., 1996; Rixon and McNab, 1999). In order to test whether or not this thermolability, and consequent disassembly at 0°C, was due to the disintegration of VP23 dimers, purified VP23His in buffer O was analysed by size exclusion chromatography before and after incubation at 4°C. Size exclusion chromatography was carried out on VP23His in buffer O and the peak elution fraction was collected and incubated o/n at 4°C to allow any disassociation to occur. This sample was subsequently re-analysed by size exclusion chromatography in buffer O at RT. Fig. 3.3.12 shows a compilation plot of the size exclusion chromatography profiles of dimeric VP23His purified in buffer O and the reanalysis of isolated VP23His dimers after a 4°C incubation. Both samples have the same peak elution volume. This would therefore indicate that VP23 dimers are not thermolabile at 4°C, as any VP23 monomers would have eluted at the approximate position indicated by the arrow on fig.3.3.12. The reduction in the size of the peak can be attributed to the dilution of the sample during its first passage through the column.

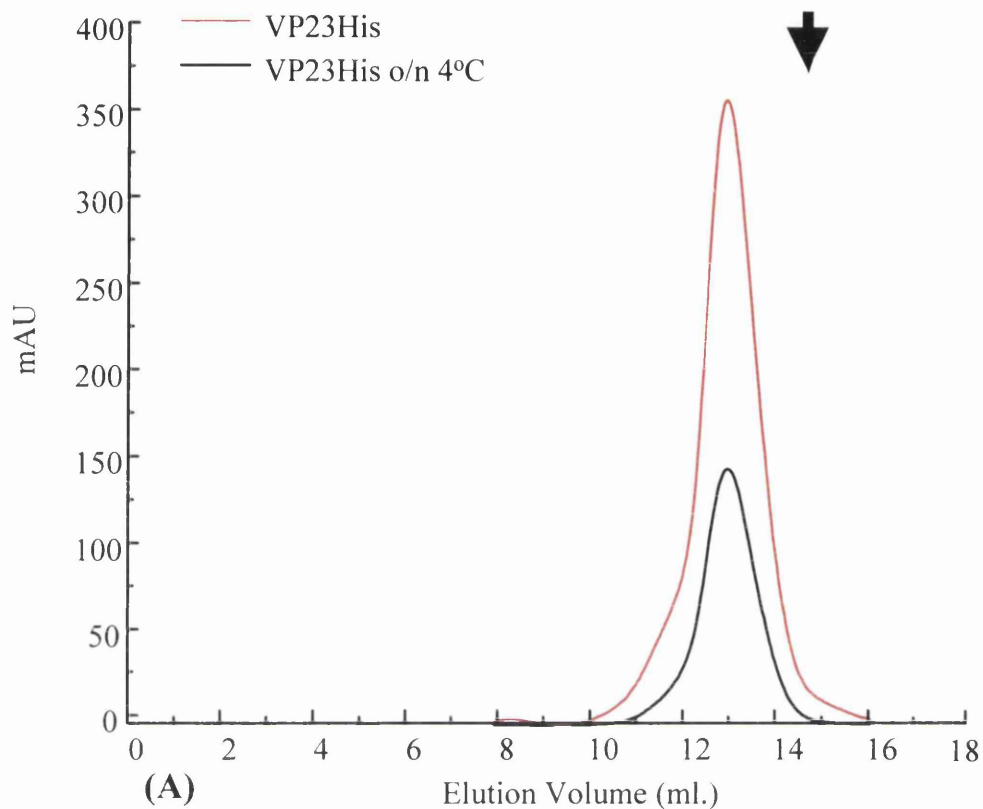


Fig. 3.3.12: Size exclusion chromatography of Ni-NTA agarose purified VP23His in buffer O before and after incubation at 4°C.

VP23His was purified in buffer O as described in Methods and fig. 3.3.5. Purified VP23His in buffer O was analysed by size exclusion chromatography using a 1ml superloop and fractions collected (as described in Methods). The peak fraction was collected and subsequently incubated o/n at 4°C before being reanalysed. The arrow indicates the position of the protein standard carbonic anhydrase (29,000 Da).

### 3.3.7 Disulphide linkage analysis of VP23

#### 3.3.7.1 VP23 dimer formation in the absence of reducing agents

Initial observations made by Dr Andrew Davison on purified B-capsids analysed by SDS-PAGE showed that VP23 migrated differently in the presence and absence of the reducing agent  $\beta$ -mercaptoethanol. Fig. 3.3.13 shows the protein profiles of purified B-capsids and of VP23His purified in sonication buffer analysed by SDS-PAGE in the presence or absence of 20mM  $\beta$ -mercaptoethanol. A distinct shift can be observed both for VP23 present in B-capsids and for purified VP23His. Although no obvious dimeric band could be observed in the purified B-capsid sample when analysed in the absence of  $\beta$ -mercaptoethanol (fig. 3.3.13, lane A), a distinct dimeric band could be detected for purified VP23His (fig. 3.3.13, lane B and C). This dimeric band was the same MW as the dimeric bands observed by SDS-PAGE analysis of purified VP23His in buffer O (fig.3.3.9). However, it is interesting to note that not all the purified VP23His analysed by SDS-PAGE in the absence of  $\beta$ -mercaptoethanol showed a mobility shift from monomer to dimer. The majority of the purified VP23His remained in the monomeric form but appeared as multiple bands rather than the single species seen in the presence of  $\beta$ -mercaptoethanol. These observations suggest the possibility of intra-molecular disulphide bonds within VP23 rather than an inter-molecular disulphide bond between VP23 dimeric molecules. The apparent dimerisation of purified VP23His in the absence of  $\beta$ -mercaptoethanol may be due to an increased proportion of VP23 dimers being resistant to SDS denaturation as a direct result of the conformational stability generated by non-reduced internal disulphide bonds. The VP23His monomer doublet which is observed, could be due to different types of intra-molecular disulphide linkages, generating a population of VP23His molecules which have a different migratory speed through the acrylamide gel. Zweig et al., (1979) demonstrated using two dimensional gel electrophoresis, both in a reducing and a non-reducing plane, that the only inter-molecular disulphide linkages within HSV-2 capsids were those between VP5 and VP19c and those between molecules of the scaffold protein VP22a. This supports the conclusion that dimerisation of VP23 is not due to inter-molecular disulphide linkage.

In order to analyse further the suspected intra-molecular disulphide linkages within VP23, purified VP23His in buffer O was analysed by size exclusion chromatography in the absence or presence of the reducing agent DTT. Size exclusion chromatography was carried out on VP23His in buffer O and the peak elution fraction was collected. 1M DTT was added to this fraction to a final concentration of 10mM and incubated at RT for 30 minutes to allow for disulphide bond reduction. This sample was subsequently re-analysed by size exclusion chromatography in buffer O. Fig. 3.3.14 shows a compilation plot of the size exclusion chromatography profiles of dimeric VP23His purified in buffer O (unreduced) and the reanalysis after DTT treatment. Both samples gave the same elution peak volume with no shift to the position expected for monomers being seen. This further confirms that inter-molecular disulphide linkages between VP23 molecules are not the cause of dimerisation. It cannot be ruled out however that intra-molecular disulphide linkages influence dimer stability as it is unlikely that reduction of buried disulphide linkages would occur. The reduction in the size of the peak can be attributed to the dilution of the sample during passage down the column. SDS-PAGE analysis in the presence of  $\beta$ -mercaptoethanol of the collected dimeric VP23His fraction before DTT reduction is shown in fig. 3.3.14 (panel B) and clearly demonstrates the presence of SDS resistant VP23His dimers (indicated by an \*).

### 3.3.7.2 VP23 sequence analysis

Comparison of the VP23 related proteins from the alphaherpesvirus subfamily demonstrated relatively high sequence homology. The closest homologue of VP23 from HSV-1 is the HSV-2 UL18 protein, demonstrating 92% amino acid sequence identity. For the other viruses the sequence identities were significantly lower. These include; EHV-1 43%, BHV-1 47 %, VZV 44% and PRV 48%. The full sequence alignment is shown in fig. 3.3.15. Examination of the pattern of cysteine residues in these proteins reveals several interesting trends. HSV-2 VP23 demonstrated 100% cysteine homology when compared to the HSV-1 protein. This is not unexpected due to the close relationship of these two viruses. However, comparison with the other four alphaherpesviruses revealed that only two out of the four cysteine residues in HSV-1 VP23 are conserved throughout. These are amino acid residues Cys27 and Cys297 (highlighted in red in fig. 3.3.15). Cys110 was conserved in five out of the six alphaherpesviruses tested but was not present

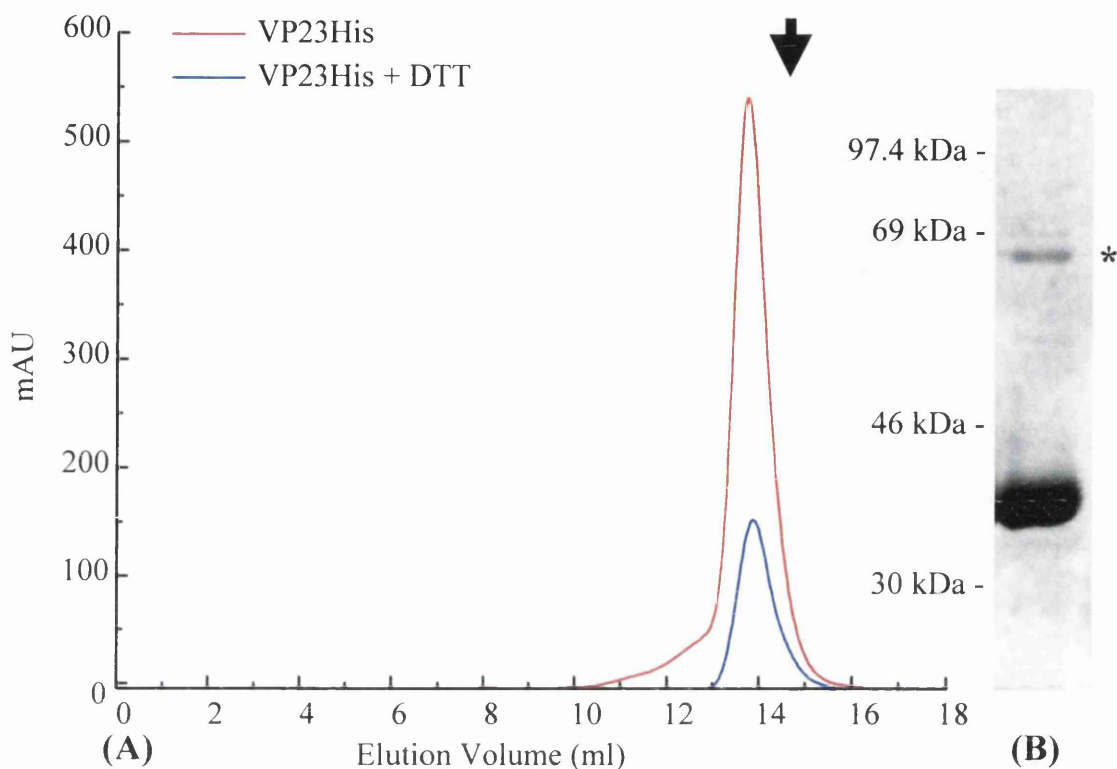


Fig. 3.3.14: Size exclusion chromatography of Ni-NTA agarose purified VP23His in buffer O before and after incubation in the presence of 10mM DTT.

VP23His was purified in buffer O as described in Methods and fig. 3.3.5. Purified VP23His in buffer O was analysed by size exclusion chromatography (as described in Methods and fig. 3.3.7) using a 1ml superloop and 1.5ml fractions were collected. The peak fraction incubated in the presence of 10mM DTT for 30 minutes before being reanalysed. The arrow indicates the predicted position of the protein standard carbonic anhydrase (29,000 Da) (A). (B) 20 $\mu$ l of the peak elution fraction collected before DTT treatment was analysed by SDS-PAGE and stained with Coomassie Brilliant Blue. \* indicates the presence of dimeric VP23His. The positions of the size markers are shown.

### 27 (CYS1)

HSV1 MLADGFETDIAIPSGISRPDAAALQRCEGRVVFLLPTIRRQLTLADVAHESFVSGGVSPDT  
HSV2 MITDCFEADIAIPSGISRPDAAALQRCEGRVVFLLPTIRRQLALADVAHESFVSGGVSPDT  
HSVEB MASAAFEIDILLPSDLSPADLSALQKCEGKLVFLTALRRRVMLSSVTLSSYYVNGAPPDT  
VZVD -MAMPFEIEVLLPGELSPAETSALQKCEGKIITFSTLRHRASLVDIALSSYYINGAPPDT  
BHV1 MAQPEAFEVEIVLPGDLSHGDLAALQKCEGKVVFFTTLRRRVPLADVALASFVNGVAPDT  
PRV -----MEVDIALPT-LSPGDLSALQKCEGRVVFLET LRRHATLREVA---LPCGG---DV  
Con. -----E-----LP--LS-----ALQ-CEG-----R---L-----G---D-

### 86 (CYS 2)

### 110 (CYS 3)

HSV1 LGLLLAYRRRFPVAVITRVLPTTRIVACPLDVGLTHAGTVNLRNTSPVDLCNGDPISLVPPV  
HSV2 LGLLLAYRRRFPVAVITRVLPTTRIVACPVDLGLTHAGTVNLRNTSPVDLCNGDPVSLVPPV  
HSVEB LSLMAAFRRRFPVAVITRVLPTTRIVACPLDVGLTHAGTVNLRNTSPVDLCNGDPSVLPPI  
VZVD LSLLEAYRMRFAAVITRVI PGKLLAHAIGVGTPTPGLF-IQNTSPVDLCNGDYICLLPPV  
BHV1 LGLMAAYRCRFPVAVLVRVAPGRMMAAPLVGVPMPRGAF-LQNTGPFDL CNGDAVCLLPPL  
PRV LAAM-ADRRRFAAVITRVT PHRMLATPLGVGGGRQSLV-LQNTGPFDLTNGDHVCLVPPL  
Con. L----A-R-RF-AV--RV-P-----A-----NT-P-DL-NGD-----PP-

HSV1 FEGQATDVRLDSLDTLRFVPLPSPLAREIVARLVARGI-RDLNPSPRNPGG-LP--DL  
HSV2 FEGQATDVRLESDDLTLRFVPLPTPLAREIVARLVARGI-RDLNPDPRTPGE-LP--DL  
HSVEB LDVE-DKLR LGSVGEIILFPLTVPLAQARELIARLVARAV-QALT PNAQAQRG-A-----  
VZVD F-GSADSIRLDSVGL EIVFPLTIPQTLMRI IAKVVARAVERTAAGA QILPHEVLR--GA  
BHV1 L-GPARALALASAGAELLFPMTVPLPQARALVARVVARAV-EALGDRAAAAARA-RA--A-  
PRV LGDEC--LRLTSANLELRFPM TPLPLAQARELTARVVARAAETLR-----GGAPAR--GA  
Con. -----L-S-----FP---P---R---A--VAR-----

HSV1 NVLYYNGSRLSLLADVQQLGPNVNAELRSLV LNMVYSITEGTTIILT LI PRLFALSAQDGY  
HSV2 NVLYYNGARLSLVADVQQLASVNT ELRSLV LNMVYSITEGTTIILT LI PRL LALSAQDGY  
HSVEB EVMFYNGRKYNVTPDLRHRDAVNGVARSLV LNMIFAMNEGSLVLLSLIPNLLT LGTQDGF  
VZVD DVICYNGRRYELETNLQHRDGS DAAIRTLV LNMFSINEGCLLLLLALIP TLLVQGAHDGY  
BHV1 DVMYHNGRRYQVTPDVLCREGADAAARTL V LNMVFNVNEGSL LLLSLIPNLLT QGLQDGV  
PRV DVVFSNGRRYQL--PPPHRDNAEAAT RSLV LNMIFLLNEGAVILLSLIPNLLT LGAQDGY  
Con. -V---NG-----R-LVLN-----EG-----LIP-L-----DG-

HSV1 VNALLQMQSVTREA AQLIH-PEAPALMQDGERRLPLYEALVAWLTHAGQLGDTLALAPVV  
HSV2 VNALLQMQSVTREA AQLIH-PEAPMLMQDGERRLPLYEALVAWLAHAGQLGDI LALAPAV  
HSVEB VNAI IQMG SATREVGQLVH-QQPVPQPQDGARRFCVYDALMSWISVASRLGDVVGKPLV  
VZVD VNLLIQ TANCVRETGQLINIPMPRI-QDGHRRFP IYETISSWISTSSRLGDTLGTRAIL  
BHV1 ANAIVQLGSASREAGQLLR-LEPAEPRQDGGRRFCLYGALA AWISSATRLGDAVGARPLA  
PRV ANAVIQ LGSATRELGQLVR-QPPPPLPQDHARRFCVFEALEAWIASASRLGDTLGTRPVA  
Con. -N---Q-----RE--QL-----QD--RR-----W-----LGD-----

### 297 (CYS 4)

HSV1 RVCTFDGA AVVRSGDMAPVIRYP  
HSV2 RVCTFDGA AVVQSGDMAPVIRYP  
HSVEB RICTFEGQATISRGEKAPVIQTLL  
VZVD RVCVFDGPSTVHPGDRTAVIQV  
BHV1 KVCTFDG PSVVRVGEKAPIVVPL  
PRV RVCIFDGPPTVPPGEKAAVVEV  
Con. --C-F-G-----G-----

Fig. 3.3.15: Amino acid sequence alignment of VP23 homologues.

Compilation of the amino acid sequence alignment of VP23 homologues from the alphaherpesvirus subfamily. HSV1 (Herpes Simplex virus type-1, strain 17), HSV2 (Herpes Simplex virus type-2, strain HG52), EHV1 (equine herpesvirus type-1, strain AB4P), VZV (Varicella-Zoster virus, strain Dumas), BHV1 (Bovine Herpesvirus type-1), PRV (Pseudorabies virus (Suid herpesvirus 1)), and Con. (consensus sequence alignment). Cysteine residue are highlighted in red.

in PRV, whereas Cys86 was only conserved in HSV-2. Several other cysteine residues were found in the other alphaherpesvirus VP23 homologues, which are not present in either HSV-1 or HSV-2. This high degree of conservation of Cys residues 27 and 297 suggests that they may perform a specific functional role within the protein, which has been conserved despite the divergence of the alphaherpesvirus sequences. It is interesting to note that the Cys residue at 116 is conserved in all the alphaherpesviruses, except HSV-1 and HSV-2 where it is replaced by Ser.

### 3.3.8 VP23 cysteine mutagenesis

In order to determine whether or not the cysteine residues in VP23 were functionally important, site directed mutagenesis was performed on pETUL18 (as described in Methods). The synthetic oligonucleotides used in each case were designed to convert the cysteine residues to serine residues. This is a structurally conservative change since the only difference is that the S-H of cysteine is an O-H in serine. In order to select plasmids containing the mutations, unique restriction sites were incorporated into the oligonucleotide sequences (fig.3.3.16, panel A), which did not introduce any other changes into the primary amino acid sequence. Recombinant colonies were isolated and plasmid DNA purified as described in Methods. Clones were analysed by restriction enzyme mapping, utilising the appropriate unique restriction sites (data not shown). Colonies that proved positive by restriction digest were subsequently confirmed by sequencing using generic oligonucleotides for the T7 promoter (as described in Methods). The automated sequence analysis of their respective sequence changes is shown in fig. 3.3.16 (panels B-E).

#### 3.3.8.1 Expression of VP23His cysteine mutants.

In order to determine whether the cysteine mutants were expressed efficiently within induced BL21 DE3 bacteria, Western blot analysis was performed. Fig. 3.3.17 (panel A) shows the results of the Western blot analysis using a polyclonal VP23 antibody (187). Mutants pETUL18CYS-1, -3, and -4 expressed efficiently reaching levels comparable to that of the WT pETUL18. However, there was no detectable expression of

BglII  
|

(1) 5' ATACCACCCGCCCTTCAGATCTCTGCAGCGCCGCCGCATCGGGGC 3'

NheI  
|

(2) 5' GCCCACGTCCAGGGGGCTAGCGACGATTCGCGTGGG 3'

BstBI  
|

(3) 5' GATGGGGTCCCCGTTCGAAAGATCAACGGGGGAGGTGTTG 3'

MluI  
|

(4) 5' CGCGCCGTCAAAGGTAGAAACGCGTACCACGGGAGCCAGGG 3'

(A)

pETUL18 (Fwd)

R P D A A A L Q R C E G R V V  
5' CGCCCCGATGCGGCGGCGCTGCAGCGCTGCGAAGGGCGGGTGGTA 3'  
5' CGCCCCGATGCGGCGGCGCTGCAGAGATCTGAAGGGCGGGTGGTA 3'  
R P D A A A L Q R S E G R V V

pETUL18CYS1 (Fwd)

(B)

pETUL18 (Fwd)

V L P T R I V A C P L D V G L  
5' GTGCTTCCCACGCGAATCGTCGCCTGCCCCCTGGACGTGGGCCTC 3'  
5' GTGCTTCCCACGCGAATCGTCGCCTAGCCCCCTGGACGTGGGCCTC 3'  
V L P T R I V A S P L D V G L

pETUL18CYS2 (Fwd)

(C)

pETUL18 (Fwd)  
 R N T S P V D L **C** N G D P I S  
 5' CGCAACACCTCCCCCGTAGATCTCTGTAACGGGGACCCCATCAGC 3'  
 5' CGCAACACCTCCCCCGTTGATCTTTCGAACGGGGACCCCATCAGC 3'  
 R N T S P V D L **S** N G D P I S  
 pETUL18CYS3 (Fwd)

**(D)**

pETUL18 (Rev)  
 V V A A G D F T **C** V R V V P A  
 3' CACAACGGCCGCGCCGTCAAAGGTGCACACCCGAACCACGGGAGC 5'  
 3' CACAACGGCCGCGCCGTCAAAGGTAGAAACGCGTACCACGGGAGC 5'  
 V V A A G D F T **S** V R V V P A  
 pETUL18CYS4 (Rev)

**(E)**

Fig. 3.3.16: Cysteine mutagenesis of UL18

(A) Oligonucleotides used in the site directed mutagenesis of 4 cysteine residues within the UL18 ORF (numbered 1-4 respectively from the VP23 N-termini). The unique restriction sites incorporated into each oligonucleotide are highlighted in red. (B-E) Automated sequence analysis using standard T7 primers of pETUL18CYS mutants compared to the WT pETUL18 sequence. FWD (forward) and REV (reverse) indicate the direction of sequence analysis. Above and below each nucleotide sequence is the appropriately encoded amino acid sequence (site specific amino acid changes are highlighted in red).

pETUL18CYS-2. It seemed possible that regeneration of the pET28MOD expression vector by T7 polymerase may have generated mutations outwith those desired in the UL18 ORF, and consequently abolished expression activity. Therefore the UL18CYS2 ORF was subcloned out of its existing pET28MOD backbone vector, ligated into a new pET28MOD vector, and reanalysed for the expression of VP23HisCYS2 by SDS-PAGE and Western blot analysis (data not shown). However, this failed to produce detectable levels of full length VP23HisCYS2. Various strategies were employed in order to generate a functional expressing pETUL18CYS2 vector, but all failed to produce detectable levels of full length protein. This would seem to suggest therefore that during mutagenesis a frame shift and/or the incorporation of a stop codon may have occurred within the UL18CYS2 ORF and thus preventing protein expression.

#### 3.3.8.2 Ni-NTA purification of VP23 cysteine mutants

VP23HisCYS mutants -1, -3, and -4 were readily purifiable from bacteria using Ni-NTA agarose affinity chromatography. Fig. 3.3.17 (panel B) shows the SDS-PAGE profile of elution fraction 1 from each of the VP23HisCYS mutants -1, -3, and -4 compared to that of WT VP23His. The samples were purified in sonication buffer and analysed by SDS-PAGE in the presence or absence of 20mM  $\beta$ -mercaptoethanol. In the presence of  $\beta$ -mercaptoethanol a single prominent band was present both in VP23His and the VP23HisCYS mutants. A faint 70kDa band could be detected in mutants 1 and 3 (fig.3.3.17, panel B, lane 2 and 3 (+)  $\beta$ -mercaptoethanol respectively). This band migrates with the same MW as dimeric VP23His (described in section 3.3.3.2 and figs.3.3.9 and 3.3.10). The presence of dimeric VP23His could be seen clearly when the VP23HisCYS mutants were analysed in the absence of  $\beta$ -mercaptoethanol (fig.3.3.17, lanes 2, 3, and 4 (-)  $\beta$ -mercaptoethanol). However, rather than the single band usually associated with dimeric VP23, two bands could be detected that were also present in the WT VP23His (fig. 3.3.17, lane 1). This probably represents different disulphide linkages within VP23. Differences in the oligomeric status of the VP23HisCYS mutants were further highlighted when they were purified in buffer O (fig. 3.3.18). Numerous prominent bands could be detected by SDS-PAGE analysis in the presence of  $\beta$ -mercaptoethanol which were absent from VP23His purified in sonication buffer (fig. 3.3.5, lane 2) and buffer O (figs. 3.3.9, panel A and 3.3.14, panel B), which resulted in the appearance of a single dimeric band.

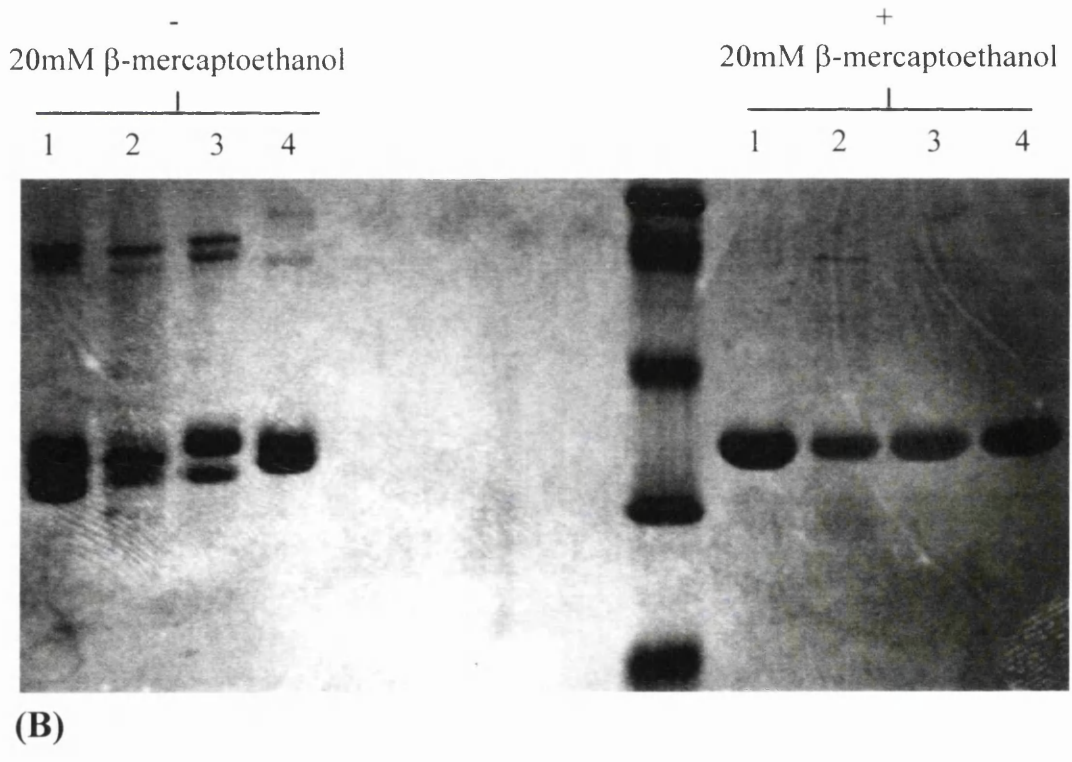
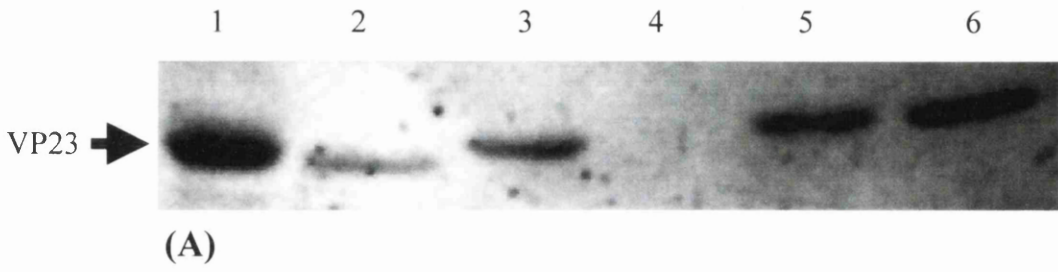


Fig. 3.3.17: Western blot and SDS-PAGE analysis of VP23His and VP23His cysteine mutants

(A) BL21 DE3 bacteria containing either pETUL18 (lane 1) or a pETUL18CYS1-4 (lanes 3-6 respectively) mutant plasmid were grown and induced (as described in Methods). 1.5 ml of the culture supernatant was centrifuged at 14,000 r.p.m. for 30 seconds. The supernatant was removed and the bacterial pellet was resuspended in 200 $\mu$ l of BM and heated for 2 minutes at 100°C in a dry block. 20 $\mu$ l of each sample were analysed by SDS-PAGE against purified B-capsids (lane 2) and transferred to a nitro-cellulose membrane (as described in Methods). The nitro-cellulose membrane was probed with a 1:1000 dilution of a polyclonal VP23 antibody (187). The position of VP23 is indicated by the arrow. (B) VP23His (lane 1) and VP23HisCYS mutants 1, 3, and 4 (lanes 2-4 respectively) were purified in sonication buffer (as described in Methods and fig. 3.3.5). 20 $\mu$ l of each elution fraction 1 was analysed by SDS-PAGE against Rainbow markers in the presence (+) or absence (-) of 20mM  $\beta$ -mercaptoethanol and stained with Coomassie Brilliant Blue.

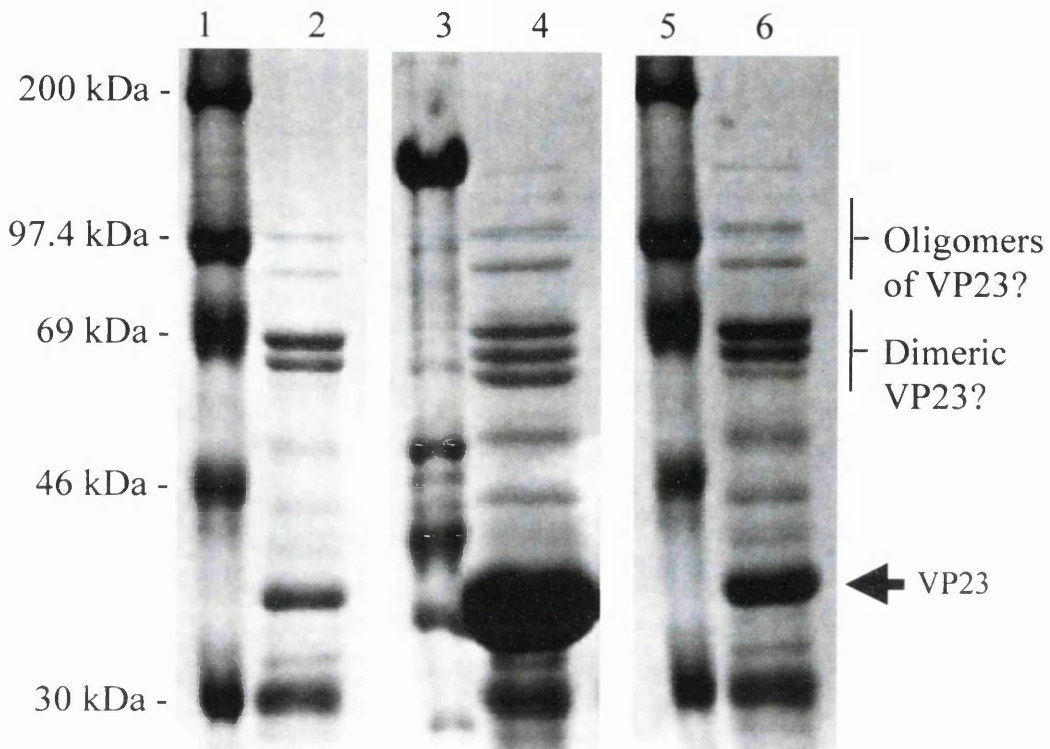


Fig. 3.3.18: SDS-PAGE analysis of purified VP23His Cysteine mutants -1, -3, and -4 in buffer O.

VP23His cysteine mutants -1 (lane 2), -3 (lane 4), and -4 (lane 6) were purified by Ni-NTA affinity chromatography (as described in Methods and fig. 3.3.5) in buffer O. 20 $\mu$ l of the appropriate VP23HisCYS elution fraction 1 was analysed by SDS-PAGE against Rainbow markers (lanes 1 and 5) and purified B-capsids (lane 3), and stained with Coomassie Brilliant Blue.

Western blot analysis of purified VP23HisCYS mutants failed to detect the presence of these higher MW bands (data not shown), unlike that of the dimeric VP23His band purified in buffer O (3.3.9, panel B). It is possible, but unlikely, that the epitope specificity of the antibody used did not recognise the oligomeric forms of purified VP23HisCYS protein. However, a more plausible explanation for the presence of these additional higher MW bands is that the cysteine mutagenesis resulted in non-specific disulphide bond formation between unlinked cysteine residues within VP23 and those present in bacterial proteins. In order to further characterise VP23HisCYS mutants and to determine whether or not they could interact with VP19c, the mutated UL18 ORFs were subcloned into the pCMV<sub>10</sub> expression vector and analysed for their intracellular localisation by immunofluorescence.

### 3.3.9 Immunofluorescence analysis of VP23 and VP23CYS mutants

#### 3.3.9.1 Cloning of UL18 and UL18CYS mutant ORFs into pCMV<sub>10</sub>

The construction of the pCMV<sub>10</sub> expression vector is described by Stow et al., (1993). It utilises the immediate-early promoter from HCMV to regulate recombinant gene expression in mammalian cells. The appropriate UL18 ORFs were subcloned individually from their pET vector as XbaI/HindIII fragments. This retained the 5' sequences encoding the 6x His epitope tag. The DNA fragments were purified from a 1% agarose TAE gel (as described in Methods) and ligated into XbaI/HindIII digested and CIP treated pCMV<sub>10</sub> to generate pE18H and pE18HCYS-1, -3, and -4. Single colonies were screened for the presence of the UL18 ORF by XbaI/HindIII digestion. The identity of mutant UL18 ORFs in each construct was confirmed by restriction mapping using restriction enzymes that recognised the unique sites incorporated into the CYS mutant primers (described in section 3.3.8 and fig. 3.3.16, panel A). The cloning strategy is summarised schematically in fig. 3.3.19. The cloning of the UL38 ORF into the pCMV<sub>10</sub> expression vector to generate pE38 was performed by Dr Frazer Rixon and is described in Rixon et al., (1996).

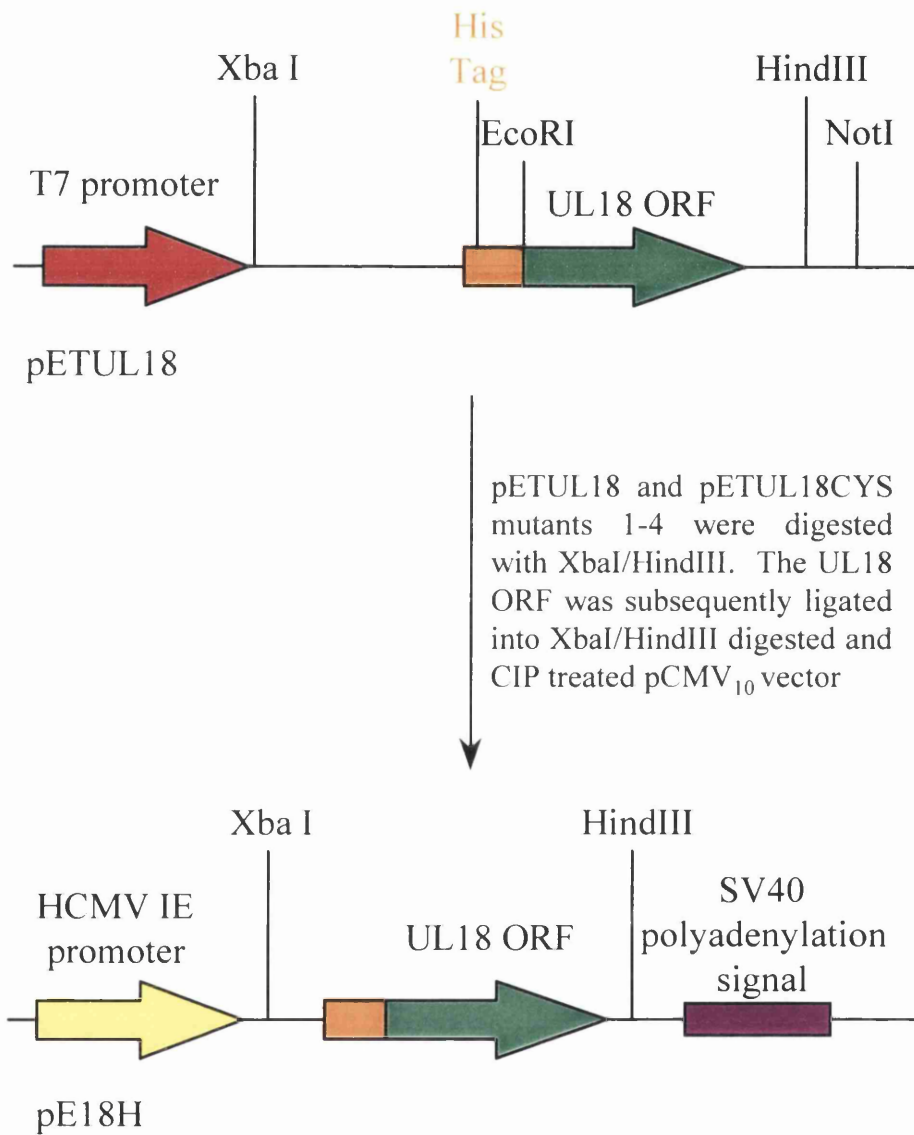


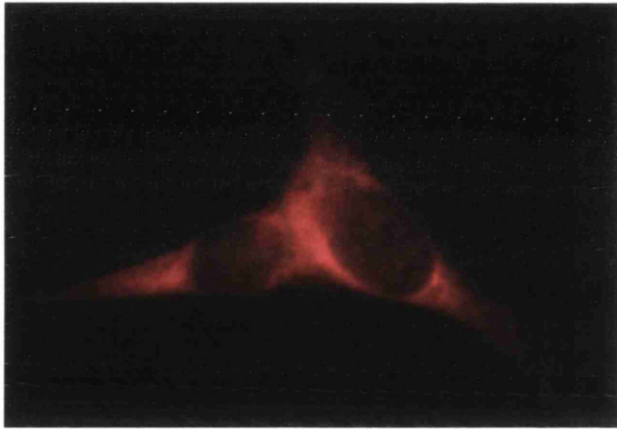
Fig. 3.3.19: Schematic representation of the cloning strategy for UL18 ORF and mutant UL18CYS ORFs into pCMV<sub>10</sub>

### 3.3.9.1 Intracellular localisation of VP23His and VP19c.

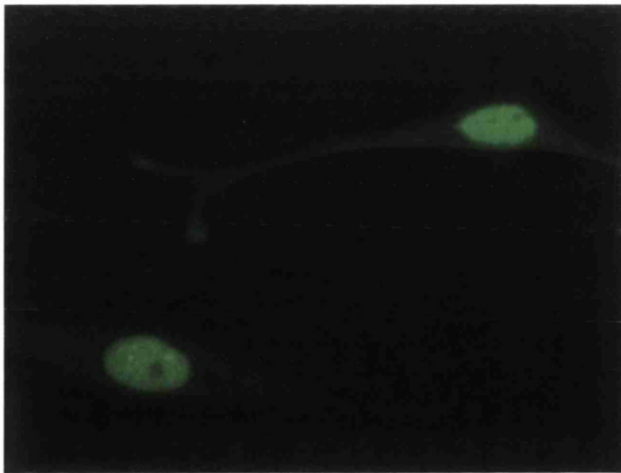
The intracellular localisation of both VP23 and VP19c within BHK-21 C13 cells has been reported previously (Nicholson et al., 1994; Rixon et al., 1996). These experiments demonstrated that VP23, when expressed on its own, was present throughout the cell, whereas VP19c had a predominantly nuclear localisation. When VP19c and VP23 were co-expressed the localisation of VP23 altered to a predominantly nuclear distribution. This led the authors to conclude that VP19c could interact with VP23 and redirect it to the nucleus where it would be required for capsid assembly. In order to confirm this behaviour and to examine the ability of VP19c to direct VP23His to the nucleus, BHK cells were transformed with the appropriate plasmids expressing either VP19c or VP23His (as described in Methods). The polyclonal VP23 antibody (187) and the monoclonal VP19c antibody (CB2040) were used in conjunction with the appropriate secondary antibodies. Fig. 3.3.20 shows the distribution of VP23His when expressed individually within BHK cells. In the majority of cells VP23His could be detected throughout the cell (panel A). However, a few cells demonstrated a predominantly cytoplasmic VP23His distribution (fig. 3.3.20, panel B). When expressed alone, VP19c was only found in the nucleus (fig. 3.3.20, panel C). Fig. 3.3.21 (panels A and C) show that VP23His was present within the nucleus of cells co-expressing both VP23His and VP19c. These results repeat the observations of Nicholson et al., (1994) and Rixon et al., (1996) and show that the 6xHis tag does not alter the behaviour of the protein. BHK cells transformed with plasmids individually expressing VP23HisCYS mutants demonstrated the same cellular distribution as that of the parental VP23His (fig. 3.3.22, panels A, C, E, and G). Similarly, when co-expressed with VP19c, all three cysteine mutants demonstrated a WT VP23 like nuclear distribution (fig. 3.3.22, panels B, D, F, and H). This therefore indicates that mutating the cysteine residues within VP23 does not affect the proteins ability to interact with VP19c within the cytoplasm of BHK cells and become translocated to the nucleus. Furthermore, the 6xHis epitope tag present on the N-terminus of VP23 does not appear to affect the interaction with VP19c. Since, the N-terminal tag on VP23 is probably present on the exterior of the protein this suggests that the N-terminus of VP23 is not directly involved in the interaction with VP19c.



(A)



(B)



(C)

Fig. 3.3.20: Immunofluorescence analysis showing the intracellular localisation of VP23 and VP19c.

BHK21 C13 cells were transfected with plasmids either expressing VP23His (pE18H) or VP19c (pE38, panel C) as described in Methods. The cellular distribution of VP23 (panels A and B) was detected by using a polyclonal VP23 antibody (187). The immunofluorescence observed was due to a secondary goat-anti rabbit IgG conjugated to CY3. The cellular distribution of VP19c (panel C) was detected using a monoclonal VP19c antibody (CB2040). The immunofluorescence observed was due to a goat anti-mouse IgG secondary antibody that was conjugated to FITC. Specific details on antibody dilutions, transfection, and immunofluorescence procedures are detailed in Methods.

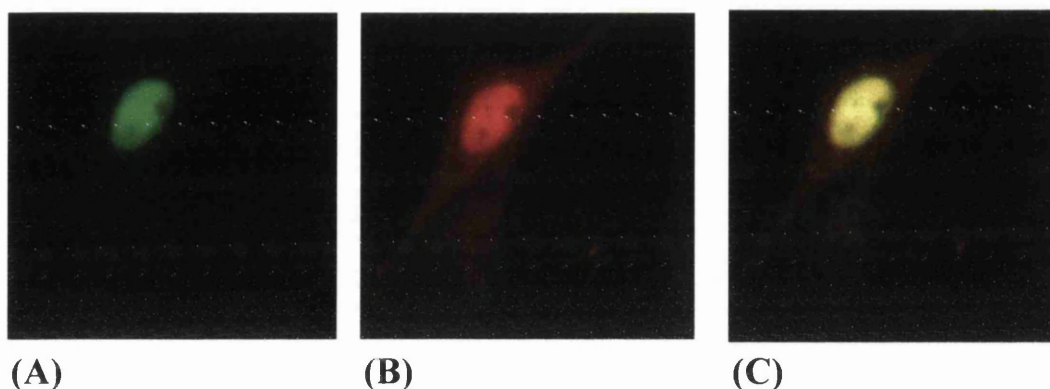


Fig. 3.3.21: Immunofluorescence analysis showing intracellular localisation of VP23 and VP19c co-expressed within BHK-21 C13 cells.

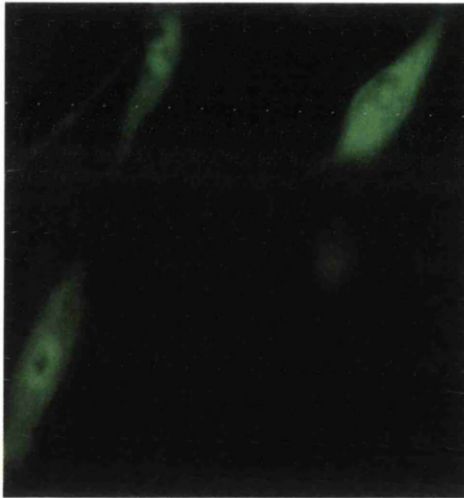
BHK-21 C13 cells were co-transfected with plasmids expressing VP23His (pE18H) and VP19c (pE38), as described in Methods. The cellular distribution of VP23 and VP19c was analysed by double immunolabelling. VP23 was detected using a polyclonal VP23 antibody (187). VP19c was detected using a monoclonal VP19c antibody (CB2040). Immunofluorescence observed was due to goat anti-mouse, and goat anti-rabbit IgG conjugated to FITC and CY3 respectively. Both primary and secondary antibodies were mixed at the appropriate dilutions (as described in Methods). Panels A shows the cellular distribution of VP23His. Panels B shows the cellular distribution of VP19c. Panel C shows a merged image of panels A and B.



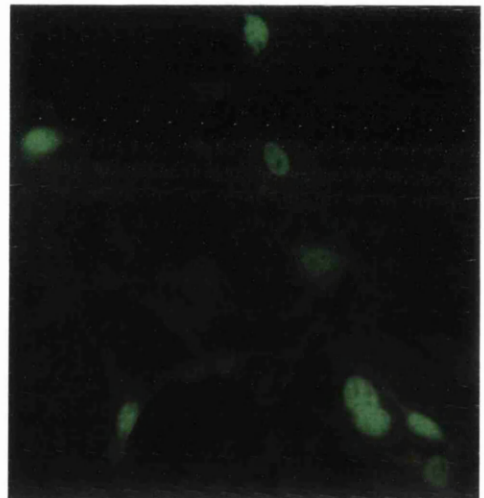
(A)



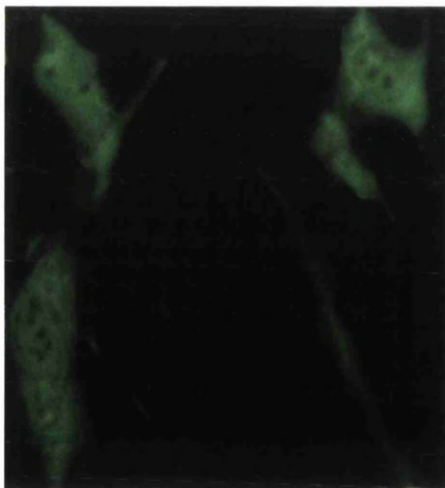
(B)



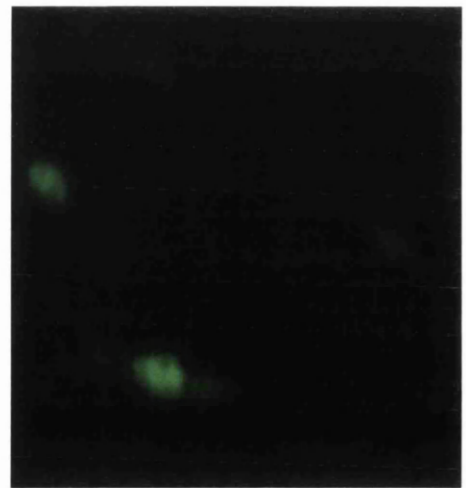
(C)



(D)



(E)



(F)

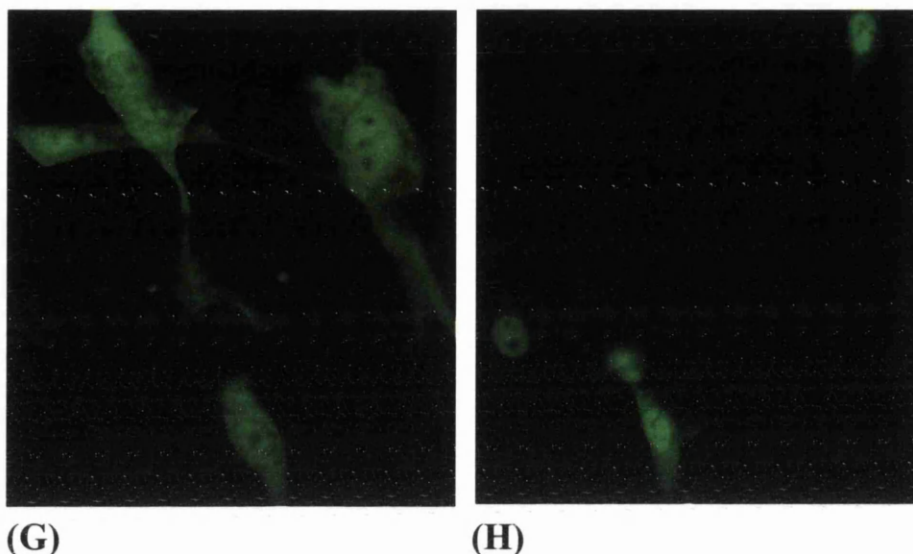


Fig. 3.3.22: Immunofluorescence analysis showing the intracellular distribution of VP23His and VP23HisCYS mutants 1, 3, and 4 with VP19c.

BHK-21 C13 cells were transfected singly with plasmids pE18H (VP23His), pE18HCYS1 (VP23HisCYS1), pE18HCYS3 (VP23HisCys3), or pE18HCYS4 (VP23HisCys4), or co-transfected with pE38 (VP19c) as described in Methods. The cellular distribution of VP23His and VP23HisCYS mutants was detected using a monoclonal VP23 antibody (CB0040) and goat anti-mouse IgG conjugated to FITC. Panels A, C, E, and G show the cellular distribution of VP23His, VP23HisCYS1, VP23HisCYS3, and VP23HisCYS4 respectively. Panels B, D, F, and H show the cellular distribution of VP23His, VP23HisCYS1, VP23HisCYS3, and VP23HisCYS4 respectively when co-expressed with VP19c.

### 3.3.10 Viral growth analysis of UL18CYS mutants

Desai et al., (1993) performed experiments utilising a permissive Vero cell line expressing VP23 (G5-11 Vero cells) to demonstrate that a *lacZ* insertion mutant (K23Z) within the UL18 ORF of HSV-1 abolished capsid formation. Saad et al., (1999) have recently shown VP23 may play a role in development of the capsid floor after procapsid formation. It was therefore decided to test whether or not VP23 cysteine mutants were able to sustain capsid formation. A complementation assay was performed utilising the K23Z mutant and the permissive G5-11 Vero cell line to test the ability of VP23HisCYS mutants to produce infectious progeny virus. The construction of K23Z VP23 null mutant virus and the permissive G5-11 Vero cell line expressing VP23 is described in Desai et al., (1993).

To test the functionality of the VP23CYS mutants, BHK-21 C13 cells were transfected with 1 µg of the appropriate pCMV10 plasmid DNA expressing either VP23His or a VP23HisCYS mutant protein (as described in Methods). 24 hours post-transfection the cells were infected with the K23Z VP23 null mutant virus at a m.o.i of 3. Progeny viruses were harvested at 24 hours post infection and titred on both permissive and non-permissive Vero cells (as described in Methods). Fig. 3.3.23 shows the titres of harvested virus in both permissive and non-permissive cells. No significant amount of revertant K23Z virus was isolated from the complementation assay, as shown by the very low titres of all the progeny virus on non-permissive Vero cells. Both WT and UL18CYS mutants were able to complement growth of K23Z. However, a considerable contrast was observed in the ability for the UL18CYS mutant 1 to produce infectious virus progeny compared to that of the WT and UL18CYS mutants 3 and 4. The assay was repeated and produced a similar titration profile (data not shown). It is possible that the VP23HisCYS1 mutant is more efficient in capsid assembly leading to an increase in the number of infectious progeny produced and consequently a higher titre. However, it is more likely the differences reflect differing transfection efficiencies of the individual plasmid DNAs. Further analysis has to be performed in order to substantiate these findings.

### 3.3.11 Conclusions

#### 3.3.11.1 VP23 dimerisation

Newcomb et al., (1993) were the first group to demonstrate that VP23 was a component of the triplex of HSV-1 capsids and that it was present in two copies per triplex. However, it was not known whether VP23 within the triplex occurred as a dimer or two separate monomeric subunits interacting separately with VP19c. Examining purified VP23 by size exclusion chromatography and sucrose gradient sedimentation has shown that it can exist as a stable dimer (figs. 3.3.10 and 3.3.11). The dimer is not held together by intermolecular disulphide linkages and is stable at 4°C (figs. 3.3.12 and 3.3.14). Therefore, findings that capsid formation is inhibited in the presence of DTT (Newcomb et al., 1994) and procapsid disassociation is induced upon incubation at 0°C (Newcomb et al., 1996) cannot be attributed to VP23 dimer disassociation. Cryo-EM has also provided additional evidence that VP23 forms dimers in the capsid (Zhou et al., 2000). Utilising cryo-EM and difference mapping of HSV-1 B-capsids and VP5-VP19c particles, Saad et al., (1999) determined the position of VP19c within WT B-capsids. From these data they concluded that VP19c was located on the top of the triplex, interconnecting adjacent capsomers. The remaining mass, forming the two legs of the triplex which connect to the capsid floor, was proposed to be VP23. These two legs had an extensive interface suggesting that the two copies of VP23 formed a dimer within the triplex (discussed further within section 4.0).

Desai and Person (1996) demonstrated that the deletion of the N-terminal 77 residues of VP23 prevented VP23 from interacting with VP19c (as determined by the yeast two hybrid system). Similar deletion mutagenesis performed by Spencer et al., (1998) upon the N-terminus of VP23 also demonstrated that mutated VP23 inhibited *in vivo* capsid assembly within insect cells. These experiments clearly indicate an essential role for the N-terminal region of VP23. However, the removal of such a large number of residues from the N-terminus makes it difficult to determine whether these residues are required for a direct protein-protein interaction with VP19c or simply to maintain the protein conformation required for interaction. Furthermore, interpretation of results from mutagenesis on VP23 is complicated by the fact that VP23 forms dimers. Therefore, it is difficult to assess

---

whether or not mutations in VP23 which prevent the interaction with VP19c specifically disrupt this interaction or disrupt VP23 dimer formation leading to a shift in conformational stability. Functional analysis demonstrated that both dimeric and monomeric VP23 can form capsids which resemble those of WT B-capsids (discussed in section 3.6 and fig. 3.6.1). This would suggest that dimerisation of VP23 may not be essential for initial capsid protein interactions and procapsid assembly. However, the maturation into a polyhedral capsid would appear to require some form of VP23 dimerisation as the mature triplex clearly show VP23 molecules in close proximity (discussed further in section 4.0, Saad et al., 1999). Desai and Person (1996) were unable to detect any such self-interaction between VP23 molecules utilising the yeast two-hybrid system. This could possibly be attributed to the GAL4 domains which are fused to the N-terminus of VP23 molecules which may interfere with dimerisation. It is interesting to note that the N-terminal 6xHis tag used in the purification of VP23His does not interfere with the dimerisation of VP23, or with its interaction with VP19c (fig. 3.3.10 and 3.6.1). This would suggest that the N-terminus itself might not be involved in these interactions but that steric inhibition may occur when larger domains are fused to the N-terminus.

Immunofluorescence analysis performed on BHK cells expressing pE18H demonstrated a small population of cells that had no intranuclear VP23 (fig. 3.3.20, panel B). It could be speculated that this distribution of VP23 to the nucleus is prevented due to the dimerisation of VP23 within the cytoplasm and as a consequence the increase in mass preventing diffusion through the nuclear pore into the nucleus. Immunofluorescent studies performed by Nicholson et al., (1994) and Rixon et al., (1996) on the cellular distribution of VP23 within cells did not present any evidence to support this observation. However, it is unlikely that the cellular distribution of VP23 in these cells is an *in vivo* artefact due to the co-localisation of VP23 to the nucleus when expressed in BHK cells containing the pE38 plasmid expressing VP19c. The variation in the cellular distribution of VP23His is more likely to reflect differences in the level of expression of VP23His from the pCMV<sub>10</sub> vector within particular cells.

### 3.3.11.2 VP23 cysteine analysis

Many viruses rely heavily on disulphide bonding to stabilise large capsid protein structures. Li et al., (1998) showed that mutating the papillomavirus capsid protein L1 carboxy terminal Cys424 residue to a Gly prevented the formation of icosahedral capsids *in vitro*. The change from Cys to Gly did not prevent pentamer assembly but prevented papillomavirus capsids from forming stable structures via an inter-pentamer disulphide bond. Similarly, the simian virus 40 (SV40) Vp1 capsid protein has a large network of cysteine linkages. Jao et al., (1999) demonstrated by mutating all 7 cysteine residues, that Cys residues at Cys9, Cys104, and Cys207 were essential for the formation of multi-pentameric complexes through inter-pentamer disulphide bonds. Examination of the published X-ray crystal structure of Vp1 (Liddington et al., 1991) revealed that residues Cys104 and Cys207 reside in interconnecting pentamer loops positioning them in an ideal situation for capsid stabilisation through disulphide bonding. The Cys9 residue is located in the amino terminal arm of Vp1 which is exposed on a Vp1 pentamer. Although not visualised by X-ray crystallography it is proposed to be involved in disulphide bonding through interconnections at the pentamer base. Conversely, Fox et al., (1997) characterised the isolation of a mutant of the cowpea chlorotic mottle virus (CCMV) which was unable to disassemble during infection and therefore was uninfecious. Subsequent analysis revealed an Arg to Cys change at residue 26 within the coat protein. The N-terminus of the coat protein is directly involved in hexameric capsomer formation and demonstrated a six-fold related symmetry. The mutation of residue 26 to a Cys generates a disulphide bond at a three-fold axis and consequently increases virion stability to a point where it became non-infectious.

Comparison of VP23 homologues from the alphaherpesvirus demonstrated a strong conservation for three out of the four cysteine residues within the HSV-1 VP23. Size exclusion chromatography of purified dimeric VP23His following DTT reduction showed that the VP23 dimer was not held together by inter-molecular disulphide linkages (fig. 3.3.14). Furthermore, site directed mutagenesis and functional analysis of three of these cysteine residues had no detectable effect on the ability of VP23 to interact with VP19c or to produce infectious virus progeny (figs. 3.3.22 and 3.3.23). Analysis of purified VP23HisCYS mutants by non-reducing SDS-PAGE demonstrated that mutating the

---

cysteine residues within VP23 did not prevent dimer formation but did result in slightly different banding patterns which might be attribute to different intra-molecular disulphide linkages formed within the VP23 dimer (figs. 3.3.17 and 3.3.18).

Although these cysteine residues do not play an essential role in the capsid assembly pathway of HSV-1, disulphide bond formation may help to strengthen the capsid post-assembly and thus stabilise progeny virions. Lee et al., (1996) reported similar findings during the dimerisation of the rubella virus capsid protein (C protein). Site directed mutagenesis on either Cys152 or Cys196 prevented dimerisation of the C protein but did not prevent virion assembly. They speculated that the disulphide mediated C protein association might be required for fixing the intersubunit interface, therefore locking the dimer into a specific conformation. The conservation of the 3 cysteine residues within the VP23 homologues would suggest some kind of structural involvement. Locking of the VP23 conformation may be an appropriate role due to its molten globule nature (discussed in section 3.6). However, to identify any specific requirement for these conserved cysteine residues and their possible implication in the folding of VP23 requires further analysis.

#### *3.3.11.3 Future Work.*

Further analysis is required to specifically identify the oligomeric status of VP23HisCYS mutants when purified in buffer O. The likelihood is that they are different disulphide linked oligomeric complexes of VP23, as VP23HisCYS mutants purified in sonication buffer yield similar but yet reducible bands corresponding to the same MWs. It would also be interesting therefore to analyse these complexes by two-dimensional gel electrophoresis, both in reducing and non-reducing conditions, in order to determine the exact composition of these higher MW complexes.

Deletion of individual cysteine residues might lead to non-specific disulphide bond formation with bacterial proteins present within lysed extracts. It would be interesting therefore to perform multiple mutagenesis to replace several or all of the cysteine residues within VP23, particularly those conserved throughout the alphaherpesvirus family, for example cysteine residues 27 (CYS1) and 297 (CYS2).

Results presented within this thesis (section 3.1) and those by Desai and Person (1996) demonstrated that VP23 and VP19c interact sufficiently within the yeast two-hybrid system to induce the transcriptional activation of GAL4. It would be interesting, therefore, to analyse the strength of interaction between VP23CYS mutants and VP19c utilising the yeast two-hybrid system. Using this system any interactions detected could be accessed for their strength of association and compared to that of the WT interactions utilising a  $\beta$ -galactosidase liquid culture assay. This would therefore provide additional evidence as to the specific requirement of these conserved cysteine residues for the formation of capsid protein interactions.

It would also be interesting to map the positions of the cysteine residues within the triplex structure. This could be accomplished through the use of colloidal gold mapping and cryo-EM analysis on in vitro assembled capsids where VP23HisCYS protein(s) have been substituted in place of VP23His. This could provide additional structural information on the folding of VP23 within the triplex.

## 3.4 Characterisation of the triplex protein VP19c

### 3.4.1 Construction and expression of pETUL38.

#### 3.4.1.1 Cloning of the UL38 ORF into pET28MOD

The cloning of UL38 ORF into the modified bacterial expression vector pET28MOD was carried out by David McNab. Briefly, the UL38 ORF was subcloned out of the transfer vector pBJ382 (constructed by Peter Nicholson and described in Nicholson, 1992) as a BamHI/HindIII fragment and ligated into a BamHI/HindIII digested pET28a bacterial expression vector to generate pETBJ382. pETBJ382 was then digested with BsrD1/EcoRV and ligated with a dsDNA oligonucleotide. This introduced a unique EcoRI site at the 5' end of the UL38 ORF to generate pET38oli. The UL38 ORF was subcloned out of pET38oli as an EcoRI/HindIII fragment and ligated into pET28MOD to generate pETUL38. The construction of pET28MOD is described in Kirkitadze et al., (1998) and schematically illustrated in section 3.3.1 (fig. 3.3.1). The expression plasmid pETUL38 is illustrated in fig. 3.4.1.

#### 3.4.1.2 Bacterial expression of VP19cHis

BL21 DE3 bacteria were electroporated in the presence of approximately 1µg of pETUL38 or pET28MOD vector DNA and recombinant colonies were isolated (as described in Methods). Single recombinant colonies were grown and induced, as described in methods and fig. 3.4.2, and analysed for the expression of VP19cHis by SDS-PAGE analysis. Fig. 3.4.2 (panel A) shows the comparative protein profiles of induced pETUL38 and pET28MOD transformed BL21 DE3 bacteria. No novel 50kDa band corresponding to VP19cHis could be detected in the pETUL38 sample by SDS-PAGE analysis and Coomassie Brilliant Blue staining (fig. 3.4.2, lanes 3 and 4). The absence of a 50kDa VP19cHis band suggests a poor level of expression from the pETUL38 vector. In order to ascertain whether there was any expression of VP19cHis in the induced cultures, Ni-NTA agarose affinity chromatography was performed (as described in Methods) and the

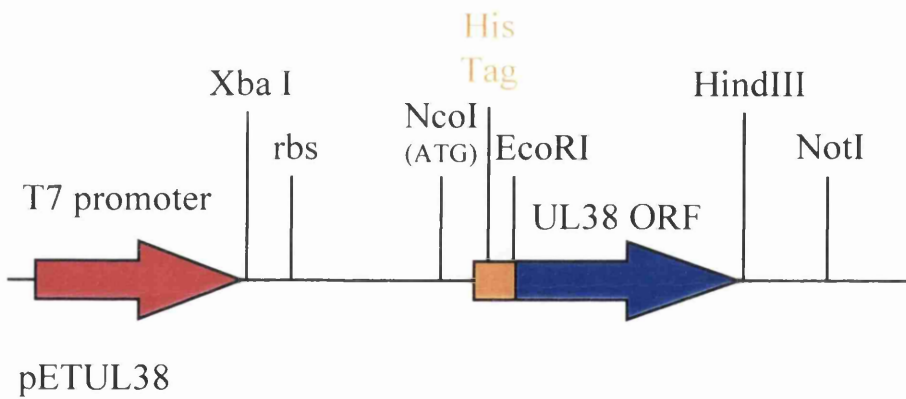
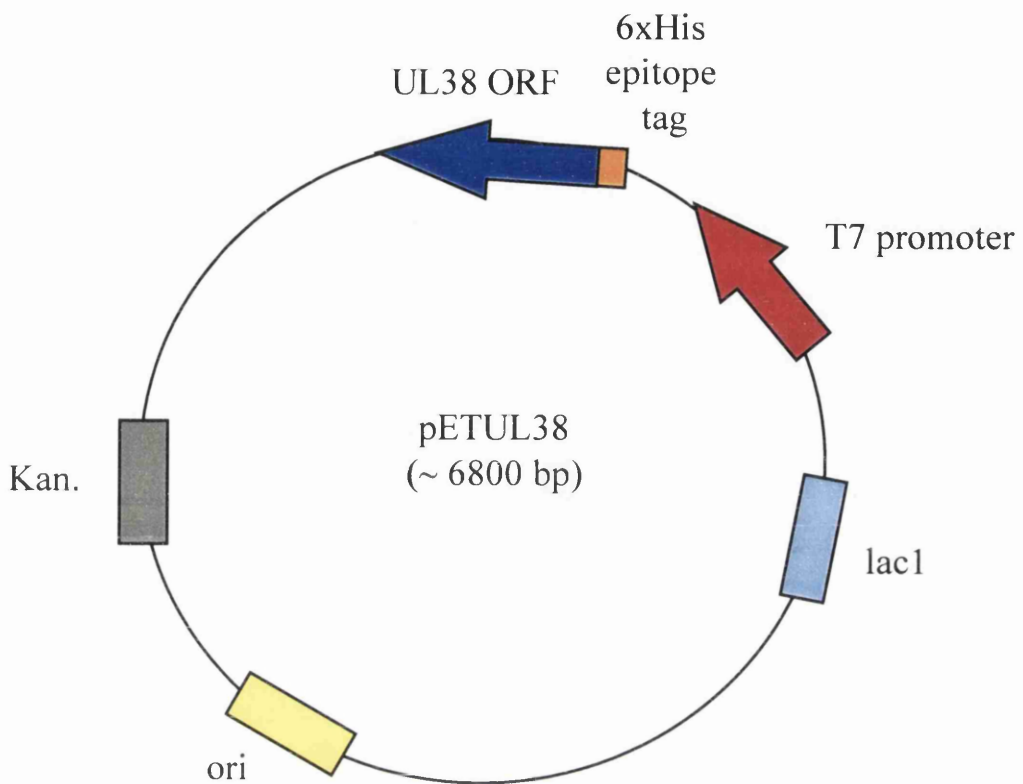


Fig. 3.4.1: Schematic representation of the bacterial expression vector pETUL38

protein(s) bound to the Ni-NTA agarose were eluted and analysed by Western blot. The principles of Ni-NTA chromatography are discussed in section 3.3. Due to the lack of a monoclonal antibody against VP19c, a monoclonal Penta His antibody, which specifically recognises the 6xHis epitope tag, was used to detect purified VP19cHis. Fig. 3.4.2 (panel B) shows the presence of a band with an approximate MW of 50kDa. The MW of 50kDa is in good agreement with the predicted 50260Da MW of VP19c from the amino acid sequence (McGeoch et al., 1988). This band was strongest in the Ni-NTA agarose elution fraction 1 (fig. 3.4.2, lane 4). However, low levels could be detected in the crude bacterial extracts, bacterial pellet and bacterial supernatant samples collected before Ni-NTA agarose purification. This suggests that the expression of the VP19cHis is extremely inefficient. The low recovery of VP19cHis was not due to the formation of insoluble inclusion bodies as little protein could be detected by Western blot analysis in either crude bacterial extracts or bacterial pellet samples post lysis. In an attempt to increase the efficiency of transcription and/or translation of pETUL38 within BL21 DE3 bacteria various induction conditions were tested. However, none of the conditions tested increased the level of VP19cHis expression (data not shown). The low level of expression of VP19cHis compared to that of VP23His, which is expressed from the same plasmid vector, may indicate a predominance of certain codons which are not recognised by the BL21 DE3 bacteria. Alternatively, VP19cHis expression may be toxic. This could possibly be attributed to the presence of hydrophobic domains on the exterior of the VP19cHis protein leading to its incorporation into bacterial membranes thereby generating a toxic phenotype (Qiagen Ni-NTA trouble shooting protocol, 1998). Alternatively, VP19cHis expressed within bacteria may be broken down or degraded. Smaller MW bands are detected in the Ni-NTA VP19cHis elution fraction 1 (see fig. 3.4.2, lane 4) which could represent breakdown products. However, at the time no monoclonal antibody to VP19c was available to conclusively demonstrate this.

### **3.4.2 VP19cHis isolation from recombinantly expressed triplexes**

Due to the difficulty in preparing VP19c from bacteria it was decided to investigate whether or not it would be possible to isolate VP19cHis from triplexes purified from SF21 cells infected with Ac18386. Triplex purification from Ac18386 infected cells is discussed

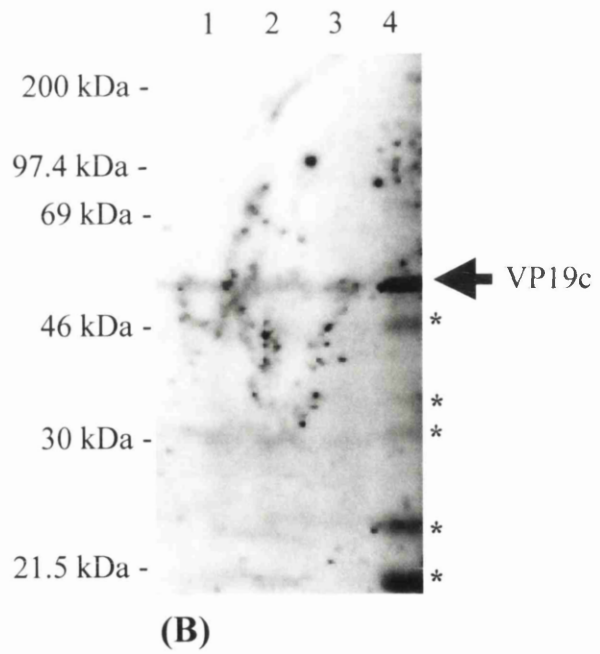
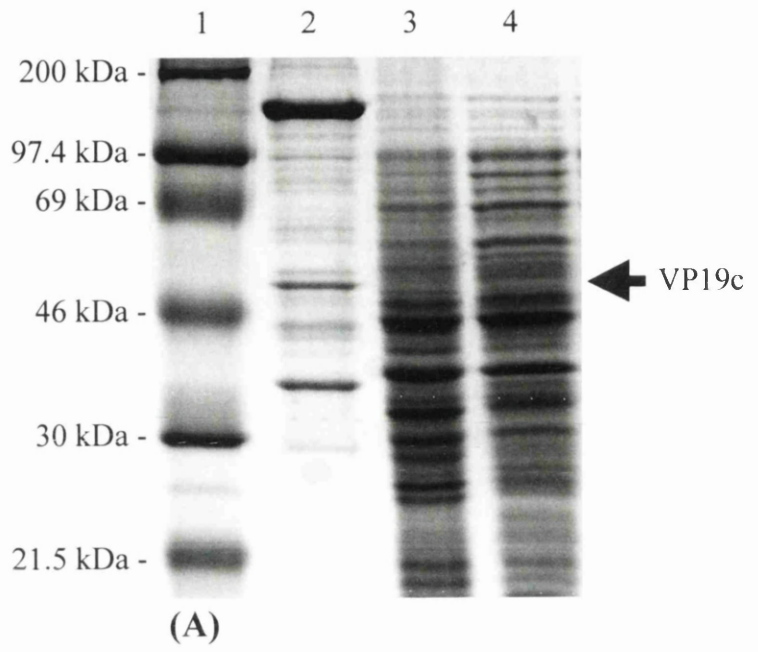


Fig. 3.4.2: SDS-PAGE and Western blot analysis of VP19cHis expression in BL21 DE3 bacteria.

BL21 DE3 bacterial cultures containing either pET28MOD vector (lane 3) or pETUL38 (lane 4) were grown and induced (as described in Methods). 1.5 ml of the culture supernatant was centrifuged at 14,000 r.p.m. for 30 seconds. The supernatant was removed and the bacterial pellet was resuspended in 200µl of BM and heated for 2 minutes at 100°C in a dry block. 15µl of each sample was analysed against purified C-capsids (lane 2) and Rainbow markers (lane 1) by SDS-PAGE and stained with Coomassie Brilliant Blue. Arrow indicates the position of VP19c as determined from the C-capsid profile (A). VP19cHis was purified from a 1200ml culture of induced BL21 DE3 bacteria containing pETUL38 using 700µl of Ni-NTA agarose equilibrated in sonication buffer (as described in Methods). VP19cHis was eluted from the agarose in 3x 1ml fractions of 250mM imidazole in sonication buffer. Western blot analysis was performed to detect the presence of purified VP19cHis using a monoclonal Penta His antibody (Qiagen; 1:1000 dilution) which specifically recognises the 6x His epitope tag. Lane 1; induced BL21 DE3 bacteria containing pETUL38. Lane 2; pETUL38 pellet fraction after lysis. Lane 3; pETUL38 supernatant fraction after lysis. Lane 4; 20µl of elution fraction 1 of Ni-NTA agarose purified VP19cHis. The position of VP19c is indicated by an arrow. \* indicates possible break down products of VP19c.

in detail in section 3.5. The 6xHis epitope tag is located on the N-terminus of the VP19c component of the heterotrimer protein complex. This means that VP19cHis will bind to Ni-NTA agarose but VP23 will not if affinity chromatography is carried out on denatured triplexes. Fig. 3.4.3 shows the elution profile of VP19cHis following treatment of the Ni-NTA agarose with 3M urea. 3M urea was sufficient to disassociate the majority of VP23 from triplexes. However, some VP23 could still be detected by Coomassie staining indicating substantial but not complete disassociation of triplexes in 3M urea.

Purified VP19cHis was dialysed against buffer O to remove any residual urea and to allow the VP19cHis the opportunity to undergo refolding. Fig. 3.4.4 (panel A) shows the SDS-PAGE profile of purified VP19cHis before and after dialysis (lanes 2 and 3 respectively). In order to analyse the conformational effects of urea denaturation on the VP19cHis purified by this method, fluorescence spectroscopy was performed (as described in Methods). Fluorescence spectroscopy can be used to measure the extent to which tryptophan side chains are buried within the interior of a protein molecule. Fig. 3.4.4 (panel B) shows the intrinsic tryptophan fluorescence spectra of the dialysed VP19cHis sample following excitation at 295nm. An emission maximum ( $\lambda_{\max}$ ) at approximately 356nm corresponds to the intrinsic  $\lambda_{\max}$  value associated with tryptophan residues within small model compounds that are exposed to the solvent. A shift in  $\lambda_{\max}$  towards 330nm indicates tryptophan residues which are buried or partially buried within the interior of a folded protein molecule (Freifelder 1982; Grimmel et al., 1983). The  $\lambda_{\max}$  obtained from the fluorescence profile for VP19cHis purified by denaturation of triplexes was around 360nm. This indicates that the tryptophan residues were exposed to the solvent and suggests that the urea treatment used in the isolation procedure for VP19cHis, denatured the molecule and that dialysis alone was not sufficient to induce the refolding of VP19cHis. Fluorescence spectroscopy analysis carried out subsequently on VP19cHis purified from SF21 cells infected with Ac381 gave a  $\lambda_{\max}$  of around 330nm showing that VP19cHis can be purified as a folded molecule (discussed in section 3.6, fig. 3.6.2).

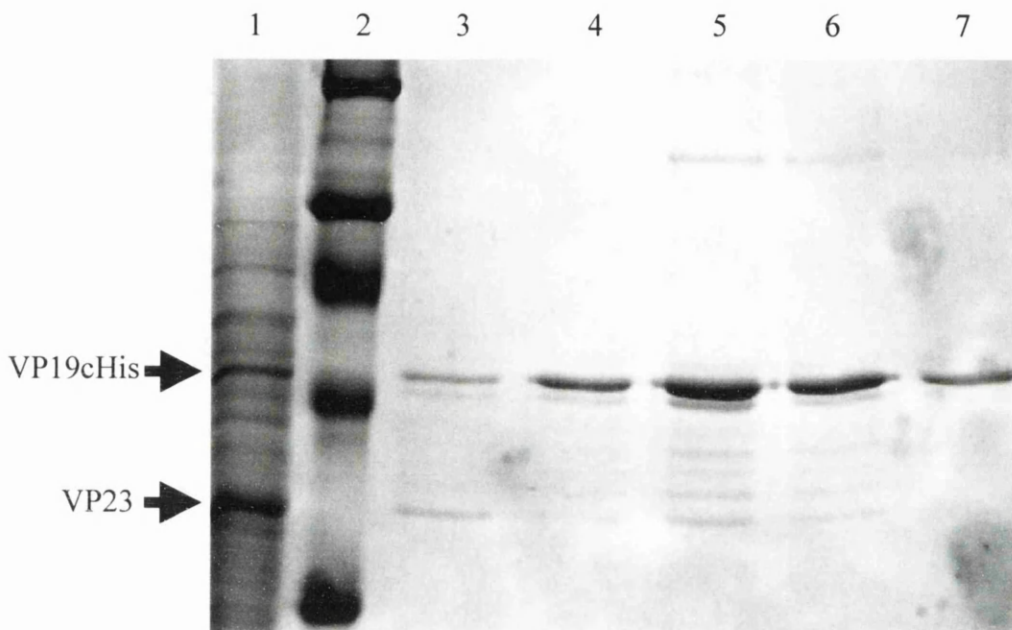
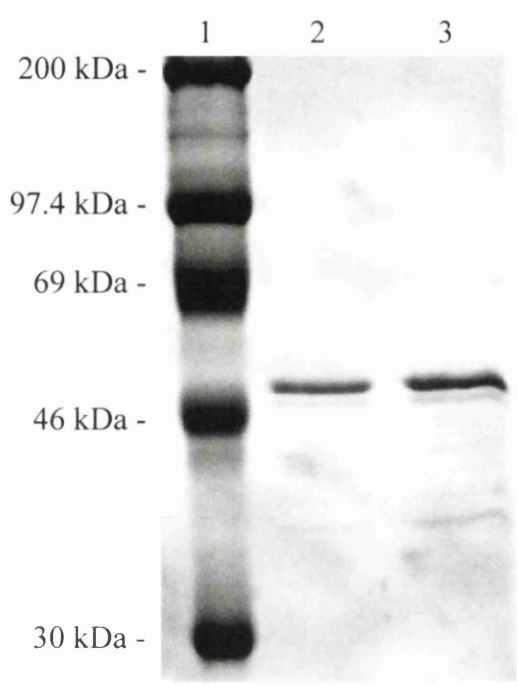
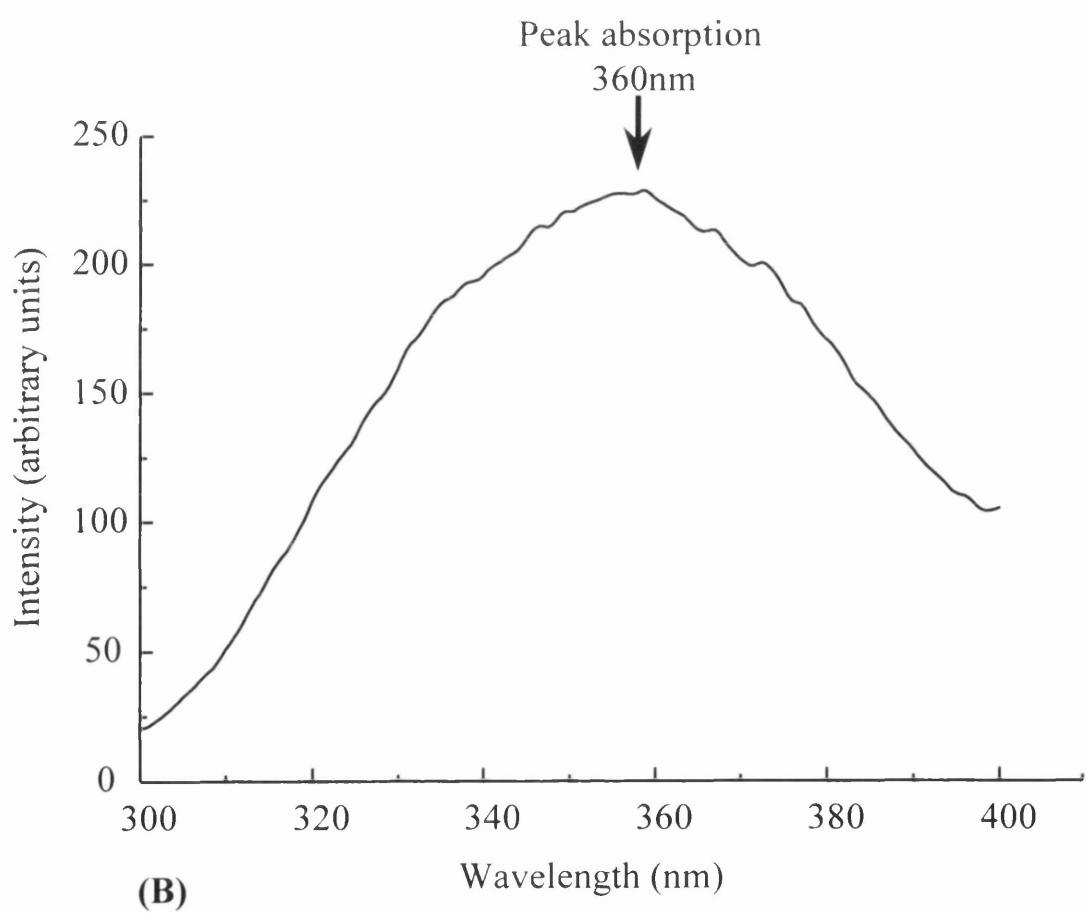


Fig. 3.4.3: SDS-PAGE analysis of VP19cHis isolated from Ni-NTA agarose purified triplexes denatured in 3M urea.

300ml of SF21 cells ( $1 \times 10^6$  cells/ml) were infected with the recombinant baculovirus Ac18386 co-expressing the triplex proteins VP23 and VP19cHis (as described in Methods). Triplexes were purified using 700 $\mu$ l of Ni-NTA agarose equilibrated in buffer O. The Ni-NTA agarose was washed with 5 ml of buffer O containing 15mM imidazole to remove weakly bound cellular proteins from the agarose resin. The Ni-NTA agarose and associated proteins were then resuspended in 5ml of buffer OU (buffer O containing 10% glycerol + 3M urea) and incubated for 30 minutes at RT. The supernatant was removed and the Ni-NTA agarose washed with a further 5ml of buffer O. Proteins were eluted from the Ni-NTA agarose by stripping the Ni<sup>2+</sup> atoms in 500 $\mu$ l of buffer O containing 250mM EDTA (pH8.0). 20 $\mu$ l of elution fractions 1-5 (lanes 3-7 respectively) and 5 $\mu$ l of Ac18386 infected SF21 cell supernatant (lane 1) were analysed by SDS-PAGE against Rainbow markers (lane 2) and stained with Coomassie Brilliant Blue. The positions of VP19c and VP23 are indicated by the arrows.



(A)



(B)

Fig. 3.4.4: SDS-PAGE and fluorescence spectroscopy analysis of Ni-NTA agarose purified VP19cHis isolated from denatured triplexes in 3M urea

VP19cHis was purified in buffer O (as described in Methods and fig. 5.4.3). (A) SDS-PAGE analysis of VP19c stripped from triplexes, before and after dialysis (lane 2 and 3 respectively). 20 $\mu$ l of each sample was analysed against Rainbow markers and stained with Coomassie Brilliant Blue. (B) Intrinsic tryptophan fluorescence profile of dialysed VP19cHis (0.1 mg/ml) in buffer O following excitation at 295nm. Trace was corrected for the effect of buffer by subtraction of a blank buffer control spectrum.

### 3.4.3 Purification of recombinantly expressed VP19cHis from SF21 cells infected with Ac381

Attempts were made throughout my PhD to purify VP19cHis by Ni-NTA agarose affinity chromatography using a variety of purification buffers. Generally these attempts proved unsuccessful until the phosphate based purification buffer (buffer O), which was found to stabilise the solubility of Ni-NTA agarose purified triplexes from SF21 cells infected with either Ac18638 or Ac18386, was utilised in the purification of VP19cHis from SF21 cells infected with Ac381.

#### 3.4.3.1 Cloning of the UL38 ORF into pAcCL29-1

Cloning of the UL38 ORF into the baculovirus expression vector pAcCL29-1 was carried out by A. McGregor. Briefly, the UL38 ORF was amplified by PCR using forward and reverse primers, which encoded the unique restriction sites BamHI and PstI respectively. PCR amplification removed sequences which encoded the 13 N-terminal amino acids of VP19c and replaced them with sequences encoding amino acids which reconstituted the methionine start codon followed by Arg, Ser and 6x His residues. The PCR product was subcloned into the pAcCL29-1 baculovirus transfer vector as a BamHI/PstI fragment. This transfer vector was then used to generate recombinant baculoviruses by co-transformation into SF21 cells with parental baculovirus (PAK6) DNA (as described in Methods). Recombinant viruses were isolated and used to generate virus stocks. Virus stock 1 (Ac381) was selected for the production of high titre virus stocks which were used for the recombinant expression of VP19cHis. The pAcCL29381 transfer vector is schematically represented in fig. 3.4.5.

#### 3.4.3.2 Expression and purification of VP19cHis

Fig. 3.4.6 shows the SDS-PAGE protein profiles of SF21 cells infected with Ac18386 or Ac381 which express the same UL38His ORF. The level of VP19cHis expression within Ac381 infected SF cells is comparable to that of VP19cHis when co-expressed with VP23 in Ac18386 infected cells (fig. 3.4.6, lanes 3 and 2 respectively). Early attempts to purify

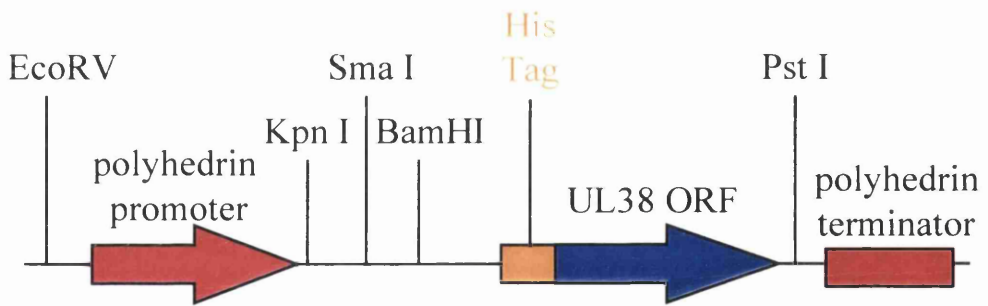
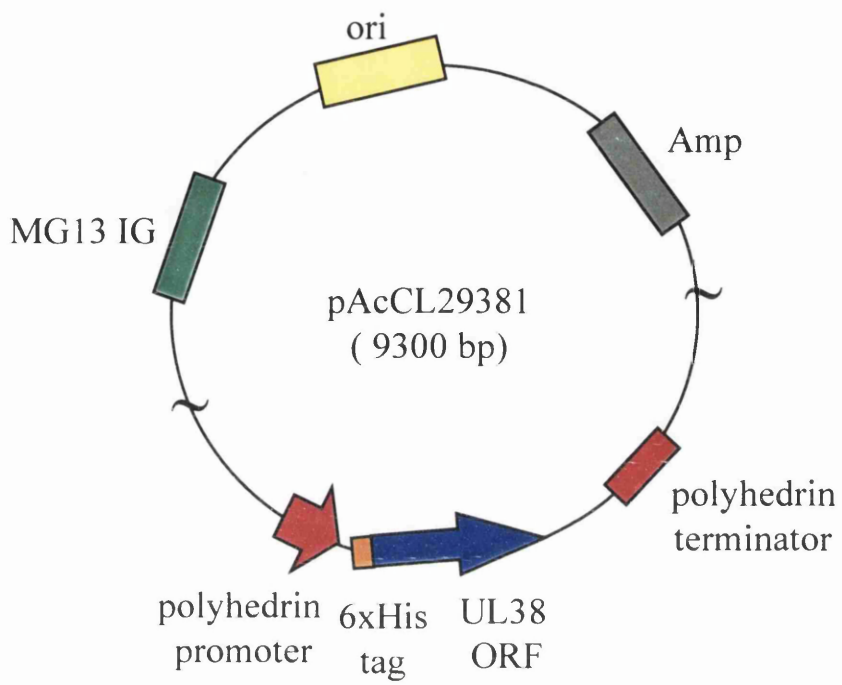


Fig. 3.4.5: Schematic representation of pAcCL29381

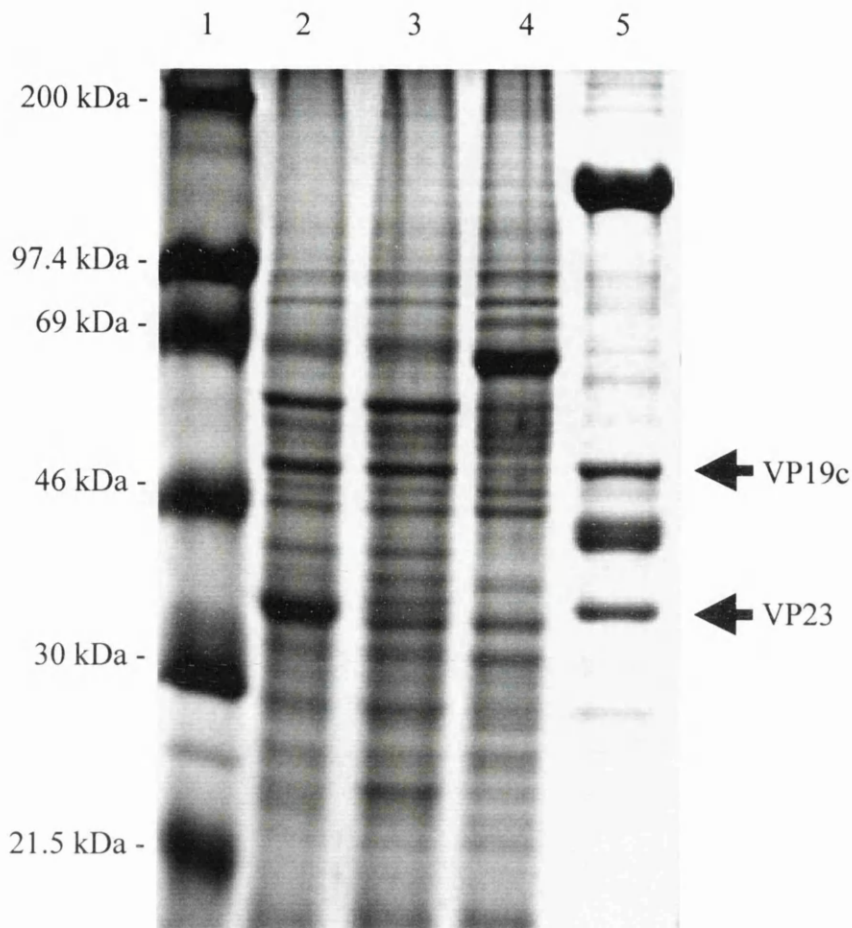


Fig. 3.4.6: SDS-PAGE analysis of SF21 cells infected with Ac381

60mm dishes containing approximately 70% confluent SF21 cells were infected at an m.o.i. of 5 with either Ac18386 (lane 2), Ac381 (lane 3), or mock infected (lane 4) (as described in Methods). 48 hours post infection SF21 cells were harvested (as described in Methods) and pelleted by centrifugation at 14,000 r.p.m. for 5 minutes at RT. The supernatant was removed and the cell pellet resuspended in 200 $\mu$ l of BM buffer and heated for 2 minutes at 100°C in a dry block. 5 $\mu$ l of each sample and purified B-capsids (lane 5) were analysed by SDS-PAGE against Rainbow markers and stained with Coomassie Brilliant Blue. The positions of VP19c and VP23 are indicated by the arrows.

VP19cHis through Ni-NTA agarose chromatography resulted in low levels of recovery. Fig. 3.4.7 shows a typical SDS-PAGE profile of VP19cHis purified in buffer O (150mM Na<sub>2</sub>HPO<sub>4</sub> (pH7.5), 0.1% Octyl-β-glucoside, 0.1% glycerol). The recovery of VP19cHis was significantly improved when the cell lysis was carried out in buffer OL (buffer O containing 150mM NaCl and 0.05% NP40). Fig. 3.4.8 (panel A) shows the typical SDS-PAGE profile of VP19cHis purified from SF21 cells infected with Ac381 when buffer OL was utilised in cell lysis. The presence of NaCl and NP40 in buffer OL evidently increases the availability of VP19cHis to the Ni-NTA agarose resin compared to that of buffer O (fig.3.4.7). Although the mechanism by which buffer OL accomplishes this is unclear, the presence of NaCl or NP40 within the buffer may increase the efficiency of cell lysis or prevent the aggregation of VP19c during purification. Using buffer OL during the lysis of SF21 cells infected with the Ac381 results in the co-purification of a 90kDa protein that typically elutes from the Ni-NTA resin in the first elution fraction (see fig. 3.4.8, lane3). Western blot analysis using a VP19c polyclonal antibody (TrpE/VP19c fusion) demonstrates that the prominent 50kDa protein band is VP19c and but failed to detect the co-purified 90kDa protein. Purification of VP19cHis often resulted in the co-purification of breakdown products of VP19c. The presence of such breakdown products is highlighted in fig. 3.8.4 (panels B and C). A prominent 40kDa MW band is readily detected as well as smaller breakdown products (indicated by \*). Western blot analysis using the Penta His monoclonal antibody (Qiagen) demonstrated that the major breakdown product was formed by the loss of the C-terminal portion of VP19c as the N-terminal His tag was readily detected (fig. 3.4.8, panel C). It is interesting to note the presence of similar MW VP19c related breakdown bands within purified B-capsids (fig. 3.4.8, panel B, lane 1). Other groups have also described the formation of C-terminally truncated VP19c products (Newcomb et al., 1996; Spencer et al., 1998). This suggests that the C-terminal truncation described here is not a direct result of the incorporation of the 6x His epitope tag making VP19cHis susceptible to proteolytic cleavage. The inclusion of a cocktail of protease inhibitors (see Materials and Methods for details) during the purification of VP19cHis did not prevent the accumulation of the C-terminally truncated VP19c molecules. This does not preclude the generation of the C-terminally truncated forms of VP19c by proteolytic digestion. One of the disadvantage in utilising Ni-NTA agarose affinity chromatography is that metal chelators, such as EDTA or EGTA that can inhibit metalloproteases, cannot be used as they strip Ni<sup>2+</sup> ions from the NTA matrix.

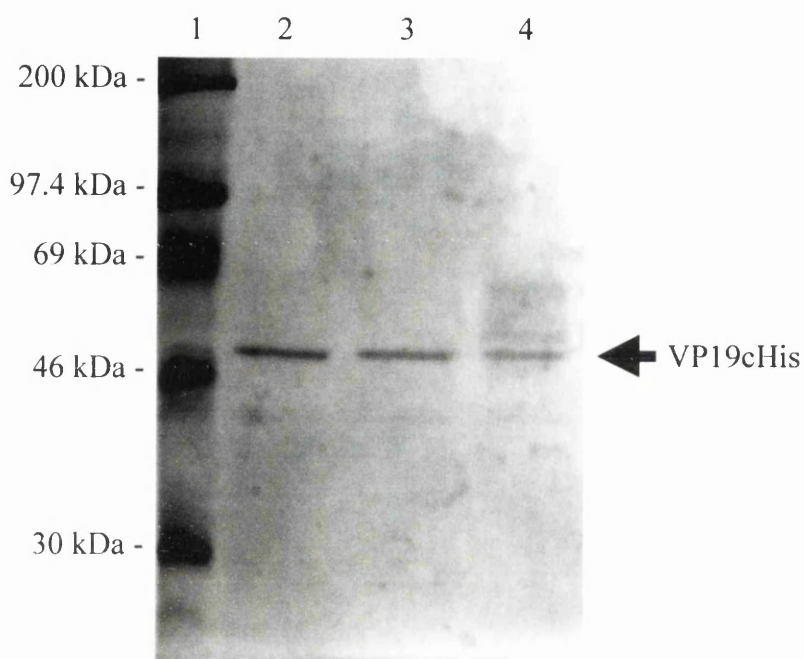
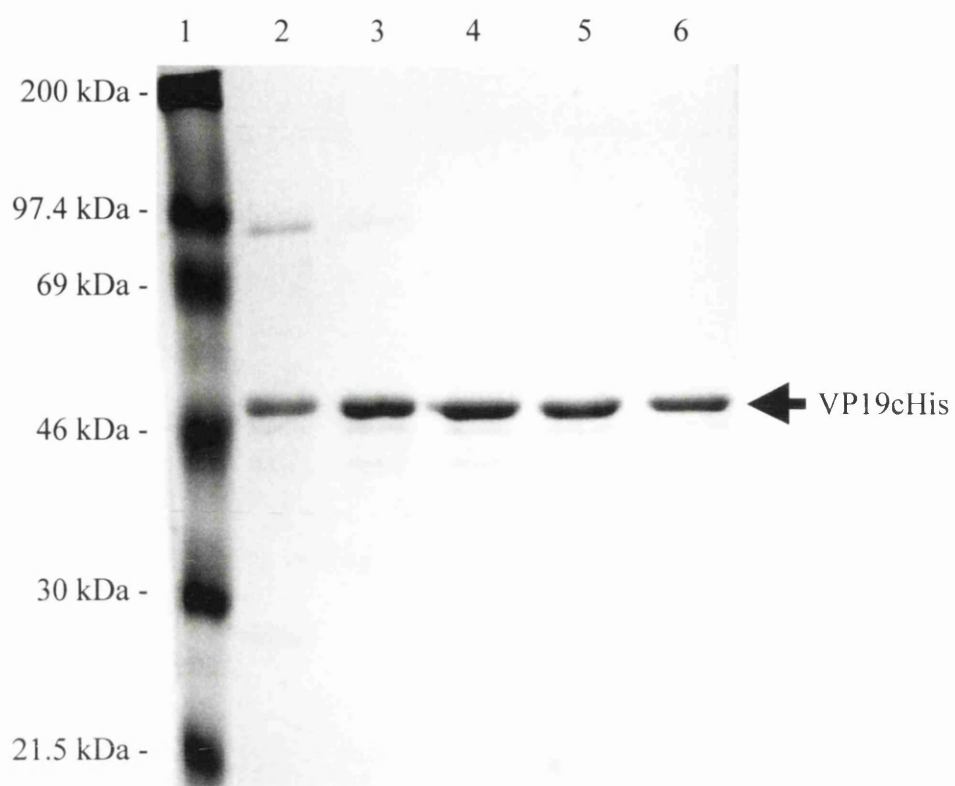
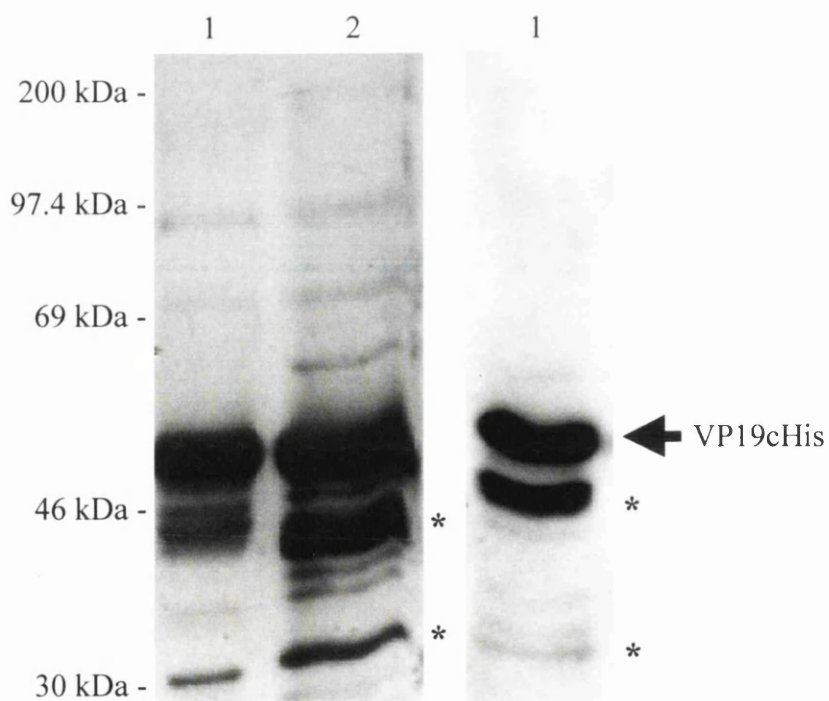


Fig. 3.4.7: SDS-PAGE analysis of VP19cHis purified in buffer O.

VP19cHis was purified from 300mls of SF21 cells ( $1 \times 10^6$  cells/ml) infected with Ac381at an m.o.i. of 5. Cells were resuspended in buffer O (150mM  $\text{Na}_2\text{HPO}_4$  (pH7.5), 0.1% glycerol, 0.1% Octyl- $\beta$ -glucoside ) + protease inhibitors and lysed by bath sonication (as described in Methods). VP19cHis was purified using 500 $\mu$ l of Ni-NTA agarose equilibrated in buffer O. The Ni-NTA agarose was washed in 2x 10 ml of buffer O before VP19cHis was eluted in 3x 350 $\mu$ l fractions of 100mM imidazole in buffer O. 20 $\mu$ l of each elution fraction (lanes 2-4) was analysed by SDS-PAGE against Rainbow markers and stained with Coomassie Brilliant Blue. The arrow indicates the position of VP19cHis.



(A)



(B)

(C)

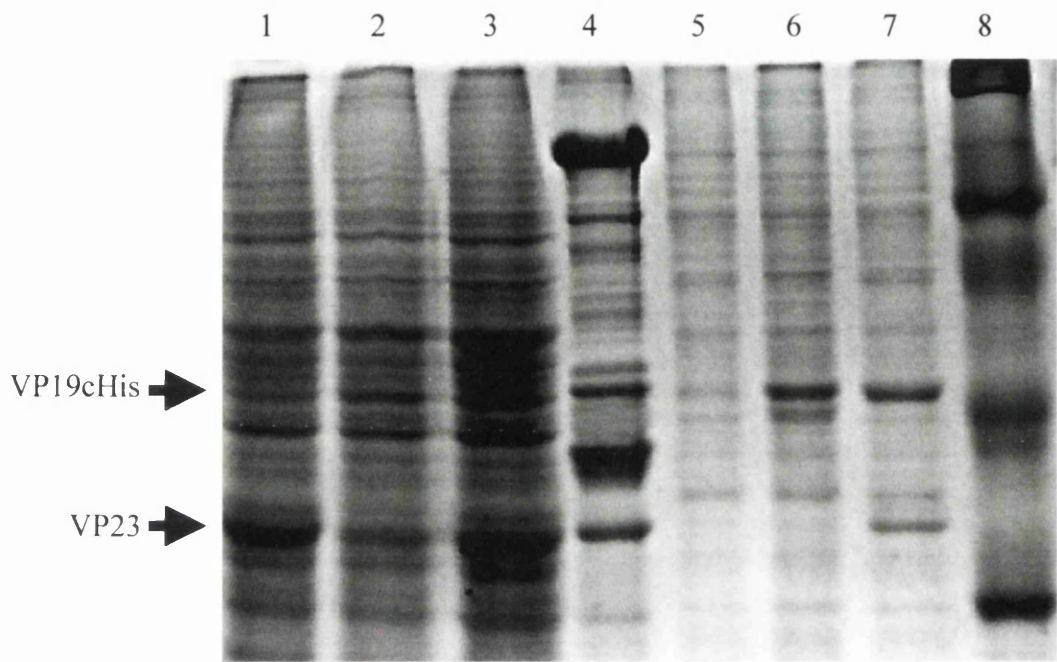
Fig. 3.4.8: SDS-PAGE and Western blot analysis of Ni-NTA agarose purified VP19cHis.

VP19cHis was purified from 300mls of SF21 cells ( $1 \times 10^6$  cells/ml) infected with Ac381 (as described in Methods and fig. 5.4.7). Cells were resuspended and lysed in buffer OL (buffer O containing 150mM NaCl and 0.1% NP40) + protease inhibitors (as described in Methods). Subsequent steps in VP19cHis purification were carried out in buffer O (as described in fig.5.4.7). VP19cHis was eluted from the Ni-NTA agarose in 350 $\mu$ l fractions of 100mM imidazole in buffer O. 20 $\mu$ l of each elution fraction (lanes 2-6) was analysed by SDS-PAGE against Rainbow markers (lane 1) and stained with Coomassie Brilliant Blue (A). (B) Western blot analysis of purified VP19cHis (lane 2) and purified B-capsids (lane 1). The nitro-cellulose membrane was probed with a 1:1000 dilution of a polyclonal UL38 antibody (TrpE/VP19c fusion). The position of VP19cHis is indicated by an arrow. (C) Western blot analysis of purified VP19cHis. The nitro-cellulose membrane was probed with 1:1000 dilution of the monoclonal Penta His antibody (Qiagen) which specifically recognises the 6x His epitope tag. (\*) indicates the position of prominent break down products of VP19cHis.

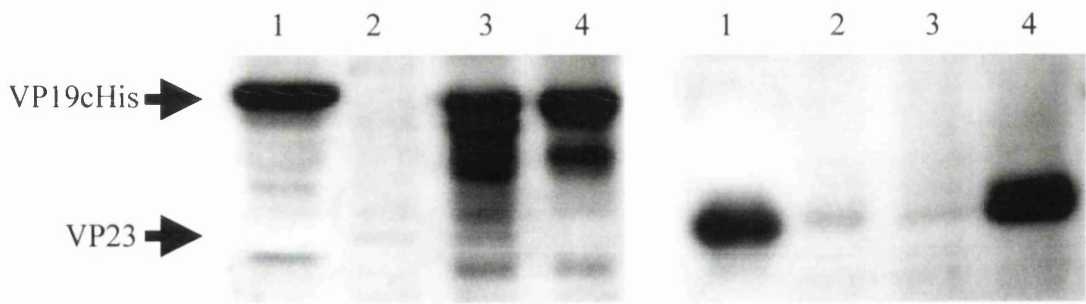
Attempts to remove the 90kDa protein which co-purified with VP19cHis by washing the Ni-NTA agarose with low concentrations of imidazole in buffer O failed since washing with imidazole at concentrations as low as 5mM resulted in the elution of both the 90kDa protein and VP19cHis (data not shown). The relatively weak binding of VP19cHis to the Ni-NTA agarose could possibly be attributed to the N-terminal 6x His tag being partially buried within the interior of the VP19cHis molecule and therefore not totally accessible to the Ni-NTA agarose. Biophysical experiments described in section 3.6 were performed on third and subsequent VP19cHis elution fractions that were checked for the presence of the contaminating 90kDa higher MW protein by SDS-PAGE and Coomassie Brilliant Blue staining before analysis.

### 3.4.4 Ni-NTA pull down assays

In order to determine if purified VP19cHis could interact *in vitro* with VP23, a pull down assay was developed. Lysates from SF21 cells infected individually with Ac381 or AcUL18 expressing VP19cHis and VP23 respectively were mixed together with Ni-NTA agarose and pelleted (as described in Methods). Fig. 3.4.9 (panel A) shows the SDS-PAGE analysis of a Ni-NTA pull down assay using VP19cHis as bait to fish VP23 from the appropriately infected SF21 cell lysate. A novel band of approximately 34kDa was purified from mixed Ac381 and AcUL18 infected cell lysates that was not present in Ni-NTA agarose pull downs of individually infected AcUL18 or Ac381 infected cell lysates. Western blot analysis using a polyclonal anti VP23 antibody (187) confirmed that this 34kDa band corresponded to VP23 (fig. 3.4.9, panel C). It is interesting to note that the 40kDa C-terminal truncated version of VP19cHis (described above) was more abundant in Ni-NTA pull downs from infected cell lysates which contained VP19cHis alone compared to those from lysates containing both VP23 and VP19cHis (fig. 3.4.9, lanes 6 and 7 respectively). This would suggest that VP23 may be able to protect full length VP19cHis from protease digestion. This result also confirms that the 13 amino acid residues deleted from the N-terminus of VP19c during the construction of VP19cHis are not required for interaction with VP23 and that the 6x His epitope tag on the N-terminus of VP19c does not inhibit this interaction.



(A)



(B)

(C)

Fig. 3.4.9: SDS-PAGE and Western blot analysis of Ni-NTA agarose VP19cHis pull down of VP23.

Pellets from 60mm plates of SF cells infected singly with either AcUL18 (VP23) or Ac381 (VP19cHis) (as described in Methods) were resuspended in 150µl of buffer O containing 100mM NaCl and 1% NP40. After incubating on ice for 15 minutes with intermittent vortexing they were clarified by ultracentrifugation at 35,000 r.p.m. for 10 minutes. 200µl of each extract was mixed or an additional 200µl of buffer O was added before being incubated for 1 hour at 28°C (as described in Methods). 30µl of Ni-NTA agarose equilibrated in buffer O was added to each sample and incubated for an additional 15 minutes at RT with intermittent vortexing. The Ni-NTA agarose was pelleted and washed (as described in Methods), resuspended in 30µl of BM loading buffer containing 250mM imidazole and heated for 10 minutes in a dry block at 100°C. 15µl of each sample was used for SDS-PAGE analysis or Western blotting. (A) SDS-PAGE analysis of cell lysates containing VP23 (lane 1), VP19cHis (lane 2), or mixed cell lysates containing VP23 and VP19cHis (lane 3). Ni-NTA pull downs were carried out on lysates containing either VP23 (lane 5) or VP19cHis (lane 6) or following mixing of VP23 and VP19cHis (lane 7). 5µl of cell lysate was analysed by SDS-PAGE against purified B-capsids (lane 4) and Rainbow markers (lane 8). Proteins were visualised by Coomassie Brilliant Blue staining. (B and C) Western blot analysis of purified B capsids (lane 1) and 15µl of samples from the Ni-NTA pull down assay. Ni-NTA pull downs were carried out on lysates containing either VP23 (lane 2) or VP19cHis (lane3), or following mixing of VP23 and VP19cHis (lane 4). (B) Nitro-cellulose membrane was probed with a 1:1000 dilution of the polyclonal VP19c antibody (TrpE/VP19c fusion). (C) Nitro-cellulose membrane probed with a 1:1000 dilution of the polyclonal VP23 antibody (187). Arrows indicate the positions of VP19cHis and VP23.

#### 3.4.4.1 Characterisation of *in vitro* triplex formation

The *in vitro* pull down assay (described above) was used to analyse the association of VP19cHis and VP23 in the presence of high concentrations of NaCl. High NaCl concentrations have been reported to disrupt capsid protein interactions in other viruses. Parker and Prevelige (1998) demonstrated that procapsid assembly of P22 could be inhibited by 1M NaCl. They went on to demonstrate that this inhibition was specifically due to the disruption of electrostatic interactions between the C-terminus of the scaffold molecule and the coat protein of P22. Similarly, Fox et al., (1997) characterised the isolation of a mutant of cowpea chlorotic mottle virus (CCMV, K42R) which produced virions that were more stable in high NaCl concentrations than WT CCMV virions which disassembled in 1M NaCl. Preliminary experiments in our laboratory demonstrated that HSV-1 capsid assembly could also be inhibited by 1M NaCl thereby suggesting the involvement of electrostatic interactions between capsid proteins during capsid assembly. In order to examine whether or not the interaction between VP23 and VP19c was affected, an Ni-NTA pull down assay was performed in the presence and absence of 1M NaCl (fig. 3.4.10). This showed that VP23 could be co-purified with VP19cHis when lysates from SF21 cells individually infected with AcUL18 and Ac381 were mixed in the presence of 1M NaCl (fig. 3.4.10, lanes 4 and 5 respectively). This result suggests that VP19cHis and VP23 do not interact primarily through electrostatic interactions.

Newcomb et al., (1996) and Rixon and McNab (1999) demonstrated that HSV-1 procapsids disassemble at temperatures of 0°C (discussed further within the introduction of this thesis, section 1.9). It was therefore decided to examine the association of VP19cHis and VP23 at 0°C. Fig. 3.4.11 shows the protein profiles of Ni-NTA agarose pull downs carried out on extracts of VP23 and VP19cHis incubated for 1 hour at 28°C or at 0°C. Co-purification of VP23 with VP19cHis was greatly reduced at 0°C (fig. 3.4.11, panel A, lane 5) compared to 28°C (fig. 3.4.11, panel A, lane 4). However, Western blot analysis using the polyclonal VP23 antibody 187 did detect VP23 in the 0°C sample (fig. 3.4.11, panel B, lane 5). This suggests that the association of VP19cHis with VP23 is partially inhibited at 0°C. It is interesting to note that once triplexes have formed they are not destabilised by incubation at 0°C (fig.3.4.11, panel C). Therefore, although the association of VP19cHis

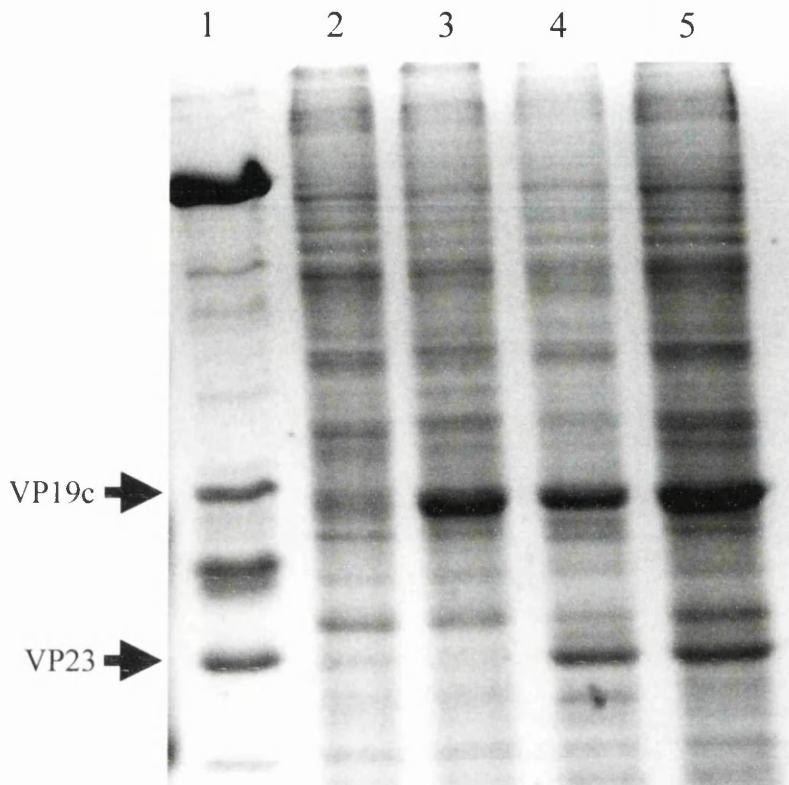
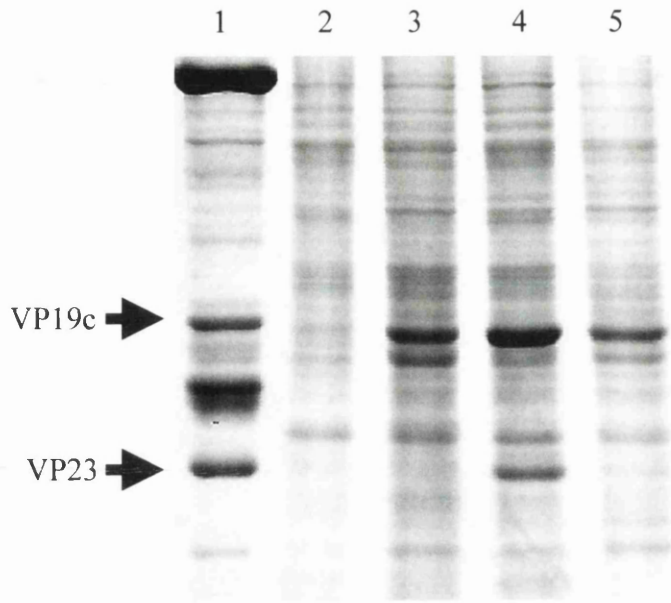


Fig. 3.4.10: SDS-PAGE analysis of VP19cHis/VP23 interaction in the presence or absence of 1M NaCl.

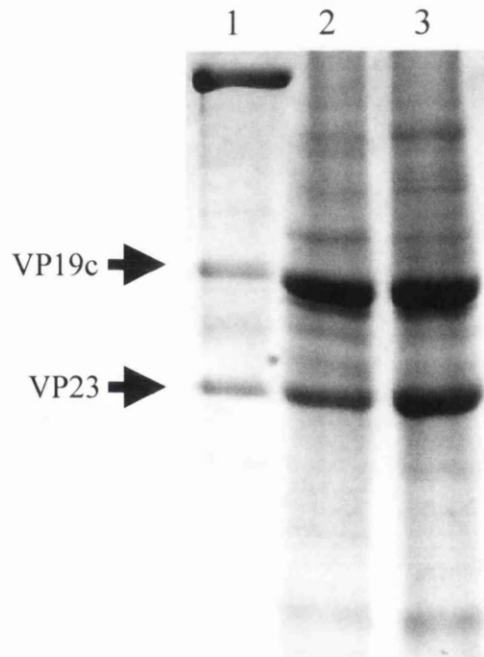
Ni-NTA agarose pull downs were performed (essentially as described in Methods and fig. 5.4.9) with 1M NaCl present in (lanes 2, 3, and 4) or absent (lane 5) all purification buffers. 15 $\mu$ l of each sample was analysed by SDS-PAGE against purified B-capsids (lane 1) and stained with Coomassie Brilliant Blue. SF cells were infected singly with either AcUL18 (VP23) or Ac381 (VP19cHis). Ni-NTA pull downs were carried out on lysates containing either VP23 (lane 2) or VP19cHis (lane 3) or following mixing of VP23 and VP19cHis (lanes 4 and 5). Arrows indicate the positions of VP19c and VP23



(A)



(B)



(C)

Fig. 3.4.11: SDS-PAGE analysis of VP19cHis/VP23 interaction at 0°C.

Ni-NTA pull downs were performed essentially as described in Methods and fig. 5.4.9. Incubations were either carried out at 0°C on ice (lane 5) or 28°C (lanes 2, 3, and 4) for 1 hour. For reactions carried out at 0°C all buffers were prechilled before use with clarification and washing stages performed at 4°C. 15µl of each sample was analysed by SDS-PAGE against purified B-capsids (lane 1) and stained with Coomassie Brilliant Blue (A). SF cells were infected singly with either AcUL18 (VP23) or Ac381 (VP19cHis). Ni-NTA pull downs were carried out on lysates containing either VP23 (lane2) or VP19cHis (lane 3) or following mixing of VP23 and VP19cHis (lanes 4 and 5) at the appropriate temperatures. (B) Western blot analysis of Ni-NTA pull downs carried out at 0°C or 28°C. Samples were analysed by SDS-PAGE (as described for A) and transferred to a nitro-cellulose membrane. The membrane was probed with a 1:1000 dilution of the polyclonal VP23 antibody (187). (C) SDS-PAGE analysis of Ni-NTA purified triplexes carried out at 28°C (lane 2) or 0°C (lane 3). SF cells were infected with Ac18386 co-expressing VP19cHis and VP23. Ni-NTA triplex purifications were carried out at 28°C or 0°C and analysed by SDS-PAGE against purified B-capsids and stained with Coomassie Brilliant Blue. The positions of VP19c and VP23 are indicated by the arrows.

and VP23 may be less efficient at 0°C, the intact triplexes are not cold labile, in as much that they do not disassemble at 0°C. It is unlikely therefore, that this accounts for the thermolability of the procapsid.

### 3.4.5 Size exclusion chromatography of VP19cHis

In order to determine an accurate native MW, size exclusion chromatography was carried out on purified VP19cHis utilising a 25ml (1 by 30 cm) Superose 12 gel filtration column (Pharmacia), as described in Methods. Fig. 3.4.12 (panel A) shows the elution profile of VP19cHis analysed in buffer O. No distinct elution peak could be detected. SDS-PAGE analysis confirmed that the material loaded onto the column contained purified VP19cHis (fig. 3.4.12, panel B, lane 1). The small peak (indicated by an arrow in fig. 3.4.12, panel A) was collected and TCA precipitated (as described in Methods). SDS-PAGE analysis of this peak demonstrated that it corresponded to VP19cHis (fig. 3.4.12, panel B, lane 3). However, the amount of VP19c in this peak was far less than the amount injected onto the column for analysis. The poor recovery of VP19cHis may be due to non-specific binding to the Superose or formation of aggregates which could not pass through *in situ* filters before entering the column. However, purified VP19cHis was clarified by ultracentrifugation before size exclusion chromatography analysis to remove insoluble aggregated material and no detectable precipitate was recovered. Numerous attempts were made to determine the native MW for VP19cHis by size exclusion chromatography including the addition of 150mM NaCl to the purification and column buffers to minimise non-specific binding to the Superose (as recommended by the manufacturer's guidelines). However, all attempts failed to generate a reproducible elution spectrum for VP19cHis. Indeed, consecutive attempts to size purify VP19cHis in buffer O resulted in an increase of column pressure above the limits recommended by the manufacturer. Since VP19cHis is reasonably stable in buffer O and shows good solubility over the time periods required for size exclusion chromatography analysis, these results suggest that VP19cHis is non-specifically binding to the Superose.

In order to determine if the cysteine residues within VP19c were forming random intermolecular disulphide bonds which could be responsible for generating protein

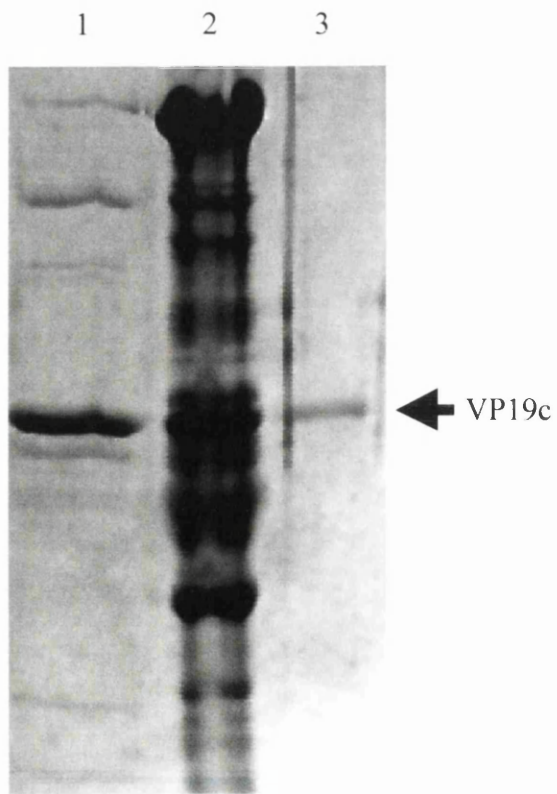
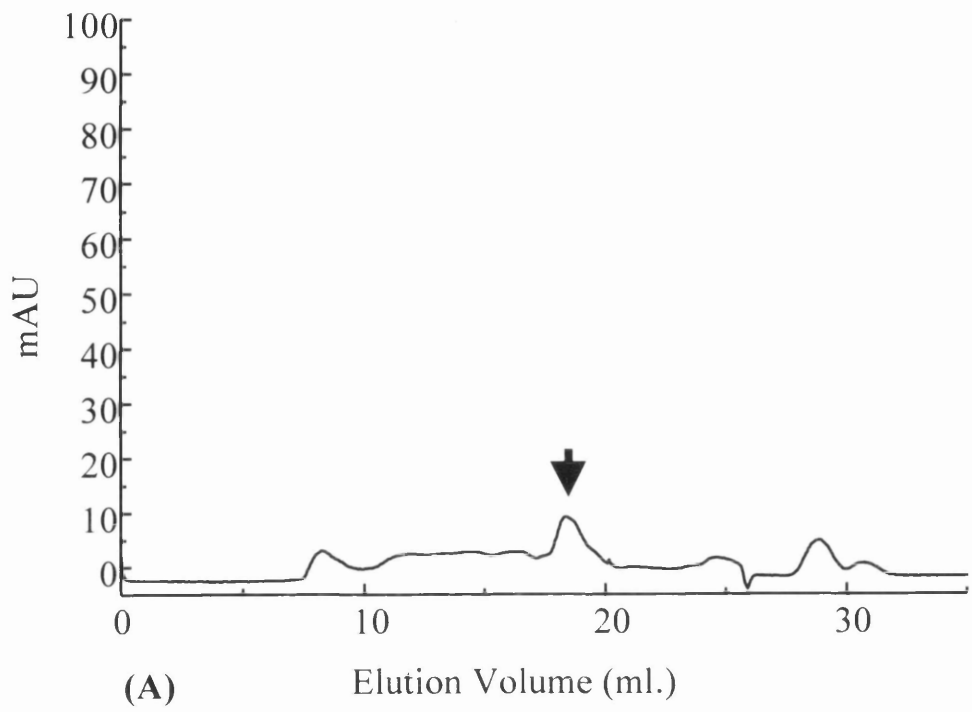


Fig. 3.4.12: Size exclusion chromatography and SDS-PAGE analysis of Ni-NTA agarose purified VP19cHis in buffer O.

VP19cHis was purified in buffer O from 300ml of SF cells ( $1 \times 10^6$  cells/ml) infected with Ac381 (as described in Methods and in fig. 5.4.7). Elution fractions 1-4 were combined (total concentration of 0.3mg/ml), and analysed on a 25 ml (1 by 30 cm) Superose 12 gel filtration column (Pharmacia) using a 1 ml injection superloop (as described in Methods). (A) Size exclusion chromatography profile for VP19cHis purified and analysed in buffer O. The fractions containing the peak marked with the arrow were TCA precipitated and the protein pellet was resuspended in 20 $\mu$ l of BM. (B) 20 $\mu$ l of purified VP19cHis combined elution fractions 1-4 (lane 1) and 20 $\mu$ l of the TCA precipitated size exclusion chromatography peak elution fraction (lane 3) were analysed by SDS-PAGE against purified B-capsids (lane 2) and stained with Coomassie Brilliant Blue.

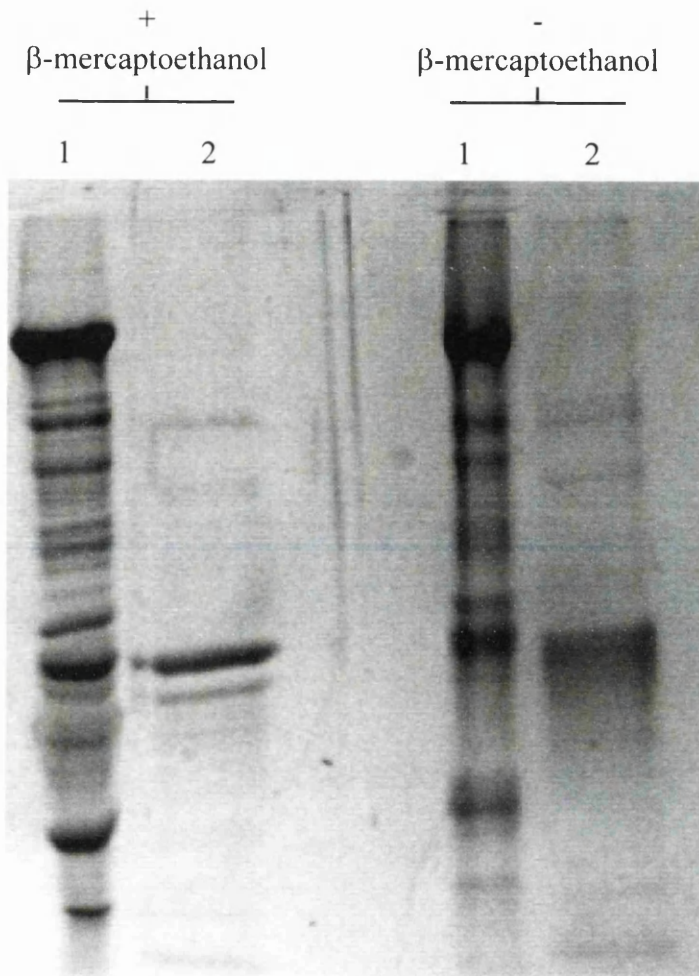


Fig. 3.4.13: SDS-PAGE analysis Ni-NTA agarose purified VP19cHis in the presence or absence of 20mM β-mercaptoethanol.

VP19cHis was purified from 300mls of SF21 cells ( $1 \times 10^6$  cells/ml) infected with Ac381 (as described in Methods and fig. 5.4.7). 20 $\mu$ l of elution fraction 1 (lane 2) was analysed by SDS-PAGE and Coomassie Brilliant Blue staining in the presence (+) or absence (-) of 20mM β-mercaptoethanol. Purified B capsids (lane 1) were analysed in the presence or absence of 20mM β-mercaptoethanol for comparison.

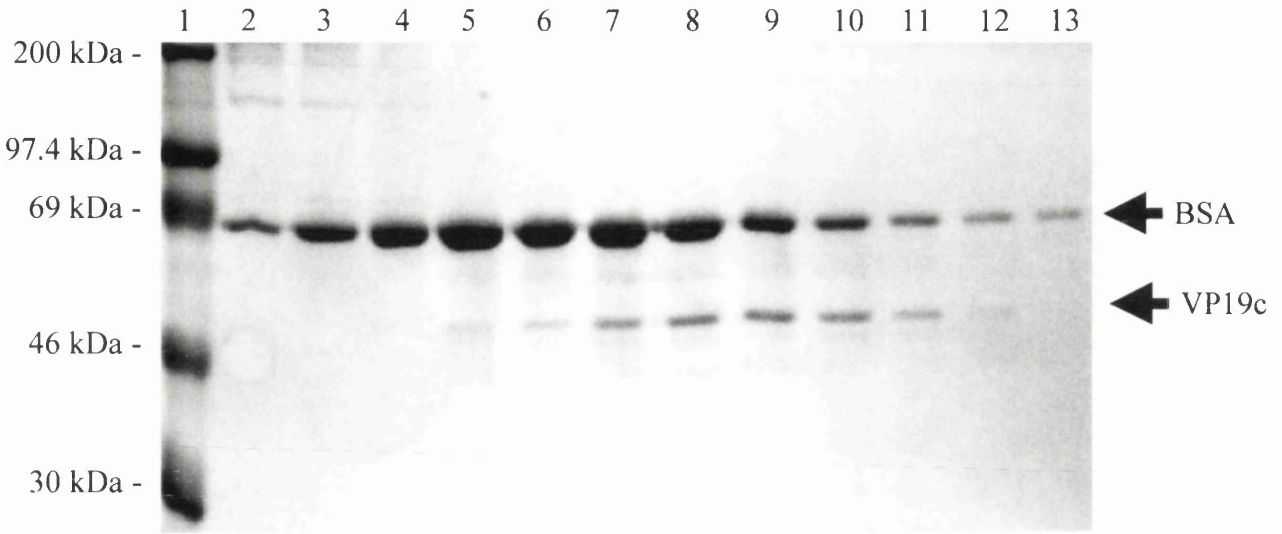
aggregates and thereby preventing effective sizing, SDS-PAGE analysis was performed on purified VP19cHis in the presence and absence of  $\beta$ -mercaptoethanol (fig. 3.4.13). No VP19cHis oligomers were detected in the absence of  $\beta$ -mercaptoethanol suggesting that inter-molecular disulphide bonds were not formed. VP19cHis also appeared to behave in a similar manner to VP19c from purified B-capsids during SDS-PAGE analysis in the absence of reducing agents (fig. 3.4.13, lanes 1 and 2, no  $\beta$ -mercaptoethanol).

### 3.4.6 Sucrose gradient sedimentation

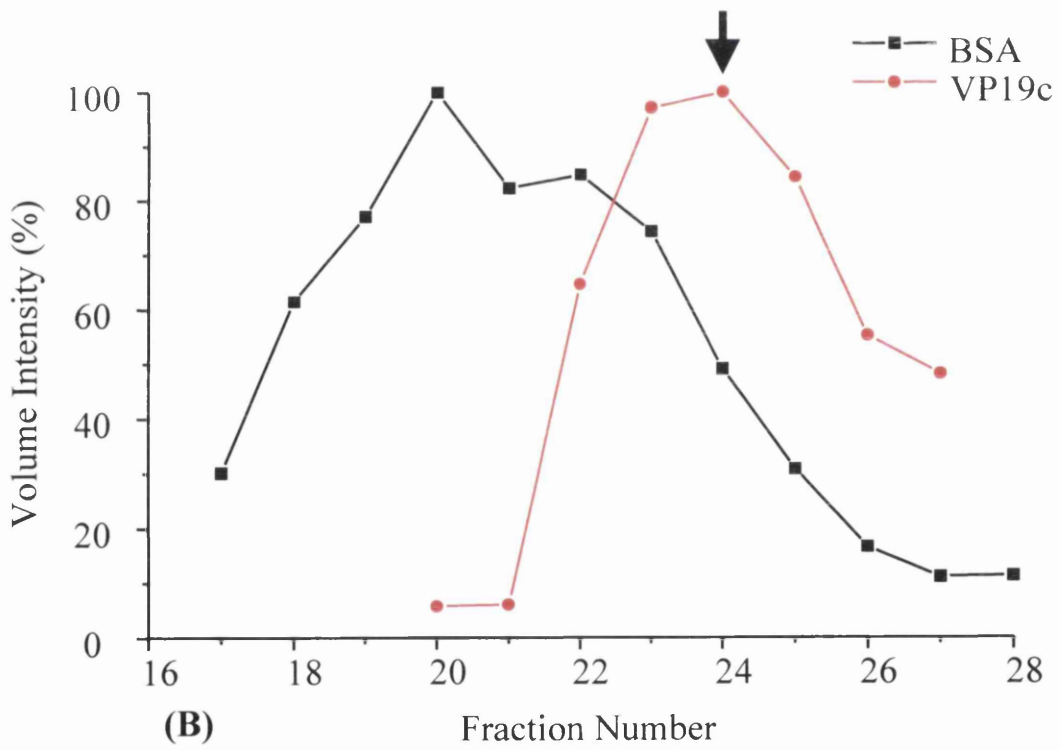
Sucrose gradient sedimentation was employed to analyse the native MW of purified VP19cHis in buffer O. Purified VP19cHis was co-sedimented with the protein standard, BSA (66kDa) through a 5ml 5-25% sucrose gradient made in buffer O and 150 $\mu$ l fractions were collected (as described in Methods). The fraction distribution of VP19cHis was determined by Western blot analysis of every third fraction (data not shown). Fig. 3.4.14 (panel A) shows the SDS-PAGE analysis of fractions 17 to 28, out of a total of 35 fractions, collected from the gradient. The relative intensities were calculated for each fraction for both VP19cHis and BSA and plotted as a percentage (%) change in volume intensity against the appropriate fraction number for each individual protein profile (fig. 3.4.14, panel B). BSA was detected over a number of fractions with the peak intensity corresponding to fraction 20. VP19cHis sedimented through the gradient as a single species which had a peak intensity in fraction 24. Therefore, VP19cHis demonstrated a four fraction shift in peak intensity compared to BSA. As fractions were collected from the bottom of the gradient this indicates that VP19cHis has a lower MW than BSA (66kDa). This would suggest that the native MW for VP19cHis cannot be significantly different from the predicted 50kDa MW derived amino acid sequence (McGeoch et al., 1988). On this basis, purified VP19cHis is likely to be in the form of a monomer of approximately 50kDa rather than a dimer (100kDa) or larger complex.

#### 3.4.6.1 *in vitro* formation of triplexes from purified proteins

In order to determine whether purified VP19cHis and purified bacterially expressed VP23His could form triplexes *in vitro*, the proteins were mixed and analysed by sucrose



(A)

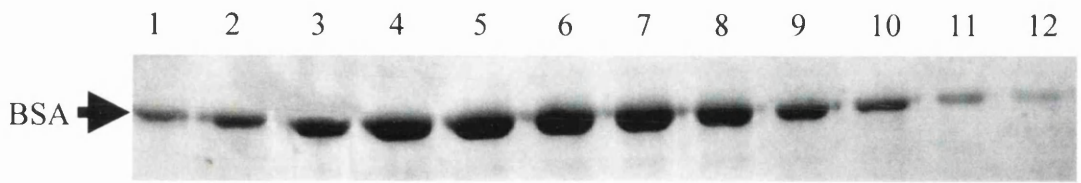


(B)

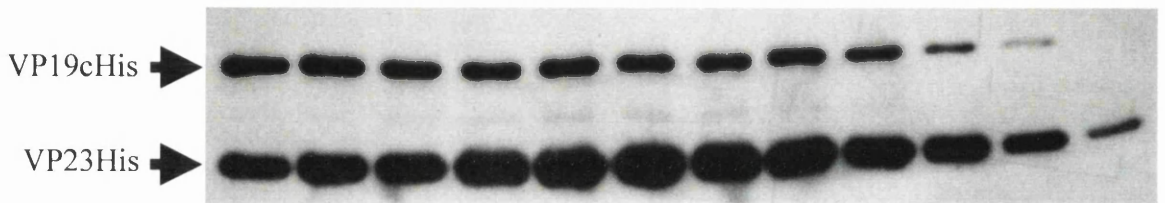
Fig. 3.4.14: Sucrose gradient sedimentation and SDS-PAGE analysis of Ni-NTA purified VP19cHis in buffer O.

VP19cHis was purified in buffer O from 300mls of SF cells ( $1 \times 10^6$  cells/ml) infected with Ac381 (as described in Methods and fig. 5.4.7). 300 $\mu$ l of purified VP19cHis from elution fraction 1 and 50 $\mu$ l BSA (5mg/ml) resuspended in buffer O were mixed and sedimented together on a 5ml 5-25% sucrose gradient at 40,000 r.p.m. for 16 hours at 4°C in a AH650 rotor and fractions collected (as described in Methods). (A) 20 $\mu$ l of fractions 17-28 (lanes 2-13 respectively) were analysed by SDS-PAGE against Rainbow markers (lane 1) and stained with Coomassie Brilliant Blue. The positions of BSA and VP19cHis are indicated by the appropriate arrows. The relative intensity of the Coomassie stained bands was calculated individually for both VP19cHis and BSA protein profiles using Quantity ONE software (Bio-Rad) as described in Methods. The data for VP19cHis and BSA was plotted as percentage (%) change in volume intensity for each individual protein profile against their eluted fraction number (B). The peak fraction for VP19cHis is indicated by an arrow.

gradient sedimentation in buffer O. Purified VP23His was added in excess to encourage all VP19cHis molecules to participate in triplex formation. Therefore, VP23His and VP19cHis were mixed in a 3:1 ratio and incubated for 1 hour at 28°C to allow the formation of triplexes to occur. The samples were subsequently sedimented together with the internal protein standard BSA (66kDa) through a 5ml 5-25% sucrose gradient made in buffer O and 150µl fractions were collected (as described in Methods). Fig. 3.4.15 (panel A) shows the SDS-PAGE profile of BSA for fractions 17-28 collected from the gradient. Western blot analysis was performed on the same fractions using the Penta His monoclonal antibody (Qiagen) which specifically recognises the 6xHis epitope tags on VP23His and VP19cHis. Fig. 3.4.15 (panel B) shows the Western blot analysis of fractions 17-28. Both VP23His and VP19cHis sedimented profiles are visible. The relative intensities of each fraction were calculated for both VP19cHis and BSA and plotted as a percentage (%) change in volume intensity against the appropriate fraction number (fig. 3.4.13, panel B). When mixed with VP23His, VP19cHis was found throughout a large proportion of the gradient. The peak intensity was in fraction 18, which in contrast to VP19cHis alone (fig. 3.4.14, panel B), is further down the gradient than the BSA peak fractions (fractions 21-22). The position of this peak with respect to the BSA standard is similar to that of purified triplexes (fig. 3.5.16) and suggests that the purified VP19cHis and VP23His are able to interact to form heterotrimeric complexes in the absence of other capsid proteins. It is interesting to note that two additional peaks could be detected (arrows b and c respectively in fig. 3.4.15). Peak b could correspond to VP19cHis interacting with a single copy of VP23His generating a protein complex which sediments further through the gradient than BSA. Peak c probably corresponds to uncomplexed VP19cHis as its positions on the gradient is similar to that of purified VP19cHis when sedimented without VP23. The fact that some of VP19cHis remained uncomplexed, in the presence of excess VP23His, suggests that either the interaction between VP23 and VP19c is in an equilibrium or that the interaction *in vitro* is not particularly efficient. Size exclusion chromatography of triplexes purified from SF21 cells infected with Ac18386 and analysed in buffer O (section 3.5, fig. 3.5.15, panel A) suggests that triplexes do not exist in equilibrium with their constituent proteins. This would seem to suggest therefore either that a proportion of VP19cHis maybe mis-folded and unable to interact with VP23His, or that, the association of purified VP19cHis and VP23His *in vitro* may require additional factors, such as chaperones, for efficient complex formation.



(A)



(B)

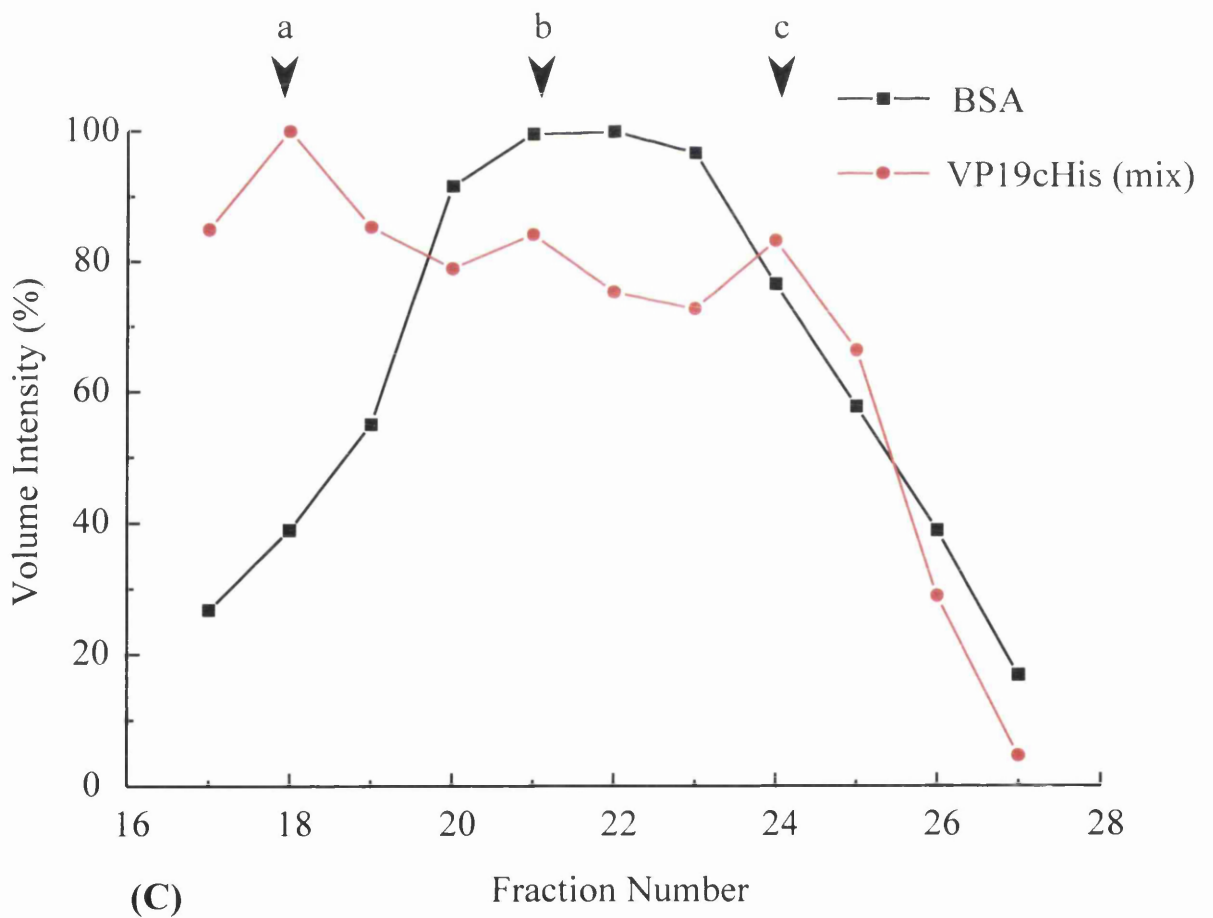


Fig. 3.4.15: Sucrose gradient sedimentation and SDS-PAGE/Western blot analysis of Ni-NTA purified VP19cHis and VP23His in buffer O.

VP19cHis and bacterially expressed VP23His were purified in buffer O (as described in Methods and figs. 5.4.7). VP23His and VP19cHis were mixed in a 3:1 ratio to a final volume of 300 $\mu$ l and incubated for 1 hour at 28°C. 50 $\mu$ l of BSA (5mg/ml resuspended in buffer O) was then added to the VP23His/VP19cHis mixture, which was sedimented on a 5ml 5-25% sucrose gradient at 40,000 r.p.m. for 16 hours at 4°C in a AH650 rotor and fractions collected (as described in Methods). (A) SDS-PAGE profile of fractions 17-28 (lanes 1-12 respectively) stained for BSA with Coomassie Brilliant Blue (20 $\mu$ l/fraction analysed). (B) Western blot analysis of fractions 17-28 (lanes 1-12 respectively) probed with a monoclonal Penta His antibody (at a 1:1000 dilution, Qiagen) which specifically recognises the 6xHis epitope tag on VP23His and VP19cHis. The position of BSA, VP19cHis and VP23His are indicated by the appropriate arrow. The relative intensities of the Coomassie stained protein profile for BSA and of the VP19cHis detected by Western blot was calculated individually using Quantity ONE software (Bio-Rad) as described in Methods. The data for VP19cHis and BSA profiles was plotted as percentage (%) change in volume intensity for each individual protein profile against their eluted fraction number (B). The peak intensities for VP19cHis are indicated by arrows a-c.

### 3.4.7 Conclusions

Recombinantly expressed VP19cHis has consistently proven to be difficult to purify utilising Ni-NTA agarose affinity chromatography from either bacterial or baculovirus expression systems. Newcomb described similar difficulties when attempting to purify untagged VP19c from insect cells (personal communication, Newcomb, 1998). The reason why VP19c is difficult to purify is unclear but sensitivity to proteolytic digestion and poor solubility seem to be consistent factors. Published observations by Spencer et al., (1998) and Newcomb et al., (1996) demonstrated by SDS-PAGE and Western blot analysis, that purified VP19c samples consistently contained a smaller product. This is probably due to proteolytic digestion of VP19c as opposed to poor translation of the UL38 ORF since a similar sized form of VP19c can be found within purified capsids (fig. 3.4.8, panel B). The same UL38 ORF when present in both Ac381 and Ac18386 results in similar levels of recombinant expression of VP19cHis. Despite this it is much easier to purify triplexes than isolate VP19c. This suggests that VP23 may stabilise recombinantly expressed VP19cHis. In part this seems to be due to the reduction of proteolytic digestion by endogenous protease's since less of the 40kDa breakdown product is seen when VP23 present. However, another major factor appears to be the increased solubility of triplexes compared to VP19c.

Chowdhury and Batterson (1994) fused small segments of VP19c to  $\beta$ -galactosidase and demonstrated that two domains (amino acid residues 1-30 and 302-327) could translocate  $\beta$ -galactosidase to the nucleus of Vero cells. Analysis of the amino acid sequence between residues 1-30 of VP19c identified a sequence homology to a small canonical sequence responsible for transporting proteins to the endoplasmic reticulum (ER). From this and immunofluorescence data the authors concluded that VP19c was transported from the perinuclear space into the nucleus via the inner nuclear membrane and therefore bypassed the nuclear pore complex. If this is correct it could provide an explanation of why VP19cHis is difficult to purify, since VP19c might be aggregating at membrane sites within or around the nucleus and therefore become immobilised and prevented from entering the soluble fraction of cell lysates used during Ni-NTA agarose affinity purification. However, it should be noted that this would be an unprecedented route for transport to the nucleus and seems especially unlikely as VP19c is also partly responsible

for the selective nuclear localisation of VP5 and VP23 (Nicholson et al., 1994; Rixon et al., 1996). An alternative explanation of Chowdhury and Batterson's results could be due to the instability and mis-folding of over expressed VP19c within Vero cells. The ER lumen has been shown to be the site at which mis-folded or unfolded proteins are directed for corrective folding by the 'unfolded protein response' (UPR) pathway. Here, ER-resident proteins, such as heat shock chaperone proteins, assist the refolding of proteins, or induce the specific degradation of incorrectly folded proteins thereby removing them from the cell (reviewed by Hampton, 2000). As VP19c appears to be less stable in the absence of other capsid proteins, in particular VP23, over expressed VP19c may become mis-folded and as a consequence become directed to the ER for refolding. Such mis-folding could itself contribute to the difficulty in purifying VP19cHis in the absence of VP23.

Immunofluorescence studies performed by Ward et al., (1996) and de Bruyn Kops et al., (1998) have also demonstrated that VP19c can localise to specific sites within the nucleus near the nuclear membrane where capsid assembly is thought to take place. The presence of NP40 and NaCl in buffer OL, compared to buffer O, may therefore be sufficient to disassociate or disrupt any VP19c associated with membrane structures, for example mis-folded VP19c within the ER or nuclear membranes. Alternatively, the presence of NaCl or NP40 within buffer OL may be sufficient to disassociate any aggregated complexes of VP19cHis and/or increase the solubility of VP19cHis during Ni-NTA agarose purification. The cloning strategy for VP19cHis involved the deletion of the N-terminal 13 amino acids of VP19c. Removing these residues and incorporating the 6x His tag in their place did not affect the protein's ability to interact with VP23 *in vitro* as demonstrated by Ni-NTA pull downs (fig. 3.4.9). Nor did it prevent the formation of triplexes that could be purified by Ni-NTA agarose affinity chromatography (fig. 3.4.11, panel C). This indicates that the N-terminus of VP19c is not essential for the interaction with VP23 and is not deeply buried within the interior of the protein molecule. These findings are supported by deletion mutagenesis performed by Spencer et al., (1998) who demonstrated that the N-terminal 45 amino acids were not required for VP19c to participate effectively in the production of capsids *in vivo*.

The isolation of VP19cHis from purified triplexes by denaturation in urea yields interesting structural data. Newcomb et al., (1993) tested the resistance of purified B-

capsids to denaturation by both urea and GdnHCl. Using SDS-PAGE and cryo-EM analysis they could not detect any significant structural changes in B-capsids when analysed in the presence of 3M urea. However, treating capsids with 6M urea resulted in the loss of the pentons and the triplexes  $T_a$  and  $T_c$ . Urea denaturation experiments performed during my project on recombinantly purified triplexes to isolate VP19cHis, demonstrated that VP23 and VP19c disassociated when they were incubated in the presence of 3M urea for 30 minutes at RT (fig. 3.4.3). This suggests that the extra stability of the triplex to urea induced denaturation in the context of the capsid may come from contacts formed between the triplex and VP5 from surrounding capsomers. Such contacts may enforce a greater stability upon the triplex and therefore increase the resistance of the triplex to denaturation. Denaturation of triplexes is discussed in further detail in section 3.6.

It is interesting to note that VP19cHis isolated by urea denaturation of triplexes remained unfolded even when dialysed to remove residual urea, as shown by the intrinsic tryptophan fluorescence spectra (fig. 3.4.4). This implies that the 50kDa VP19c molecule is unable to refold by itself *in vitro*.

Although no reproducible data could be obtained from size exclusion chromatography analysis of purified VP19cHis, the native MW could be estimated from sucrose gradient sedimentation analysis. This suggests that VP19cHis was purified as a monomer with a native MW smaller than that of the 66kDa internal protein standard, BSA (fig. 3.4.14, panel B). This is in agreement with published GdnHCl denaturation experiments on HSV-1 B-capsids (Newcomb et al., 1993). From these experiments Newcomb and co-workers proposed that the triplexes are composed of a single copy of VP19c and two copies of VP23. More recently, Spencer et al., (1998) demonstrated through sucrose gradient sedimentation analysis of baculovirus infected SF9 extracts that contained VP19c and VP23 that *in vivo* formed triplexes had a native MW greater than that of BSA. The calculated sedimentation co-efficient was consistent with the formation of a heterotrimer complex composed of one copy of VP19c and two copies of VP23. Data presented within this chapter utilising similar sucrose gradient sedimentation analyses upon complexes formed from purified VP23His and VP19cHis showed that these two proteins could indeed form triplexes in the absence of other capsid and cellular proteins (fig.3.4.15, panel B).

However, the interaction did not appear particularly efficient with two secondary peaks being detected (fig. 3.4.15, panel B, peaks b and c). Newcomb et al., (1999) reported that capsids could be formed from individually purified capsid components. However, they used pre-assembled purified triplexes and their conclusion, that capsids could be formed in the absence of other cellular proteins, in particular chaperone proteins, cannot be applied to the formation of triplexes. The results presented within this thesis do suggest that cellular proteins are not required for triplex formation and the low efficiency of the process in this case may simply reflect the conditions under which the experiments were performed. For example, the use of detergents within the purification protocol may hinder possible hydrophobic interactions that are required for triplex formation. Alternatively, since sucrose has also been shown to disassemble procapsids (Newcomb et al., 1999), some of the triplexes which had not completely folded into a stable conformation may have disassembled during sucrose sedimentation analysis. Furthermore, Ni-NTA pull downs have shown that triplex formation is partially inhibited at 0°C (fig. 3.4.11). This raises the possibility that complexes, which are not conformationally stable, may disassemble during the 4°C sedimentation analysis. The complexities of triplex formation are discussed in subsequent chapters within this thesis.

#### *3.4.7.1 Future work*

Further investigation of the conditions for purifying of VP19cHis may be required in order to purify it at high enough concentrations to perform comprehensive biophysical characterisation experiments (discussed within section 3.6). It would also be interesting to characterise the 90kDa MW band which co-purified with VP19cHis using Ni-NTA agarose affinity chromatography (fig. 3.4.8, panel A). Since this band was not detected by Western blotting with a polyclonal VP19c antibody it is unlikely to represent an oligomeric/aggregated form of purified VP19cHis which is resistant to SDS denaturation. It would be interesting therefore to determine whether or not this 90kDa protein interacts specifically with VP19cHis.

## 3.5 Characterisation of the HSV-1 triplex

Triplexes can be stripped from purified capsids, in particular the triplexes T<sub>a</sub> and T<sub>c</sub>, in low concentrations of GdnHCl (Newcomb et al., 1991; Newcomb et al., 1993). It was considered unlikely that this technique would provide sufficient quantities of material in a suitable condition for subsequent analyses following purification. Therefore, attempts were made to co-express triplex proteins utilising both prokaryotic and eukaryotic expression systems.

### 3.5.1 Construction and expression of pETUL1838.

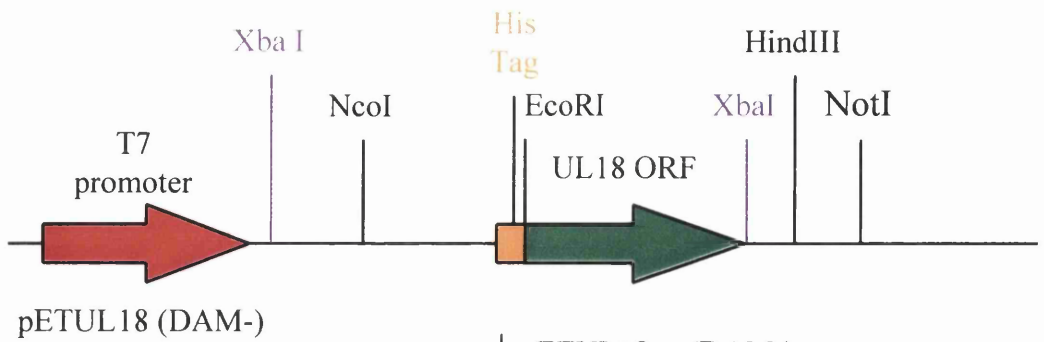
Recombinant expression of the single triplex protein VP19cHis within induced BL21 DE3 bacteria was very poor (previously described in section 3.4). In an attempt to increase the protein production and/or stability of VP19cHis within bacteria it was decided to co-express both VP23His and VP19cHis from the same expression vector.

#### 3.5.1.1 Cloning of the 6xHis tagged UL18 ORF into pETUL38.

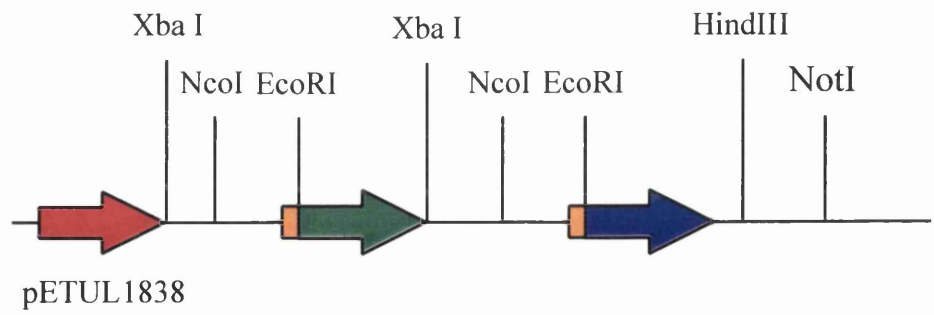
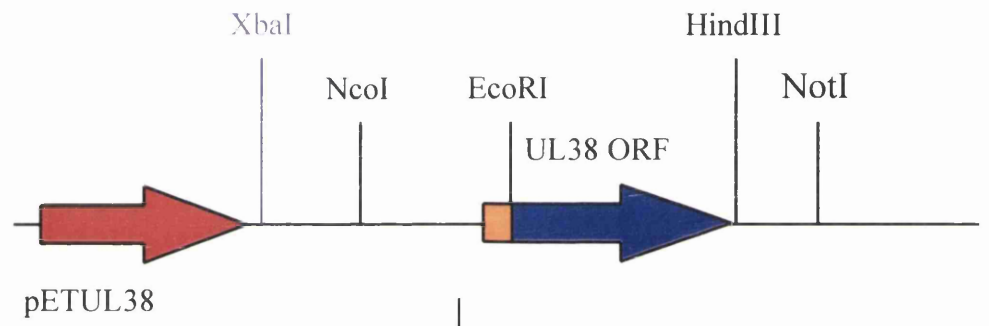
As the cloning strategy required the use of a methylation sensitive XbaI restriction site at the 3' end of the UL18 ORF, pETUL18 was electroporated into GM48 (DAM-) bacteria and unmethylated pETUL18 DNA was isolated (as described in Methods). The UL18 ORF, including sequences encoding the 6xHis epitope tag, was subcloned out of pETUL18 as an XbaI fragment and ligated into XbaI digested and CIP treated pETUL38 to generate pETUL1838. The strategy for cloning the UL18 ORF into pETUL38 is illustrated schematically in fig. 3.5.1.

#### 3.5.1.2 Expression of triplex proteins VP23His and VP19cHis in BL21 DE3 bacteria.

BL21 DE3 bacteria were electroporated in the presence of approximately 1µg of pETUL1838 or pET28MOD DNA and colonies were isolated from a L-broth agar plate containing kanamycin (50mg/ml). Single colonies were grown and induced (as described



pETUL18 (DAM-) was digested with XbaI the UL18 ORF isolated and ligated into XbaI digested and CIP treated pETUL38 to generate pETUL1838



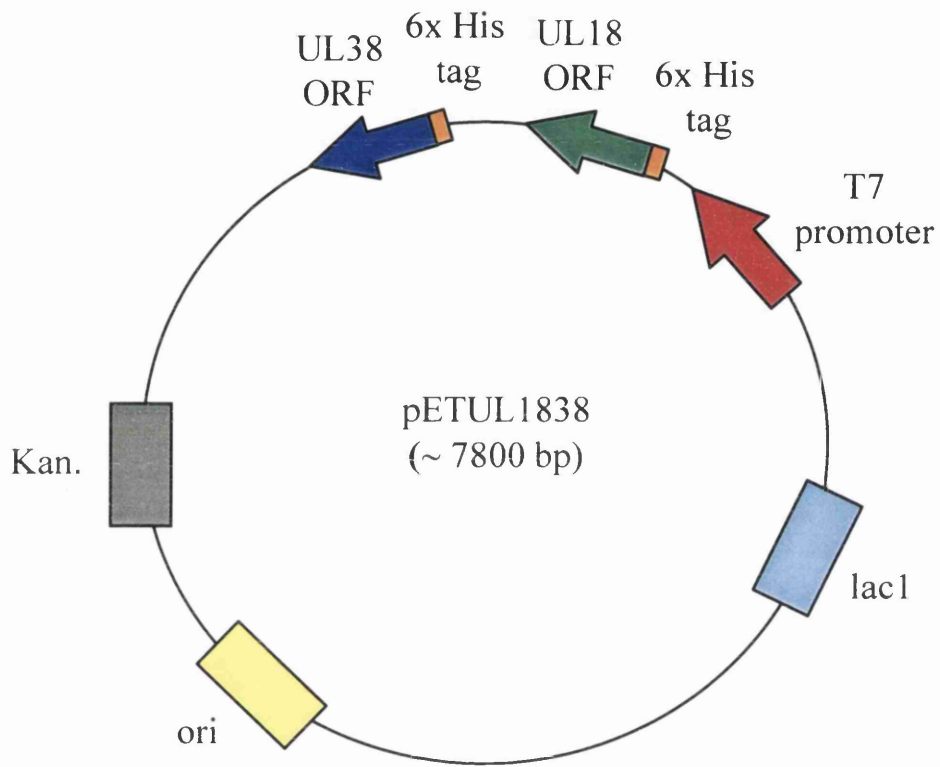


Fig. 3.5.1: Schematic representation of the cloning strategy for UL18 ORF into pETUL38 to generate pETUL1838

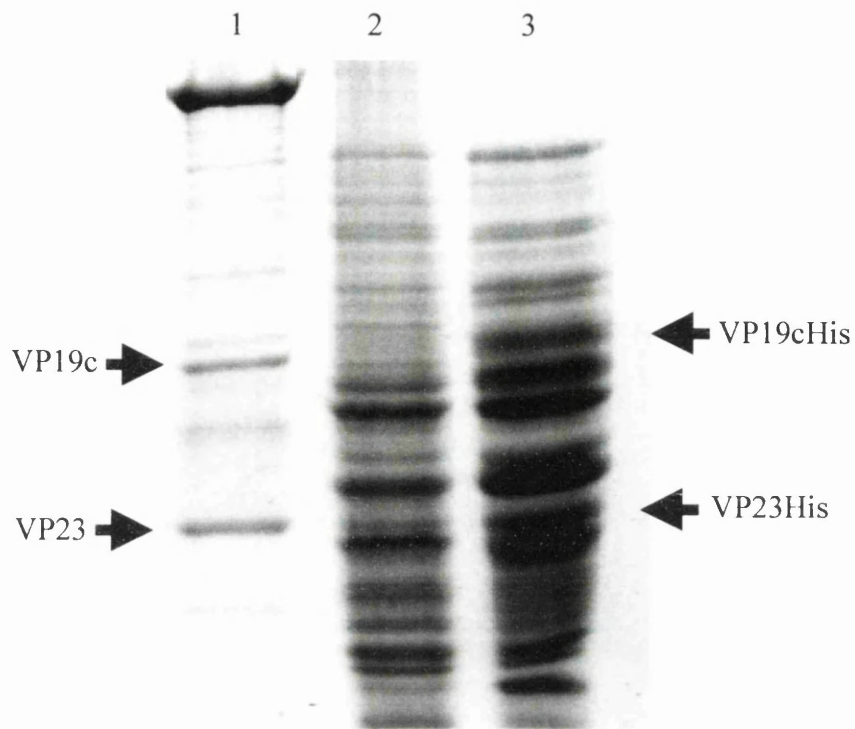
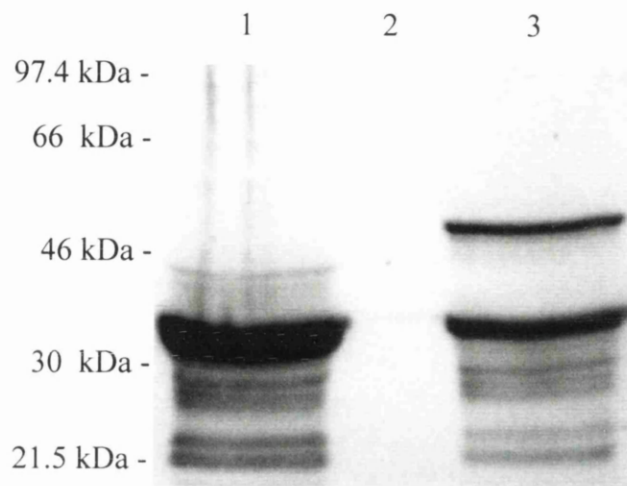
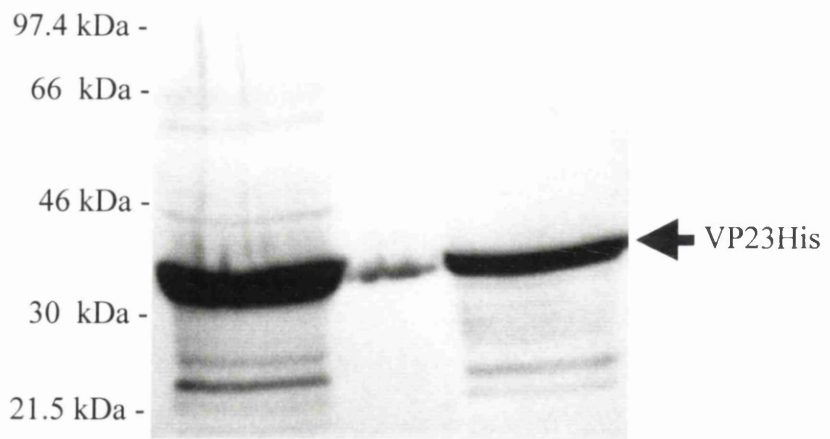


Fig. 3.5.2: SDS-PAGE analysis of pETUL1838 expression in BL21 DE3 bacteria.

BL21 DE3 bacterial cultures containing either pET28MOD (lane 2) or pETUL1838 (lane 3) were grown and induced (as described in Methods). 1.5 ml of the culture was centrifuged at 14,000 r.p.m. for 30 seconds in a microfuge. The supernatant was removed and the bacterial pellet was resuspended in 200 $\mu$ l of BM and heated for 2 minutes at 100°C in a dry block. 15 $\mu$ l of each sample was analysed against purified C-capsids (lane 1) by SDS-PAGE and stained with Coomassie Brilliant Blue. The presence of novel bands is indicated by arrows.



(A)



(B)

Fig. 3.5.3: Western blot analysis of pETUL18 and pETUL1838 expression in BL21 DE3 bacteria.

BL21 DE3 bacterial cultures containing either pETUL18 (lane 1) or pETUL1838 (lane 3) were grown and induced (as described in Methods). 1.5 ml of the culture was centrifuged at 14,000 r.p.m. for 30 seconds in a microfuge. The supernatant was removed and the bacterial pellet was resuspended in 200 $\mu$ l of BM and heated for 2 minutes at 100°C in a dry block. Western blot analysis was performed on 40 $\mu$ l of each sample and purified C-capsids (lane 2). (A) Nitrocellulose membrane was probed with 1:1000 dilution of the Penta His monoclonal antibody (Qiagen). (B) Nitrocellulose membrane was stripped (as described in Methods) and re-probed with a 1:1000 dilution of the polyclonal VP23 antibody 187. The arrow indicates the position of VP23His.

in Methods) and analysed for the expression of VP19cHis and VP23His by SDS-PAGE and Coomassie Brilliant Blue staining. Fig. 3.5.2 shows the comparative protein profile of induced BL21 DE3 bacteria containing either the pETUL1838 or pET28MOD bacterial expression vectors. Two bands could be detected by Coomassie Brilliant Blue staining in the pETUL1838 sample that were not present in the pET28MOD sample (indicated by a (+) in fig. 3.5.2). These bands migrated with a MW just higher than that of VP23 and VP19c from purified C-capsids (indicated by arrows in fig. 3.5.2) and reflects the addition of extra sequences on their respective N-termini. Western blot analysis utilising a commercial Penta His monoclonal antibody (Qiagen) detected the presence of two protein bands in bacterial extracts expressing pETUL1838 (fig.3.5.3, panel A, lane 3). In comparison, only a single band could be detected within bacterial extracts expressing pETUL18 (fig.3.5.3, panel A, lane 1). Western blot analysis utilising a polyclonal VP23 antibody (187) confirmed this lower MW band within the pETUL1838 sample was VP23His (fig.3.5.3, panel B, lane 3). This data therefore confirms that the successful cloning and expression of the UL18 ORF within the pETUL1838 expression vector. However, due to the lack of a specific antibody against VP19c it was not possible at this time to determine whether or not the higher MW band detected by the monoclonal Penta HIS antibody corresponded to the bacterial expression of VP19cHis. Nevertheless, the estimated MW of 50kDa and the co-migration with VP19c from purified C-capsids supported the case for this being VP19cHis.

### *3.5.1.3 Ni-NTA agarose purification of VP23His and VP19cHis from induced BL21 DE3 bacteria expressing pETUL1838.*

Various attempts were made to purify the bacterially expressed triplex proteins utilising different buffers (data not shown). However, in each case only VP23His could be purified by Ni-NTA agarose affinity chromatography with little or no purification of VP19cHis detectable by Coomassie Brilliant Blue staining. Fig. 3.5.4 shows a typical SDS-PAGE profile of Ni-NTA purified triplex proteins in PBSa. No VP19cHis could be observed in either the 20mM imidazole washes (lanes 1 and 2) or 250mM imidazole elution fractions 1 and 2 (lanes 4 and 5). In subsequent experiments attempts were made to purify triplex proteins without washing the Ni-NTA agarose in 20mM imidazole to ensure that VP19cHis was not eluted from the Ni-NTA resin in low concentrations of imidazole.

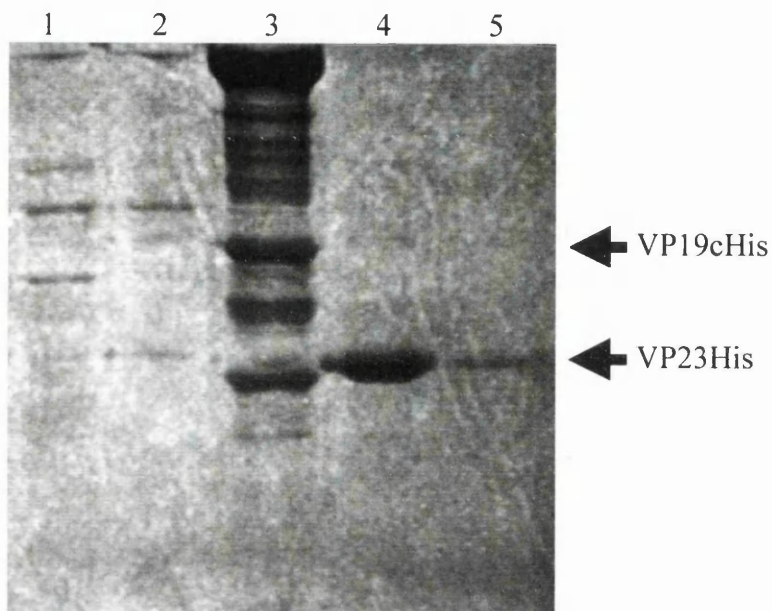


Fig. 3.5.4: SDS-PAGE analysis of Ni-NTA agarose purified bacterially expressed triplex proteins (VP23His+VP19cHis).

BL21 DE3 bacteria cultures containing the pETUL1838 were grown and induced (as described in Methods). Proteins purified using 700 $\mu$ l of Ni-NTA agarose equilibrated in PBSa. The Ni-NTA agarose was washed in 10ml (10x 1ml) of 20mM imidazole in PBSa to remove non-specifically bound proteins from the Ni-NTA matrix. Samples were eluted from the Ni-NTA agarose in 3ml (3x 1ml fractions) of 250mM imidazole in PBSa. 20 $\mu$ l of the 20mM imidazole wash fractions 1 and 2 (lanes 1 and 2 respectively) and 20 $\mu$ l of the 250mM elution fractions 1 and 2 (lanes 4 and 5 respectively) were analysed by SDS-PAGE and stained with Coomassie Brilliant Blue. Eluted Ni-NTA agarose proteins were analysed against purified B-capsids (lane 3).

However, in all cases SDS-PAGE analysis and Coomassie Brilliant Blue staining failed to reveal the presence of a 50kDa protein band corresponding to VP19cHis (data not shown).

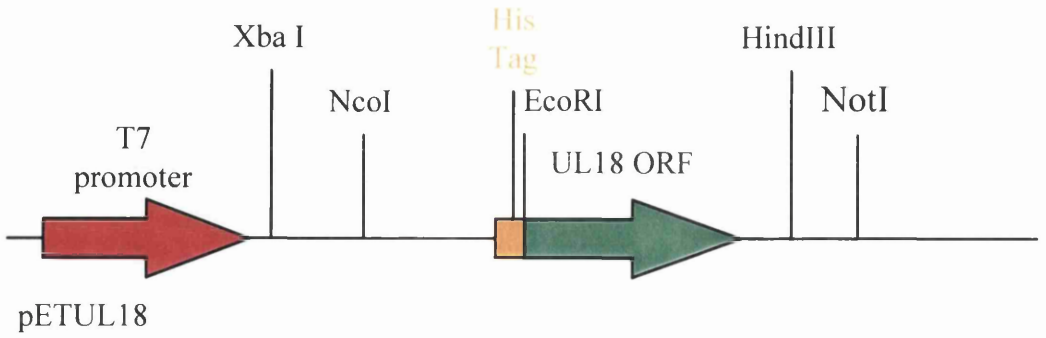
Previous Western blot analysis utilising the monoclonal Penta His antibody (Qiagen) did not detect the presence of a 50kDa MW protein in bacterial extracts expressing pETUL38 (discussed in section 3.4). Therefore, the detection of a 50kDa band in bacterial extracts expressing the pETUL1838 seems to imply that the expression and/or stability of this 50kDa protein is enhanced when co-expressed in the presence of VP23His. This resembles the stabilisation of VP19cHis by VP23 seen in the recombinant baculovirus expression (discussed below). The difficulty associated with the purification of bacterially expressed VP19cHis suggests that it may be forming insoluble aggregates which may prevent its purification under the buffering conditions employed. Attempts to purify VP23His and VP19cHis under denaturing conditions, for example in 8M urea, which could solubilise any aggregated and insoluble proteins, were not pursued. Instead efforts were directed towards the expression and purification of triplex proteins within SF21 cells utilising recombinant baculoviruses.

### **3.5.2 Co-expression of VP23 and VP19c triplex proteins within SF21 cells.**

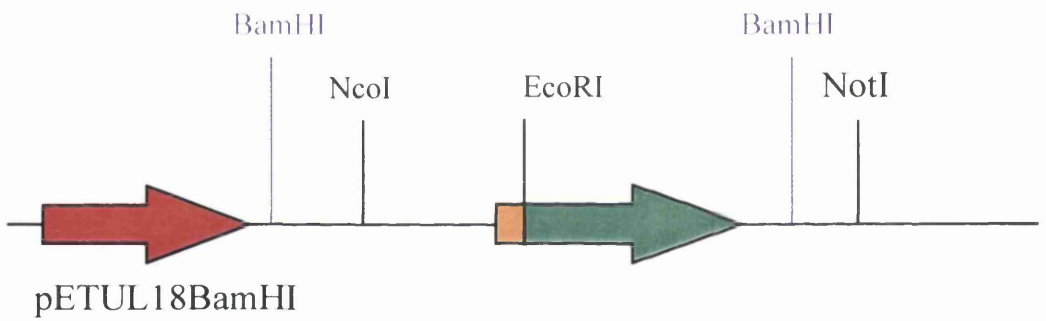
Due to the apparent insolubility of VP19cHis within the prokaryotic expression system it was decided to co-express VP19c and VP23His within the eukaryotic baculovirus expression system in an attempt to produce triplexes for purification and analysis.

#### *3.5.2.1 Cloning of the UL18 ORF into the baculovirus transfer vector pAcAB3 containing the UL38 ORF (pAcAB3.10).*

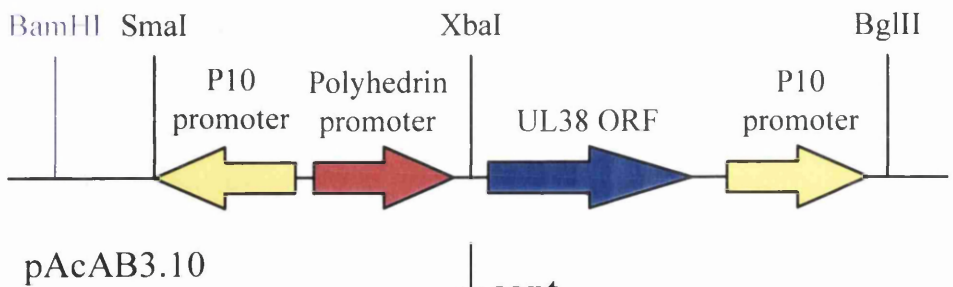
The UL18 ORF plus sequences containing the 6xHis tag was subcloned out of the bacterial expression vector pETUL18. The pETUL18 plasmid was XbaI digested at a unique XbaI restriction site. Following digestion, the DNA was phenol/chloroform extracted and ethanol precipitated (as described in Methods). The linear DNA molecule was then blunt ended using T4 polymerase and BamHI linkers were inserted (as described in Methods).



Endonuclease restriction digestion and BamHI linker ligation performed individually upon XbaI and HindIII cloning sites.



pETUL18BamHI digested with BamHI, the UL18 ORF BamHI fragment purified and ligated into BamHI digested and CIP treated pAcAB3.10 to generate pAcABUL18638.



cont.

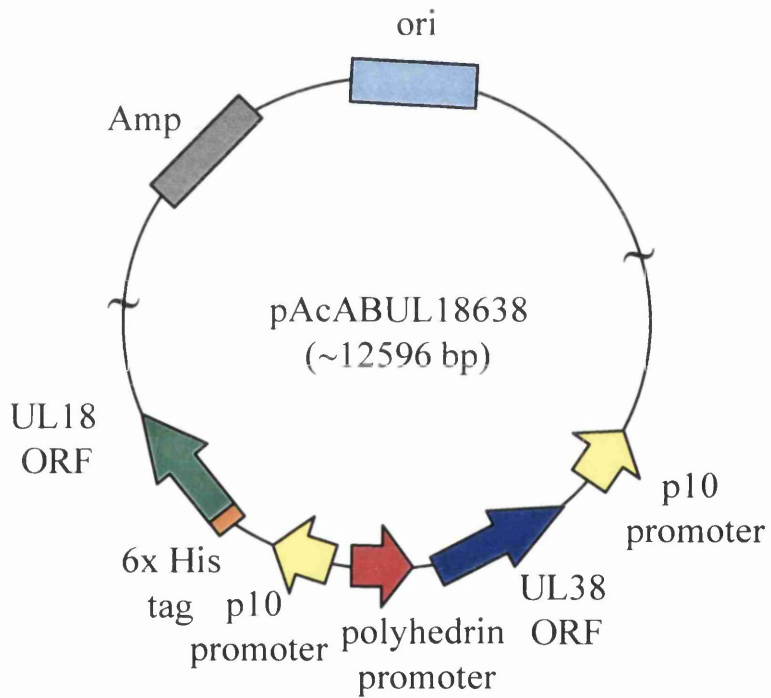
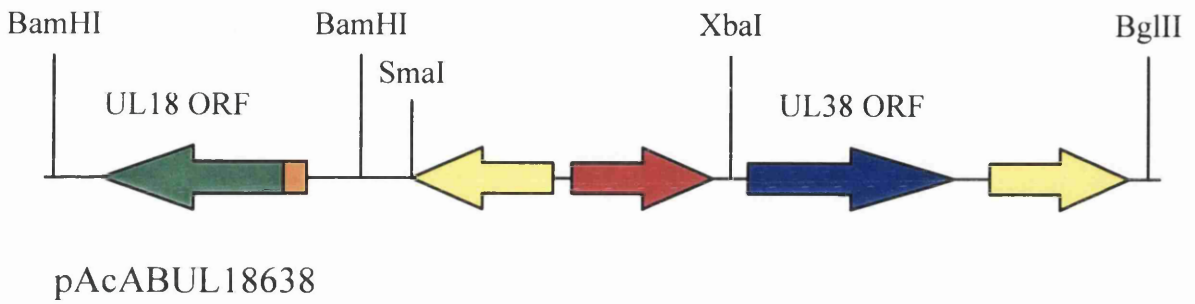


Fig. 3.5.5: Schematic representation of the cloning strategy for the insertion of the UL18 ORF into the baculovirus transfer vector pAcAB3.10 to generate pAcABUL18638 (Ac18638).

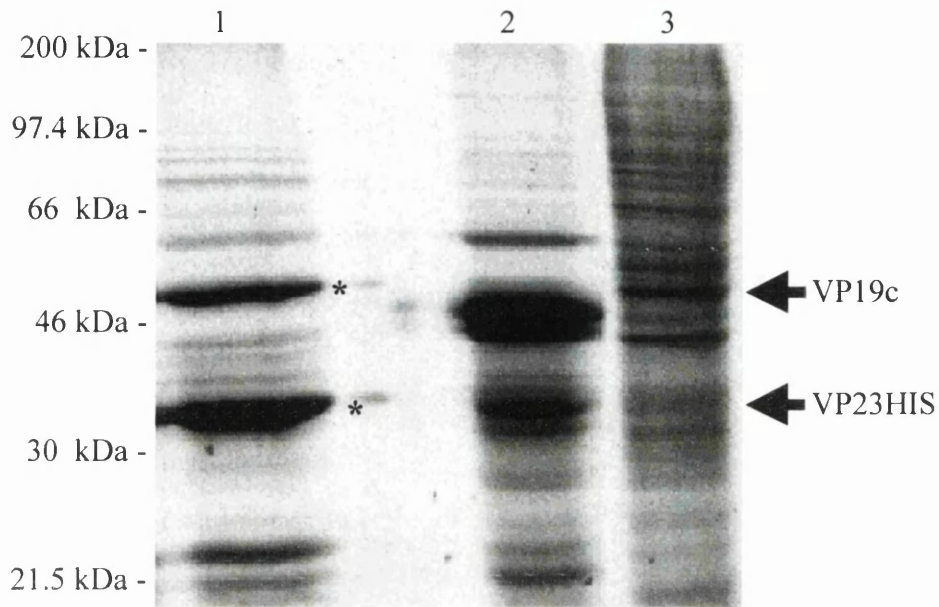


Fig. 3.5.6: SDS-PAGE analysis of [ $^{35}\text{S}$ ]methionine-labelled SF21 cell infected with the recombinant baculovirus Ac18638 co-expressing VP23His and VP19c.

35mm dishes containing approximately 70% confluent SF21 cells were infected with 100 $\mu\text{l}$  of plaque purified Ac18386 recombinant baculovirus (lane 1), AcUL26.5 at an m.o.i. of 5 (lane 2), or mock infected (lane 3). 24 hours post infection SF21 cells were labelled with [ $^{35}\text{S}$ ]methionine (as described in Methods) and incubated for a further 24 hours. The cells were harvested and pelleted by centrifugation in a 1.5ml reaction vial at 14,000 r.p.m. for 5 minutes at RT in a microfuge. The supernatant was removed and the cell pellets resuspended in 200 $\mu\text{l}$  of BM buffer and heated for 2 minutes at 100 $^{\circ}\text{C}$  in a dry block. 20 $\mu\text{l}$  of each sample and 3 $\mu\text{l}$  of Rainbow markers were analysed by SDS-PAGE and stained with Coomassie Brilliant Blue. The gel was dried onto Whatmann 3mm paper and [ $^{35}\text{S}$ ]methionine labelled proteins were detected by exposing the gel o/n to Kodak film (as described in Methods). The arrows mark the position of recombinantly expressed triplex proteins VP19c and VP23His. The positions of the size markers are indicated.

The BamHI linker insertion procedure was repeated utilising a unique HindIII restriction site (fig. 3.5.5) to generate pETUL18BamHI. The UL18 ORF and sequences encoding the 6xHis epitope tag was then subcloned out of the pETUL18BamHI vector as a BamHI fragment and ligated into a BamHI digested and CIP treated baculovirus transfer vector (pPACAB3.10), which already contained the UL38 ORF. This generated pAcABUL18638. The cloning strategy for the insertion of the UL18 ORF into pAcAB3.10 is schematically illustrated in fig. 3.5.5. The cloning of the UL38 ORF into the baculovirus transfer vector pAcAB3 was performed by Jacqueline Tatman (previously described in Tatman, 1996). Briefly, the UL38 ORF was cloned out of pBJ382 (described in section 3.4) as a XbaI/HincII fragment and ligated into XbaI/StuI digested and CIP treated pPACAB3 (Pharmingen) baculovirus transfer vector to generate pAcAB3.10.

#### *3.5.2.2 Expression of Ac18638 within SF21 cells.*

Recombinant baculoviruses expressing VP23His and VP19c were obtained by co-transforming SF21 cells with the pAcABUL18638 baculovirus transfer vector and parental baculovirus (PAK6) DNA (as described in Methods). Fig. 3.5.6 shows the [<sup>35</sup>S] methionine-labelled profiles of SF21 cells infected with a third round plaque purified isolate of Ac18638 virus (lane 1). For comparison AcUL26.5 (lane 2) and mock (lane 3) infected samples are shown. In Ac18638 infected SF21 cells two novel protein bands of 34 and 50kDa (corresponding to VP23His and VP19c respectively) could be detected which were not present in either the mock or AcUL26.5 infected SF21 cells.

### **3.5.3 Cloning and expression of Ac18386**

During the course of working out a solubilisation strategy for Ni-NTA agarose purified triplex proteins from SF21 cells infected with Ac18638, it was noted that the ratio of VP23His to VP19c was higher than the predicted 2:1 ratio of VP23 and VP19c in triplexes (Newcomb et al., 1993). Furthermore, purification of triplexes utilising the 6xHis epitope tag on VP23 resulted in the co-purification of truncated forms of VP19c (indicated by \* in fig. 3.5.7). In an attempt to produce a homogenous population of recombinant triplexes and avoid an excess purification of VP23, it was decided to express the 6xHis tag on

VP19c rather than VP23. Purification of triplexes through the use of Ni-NTA agarose affinity chromatography would therefore result in the co-purification of only those VP23 molecules that were associated with VP19c as part of a heterotrimer complex.

### *3.5.3.1 Cloning of the 6x His epitoped tagged UL38 ORF and UL18 ORF into the baculovirus transfer vector pAcAB3.*

The cloning of the UL18 ORF and the UL38 ORF, which contained sequences encoding the 6xHis epitope tag, was performed by D. McNab. The UL38 ORF was cloned by PCR amplification and ligated into the transfer vector pTZ18U as a BamHI/PstI fragment (described in section 3.4 and Nicholson, 1992) to generate pTZ386. The UL38 6xHis ORF was then subcloned out of pTZ386 as a HindIII fragment and filled in using Klenow (as described in Methods). BamHI linkers were inserted and the fragment ligated into a BamHI digested and CIP treated pTZ18U to generate pTZ386BamHI. The UL38 6xHis ORF was then isolated from pTZ386BamHI as a BamHI fragment and ligated into a BamHI digested and CIP treated pAcAB3 baculovirus transfer vector (PharMingen) to generate pAcAB386. The UL18 ORF had been previously cloned into the pT3T7 vector (described in Tatman, 1996). The pT3T7 vector containing the UL18 ORF was digested with Sall and filled in using Klenow (as described in Methods). A BamHI linker was inserted and the vector ligated to generate pT3T7UL18BamHI. The UL18 ORF was then subcloned out of pT3T7UL18BamHI as a BamHI fragment and ligated into a BglII digested and CIP treated pAcAB386 transfer vector to generate pAcABUL18386. The baculovirus transfer vector pAcAB3 and the pAcABUL18386 transfer vector are schematically illustrated in fig. 3.5.8 and 3.5.9.

### *3.5.3.2 Expression of Ac18386 in SF21 cells*

Recombinant baculovirus (Ac18386) co-expressing VP19cHis and VP23 was obtained by co-transforming SF21 cells with pAcABUL18386 and parental baculovirus (PAK6) DNA (as described in Methods). Fig.3.5.10 shows the SDS-PAGE protein profile of SF21 cells either mock infected (lane 2), infected with Ac18386 (lane 3), or infected with AcUL26.5 (lane 4). Two proteins (indicated by the appropriate arrows) could be detected by Coomassie Brilliant Blue staining which were not present in either mock infected or

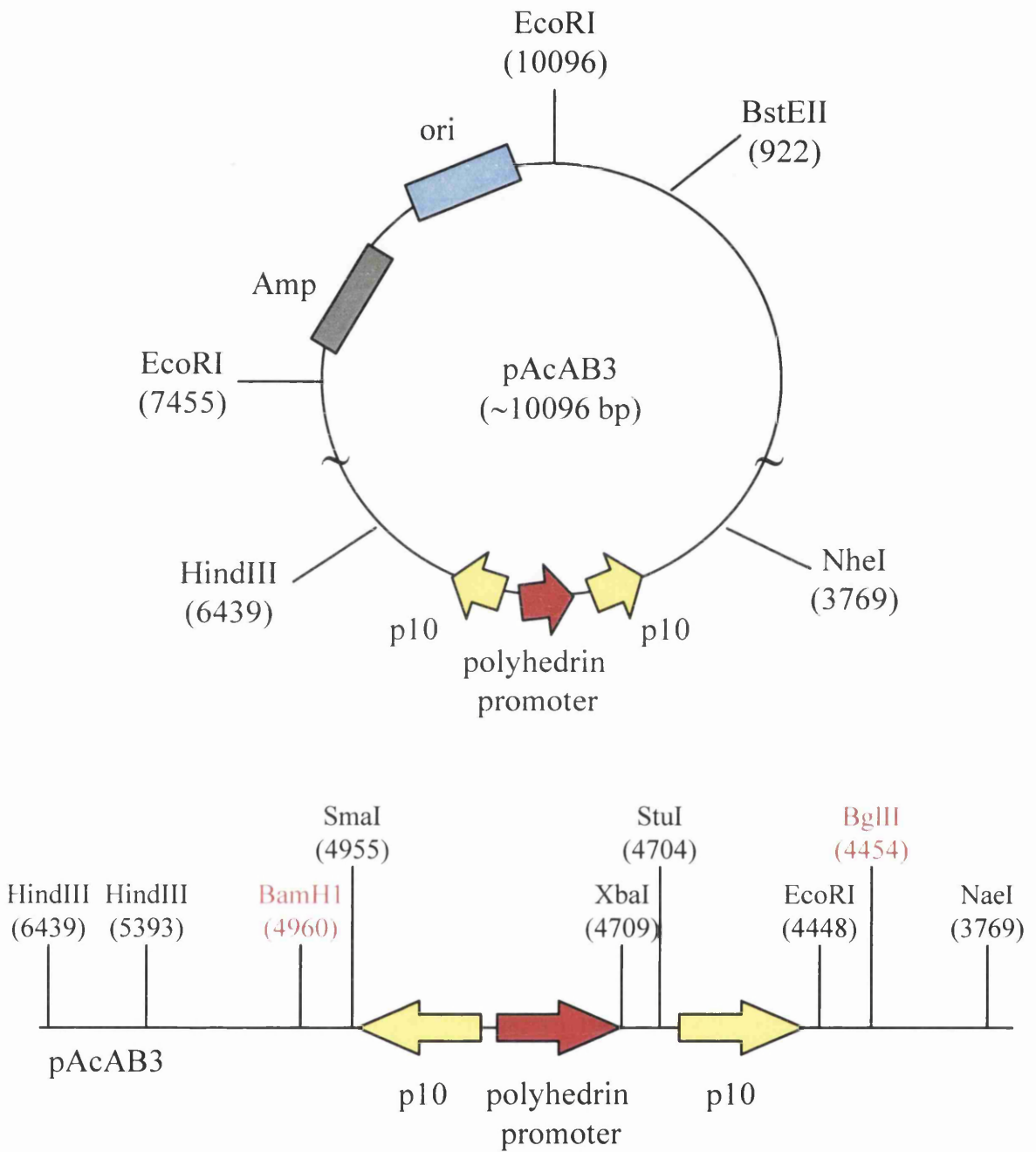


Fig. 3.5.8: Schematic representation of the baculovirus transfer vector pAcAB3. The red sites indicate the unique restriction sites used in the construction of pAcABUL18386

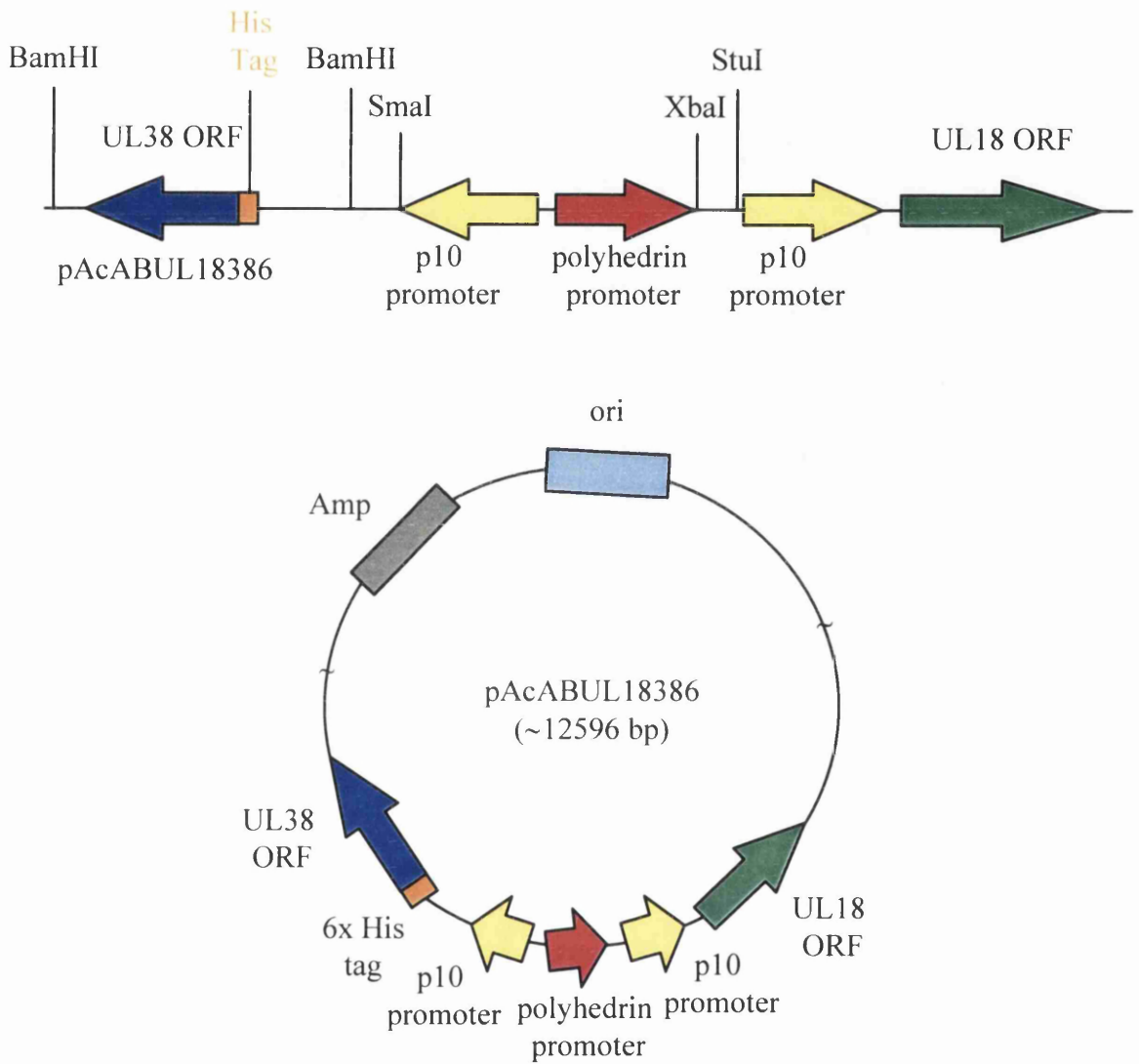


Fig. 3.5.9: Schematic representation for the orientation of the UL18 and UL38 ORFs within the baculovirus transfer vector pAcAB3 to generate pAcABUL18386 (Ac18386).

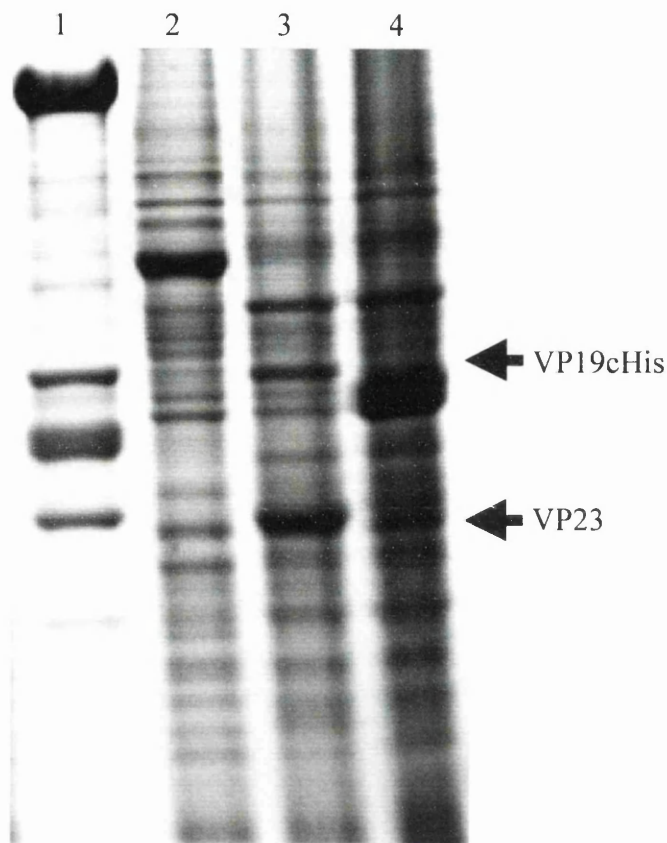


Fig. 3.5.10: SDS-PAGE analysis of SF21 cells infected with Ac18386 co-expressing the triplex proteins VP19cHis and VP23.

60mm dishes containing approximately 70% confluent SF21 cells were infected at an m.o.i. of 5 with either Ac18386 (lane 3), AcUL26.5 (lane 4), or mock infected (lane 2). 48 hours post infection SF21 cells were harvested (as described in Methods) and the cells pelleted by centrifugation at 14,000 r.p.m. for 5 minutes at RT in a microfuge. The supernatant was removed and the cell pellet resuspended in 200 $\mu$ l of BM buffer and heated for 2 minutes at 100°C in a dry block. 5 $\mu$ l of each sample and 3 $\mu$ l of purified B capsids (lane 1) were analysed by SDS-PAGE and stained with Coomassie Brilliant Blue. The arrows indicate the positions of VP23 and VP19cHis.

AcUL26.5 infected, SF21 cell extracts. These protein bands migrated with the same MW as VP19c and VP23 from purified B-capsids (lane 1). This would, therefore, imply that infection of SF21 cells with Ac18386 results the successful co-expression of VP23 and VP19cHis.

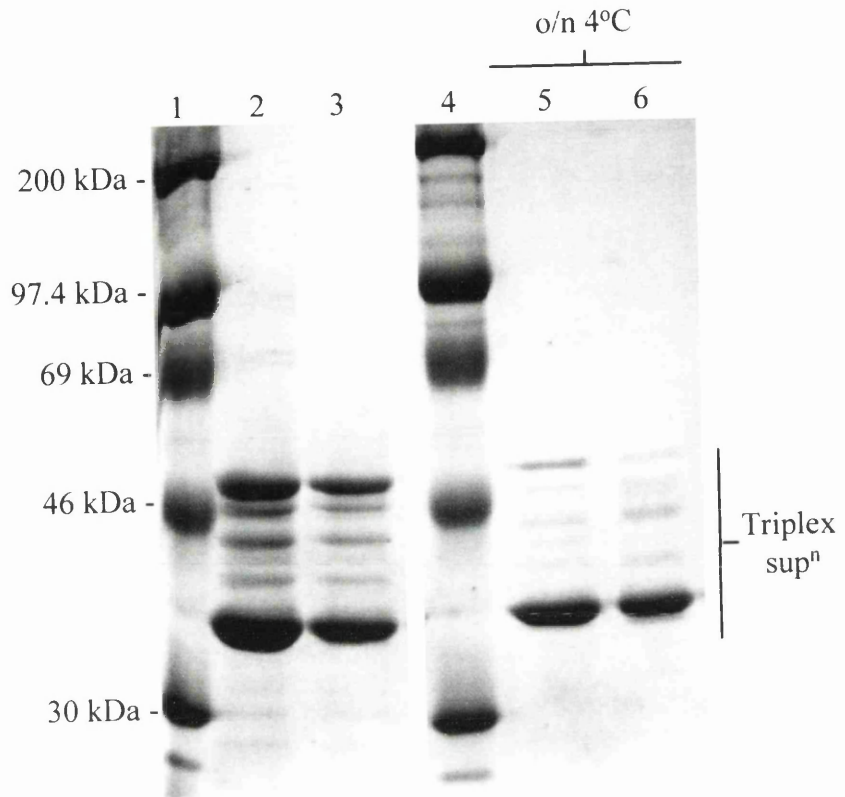
### **3.5.4 Ni-NTA agarose purification of triplex proteins expressed within SF21 cells infected either with Ac18638 or Ac18386.**

#### *3.5.4.1 Purification of triplexes*

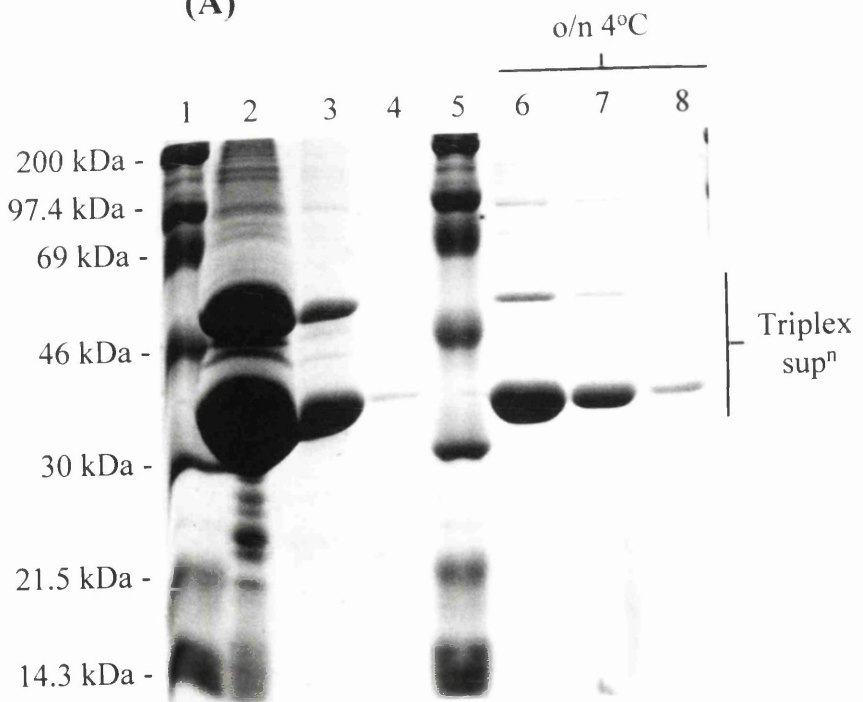
Utilising Ni-NTA agarose affinity chromatography, triplex proteins were readily purified from SF21 cells infected with either Ac18638 or Ac18386 (fig. 3.5.11, panel A lanes 2 and 3; panel B lanes 2-4 respectively) at protein concentrations of 0.5-2.0 mg/ml for elution fraction 1 (as determined by OD<sub>280</sub>). This would imply, therefore, that the N-terminus of both VP23His (Ac18638) and VP19cHis (Ac18386), where the 6xHis epitope tags are located are freely exposed to the solvent and readily available to bind to the Ni-NTA agarose. This suggests that the N-termini of these proteins are neither directly involved in the interaction with their appropriate triplex partner nor buried within the interior of their respective proteins. Furthermore, in each case, co-purification of the untagged triplex protein partner demonstrated that these proteins can interact in the absence of other capsid proteins and confirms previous experimental findings from Ni-NTA pull downs (described in section 3.4).

#### *3.5.4.2 Solubility of triplexes at 4°C*

Although the triplex proteins could be readily purified their long-term solubility, in particular that of VP19c, at either RT or 4°C was poor. Visible precipitates were observed over different periods of time post column elution, ranging from a few minutes to several hours depending on the purification buffer employed and their initial concentration of the eluted samples. Fig. 3.5.11 (panels A and B) shows the solubility of Ni-NTA agarose purified triplex proteins from SF21 cells infected with Ac18638 (panel A) or Ac18386 (panel B) respectively. Purified triplex proteins were incubation o/n at 4°C. Precipitates



(A)



(B)

Fig. 3.5.11: SDS-PAGE analysis of Ni-NTA agarose purified triplex proteins upon incubation at 4°C.

Triplex proteins were purified from SF21 cells infected with either Ac18638 (panel A) or Ac18386 (panel B), as described in Methods and fig. 3.5.7. Triplex proteins in (A) were purified in TB2 buffer (100mM Na<sub>2</sub>HPO<sub>4</sub>, 50mM NaCl, 0.1% glycerol, 1% DMSO, 0.05% Triton X-100). The Ni-NTA agarose was washed with 25ml of 20mM imidazole and the proteins were eluted in 6ml (4x 1.5ml fractions) of 250mM imidazole in buffer TB2. Triplex proteins in (B) were purified in TB3 buffer (20mM Na<sub>2</sub>HPO<sub>4</sub>, 100mM Na<sub>2</sub>SO<sub>4</sub>, 0.05% NP40). The Ni-NTA agarose was washed with 25ml of 20mM imidazole and the proteins eluted in 5ml (5x 1ml fractions) of 250mM imidazole in TB3 buffer. In each instance 20µl of the appropriate elution fraction was immediately transferred into BM and stored at -20°C. The elution fractions were then stored o/n at 4°C. Precipitated proteins were sedimented by ultracentrifugation either at 50,000 r.p.m. for 5 minutes at 4°C in a Beckman TLA100.2 rotor (A) or at 14,000 r.p.m. for 5 minutes at RT in a bench top microfuge (B). The supernatant containing the soluble protein fraction was transferred to a fresh 1.5ml reaction vial immediately following centrifugation. 20µl of the appropriate soluble protein fractions were compared with 20µl of the original protein elution fractions by SDS-PAGE and stained with Coomassie Brilliant Blue. (A) Lanes 1 and 4: Rainbow markers. Lanes 2 and 3: 250mM imidazole elution fractions 1 and 2 respectively. Lanes 5 and 6: soluble protein fraction from elution fractions 1 and 2 respectively after incubation o/n at 4°C. (B) Lanes 1 and 5: Rainbow markers. Lanes 2-4: 250mM imidazole elution fractions 1-3 respectively. Lanes 6-8: soluble protein fraction from elution fractions 1-3 respectively after incubation o/n at 4°C.

were sedimented by centrifugation (as described in legend) and the soluble protein fractions were analysed by SDS-PAGE to investigate which triplex protein constituents had precipitated out of solution during their respective incubations. In all incidences precipitation primarily affected VP19cHis and VP19c, while VP23His and VP23 generally remained more soluble (fig. 3.5.11, panel A, lanes 5 and 6, panel B, lanes 6-7). In an attempt to increase the solubility and stability of the purified triplexes a range of purification buffers were tested. It should be noted that in some instances purification buffers, although retaining triplex solubility, were unsuitable for many biophysical characterisation experiments (described in section 3.6), in particular Far-UV CD. These buffers tended to include comparatively high concentrations of NaCl (typically >150mM) and/or glycerol (>1%) which can lead to excessive noise within absorption spectra. In particular, Cl<sup>-</sup> ions absorb strongly below 195nm (Kelly and Price, 1996; Price, 1995). Such affects could be countered in most instances by analysis and subtracting buffer control spectra. However, buffer constituents including certain detergents, such as Triton X-100, and imidazole were completely unsuitable for Far-UV CD analysis. Table 3.5.1 shows a summary of the buffers used in the analysis of purification and solubilisation of Ni-NTA agarose purified triplex proteins.

Comparatively good triplex solubility was maintained utilising buffer OG (150mM Na<sub>2</sub>HPO<sub>4</sub> (pH7.5), 0.1% octyl-β-glucoside, 5% glycerol). Fig. 3.5.12 shows the solubility following a 48 hour incubation at 4°C of Ni-NTA agarose purified triplex proteins from SF21 cells infected with Ac18386. The triplex proteins appeared to remain completely soluble under these conditions. Further analysis revealed that the triplex proteins purified in buffer OG remained soluble for up to 4-5 days at 4°C (data not shown). However, far-UV CD analysis of triplex proteins in buffer OG (in the absence of imidazole) still proved problematic, possibly due to the high absorption factor of the glycerol component of buffer. Reduction in the concentration of glycerol from 5% to 0.1% (buffer O) removed this problem and still permitted triplex purification while maintaining good solubility. Buffer O was, therefore, used for all biophysical characterisation experiments employed.

Buffer composition	Purification of VP23	Purification of VP19c	Analysis	Comments
<b>Sonication buffer</b> (20 mM Tris (pH 7.0), 10% Glycerol, 0.1% NP40)	+++	+	SDS- PAGE	
<b>PBSa</b> (170mM NaCl, 3.5mM KCl, 10mM NaH <sub>2</sub> PO <sub>4</sub> , 3mM KH <sub>2</sub> PO <sub>4</sub> )	+++	++	SDS- PAGE	ppt. at RT
<b>G-150 buffer</b> (150mM NaCl, 20mM Tris (pH 8.0), 0.1% Tween)	+	+	SDS- PAGE	
30mM Tris (pH 8.0), 2M urea, 200mM NaCl, 10% glycerol	++++	+	SDS- PAGE	
G-150 + 1M urea	++	+	SDS- PAGE	
500mM NaCl, 20mM Tris, 3M Urea, 0.5% NP40, pH 7.0	+	+	SDS- PAGE	
<b>TB4: 20mM Tris (pH 7.5), 0.1% NP40, 1M Urea</b>	+++	++	SDS- PAGE FPLC	o/n 4°C VP19c ppt.
20mM Tris (pH7.5), 0.25M Urea, 0.05% NP40	+++	+++	SDS- PAGE	CD -VE
0.5M Urea, 20mM Tris (pH7.5), 0.05% NP40	+++	+++	SDS- PAGE FPLC	CD -VE
20mM Tris (pH7.5), 0.05% NP40, 500mM NaCl	++++	++++	SDS- PAGE FPLC DSC	CD -VE
20mM Tris (pH7.5), 0.05% NP40, 500mM NaCl, 8M Urea	++++	-	SDS- PAGE	No inter- disulphide bond
20 mM Tris (pH7.5), 250mM NaCl, 0.05% NP40	++++	++++	SDS- PAGE FPLC	Peak frac. (2 mg/ml)
20mM Na <sub>2</sub> HPO <sub>4</sub> (pH 7.5), 0.1% glycerol, 0.05% NP40	++++	++++	SDS- PAGE FPLC	o/n 4°C VP19c ppt.

**Cont.**

20mM Na <sub>2</sub> HPO <sub>4</sub> (pH6.0), 100mM Na <sub>2</sub> SO <sub>4</sub> , 0.05% NP40	N/A	N/A	FPLC	o/n RT & 4°C VP19c ppt.
<b>TB3:</b> 20mM Na <sub>2</sub> HPO <sub>4</sub> (pH8.0), 100mM Na <sub>2</sub> SO <sub>4</sub> , 0.05% NP40	++++	++++	SDS- PAGE	o/n RT & 4°C VP19c ppt.
20mM Na <sub>2</sub> HPO <sub>4</sub> , 0.05% triton, 0.1% glycerol, 10% DMSO	++++	+++	SDS- PAGE	o/n RT & 4°C VP19c ppt.
<b>TB1:</b> PBScomplete, 1%glycerol, 10mM Na <sub>2</sub> SO <sub>4</sub> , 2.5% DMSO, 0.05% Triton X-100	++++	+++	SDS- PAGE FPLC: +++	Low 4°C VP19c ppt. CD -VE
<b>TB2:</b> 100mM Na <sub>2</sub> HPO <sub>4</sub> , 50mM NaCl, 0.1% glycerol, 1 % DMSO, 0.05% Triton X-100	++++	++++	SDS- PAGE	o/n 4°C VP19c ppt.
100mM Na <sub>2</sub> HPO <sub>4</sub> , 0.1% glycerol, 1 % DMSO, 0.05% Triton X-100	++++	++++	SDS- PAGE FPLC	CD -VE
100mM Na <sub>2</sub> HPO <sub>4</sub> , 0.001% NP40 (pH 8.65)	++++	+	SDS- PAGE	
100mM Na <sub>2</sub> HPO <sub>4</sub> , 0.001% Octyl-β-glucoside, 0.1% glycerol, 1% DMSO, 30mM NaCL (pH 8.65)	+++	+	SDS- PAGE	
20mM Tris, 0.1% Octyl-β- glucoside, 20mM NaCl, 1% glycerol	++++	+++	SDS- PAGE	VP19c ppt. on dialysis
<b>Buffer OG</b> 150mM Na <sub>2</sub> HPO <sub>4</sub> , 0.1% Octyl-β-glucoside, 5% glycerol (pH7.75)	++++	++++	SDS- PAGE FPLC	VP19c Soluable o/n at 4°C CD -VE
<b>Buffer O</b> 150mM Na <sub>2</sub> HPO <sub>4</sub> , 0.1% Octyl-β-glucoside, 0.1% glycerol (pH7.75)	++++	++++	SDS- PAGE FPLC	CD +VE DSC +VE

Table 3.5.1: Summary table of buffers used in the solubilisation of Ni-NTA agarose purified triplex proteins. Triplex proteins were purified from SF cells infected with either Ac18638 or Ac18386 (as described in Methods and fig. 3.5.7). Purified proteins were analysed (as described in table) and rated for the presence of both VP19c and VP23; ++++ (very good), +++ (good), ++ (poor), + (detectable), - (not detectable).

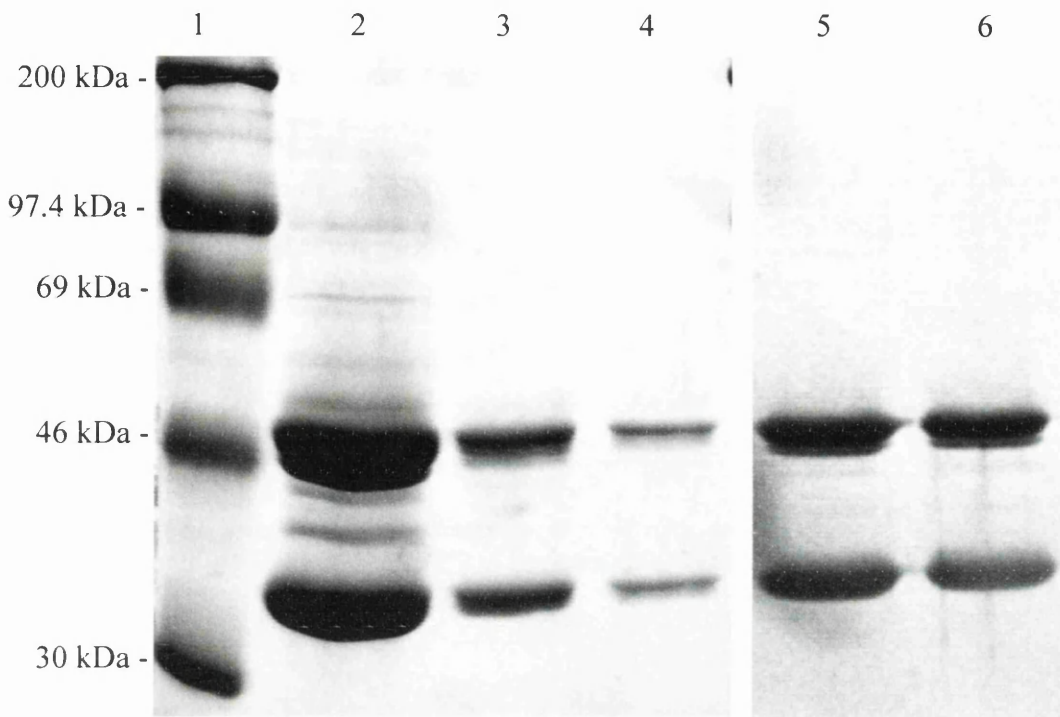


Fig. 3.5.12: SDS-PAGE analysis of Ni-NTA agarose purified triplex proteins in buffer OG before and after o/n storage at 4°C.

Triplex proteins were purified from SF21 cells infected with Ac18386 in buffer OG (as described in Methods and fig. 3.5.7). 20µl of each 250mM imidazole elution fraction 1-3 (lanes 2-4 respectively) and Rainbow markers (lane 1) were analysed by SDS-PAGE and stained with Coomassie Brilliant Blue. Elution fraction 2 was subsequently incubated at 4°C for 48 hours. Following incubation, 25µl of elution fraction 2 was transferred into BM buffer. Precipitated proteins were sedimented by ultracentrifugation at 80,000 r.p.m. for 5 minutes at 4°C in a Beckman TLA 100.2 rotor. The supernatant fraction containing soluble proteins was immediately transferred to a fresh 1.5ml reaction vial. 25µl of the pre-incubation elution fraction 2 and 25µl of the supernatant fraction post incubation was analysed by SDS-PAGE (lanes 5 and 6 respectively) and stained with Coomassie Brilliant Blue.

### 3.5.5 Disulphide bond analysis of purified triplex proteins.

Zweig et al., (1979) demonstrated through the use of non-reducing SDS-PAGE analysis that VP19c and VP5 from purified HSV-2 capsids were disulphide linked. In order to determine whether or not HSV-1 encoded VP19c and VP23 were also disulphide linked, the triplex proteins were purified from SF21 cells infected with Ac18638 in the presence (fig. 3.5.13, lanes 4 and 6) or absence (fig. 3.5.13, lanes 3 and 5) of 8M urea. Only a single prominent band corresponding to VP23His was purified in the presence of 8M urea. This indicates that inter-molecular disulphide bonds do not link VP19c and VP23His. This result is in agreement with published observations by Zweig et al., (1979) who could not detect any alteration in the behaviour of VP23 from purified HSV-2 capsids when analysed by non-reducing SDS-PAGE. This result also demonstrates that interaction between VP23His and VP19c is specific and conformation dependent and not a result of VP19c non-specifically binding to the Ni-NTA agarose.

SDS-PAGE analysis of purified triplex proteins in the presence and absence of  $\beta$ -mercaptoethanol demonstrated a minor shift in migratory position of these purified complexes. Fig. 3.5.14 shows the non-reducing SDS-PAGE analysis of Ni-NTA agarose purified triplex proteins from SF21 cells infected with Ac18386. In the absence of 20mM  $\beta$ -mercaptoethanol two faint bands, corresponding to approximately 150 and 175kDa, can be observed by Coomassie Brilliant Blue staining (fig. 3.5.14, lanes 2 and 3, (-)  $\beta$ -mercaptoethanol). The homogeneity of the reduced triplex proteins (fig. 3.5.14, lanes 2 and 3, (+)  $\beta$ -mercaptoethanol) strongly suggests that these bands are related to the VP23/VP19cHis complexes but their nature is unclear. This data, therefore, supports the evidence from triplex purification in 8M urea (fig. 3.5.13) and suggests that no intra-molecular disulphide linkages are formed between VP23 and VP19c within the triplex. However, there may be cysteine residues within either VP23 or VP19cHis that are required for the formation of intra-molecular disulphide linkages. Such linkages may be required for maintaining a suitable conformation for the interaction with the complementing triplex protein partner and as a consequence generating SDS resistant complexes, as seen by SDS-PAGE in the absence of  $\beta$ -mercaptoethanol.

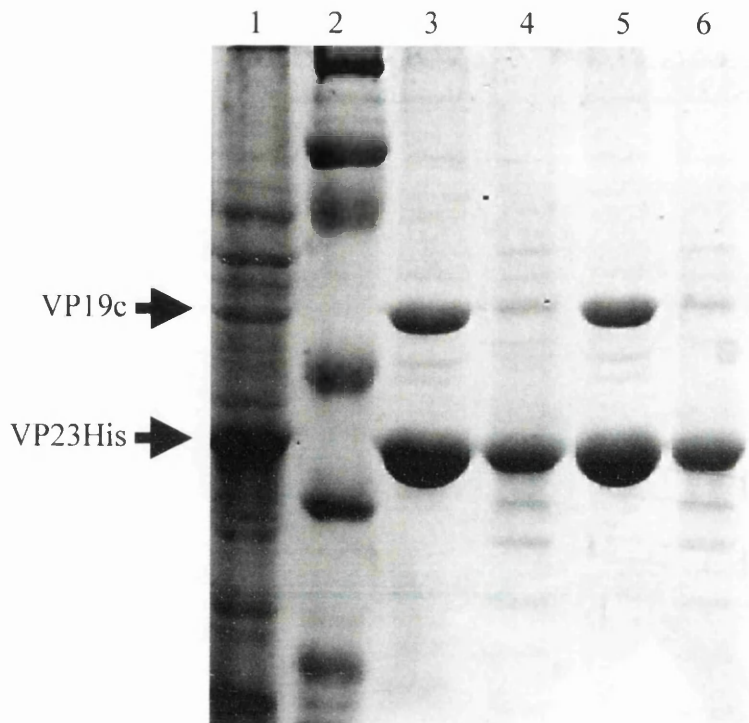


Fig. 3.5.13: Ni-NTA agarose purification of triplex proteins in the presence of 8M urea.

Triplex proteins were purified from SF21 cells infected with Ac18638 as described in Methods. The cells were split into two fractions and sedimented by centrifugation at 3,000 r.p.m. in a Sorval RT7 centrifuge for 5 minutes at RT. The supernatants were removed and the cell pellets resuspended in either TB4 buffer (20mM Tris pH7.5, 0.1% NP40, 500mM NaCl) (lanes 3 and 5) or TB4 buffer + 8M urea (lanes 4 and 6). Triplex proteins were subsequently purified (as described in Methods and fig. 3.5.7) in their respective buffers. The Ni-NTA agarose was sequentially washed in 10ml of TB4 buffer and 5ml of 20mM imidazole in TB4 buffer to remove any non-specifically bound proteins and residual urea from the Ni-NTA matrix. Proteins were eluted in 1.5ml (5x 300 $\mu$ l) of 250mM imidazole in buffer TB4. 20 $\mu$ l of the appropriate elution fraction and 5 $\mu$ l of Ac18638 infected SF21 total cell extract (lane 1) was analysed against Rainbow markers (lane 2) by SDS-PAGE and stained with Coomassie Brilliant Blue.

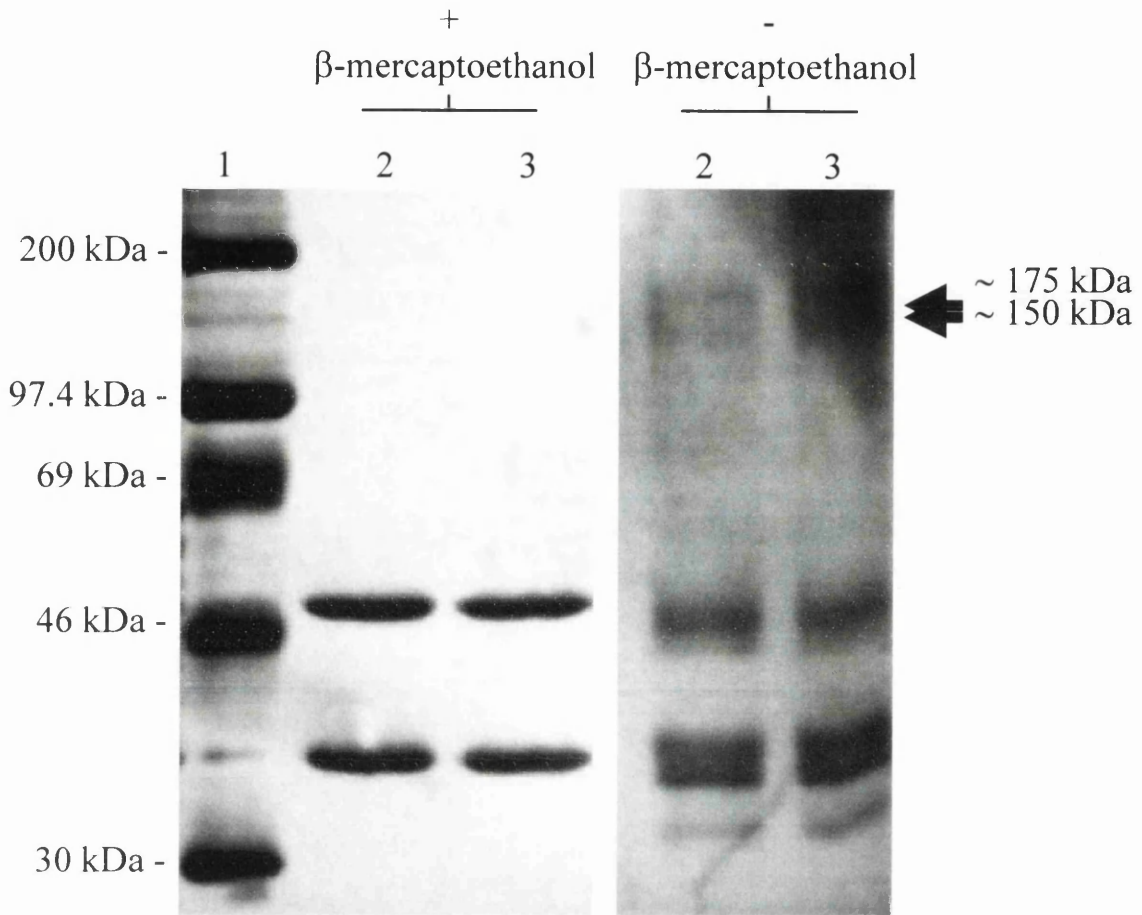


Fig. 3.5.14: SDS-PAGE analysis of Ni-NTA agarose purified triplex proteins in the presence (+) or absence (-) of 20mM  $\beta$ -mercaptoethanol.

Triplex proteins were purified from SF21 cells infected with Ac18386 as described in Methods and fig. 3.5.7 in buffer OG. Rainbow markers (lane 1) and 20 $\mu$ l of elution fractions 1 and 2 (lanes 2 and 3 respectively) were analysed in the presence (+) or absence (-) of 20mM  $\beta$ -mercaptoethanol. Samples were analysed by SDS-PAGE and stained with Coomassie Brilliant Blue.

### 3.5.6 Size exclusion chromatography analysis of purified triplex proteins

In order to determine whether or not Ni-NTA agarose purified triplex proteins formed heterotrimeric complexes and to determine an accurate native MW for the triplex size exclusion chromatography analysis was performed on Ni-NTA agarose purified triplex proteins in buffer O. Fig. 3.5.15 (panel A) shows a single elution peak obtained with Ni-NTA agarose purified triplexes purified from SF21 cells infected with Ac18386. The elution profile is plotted against a standard curve generated by analysis of protein standards (as described in Methods). The elution volume of the single peak detected corresponded to a native MW of 103kDa. This is a shift from the predicted MW of approximately 118kDa estimated from the amino acid sequence of VP23 and VP19c in a 2:1 ratio (McGeoch et al., 1988). Furthermore, the native MW of 103kDa for purified triplexes is also considerably different from the estimated triplex mass determined by Newcomb and co-workers of 115kDa to 135kDa by STEM density mapping of hexon associated triplexes (Newcomb et al., 1993). Although several N-terminal amino acids of VP19c were removed during the cloning of the UL38 ORF this would not account for a 15kDa shift in observed and predicted triplex MW. The shift in MW may represent resolving limitations in separation of the Superose 12 column or alternatively reflect the compact native structure of *in vivo* preformed triplexes. A more likely explanation for the apparent low MW of the triplexes is the anomalous behaviour of the BSA protein standard (66kDa, highlighted in red in fig. 3.5.15). The elution volume from this standard reduces the slope of the standard curve away from that of the other protein standards and therefore alters the  $\text{Log}_{10}$  MW reading derived from the triplex elution volume. Indeed, if the standard curve is plotted without BSA elution volume the triplex MW increases to approximately 115kDa. Recently, Spencer et al., (1998) published data on the sedimentation coefficients of triplexes and triplex proteins analysed on sucrose gradients. The triplexes analysed were formed *in vitro* by mixing SF9 cell extracts individually expressing VP23 and VP19c. Sedimentation analysis determined their triplexes to have a MW of 129kDa, 11kDa larger than that of the predicted MW derived from the amino acid sequence. However, experiments performed by Spencer et al., (1998) relied on a single protein standard (BSA) to act as a MW marker during sedimentation analysis and therefore inaccuracies in estimating the MW of triplexes may have occurred.

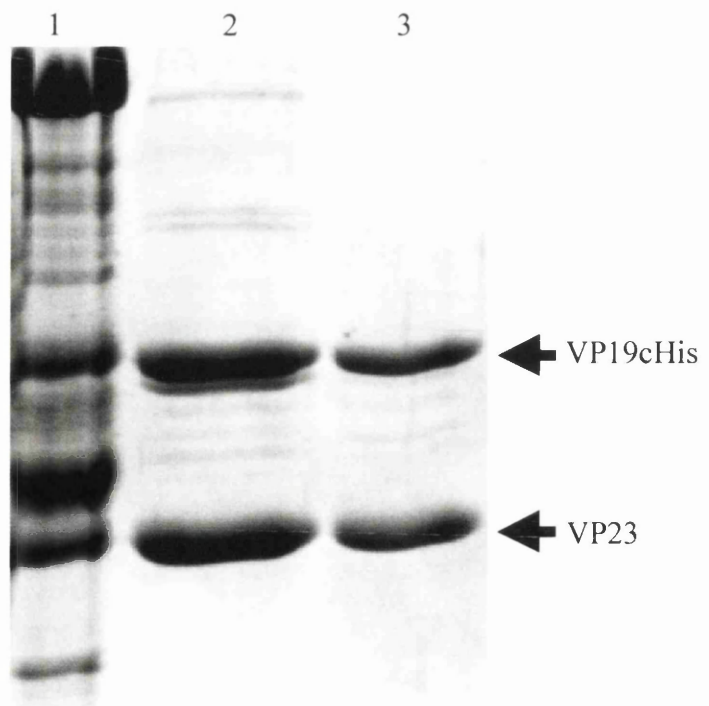
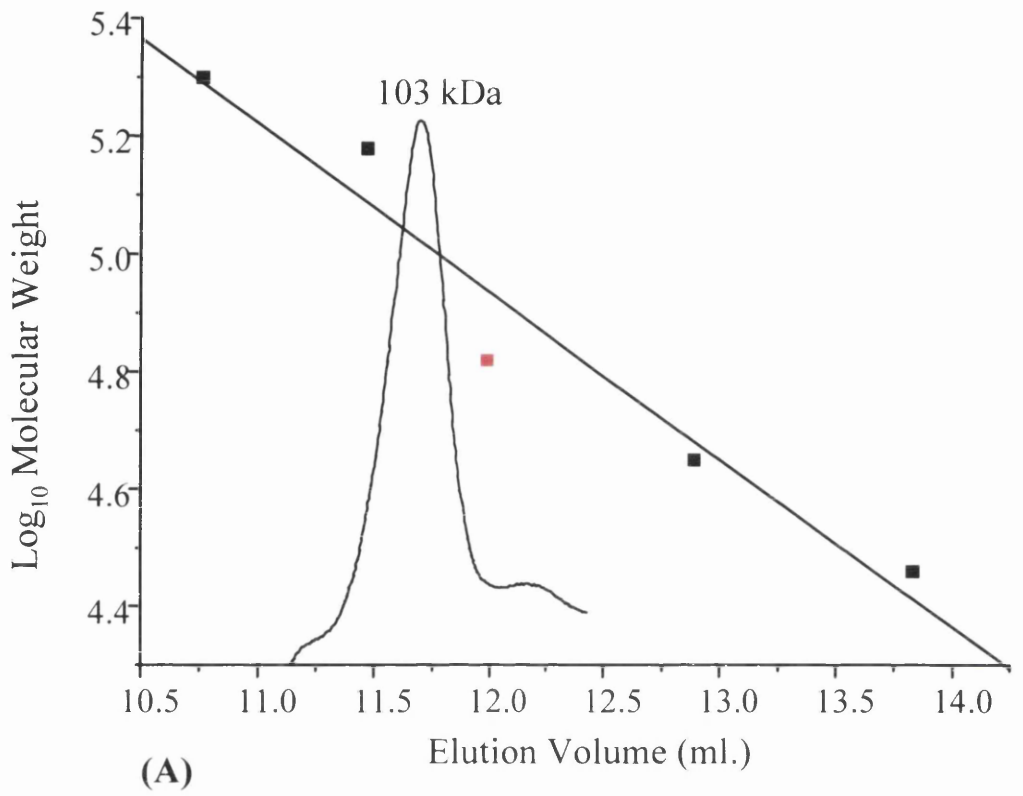
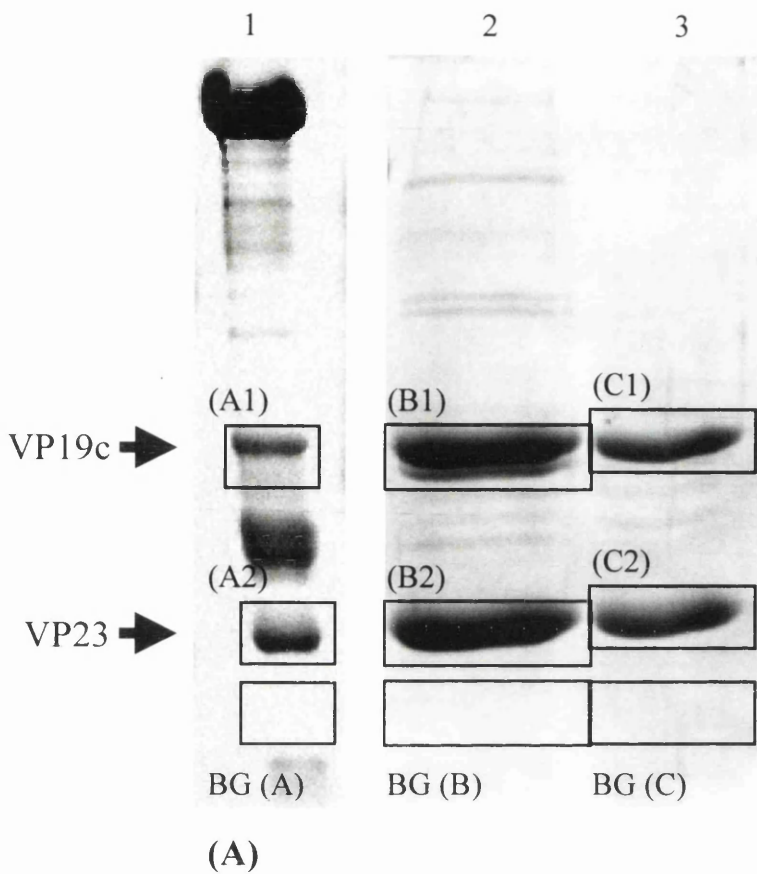


Fig. 3.5.15: Ni-NTA agarose purification of triplex proteins and size exclusion chromatography.

(A) Triplexes were purified in buffer O from SF21 cells infected with Ac18386 (as described in Methods and in fig. 3.5.7). Triplex proteins (0.5mg/ml) were analysed on a 25ml (1 by 30 cm) Superose 12 gel filtration column (Pharmacia) using a 1ml injection superloop. The column was equilibrated and run in buffer O at a constant flow rate of 0.5 ml/min. 0.5 mg/ml of commercially available protein standards;  $\beta$ -amylase (MW, 200,000), alcohol dehydrogenase (MW, 150,000), bovine serum albumin (MW, 66,000), ovalbumin (MW, 45,000), and carbonic anhydrase (MW, 29,000) were analysed individually in buffer O (as described in Methods and fig. 3.3.7). A standard curve was generated plotting  $\text{Log}_{10}$  MW against peak elution volume using Origin 3.5 software. The triplex MW was calculated using linear regression analysis software within the Origin 3.5 software package from the standard curve using the peak elution volume from the triplex elution profile. The position of the BSA standard is highlighted by a red square. (B) 20 $\mu$ l of the Ni-NTA agarose purified triplexes ( lane 2) and 20 $\mu$ l of the peak elution fraction (lane 3) following gel filtration was analysed against purified B-capsids by SDS-PAGE and Coomassie Brilliant Blue staining. The arrows indicate the position of the triplex proteins VP23 and VP19cHis.

By size exclusion chromatography analysis only a single peak could be detected corresponding to purified triplexes. This would imply therefore that preformed VP19cHis/VP23 complexes do not exist in equilibrium with their individual components. SDS-PAGE analysis of the peak elution fraction (fig. 3.5.15, panel B, lane 3) indicated the presence of both VP19cHis and VP23 and confirms that the triplex proteins VP19cHis and VP23 are interacting to form a specific complex. The calculated native MW of 103kDa suggests a 2:1 ratio of VP23 to VP19c within the triplex using the predicted MWs of 34268 (VP23) and 50260 (VP19c) Da respectively (McGeoch et al., 1988). In order to confirm this ratio the intensity of Coomassie Brilliant Blue staining was compared for triplex proteins within purified B-capsids, Ni-NTA agarose purified triplex proteins, and triplex proteins collected from the peak fraction collected during size exclusion chromatography. Fig. 3.5.16 (panel A) shows the SDS-PAGE elution profiles used in the analysis and (panel B) shows the quantitative estimates of Coomassie Brilliant Blue bound to the triplex proteins. Using these analyses and determining their intensities relative to the total predicted triplex mass, copy numbers could be estimated for VP19c and VP23 within the triplex. Analysis of triplex proteins from purified B-capsids demonstrated that VP23 and VP19c exist in a 1.8:1.0 ratio which is in agreement with the 2:1 ratio reported by Newcomb et al, (1993). Analysis of the peak fraction from size exclusion chromatography showed a similar ratio (1.7:1.0) of VP23 to VP19c to that obtained from purified B-capsids. This therefore confirms that the single triplex peak seen by size exclusion chromatography represents a VP23/VP19cHis 2:1 heterotrimeric complex.

Analysis of the Ni-NTA purified triplex protein profile before size exclusion chromatography demonstrated a 1.4:1.0 ratio of VP23 to VP19cHis. The slight increase in the proportion of VP19cHis compared to that within purified B-capsids is probably due to the presence of a truncated VP19c molecule which co-purifies with the full length VP19cHis. It is interesting to note that the truncated VP19c protein was not present in the peak fraction purified by size exclusion chromatography. This suggests it is not a component of a triplex complex. The retention in the ability to bind to Ni-NTA agarose would imply that this lower MW form of VP19c is due to the truncation of the C-terminus, resembling those truncation forms of VP19cHis from Ac381 infected cells (section 3.4). The fact that the truncated VP19c molecule does not produce an elution peak during size exclusion chromatography is probably due to the non-specific binding of VP19c to the



Sample	% Adj. Vol.		Relative intensity to triplex mass (%)		Copy number per triplex	
	VP19c	VP23	VP19c	VP23	VP19c	VP23
B-Capsid	(A1)	(A2)	(A1)	(A2)	(A1)	(A2)
	45.14	54.86	53.63	65.17	<b>1.0</b>	<b>1.8</b>
Elution frac. 1	(B1)	(B2)	(B1)	(B2)	(B1)	(B2)
	50.88	49.12	60.44	58.35	<b>1.0</b>	<b>1.4</b>
FPLC peak frac.	(C1)	(C2)	(C1)	(C2)	(C1)	(C2)
	45.84	54.16	54.46	64.34	<b>1.0</b>	<b>1.7</b>

(B)

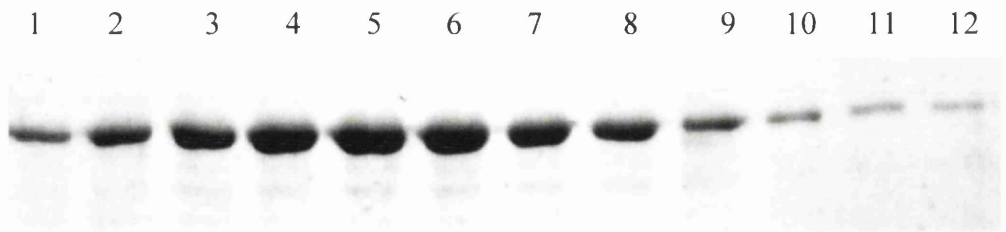
Fig. 3.5.16: SDS-PAGE and ratio analysis of triplex proteins.

Triplexes were purified in buffer O from SF21 cells infected with Ac18386 (as described in Methods and in fig. 3.5.7). (A) 20 $\mu$ l of purified triplex proteins (lane 2) and 20 $\mu$ l of the peak elution fraction collected post gel filtration (lane 3) were analysed against purified B-capsids (lane 1) by SDS-PAGE and stained with Coomassie Brilliant Blue. (B) Using Quantity ONE software (BIO-Rad) the intensity of Coomassie Brilliant Blue binding to the triplex proteins was analysed and adjusted against the appropriate background (BG) control. Using the predicted MWs for triplex proteins (McGeoch et al., 1988) in a 2:1 ratio of VP23 (34268 Da) to VP19c (50260 Da) a total predicted MW could be calculated for a single triplex molecule (118796 Da). Using the predicted MW of the triplex a percentage (%) intensity relative to triplex mass could be calculated for each band analysed. Using the individual predicted MW for the corresponding triplex protein the copy number per triplex could be calculated. Copy numbers are highlighted in bold type.

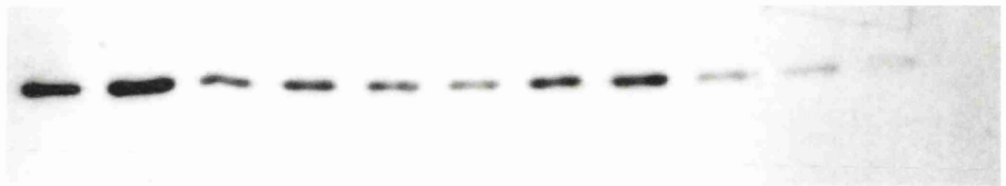
Superose column (discussed in the size exclusion chromatography of VP19cHis in section 3.4). Taken together, these observations suggest that the C-terminus of VP19c is required for interaction with VP23 and confirms published deletion mutagenesis studies performed by Desai and Person (1996) and Spencer et al., (1998). Spencer et al., (1998) demonstrated that the removal of 15 amino acids from the C-terminus of VP19c, abolished the interaction with VP23 and as a consequence prevented capsid formation.

### 3.5.7 Sucrose gradient sedimentation analysis of Ni-NTA agarose purified triplexes

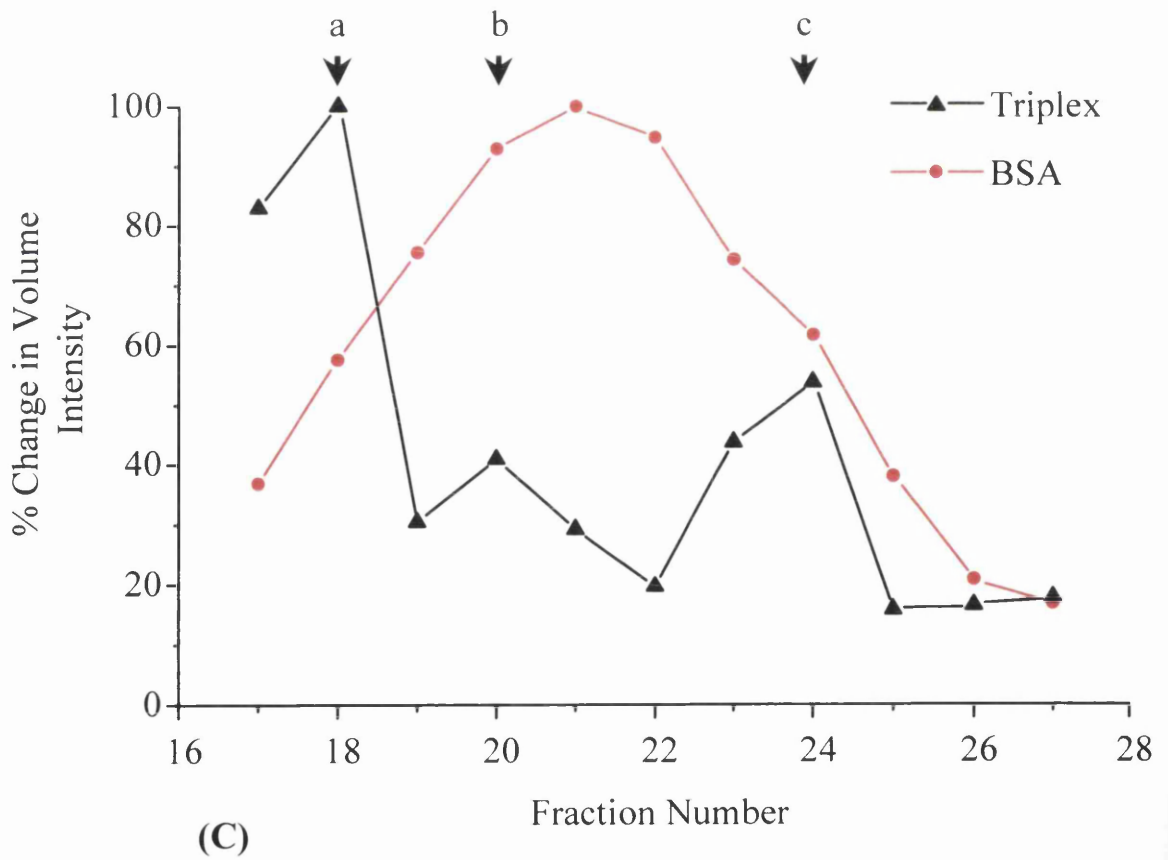
Sucrose gradient sedimentation of Ni-NTA agarose purified triplex proteins from SF21 cells infected with Ac18386 generated a profile which resembled that of individually purified and mixed VP23His and VP19cHis triplex proteins in buffer O (fig. 3.5.17, panel C compared to fig. 3.4.15, panel C). Fig. 3.5.17 (panels A and B) shows the SDS-PAGE and Western blot profiles of BSA and purified triplexes respectively following sucrose gradient centrifugation. The relative intensities were calculated for each fraction for both BSA and VP19cHis and plotted as a percentage (%) change in volume intensity against their appropriate fraction number (fig. 3.5.17, panel C). As with the *in vitro* mixing of individually purified triplex proteins the Ni-NTA co-purification of VP19cHis and VP23 gave rise to three detectable peaks (arrows a-c) with the peak intensity occurring in fraction 18 (indicated by arrow a). This peak sediments substantially further through the gradient than BSA and represents the majority of the purified protein present on the gradient. This presumably represents the expected heterotrimeric triplex complex. The two additional peaks (arrows b and c) could represent partially assembled triplexes (a 1:1 ratio of VP23/VP19cHis for peak b) or uncomplexed VP19cHis (peak c). Indeed, peak c corresponds exactly to the position on the sucrose gradient (fraction 24) of individually purified VP19cHis in buffer O (fig. 3.4.14, panel B). Size exclusion chromatography analysis of purified triplexes demonstrated that triplexes do not exist in equilibrium with their basic protein constituents. Furthermore, Coomassie Brilliant Blue binding analysis demonstrated that the Ni-NTA purified triplex proteins existed primarily in a 2:1 ratio if the C-terminal break down product of VP19c is taken into consideration. As no evidence of the C-terminal truncated product could be detected by Western blot analysis the two



(A)



(B)



(C)

Fig. 3.5.17: Sucrose gradient sedimentation analysis of Ni-NTA purified triplex proteins.

Triplexes were purified in buffer O from SF cells infected with Ac18386 (as described in Methods and fig. 3.5.7). 300µl of purified protein (~0.2mg/ml) and 50µl BSA (5mg/ml) resuspended in buffer O was layered onto a 5ml 5-25% sucrose gradient. The proteins were centrifuged at 4°C for 16 hours at 40,000 r.p.m. in a AH650 rotor and 150µl fractions collected (as described in Methods). To analyse the distribution of BSA across the gradient 20µl of fractions 17-28 (lanes 1-12) were analysed by SDS-PAGE and stained with Coomassie Brilliant Blue (A). To analyse the distribution of triplexes across the gradient 20µl of fractions 17-28 were resolved by SDS-PAGE and analysed by Western blotting (B). VP19cHis distribution was detected by probing the Nitrocellulose membrane with a 1:1000 dilution of the Penta His antibody (Qiagen). The relative intensity of the protein profiles was calculated individually for both VP19cHis and BSA using Quantity ONE software (BIO-Rad) (as described in Methods). The data for the triplex and BSA protein profiles was individually plotted as % change in relative intensity against their appropriate elution fraction number (C). The arrows (a-c) mark the peak intensities in the distribution of VP19cHis across the gradient.

additional peaks observed (peaks b and c) might represent the break up of *in vivo* formed Ni-NTA purified triplexes. As previously discussed in section 3.4 sucrose has been implicated in the disassembly of procapsids isolated by immune precipitation and centrifugation through a 30% sucrose cushion (personal communication, Newcomb, 1999; Newcomb et al., 1999; Newcomb et al., 2000). Taking this into consideration sucrose may be able to disrupt triplex protein-protein interactions. Although the sedimentation analysis demonstrated a distinct triplex peak (fig. 3.5.17, peak a), the sucrose in the gradient may be able to disassemble complexes, which have not completely associated, or complexes that have not correctly folded into a native heterotrimeric complex. Alternatively, Ni-NTA agarose purification of triplexes from Ac18386 infected SF cells may result in the purification of uncomplexed VP19cHis. Although, the expression of VP19cHis is generally lower than that of VP23 (as determined by Coomassie Brilliant Blue staining), some of the VP19cHis molecules may be mis-folded as individual molecules. Thus, although these molecules may not be able to form triplexes they could be purified using Ni-NTA agarose. Size exclusion chromatography would be unable to detect the presence of such mis-folded molecules due to the non-specific binding of VP19c to the Superose column (discussed in section 3.4). However, further analysis is required in order to specifically identify these lower MW peaks.

### 3.5.8 Conclusions

Triplexes could be readily purified from SF21 cells infected with either Ac18638 or Ac18386 utilising Ni-NTA agarose affinity chromatography that maintained reasonable solubility in buffer O. The insolubility of the purified triplex proteins in other purification buffers probably reflects the aggregation of triplexes and/or VP19c molecules due to non-specific hydrophobic interactions. The non-ionic detergent octyl- $\beta$ -glucoside is apparently able to bind to exposed hydrophobic domains and prevent the aggregation of triplexes during purification. Indeed, octyl- $\beta$ -glucoside has been shown to be efficient in the solubilisation of a number of membrane associated glycoproteins (Rohrer et al., 1990). The generally poor solubility of purified triplexes is not surprising considering the number of functions VP19c performs during procapsid formation, capsid maturation, and ultimately virion assembly. VP19c has been shown not only to form extensive interactions

with VP23 within the triplex but also to interact with VP5 from adjacent capsomers (Zhou et al., 1994; Saad et al., 1999; Zhou et al., 2000). Recent cryo-EM analysis has revealed that VP19c may also play an integral role within the structural organisation of the tegument that surrounds the capsid during virus infection (Zhou et al., 1999). Although the relevant tegument proteins have yet to be identified, cryo-EM analysis has revealed extensive interactions between tegument proteins and the triplexes ( $T_a$  and  $T_c$ ). Furthermore, cryo-EM can only detect those protein-protein interactions that display an icosahedrally ordered symmetry. It is possible therefore that the other triplexes ( $T_b$ ,  $T_d$ ,  $T_e$  and  $T_f$ ) may also play a role in the structural organisation of the tegument. Indeed, cryo-EM analysis of the SCMV virion has established that the triplex protein homologues within SCMV B-capsids binds to a tegument protein dimer postulated to be the 119kDa basic phosphoprotein (BPP). These protein dimers were present on all of the triplexes within the SCMV B-capsid (Trus et al., 1999). Furthermore, cryo-EM analysis of HCMV virions demonstrates that the VP19c homologue component within the triplex of HCMV capsid, the minor capsid protein (mCP), also demonstrates a significant amount of interaction with as yet unknown HCMV tegument capsid proteins. Although the mCP binding protein is 17kDa smaller than its HSV counterpart VP19c (50kDa), the function of the mCP binding protein within the HCMV capsid as part of a heterotrimeric complex appears similar (Butcher et al., 1998). The mCP binding protein interacts with and joins adjacent pentons and hexons through the interaction with the major capsid protein (MCP), the homologue to VP5 within the HSV capsid, within the HCMV capsid. The mCP binding protein also interacts with several tegument proteins within the HCMV virion in the same manner in which VP19c appears to within the HSV-1 virion and therefore demonstrates the conserved nature of the triplex function throughout the herpesvirus family.

Ni-NTA agarose purification in the presence of 8M urea showed that the triplex proteins VP23 and VP19c were not linked by inter-molecular disulphide bonds (fig. 3.5.13). However, non-reducing SDS-PAGE analysis demonstrated that there may be some intra-molecular disulphide bonding in triplexes (fig. 3.5.14). Size exclusion chromatography analysis of Ni-NTA purified triplexes gave a native MW of 103kDa and suggested that triplexes do not exist in equilibrium with their constituent protein. Measuring the intensity of Coomassie Brilliant Blue stain binding to triplex proteins from purified B-capsids and

from the peak elution fraction from size exclusion chromatography analysis of Ni-NTA purified triplex proteins confirmed that the triplex was indeed composed of one copy of VP19c to two copies of VP23. This is in agreement with the 2:1 ratio of VP23 to VP19c determined by comparing 2M GdnHCl treated B-capsids with WT B-capsid by STEM analysis (Newcomb et al., 1993). More recently, high-resolution cryo-EM analysis of HSV-1 B capsids and difference mapping using VP5-VP19c particles has determined the locations of VP19c and VP23 proteins within the triplex (Saad et al., 1999). By computationally comparing the triplex and VP19c connecting densities, Saad and co-workers could identify masses within the triplex that corresponded to a single copy of VP19c and two copies of VP23 (discussed in detail within section 4).

#### *3.5.9.1 Future work*

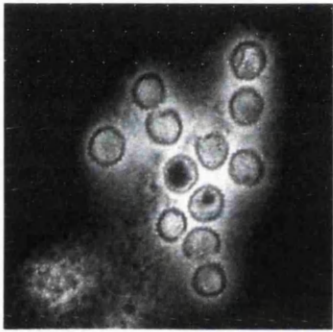
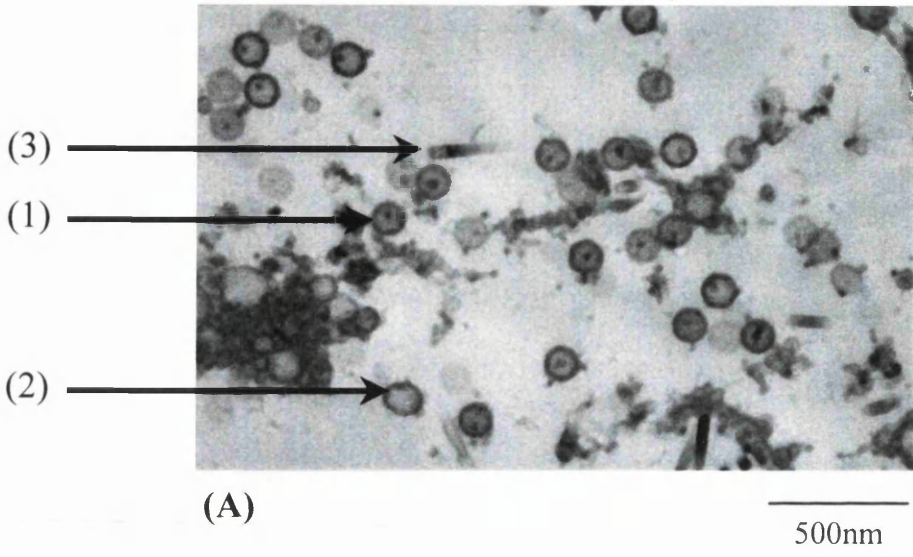
Much work has been done to solubilise the Ni-NTA purified triplexes from both Ac18638 and Ac18386 infected SF cells (table 3.5.1). It would be interesting, therefore, to continue and improve upon this solubilisation strategy utilising octyl- $\beta$ -glucoside in order to produce higher concentrations of purified triplexes. This would allow further structural analysis to be performed, such as NMR or X-ray crystallography, which could provide further information into the triplexes unique asymmetrical structure within the HSV-1 capsid.

## 3.6 Functional and biophysical characterisation of purified triplexes and triplex proteins

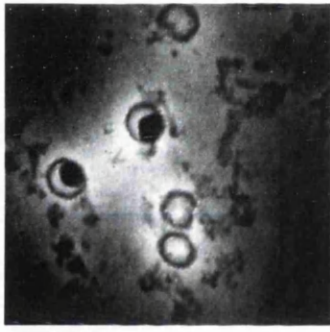
### 3.6.1 *In vivo* and *in vitro* capsid assembly analysis

To test whether or not recombinantly expressed and Ni-NTA agarose purified 6xHis tagged proteins were functional, purified triplexes and triplex proteins were analysed for their ability to participate in the formation of capsid particles *in vitro*. Tatman et al., (1994) and Thomsen et al., (1994) characterised the formation of capsid particles *in vivo* by co-infecting insect cells with panels of recombinant baculoviruses individually expressing the major structural capsid proteins. Newcomb et al., (1994) went on to demonstrate that capsid assembly could occur *in vitro* when lysed, individually infected SF9 cell extracts expressing VP5, VP19c, VP23, and preVP22a were mixed and incubated o/n at 27°C. Subsequently, Newcomb et al., (1999) has shown that *in vitro* assembly could occur using purified VP5, preVP22a and VP23/VP19c (triplexes), and concluded that capsid assembly did not require additional cellular proteins.

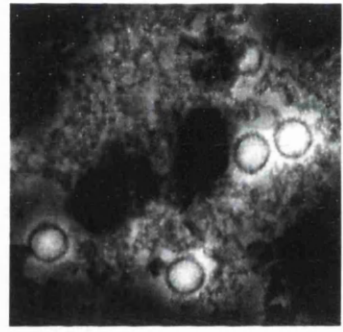
In order to test whether or not the 6xHis tag affected essential protein-protein interactions required for capsid assembly, *in vivo* capsid assembly was examined in SF21 cells, which were co-infected with the appropriate set of recombinant baculoviruses (as described in Methods and fig. 3.6.1). Thin sections were obtained from SF21 cell pellets harvested 48 hours post infection and analysed for the presence of capsids by EM (as described in Methods). The presence of the 6xHis tag on either VP23 or VP19c, when co-expressed together (Ac18638 or Ac18386) or expressed individually in the case of VP19cHis (Ac381), did not appear to effect the formation of capsids *in vivo*. Fig. 3.6.1 (panel A), shows a typical thin section micrograph of *in vivo* formed capsids from SF21 cells co-infected with a three baculoviruses expressing the capsid proteins VP5 (AcUL19), preVP22a (AcUL26.5) and co-expressing VP23His and VP19c (AcUL18638) respectively. *In vivo* formed capsids had similar morphological characteristics to those of WT HSV-1 capsids. Most contained either a scaffold core (panel A, arrow 1), although a small number of coreless particles were also observed (panel A, arrow 2).



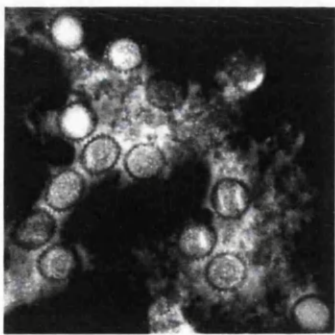
(B)



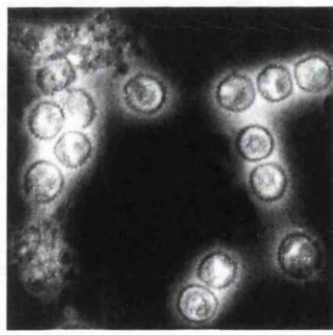
(C)



(D)



(E)



(F)

Fig. 3.6.1: Functional analysis of recombinantly expressed 6xHis tagged proteins.

Capsid assembly was performed either *in vivo* (panels A and F) or *in vitro* (panels B to E) (as described in Methods). Capsid particles were detected by electron microscopy either from thin sections of pelleted infected cells (panel A) or by negative stain of pelleted material (panels B to F) as described in Methods. Panel A; SF21 cells were co-infected with a panel of recombinant baculoviruses, AcUL19 (VP5), AcUL26 (VP21/VP24), and Ac18638 (co-expressing VP23His and VP19c). 48 hours post infection the cells were harvested, fixed and analysed by thin section for the presence of capsid particles. Small cored B-capsids (1), empty A-capsids (2) and baculovirus capsids (3) are indicated by the appropriate arrows. Panels B to E represent negative stained images of capsid particles assembled *in vitro* from lysed crude SF cell extracts individually infected with; AcUL19 (VP5), AcUL26.5 (preVP22a), and Ac18386 (co-expressing VP19cHis and VP23) (panel B); AcUL19 (VP5) and AcUL26.5 (preVP22a), supplemented with purified (VP19cHis/VP23) triplexes (Panel C); AcUL19 (VP5), AcUL26.5 (preVP22a), AcUL18 (VP23), supplemented with purified VP19cHis (Ac381) (Panel D); AcUL19 (VP5), AcUL26.5 (preVP22a), supplemented with individually purified VP19cHis (Ac381) and VP23His (bacterially expressed) (Panel E). (Panel F) Positive control of capsids prepared from SF cells that were co-infected with a panel of baculoviruses, AcUL19 (VP5), AcUL26.5 (preVP22a), AcUL18 (VP23), and AcUL38 (VP19c), which expressed recombinant proteins without any epitope tags. Capsid particles assembled *in vivo* were released from cells by bath sonication and prepared for EM analysis (as described in Methods). Scale bars represent 500 nm.

Utilising the *in vitro* assembly procedure described by Newcomb et al., (1994) Ni-NTA agarose purified triplexes and triplex proteins were analysed for their ability to form capsids. *In vitro* capsid assembly analysis was particularly important for purified VP23His since it was expressed in bacteria and its functionality *in vivo* could not be analysed. It was also important to establish that purification of the proteins did not inhibit their ability to participate in capsid assembly. Typically, 1/10<sup>th</sup> of an SF21 burrler extract(s) was used to supplement the appropriately purified capsid protein(s) under analysis (as described in Methods). Mixed extracts were left o/n at 28°C before the sample was prepared for electron microscopy (as described in Methods). Fig. 3.6.1 (panel B) shows a negative stained image of capsids assembled *in vitro* from lysed SF21 cell extracts individually infected with recombinant baculoviruses expressing VP5 (AcUL19), preVP22a (AcUL26.5), and triplexes (AcUL18386). Distinctive capsid particles are evident, which are identical to those of *in vivo* formed negatively stained capsids (fig. 3.6.1, panel F). Fig. 3.6.1 (panels C-E) show typical examples of the negative stained images obtained from *in vitro* assembled capsids when purified triplexes (VP19cHis/VP23, panel C), purified VP19cHis (panel D), and separately purified VP23His (bacterially expressed pETUL18) + purified VP19cHis (panel E), were mixed with the appropriate infected SF21 cell extracts. In all incidences capsid assembly only occurred when Ni-NTA agarose purified protein(s) were supplemented with the appropriate complementing infected SF21 cell extracts. This clearly demonstrates that the 6x His tag does not inhibit the formation of capsids *in vitro*. The bacterially expressed and purified VP23His participated in *in vitro* capsid assembly in both of the purification buffers used. This suggests that both monomeric (purified in sonication buffer, see section 3.3.3.1) and dimeric (purified in Buffer O, see section 3.3.3.2) VP23His participate effectively in capsid assembly. Furthermore, individually purified VP23His (bacterially expressed) and VP19cHis (baculovirus expressed) were shown to participate in *in vitro* capsid assembly when mixed together (fig. 3.6.1, panel E). Therefore, the purified VP23His and VP19cHis must be capable of forming functional triplexes *in vitro*. Table 3.5.1 summarises both the *in vivo* and *in vitro* capsid assembly data for the Ni-NTA agarose purified triplexes and triplex proteins, and the purification buffers in which the analyses were performed.

Test Sample	Buffer	<i>In vitro</i> capsid assembly	<i>In vivo</i> capsid assembly
Purified VP23His	Sonication buffer	+	N/A
Purified VP23His	Buffer O	+	N/A
Ac18638 infected SF21 cells/extracts	PBSa	+	+
Ac18386 infected SF21 cells/extracts	PBSa	+	+
Purified triplexes (Ac18638)	Buffer O	+	N/A
Purified triplexes (Ac18386)	Buffer O	+	N/A
Ac381 infected SF21 cells/extracts	Buffer O	+	+
Purified VP23His + purified VP19cHis	Buffer O	+	N/A

Table 3.6.1: Functional analysis of triplexes and triplex protein samples to support *in vitro* and *in vivo* capsid formation

It should be noted that *in vitro* capsid formation using Ni-NTA agarose purified triplexes and triplex proteins was particularly sensitive to protein concentration. The formation of capsids *in vitro* was much less efficient when purified protein samples were <0.3mg/ml. This probably represents a limiting factor during the formation of capsids and/or the polymerisation of capsid protein subunits. Thus, although capsid assembly may begin there may not be a sufficient local concentrations of uncomplexed purified protein immediately available to drive capsid assembly to completion (Zlotnick, 1994). Indeed, concentration dependent *in vitro* capsid assembly has also been reported for P22 and  $\phi$ 29 bacteriophages (Prevelige et al., 1993b; Lee and Guo, 1995).

### **3.6.2 Biophysical characterisation of the HSV-1 triplexes and triplex protein constituents**

Although the individual protein components of the HSV-1 capsid have been known for some time (Gibson and Roizman, 1972) virtually nothing is known about their properties before they become associated within the mature icosahedral capsid. It is now becoming clear that capsid assembly in icosahedral viruses requires numerous complex folding stages where a capsid protein's conformation may change throughout the course of capsid assembly (Johnson, 1996; Tuma et al., 1998). Techniques such as fluorescence, near/far-UV circular dichroism (CD), nuclear magnetic resonance (NMR), differential scanning calorimetry (DSC), and 8-anilino-1-naphthalenesulfonate (ANS) binding studies are becoming increasingly popular for studying the dynamics of protein folding and conformational stability of proteins. These techniques were applied whenever possible to Ni-NTA agarose purified triplexes and triplex proteins in an attempt to understand their properties better.

#### *3.6.2.1 Homogeneity of Ni-NTA agarose purified triplexes and triplex proteins used for biophysical experimental analysis*

Purification protocols for the isolation and solubilisation of triplexes and triplex proteins have been discussed in detail in previous sections. Biophysical characterisation experiments were carried out on Ni-NTA agarose purified triplexes from SF21 cells

infected with Ac18386. To ensure an accurate 2:1 ratio of VP23 to VP19cHis within the heterotrimer complex, triplexes were further purified by size exclusion chromatography. The peak elution fraction was collected and used for biophysical analysis. In Ni-NTA agarose purified VP19cHis samples a 90kDa protein typically eluted from the Ni-NTA agarose in the first and second elution fractions. Therefore, for all VP19c biophysical characterisation experiments only the third and subsequent elution fractions were used for experimental analysis. Due to the importance of maintaining protein sample homogeneity in order to obtain consistent and reproducible biophysical data, all Ni-NTA agarose purified samples were analysed by SDS-PAGE and Coomassie Brilliant Blue staining. Accurate protein concentrations were obtained by measuring protein absorbance at OD<sub>280</sub> using a Beckman DU-60 spectrophotometer (as described in Methods).

### *3.6.2.2 Ni-NTA purified triplexes and triplex proteins are folded protein molecules*

As previously discussed in section 3.4, fluorescence spectroscopy can be used to measure the extent of which tryptophan (Trp) side chains are buried within the interior of a protein molecule. Fig. 3.6.2 (panels A-C) shows the fluorescence emission spectra for purified VP23His, VP19cHis, and purified triplexes following excitation at 295nm. The emission spectra all demonstrate a significant shift in  $\lambda_{\max}$  from the value of 356nm which is associated with exposed Trp side chains within small model compounds. This indicates that the single Trp residue within VP23His and the 7 Trp residues within VP19cHis are buried or partially buried within the interior of a folded protein molecule. This is confirmed by comparing the  $\lambda_{\max}$  value of 335nm for purified native VP19cHis (fig. 3.6.2, panel B) with the value of approximately 360nm for VP19cHis purified by urea denaturation of triplexes isolated from SF21 cells infected with Ac18386 (fig.3.4.4, panel B). The  $\lambda_{\max}$  for purified triplexes (331nm) also demonstrates that the 9 Trp residues (2 Trp residues from 2x VP23 molecules and 7 from 1x VP19c molecule) are buried or partially buried within the interior of the complex. This implies that the protein-protein interaction between VP23 and VP19cHis within the triplex does not lead to conformational rearrangements that result in the exposure of these Trp residues to the solvent.

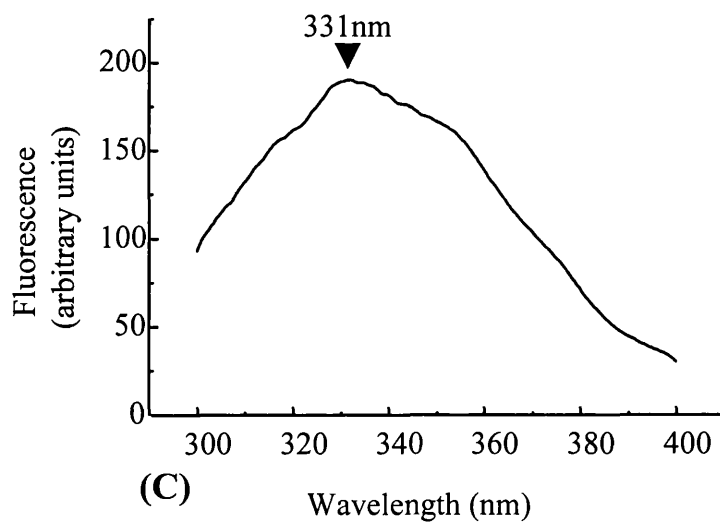
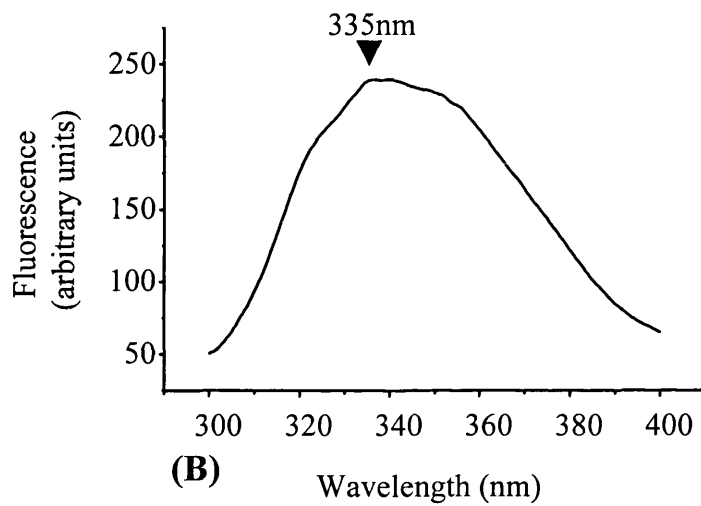
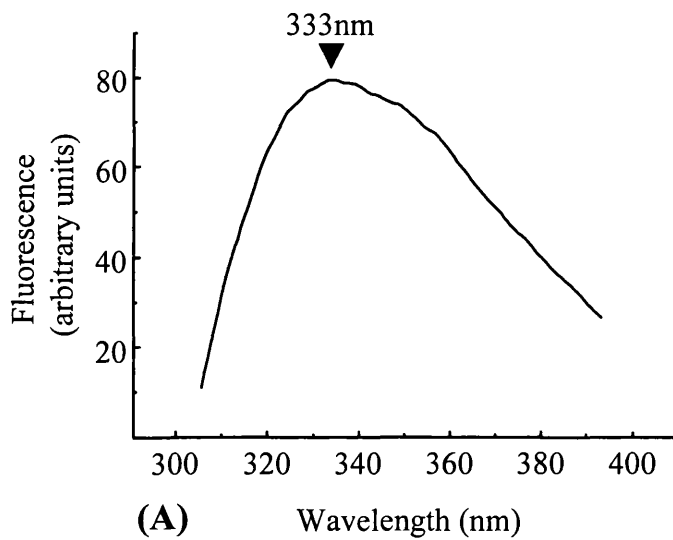
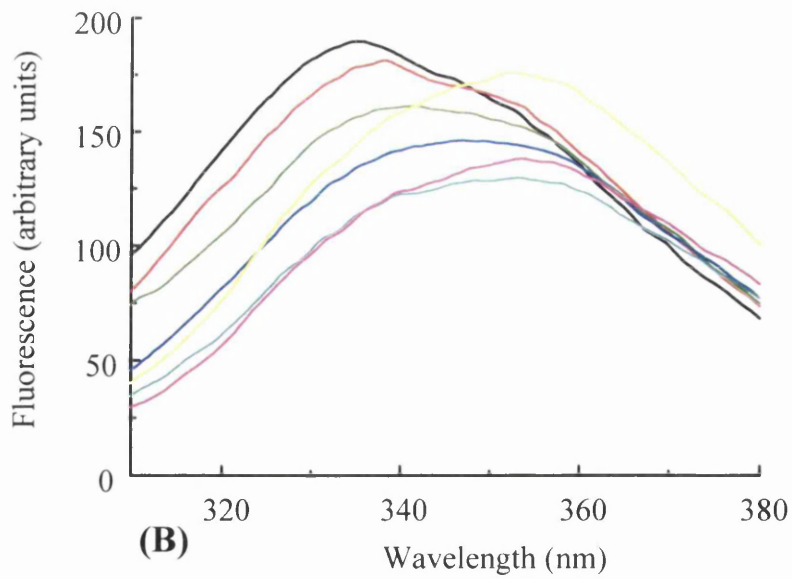
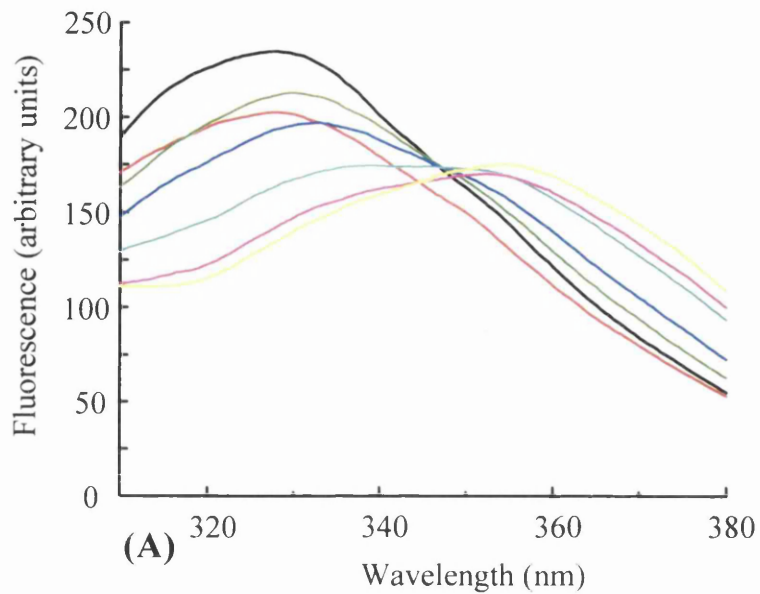


Fig. 3.6.2: Intrinsic fluorescence spectra of Ni-NTA agarose purified VP23His, VP19cHis and triplexes.

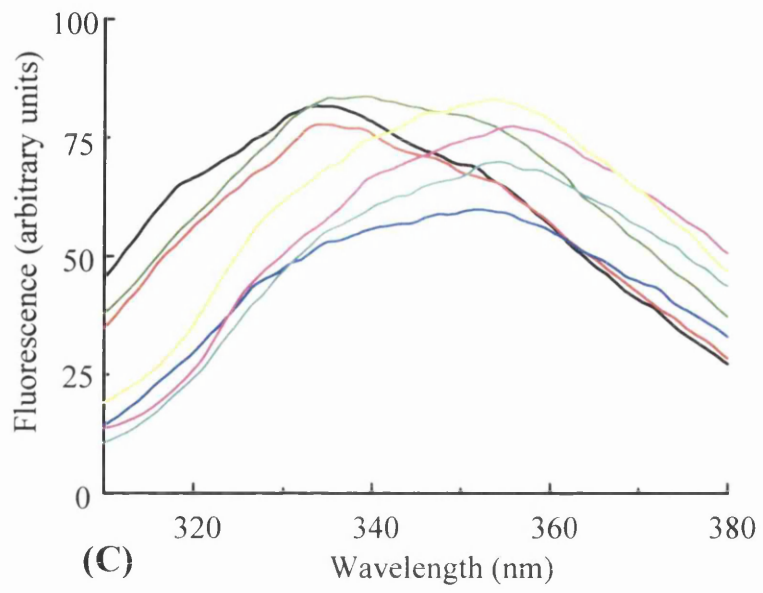
Fluorescence profiles for purified VP23His (0.2mg/ml) in buffer P (A), purified VP19cHis (0.1 mg/ml) in buffer O (B), purified triplexes (0.2 mg/ml) in buffer O (C) were monitored following excitation at 295nm (as described in Methods). All spectra were corrected for buffer absorbance by subtraction of the appropriate buffer-only spectra. The peak values are marked by the appropriate arrows.

### 3.6.2.3 *GdnHCl* induced unfolding of triplexes and triplex proteins

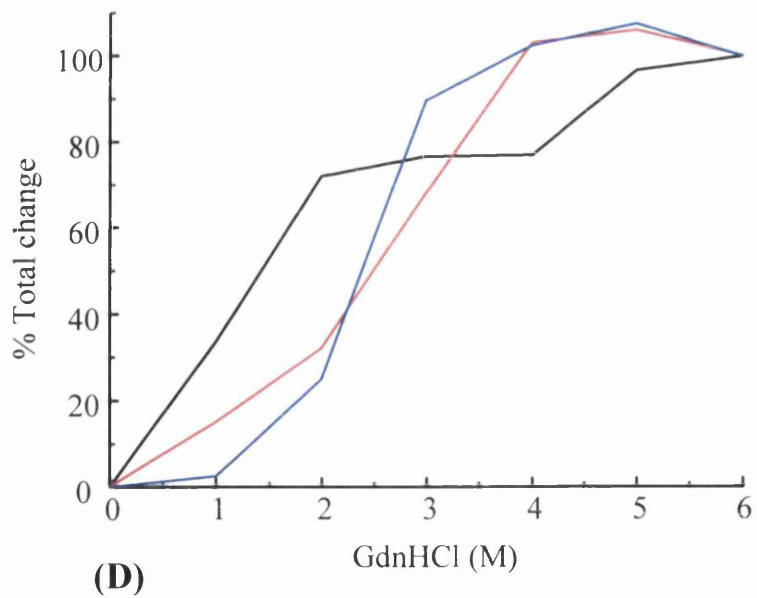
Fluorescence spectroscopy can also be used to monitor the induced unfolding of protein molecules and complexes by measuring the fluorescence of a protein or protein complex in the presence of guanidine hydrochloride (GdnHCl). Exposure to increasing concentrations of GdnHCl results in the loss of protein structure and will eventually lead to a protein molecule adopting a random coil conformation where all the Trp residues are exposed to the solvent (Nishina et al., 1977). Unfolding of purified triplexes and triplex proteins induced by GdnHCl denaturation was therefore monitored by measuring their intrinsic Trp fluorescence. Fig. 3.6.3 (panels A-C) shows the spectra of purified VP23His, VP19cHis and triplexes in the presence of increasing concentrations of GdnHCl. VP23His, VP19cHis, and triplexes all demonstrated a shift in  $\lambda_{\max}$  towards 356nm which clearly indicates the progressive unfolding of protein structure, resulting in the increased exposure of Trp side chains to the solvent. Fig. 3.6.3 (panel D) shows the profile of GdnHCl induced protein unfolding of as a plot of the percentage change in  $\lambda_{\max}$  against the molarity of GdnHCl. VP23His exhibited a rapid loss in protein structure with 70% of the total shift occurring in the presence of 2M GdnHCl, compared to a shift of 30% and 20% for VP19His and triplexes respectively. Increasing the concentration of GdnHCl to 4M resulted in little further shift in  $\lambda_{\max}$  for VP23His but had a major effect on protein structure for VP19cHis and triplexes. Increasing the GdnHCl concentration above 4M GdnHCl resulted in a gradual loss of the remaining protein structure for VP23His with little further effect on VP19cHis and triplexes. These data suggest that VP23His unfolds in the presence of low concentrations of GdnHCl (1-2M GdnHCl), while the induced protein unfolding of triplexes and VP19cHis proves to be more resistant to GdnHCl denaturation with the loss of the majority of protein structure occurring between 2-3 M GdnHCl. Ni-NTA agarose purification experiments of VP19cHis performed by denaturation of triplexes in 3M urea (approximately 1.5M GdnHCl) resulted in the almost complete loss of the VP23/VP19cHis heterotrimer interaction, as determined by SDS-PAGE and Coomassie Brilliant Blue staining (fig. 3.4.3). This suggests that the transition observed for purified triplexes between 1-2M GdnHCl might be attributed to the denaturation of structural elements that are involved in the association of VP23 with VP19cHis. Furthermore, VP19cHis can be seen to begin unfolding in 1M GdnHCl whereas triplexes do not appear to undergo any significant transitions in unfolding until



— 0M GdnHCl    — 1M GdnHCl    — 2M GdnHCl  
— 3M GdnHCl    — 4M GdnHCl    — 5M GdnHCl    — 6M GdnHCl



— 0M GdnHCl    — 1M GdnHCl    — 2M GdnHCl  
 — 3M GdnHCl    — 4M GdnHCl    — 5M GdnHCl    — 6M GdnHCl



— VP23    — VP19c    — Triplexes

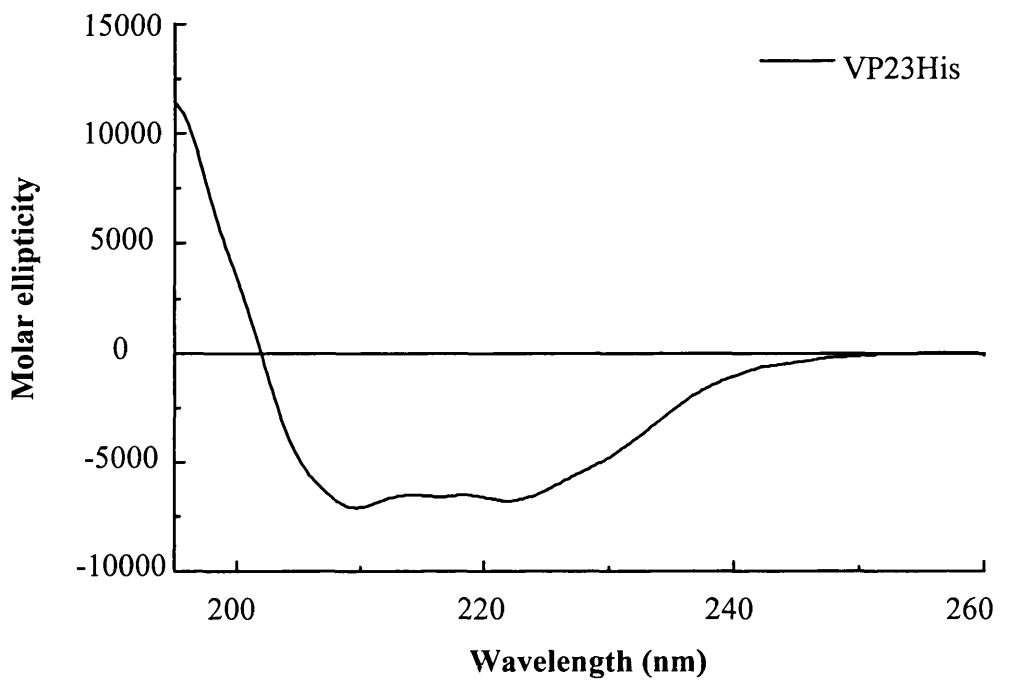
Fig. 3.6.3: Structural stability analysis of Ni-NTA agarose purified VP23His, VP19cHis and triplexes by GdnHCl induced unfolding.

Trp fluorescence was monitored for purified VP23His (0.2mg/ml) in buffer P (A); VP19cHis (0.2mg/ml) in buffer O (B); triplexes (0.2mg/ml) in buffer O (C); in the presence of increasing concentrations of GdnHCl (0-6M). (D) The observed change in  $\lambda_{\text{max}}$  was plotted as a percentage change in  $\lambda_{\text{max}}$  against the appropriate concentration of GdnHCl used to induce unfolding. All traces were corrected for buffer absorbance by subtraction of the appropriate buffer only spectra.

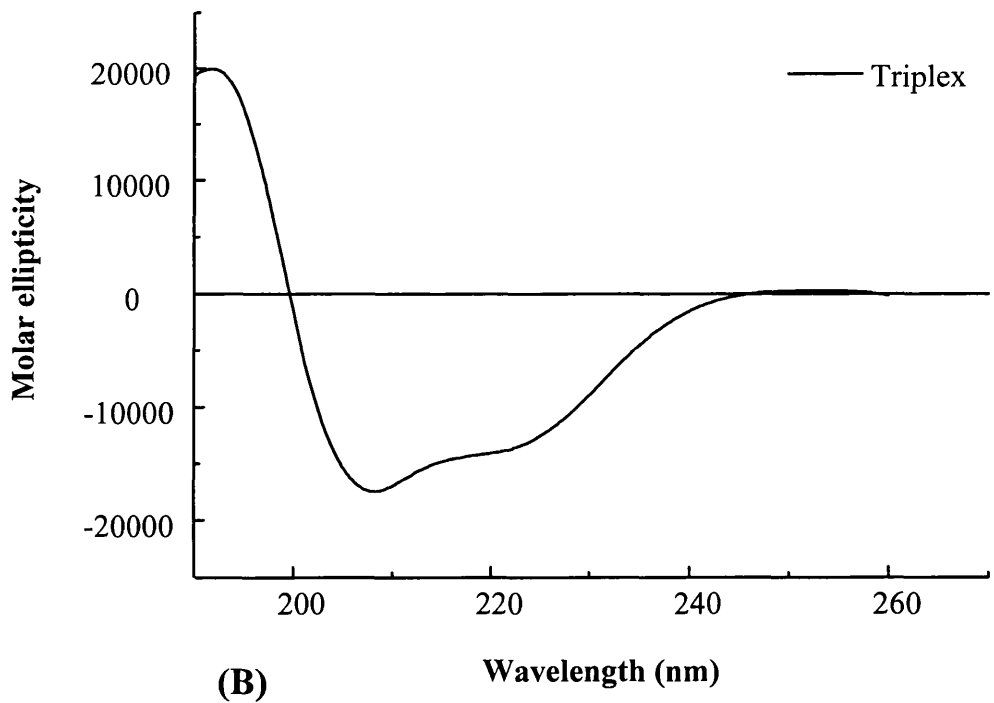
incubated in the presence of 2M GdnHCl. It is interesting to note that GdnHCl denaturation experiments performed by Newcomb et al., (1993) on purified B-capsids resulted in the loss of pentons and the triplexes T<sub>a</sub> and T<sub>c</sub> in the presence of 2M GdnHCl. Newcomb and co-workers further reported that increasing the GdnHCl concentration to 2.5M GdnHCl did not lead to the additional loss of triplexes from the capsid but did result in the partial disintegration in hexon structure, although no hexons were removed from the capsids. Incubating purified B-capsids in the presence of 3M GdnHCl resulted in the complete solubilisation of capsids (Newcomb and Brown, 1991). Incubating purified triplexes in the presence of 2-3M GdnHCl resulted in the largest shift in  $\lambda_{max}$ . Although it is tempting to speculate that the loss of T<sub>a</sub> and T<sub>c</sub> triplexes in 2M GdnHCl was a direct result of triplex unfolding not all triplexes were disassociated from treated capsids (Newcomb et al., 1993). This implies that the stability of the triplex varies depending upon their position within the capsid. Observations made by cryo-EM analysis of HSV-1 capsids demonstrates that this stability may be attributable to significant differences in the intercapsomeric connections formed by the triplexes T<sub>a</sub>-T<sub>f</sub> with their surrounding capsomers (Zhou et al., 1994; Zhou et al., 1998; Zhou et al., 2000). Furthermore, triplexes have recently been shown to form substantial interactions with the capsid floor (Saad et al., 1999; Zhou et al., 2000). Although these interactions have yet to be fully characterised, the observed differences in the various triplex connections highlights the increased conformational stability that could to be gained by the triplex when in association with other capsid proteins.

#### *3.6.2.4 Far-UV CD analysis of the secondary structure within triplexes and triplex proteins*

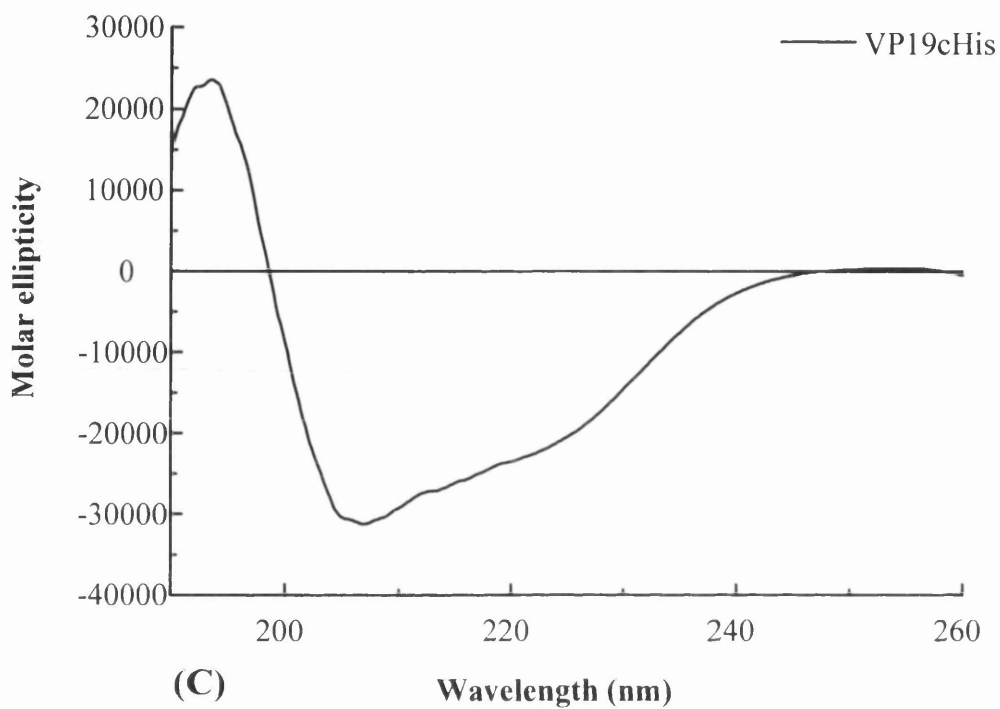
Circular dichroism (CD) can be used to determine the extent of secondary and tertiary structure within a protein molecule or complex by measuring the differential absorbance of chromophores. The chirality of these chromophores can either be intrinsic or because they are placed within an asymmetric environment within the protein structure. Proteins contain a range of chromophores, in particular the aromatic amino acid side chains of phenylalanine (Phe), tyrosine (Try), and tryptophan (Trp). Such aromatic side chains and the disulphide bonds between cysteine residues absorb strongly over the near-UV region of 250-290nm.



(A)



(B)



	PHD			CD		
	$\alpha$ -Helix	$\beta$ -Sheet	Loop	$\alpha$ -Helix	$\beta$ -Sheet	Loop
VP23	31.8%	22.6%	45.6%	24%	30%	46%
Triplex	34.6%	17.7%	47.7%	35%	30%	35%
VP19c	23.2%	15.5%	61.3%	13%	56%	31%

(D)

Fig. 3.6.4: Far-UV CD analysis and CONTIN estimation of secondary structure of purified VP23His, VP19cHis, and triplex.

Absorbance spectra in the Far-UV CD region (180-240nm) for purified VP23His (0.2mg/ml) in buffer P (A); triplexes (0.05mg/ml) in buffer O (B); VP19cHis (0.1mg/ml) in buffer O (C). All traces were corrected for buffer absorbance by subtraction of the appropriate buffer-only spectra. (D) Comparison of secondary structure content of purified triplexes and triplex proteins derived from amino acid sequences submitted to PHD predict ([WWW.embl-heidelberg.de/predictprotein](http://WWW.embl-heidelberg.de/predictprotein)) and CONTIN estimations of secondary structure content of  $\alpha$ -helix and  $\beta$ -sheet from Far-UV CD analysis of A, B, and C.

However, the strongest absorption within the UV range is that of peptide bonds which absorb in the far-UV region (180-240nm) (Price, 1995; Kelly and Price, 1996). Far-UV CD analysis can be used to assess quantitatively the overall secondary structure content of a protein due to the characteristically different absorption's of  $\alpha$ -helix and  $\beta$ -sheet within the far-UV region. For example,  $\alpha$ -helices give characteristic absorption peaks at 208 and 222nm (Hirst and Brooks, 1994). By applying the CONTIN procedure of Provencher and Glöckner (1981) the amount of secondary structure within a protein molecule can be determined. The CONTIN procedure utilises the far-UV CD absorption spectrum and applies a linear combination of CD spectra from 16 proteins that have had their structures resolved by X-ray crystallography. Within this procedure greater weight is automatically applied to those reference spectra that closely resemble those of the analysed sample. This therefore allows reliable and quantitative measurement of the amount of secondary structure a protein molecule or protein complex contains. Fig. 3.6.4 (panels A-C) shows the far-UV CD spectra for Ni-NTA purified VP23His, VP19cHis and triplexes after subtraction of the appropriate buffer control spectra. VP23His, VP19cHis and triplexes all produce absorption spectra that demonstrate significant amounts of secondary structure associated with folded protein molecules (Kelly and Price, 1996). Application of the CONTIN procedure to these spectra provides a quantitative assessment of the secondary structure content of  $\alpha$ -helix and  $\beta$ -sheet within these protein molecules. Fig. 3.6.4 (panel D) shows the comparison between the estimated secondary structures determined from the application of the CONTIN procedure and the predicted secondary structures from the secondary structure prediction program PHD (Rost and Sander, 1993). PHD predictions were acquired by submitting the amino acid sequences of VP23 and VP19c, or in the case of the triplex a compilation made by assembling a VP19c and two VP23 sequences. It should be noted that experimental values obtained by CD can be affected by small errors in protein concentration determination and high levels of noise, particularly in the absorption region below 190nm, which may be brought about by components within purification buffers, especially imidazole and  $\text{Cl}^-$  ions. Utilising Ni-NTA agarose affinity chromatography to purify recombinantly expressed 6x His tagged proteins resulted in the presence of imidazole within the elution buffer (typically >100mM). In all incidences the imidazole was removed from the protein samples prior to analysis by dialysis or gel filtration of purified protein samples. Far-UV CD analysis was repeated multiple times on different samples. Both VP23His and triplexes gave reproducible spectra and consistent

CONTIN estimations for the content of secondary structure (fig.3.6.4, panel D). However, attempts to obtain a reproducible far-UV CD spectra for VP19cHis proved difficult. Dialysis of purified VP19cHis (o/n at 4°C) to remove imidazole from the elution buffer resulted in the majority of VP19cHis precipitating out of solution. Shorter periods of dialysis were employed, both at RT and 4°C, but either resulted in the protein precipitating out of solution or were ineffective in lowering the concentration of imidazole sufficiently to reduce the high level of noise in the far-UV absorption region. Attempts to remove imidazole from purified VP19cHis protein samples by size exclusion chromatography also failed due to the non-specific binding of VP19cHis to the Superose matrix (discussed in section 3.4.5). Similarly, attempts to remove imidazole through the use of desalting columns failed due to non-specific binding of VP19cHis to the various column matrices (data not shown). A CONTIN prediction of secondary structure obtained from a successful scan of purified and dialysed VP19cHis is shown in fig. 3.6.4 (panel D highlighted in red). However, it should be noted that this result has yet to be confirmed.

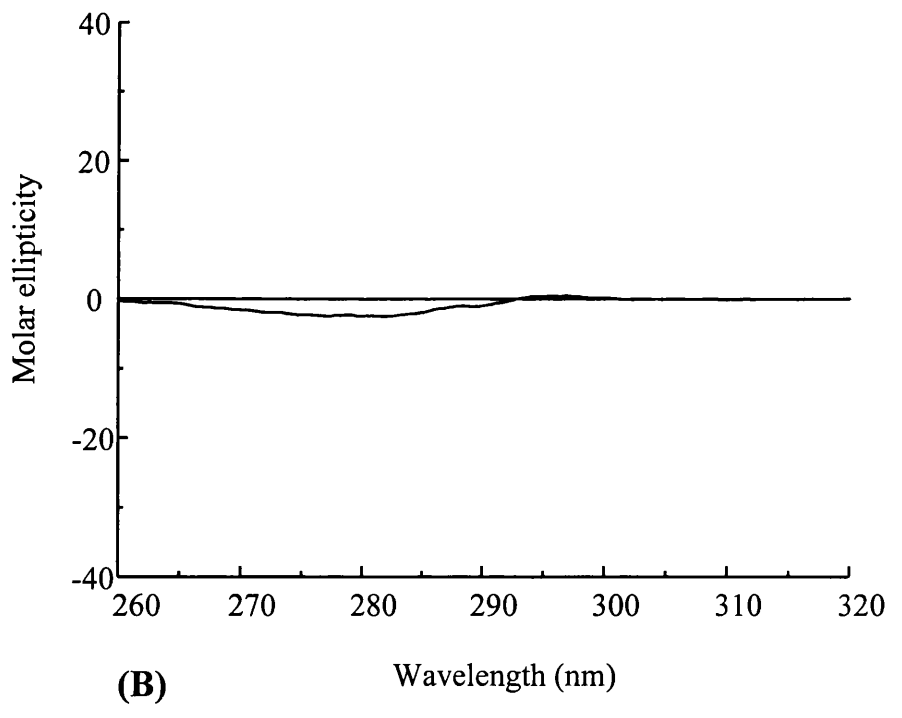
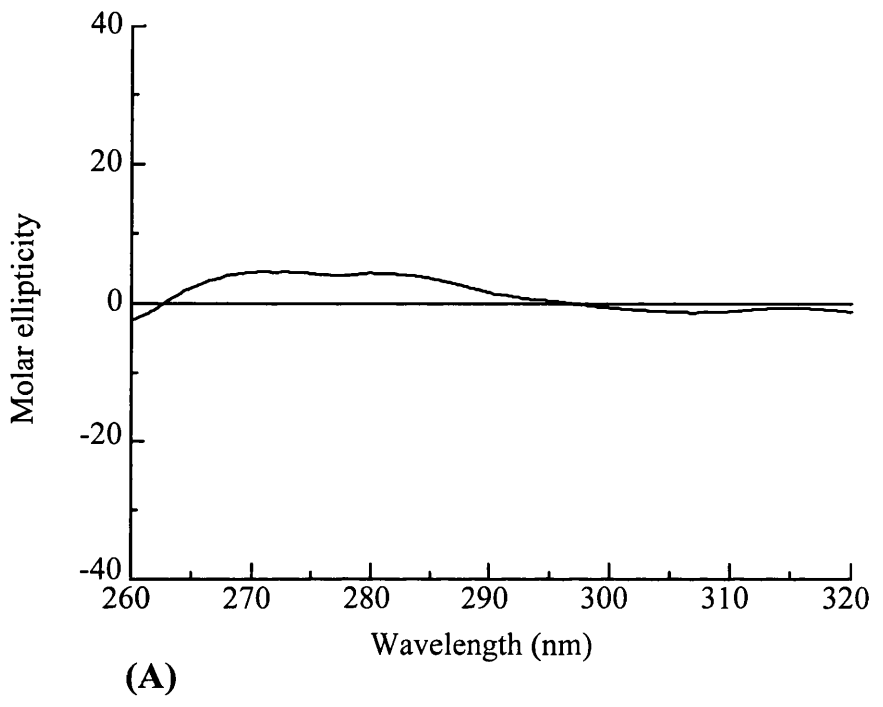
Furthermore, it should also be noted that protein prediction programs such as PHD rely heavily on the degree of similarity between the submitted amino acid sequences and that of protein sequences compiled within the database. Therefore, errors in the estimation of secondary structure content for a given amino acid sequence may occur due to no suitable sequence counterpart within the database.

Comparison of the secondary structure of VP23His and triplexes derived experimentally from far-UV CD/CONTIN analysis with the predicted secondary structure reveals a reasonably close correlation although the figures for VP19c are more divergent. Nevertheless, the spectra for both VP23His and triplexes, as well as the spectra obtained for purified VP19cHis, demonstrated that triplexes and individual triplex proteins contain a significant degree of secondary structure. Purified triplexes and triplex proteins therefore represent, at least, partially folded protein molecules. Although difficulties were experienced in obtaining far-UV CD spectra for VP19cHis, the CONTIN prediction for secondary structure for purified triplexes has approximately 10% more  $\alpha$ -helix content compared to that of purified VP23His. This would suggest, therefore, that VP19cHis is contributing to the level of secondary structure within the triplex.

### 3.6.2.5 Near-UV CD analysis of the tertiary structure within triplexes and triplex proteins

Near-UV CD (250-320nm) can be used to analyse the tertiary structure of a protein molecule by measuring the absorbance of the aromatic amino acid side chains, principally those of Phe (255nm), Tyr (275nm), and Trp (290nm). The folding of a polypeptide chain places the aromatic amino acids side chains of these amino acids in a variety of environments which affect their ability to absorb in the near-UV region. The intensity of absorbance by these aromatic side chains reflects the degree to which they are incorporated within a given protein structure. If the protein contains rigid tertiary structure and tightly packed aromatic amino acid side chains then their absorbance within the near-UV CD region is high. Conversely, if the protein lacks substantial tertiary structure and the aromatic side chains can move more freely, then the intensity of absorbance is lower (Kelly and Price, 1996). The near-UV CD spectrum therefore reflects the degree to which stable interactions occur between amino acids and provides a measure of the tertiary structure of a protein molecule.

Fig. 3.6.5 shows the near-UV CD spectra for monomeric and dimeric VP23His and triplexes. The near-UV CD spectra for both monomeric and dimeric VP23His (panels A and B) appear as flat traces. There is no evidence of the distinct peaks expected if the aromatic amino acid side chains occupy fixed positions within the protein structure. This suggests that any tertiary interactions within VP23His are weak and do not result in the formation of rigid tertiary structural domains. Conversely, the near-UV CD spectrum for purified triplexes (fig. 3.6.5, panel C) demonstrated a strong absorbance peak. Therefore, some or all of the aromatic amino acid side chains within the heterotrimeric protein complex occupy fixed positions suggesting that defined tertiary structure exists within the triplex. Because of the relatively high protein concentrations required for near-UV CD analysis, typically 0.5-2 mg/ml, no trace could be obtained for purified VP19cHis due to its relative poor recovery from SF21 cells infected with Ac381 (discussed previously in section 3.4). Therefore, it was impossible to determine whether the near-UV CD spectrum of the triplex solely represents the contribution of VP19c to the heterotrimer complex, or if the tertiary structure observed is at least partly a result of the interaction between the



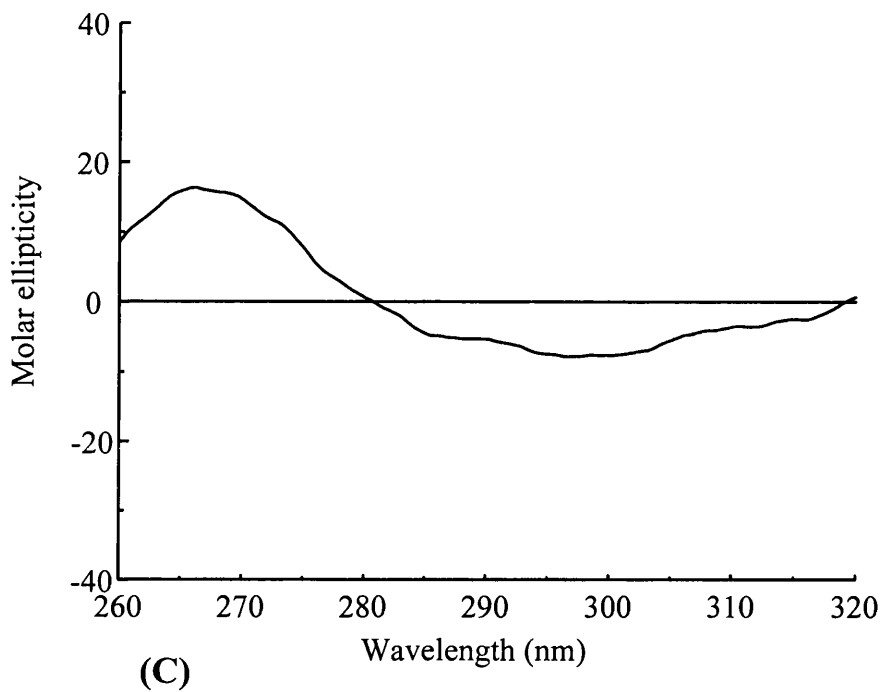


Fig. 3.6.5: Near-UV CD analysis of monomeric, and dimeric VP23His and triplexes

Near-UV CD absorbance spectra for purified monomeric VP23His (1.5mg/ml) in buffer P (A), dimeric VP23His (1.5mg/ml) in buffer O (B), and triplexes (1.5mg/ml) in buffer O (C). All traces were corrected for buffer absorbance by subtraction of the appropriate buffer-only spectra.

VP19c and VP23 protein molecules. For example, if tertiary structure within the triplex is developed through mutual co-folding of VP19c and VP23 during triplex formation.

### 3.6.2.6 DSC analysis of the tertiary structure within triplexes and triplex proteins

The tertiary structure of protein molecules and protein complexes can also be analysed by temperature-induced denaturation through the use of differential scanning calorimetry (DSC). Analysing the heat capacity of a protein molecule provides a thermodynamic description of its conformational stability and provides valuable information on the state of folding adopted under specific conditions (Privalov et al., 1995). The presence of an endothermic transition on a plot of heat capacity versus temperature is usually considered to be a result of co-operative melting of a protein's tertiary structure (Privalov and Potekhin, 1986). A positive enthalpy transition primarily represents the exposure of buried hydrophobic amino acids to the solvent due to the heat induced disruption of van der Waals interactions within the interior of a protein molecule (Dill, 1990; Murphy et al., 1990; Makhatadze and Privalov, 1993; Privalov, 1997). Fig. 3.6.6 (panel A) shows the DSC profile obtained for monomeric VP23His (0.7 mg/ml) purified in buffer P. The profile shows no heat absorption peak suggesting that no endothermic transition has occurred due to the co-operative melting of tertiary structure. The decline in heat capacity above 60°C is due to the irreversible exothermic aggregation of VP23His molecules post-denaturation and reflects the precipitation of unfolded VP23His molecules out of solution (Cooper, 1999). The DSC spectrum for VP23His therefore confirms observations made by near-UV CD analysis and indicates the lack of a rigid tertiary structure within the VP23His protein molecule. Hydrodynamic studies performed by Marina Kirkitadze (Kirkitadze et al., 1998) demonstrated that Ni-NTA agarose purification of VP23His in sonication buffer and subsequent dialysis into buffer P resulted in a predominantly monomeric population of VP23His molecules at concentrations below 0.8mg/ml. Therefore, the DSC analysis described above for VP23His in buffer P represents the native level of tertiary structure within a single monomeric molecule of VP23His. Ni-NTA agarose purification of VP23His in buffer O resulted in the isolation of VP23His dimers (discussed in section 3.3). Fig. 3.6.6 (panel B) shows the DSC profile for dimeric VP23His (0.5mg/ml) purified in

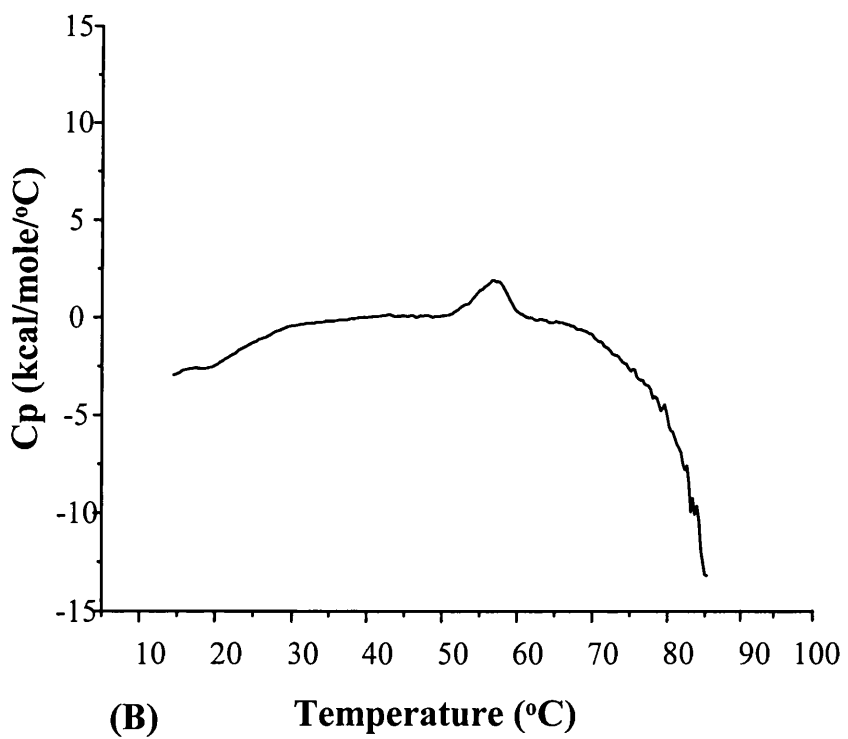
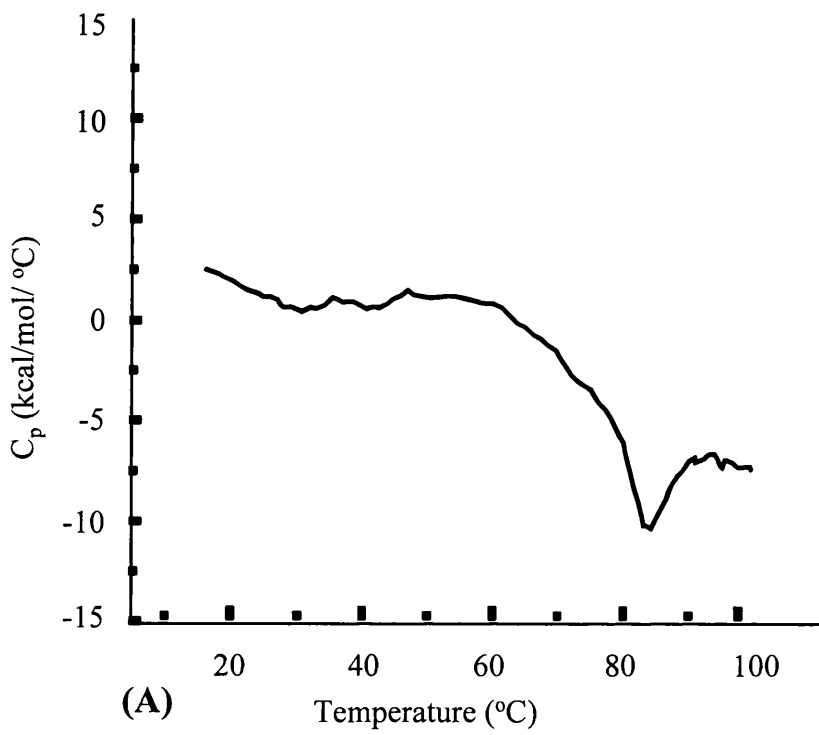


Fig. 3.6.6: Differential scanning calorimetry (DSC) of Ni-NTA agarose purified VP23His.

Heat absorption profiles of VP23His (0.7mg/ml) purified in buffer P (A), and VP23His (0.5mg/ml) purified in buffer O + 250mM imidazole (B). Profiles were obtained by heating the protein solutions through a temperature range of 10 to 100°C at a scan rate of 1°C/min. The spectrum was corrected by subtracting the buffer control spectrum for the appropriate buffer heated in the same manner.

buffer O. A small heat absorption peak was observed at approximately 58°C suggesting that a small endothermic transition had occurred. However, as the near-UV CD trace for dimeric VP23 in buffer O was flat, suggesting an absence of tertiary structure within dimeric VP23, the endothermic transition observed probably represents the exposure of hydrophobic surfaces at the interface between the VP23 molecules and not the co-operative melting of tertiary structure. As with the monomeric VP23His DSC spectra, dimeric VP23His also showed a sharp decline in heat capacity above 60°C demonstrating the irreversible unfolding of VP23His molecules during temperature denaturation.

One of the advantages of DSC analysis over far-UV and near-UV CD analysis, is that the experimental procedure can be carried out in the presence of imidazole. DSC therefore provides a means of analysing of the conformational stability of purified VP19cHis, which circumvents the difficulties associated with removing imidazole from the protein sample. Fig. 3.6.7 shows the DSC profile of Ni-NTA agarose purified VP19cHis (0.5mg/ml) in buffer O. The temperature-induced denaturation of VP19cHis produced an uncharacteristic, but reproducible, DSC spectrum. Typically, a buffer normalised DSC profile for a compact globular protein is comparatively flat with a defined peak, or peaks, representing the co-operative unfolding of tertiary structure upon temperature induced denaturation. However, no distinctive peak could be detected from DSC analysis of purified VP19cHis, with different samples consistently producing a similar curve. Throughout the purification procedure and preceding DSC analysis the solubility of the VP19cHis was examined to ensure that it had not precipitated out of solution. Special care was also taken during loading of the sample into the cell to prevent complications, for example the presence of air bubbles within the cell, that could have affected the DSC analysis. Despite this, different batches of VP19cHis produced the same profile over a range of protein concentrations (0.2-0.5mg/ml, data not shown). Therefore, the DSC profiles generated for purified VP19cHis must be assumed to provide an indication of the native conformational stability of VP19cHis during temperature induced denaturation. As no endothermic transition was observed for purified VP19cHis this would suggest that VP19cHis has little or no stable tertiary structure.

The uncharacteristic DSC profiles could possibly be explained by conformational instability of purified VP19cHis molecules. If the native state of purified VP19cHis molecules is never fully populated by a particular conformation, due to the protein's

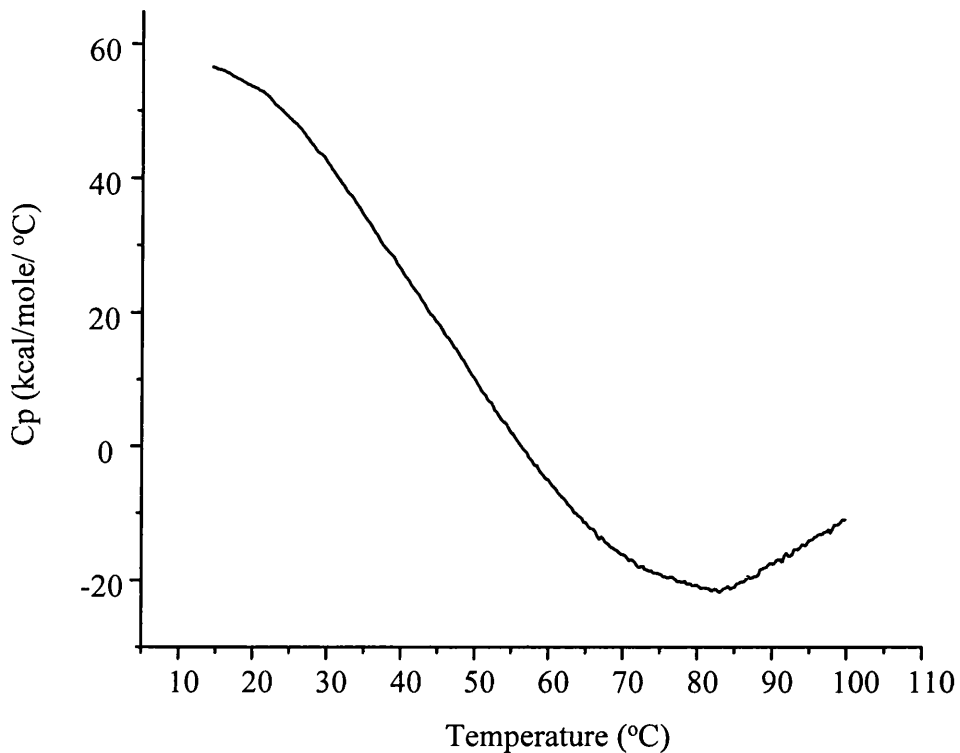


Fig. 3.6.7: Differential scanning calorimetry (DSC) of Ni-NTA agarose purified VP19cHis.

Heat absorption profile of VP19cHis (0.5mg/ml) purified in buffer O + 100mM imidazole. The profile was obtained by heating the protein solution through a temperature range of 10 to 100°C at a scan rate of 1°C/min. The spectrum was corrected by subtracting the control spectrum for the purification buffer heated in the same manner.

conformational instability, then the conventional baseline subtraction cannot be performed to provide accurate temperature transitions (Privalov et al., 1995). Indeed, this can be seen to occur in proteins that show cold denaturation, very specific and strong temperature-dependent interactions of non-polar groups with water. Hydration of these residues is atypical, in that it is thermodynamically favourable, and as a result a cold sensitive protein will unfold at sufficiently low temperatures exposing its internal non-polar residues to the environment (Privalov, 1990). Experiments performed by Privalov et al., (1986) demonstrated that the tertiary structure of metmyoglobin unfolds completely upon cooling. This results in the polypeptide demonstrating similar characteristics to those of a random coil with only residual helicity remaining in the unfolded polypeptide, as determined by NMR and CD analysis. The transition in unfolding of metmyoglobin due to cold denaturation was monitored by DSC and was shown to occur when metmyoglobin was cooled between 10°C and -7°C. A transition could be detected between 10 and 0°C, similar to, but not as broad as, the DSC profile of VP19cHis. Although there is no direct evidence to show that purified VP19cHis undergoes cold denaturation there may be exposed hydrophobic residues, which might be required for future protein interactions with VP23, VP5, and HSV-1 tegument proteins. These may promote protein instability in the absence of these other proteins. *In vitro* purification of VP19cHis is also likely to promote the possible hydration of non-polar residues, due to the removal of cellular factors within the cytosol that could maintain protein conformation and stability, for example cellular chaperones. Chaperone proteins have been implicated in the stabilisation of cold labile proteins, in preventing irreversible aggregation by stabilising intermediate folded protein structures during their assembly, and in some circumstances disassembly, of oligomeric complexes (Guy et al., 1998). Indeed, molecular chaperones GroEL and GroES have been implicated in the *in vivo* capsid assembly pathway of *ts* mutants of P22 bacteriophage (Nakonechny and Teschke, 1998). Thus, the instability of purified VP19cHis *in vitro* may result in a population of protein molecules in different states of unfolding which do not conform to a particular conformation and therefore are unable to provide a uniform endothermic transition to which a buffer base line can be subtracted.

It is noteworthy that Ni-NTA agarose pull downs have shown that the interaction between VP23 and VP19c is partially inhibited at 0°C (discussed in section 3.4 and fig. 3.4.11). This could be explained if the conformational stability of VP19cHis is altered at low

temperatures. However, it should be emphasised that further analysis is required in order to accurately determine the conformational stability of purified VP19cHis and determine whether it undergoes cold-denaturation similar to that of previously characterised cold labile proteins.

Fig. 3.5.8 (panel A) shows the DSC profile for triplexes (0.5mg/ml) purified in buffer O. A distinct heat absorption peak was observed at approximately 60°C. This represents a substantial endothermic transition indicating the co-operative melting of tertiary structure leading to the exposure of non-polar residues to the solvent. This confirms the experimental observations made by near-UV CD analysis, which suggested that the triplex contains rigid tertiary structure. DSC analyses of multi-domain proteins sometimes demonstrate the presence of several endothermic transitions during heat denaturation. Experiments performed by Novokhatny et al., (1984) on plasminogen, demonstrated seven independent co-operative transitions which were specifically associated with the co-operative unfolding of structural domains linked together by disulphide bonds. In contrast, only a single endothermic transition was detected during the heat denaturation of the triplex. This would suggest that the purified triplexes may only contain a single rigid tertiary structural domain which co-operatively unfolds in a manner similar to that of small compact globular proteins (Privalov, 1997). If the VP23 and VP19cHis molecules within the triplex had independent rigid tertiary structures, then two or more endothermic transitions might be expected due to the co-operative unfolding of the complex followed by the unfolding of tertiary structure within the individual triplex protein molecules. The fact that only a single transition was detected would further imply that VP19cHis and VP2His lack any rigid tertiary structure as individual triplex proteins. It is likely therefore that some form of mutual co-folding between VP19c and VP23 triplex proteins is occurring during triplex formation.

In order to analyse the association of purified VP23His and VP19cHis molecules, DSC analysis was performed on *in vitro* formed triplexes. VP23His and VP19cHis were individually purified by Ni-NTA agarose affinity chromatography in buffer O, mixed in a 2:1 molar ratio to a final protein concentration of 0.5mg/ml and allowed to associate for 1 hour at 28°C. Fig. 3.6.8 (panel B) shows the DSC profile of the samples, following this procedure. A distinctive heat absorption peak could be detected at approximately 55°C. Although this peak is smaller than that for an equivalent amount of purified *in vivo* formed

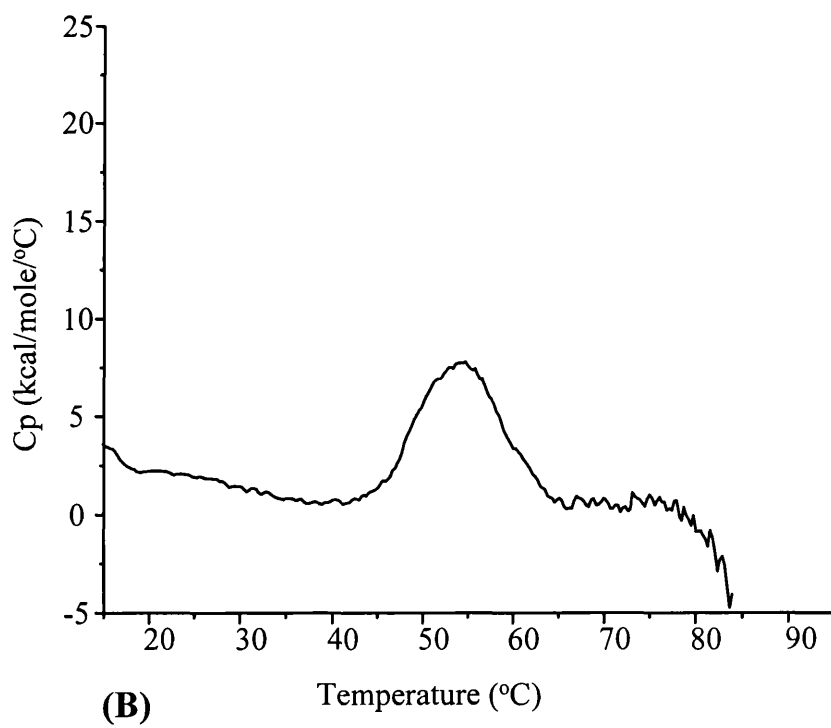
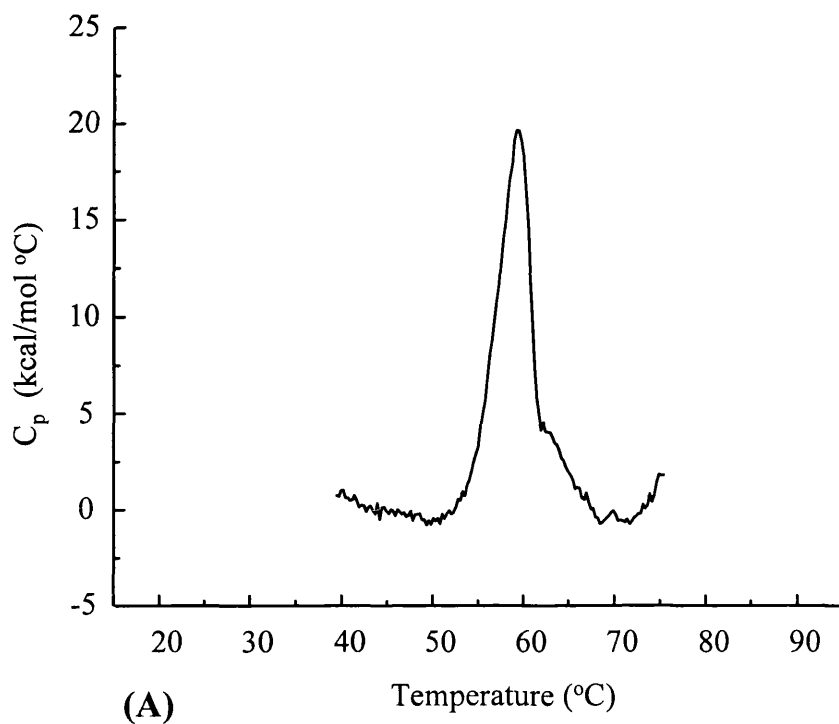


Fig. 3.6.8: Differential scanning calorimetry (DSC) of Ni-NTA agarose purified triplexes

Heat absorption profile of triplexes (0.5mg/ml) purified in buffer O (A) and *in vitro* assembled triplexes (0.5mg/ml) (B). *In vitro* assembled triplexes were made by mixing a 2:1 ratio of individually purified VP23His and VP19cHis in buffer O + 250mM imidazole for 1 hour at 28°C before analysis. Profiles were obtained by heating the protein solutions through a temperature range of 10 to 100°C at a scan rate of 1°C/min. The spectrum was corrected by subtracting the control spectrum for the appropriate buffer heated in the same manner.

triplexes, it demonstrates that individually purified triplex proteins can interact to form complexes that have tertiary structure which undergoes co-operative unfolding upon heat denaturation. The endothermic transition occurs at a slightly lower temperature than that of purified *in vivo* formed triplexes (60°C). The smaller heat absorption peak seen with the *in vitro* formed complexes could mean that some, but not all, of the individually purified triplex proteins form complexes *in vitro*. This would appear to mirror the behaviour of the *in vitro* assembled triplexes analysed on sucrose gradients (fig. 3.4.15). The reason for the incomplete association of purified triplex proteins and the observed lower temperature of co-operative unfolding remains unclear.

Sucrose gradient sedimentation analysis has shown that individually purified triplex proteins mixed *in vitro* form complexes which sediment to the same position as purified *in vivo* formed triplexes (section 3.4.6, fig. 3.4.15). This, together with their ability to support *in vitro* capsid assembly, demonstrates that the individual proteins are capable of assembling into functional heterotrimeric complexes. Protein concentration has been shown to be important for the successful formation of capsid structures. Prevelige et al., (1993b) demonstrated that P22 capsid assembly could not occur below a critical protein concentration (0.3mg/ml) due to the unsuccessful polymerisation of coat and scaffold protein subunits. The same could be true for triplex formation. The equilibrium established between individual protein subunits (VP23His and VP19cHis) and polymerised complexes (triplexes) may be stalled when the concentration of free triplex subunits required to drive the formation of triplexes falls below a concentration critical for subunit polymerisation (Zlotnick, 1994). Alternatively, the purification procedure of VP23His and VP19cHis may affect their ability to form complexes. For example, the presence of detergents may inhibit formation by concealing external hydrophobic residues required for efficient complex formation. The purification of individual triplex proteins could also remove cellular components required for efficient interaction.

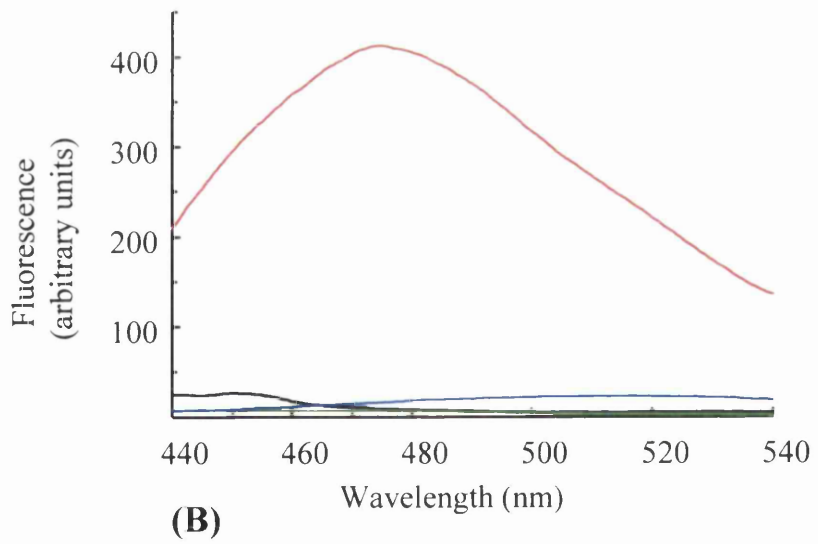
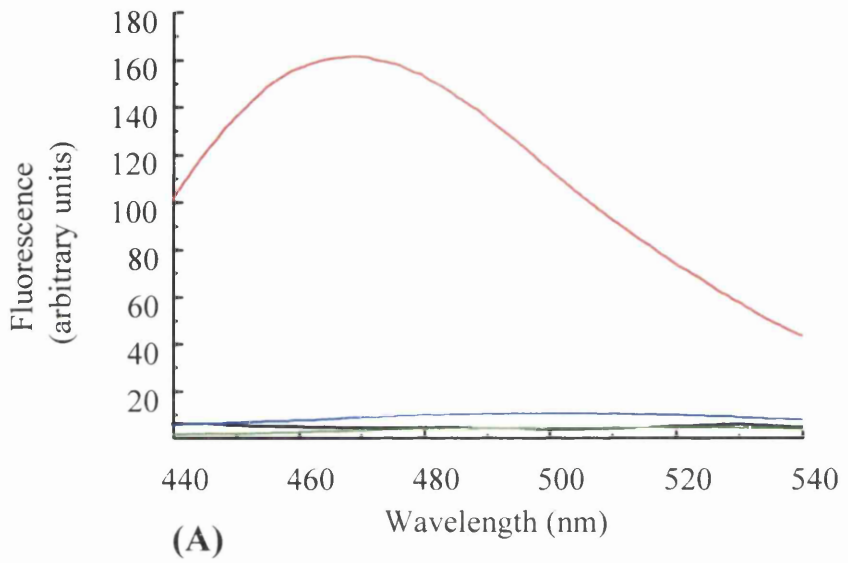
The endothermic transition of *in vitro* assembled triplexes occurs at a slightly lower temperature than for triplexes formed *in vivo*. This implies that the tertiary structure of *in vitro* formed triplexes is not as stable as that of purified *in vivo* triplexes. Alternatively, the lack of a sharp transition may indicate that *in vitro* triplexes represent a partially folded intermediate state in triplex assembly. Fuchs et al., (1991) demonstrated that the refolding of the trimeric tail spike of P22 bacteriophage produced a non-native trimer intermediate

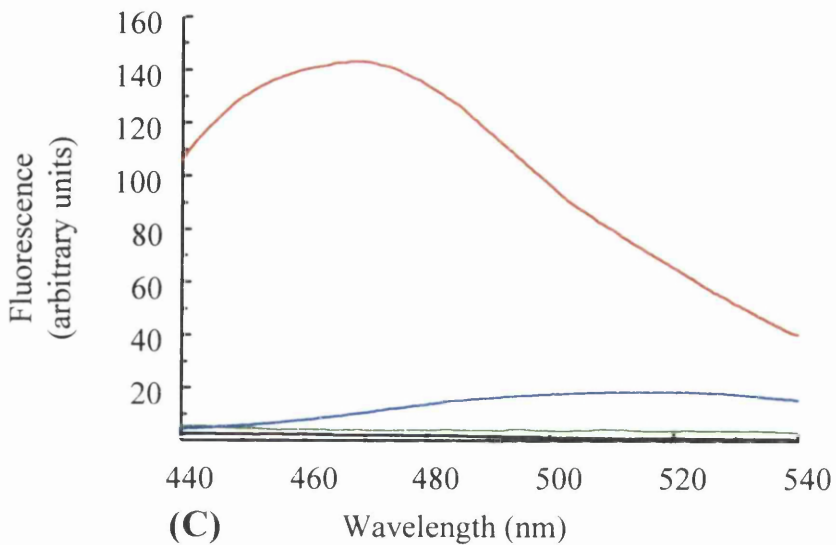
(T<sub>p</sub>). Although the monomeric subunits associated into trimers comparatively quickly (1.5 hours) without passing through a detectable dimeric intermediate state, the native SDS-resistant trimers took 3 days to form at 10°C. The formation of triplexes *in vitro* may therefore require longer periods of incubation. Although, incubation for 1 hour at 28°C may be sufficient time to allow the association of triplex protein molecules, which may undergo some degree of co-operative folding, but insufficient to form the specific native tertiary structure as seen within the *in vivo* formed purified triplexes. One of, or a combination of, these factors may be responsible for the incomplete polymerisation of all the individual purified triplex protein constituents and consequently a reduction in the heat absorption capacity of *in vitro* formed triplexes compared to that of purified *in vivo* formed triplexes.

#### 3.6.2.7 Partial folding within purified triplexes and triplex proteins

The use of non-covalent probes, such as 8-anilino-1-naphthalenesulfonate (ANS), has become increasingly popular in analysing protein conformation. The binding of ANS to a protein molecule was generally regarded as a sensitive test for partial folding which allows ANS access to the hydrophobic interior of a protein molecule where it can become fluorescent upon excitation at 370nm. Indeed, ANS has been used in the detection and analysis of molten globules (protein molecules in an intermediate state of protein folding) which have a compact conformation with pronounced secondary structure but with little or no rigid tertiary structure (Semisotnov et al., 1991; Ptitsyn, 1995a). The increased ability of ANS to bind to proteins that are in a molten globule-like state, which can become fluorescent upon excitation, is primarily due to an increase in the number of exposed binding sites within the hydrophobic core of molten globule-like proteins where ANS is not exposed to the quenching effect of the surrounding solvent.

Fig. 3.6.9 (panels A-C) shows the ANS binding profiles of Ni-NTA agarose purified VP23His, VP19cHis and triplexes respectively. Triplexes and the individual triplex proteins all demonstrated a large increase in ANS fluorescence at 470nm over that seen for ANS in buffer or for protein samples analysed in the absence ANS. This indicates that ANS molecules were binding to the protein molecules and that the organic moiety responsible for ANS fluorescence was buried within their hydrophobic interiors. As





— Protein + ANS      — Buffer  
— Protein      — Buffer + ANS

Fig. 3.6.9: ANS binding analysis to Ni-NTA agarose purified VP23His, VP19cHis, and triplexes.

ANS fluorescence at 440-540nm was monitored following excitation at 370nm (as described in Methods). ANS was mixed (to a final concentration of 20 $\mu$ M) with purified VP23His (0.2mg/ml) in buffer P (A); purified VP19cHis (0.1mg/ml) in buffer O (B); and purified triplexes (0.2mg/ml) in buffer O (C). Control fluorescence spectra were measured for ANS in the appropriate buffer and for protein samples in the absence of ANS.

purified triplexes demonstrate ANS fluorescence, there must be additional accessible internal areas of hydrophobicity within VP23 and VP19cHis, which are not lost due to the interactions between VP19cHis and VP23. This would indicate that triplexes still contain a degree of partial folding allowing ANS access to hydrophobic pockets away from the quenching environment of the solvent. It should be noted that recent studies have shown that ANS can bind to solvent accessible polar groups on native, non-molten globular proteins through electrostatic interactions. However, the fluorescence of such ANS molecules binding to exposed sites is typically quenched by water molecules within the solvent (Matulis and Lovrien, 1998; Matulis et al., 1999). Denatured VP23His and VP5, unfolded in the presence of 6M GdnHCl, have been shown not to produce an increase in ANS fluorescence following excitation (Kirkitadze et al., 1998). This would suggest that ANS only becomes fluorescent following excitation when in association with capsid proteins that have a degree of folding, where ANS molecules can gain access to a hydrophobic core.

### 3.6.3 Conclusions

#### 3.6.3.1 Ni-NTA agarose purified triplexes and triplex proteins are functionally active.

Utilising *in vitro* capsid assembly analyses it has been demonstrated that Ni-NTA agarose purified triplexes and triplex proteins are capable of participating in the formation of capsid particles that morphologically resemble WT HSV-1 capsids (as determined by electron microscopy). Capsid formation only occurred when VP5, VP19c, VP23, and the scaffold component preVP22a were present as purified proteins or in SF21 whole cell extracts. This confirms previously published observations which reported that the *in vitro* formation of capsids does not require the presence of VP26 (UL35) (Newcomb et al., 1994; Newcomb et al., 1999; Newcomb et al., 2000).

*In vitro* capsid assembly utilising purified triplexes and triplex proteins demonstrated that the 6x His epitope tag located on the N-terminus of VP19cHis or VP23His, either as an individual protein molecule or as part of the heterotrimer complex, did not affect protein

functionality. This ability to form capsid particles indicates that the N-termini are not directly involved in the interactions occurring during capsid assembly. Indeed, Desai and Person (1996) and Spencer et al., (1998) have shown that small deletions from the N-termini of VP23 and VP19c do not affect protein functionality, as determined by the yeast two hybrid system and *in vivo* capsid assembly respectively.

The purification protocols/buffers used in the isolation of the recombinantly expressed proteins do not appear to affect protein functionality. However, in the case of VP23His, the oligomeric status of VP23 appears to be buffer dependent. Both monomeric VP23His (purified in sonication buffer) and dimeric VP23His (purified in buffer O), appeared equally efficient at forming capsids. The buffer dependency on the oligomeric status of VP23His would imply that the VP23His molecules within the dimer are weakly associated and that dimer formation is not specifically required for triplex and capsid formation. This relatively weak intra-molecular association is highlighted by the absence of a near-UV CD signal and the small endothermic transition observed during DSC analysis of dimeric VP23His purified in buffer O (figs. 3.6.5, panel B and 3.6.6, panel B respectively).

### 3.6.3.2 Molten globularity of purified VP23His and VP19cHis

Far-UV CD and fluorescence analysis of purified VP23His and VP19cHis demonstrated that these molecules are folded and contain pronounced secondary structure. However, DSC and near-UV CD revealed that both these proteins lacked rigid tertiary structure. Moreover, both VP23His and VP19cHis bound ANS and demonstrated an increase in fluorescence following excitation. These data, taken together, indicate that both VP23His and VP19cHis are in partially folded states and fit the defining criteria of molten globule like-proteins. Molten globule-like proteins are partially folded protein molecules that have a compact state with distinct secondary structure elements but lack rigid tertiary structure (Ptitsyn, 1995a; Privalov, 1996). The lack of rigid tertiary structure in the molten globule-like state is generally considered to reflect the absence of tight packing of amino acid side chains within the hydrophobic core of the protein molecule (Ptitsyn, 1995a; Privalov, 1996). This allows a greater degree of domain flexibility, in particular by allowing the secondary structural elements to move in relation to each other (Semisotnov et al., 1991).

Many proteins have been shown to adopt a molten globular state during induced protein unfolding under non-physiological conditions, for example at low pH and/or in the presence of denaturants. The partially folded state is thought to represent an equilibrium intermediate in the protein folding pathway (Ptitsyn et al., 1990). One of the most extensively studied proteins to demonstrate a partially folded intermediate state, is apo- $\alpha$ -lactalbumin, which adopts a molten globule-like form when incubated in the presence of denaturants such as GdnHCl or low pH. Yutani et al., (1992) also demonstrated that apo- $\alpha$ -lactalbumin could form a molten globule-like state at neutral pH in the absence of  $\text{Ca}^{2+}$  ions. Utilising DSC and CD analysis they characterised this partially folded intermediate state and demonstrated that it contained no detectable tertiary structure. However, it retained a comparable amount of secondary structure to that of the native apo- $\alpha$ -lactalbumin when analysed by Far-UV CD. Similar observations were reported when structural studies were performed by Uversky et al., (1995) on the glycoprotein  $\alpha$ -fetoprotein (AFP). AFP demonstrates significant conformational rearrangements when subject to low pH (pH3.1) which lead to the development of attributes characteristic of a molten globule-like state. Far-UV CD analysis demonstrated that AFP contained similar levels of secondary structure at pH 3.1 to that of native AFP, while AFP denatured in 9M urea contained no detectable secondary structure. Conversely, the lack of a distinct endothermic transition detectable by DSC analysis showed that at pH 3.1 AFP contained no rigid tertiary structure. This was in contrast to native AFP molecules analysed at pH 7.2. This led the authors to conclude that the transition from native to molten globule-like state for AFP might play an important role in the proteins functionality. They hypothesised that the increased flexibility of the molten globule state could facilitate ligand disassociation at membrane structures, where the intracellular pH is lower than that of the cytosol.

Molten globule-like states have not been widely characterised within virus structural proteins. This is probably due to the relatively limited investigations of the folding pathways of such proteins compared to those of smaller more amenable globular proteins. However, a partially folded intermediate state has been proposed for the coat protein subunit of P22 bacteriophage. Teschke and King (1993) analysed the ability of denatured P22 coat protein to refold *in vitro*. Upon refolding the coat protein molecule was fully functional and actively participated in capsid assembly when associated with its scaffold

protein counterpart. During refolding an intermediate was identified which exhibited an increase in both intrinsic fluorescence and the number of sites that bound ANS compared with the fully folded form. The increased number of ANS sites led the authors to propose that this folding intermediate was in an molten globule-like transitional state. They further proposed that the native coat protein, which had not associated with a scaffold subunit, was in a partially folded intermediate state and only became fully folded when polymerised within the capsid during assembly in association with scaffold protein molecules.

### 3.6.3.3 *Mutual protein co-folding within the triplex*

DSC analysis of purified VP19cHis and VP23His demonstrated that they contain little or no rigid tertiary structure. Conversely, DSC analysis of purified *in vivo* and *in vitro* formed triplexes, and near-UV CD analysis of *in vivo* purified triplexes, showed that they contain considerable tertiary structure. As the individual triplex proteins appear to lack any independent tertiary structure, the tertiary structure within the triplex would appear to be formed by the association of VP19c and VP23 during triplex formation. The formation of such rigid tertiary structure is probably a direct result of mutual co-folding of secondary structural elements from each protein during complex formation (discussed further in section 4).

### 3.6.3.4 *Partial folding within the triplex*

Although the classical definition of the molten globule-like state does not apply to the triplex, it still binds the hydrophobic probe ANS strongly and shows enhanced fluorescence following excitation (fig. 3.6.9, panel C). This indicates that ANS has access to the hydrophobic interior of the heterotrimer and suggests that although the triplex is fully folded and contains rigid tertiary structure, other regions within the complex still retain the characteristics of a partially folded molten globule-like intermediate.

Although there are few examples of trimeric protein complexes that exhibit partial folding, one example is that of the cytokine tumour necrosis factor- $\alpha$  (TNF $\alpha$ ). TNF $\alpha$  is a 52kDa

globular trimeric protein composed of identical subunits of approximately 17.3kDa (Wingfield et al., 1987). TNF $\alpha$  has been shown to partially unfold at low pH and demonstrates the usual characteristics of an acid induced molten globule-like state (Hlodan and Pain, 1994). Experiments performed by Hlodan and Pain (1995) demonstrated that TNF $\alpha$  could be denatured into unfolded monomers in 3M GdnHCl and upon refolding passed through a transient trimeric intermediate ( $I_3$ ) molten globule-like state. This  $I_3$  intermediate bound ANS more effectively than the native compact conformation. During refolding there was desorption of ANS which was thought to reflect the conformational rearrangement and re-packing of side chains into the native trimeric conformation. The fact that HSV triplexes still retain the ability to bind strongly to ANS could therefore indicate that further conformational rearrangements have yet to occur within the triplex. The triplex itself may therefore represent a partially flexible intermediate in respect to capsid assembly, which only adopts its final native conformation following capsid maturation (discussed further in section 4.0).

Although the classical definition of the molten globule is associated with a lack of rigid tertiary structure, some proteins have been shown to have a bipartite structure comprised of both molten globule-like and fully folded protein domains. For example, the molten globule-like state of  $\alpha$ -lactalbumin contains two domains, an  $\alpha$ -helical and  $\beta$ -sheet domains, which exhibit different degrees of folding. The  $\beta$ -sheet domain is largely unstructured whilst the structure of the  $\alpha$ -helical domain closely resembles that of the native protein (Peng et al., 1995). This folded structure is thought to be due to a small subset of hydrophobic residues within the  $\alpha$ -helical domain which form a densely packed core. This step is thought to direct the overall folding of the protein molecule in the early stages of folding before specific packing of amino acid side chains occurs (Peng and Kim, 1994; Wu and Kim, 1998; Song et al., 1998). Therefore, in a multi-domain polypeptide, molten globule properties can be limited to portions of the polypeptide with individual domains folding independently (Peng and Kim, 1994; Peng et al., 1995). Indeed, it is now becoming clear that folding of some protein molecules requires a number of folding stages with the protein molecule passing through several conformational intermediates before it takes on its final native structure. For example, interleukin-4 at low pH has been shown by NMR studies to take on a late folding intermediate conformation that contains extensive tertiary interactions within a highly ordered hydrophobic core but still displays extensive

disorder within regions which link the structural domains. This has led to the terminology of the 'highly ordered molten globule' (Redfield et al., 1994). Similar NMR analysis of cytochrome  $b_{562}$ , with (halo-) and without (apo-) the prosthetic haem group, has revealed that the overall topology of the molecule is conserved between apo- and halo-forms (Feng et al., 1994). However, significant differences were detected in the helix-helix packing, in particular around the haem-binding pocket of apo-cytochrome  $b_{562}$  which, although conserved, was exposed to the solvent.

Purified *in vivo* formed triplexes seem to belong to this class of proteins which contains both highly structured and flexible domains. The flexible domains may assist further protein folding events during the course of capsid assembly (discussed further in section 4.0). In the absence of a high resolution structure, it is difficult to speculate where the structured and flexible portions are located within the triplex. The highly structured component of the triplex may represent the product of mutual co-folding between VP23 and VP19c and/or be the direct result of tertiary structure developed within the individual triplex proteins during triplex formation. Cryo-EM analysis to 8Å resolution has shown that the triplex appears as a compact globular heterotrimer (Zhou et al., 2000). However, this triplex structure is derived from a mature icosahedral B-capsid and is likely to differ from that of isolated triplexes, due to possible additional conformational rearrangements that occur during association of the triplex with other capsid protein subunits during capsid assembly. Indeed, as described in the introduction to this thesis, such conformational changes are evident, albeit at comparatively low resolution, when comparing the triplex conformation within procapsids to that of mature capsids (triplex conformational flexibility is discussed in further detail within section 4.0).

#### 3.6.3.5 Future work

The stability of purified VP19cHis *in vitro* is poor compared to that of VP23His and triplexes. It has therefore been consistently difficult to perform biophysical analysis upon VP19cHis due to the low concentrations of homogenous samples. Further biophysical analysis is therefore required on VP19cHis, such as near and far-UV CD, in order to accurately determine the degree of secondary and tertiary structure. Although attempts to

concentrate purified VP19cHis have failed, primarily due to non-specific binding to various agarose matrixes, it would be worth attempting to concentrate VP19cHis through other methods, such as micro-dialysis. Similarly, it would also be beneficial to develop other suitable purification buffers utilising octyl- $\beta$ -glucoside in order to increase the solubility of VP19cHis at higher concentrations.

Teschke and King (1993) demonstrated that the coat protein of bacteriophage P22 passed through a kinetic molten globule-like intermediate and that the binding of ANS to either the coat protein or scaffold subunits prevented the formation of icosahedral capsid particles *in vitro*. Although the binding of ANS had no effect upon the overall secondary structure of the coat protein, it did induce conformational changes within the secondary structure of the scaffold protein molecule, which altered its ability to undergo maturation. It would be interesting, therefore, to compare the number of ANS molecules that bound to VP23 and VP19c with the number bound to triplexes and to determine whether or not ANS prevented triplex polymerisation. This might provide a clearer insight into how these two triplex proteins interact and to further elucidate the role in which the triplex plays within capsid assembly. Similarly, it would be interesting to determine, as with P22 capsid assembly, whether or not ANS inhibited the polymerisation of capsid particles, as little is currently known about the folding processes of other HSV-1 capsid proteins molecules, in particular VP5.

Furthermore, it would also be interesting to analyse by DSC the endothermic transition of triplexes in the presence of increasing concentrations of denaturants such as urea and GdnHCl. 3M urea has been shown to disassociate triplex molecules into their basic constituent proteins (section 5.42). DSC analysis of triplexes in the presence of denaturants would therefore provide more information upon the co-operative unfolding of these two molecules and might reveal whether or not the tertiary structure within the triplex is derived specifically from the association of VP23 with VP19c. Similarly, it would be interesting to follow the changes in the tertiary structure of purified capsid proteins in real time by near-UV CD analysis. This could be accomplished by separately purifying individual capsid proteins and mixing them just prior to analysis. This would provide a sequence of folding events involved during procapsid assembly and subsequent procapsid maturation.

# Chapter 4

## Discussion

## 4.0 Discussion

### 4.1 Quasi-equivalence and conformational flexibility within the HSV-1 capsid.

The HSV-1 capsid is among the largest and most complex of virus particles and as such there has been considerable interest in analysing its three dimensional structure. However, to date there has been no X-ray crystallography structure published of the complete capsid, nor any of its individual outer shell structural components. This, in part, reflects the complexity of the HSV-1 capsid, in particular its size (~1250Å in diameter), and the difficulties associated with acquiring high concentrations of homogenous and intact samples from infected cell nuclei (Gibson and Roizman, 1972; Steven et al., 1997). Attempts to recombinantly express and purify individual full length capsid polypeptides at concentrations required for X-ray crystallography (typically >10mg/ml) have also proved to be difficult due to their relative insolubility at high concentrations (personal communication, Bowman, 1999). Consequently, the majority of the structural information derived from the HSV-1 capsid has been determined through the use of cryo-EM examination in conjunction with image processing and computer reconstruction analysis (Schrag et al., 1989; Booy et al., 1991; Newcomb et al., 1993; Zhou et al., 1994, Zhou et al., 1995, Zhou et al., 1998; Zhou et al., 2000). Through the use of cryo-EM the structure of the HSV-1 B capsid has recently been resolved to a resolution of 8.5Å (fig. 4.1, Zhou et al., 2000). Although the strict bonding relationships between protein molecules within the HSV-1 capsid still remains unresolved at this resolution, it has been possible to determine mass boundaries of individual protein molecules and predict secondary structural elements, in particular  $\alpha$ -helices, within subunit structures. EM and cryo-EM analysis has long since established that the outer capsid shell of the HSV-1 capsid is composed of 150 hexons and 12 pentons that are interconnected by 320 triplexes (Wildy et al., 1960; Schrag et al., 1989). The interactions between these individual capsomeric subunits, in particular the triplexes, within the T=16 icosahedral lattice and their deviations away from their predicted quasi-equivalent bonding arrangements are discussed below in relation to the molten globule-like characteristics of the triplex and triplex protein constituents.

## 4.2 Non-equivalent interactions of triplexes within the HSV-1 capsid

Cryo-EM analysis of the HSV-1 capsid has established that triplexes occupy the local and, with respect to the triplex 'T<sub>f</sub>', global 3-fold rotational symmetry axes. However, the asymmetry of the triplex and its heterotrimeric nature (2 copies of VP23:1 copy of VP19c) make it difficult to envisage how this complex can occupy a position of 3-fold rotational symmetry, since rotation of a triplex around its axis would not lead to equivalent 3-fold symmetries and bonding arrangements with adjacent capsomers (Schrag et al., 1989; Booy et al., 1991; Conway et al., 1993; Zhou et al., 1994; Zhou et al., 1998). The apparent 3-fold symmetry observed for triplex 'T<sub>f</sub>' is a direct result of 3-fold averaging during the computer reconstruction process. The inter-capsomeric bonding of triplex 'T<sub>f</sub>' within the HSV-1 capsid is, therefore, currently unresolved and shall not be discussed further here (Schrag et al., 1989; Conway et al., 1993; Zhou et al., 1994).

Early low-resolution cryo-EM analysis of the HSV-1 capsid demonstrated different bonding interfaces between the triplexes 'T<sub>a</sub>-T<sub>e</sub>' and their surrounding capsomers. The most different of these inter-capsomeric connections is that of the triplex 'T<sub>a</sub>' compared to that of triplexes 'T<sub>b</sub>-T<sub>e</sub>'. Triplex 'T<sub>a</sub>' appears to make a single prominent head connection compared to that of two head connections observed for triplexes 'T<sub>b</sub>-T<sub>e</sub>' to their respective capsomers (fig. 4.1) (Zhou et al., 1994; Zhou et al., 1998; personal communication, Zhou, 1999). The substantial differences in the inter-capsomeric bonding arrangements of triplexes 'T<sub>a</sub>-T<sub>e</sub>' and the general asymmetry of these complexes clearly violate the rules depicted by the theory of quasi-equivalence proposed by Caspar and Klug (1962). Furthermore, this degree of variation in triplex inter-capsomeric bonding can be detected biochemically. Structural and biochemical analysis performed by Newcomb et al., (1993) on purified HSV-1 B capsids treated with various concentrations of denaturants demonstrated that the peripentonal triplex 'T<sub>a</sub>' and the perihexonal triplex 'T<sub>c</sub>' were more readily disassociated from capsids than those perihexonal 'T<sub>b</sub>, T<sub>d</sub>, T<sub>e</sub>, T<sub>f</sub>' triplexes. Conway et al., (1993) reported similar observations when comparing low and high dose irradiated HSV-1 B-capsids. It is clear therefore from both biochemical and structural analysis of HSV-1 capsids that triplexes 'T<sub>a</sub>-T<sub>f</sub>' have distinctly different inter-capsomeric bonding arrangements to their surrounding capsomeric subunits within the HSV-1 capsid.

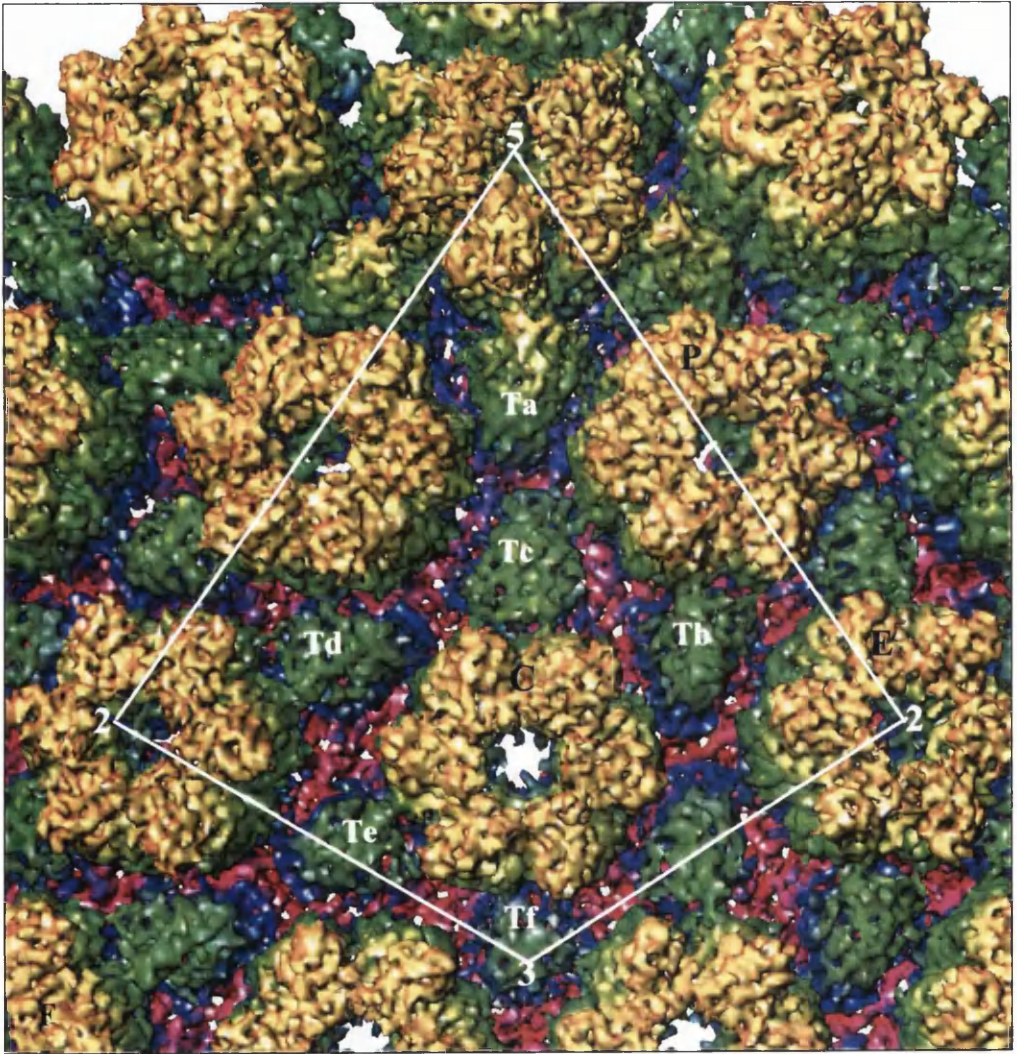


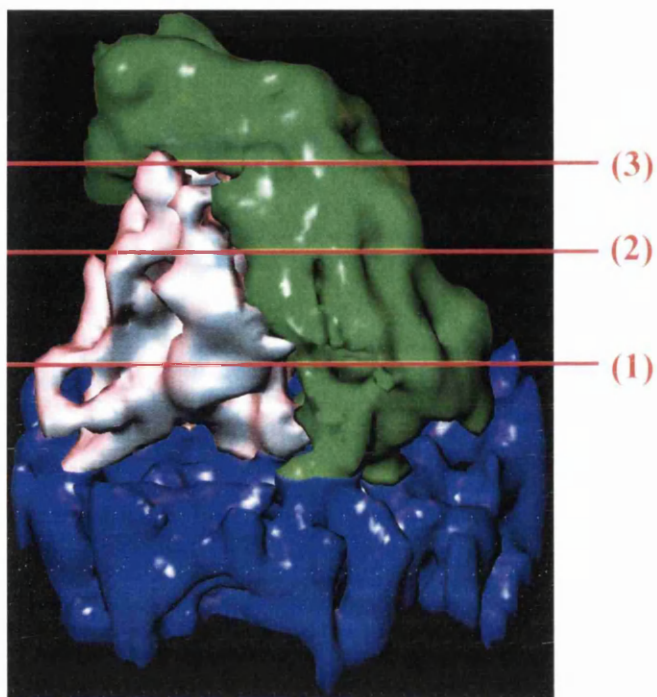
Fig. 4.1: Surface reconstruction of the HSV-1 capsid at 8.5Å resolution

Radially colour-coded representation of the HSV-1 capsid at 8.5Å (dark to light colours represent low to high positions of mass density respectively). A single asymmetric unit is enclosed by the white outline connecting the five, three, and two-fold axes (indicated by 5, 3, and 2 respectively). The penton (at the 5-fold axes), the three types of hexon (designated P, E, and C) and the six types of triplexes ( $T_a$ ,  $T_b$ ,  $T_c$ ,  $T_d$ ,  $T_e$ , and  $T_f$ ) are appropriately labelled.

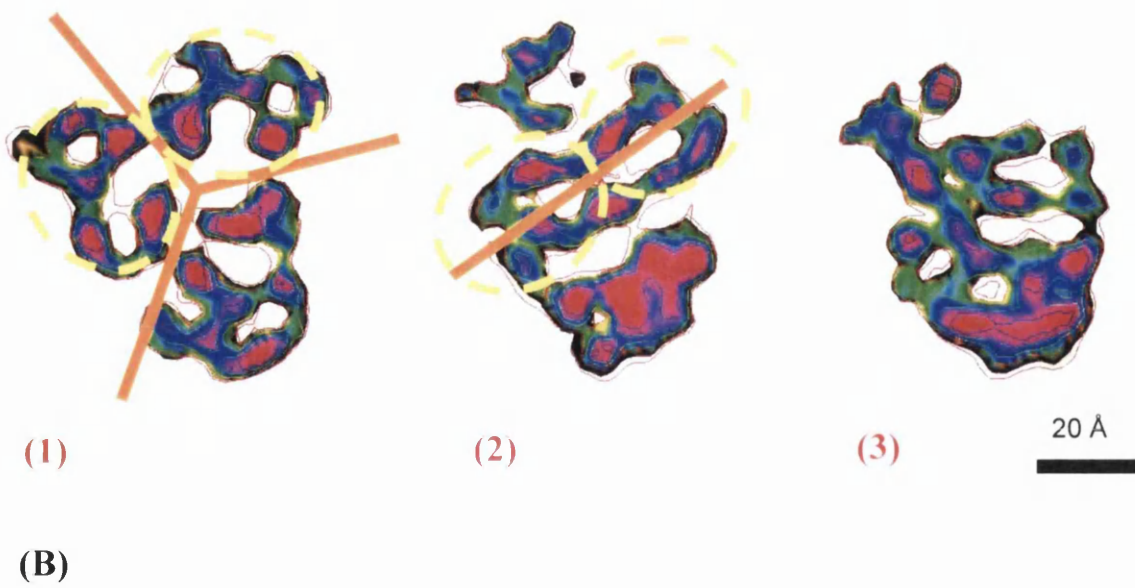
This picture was reproduced with permission from W. Chiu, Baylor college of medicine, USA.

### 4.3 How do the triplexes occupy a 3-fold rotational axis?

Cryo-EM and computer image processing analysis of the triplex connections to the capsid floor at 8.5Å resolution has suggested how the asymmetrical triplex occupies a 3-fold symmetrical position. The densities at the base of the triplex appear to exhibit a limited 3-fold symmetry. The lower third of the triplex molecule consists of two legs, assigned to VP23, and a tail formed by VP19c. These are triangularly related with two copies of VP23 forming an angle of approximately 120° and VP19c occupying the third triangular position (fig. 4.2, panel B(1)). The triplex therefore forms a pseudo-trimer at its base with each of the triplex proteins interacting with the floor densities provided by surrounding hexon capsomer subunits (Zhou et al., 2000). However, the pseudo-trimer relationship within the triplex becomes significantly altered further up the triplex away from the capsid floor. Within the middle domain of the triplex the triangular arrangement of the triplex proteins is lost and the dimeric relationship between the VP23 molecules becomes more evident. The relative angle between VP23 molecules within the middle domain changes from 120° to approximately 180° with the mass density attributed to VP19c no longer having an equivalent relationship to that of the dimer of VP23 molecules (fig. 4.2, panel B(2)). The upper domain of the triplex is entirely composed of protein mass relating to VP19c and is responsible for interconnecting adjacent capsomers above the capsid floor (fig. 4.2, panel A and panel B(3)) (Saad et al., 1999, Zhou et al., 2000). Computer analysis of the local symmetry within the hexon demonstrated a high 6-fold local symmetry running throughout the entire structure with the tower region being particularly conserved (personal communication, Jing He, 2000). Computer analysis of the local symmetry within the triplex has demonstrated that they have no detectable mathematical local 3-fold symmetry (personal communication, Jing He, 2000). However, there does appear to be some functional symmetry between the triplex proteins, especially at the points of contact the triplex makes with the capsid floor (personal communication, Jing He, 2000). The 'T<sub>a</sub>-T<sub>f</sub>' triplexes therefore represent highly unusual but essential building blocks within the mature HSV-1 capsid particle (Tatman et al., 1994, Thomsen et al., 1994, Zhou et al., 2000).



(A)



(1)

(2)

(3)

20 Å

(B)

Fig. 4.2: Heterotrimeric arrangement of VP23 and VP19c interactions within the triplex

(A) Side view of a triplex obtained by averaging the four triplexes ( $T_b$ ,  $T_c$ ,  $T_d$ ,  $T_e$ ) around the C-hexon. The different colours represent individual capsid proteins; VP19c (green), VP23 (white), and the capsid floor composed of VP5 (blue). Red lines numbered 1-3 represent the position of cross sections taken through the averaged triplex shown in panel B.

(B) Three cross sections representing 1.4Å slices through the averaged triplex at positions 1-3 (indicated by red lines above). Contour colouring represents high (red), median (purple) and low (green) density levels. Slice (1) illustrates the pseudo 3-fold symmetry at the base of the triplex (highlighted by the orange lines). The two copies of VP23 (highlighted by yellow dotted circles) have an approximate 120° relationship to one another with the single copy of VP19c occupying the third position. Slice (2) indicates the conformation change in the orientation of VP23 molecules which now have an approximate 180° relationship to one another (highlighted by the orange line). Slice (3) shows the asymmetric appearance of the density at the top of the averaged triplex mass relating to VP19c. The scale bar represents 20Å in length.

This picture was reproduced with permission from W. Chiu, Baylor College of medicine, USA.

#### 4.4 Conformational flexibility within the triplex

Computational averaging of triplexes resolved to 8.5Å has demonstrated that triplexes contain a degree of domain variation between the two VP23 molecules within each individual triplex. Computational alignment of the individual VP23 molecules obtained from averaging triplexes 'T<sub>a</sub>-T<sub>e</sub>' demonstrated an overall conservation of the gross conformation and putative  $\alpha$ -helical content. However, significant domain movements were evident between individual VP23 molecules within the triplex, in particular the degree of orientation for the predicted upper  $\alpha$ -helix (fig. 4.3). This implies that these protein molecules have non-equivalent bonding relationships within individual triplexes and therefore must possess a degree of conformational flexibility in order to accommodate the observed domain movements. Indeed, the non-equivalent relationship between VP23 molecules within the triplex is particularly highlighted by their respective interfaces with VP19c. One side of a VP23 molecule (coloured in white in fig. 4.4) forms an extensive protein interface with VP19c, while the equivalent side of the other VP23 molecule (coloured in grey in fig. 4.4) interacts directly with the opposing VP23 molecule (also highlighted in fig. 4.2, panel B(1)). Thus, the dimer of VP23 within the heterotrimer is itself asymmetrical with the VP23 molecules taking on different conformations and presumably different bonding attributes within the triplex. This arrangement is structurally irregular as dimeric molecules, or subunits composed of dimers, generally demonstrate identical bonding interfaces. Furthermore, the few instances where such non-equivalent dimeric interfaces occur necessitate the appropriate subunit to have a degree of flexibility. For example, the inner subcore of BTV forms a T=2 shell from dimers of the polypeptide VP3. The VP3 interacts through non-equivalent interfaces and these provide the flexibility to form a closed spherical shell. The inherent flexibility of VP3 therefore circumvents the geometrical constrictions placed upon capsomer subunits within spherical particles predicted by Caspar and Klug (1962) (discussed in further detail within the introduction of this thesis and in Grimes et al., 1998). Such asymmetry within dimeric molecules can also be seen within the black widow neurotoxin  $\alpha$ -latrotoxin (LTX). LTX is a hydrophilic pore-forming toxin where the pore subunit is a tetramer composed of two asymmetrical dimers of LTX. In the presence of divalent cations the dimers associate to form a pore complex that contains a 25Å channel running through its centre. Although the relative

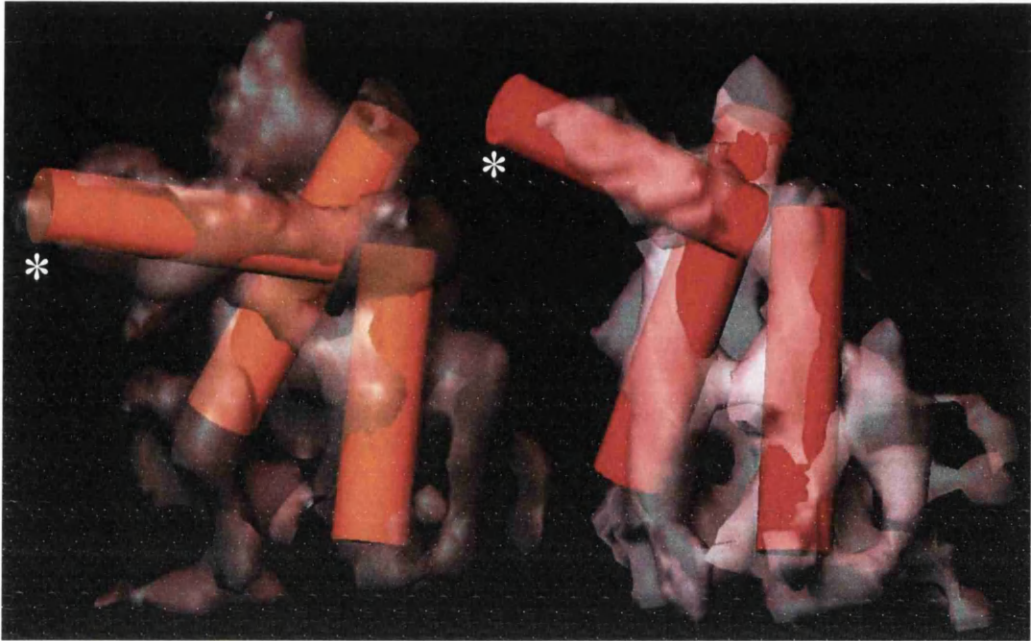
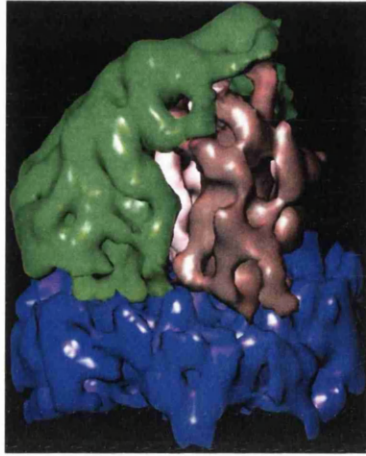


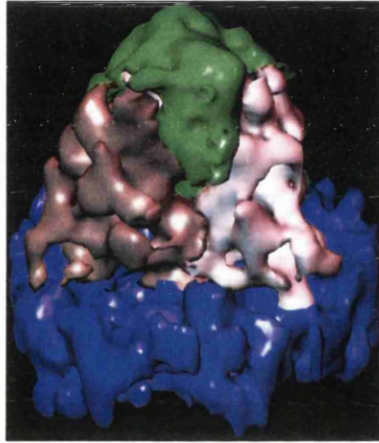
Fig. 4.3: Predicted  $\alpha$ -helices within the two VP23 molecules of an averaged triplex

The putative  $\alpha$ -helices within the two VP23 molecules of an averaged triplex are indicated as red and orange cylinders respectively of  $5\text{\AA}$  in diameter. Protein mass densities relating to the capsid floor (composed of VP5) and VP19c have been removed. The remaining mass density attributed to the VP23 dimer was extracted and the two VP23 molecules aligned to a similar orientation. The white \* highlights the difference in the angle of the upper  $\alpha$ -helix between VP23 molecules.

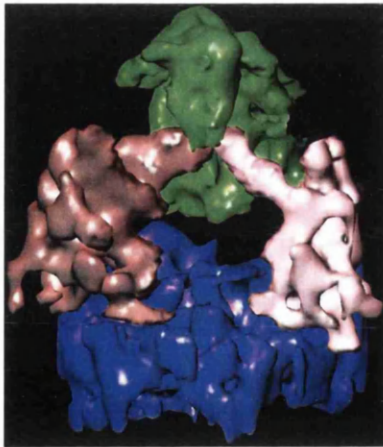
This picture was reproduced with permission from W. Chiu, Baylor College of medicine, USA.



(A)



(B)



(C)

Fig. 4.4: Visualisation of the heterotrimeric interactions within the triplex

(A) Side view of an averaged triplex obtained by averaging the four triplexes ( $T_b$ ,  $T_c$ ,  $T_d$ ,  $T_e$ ) around the C-hexon (opposite view from fig. 4.2). The different colours represent individual capsid proteins; VP19c (green), VP23 (white and grey), and the capsid floor composed of VP5 (blue). (B) Averaged triplex rotated  $120^\circ$  around the 3-fold local axis from position (A). (C) Same view of the averaged triplex as in (B) but VP19c and VP23 molecules separated to demonstrate their conformational organisation within the triplex.

This picture was reproduced with permission from W. Chiu, Baylor College of medicine, USA.

structural domains are similar within the dimer and tetramer, consisting of body, head and wing domains, the relative angle of orientation of these domains between dimer and tetramer is considerably different, ranging between 10-20° (Saibil, 2000). Thus, oligomerisation from dimer to tetramer must require flexibility within the dimeric subunit in order to accommodate these domain movements. The need for this substantial conformational change remains ambiguous but may reflect a functional role in the penetration of the pore complex through membrane structures (Orlova et al., 2000).

#### **4.5 Molten globule characteristics of the triplex**

As previously discussed (within section 3.6) the individual triplex protein molecules represent partially folded protein structures that contain a high degree of secondary structure with little or no stable tertiary structure. These characteristics are similar to those of molten globules, proteins that are in an intermediate state of protein folding. The lack of rigid tertiary structure within proteins in this partially folded state is thought to be necessary to accommodate the arrangement of certain secondary structural elements, such as  $\alpha$ -helices, during folding (Ptitsyn, 1995b). The protein-protein interactions that occur upon association of VP19c and VP23 during triplex formation, result in the development of rigid tertiary structure (as determined by DSC analysis). The generation of this tertiary structure appears to involve the mutual co-folding of protein domains from both VP23 and VP19c, as dimeric VP23 has little rigid tertiary structure of its own. However, the triplexes still appear to retain a degree of partial folding, with the fluorescent hydrophobic probe ANS having access to the interior of the triplex molecule. Thus, although at least some domains of the triplex have defined tertiary structure, the triplex as a whole retains flexible elements that can undergo further conformational rearrangement and folding. In relation to the macromolecular assembly of the capsid the triplex would therefore represent a flexible intermediate protein subunit and as such could be defined as a 'highly ordered molten globule-like' protein complex (Redfield et al., 1994). The plasticity inherent in such from such a molten globule-like state would provide the flexibility necessary to attain such non-equivalent interactions as those seen within the mature polyhedral HSV-1 capsid.

## 4.6 Gross conformational rearrangements and the capsid floor

One of the largest conformational changes to regularly occur during virus assembly is the transition from procapsid to mature capsid (figs. 1.13 and 1.15). Procapsids have been documented in a number of dsDNA viruses, such as the bacteriophage P22 (discussed in the introduction of this thesis), and more recently within HSV-1 capsids (Newcomb et al., 1996; Trus et al., 1996; Tuma and Thomas, 1997; Newcomb et al., 2000). However, procapsids are not limited to dsDNA viruses and have recently been observed as assembly intermediates of non-enveloped small RNA viruses such as *Nudaurelia capensis*  $\omega$  virus (Canady et al., 2000). In dsDNA viruses, procapsids are thought to represent an intermediate capsid assembly stage at which point the scaffold protein subunits are removed from the precursor capsid shell before the packaging of the nucleic acid genome (King et al., 1976; Prevelige and King, 1993; Iiag et al., 1995). DNA packaging during bacteriophage assembly has been demonstrated to occur specifically during the procapsid transition and this is also thought to be the stage at which DNA packaging occurs within the HSV-1 capsid. During assembly, the HSV-1 capsid has been shown to be progressively built up by the incremental addition of VP5 and scaffold subunits inter-linked by triplexes. The increasing addition of subunits to the growing structure leads to the formation of partial capsids and eventually to closed spherical particles ‘procapsids’ (fig. 1.14) (Newcomb et al., 1996; Newcomb et al., 1999). Procapsids are spherical, lacking the flat facets, angular edges and vertices associated with the mature polyhedral form. They exhibit no local 6-fold symmetry, for example the P, E, and C hexon capsomer subunits taking on oval, highly oval, and triangular appearances respectively, and their respective protomers have little or no interconnecting density. In comparison, their structures within the mature polyhedral capsid are hexagonal and tightly packed in appearance, with strong interconnecting densities (Trus et al., 1996; Zhou et al., 1994; Zhou et al., 1998). Thus, the procapsid of HSV-1 could in itself be considered as a flexible protein intermediate on a macromolecular scale where considerable protein rearrangements occur upon procapsid maturation.

One of the most significant differences between procapsids and mature polyhedral capsid is within the floor domain. Capsomers in the HSV-1 procapsid have little contact with each other except through the triplexes located at the 3-fold axes. The capsid floor is

largely undefined and contains large gaps between the capsomeric subunits. The triplexes connecting adjacent capsomers appear to make no contact with the floor domain unlike triplexes within the mature capsid. Furthermore, triplexes in the procapsid appear to interact triangularly with all three adjacent capsomers. Maturation of the procapsid therefore results in large-scale conformational changes. Individual capsomeric subunits become more compact taking on their respective hexavalent or pentavalent structures and develop connections leading to the formation of the capsid floor, thought in part to be interconnected by the N-terminal  $\alpha$ -helices of VP5 protomers (Zhou et al., 2000). The triplexes become anchored to the capsid floor and develop their unique non-equivalent connections between capsomeric subunits (Trus et al., 1996; Zhou et al., 2000). At the current resolution of the HSV-1 procapsid structure the processes involved in such radical conformational changes remain unclear. However, it is clear that the observed changes would require particular flexibility within subunit structures in order to accommodate such gross conformational rearrangements in inter/intra-capsomer interactions. Therefore, the experimental findings described above, that the triplex forms a partially flexible protein subunit with both highly ordered and molten globule-like characteristics, are consistent with the known procapsid and mature HSV-1 capsid structures.

Once maturation is complete further stability may be provided through the formation of disulphide bonds. Zweig et al., (1979) demonstrated that VP5 and VP19c were disulphide linked within mature HSV-2 icosahedral capsids. Although the VP5/VP19c disulphide linkage has yet to be identified within HSV-1 capsid, significant band shifts can be detected when analysing purified HSV-1 capsids by non-reducing SDS-PAGE analysis (for an example see fig. 3.3.13). This would therefore indicate a role for disulphide bonding within the HSV-1 capsid. However, Newcomb et al., (1994) demonstrated that the assembly of capsids could occur in the presence of 10mM DTT, which would imply that disulphide bond formation is not essential for capsid polymerisation to occur. As disulphide bond formation is generally considered to occur as a late event in the protein-folding pathway, these disulphide connections could be seen to fix the partially flexible structures into rigid conformations in order to provide structural reinforcement leading to a more robust capsid structure. Cysteine residues within the triplex, in particular those conserved cysteines within VP23 molecules, might also aid the inter-molecular locking of the triplex structure through the formation of intra-molecular disulphide bonds once

maturation is completed and stability is required over flexibility. Such a late role could explain why the highly conserved cysteine residues within VP23 are not essential for capsid formation (discussed further in the conclusion of section 3.3).

#### **4.7 Heterotrimer opposed to homotrimer, the requirement for VP23 within the triplex**

Ever since the composition of the triplex was postulated by Newcomb et al., (1993) to be a ratio of 2:1 of VP23 to VP19c, one of the fundamental questions in respect to HSV-1 capsid structure has been; ‘why are triplexes organised as heterotrimers rather than homotrimers’? Viruses have strict limitations in their coding capacity and therefore the evolution of the triplex as a heterotrimer of two unrelated proteins seems inefficient. Furthermore, small homotrimers have been identified at those local 3-fold symmetry positions interconnecting hexons in other icosahedral virus capsids, for example bacteriophages T4 (*soc*) and  $\lambda$  (*gpD*), and animal viruses such as adenovirus (polypeptide IX) (Ishii and Yanagida, 1977; Colby and Shenk, 1981; van Oostrum and Burnett, 1985; Perucchetti et al., 1988; Dokland and Murialdo, 1993). In such cases these homotrimers have been shown to bind to their respective capsids post-assembly and although not specifically required for assembly are thought to stabilise the capsid by providing structural reinforcement (Furcinitti et al., 1989). DSC analysis on T4 capsids showed that the presence or absence of *soc* proteins altered their thermostability during temperature denaturation, reinforcing the idea that these homotrimeric proteins are specifically involved in capsid stabilisation (Ross et al., 1985; Steven et al., 1992).

However, all herpes viruses studied to date contain triplexes at all local 3-fold positions and where the capsid composition is known they are composed of heterotrimers of two unrelated proteins (Davison, 1993; Davison 1995). Although their relative sequence homology is not particularly conserved their structural position at the 3-fold symmetry axis and their stoichiometry within their appropriate capsid structures appears to be well conserved in those capsid structures analysed to date (Baker et al., 1990; Booy et al., 1996; Davison et al., 1995).

#### 4.7.1 *The function of VP23 within the triplex*

It has been established through cryo-EM analysis that one of the primary functions of VP19c during capsid assembly is to interconnect adjacent capsomers and that this function is essential for the assembly of capsids. Indeed, the expression of VP5 and VP19c in the baculovirus system has been shown to lead to the production of smaller icosahedral particles with T=7 symmetry (Tatman et al., 1994; Saad et al., 1999). One might assume therefore that the addition of the scaffold protein subunits would be sufficient to direct capsid assembly to produce T=16 icosahedral particles. However, the baculovirus system has demonstrated that the co-expression of VP5, VP19c, and scaffold (either preVP22a or VP21/VP24) without VP23 results in the formation of irregular capsids. VP23 is therefore essential for the production of mature T=16 polyhedral capsids (Tatman et al., 1994; Thomsen et al., 1994).

Analysis of VP5/VP19c particles has also demonstrated that T=7 particles lack the intricate network of interactions found within the capsid floor of polyhedral HSV-1 capsids (Saad et al., 1999). Procapsids have also been shown to lack such interconnecting densities within the capsid floor (Trus et al., 1996; Newcomb et al., 2000). As VP23 appears to make contact with VP5 within the floor domain of mature capsids, VP23 may be responsible for initiating or directing the conformational rearrangements of protein densities within the capsid floor from surrounding capsomers during procapsid maturation.

It is of interest to note that homotrimers associated with capsid assembly, for example polypeptide IX homotrimers from adenovirus capsids, have only been shown to interact around the local 3-fold axes of symmetry surrounding hexon capsomeric subunits (van Oostrum and Burnett, 1985). The conformational differences in the bonding arrangements within the floor domains surrounding pentons and hexons may therefore require additional flexibility within subunits occupying the 3-fold symmetry axes surrounding the penton capsomers. The non-equivalent nature of VP23 molecules within the triplex and their molten globule like structure may provide the conformational flexibility needed to direct folding events during floor development at all 3-fold axes surrounding both pentons and hexons. In a similar manner to the homotrimers found in other icosahedral capsids, the contacts made by VP23 and VP19c to the capsid floor act as cement by interlocking the

floor protein interfaces and providing increased rigidity throughout the capsid. Such conformational variation in protein interfaces within the capsid floor between pentons and hexons, and between the different quasi-equivalent hexons, may also account for the observed differences in the bonding of VP19c within triplexes 'T<sub>a</sub>-T<sub>e</sub>' to their respective capsomers. For example, although the triplex appears to be partially flexible the constrictions placed upon VP23 during floor maturation could force VP19c to alter its triangular capsomeric arrangement within the procapsid so that VP19c becomes anchored to the capsid floor. The differences observed in the binding of VP19c to its surrounding capsomers would therefore reflect the degree of conformational variation in VP23 interactions made during floor development. Indeed, those triplexes that appear to have the most variation in their VP19c capsomer binding interfaces, namely 'T<sub>a</sub>' and 'T<sub>c</sub>', are located at peripentonal or close to peripentonal positions respectively within the icosahedral lattice (Zhou et al., 2000). The flexibility derived from the molten globule-like state of individual triplex protein molecules, in particular VP23, would provide the conformational flexibility to form contacts at all positions 3-fold axes of symmetry within the icosahedral lattice.

It seems reasonable to speculate that, as a trimeric complex appears essential at all positions of 3-fold symmetry within the HSV-1, the virus has evolved the triplex complex as a conformationally flexible heterotrimer. The development of such conformational flexibility through the association of VP23 and VP19c as a heterotrimer allows the triplex to play an essential and dynamic role in the assembly and maturation of the HSV-1 capsid. The transitions in triplex conformation during capsid assembly are schematically illustrated in fig. 4.5.

#### **4.8 VP5 capsomer flexibility**

As previously discussed in the introduction to this thesis VP5 makes up the entire mass of pentons (5 copies of VP5) and the majority of the mass of hexons (6 copies of VP5). Computational comparison of VP5 molecules from pentons and hexons has demonstrated that they have similar overall conformations. However, pentons and hexons have distinctly different properties. For example, pentons interact with tegument proteins

following capsids assembly while VP26 only binds to hexons (Zhou et al., 1995; Zhou et al., 1999). Such differences in biological properties between pentons and hexons can be attributed to conformational differences between their VP5 subunits. These differences are evident post-assembly and consequently when VP5 is fully folded. Thus, the attachment of VP26 to the tips of the hexons requires VP5 molecules within the hexavalent capsomers to have undergone their conformational rearrangement, as VP26 molecules do not associate with the hexons in purified HSV-1 procapsids (Newcomb et al., 1999; Newcomb et al., 2000; Chi and Wilson, 2000). The conformational differences between VP5 protomers in hexons and pentons have also been detected immunogenically. Trus et al., (1992) demonstrated that monoclonal antibodies raised against purified VP5 recognised specific capsomer epitopes on hexons or pentons but not both.

VP5 molecules within pentons have also been shown to contain an extra density of mass within the middle domain of the penton that is absent from hexons thought to be attributed to the closure of the penton channel following the packaging of viral DNA. This extra density has been attributed to the movement of a bundle of short  $\alpha$ -helices, which constricts and thus closes the 25Å channel running through the penton (Zhou et al., 1994; Zhou et al., 2000; personal communication, Frazer Rixon, 2000). Further differences have been seen within the lower domain of the VP5 molecule, in particular the orientation of the predicted long N-terminal  $\alpha$ -helix. Differences in the angle of this  $\alpha$ -helix can be seen not only between VP5 molecules from pentons and hexons but also seen between VP5 molecules from P, E and C hexons (Zhou et al., 1994; Zhou et al., 2000). The conformational differences between VP5 molecules from hexons and pentons, and between the various quasi-equivalent hexons would therefore require a degree of flexibility within specific domains of VP5 during capsid assembly and procapsid maturation. Like the triplex, VP5 must be partially folded as an individual capsid protein in order to account for such conformational flexibility. Indeed, VP5 has been shown to bind ANS and to produce a characteristic increase in fluorescence following excitation (McCelland, 1999 unpublished observations). This would therefore imply that the hydrophobic core of VP5, like that of the triplex, is exposed or partially exposed to the solvent and can undergo further folding. As purified VP5 has been shown to exist as a monomer in solution (Newcomb et al., 1999) this would indicate that VP5 forms hexons and pentons as a partially folded intermediate within the nucleus during the progressive assembly of the

capsid. This is consistent with the evidence generated through cryo-EM analysis of procapsids where individual capsomers appear rounded making little or no intracapsomeric connections (Trus et al., 1996; Newcomb et al., 2000) and supports the notion that VP5 must be able to form a flexible intermediate that can undergo conformational rearrangements during capsid maturation. Like the triplex, VP5 is likely to undergo several changes in conformation before mature capsomers are formed and take on their respective appearances as hexons and pentons within the polyhedral capsid. The final step in the conformational maturation of VP5 protomers presumably creates the structural epitope specificity required for VP26 subunits to bind to the tips of hexons, thereby completing the procapsid maturation transition into WT polyhedral capsids.

Protein synthesis:

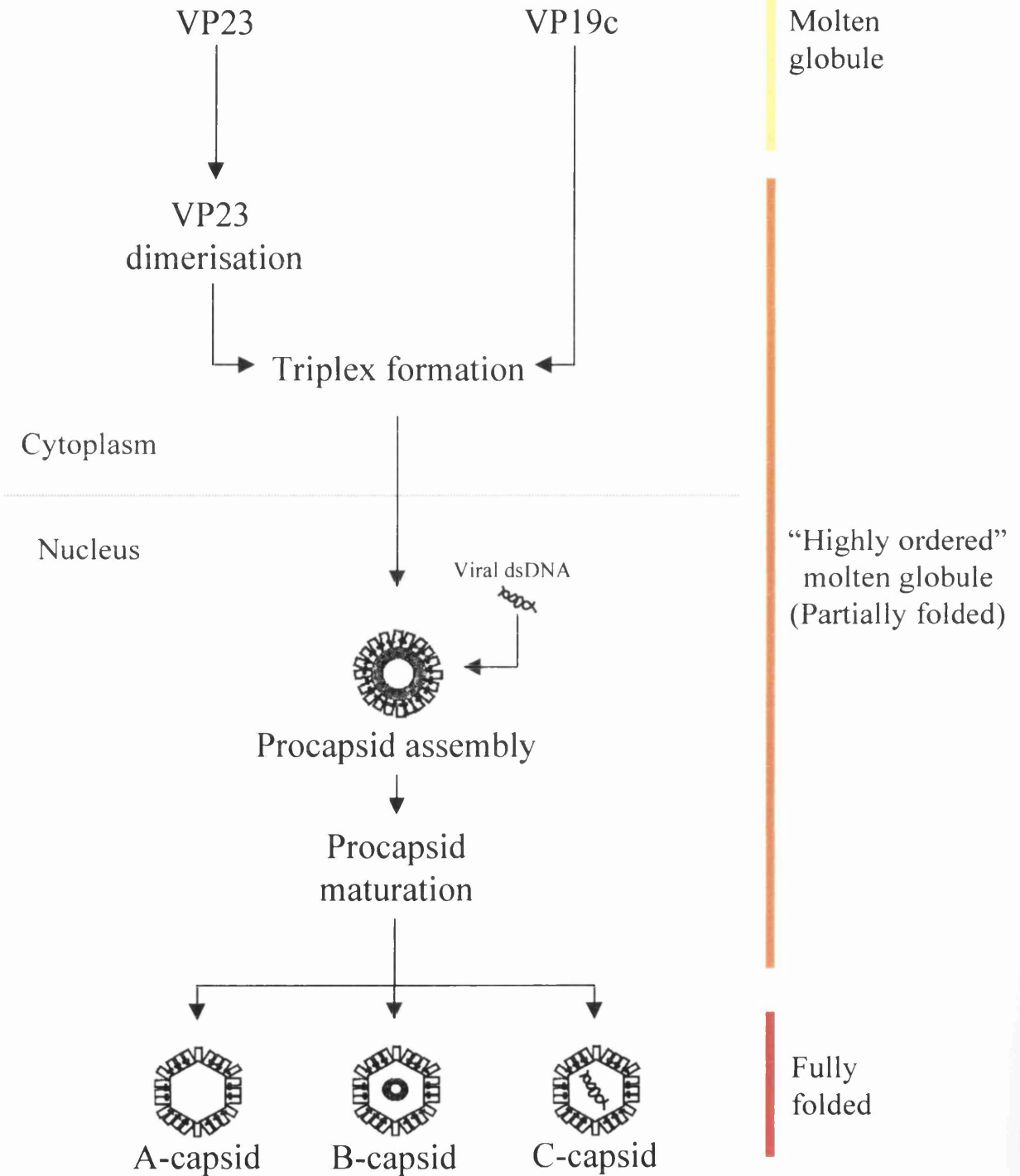


Fig. 4.5: Model for the folding events and cellular localisation of the triplex proteins during capsid assembly

Late gene expression results in the translation of triplex proteins VP23 and VP19c within the cytoplasm of infected cells. Individual triplex proteins are partially folded and take on their respective molten globule like conformations with no rigid tertiary structure. VP23 dimerises, developing some independent tertiary structure, and associates with VP19c resulting in further folding and the development of significant tertiary structure possible through mutual co-folding. Triplexes become localised to the nucleus and associate with VP5 and scaffold proteins resulting in the initiation of capsid assembly. Progressive assembly of triplexes, VP5 complexes, and scaffold occurs until procapsid formation is complete. Scaffold particles exit the procapsid and maturation begins resulting in the angularisation of the capsid and the packaging of the viral dsDNA genome at an unknown point during maturation. Successful packaging of the genome results in mature polyhedral C-capsids that can then go on to produce infectious progeny virions. Unsuccessful attempts in the packaging of the viral DNA or scaffold disassembly results in the production of A and B-capsids respectively. The coloured bar represents the transitions in folding of the triplex proteins during capsid assembly from molten globule (yellow), to “highly ordered molten globule” (orange), to fully folded (red).

# Chapter 5

## Summary

## 5.0 Summary

### 5.1 Partial folding and capsid assembly

High-resolution analysis of various viral capsid structures, either by X-ray crystallography or cryo-EM, has demonstrated that capsids are architecturally complex macromolecular assemblies. It is becoming increasingly evident that the assembly of such capsids does not represent the straightforward geometrical association of static protein subunits. In other words, it is becoming appreciated that capsid assembly is a dynamic folding cascade on a macromolecular level and not just the progressive association of fully folded rigid building blocks. This is particularly evident in those capsid structures that do not conform to the classic quasi-equivalence model, such as the SV40 capsid (Liddington et al., 1991). The nature of the association between subunits within such structures requires that individual molecules must have a degree of flexibility in order to accommodate the differing interactions with their surrounding subunits that are required to produce a closed spherical particle. Similarly, the intricate network of associations between complex subunit or protomer structures seen within a number of viral capsids must require the association of these capsomer structures to pass through a series of partially folded intermediate stages before forming the conformationally mature structures seen in a high-resolution image. For example, X-ray crystallography analysis of the adenovirus type-2 hexon has demonstrated that it is composed of three copies of the major coat protein. The three major coat protein molecules have been shown to interpenetrate each other to form a compact homotrimer (Athappilly et al., 1994). The association of rigid coat protein subunits could not account for such an intricate association, which could only be achieved by extensive mutual co-folding of individual coat protein molecules during hexon formation. Therefore, it is likely that individual hexon protein molecules are partially folded and pass through a number of intermediate folding stages to form a conformationally mature hexon subunit structure. In addition, all capsids that undergo large-scale conformational changes during assembly, for example during procapsid maturation, must by definition, contain flexible elements in order to accommodate the necessary domain movements. Partial folding of individual capsid protein components could provide the flexibility required for such gross conformational rearrangements during capsid assembly.

## 5.2 Partial folding and HSV-1 capsid assembly

Unlike the adenovirus hexon and SV40 capsid, the structure of the HSV-1 capsid has yet to be resolved by X-ray crystallography and therefore little can be specifically concluded about the exact protein-protein interactions within the mature polyhedral capsid. However, high-resolution cryo-EM analysis has provided clear indications of specific protein mass densities within the HSV-1 capsid and has highlighted significant differences in capsomer interactions throughout the icosahedral lattice. Although it is difficult to speculate whether or not the differences in bonding arrangements of quasi-equivalent VP5 protomers between hexons and pentons exceeds those predicted by quasi-equivalence, it is clear that domain flexibility throughout individual VP5 molecules is required. Such flexibility could be achieved by individual VP5 molecules existing in a 'highly ordered molten globule-like' state post-translation (currently under analysis within our laboratory).

However, it is clear from cryo-EM analysis of HSV-1 capsids that the asymmetry of the 'T<sub>a</sub>-T<sub>e</sub>' triplexes and the transitions observed from procapsid to polyhedral capsid do violate the rules of deformable bonds predicted by the theory of quasi-equivalence (Caspar and Klug, 1962). The assembly of the HSV-1 capsid has been shown to occur through the progressive addition of subunits to a growing shell (Newcomb et al., 1996). As discussed above, proteins within this growing macromolecular structure must possess a degree of domain flexibility in order to assemble efficiently and mature into polyhedral capsids that are capable of packaging the viral nucleic acid. Triplexes play a fundamental role in the assembly of the HSV-1 capsid from the initiation of precursor shells, to procapsid formation, and eventually to the maturation into polyhedral capsids. Although the energetics of the folding transitions of proteins involved in the assembly of the HSV-1 capsid have yet to be analysed, folding through flexible intermediates would provide a basis for efficient polymerisation of viral capsids without resulting in cumulative dead end abortive structures incapable of producing infectious progeny virions. The molten globule-like characteristics of the individual triplex proteins and the highly ordered molten globule-like characteristics of the triplex provide some explanation to how these observed structural transitions can occur and provide a deeper insight into the complexities of folding pathways for large macromolecular structures.

---

## References

- Addison, C., Rixon, F. J., Palfreyman, J. W., O'Hara, M. & Preston, V. G. (1984). Characterisation of a herpes simplex virus type 1 mutant which has a temperature-sensitive defect in penetration of cells and assembly of capsids. *Virology* **138**, 246-59.
- Addison, C., Rixon, F. J. & Preston, V. G. (1990). Herpes simplex virus type 1 UL28 gene product is important for the formation of mature capsids. *J Gen Virol* **71**, 2377-84.
- Allen, K. E. & Everett, R. D. (1997). Mutations which alter the DNA binding properties of the herpes simplex virus type 1 transactivating protein Vmw175 also affect its ability to support virus replication. *J Gen Virol* **78**, 2913-22.
- Athappilly, F. K., Murali, R., Rux, J. J., Cai, Z. & Burnett, R. M. (1994). The refined crystal structure of hexon, the major coat protein of adenovirus type 2, at 2.9 Å resolution. *J Mol Biol* **242**, 430-55.
- Baines, J. D., Koyama, A. H., Huang, T. & Roizman, B. (1994). The UL21 gene products of herpes simplex virus 1 are dispensable for growth in cultured cells. *J Virol* **68**, 2929-36.
- Baines, J. D. & Roizman, B. (1992). The UL11 gene of herpes simplex virus 1 encodes a function that facilitates nucleocapsid envelopment and egress from cells. *J Virol* **66**, 5168-74.
- Baker, T. S., Newcomb, W. W., Booy, F. P., Brown, J. C. & Steven, A. C. (1990). Three-dimensional structures of maturable and abortive capsids of equine herpesvirus 1 from cryoelectron microscopy. *J Virol* **64**, 563-73.
- Batterson, W., Furlong, D. & Roizman, B. (1983). Molecular genetics of herpes simplex virus. VIII. further characterization of a temperature-sensitive mutant defective in release of viral DNA and in other stages of the viral reproductive cycle. *J Virol* **45**, 397-407.
- Bazinet, C. & King, J. (1988). Initiation of P22 procapsid assembly in vivo. *J Mol Biol* **202**, 77-86.
- Berk, A. J., Boyer, T. G., Kapanidis, A. N., Ebright, R. H., Kobayashi, N. N., Horn, P. J., Sullivan, S. M., Koop, R., Surby, M. A. & Triezenberg, S. J. (1998). Mechanisms of viral activators. *Cold Spring Harb Symp Quant Biol* **63**, 243-52.
- Boehmer, P. E. & Lehman, I. R. (1997). Herpes simplex virus DNA replication. *Annu Rev Biochem* **66**, 347-84.
- Booy, F. P., Newcomb, W. W., Trus, B. L., Brown, J. C., Baker, T. S. & Steven, A. C. (1991). Liquid-crystalline, phage-like packing of encapsidated DNA in herpes simplex virus. *Cell* **64**, 1007-15.
- Booy, F. P., Trus, B. L., Davison, A. J. & Steven, A. C. (1996). The capsid architecture of channel catfish virus, an evolutionarily distant herpesvirus, is largely conserved in the absence of discernible sequence homology with herpes simplex virus. *Virology* **215**, 134-41.
- Booy, F. P., Trus, B. L., Newcomb, W. W., Brown, J. C., Conway, J. F. & Steven, A. C. (1994). Finding a needle in a haystack: detection of a small protein (the 12-kDa VP26) in a large complex (the 200-MDa capsid of herpes simplex virus). *Proc Natl Acad Sci U S A* **91**, 5652-6.
-

- Brandimarti, R. & Roizman, B. (1997). Us9, a stable lysine-less herpes simplex virus 1 protein, is ubiquitinated before packaging into virions and associates with proteasomes. *Proc Natl Acad Sci U S A* **94**, 13973-8.
- Bronstein, J. C., Weller, S. K. & Weber, P. C. (1997). The product of the UL12.5 gene of herpes simplex virus type 1 is a capsid-associated nuclease. *J Virol* **71**, 3039-47.
- Browne, H., Bell, S., Minson, T. & Wilson, D. W. (1996). An endoplasmic reticulum-retained herpes simplex virus glycoprotein H is absent from secreted virions: evidence for reenvelopment during egress. *J Virol* **70**, 4311-6.
- Buckmaster, A. E., Scott, S. D., Sanderson, M. J., Boursnell, M. E., Ross, N. L. & Binns, M. M. (1988). Gene sequence and mapping data from Marek's disease virus and herpesvirus of turkeys: implications for herpesvirus classification. *J Gen Virol* **69**, 2033-42.
- Butcher, S. J., Aitken, J., Mitchell, J., Gowen, B. & Dargan, D. J. (1998). Structure of the human cytomegalovirus B capsid by electron cryomicroscopy and image reconstruction. *J Struct Biol* **124**, 70-6.
- Campadelli-Fiume, G., Farabegoli, F., Di Gaeta, S. & Roizman, B. (1991). Origin of unenveloped capsids in the cytoplasm of cells infected with herpes simplex virus 1. *J Virol* **65**, 1589-95.
- Canady, M. A., Tihova, M., Hanzlik, T. N., Johnson, J. E. & Yeager, M. (2000). Large conformational changes in the maturation of a simple RNA virus, nudaurelia capensis omega virus (NomegaV). *J Mol Biol* **299**, 573-84.
- Casjens, S. (1997). Principles of virion structure, function, and assembly. In *Structural biology of viruses*. W. Chiu, R. Burnett, and R. Garcea (Eds): Oxford University Press, New York., 3-37.
- Caspar, D. & Klug, A. (1962). Physical principles in the construction of regular viruses. *Cold Spring Harbour Symp. Quant. Biol.* **27**, 1-24.
- Cavalcoli, J. D., Baghian, A., Homa, F. L. & Kousoulas, K. G. (1993). Resolution of genotypic and phenotypic properties of herpes simplex virus type 1 temperature-sensitive mutant (KOS) tsZ47: evidence for allelic complementation in the UL28 gene. *Virology* **197**, 23-34.
- Cerritelli, M. E., Cheng, N., Rosenberg, A. H., McPherson, C. E., Booy, F. P. & Steven, A. C. (1997). Encapsidated conformation of bacteriophage T7 DNA. *Cell* **91**, 271-80.
- Chen, D. H., Jiang, H., Lee, M., Liu, F. & Zhou, Z. H. (1999). Three-dimensional visualization of tegument/capsid interactions in the intact human cytomegalovirus. *Virology* **260**, 10-6.
- Chevray, P. M. & Nathans, D. (1992). Protein interaction cloning in yeast: identification of mammalian proteins that react with the leucine zipper of Jun. *Proc Natl Acad Sci U S A* **89**, 5789-93.
- Chi, J. H. & Wilson, D. W. (2000). ATP-Dependent localization of the herpes simplex virus capsid protein VP26 to sites of procapsid maturation. *J Virol* **74**, 1468-76.
- Chowdhury, S. I. & Batterson, W. (1994). Transinhibition of herpes simplex virus replication by an inducible cell-resident gene encoding a dysfunctional VP19c capsid protein. *Virus Res* **33**, 67-87.
- Cohen, G. H., Ponce de Leon, M., Diggelmann, H., Lawrence, W. C., Vernon, S. K. & Eisenberg, R. J. (1980). Structural analysis of the capsid polypeptides of herpes simplex virus types 1 and 2. *J Virol* **34**, 521-31.
- Colby, W. W. & Shenk, T. (1981). Adenovirus type 5 virions can be assembled in vivo in the absence of detectable polypeptide IX. *J Virol* **39**, 977-80.

- Conway, J. F., Trus, B. L., Booy, F. P., Newcomb, W. W., Brown, J. C. & Steven, A. C. (1993). The effects of radiation damage on the structure of frozen hydrated HSV-1 capsids. *J Struct Biol* **111**, 222-33.
- Cooper, A. (1999). Thermodynamics of protein folding and stability. In *Protein: A comprehensive treatise*. JAI Press, Inc. Vol.2, 217-270.
- Costa, R. H., Cohen, G., Eisenberg, R., Long, D. & Wagner, E. (1984). Direct demonstration that the abundant 6-kilobase herpes simplex virus type 1 mRNA mapping between 0.23 and 0.27 map units encodes the major capsid protein VP5. *J Virol* **49**, 287-92.
- Crick, F. & Watson, J. (1956). The structure of small viruses. *Nature* **177**, 473-475.
- Dargan, D. J. & Subak-Sharpe, J. H. (1997). The effect of herpes simplex virus type 1 L-particles on virus entry, replication, and the infectivity of naked herpesvirus DNA. *Virology* **239**, 378-88.
- Davison, A. J. (1993). Herpesvirus genes. *Reviews in medical virology* **3**, 237-244.
- Davison, A. J. & Davison, M. D. (1995). Identification of structural proteins of channel catfish virus by mass spectrometry. *Virology* **206**, 1035-43.
- Davison, M. D., Rixon, F. J. & Davison, A. J. (1992). Identification of genes encoding two capsid proteins (VP24 and VP26) of herpes simplex virus type 1. *J Gen Virol* **73**, 2709-13.
- de Bruyn Kops, A. & Knipe, D. M. (1994). Preexisting nuclear architecture defines the intranuclear location of herpesvirus DNA replication structures. *J Virol* **68**, 3512-26.
- de Bruyn Kops, A., Uprichard, S. L., Chen, M. & Knipe, D. M. (1998). Comparison of the intranuclear distributions of herpes simplex virus proteins involved in various viral functions. *Virology* **252**, 162-78.
- Desai, P., DeLuca, N. A., Glorioso, J. C. & Person, S. (1993). Mutations in herpes simplex virus type 1 genes encoding VP5 and VP23 abrogate capsid formation and cleavage of replicated DNA. *J Virol* **67**, 1357-64.
- Desai, P., DeLuca, N. A. & Person, S. (1998). Herpes simplex virus type 1 VP26 is not essential for replication in cell culture but influences production of infectious virus in the nervous system of infected mice. *Virology* **247**, 115-24.
- Desai, P. & Person, S. (1996). Molecular interactions between the HSV-1 capsid proteins as measured by the yeast two-hybrid system. *Virology* **220**, 516-21.
- Desai, P. & Person, S. (1998). Incorporation of the green fluorescent protein into the herpes simplex virus type 1 capsid. *J Virol* **72**, 7563-8.
- Desai, P. & Person, S. (1999). Second site mutations in the N-terminus of the major capsid protein (VP5) overcome a block at the maturation cleavage site of the capsid scaffold proteins of herpes simplex virus type 1. *Virology* **261**, 357-66.
- DiIanni, C. L., Mapelli, C., Drier, D. A., Tsao, J., Natarajan, S., Riexinger, D., Festin, S. M., Bolgar, M., Yamanaka, G., Weinheimer, S. P. & et al. (1993). In vitro activity of the herpes simplex virus type 1 protease with peptide substrates. *J Biol Chem* **268**, 25449-54.
- Dill, K. A. (1990). The meaning of hydrophobicity. *Science* **250**, 297-8.
- Dokland, T. & Murialdo, H. (1993). Structural transitions during maturation of bacteriophage lambda capsids. *J Mol Biol* **233**, 682-94.
- Durfee, T., Becherer, K., Chen, P. L., Yeh, S. H., Yang, Y., Kilburn, A. E., Lee, W. H. & Elledge, S. J. (1993). The retinoblastoma protein associates with the protein phosphatase type 1 catalytic subunit. *Genes Dev* **7**, 555-69.

- Earnshaw, W. C. & Casjens, S. R. (1980). DNA packaging by the double-stranded DNA bacteriophages. *Cell* **21**, 319-31.
- Eberle, R. & Courtney, R. J. (1980). gA and gB glycoproteins of herpes simplex virus type 1: two forms of a single polypeptide. *J Virol* **36**, 665-75.
- Elgadi, M. M., Hayes, C. E. & Smiley, J. R. (1999). The herpes simplex virus vhs protein induces endoribonucleolytic cleavage of target RNAs in cell extracts. *J Virol* **73**, 7153-64.
- Elliott, G. & O'Hare, P. (1998). Herpes simplex virus type 1 tegument protein VP22 induces the stabilization and hyperacetylation of microtubules. *J Virol* **72**, 6448-55.
- Elliott, G. & O'Hare, P. (1999). Live-cell analysis of a green fluorescent protein-tagged herpes simplex virus infection. *J Virol* **73**, 4110-9.
- Evans, A. S. & Niedermen, J. C. (1991). Epstein-Barr virus. In *Viral infections of humans*. A. Evans (Ed). Plenum publishing corporation, New York, N.Y. **3rd ed.**, 265-292.
- Everett, R. D. (2000). ICP0, a regulator of herpes simplex virus during lytic and latent infection. *Bioessays* **22**, 761-70.
- Everly, D. N., Jr. & Read, G. S. (1999). Site-directed mutagenesis of the virion host shutoff gene (UL41) of herpes simplex virus (HSV): analysis of functional differences between HSV type 1 (HSV-1) and HSV-2 alleles. *J Virol* **73**, 9117-29.
- Falgout, B. & Ketner, G. (1988). Characterization of adenovirus particles made by deletion mutants lacking the fiber gene. *J Virol* **62**, 622-5.
- Feng, Y., Sligar, S. G. & Wand, A. J. (1994). Solution structure of apocytochrome b562. *Nat Struct Biol* **1**, 30-5.
- Fields, S. & Song, O. (1989). A novel genetic system to detect protein-protein interactions. *Nature* **340**, 245-6.
- Flint, S. J., Enquist, L. W., Krug, R. M., Racaniello, V. R. & Skalka, A. M. (2000). Herpesviruses. In *Principles of virology. Molecular biology, pathogenesis, and control*. American Society for microbiology, 774-777.
- Fox, J. M., Albert, F. G., Speir, J. A. & Young, M. J. (1997). Characterization of a disassembly deficient mutant of cowpea chlorotic mottle virus. *Virology* **227**, 229-33.
- Freifelder, D. (1982). *Physical Biochemistry*, 2nd edn: W. H. Freeman and Co., New York, N.Y.
- Fuchs, A., Seiderer, C. & Seckler, R. (1991). In vitro folding pathway of phage P22 tailspike protein. *Biochemistry* **30**, 6598-604.
- Fuller, M. T. & King, J. (1981). Purification of the coat and scaffolding proteins from procapsids of bacteriophage P22. *Virology* **112**, 529-47.
- Fuller, M. T. & King, J. (1982). Assembly in vitro of bacteriophage P22 procapsids from purified coat and scaffolding subunits. *J Mol Biol* **156**, 633-65.
- Furcinitti, P. S., van Oostrum, J. & Burnett, R. M. (1989). Adenovirus polypeptide IX revealed as capsid cement by difference images from electron microscopy and crystallography. *Embo J* **8**, 3563-70.
- Furlong, D. (1978). Direct evidence for 6-fold symmetry of the herpesvirus hexon capsomere. *Proc Natl Acad Sci U S A* **75**, 2764-6.
- Furlong, D., Swift, H. & Roizman, B. (1972). Arrangement of herpesvirus deoxyribonucleic acid in the core. *J Virol* **10**, 1071-4.
- Galisteo, M. L. & King, J. (1993). Conformational transformations in the protein lattice of phage P22 procapsids. *Biophys J* **65**, 227-35.
- Gao, M., Matusick-Kumar, L., Hurlburt, W., DiTusa, S. F., Newcomb, W. W., Brown, J. C., McCann, P. J., 3rd, Deckman, I. & Colonno, R. J. (1994). The protease of

- herpes simplex virus type 1 is essential for functional capsid formation and viral growth. *J Virol* **68**, 3702-12.
- Geraghty, R. J., Krumpal, C., Cohen, G. H., Eisenberg, R. J. & Spear, P. G. (1998). Entry of alphaherpesviruses mediated by poliovirus receptor-related protein 1 and poliovirus receptor. *Science* **280**, 1618-20.
- Gibson, W. & Roizman, B. (1972). Proteins specified by herpes simplex virus. 8. Characterization and composition of multiple capsid forms of subtypes 1 and 2. *J Virol* **10**, 1044-52.
- Gibson, W. & Roizman, B. (1974). Proteins specified by herpes simplex virus. Staining and radiolabeling properties of B capsid and virion proteins in polyacrylamide gels. *J Virol* **13**, 155-65.
- Gold, E. & Nankervis, G. A. (1991). Cytomegalovirus. In *Viral infections of humans. A. Evans (Ed). Plenum publishing corporation, New York, N.Y. 3rd ed.*, 169-189.
- Goldstein, J. N. & Weller, S. K. (1998). In vitro processing of herpes simplex virus type 1 DNA replication intermediates by the viral alkaline nuclease, UL12. *J Virol* **72**, 8772-81.
- Gominak, S., Cros, D. & Paydarfar, D. (1990). Herpes simplex labialis and trigeminal neuropathy. *Neurology* **40**, 151-2.
- Goshima, F., Watanabe, D., Takakuwa, H., Wada, K., Daikoku, T., Yamada, M. & Nishiyama, Y. (2000). Herpes simplex virus UL17 protein is associated with B capsids and colocalizes with ICP35 and VP5 in infected cells. *Arch Virol* **145**, 417-26.
- Greene, B. & King, J. (1994). Binding of scaffolding subunits within the P22 procapsid lattice. *Virology* **205**, 188-97.
- Grimes, J. M., Burroughs, J. N., Gouet, P., Diprose, J. M., Malby, R., Zientara, S., Mertens, P. P. & Stuart, D. I. (1998). The atomic structure of the bluetongue virus core. *Nature* **395**, 470-8.
- Grimmel, M., Zibirre, R. & Koch, G. (1983). Fluorescence spectrophotometric study of structural alterations in the capsid of poliovirus. *Arch Virol* **78**, 191-201.
- Guy, C., Haskell, D. & Li, Q. (1998). Association of proteins with the stress 70 molecular chaperones at low temperature: Evidence for the existence of cold labile proteins in spinach. *Cryobiology* **36**, 301-314.
- Haarr, L. & Skulstad, S. (1994). The herpes simplex virus type 1 particle: structure and molecular functions. Review article. *Apmis* **102**, 321-46.
- Hampton, R. Y. (2000). Getting the UPR hand on misfolded proteins. *Curr Biol* **10**, R518-21.
- Harris-Hamilton, E. & Bachenheimer, S. L. (1985). Accumulation of herpes simplex virus type 1 RNAs of different kinetic classes in the cytoplasm of infected cells. *J Virol* **53**, 144-51.
- Harrison, S. C. (1983). Packaging of DNA into bacteriophage heads: a model. *J Mol Biol* **171**, 577-80.
- Heilman, C. J., Jr., Zweig, M., Stephenson, J. R. & Hampar, B. (1979). Isolation of a nucleocapsid polypeptide of herpes simplex virus types 1 and 2 possessing immunologically type-specific and cross-reactive determinants. *J Virol* **29**, 34-42.
- Heine, J. W., Honess, R. W., Cassai, E. & Roizman, B. (1974). Proteins specified by herpes simplex virus. XII. The virion polypeptides of type 1 strains. *J Virol* **14**, 640-51.
- Hendrix, R. W. (1978). Symmetry mismatch and DNA packaging in large bacteriophages. *Proc Natl Acad Sci U S A* **75**, 4779-83.

- Hendrix, R. W. & Garcea, R. L. (1994). Capsid assembly of dsDNA viruses. *Seminars in Virology* **5**, 15-26.
- Hirst, J. D. & Brooks, C. L., 3rd (1994). Helicity, circular dichroism and molecular dynamics of proteins. *J Mol Biol* **243**, 173-8.
- Hlodan, R. & Pain, R. H. (1994). Tumour necrosis factor is in equilibrium with a trimeric molten globule at low pH. *FEBS Lett* **343**, 256-60.
- Hlodan, R. & Pain, R. H. (1995). The folding and assembly pathway of tumour necrosis factor TNF alpha, a globular trimeric protein. *Eur J Biochem* **231**, 381-7.
- Homa, F. L. & Brown, J. C. (1997). Capsid assembly and DNA packaging in herpes simplex virus. *Rev Med Virol* **7**, 107-122.
- Honess, R. W. & Roizman, B. (1974). Regulation of herpesvirus macromolecular synthesis. I. Cascade regulation of the synthesis of three groups of viral proteins. *J Virol* **14**, 8-19.
- Hong, Z., Beudet-Miller, M., Durkin, J., Zhang, R. & Kwong, A. D. (1996). Identification of a minimal hydrophobic domain in the herpes simplex virus type 1 scaffolding protein which is required for interaction with the major capsid protein. *J Virol* **70**, 533-40.
- Ilag, L. L., Olson, N. H., Dokland, T., Music, C. L., Cheng, R. H., Bowen, Z., McKenna, R., Rossmann, M. G., Baker, T. S. & Incardona, N. L. (1995). DNA packaging intermediates of bacteriophage phi X174. *Structure* **3**, 353-63.
- Ishii, T. & Yanagida, M. (1977). The two dispensable structural proteins (soc and hoc) of the T4 phage capsid; their purification and properties, isolation and characterization of the defective mutants, and their binding with the defective heads in vitro. *J Mol Biol* **109**, 487-514.
- Jao, C. C., Weidman, M. K., Perez, A. R. & Gharakhanian, E. (1999). Cys9, Cys104 and Cys207 of simian virus 40 Vp1 are essential for inter-pentamer disulfide-linkage and stabilization in cell-free lysates. *J Gen Virol* **80**, 2481-9.
- Jerome, K. R., Fox, R., Chen, Z., Sears, A. E., Lee, H. & Corey, L. (1999). Herpes simplex virus inhibits apoptosis through the action of two genes, Us5 and Us3. *J Virol* **73**, 8950-7.
- Johnson, J. E. (1996). Functional implications of protein-protein interactions in icosahedral viruses. *Proc Natl Acad Sci U S A* **93**, 27-33.
- Johnson, J. E. & Speir, J. A. (1997). Quasi-equivalent viruses: a paradigm for protein assemblies. *J Mol Biol* **269**, 665-75.
- Johnston, S. A., Salmeron, J. M., Jr. & Dincher, S. S. (1987). Interaction of positive and negative regulatory proteins in the galactose regulon of yeast. *Cell* **50**, 143-6.
- Kehm, R., Gelderblom, H. R. & Darai, G. (1998). Identification of the UL56 protein of herpes simplex virus type 1 within the virion by immuno electron microscopy. *Virus Genes* **17**, 49-53.
- Kelly, S. M. & Price, N. C. (1996). The application of circular dichroism to studies of protein folding and unfolding. *Biochimica Et Biophysica Acta-Protein Structure and Molecular Enzymology* **1338**, 161-185.
- Kennard, J., Rixon, F. J., McDougall, I. M., Tatman, J. D. & Preston, V. G. (1995). The 25 amino acid residues at the carboxy terminus of the herpes simplex virus type 1 UL26.5 protein are required for the formation of the capsid shell around the scaffold. *J Gen Virol* **76**, 1611-21.
- King, J., Botstein, D., Casjens, S., Earnshaw, W., Harrison, S. & Lenk, E. (1976). Structure and assembly of the capsid of bacteriophage P22. *Philos Trans R Soc Lond B Biol Sci* **276**, 37-49.

- King, J. & Casjens, S. (1974). Catalytic head assembling protein in virus morphogenesis. *Nature* **251**, 112-9.
- King, J. & Chiu, W. (1997). The procapsid-to-capsid transition in double stranded DNA bacteriophage. In *Structural biology of viruses*. W. Chiu, R. Burnett, and R. Garcea (Eds): Oxford Univeristy Press, New York., 288-311.
- Kirkitadze, M. D., Barlow, P. N., Price, N. C., Kelly, S. M., Boutell, C. J., Rixon, F. J. & McClelland, D. A. (1998). The herpes simplex virus triplex protein, VP23, exists as a molten globule. *J Virol* **72**, 10066-72.
- Kishore, G. M. & Shah, D. M. (1988). Amino acid biosynthesis inhibitors as herbicides. *Annu Rev Biochem* **57**, 627-63.
- Koslowski, K. M., Shaver, P. R., Casey, J. T., 2nd, Wilson, T., Yamanaka, G., Sheaffer, A. K., Tenney, D. J. & Pederson, N. E. (1999). Physical and functional interactions between the herpes simplex virus UL15 and UL28 DNA cleavage and packaging proteins. *J Virol* **73**, 1704-7.
- Krummenacher, C., Nicola, A. V., Whitbeck, J. C., Lou, H., Hou, W., Lambris, J. D., Geraghty, R. J., Spear, P. G., Cohen, G. H. & Eisenberg, R. J. (1998). Herpes simplex virus glycoprotein D can bind to poliovirus receptor-related protein 1 or herpesvirus entry mediator, two structurally unrelated mediators of virus entry. *J Virol* **72**, 7064-74.
- Kunkel, T. A. (1985). Rapid and efficient site-specific mutagenesis without phenotypic selection. *Proc Natl Acad Sci U S A* **82**, 488-92.
- Kwong, A. D. & Frenkel, N. (1987). Herpes simplex virus-infected cells contain a function(s) that destabilizes both host and viral mRNAs. *Proc Natl Acad Sci U S A* **84**, 1926-30.
- Kwong, A. D., Kruper, J. A. & Frenkel, N. (1988). Herpes simplex virus virion host shutoff function. *J Virol* **62**, 912-21.
- Lamberti, C. & Weller, S. K. (1998). The herpes simplex virus type 1 cleavage/packaging protein, UL32, is involved in efficient localization of capsids to replication compartments. *J Virol* **72**, 2463-73.
- Laurent, A. M., Madjar, J. J. & Greco, A. (1998). Translational control of viral and host protein synthesis during the course of herpes simplex virus type 1 infection: evidence that initiation of translation is the limiting step. *J Gen Virol* **79**, 2765-75.
- Lee, C. S. & Guo, P. (1995). In vitro assembly of infectious virions of double-stranded DNA phage phi 29 from cloned gene products and synthetic nucleic acids. *J Virol* **69**, 5018-23.
- Lee, J. Y., Hwang, D. & Gillam, S. (1996). Dimerization of rubella virus capsid protein is not required for virus particle formation. *Virology* **216**, 223-7.
- Lee, W. C. & Fuller, A. O. (1993). Herpes simplex virus type 1 and pseudorabies virus bind to a common saturable receptor on Vero cells that is not heparan sulfate. *J Virol* **67**, 5088-97.
- Lehman, I. R. & Boehmer, P. E. (1999). Replication of herpes simplex virus DNA. *J Biol Chem* **274**, 28059-62.
- Lepault, J., Dubochet, J., Baschong, W. & Kellenberger, E. (1987). Organization of double-stranded DNA in bacteriophages: a study by cryo-electron microscopy of vitrified samples. *Embo J* **6**, 1507-12.
- Levy, J. A. (1997). Three new human herpesviruses (HHV6, 7, and 8). *Lancet* **349**, 558-63.
- Li, M., Beard, P., Estes, P. A., Lyon, M. K. & Garcea, R. L. (1998). Intercapsomeric disulfide bonds in papillomavirus assembly and disassembly. *J Virol* **72**, 2160-7.

- Liddington, R. C., Yan, Y., Moulai, J., Sahli, R., Benjamin, T. L. & Harrison, S. C. (1991). Structure of simian virus 40 at 3.8-Å resolution. *Nature* **354**, 278-84.
- Lillicrop, K. A., Estridge, J. K. & Latchman, D. S. (1993). The octamer binding protein Oct-2 inhibits transactivation of the herpes simplex virus immediate-early genes by the virion protein Vmw65. *Virology* **196**, 888-91.
- Liu, F. Y. & Roizman, B. (1991a). The promoter, transcriptional unit, and coding sequence of herpes simplex virus 1 family 35 proteins are contained within and in frame with the UL26 open reading frame. *J Virol* **65**, 206-12.
- Liu, F. Y. & Roizman, B. (1991b). The herpes simplex virus 1 gene encoding a protease also contains within its coding domain the gene encoding the more abundant substrate. *J Virol* **65**, 5149-56.
- Lomonte, P. & Everett, R. D. (1999). Herpes simplex virus type 1 immediate-early protein Vmw110 inhibits progression of cells through mitosis and from G(1) into S phase of the cell cycle. *J Virol* **73**, 9456-67.
- Lycke, E., Hamark, B., Johansson, M., Krotochwil, A., Lycke, J. & Svennerholm, B. (1988). Herpes simplex virus infection of the human sensory neuron. An electron microscopy study. *Arch Virol* **101**, 87-104.
- Ma, J. & Ptashne, M. (1987). Deletion analysis of GAL4 defines two transcriptional activating segments. *Cell* **48**, 847-53.
- MacLean, C. A., Clark, B. & McGeoch, D. J. (1989). Gene UL11 of herpes simplex virus type 1 encodes a virion protein which is myristylated. *J Gen Virol* **70**, 3147-57.
- MacPherson, I. & Stoker, M. (1962). Polyoma transformation of hamster cell clones: an investigation of genetic factors affecting cell competence. *Virology* **16**, 147-151.
- Makhatadze, G. I. & Privalov, P. L. (1993). Contribution of hydration to protein folding thermodynamics. I. The enthalpy of hydration. *J Mol Biol* **232**, 639-59.
- Maniatis, T., Fritsch, E. & Sambrooke, J. (1982). Molecular cloning; A laboratory manual. *Cold Spring Harbour. New York*.
- Martinez, R., Sarisky, R. T., Weber, P. C. & Weller, S. K. (1996). Herpes simplex virus type 1 alkaline nuclease is required for efficient processing of viral DNA replication intermediates. *J Virol* **70**, 2075-85.
- Matulis, D., Baumann, C. G., Bloomfield, V. A. & Lovrien, R. E. (1999). 1-anilino-8-naphthalene sulfonate as a protein conformational tightening agent. *Biopolymers* **49**, 451-8.
- Matulis, D. & Lovrien, R. (1998). 1-Anilino-8-naphthalene sulfonate anion-protein binding depends primarily on ion pair formation. *Biophys J* **74**, 422-9.
- Matusick-Kumar, L., Newcomb, W. W., Brown, J. C., McCann, P. J., 3rd, Hurlburt, W., Weinheimer, S. P. & Gao, M. (1995). The C-terminal 25 amino acids of the protease and its substrate ICP35 of herpes simplex virus type 1 are involved in the formation of sealed capsids. *J Virol* **69**, 4347-56.
- McGeoch, D. J., Cook, S., Dolan, A., Jamieson, F. E. & Telford, E. A. (1995). Molecular phylogeny and evolutionary timescale for the family of mammalian herpesviruses. *J Mol Biol* **247**, 443-58.
- McGeoch, D. J., Dalrymple, M. A., Davison, A. J., Dolan, A., Frame, M. C., McNab, D., Perry, L. J., Scott, J. E. & Taylor, P. (1988). The complete DNA sequence of the long unique region in the genome of herpes simplex virus type 1. *J Gen Virol* **69**, 1531-74.
- McLauchlan, J., Addison, C., Craigie, M. C. & Rixon, F. J. (1992). Noninfectious L-particles supply functions which can facilitate infection by HSV-1. *Virology* **190**, 682-8.

- McLauchlan, J. & Rixon, F. J. (1992). Characterization of enveloped tegument structures (L particles) produced by alphaherpesviruses: integrity of the tegument does not depend on the presence of capsid or envelope. *J Gen Virol* **73**, 269-76.
- McNab, A. R., Desai, P., Person, S., Roof, L. L., Thomsen, D. R., Newcomb, W. W., Brown, J. C. & Homa, F. L. (1998). The product of the herpes simplex virus type 1 UL25 gene is required for encapsidation but not for cleavage of replicated viral DNA. *J Virol* **72**, 1060-70.
- McNabb, D. S. & Courtney, R. J. (1992). Analysis of the UL36 open reading frame encoding the large tegument protein (ICP1/2) of herpes simplex virus type 1. *J Virol* **66**, 7581-4.
- Mertens, P. P., Burroughs, J. N. & Anderson, J. (1987). Purification and properties of virus particles, infectious subviral particles, and cores of bluetongue virus serotypes 1 and 4. *Virology* **157**, 375-86.
- Mocarski, E. S. & Roizman, B. (1982). Structure and role of the herpes simplex virus DNA termini in inversion, circularization and generation of virion DNA. *Cell* **31**, 89-97.
- Montgomery, R. I., Warner, M. S., Lum, B. J. & Spear, P. G. (1996). Herpes simplex virus-1 entry into cells mediated by a novel member of the TNF/NGF receptor family. *Cell* **87**, 427-36.
- Muller, S. & Dejean, A. (1999). Viral immediate-early proteins abrogate the modification by SUMO-1 of PML and Sp100 proteins, correlating with nuclear body disruption. *J Virol* **73**, 5137-43.
- Murphy, K. P., Privalov, P. L. & Gill, S. J. (1990). Common features of protein unfolding and dissolution of hydrophobic compounds. *Science* **247**, 559-61.
- Nahmias, A. J., Keyserling, H. & Lee, F. K. (1991). Herpes simplex viruses 1 and 2. In *Viral infections of humans*. A. Evans (Ed). Plenum publishing corporation, New York, N.Y. **3rd ed.**, 393-413.
- Nakonechny, W. S. & Teschke, C. M. (1998). GroEL and GroES control of substrate flux in the in vivo folding pathway of phage P22 coat protein. *J Biol Chem* **273**, 27236-44.
- Namba, K., Pattanayek, R. & Stubbs, G. (1989). Visualization of protein-nucleic acid interactions in a virus. Refined structure of intact tobacco mosaic virus at 2.9 Å resolution by X-ray fiber diffraction. *J Mol Biol* **208**, 307-25.
- Newcomb, W. W. & Brown, J. C. (1989). Use of Ar<sup>+</sup> plasma etching to localize structural proteins in the capsid of herpes simplex virus type 1. *J Virol* **63**, 4697-702.
- Newcomb, W. W. & Brown, J. C. (1991). Structure of the herpes simplex virus capsid: effects of extraction with guanidine hydrochloride and partial reconstitution of extracted capsids. *J Virol* **65**, 613-20.
- Newcomb, W. W., Homa, F. L., Thomsen, D. R., Booy, F. P., Trus, B. L., Steven, A. C., Spencer, J. V. & Brown, J. C. (1996). Assembly of the herpes simplex virus capsid: characterization of intermediates observed during cell-free capsid formation. *J Mol Biol* **263**, 432-46.
- Newcomb, W. W., Homa, F. L., Thomsen, D. R., Trus, B. L., Cheng, N., Steven, A., Booy, F. & Brown, J. C. (1999). Assembly of the herpes simplex virus procapsid from purified components and identification of small complexes containing the major capsid and scaffolding proteins. *J Virol* **73**, 4239-50.
- Newcomb, W. W., Homa, F. L., Thomsen, D. R., Ye, Z. & Brown, J. C. (1994). Cell-free assembly of the herpes simplex virus capsid. *J Virol* **68**, 6059-63.

- Newcomb, W. W., Trus, B. L., Booy, F. P., Steven, A. C., Wall, J. S. & Brown, J. C. (1993). Structure of the herpes simplex virus capsid. Molecular composition of the pentons and the triplexes. *J Mol Biol* **232**, 499-511.
- Newcomb, W. W., Trus, B. L., Cheng, N., Steven, A. C., Sheaffer, A. K., Tenney, D. J., Weller, S. K. & Brown, J. C. (2000). Isolation of Herpes Simplex Virus Procapsids from Cells Infected with a Protease-Deficient Mutant Virus. *J Virol* **74**, 1663-1673.
- Nicholson, P. (1992). Analysis of four capsid protein genes of HSV-1. *PhD. Thesis, University of Glasgow*.
- Nicholson, P., Addison, C., Cross, A. M., Kennard, J., Preston, V. G. & Rixon, F. J. (1994). Localization of the herpes simplex virus type 1 major capsid protein VP5 to the cell nucleus requires the abundant scaffolding protein VP22a. *J Gen Virol* **75**, 1091-9.
- Nishina, Y., Horiike, K., Shiga, K. & Yamano, T. (1977). A fluorescence study of egg white riboflavin-binding protein. *J Biochem (Tokyo)* **82**, 1715-21.
- Novokhatny, V. V., Kudinov, S. A. & Privalov, P. L. (1984). Domains in human plasminogen. *J Mol Biol* **179**, 215-32.
- Ojala, P. M., Sodeik, B., Ebersold, M. W., Kutay, U. & Helenius, A. (2000). Herpes simplex virus type 1 entry into host cells: reconstitution of capsid binding and uncoating at the nuclear pore complex in vitro. *Mol Cell Biol* **20**, 4922-31.
- Orlova, E. V., Rahman, M. A., Gowen, B., Volynski, K. E., Ashton, A. C., Manser, C., van Heel, M. & Ushkaryov, Y. A. (2000). Structure of alpha-latrotoxin oligomers reveals that divalent cation-dependent tetramers form membrane pores [see comments]. *Nat Struct Biol* **7**, 48-53.
- Overton, H., McMillan, D., Hope, L. & Wong-Kai-In, P. (1994). Production of host shutoff-defective mutants of herpes simplex virus type 1 by inactivation of the UL13 gene. *Virology* **202**, 97-106.
- Parker, M. H. & Prevelige, P. E., Jr. (1998). Electrostatic interactions drive scaffolding/coat protein binding and procapsid maturation in bacteriophage P22. *Virology* **250**, 337-49.
- Patel, A. H. & MacLean, J. B. (1995). The product of the UL6 gene of herpes simplex virus type 1 is associated with virus capsids. *Virology* **206**, 465-78.
- Patel, A. H., Rixon, F. J., Cunningham, C. & Davison, A. J. (1996). Isolation and characterization of herpes simplex virus type 1 mutants defective in the UL6 gene. *Virology* **217**, 111-23.
- Pelletier, A., Do, F., Brisebois, J. J., Lagace, L. & Cordingley, M. G. (1997). Self-association of herpes simplex virus type 1 ICP35 is via coiled-coil interactions and promotes stable interaction with the major capsid protein. *J Virol* **71**, 5197-208.
- Penfold, M. E., Armati, P. & Cunningham, A. L. (1994). Axonal transport of herpes simplex virions to epidermal cells: evidence for a specialized mode of virus transport and assembly. *Proc Natl Acad Sci U S A* **91**, 6529-33.
- Peng, Z. Y. & Kim, P. S. (1994). A protein dissection study of a molten globule. *Biochemistry* **33**, 2136-41.
- Peng, Z. Y., Wu, L. C., Schulman, B. A. & Kim, P. S. (1995). Does the molten globule have a native-like tertiary fold? *Philos Trans R Soc Lond B Biol Sci* **348**, 43-7.
- Perng, G. C., Jones, C., Ciacci-Zanella, J., Stone, M., Henderson, G., Yukht, A., Slanina, S. M., Hofman, F. M., Ghiasi, H., Nesburn, A. B. & Wechsler, S. L. (2000). Virus-induced neuronal apoptosis blocked by the herpes simplex virus latency-associated transcript. *Science* **287**, 1500-3.

- Person, S. & Desai, P. (1998). Capsids are formed in a mutant virus blocked at the maturation site of the UL26 and UL26.5 open reading frames of herpes simplex virus type 1 but are not formed in a null mutant of UL38 (VP19C). *Virology* **242**, 193-203.
- Pertuiset, B., Boccara, M., Cebrian, J., Berthelot, N., Chousterman, S., Puvion-Dutilleul, F., Sisman, J. & Sheldrick, P. (1989). Physical mapping and nucleotide sequence of a herpes simplex virus type 1 gene required for capsid assembly. *J Virol* **63**, 2169-79.
- Perucchetti, R., Parris, W., Becker, A. & Gold, M. (1988). Late stages in bacteriophage lambda head morphogenesis: in vitro studies on the action of the bacteriophage lambda D-gene and W-gene products. *Virology* **165**, 103-14.
- Philipson, L., Lonberg-Holm, K. & Pettersson, U. (1968). Virus-receptor interaction in an adenovirus system. *J Virol* **2**, 1064-75.
- Prasad, B. V., Prevelige, P. E., Marietta, E., Chen, R. O., Thomas, D., King, J. & Chiu, W. (1993). Three-dimensional transformation of capsids associated with genome packaging in a bacterial virus. *J Mol Biol* **231**, 65-74.
- Preston, C. M. (2000). Repression of viral transcription during herpes simplex virus latency. *J Gen Virol* **81 Pt 1**, 1-19.
- Preston, V. G., Coates, J. A. & Rixon, F. J. (1983). Identification and characterization of a herpes simplex virus gene product required for encapsidation of virus DNA. *J Virol* **45**, 1056-64.
- Preston, V. G., Rixon, F. J., McDougall, I. M., McGregor, M. & al Kobaisi, M. F. (1992). Processing of the herpes simplex virus assembly protein ICP35 near its carboxy terminal end requires the product of the whole of the UL26 reading frame. *Virology* **186**, 87-98.
- Prevelige, P. E., Jr. & King, J. (1993). Assembly of bacteriophage P22: a model for ds-DNA virus assembly. *Prog Med Virol* **40**, 206-21.
- Prevelige, P. E., Jr., Thomas, D., Aubrey, K. L., Towse, S. A. & Thomas, G. J., Jr. (1993a). Subunit conformational changes accompanying bacteriophage P22 capsid maturation. *Biochemistry* **32**, 537-43.
- Prevelige, P. E., Jr., Thomas, D. & King, J. (1988). Scaffolding protein regulates the polymerization of P22 coat subunits into icosahedral shells in vitro. *J Mol Biol* **202**, 743-57.
- Prevelige, P. E., Jr., Thomas, D. & King, J. (1993b). Nucleation and growth phases in the polymerization of coat and scaffolding subunits into icosahedral procapsid shells. *Biophys J* **64**, 824-35.
- Price, N. C. (1995). Circular dichroism in protein analysis. In *Molecular biology and biotechnology. A comprehensive desk reference*. Ed. Meyers, R. A. VCH publishers, Inc., 179-185.
- Privalov, G., Kavina, V., Freire, E. & Privalov, P. L. (1995). Precise scanning calorimeter for studying thermal properties of biological macromolecules in dilute solution. *Anal Biochem* **232**, 79-85.
- Privalov, P. L. (1990). Cold denaturation of proteins. *Crit Rev Biochem Mol Biol* **25**, 281-305.
- Privalov, P. L. (1996). Intermediate states in protein folding. *J Mol Biol* **258**, 707-25.
- Privalov, P. L. (1997). Thermodynamics of protein folding. *Journal of chemical thermodynamics* **29**, 447-474.
- Privalov, P. L., Griko Yu, V., Venyaminov, S. & Kutysenko, V. P. (1986). Cold denaturation of myoglobin. *J Mol Biol* **190**, 487-98.

- Privalov, P. L. & Potekhin, S. A. (1986). Scanning microcalorimetry in studying temperature-induced changes in proteins. *Methods Enzymol* **131**, 4-51.
- Prod'hon, C., Machuca, I., Berthomme, H., Epstein, A. & Jacquemont, B. (1996). Characterization of regulatory functions of the HSV-1 immediate-early protein ICP22. *Virology* **226**, 393-402.
- Provencher, S. W. & Glockner, J. (1981). Estimation of globular protein secondary structure from circular dichroism. *Biochemistry* **20**, 33-7.
- Ptitsyn, O. B. (1995a). How the molten globule became. *Trends Biochem Sci* **20**, 376-9.
- Ptitsyn, O. B. (1995b). Structures of folding intermediates. *Curr Opin Struct Biol* **5**, 74-8.
- Ptitsyn, O. B., Pain, R. H., Semisotnov, G. V., Zerovnik, E. & Razgulyaev, O. I. (1990). Evidence for a molten globule state as a general intermediate in protein folding. *FEBS Lett* **262**, 20-4.
- Puvion-Dutilleul, F., Pichard, E., Laithier, M. & Leduc, E. H. (1987). Effect of dehydrating agents on DNA organization in herpes viruses. *J Histochem Cytochem* **35**, 635-45.
- Quinlan, M. P., Chen, L. B. & Knipe, D. M. (1984). The intranuclear location of a herpes simplex virus DNA-binding protein is determined by the status of viral DNA replication. *Cell* **36**, 857-68.
- Rayment, I., Baker, T. S., Caspar, D. L. & Murakami, W. T. (1982). Polyoma virus capsid structure at 22.5 Å resolution. *Nature* **295**, 110-5.
- Redfield, C., Smith, R. A. & Dobson, C. M. (1994). Structural characterization of a highly-ordered 'molten globule' at low pH. *Nat Struct Biol* **1**, 23-9.
- Reynolds, A. E., Fan, Y. & Baines, J. D. (2000). Characterization of the U(L)33 Gene Product of Herpes Simplex Virus 1. *Virology* **266**, 310-318.
- Rixon, F. J. (1993). Structure and Assembly of Herpesviruses. *Seminars in Virology* **4**, 135-144.
- Rixon, F. J., Addison, C., McGregor, A., Macnab, S. J., Nicholson, P., Preston, V. G. & Tatman, J. D. (1996). Multiple interactions control the intracellular localization of the herpes simplex virus type 1 capsid proteins. *J Gen Virol* **77**, 2251-60.
- Rixon, F. J., Addison, C. & McLauchlan, J. (1992). Assembly of enveloped tegument structures (L particles) can occur independently of virion maturation in herpes simplex virus type 1-infected cells. *J Gen Virol* **73**, 277-84.
- Rixon, F. J., Davison, M. D. & Davison, A. J. (1990). Identification of the genes encoding two capsid proteins of herpes simplex virus type 1 by direct amino acid sequencing. *J Gen Virol* **71**, 1211-4.
- Rixon, F. J. & McNab, D. (1999). Packaging-competent capsids of a herpes simplex virus temperature-sensitive mutant have properties similar to those of in vitro-assembled procapsids. *J Virol* **73**, 5714-21.
- Rodahl, E. & Haarr, L. (1997). Analysis of the 2-kilobase latency-associated transcript expressed in PC12 cells productively infected with herpes simplex virus type 1: evidence for a stable, nonlinear structure. *J Virol* **71**, 1703-7.
- Rohrer, S. P., Evans, D. V. & Bergstrom, A. (1990). A membrane associated glutamate binding protein from *Caenorhabditis elegans* and *Haemonchus contortus*. *Comp Biochem Physiol C* **95**, 223-8.
- Roizman, B. & Sears, A. (1996). Herpes simplex viruses and their replication. In *Fields Virology*, Edited by B. N. Fields, D. M. Knipe, P. M. Howley, & e. al. Philadelphia: Raven publishers., 2231-2295.
- Roizmann, B., Desrosiers, R. C., Fleckenstein, B., Lopez, C., Minson, A. C. & Studdert, M. J. (1992). The family Herpesviridae: an update. The Herpesvirus Study Group of the International Committee on Taxonomy of Viruses. *Arch Virol* **123**, 425-49.

- Roller, R. J., Monk, L. L., Stuart, D. & Roizman, B. (1996). Structure and function in the herpes simplex virus 1 RNA-binding protein U(s)11: mapping of the domain required for ribosomal and nucleolar association and RNA binding in vitro. *J Virol* **70**, 2842-51.
- Rose, J. K., Buonocore, L. & Whitt, M. A. (1991). A new cationic liposome reagent mediating nearly quantitative transfection of animal cells. *Biotechniques* **10**, 520-5.
- Ross, P. D., Black, L. W., Bisher, M. E. & Steven, A. C. (1985). Assembly-dependent conformational changes in a viral capsid protein. Calorimetric comparison of successive conformational states of the gp23 surface lattice of bacteriophage T4. *J Mol Biol* **183**, 353-64.
- Rossmann, M. G. (1984). Constraints on the assembly of spherical virus particles. *Virology* **134**, 1-11.
- Rost, B. & Sander, C. (1993). Improved prediction of protein secondary structure by use of sequence profiles and neural networks. *Proc Natl Acad Sci U S A* **90**, 7558-62.
- Saad, A., Zhou, Z. H., Jakana, J., Chiu, W. & Rixon, F. J. (1999). Roles of triplex and scaffolding proteins in herpes simplex virus type 1 capsid formation suggested by structures of recombinant particles. *J Virol* **73**, 6821-30.
- Saibil, H. R. (2000). The black widow's versatile venom [news; comment]. *Nat Struct Biol* **7**, 3-4.
- Salmon, B. & Baines, J. D. (1998). Herpes simplex virus DNA cleavage and packaging: association of multiple forms of U(L)15-encoded proteins with B capsids requires at least the U(L)6, U(L)17, and U(L)28 genes. *J Virol* **72**, 3045-50.
- Salmon, B., Cunningham, C., Davison, A. J., Harris, W. J. & Baines, J. D. (1998). The herpes simplex virus type 1 U(L)17 gene encodes virion tegument proteins that are required for cleavage and packaging of viral DNA. *J Virol* **72**, 3779-88.
- Sandri-Goldin, R. M. (1998). Interactions between a herpes simplex virus regulatory protein and cellular mRNA processing pathways. *Methods* **16**, 95-104.
- Schek, N. & Bachenheimer, S. L. (1985). Degradation of cellular mRNAs induced by a virion-associated factor during herpes simplex virus infection of Vero cells. *J Virol* **55**, 601-10.
- Schmitz, J. B., Albright, A. G., Kinchington, P. R. & Jenkins, F. J. (1995). The UL37 protein of herpes simplex virus type 1 is associated with the tegument of purified virions. *Virology* **206**, 1055-65.
- Schoehn, G., Fender, P., Chroboczek, J. & Hewat, E. A. (1996). Adenovirus 3 penton dodecahedron exhibits structural changes of the base on fibre binding. *Embo J* **15**, 6841-6.
- Schrag, J. D., Prasad, B. V., Rixon, F. J. & Chiu, W. (1989). Three-dimensional structure of the HSV1 nucleocapsid. *Cell* **56**, 651-60.
- Semisotnov, G. V., Rodionova, N. A., Razgulyaev, O. I., Uversky, V. N., Gripas, A. F. & Gilmanshin, R. I. (1991). Study of the "molten globule" intermediate state in protein folding by a hydrophobic fluorescent probe. *Biopolymers* **31**, 119-28.
- Shao, L., Rapp, L. M. & Weller, S. K. (1993). Herpes simplex virus 1 alkaline nuclease is required for efficient egress of capsids from the nucleus. *Virology* **196**, 146-62.
- Sheaffer, A. K., Newcomb, W. W., Brown, J. C., Gao, M., Weller, S. K. & Tenney, D. J. (2000). Evidence for controlled incorporation of herpes simplex virus type 1 UL26 protease into capsids. *J Virol* **74**, 6838-48.
- Shieh, M. T. & Spear, P. G. (1994). Herpesvirus-induced cell fusion that is dependent on cell surface heparan sulfate or soluble heparin. *J Virol* **68**, 1224-8.

- Sinclair, M. C., McLauchlan, J., Marsden, H. & Brown, S. M. (1994). Characterization of a herpes simplex virus type 1 deletion variant (1703) which under-produces Vmw63 during immediate early conditions of infection. *J Gen Virol* **75**, 1083-9.
- Sodeik, B., Ebersold, M. W. & Helenius, A. (1997). Microtubule-mediated transport of incoming herpes simplex virus 1 capsids to the nucleus. *J Cell Biol* **136**, 1007-21.
- Song, J., Bai, P., Luo, L. & Peng, Z. Y. (1998). Contribution of individual residues to formation of the native-like tertiary topology in the alpha-lactalbumin molten globule. *J Mol Biol* **280**, 167-74.
- Spear, P. (1993). Entry of alphaherpesviruses into cells. *seminars in Virology* **4**, 143-159.
- Spear, P. G. & Roizman, B. (1972). Proteins specified by herpes simplex virus V. Purification and structural proteins of the herpesvirion. *Journal of Virology* **9**, 143-159.
- Spencer, J. V., Newcomb, W. W., Thomsen, D. R., Homa, F. L. & Brown, J. C. (1998). Assembly of the herpes simplex virus capsid: preformed triplexes bind to the nascent capsid. *J Virol* **72**, 3944-51.
- Steiner, I. & Kennedy, P. G. (1995). Herpes simplex virus latent infection in the nervous system. *J Neurovirol* **1**, 19-29.
- Steven, A. C., Couture, E., Aebi, U. & Showe, M. K. (1976). Structure of T4 polyheads. II. A pathway of polyhead transformation as a model for T4 capsid maturation. *J Mol Biol* **106**, 187-221.
- Steven, A. C., Greenstone, H. L., Booy, F. P., Black, L. W. & Ross, P. D. (1992). Conformational changes of a viral capsid protein. Thermodynamic rationale for proteolytic regulation of bacteriophage T4 capsid expansion, co-operativity, and super-stabilization by soc binding. *J Mol Biol* **228**, 870-84.
- Steven, A. C. & Spear, P. G. (1997). Herpesvirus capsid assembly and envelopment. In *Structural biology of viruses. W. Chiu, R. Burnett, and R. Garcea (Eds): Oxford University Press, New York.*, 321-251.
- Steven, A. C., Trus, B. L., Booy, F. P., Cheng, N., Zlotnick, A., Caston, J. R. & Conway, J. F. (1997). The making and breaking of symmetry in virus capsid assembly: glimpses of capsid biology from cryoelectron microscopy. *Faseb J* **11**, 733-42.
- Stow, N. D., Hammarsten, O., Arbuckle, M. I. & Elias, P. (1993). Inhibition of herpes simplex virus type 1 DNA replication by mutant forms of the origin-binding protein. *Virology* **196**, 413-8.
- Subak-Sharpe, J. H. & Dargan, D. J. (1998). HSV molecular biology: general aspects of herpes simplex virus molecular biology. *Virus Genes* **16**, 239-51.
- Szilagyi, J. F. & Cunningham, C. (1991). Identification and characterization of a novel non-infectious herpes simplex virus-related particle. *J Gen Virol* **72**, 661-8.
- Tatman, J. D. (1996). An investigation into the structure and assembly of the herpes simplex type-1 (HSV-1) capsid using the baculovirus expression system. *PhD. Thesis, University of Glasgow.*
- Tatman, J. D., Preston, V. G., Nicholson, P., Elliott, R. M. & Rixon, F. J. (1994). Assembly of herpes simplex virus type 1 capsids using a panel of recombinant baculoviruses. *J Gen Virol* **75**, 1101-13.
- Teschke, C. M. & King, J. (1993). Folding of the phage P22 coat protein in vitro. *Biochemistry* **32**, 10839-47.
- Thomas, S. K., Gough, G., Latchman, D. S. & Coffin, R. S. (1999). Herpes simplex virus latency-associated transcript encodes a protein which greatly enhances virus growth, can compensate for deficiencies in immediate-early gene expression, and is likely to function during reactivation from virus latency. *J Virol* **73**, 6618-25.

- Thomsen, D. R., Roof, L. L. & Homa, F. L. (1994). Assembly of herpes simplex virus (HSV) intermediate capsids in insect cells infected with recombinant baculoviruses expressing HSV capsid proteins. *J Virol* **68**, 2442-57.
- Tognon, M., Furlong, D., Conley, A. J. & Roizman, B. (1981). Molecular genetics of herpes simplex virus. V. Characterization of a mutant defective in ability to form plaques at low temperatures and in a viral fraction which prevents accumulation of coreless capsids at nuclear pores late in infection. *J Virol* **40**, 870-80.
- Trus, B. L., Booy, F. P., Newcomb, W. W., Brown, J. C., Homa, F. L., Thomsen, D. R. & Steven, A. C. (1996). The herpes simplex virus procapsid: structure, conformational changes upon maturation, and roles of the triplex proteins VP19c and VP23 in assembly. *J Mol Biol* **263**, 447-62.
- Trus, B. L., Gibson, W., Cheng, N. & Steven, A. C. (1999). Capsid structure of simian cytomegalovirus from cryoelectron microscopy: evidence for tegument attachment sites [published erratum appears in *J Virol* 1999 May;73(5):4530]. *J Virol* **73**, 2181-92.
- Trus, B. L., Homa, F. L., Booy, F. P., Newcomb, W. W., Thomsen, D. R., Cheng, N., Brown, J. C. & Steven, A. C. (1995). Herpes simplex virus capsids assembled in insect cells infected with recombinant baculoviruses: structural authenticity and localization of VP26. *J Virol* **69**, 7362-6.
- Trus, B. L., Newcomb, W. W., Booy, F. P., Brown, J. C. & Steven, A. C. (1992). Distinct monoclonal antibodies separately label the hexons or the pentons of herpes simplex virus capsid. *Proc Natl Acad Sci U S A* **89**, 11508-12.
- Trus, B. L., Roden, R. B., Greenstone, H. L., Vrhel, M., Schiller, J. T. & Booy, F. P. (1997). Novel structural features of bovine papillomavirus capsid revealed by a three-dimensional reconstruction to 9 Å resolution. *Nat Struct Biol* **4**, 413-20.
- Tuma, R., Prevelige, P. E., Jr. & Thomas, G. J., Jr. (1998). Mechanism of capsid maturation in a double-stranded DNA virus. *Proc Natl Acad Sci U S A* **95**, 9885-90.
- Tuma, R. & Thomas, G. J., Jr. (1997). Mechanisms of virus assembly probed by Raman spectroscopy: the icosahedral bacteriophage P22. *Biophys Chem* **68**, 17-31.
- Uversky, V. N., Kirkitadze, M. D., Narizhneva, N. V., Potekhin, S. A. & Tomashevski, A. (1995). Structural properties of alpha-fetoprotein from human cord serum: the protein molecule at low pH possesses all the properties of the molten globule. *FEBS Lett* **364**, 165-7.
- Valpuesta, J. M. & Carrascosa, J. L. (1994). Structure of viral connectors and their function in bacteriophage assembly and DNA packaging. *Q Rev Biophys* **27**, 107-155.
- van Genderen, I. L., Brandimarti, R., Torrisi, M. R., Campadelli, G. & van Meer, G. (1994). The phospholipid composition of extracellular herpes simplex virions differs from that of host cell nuclei. *Virology* **200**, 831-6.
- van Oostrum, J. & Burnett, R. M. (1985). Molecular composition of the adenovirus type 2 virion. *J Virol* **56**, 439-48.
- Vaughn, J. L., Goodwin, R. H., Tompkins, G. J. & McCawley, P. (1977). The establishment of two cell lines from the insect *Spodoptera frugiperda* (Lepidoptera; Noctuidae). *In Vitro* **13**, 213-7.
- Vernon, S. K., Lawrence, W. C. & Cohen, G. H. (1974). Morphological components of herpesvirus. I. Intercapsomeric fibrils and the geometry of the capsid. *Intervirology* **4**, 237-48.

- Vidal, M., Brachmann, R. K., Fattaey, A., Harlow, E. & Boeke, J. D. (1996a). Reverse two-hybrid and one-hybrid systems to detect dissociation of protein-protein and DNA-protein interactions [see comments]. *Proc Natl Acad Sci U S A* **93**, 10315-20.
- Vidal, M., Braun, P., Chen, E., Boeke, J. D. & Harlow, E. (1996b). Genetic characterization of a mammalian protein-protein interaction domain by using a yeast reverse two-hybrid system [see comments]. *Proc Natl Acad Sci U S A* **93**, 10321-6.
- Vidal, M. & Legrain, P. (1999). Yeast forward and reverse 'n'-hybrid systems. *Nucleic Acids Res* **27**, 919-29.
- Wagner, E. K. & Bloom, D. C. (1997). Experimental investigation of herpes simplex virus latency. *Clin Microbiol Rev* **10**, 419-43.
- Ward, P. L., Ogle, W. O. & Roizman, B. (1996). Assemblons: nuclear structures defined by aggregation of immature capsids and some tegument proteins of herpes simplex virus 1. *J Virol* **70**, 4623-31.
- Weinheimer, S. P., McCann, P. J. d., O'Boyle, D. R. d., Stevens, J. T., Boyd, B. A., Drier, D. A., Yamanaka, G. A., Dilanni, C. L., Deckman, I. C. & Cordingley, M. G. (1993). Autoproteolysis of herpes simplex virus type 1 protease releases an active catalytic domain found in intermediate capsid particles. *J Virol* **67**, 5813-22.
- Weller, S. K., Carmichael, E. P., Aschman, D. P., Goldstein, D. J. & Schaffer, P. A. (1987). Genetic and phenotypic characterization of mutants in four essential genes that map to the left half of HSV-1 UL DNA. *Virology* **161**, 198-210.
- Whiteley, A., Bruun, B., Minson, T. & Browne, H. (1999). Effects of targeting herpes simplex virus type 1 gD to the endoplasmic reticulum and trans-Golgi network. *J Virol* **73**, 9515-20.
- Wildy, P., Russell, W. & Horne, R. (1960). The morphology of herpesvirus. *Virology* **12**, 201-222.
- Wingfield, P., Pain, R. H. & Craig, S. (1987). Tumour necrosis factor is a compact trimer. *FEBS Lett* **211**, 179-84.
- Wingfield, P. T., Stahl, S. J., Thomsen, D. R., Homa, F. L., Booy, F. P., Trus, B. L. & Steven, A. C. (1997). Hexon-only binding of VP26 reflects differences between the hexon and penton conformations of VP5, the major capsid protein of herpes simplex virus. *J Virol* **71**, 8955-61.
- Wittels, M. & Spear, P. G. (1991). Penetration of cells by herpes simplex virus does not require a low pH-dependent endocytic pathway. *Virus Res* **18**, 271-90.
- Wu, L. C. & Kim, P. S. (1998). A specific hydrophobic core in the alpha-lactalbumin molten globule. *J Mol Biol* **280**, 175-82.
- Yamada, H., Daikoku, T., Yamashita, Y., Jiang, Y. M., Tsurumi, T. & Nishiyama, Y. (1997). The product of the US10 gene of herpes simplex virus type 1 is a capsid/tegument-associated phosphoprotein which copurifies with the nuclear matrix. *J Gen Virol* **78**, 2923-31.
- Ye, G. J., Vaughan, K. T., Vallee, R. B. & Roizman, B. (2000). The herpes simplex virus 1 U(L)34 protein interacts with a cytoplasmic dynein intermediate chain and targets nuclear membrane. *J Virol* **74**, 1355-63.
- Yei, S. P., Chowdhury, S. I., Bhat, B. M., Conley, A. J., Wold, W. S. & Batterson, W. (1990). Identification and characterization of the herpes simplex virus type 2 gene encoding the essential capsid protein ICP32/VP19c. *J Virol* **64**, 1124-34.
- Yu, D. & Weller, S. K. (1998). Herpes simplex virus type 1 cleavage and packaging proteins UL15 and UL28 are associated with B but not C capsids during packaging. *J Virol* **72**, 7428-39.

- Yutani, K., Ogasahara, K. & Kuwajima, K. (1992). Absence of the thermal transition in apo-alpha-lactalbumin in the molten globule state. A study by differential scanning microcalorimetry. *J Mol Biol* **228**, 347-50.
- Zezulak, K. M. & Spear, P. G. (1984). Mapping of the structural gene for the herpes simplex virus type 2 counterpart of herpes simplex virus type 1 glycoprotein C and identification of a type 2 mutant which does not express this glycoprotein. *J Virol* **49**, 741-7.
- Zhang, X., Efstathiou, S. & Simmons, A. (1994). Identification of novel herpes simplex virus replicative intermediates by field inversion gel electrophoresis: implications for viral DNA amplification strategies. *Virology* **202**, 530-9.
- Zhang, Y. & McKnight, J. L. (1993). Herpes simplex virus type 1 UL46 and UL47 deletion mutants lack VP11 and VP12 or VP13 and VP14, respectively, and exhibit altered viral thymidine kinase expression. *J Virol* **67**, 1482-92.
- Zhang, Y., Sirko, D. A. & McKnight, J. L. (1991). Role of herpes simplex virus type 1 UL46 and UL47 in alpha TIF-mediated transcriptional induction: characterization of three viral deletion mutants. *J Virol* **65**, 829-41.
- Zhang, Z., Greene, B., Thuman-Commike, P. A., Jakana, J., Prevelige, P. E., Jr., King, J. & Chiu, W. (2000). Visualization of the maturation transition in bacteriophage P22 by electron cryomicroscopy. *J Mol Biol* **297**, 615-26.
- Zhou, Z. H., Chen, D. H., Jakana, J., Rixon, F. J. & Chiu, W. (1999). Visualization of tegument-capsid interactions and DNA in intact herpes simplex virus type 1 virions. *J Virol* **73**, 3210-8.
- Zhou, Z. H., Dougherty, M., Jakana, J., He, J., Rixon, F. J. & Chiu, W. (2000). Seeing the herpesvirus capsid at 8.5 Å. *Science* **288**, 877-80.
- Zhou, Z. H., He, J., Jakana, J., Tatman, J. D., Rixon, F. J. & Chiu, W. (1995). Assembly of VP26 in herpes simplex virus-1 inferred from structures of wild-type and recombinant capsids. *Nat Struct Biol* **2**, 1026-30.
- Zhou, Z. H., Macnab, S. J., Jakana, J., Scott, L. R., Chiu, W. & Rixon, F. J. (1998). Identification of the sites of interaction between the scaffold and outer shell in herpes simplex virus-1 capsids by difference electron imaging. *Proc Natl Acad Sci USA* **95**, 2778-83.
- Zhou, Z. H., Prasad, B. V., Jakana, J., Rixon, F. J. & Chiu, W. (1994). Protein subunit structures in the herpes simplex virus A-capsid determined from 400 kV spot-scan electron cryomicroscopy. *J Mol Biol* **242**, 456-69.
- Zlotnick, A. (1994). To build a virus capsid. An equilibrium model of the self assembly of polyhedral protein complexes. *J Mol Biol* **241**, 59-67.
- Zweig, M., Heilman, C. J., Jr. & Hampar, B. (1979). Identification of disulfide-linked protein complexes in the nucleocapsids of herpes simplex virus type 2. *Virology* **94**, 442-50.